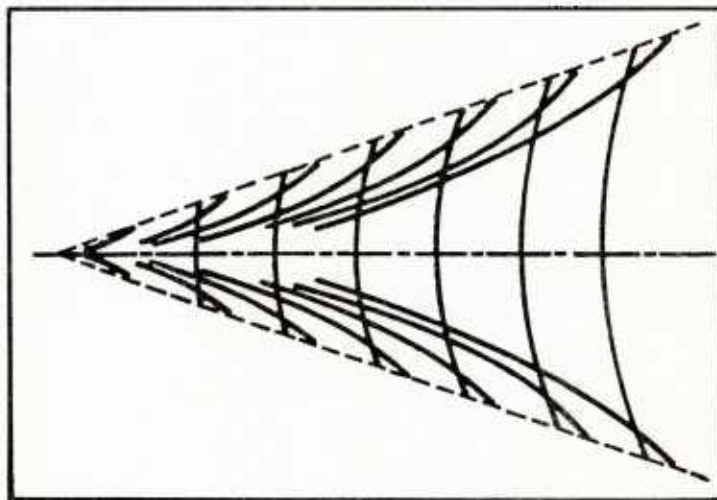


39615

THE PROCEEDINGS OF THE SECOND DTNSRDC WORKSHOP ON
SHIP WAVE-RESISTANCE COMPUTATIONS

ae

LIBRARY
RESEARCH REPORTS DIVISION
NAVAL POSTGRADUATE SCHOOL
MONTEREY, CALIFORNIA 93945



16-17 November 1983

David W. Taylor Naval Ship Research and Development Center
Bethesda, Maryland 20084
United States of America

AN (1) AD-A139 615
 FG (2) 120100
 FG (2) 131000
 FG (2) 200400
 CI (3) (U)
 CA (5) DAVID W TAYLOR NAVAL SHIP RESEARCH AND DEVELOPMENT
 CENTER BETHESDA MD
 TI (6) Proceedings of the DTNSRDC (David W. Taylor Naval Ship
 Research and Development Center) Workshop on Ship
 Wave-Resistance Computations (2nd) Held at Bethesda,
 Maryland on 16-17 November 1983,
 AU (10) Noblesse, F.
 AU (10) McCarthy, J. H.
 RD (11) Nov 1983
 PG (12) 467p
 RC (20) Unclassified report
 NO (21) For sales information of individual items see AD-P003
 Q37 - AD-P003 Q57.
 DE (23) *Water waves, *Ship hulls, *Symposia, *Mathematical
 models, *Hydrodynamics, *Resistance, Numerical methods
 and procedures, Mathematical prediction, Computerized
 simulation, Water flow, Theory, Applied mathematics,
 Computations, Workshops
 DC (24) (U)
 ID (25) *Wave resistance, Thin ship theory, Froude number,
 Singularities, Compilation Reports
 IC (26) (U)
 AB (27) A main goal of the present and previous workshops was
 to develop a bank of numerical results for a few
 selected hull forms. Creation of extensive sets of
 numerical results, together with corresponding sets of
 experimental values, is indispensable for objectively
 evaluating the merits and limitations of the various
 existing methods of wave-resistance calculation, and
 for progressing towards development of reliable and
 practical calculation methods. Five hull forms were
 suggested for the workshop. These include the Wigley
 parabolic hull and the Series 60 block coefficient 0.60
 hull. Two vertical cylinders (infinite draft), one with
 a round-ended elliptical waterline and the other with a
 sharp-ended lens-like waterline in the shape of an
 ogive ((consisting of two arcs of circle), were
 suggested for use in the low-speed theories. Both have
 beam/length ratio, b , equal to 0.15. A fully-submerged
 body may provide a useful intermediate test case for
 development of a numerical method. A prolate spheroid
 with a 5:1 ratio of length to midsection diameter and a
 ratio of submergence depth (measured from the axis of
 the spheroid to the undisturbed free-surface level) to
 the midsection diameter of 0.792, for which there
 already exist both experimental data and theoretical
 results, was proposed. Finally, a simple strut-like

Page 2

** MAY CONTAIN EXPORT CONTROL DATA **

ADAXXXXXX MICROFICHE ARE HOUSED IN THE GENERAL MICROFORMS RM

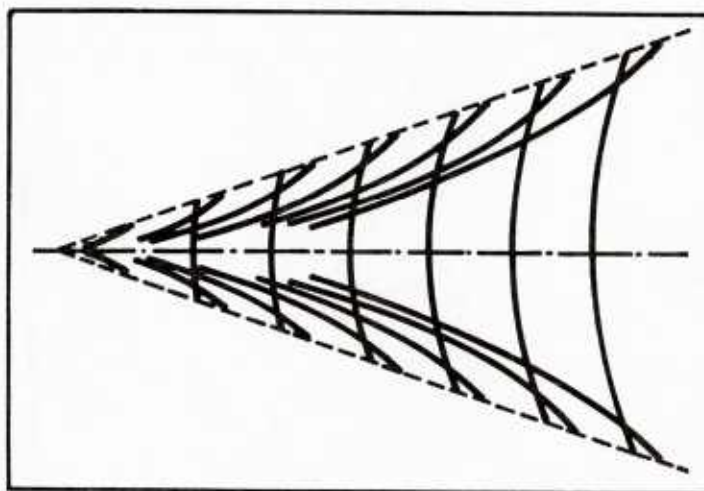
hull form having constant draft, rectangular
 framelines, and a substantial parallel middle body, and
 that is sharp at one end and round at the other end,
 was proposed.

AC (28) (U)
 DL (33) 01
 SE (34) 2
 CC (35) 387682



PROCEEDINGS OF THE SECOND DTNSRDC WORKSHOP ON SHIP WAVE-RESISTANCE COMPUTATIONS

**Edited by
Francis Noblesse
Justin H. McCarthy**



16-17 November 1983

**David W. Taylor Naval Ship Research and Development Center
Bethesda, Maryland 20084
United States of America**

Statements and opinions contained herein are those of the authors and are not to be construed as official or reflecting the views of the Navy Department or of the naval service at large.



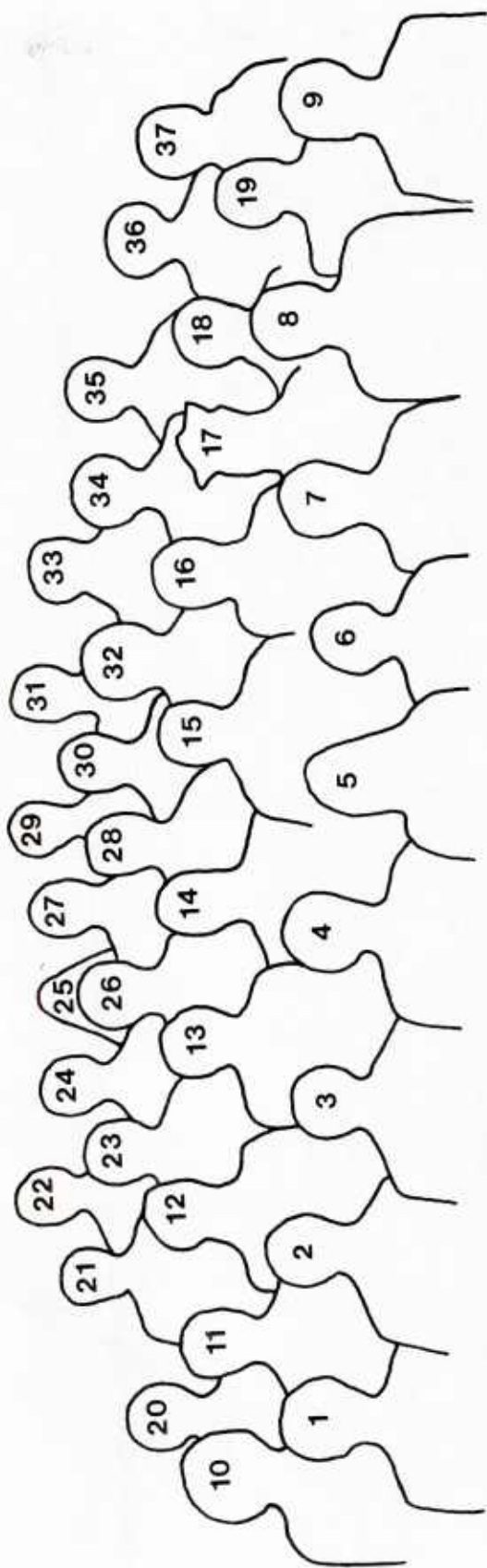


PHOTO INDEX OF WORKSHOP PARTICIPANTS AT
DAVID W. TAYLOR NAVAL SHIP RESEARCH AND DEVELOPMENT CENTER,
BETHESDA, MARYLAND, U.S.A.

1. Prof. Kazuhiro Mori, Hiroshima University, Japan
2. Dr. Bohyun Yim, DTNSRDC
3. Mr. Bill H. Cheng, DTNSRDC
4. Dr. Thomas T. Huang, DTNSRDC
5. Ms. Toby J. Nagle, DTNSRDC
6. Prof. Mitsuhisa Ikehata, Yokohama National University, Japan
7. Dr. Yoon-Ho Kim, DTNSRDC
8. Prof. Shee-Mang Yen, University of Illinois, USA
9. Mr. Chu-Yung Chen, Naval Sea Systems Command, USA
10. Mr. Steven C. Fisher, DTNSRDC
11. Prof. Hideaki Miyata, University of Tokyo, Japan
12. Mr. Seikoo Ogiwara, Ishikawajima-Harima Heavy
Industries Co., Ltd. Research Institute, Yokohama, Japan
13. Prof. Louis Landweber, University of Iowa, USA
14. Mr. Daniel F. Dementhon, TRACOR HYDRONAUTICS, USA
15. Dr. Allen V. Hershey, Naval Postgraduate School, USA
16. Prof. Kuniharu Nakatake, Kyushu University, Japan
17. Dr. John L. Jayne, DTNSRDC
18. Dr. Ki-Han Kim, DTNSRDC
19. Dr. Christian H. von Kerczek, DTNSRDC
20. Prof. Sander M. Calisal, University of British Columbia, Canada
21. Prof. Chi-Chao Hsiung, Memorial University of Newfoundland, Canada
22. Dr. Henry T. Wang, Naval Research Laboratory, USA
23. Mr. Justin H. McCarthy, DTNSRDC
24. Mr. Michael Mackay, Defence Research Establishment Atlantic, Canada

25. Ms. Janet S. Dean, DTNSRDC
26. Dr. Arthur M. Reed, DTNSRDC
27. Mr. Vidar Aanesland, Norwegian Institute of Technology, Trondheim, Norway
28. Dr. Young S. Hong, DTNSRDC
29. Dr. Francis Noblesse, DTNSRDC
30. Mr. Roderick M. Coleman, DTNSRDC
31. Ms. Joanna W. Schot, DTNSRDC
32. Mr. Seth Hawkins, DTNSRDC
33. Dr. Hans J. Lugt, DTNSRDC
34. Dr. Carl A. Scragg, Science Applications Inc., USA
35. Dr. Henry J. Haussling, DTNSRDC
36. Mr. William C. Sandberg, Naval Sea Systems Command, USA
37. Dr. Marc A. Lenoir, CNRS-ENSTA, Palaiseau, France

Workshop Participants not in photograph:

38. Dr. Robert C. Allen, DTNSRDC
39. Dr. Ming-Shun Chang, DTNSRDC
40. Mr. William G. Day, DTNSRDC
41. Dr. Choung M. Lee, Office of Naval Research, USA
42. Dr. Yu-Tai Lee, DTNSRDC
43. Dr. Cheng-Wen Lin, ORI, Inc., USA
44. Dr. Wen-Chin Lin, DTNSRDC
45. Dr. William B. Morgan, DTNSRDC
46. Dr. David D. Moran, DTNSRDC
47. Dr. A. Yucel Odabasi, British Ship Research Association, England
48. Mr. John G. Telste, DTNSRDC
49. Dr. Michael B. Wilson, DTNSRDC

PREFACE

WELCOMING REMARKS TO PARTICIPANTS

Justin H. McCarthy
David W. Taylor Naval Ship Research and Development Center
Bethesda, Maryland, USA

On behalf of the Commanding Officer, Captain Barrick F. Tibbitts, and the Technical Director, Dr. Alan Powell, I welcome you to the David W. Taylor Naval Ship Research and Development Center (DTNSRDC).

For the next two days we will be engaged in the Center's Second Workshop on Ship Wavemaking Resistance Computations. There are twenty-one papers to be presented: Seven from Japan, one from the Republic of China, one from France, one from the United Kingdom, and eleven from North America of which two are from Canada. For those of you who have travelled long distances we are very grateful, for the subject of the Workshop is truly of international interest.

The present Workshop is the third in four years. The First Workshop was held at DTNSRDC in 1979 and was soon followed by a Continued Workshop held at Shuzenji, Japan in 1980. Many impressive results were presented at the earlier Workshops. However, it was apparent that large differences existed between the predictions of wave resistance by the various methods, even when the same or closely related theories were used. The goal of the present Workshop is to shed further light on the differences and hopefully pave the way for more reliable prediction methods.

There are a number of reasons for convening workshops on the prediction of wavemaking resistance, a classical and important problem of ship hydrodynamics. First, because of the diversity of methods under development, valuable exchanges can be made between method developers in a workshop format. Second, establishment of a "Bank" of numerical predictions for a select group of hull forms can help in the evaluation of new methods, and thus promote progress. Finally, the present Workshop seems especially timely because progress has been made rapidly in the past few years and a number of first generation numerical methods are now

operational.

The goals of the present and previous Workshops have been subscribed to and enthusiastically supported by members of the Resistance Committee of the International Towing Tank Conference (ITTC). The committee is currently assembling an experimental data base on the resistance components of and flow about four baseline hull forms, using information supplied by ITTC member organizations. Some of the data are reported at the present Workshop. All of the data will be reported in 1984 and should be useful in evaluating analytical and numerical methods for predicting the components of ship resistance.

Again, I welcome you all to the Workshop, wish you success, and invite you to take part in free discussions and exchanges of ideas.

CONTENTS

	<u>Page</u>
PREFACE, Justin H. McCarthy	viii
INTRODUCTION, Francis Noblesse	1
SUMMARY OF THE COOPERATIVE EXPERIMENT ON WIGLEY PARABOLIC MODEL IN JAPAN, H. Kajitani and H. Miyata, M. Ikehata, H. Tanaka and H. Adachi, M. Namimatsu and S. Ogiwara	5
STUDY OF TOTAL AND VISCOUS RESISTANCE FOR THE WIGLEY PARABOLIC SHIP FORM, Sangseon Ju	36
A GEOMETRICALLY CONSISTENT LINEARIZATION METHOD FOR AN ELLIPTIC STRUT, S.M. Calisal	50
A SEMI-EMPIRICAL METHOD FOR WAVE RESISTANCE PREDICTION, A. Yucel Odabasi	62
COMPUTING WAVE RESISTANCE AND WAVE PROFILE FOR SIX DIFFERENT HULL FORMS, Chi-Chao Hsiung, Ge Weizhen, Jiunn-Ming Chuang	72
COMPUTATION OF NON-LINEAR WAVE RESISTANCE, Young S. Hong	104
A SLENDER-BODY SOLUTION FOR THE CENTERPLANE DISTRIBUTION FOR THE WIGLEY SHIP FORM, L. Landweber and Sangseon Ju	127
AN APPLICATION OF NEW SLENDER SHIP THEORY TO SERIES 60, $C_b = 0.60$, H. Maruo and M. Ikehata	141
A NUMERICAL INVESTIGATION OF THE SLENDER-SHIP WAVE RESISTANCE APPROXIMATION, Carl A. Scragg	161
NUMERICAL STUDY OF EIGHT WAVE-RESISTANCE APPROXIMATIONS, Francis Noblesse	179
LINEAR AND NON-LINEAR CALCULATIONS FOR THE WAVE-RESISTANCE OF SUBMERGED BODIES, M. Lenoir, J. Cahouet, C. Guttman	213
A COMPUTATION OF FLOW AROUND A SHIP, Allen V. Hershey	228
NUMERICAL SOLUTION OF THE NEUMANN-KELVIN PROBLEM AND ITS APPLICATION TO SHIP WAVE-RESISTANCE COMPUTATIONS, Wu-ting Tsai, Yeun-junn Lin and Ching-chao Liao	233
NEUMANN-KELVIN PROBLEM SOLVED BY THE ITERATIVE PROCEDURE USING HESS AND SMITH SOLVER PROGRAM, H. Adachi and H. Takeshi	281
WAVE RESISTANCE CALCULATION BY MODIFIED RANKINE SOURCE METHOD, Kazuhiro Mori and Koichi Murata	321

NUMERICAL CALCULATION OF FREE SURFACE FLOW BY MEANS OF MODIFIED RANKINE SOURCE METHOD, S. Ogiwara	341
THE XYZ FREE SURFACE PROGRAM AND ITS APPLICATION TO TRANSOM-STERN SHIPS WITH BOW DOMES, Bill H. Cheng, Janet S. Dean, John L. Jayne ...	370
A COMPARISON WITH EXPERIMENTAL RESULTS OF WAVE RESISTANCE PREDICTIONS USING A RANKINE SOURCE PANEL METHOD AND A SLENDER BODY THEORY, William C. Sandberg and Carl A. Scragg	393
WAVE RESISTANCE OF VERTICAL CYLINDERS WITH OGIVAL AND ELLIPTICAL WATER PLANES, K. Nakatake, A. Nishida and R. Yamazaki	406
NUMERICAL CALCULATIONS OF THE POTENTIAL FLOW ABOUT THE WIGLEY HULL, S.M. Yen and R.R. Chamberlain	422
NUMERICAL SIMULATION OF SHIP WAVES BY DIRECT INTEGRATION OF NAVIER-STOKES EQUATIONS, Hideaki Miyata, Shinichi Nishimura, Hisashi Kajitani	441

SECOND DTNSRDC WORKSHOP ON SHIP WAVE-RESISTANCE COMPUTATIONS

INTRODUCTION

Francis Noblesse
David W. Taylor Naval Ship Research and Development Center
Bethesda, Maryland, USA

The object of this introduction is to provide a brief overview of the studies that were presented at the Workshop and are included in these Proceedings, of the theoretical and numerical methods that were used, and of the hull forms for which calculations were performed.

HULL FORMS

A main goal of both the present and the previous Workshops was to develop a "bank of numerical results" for a few selected hull forms. The creation of extensive sets of numerical results, together with corresponding sets of experimental values, indeed is extremely important, if not indispensable, for objectively evaluating the merits and limitations of the various existing methods of wave-resistance calculation, and for progressing towards the development of reliable and practical calculation methods.

Five hull forms were suggested for the Workshop. Two of these five hull forms were easy choices since they had already been used by a large number of Participants at the first Workshop in 1979, and extensive experimental values are available. These two hulls are the Wigley parabolic hull and the Series 60 block coefficient 0.60 hull, that are defined in detail on pages 89-91 and pages 95-100, respectively, in Volume 1 of the Proceedings of the 1979 Workshop.¹ The other three "suggested hull forms" were proposed on the basis of suggestions received in response to the first announcement for the Workshop.

Two vertical cylinders (infinite draft), one with a round-ended elliptical waterline and the other with a sharp-ended lens-like waterline in the shape of an ogive (consisting of two arcs of circle), were suggested by Dr. Eiichi Baba for use in the low-speed theories (the zero-Froude-number potential is given by

simple analytical expressions for these two vertical cylinders). Both cylinders have beam/length ratio, b , equal to 0.15. Specifically, the equations of the waterlines are given by $y = \pm(b/2)(1-4x^2)^{1/2}$ and $y = \pm(1/2) \{ [(1+b^2)^2/4b^2 - 4x^2]^{1/2} - (1-b^2)/2b \}$, where $-1/2 \leq x \leq 1/2$, for the ellipse and the ogive, respectively.

A fully-submerged body was suggested by both Dr. Ming Chang and Professor Daniel Euvrard. Calculations for a fully-submerged body are far simpler than for a free-surface piercing hull since the major difficulties arising from the intersection between the hull surface and the free surface obviously are eliminated. In this sense, a fully-submerged body may provide a useful intermediate test case for the development of a numerical method. A prolate spheroid with a 5 to 1 ratio of length to midsection diameter and a ratio of submergence depth (measured from the axis of the spheroid to the undisturbed free-surface level) to the midsection diameter of 0.792, for which there already exist both experimental data by Farell and Guven² and theoretical results by Farell³, was then proposed. Specifically, the spheroid is defined by the equation $(y^2+z^2)^{1/2} = 0.1 (1-4x^2)^{1/2}$ where $-1/2 \leq x \leq 1/2$, and the mean free surface is the plane $z = 0.1584$.

Finally, a simple strut-like hull form having constant draft, rectangular framelines, and a substantial parallel middle body, and that is sharp at one end and round at the other end, was proposed. It was also suggested that calculations be performed for both cases when the hull moves with the sharp end ahead (sharp bow/round stern case) and with the round end ahead (round bow/sharp stern case). Specifically, the waterline of this strut-like hull form is defined by the equations $y = \pm(b/2)8x(1-2x)$ for $1/4 \leq x \leq 1/2$, $y = \pm b/2$ for $-1/4 \leq x \leq 1/4$, and $y = \pm(b/2) [1-16(x+1/4)^2]^{1/2}$ for $-1/2 \leq x \leq -1/4$, where the beam/length ratio, b , and the draft/length ratio, d , are taken as $b = 0.15$ and $d = 0.075$.

In these Proceedings, fourteen papers present either numerical (twelve papers) or experimental (two papers) results for the Wigley hull; eight papers provide numerical results for the Series 60 hull; and the vertical cylinders, the strut-like hull form, and the submerged spheroid are considered in five, four, and three papers, respectively. In addition, numerical results are also presented for the HSVA tanker (one paper) and the high-speed ATHENA hull (one paper) for which calculations were performed at the 1979 Workshop¹, for two hull forms having a transom stern and a bow dome (two papers), and for a bulk carrier (one paper), strut-like hull forms (two papers), vertical elliptical cylinders (one paper), and fully-submerged bodies (one paper).

NUMERICAL METHODS

Two of the twenty-one papers included in these Proceedings present experimental data for the Wigley hull and one paper presents a comparison of experimental data with numerical results obtained in two other papers by using different numerical methods. The remaining eighteen papers present theoretical and numerical results. These eighteen papers may be classified into four main groups, as follows: seven papers present results based on either a thin-ship (four papers) or a slender-ship (three papers) approximation of some kind, five papers can be grouped under the heading "Neumann-Kelvin theory", three papers make use of "Rankine-source distributions", and three papers are based on the "finite-difference method".

This classification, like most such classifications, is arbitrary to some extent, and indeed there are close similarities among the foregoing four groups of methods that might warrant a different classification. In particular, the methods classified under the headings "thin- or slender-ship approximations" and "Neumann-Kelvin theory" rely upon the use of the Green function, G , associated with the usual linearized free-surface boundary condition $\partial G / \partial z + F^2 \partial^2 G / \partial x^2 = 0$. Thus, twelve papers (7+5) out of eighteen, that is two papers out of three, make use of the Michell-Havelock Green function. The methods classified under the headings "Neumann-Kelvin theory" and "Rankine-source method" are also closely related. Indeed, both of these methods are "boundary integral equation methods" in which the Laplace equation is used to formulate an integral equation of some sort, and that integral equation is solved numerically in one way or another. The major difference between the "Neumann-Kelvin method" and the "Rankine-source method" is that the former method relies upon the Michell-Havelock Green function whereas the latter method simply uses the Rankine-source Green function $G = -1/4\pi R$. It may then be seen that eight papers (5+3) out of eighteen, that is about one paper out of two, are based upon the "boundary integral equation method".

ARRANGEMENT OF PAPERS

In these Proceedings, papers have been arranged in accordance with the foregoing classification into "experimental papers" and four groups of "theoretical papers". Specifically, the papers are ordered in the following sequence: two papers presenting experimental data for the Wigley hull, four "thin-ship approximation"

papers, three "slender-ship approximation" papers, five "Neumann-Kelvin theory" papers, three "Rankine-source method" papers, one paper that presents a comparison of experimental data with numerical predictions obtained by using the Rankine-source method and a simple slender-ship approximation, and finally three "finite-difference method" papers.

COMPARISON OF RESULTS

A major purpose of both the present and the previous Workshops is to provide a basis for comparing various sets of numerical results with one another, and with corresponding experimental values whenever available. A fairly large body of numerical results have now been obtained, notably for the Wigley hull (for which a sizable body of experimental data now also exists) and for the Series 60 $C_B = 0.60$ hull. A significant amount of time thus is required for performing a detailed comparison of all available experimental and theoretical values for the several hull forms considered at this and the previous Workshops. Preparation of such a comparison has therefore been postponed in order not to unduly delay the publication of these Proceedings.

REFERENCES

1. Proceedings of the Workshop on Ship Wave-Resistance Computations, Vol. 1, David Taylor Naval Ship Research and Development Center, Bethesda, Maryland, 13-14 November 1979.
2. Farrell, C. and O. Guven, "On Experimental Determination of the Resistance Components of a Submerged Spheroid," Journal of Ship Research, Vol. 17, June 1973, pp. 72-79.
3. Farrell, C., "On the Wave Resistance of a Submerged Spheroid," Journal of Ship Research, Vol. 17, March 1973, pp. 1-11.

The Summary of the Cooperative Experiment
on Wigley Parabolic Model in Japan

The executive members

H.Kajitani and H.Miyata
The University of Tokyo

M.Ikehata
Yokohama National University

H.Tanaka and H.Adachi
Ship Research Institute

M.Namimatsu and S.Ogiwara
Ishikawajima-Harima Heavy Industries Co.,Ltd.

Abstract

The 16th ITTC Resistance Committee made a proposal of cooperative experimental research program for ship resistance and flow around hull to construct standard data base. In Japan three organization, the University of Tokyo (UT), Ship Research Institute(SRI) and Ishikawajima-Harima Heavy Industries Co.,Ltd.(IHI) responded to the proposal of the Committee and Yokohama National University(YNU) joined this program in the later time . They conducted the experiments on Wigley parabolic model in order to investigate the scale effect of ship resistance using geosim models of a 6 m length in IHI, 4 m length in SRI, 2.5 m length in UT and 2 m length in YNU. The experiments were separately performed on the following items and cooperatively analyzed,

- (1) Resistance test
- (2) Wave pattern analysis
- (3) Wake survey
- (4) Wave profile measurement
- (5) Pressure measurement on hull surface

YNU separately performed the measurement of boundary layer around the hull. The report of the cooperative experiment was presented to the Resistance Committee of the 17th ITTC at Varna, Bulgaria in September, 1983. This paper describes the summary of the report extracting principal data of experiments in order to serve as a reference for the theoretical prediction of ship resistance.

Nomenclature

C_T	$R_T / \left(\frac{1}{2} \rho U^2 S \right)$	Total resistance coefficient
C_W	$R_W / \left(\frac{1}{2} \rho U^2 S \right)$	Wave resistance coefficient derived from towing test
C_{Wp}	$R_{Wp} / \left(\frac{1}{2} \rho U^2 S \right)$	Wave resistance coefficient derived from wave pattern analysis
C_{Fo}		Frictional resistance coefficient (Schoenherr)
C_{pR}		Resistance coefficient derived from integrating hull surface pressure
C_p		Pressure coefficient = $(p - p_o) / \left(\frac{1}{2} \rho U^2 \right)$
Fn		Froude number = U / \sqrt{gL}
S		Wetted surface area at rest defined by $S = C_s \cdot L(2D+B)$ $C_s = 0.661$
L		Waterline length (= L_{pp} for Wigley model)
B		Beam at midship
D		Draft at midship
H, H_o		Total head ($H_o = U^2/g$)
Rn		Reynolds number = LU/ν
THL		Total head loss = $(H_o - H)/H_o$
U		Model speed of advance
b		$B/2$
$d_F, \Delta d_F$		Draft at FP, its increase from the rest
$d_A, \Delta d_A$		Draft at AP, its increase from the rest
g		Gravitational acceleration = 9.8 m/sec^2
k		Three dimensional form factor on flat plate skin friction
k_o		Wave number = g/U^2

l	$L/2$
t	Trim (positive for bow up) = $(d_A - d_F)/L$
τ	$2k_o \cdot L \cdot t$
s	Sinkage = $(\Delta d_F + \Delta d_A)/2L$
σ	$2k_o \cdot L \cdot s$
ξ	Nondimensional wave elevation = $k_o \zeta(x)$
$\zeta(x)$	Wave elevation
ν	Kinematic viscosity
ρ	Mass density
x, y, z	Coordinate system fixed in space
x', y', z'	Coordinate system fixed in ship
FR	Free to sink and trim
FX	Fixed to sink and trim
S-FR.T-FX	Free to sink, fixed to trim

1. General notes

A) Model size

	IHI	SRI	UT	YNU
L (m)	6.0	4.0	2.5	2.0
B (m)	0.6	0.4	0.25	0.25
D (m)	0.375	0.25	0.156	0.125

$$\text{Hull form; } y = B/L \left[1 - (2x/L)^2 \right] \left[1 - (z/D)^2 \right]$$

B) Items of experiment

	IHI	SRI	UT	YNU
1 Resistance test	FR	FR,FX	FR,FX, S-FR.T-FX	FR,FX
2 Wave pattern analysis	FR	FR,FX	FR,FX, S-FR.T-FX	FR
3 Wake survey	FR	FR	FR	FR
4 Wave profile on hull	FR	FR,FX	FR,FX, S-FR.T-FX	
5 Pressure on hull	FR	FR	FR, FX	

C) Boundary condition

	IHI	SRI	UT	YNU
Turbulent stimulator stud				
Height*Spacing (mm) at x/l=-0.9	3*10	3*10	2*10	2*10
Tank section, BT*DT (m)	10*5	18*8	3.5*2.35	8*3.5
Towing height from keel (mm)	330	235	103	
Speed measurement	Current speed	Ground speed	Ground speed	Ground speed

2. Results of resistance test and wave analysis

Figure 1 shows the total resistance (C_T), frictional resistance (Schoenherr, C_{F0}), wave resistance (C_w) and wave pattern resistance (C_{wp}) for three models of 6.0m, 4.0m and 2.5m length on the condition of free to sink and trim (FR). Wave resistance is derived using form factor on skin friction.

Wave pattern resistance is derived by the method of Newmwn-Sharma. Distance of measuring plane of wave profile from the center line of the model is as follows,

	IHI	SRI	UT	YNU
y/l	1.667	1.0	1.4	4.0

Figure 2 shows C_T , C_{F0} , C_w and C_{wp} for two models of 4.0m and 2.5m length on the condition of FX.

Figure 3 shows C_T , C_{F0} , C_w and C_{wp} for the 2.5m length model on the condition of FR, FX and S-FR, T-FX .

Figure 4 shows the sinkage and trim of three models of 6.0m, 4.0m and 2.5m length.

Figure 5 shows C_T , C_{F0} , C_w and C_{wp} of the 2.0m length model on the condition of FR and FX.

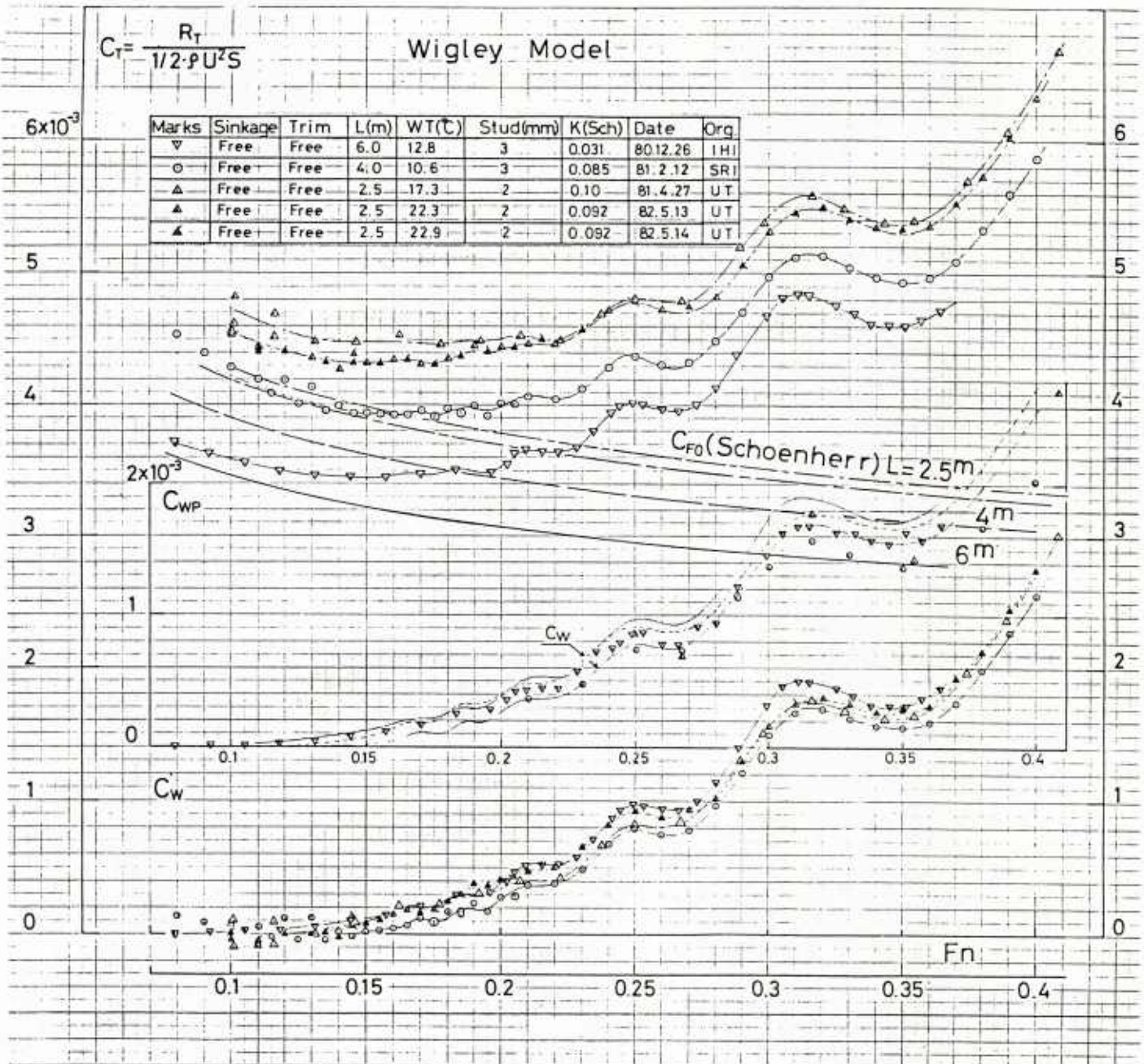


Fig.1 The results of resistance test and wave pattern analysis
(Free to sink and trim)

Wigley Model

$$C_T = \frac{R_T}{\frac{1}{2} \rho U^2 S}$$

Marks	Sinkage	Trim	L(m)	WT(°C)	Stud(mm)	K(Sch)	Date	Org.
○	Fix	Fix	4.0	15.5	3	0.095	81.5.8	SRI
△	Fix	Fix	2.5	16.9	2	0.045	81.4.24	U-T
▲	Fix	Fix	2.5	21.1	2	0.047	82.5.11	U-T
△	Fix	Fix	2.5	21.8	2	0.047	82.5.12	U-T

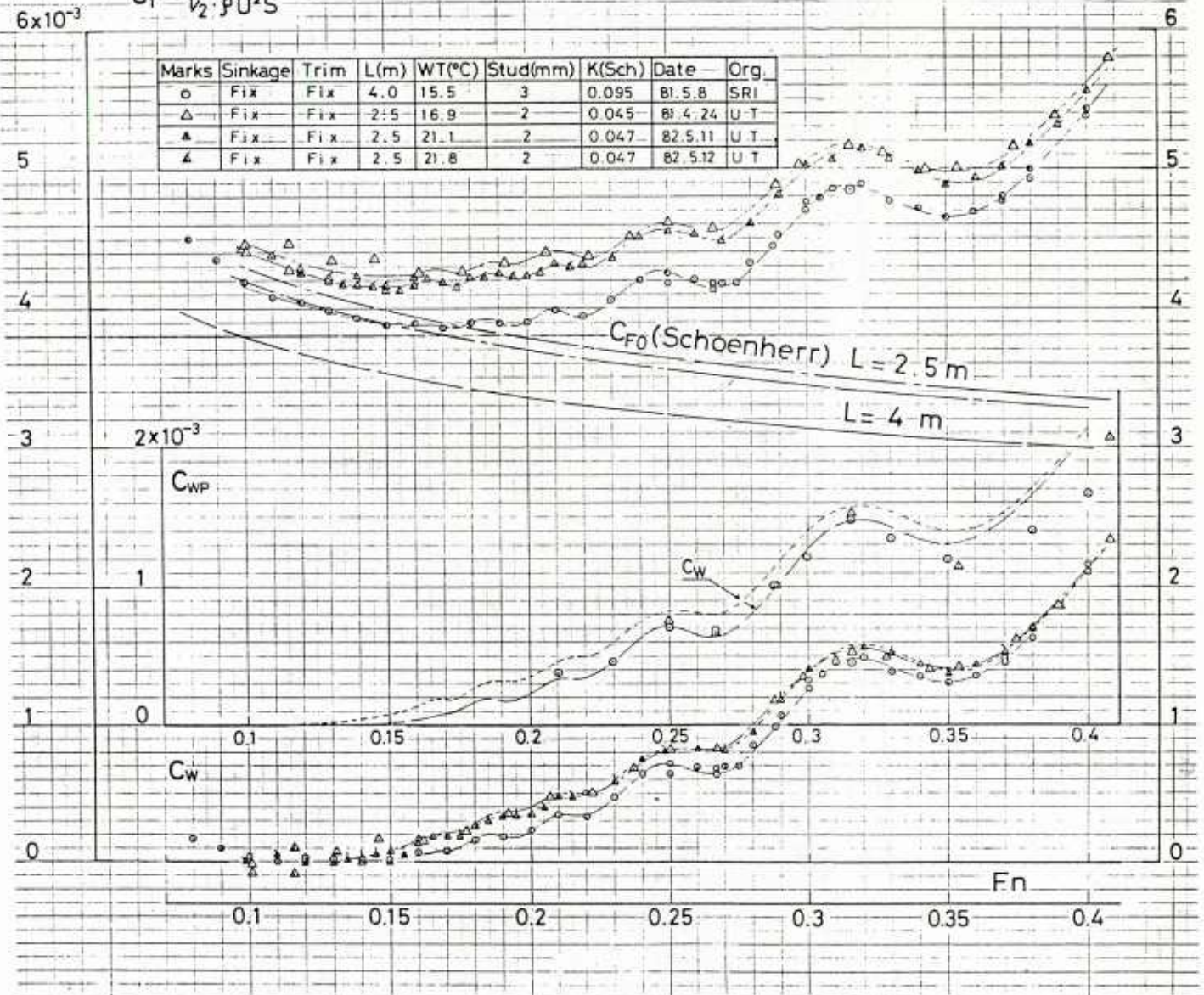


Fig.2 The results of resistance test and wave pattern analysis
(Fixed to sink and trim)

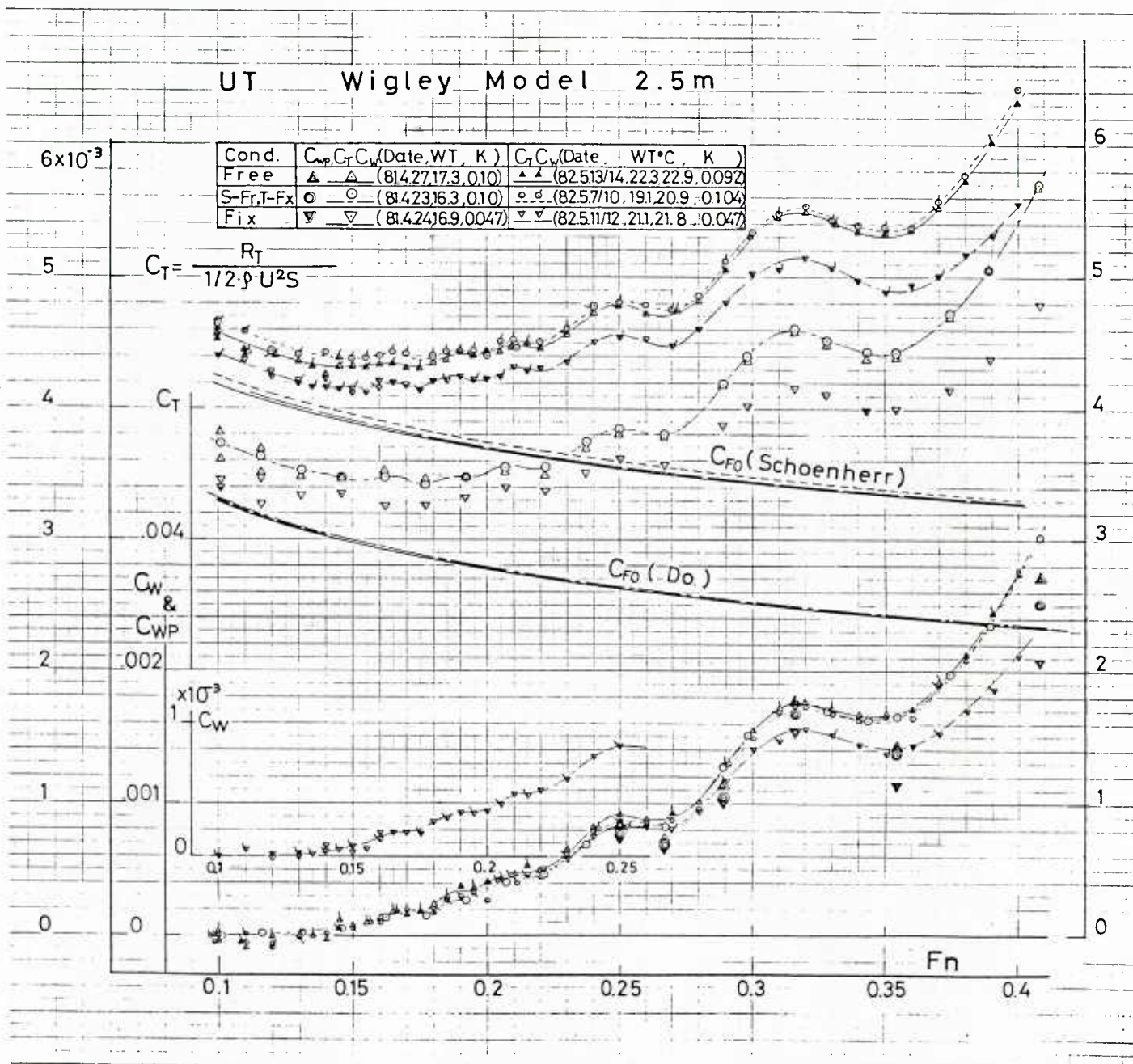


Fig.3 The results of resistance test and wave pattern analysis of 2.5m model

Wigley Model

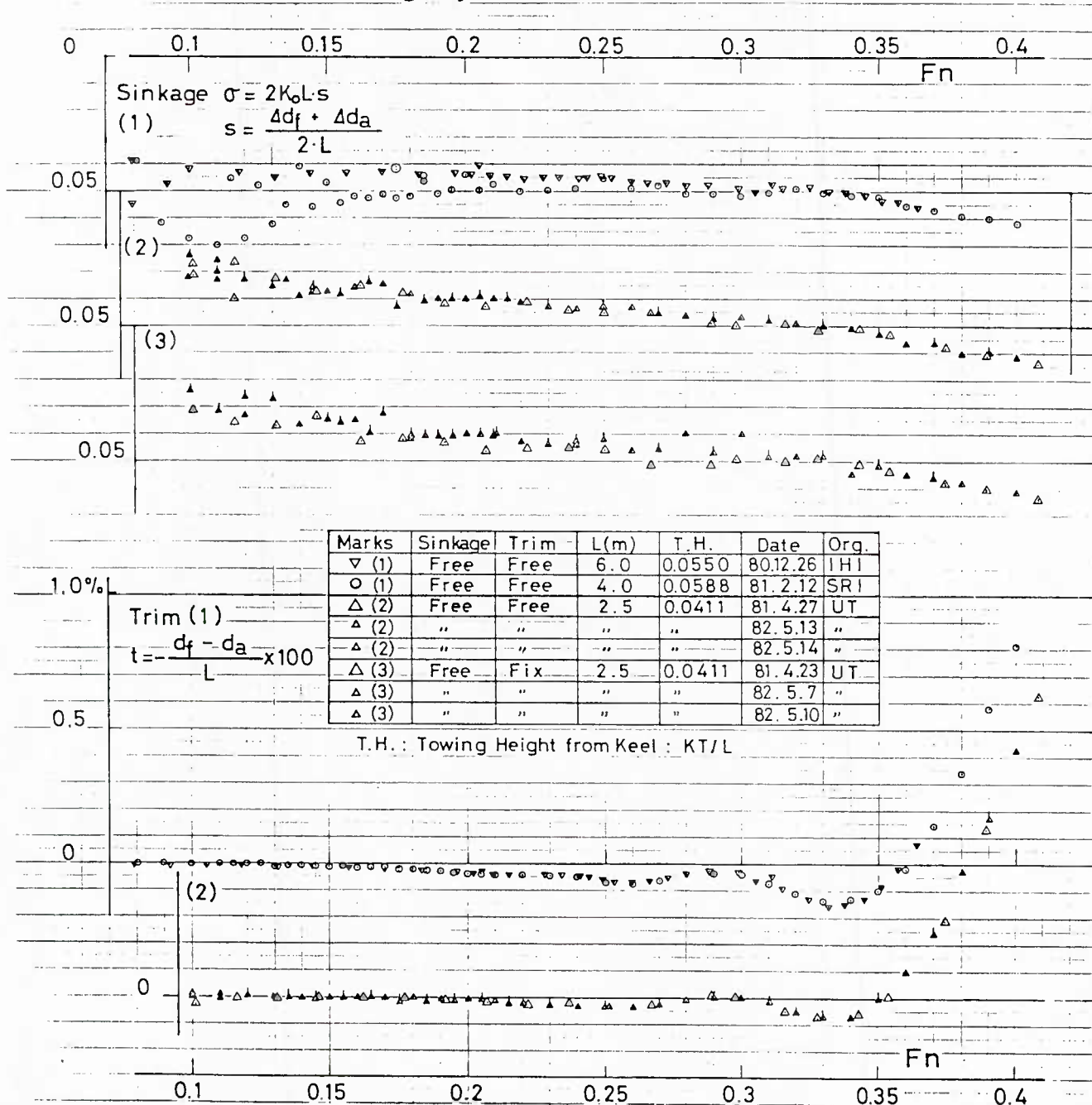


Fig.4 The results of sinkage and trim measurement

WIGLEY MODEL $L=2.0\text{ m}$ (YOKOHAMA NATIONAL UNIV.)

MARK	SINKAGE	TRIM	W.T.	k
—○—	FREE	FREE	13.3°C	0.06
—●—	FIXED	FIXED	13.3°C	0.06

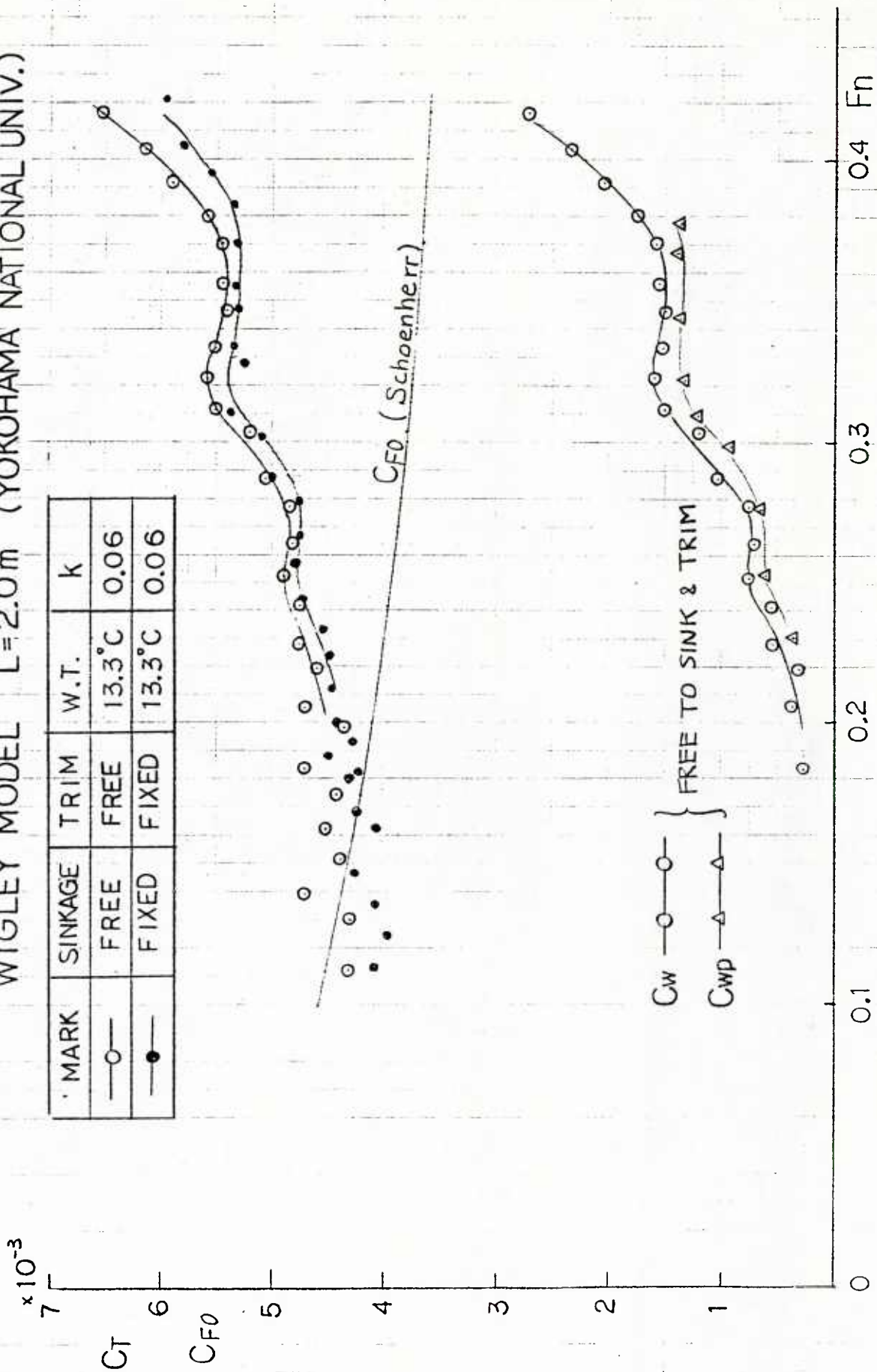


Fig.5 The results of resistance test and wave pattern analysis of 2.0m model

3. Results of wake survey

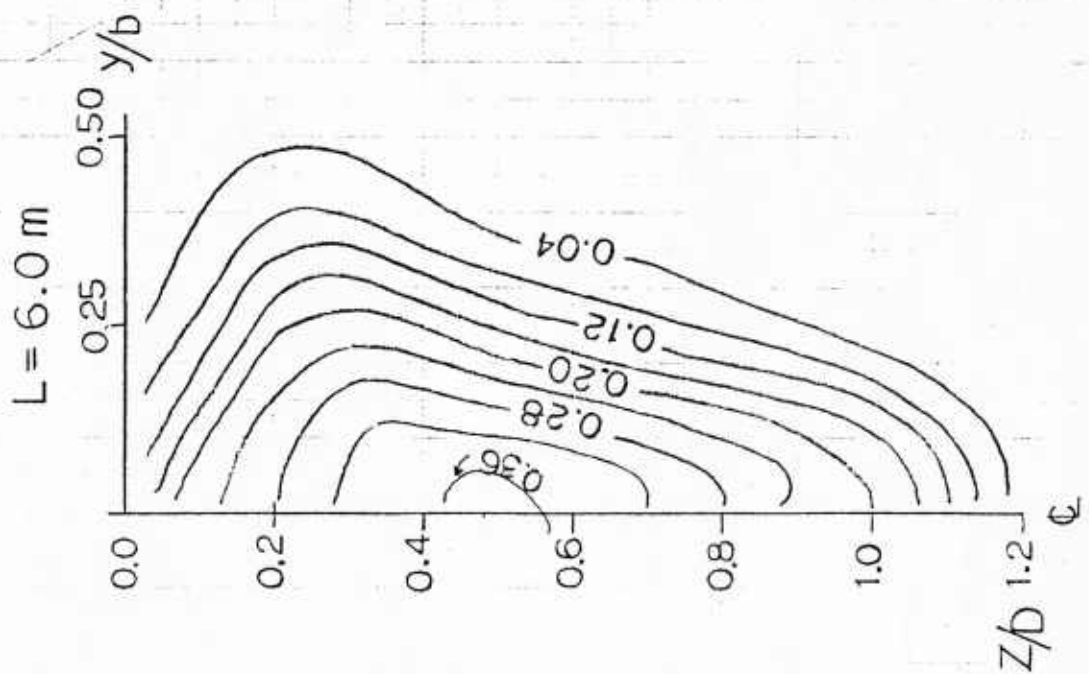
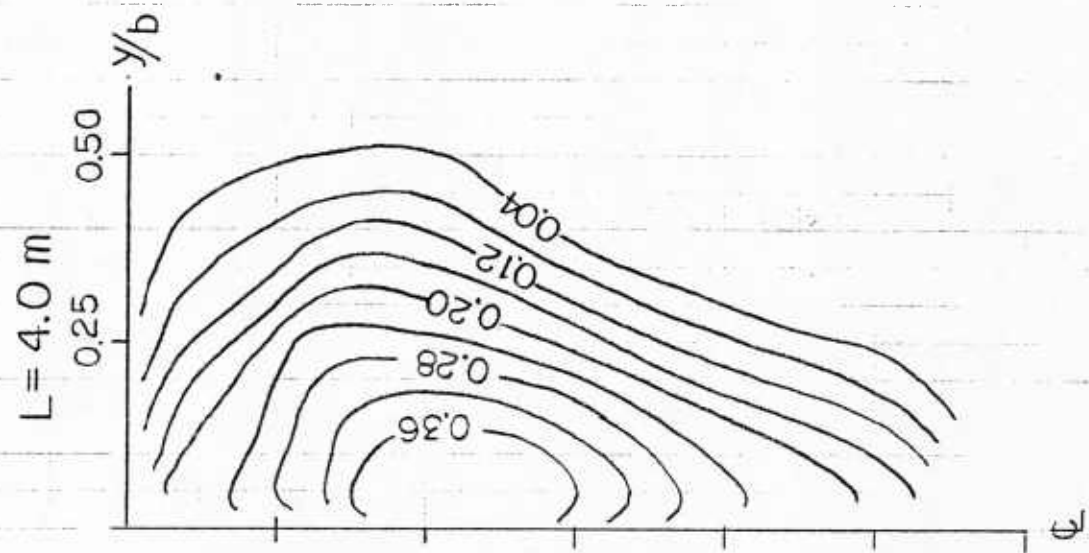
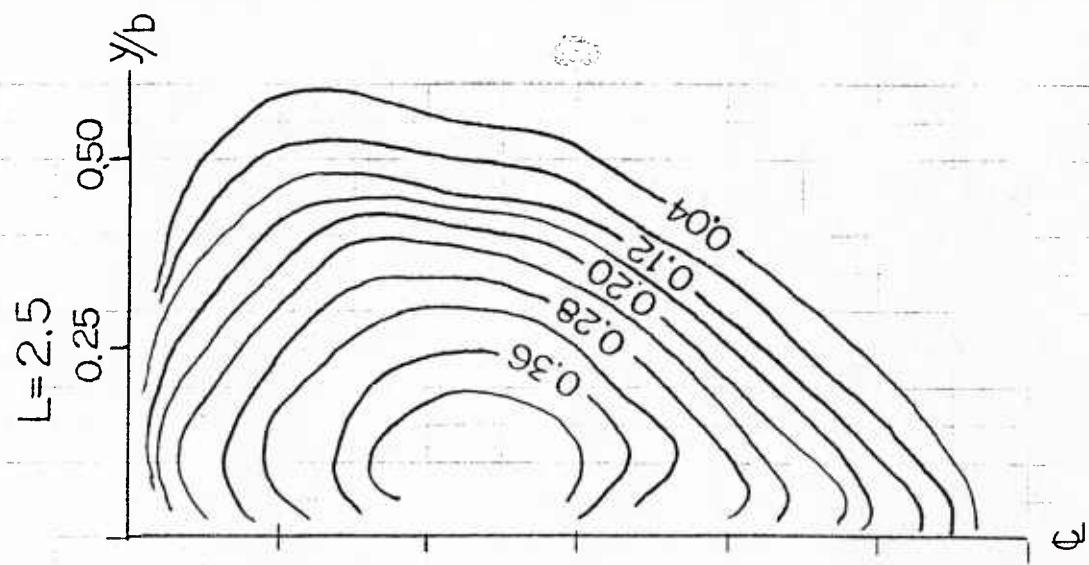
Condition of wake survey

	IHI	SRI	UT	YNU
Position of measuring section from AP (x/l)	1.0	1.0	1.0	1.0

	Froude number					Water Temp($^{\circ}$ C)
IHI (FR)	0.267			0.316		16.6
SRI (FR)	0.250	0.267	0.289	0.316		10.6
UT (FR)	0.250	0.267	0.289	0.316		20.9
YNU (FR)	0.230	0.276	0.309	0.343	0.377	

Figure 6 shows an example of the contour of nondimensional total head loss $(H - H)/H$ for three models of 6.0m, 4.0m and 2.5m length on the condition of FR.

Figure 7 shows an example of comparison of horizontally integrated total head loss for three models of 6.0m, 4.0m and 2.5m length.



FREE $F_n = 0.316$

Fig.6 The contour of total head loss $(H_o - H)/H_o$

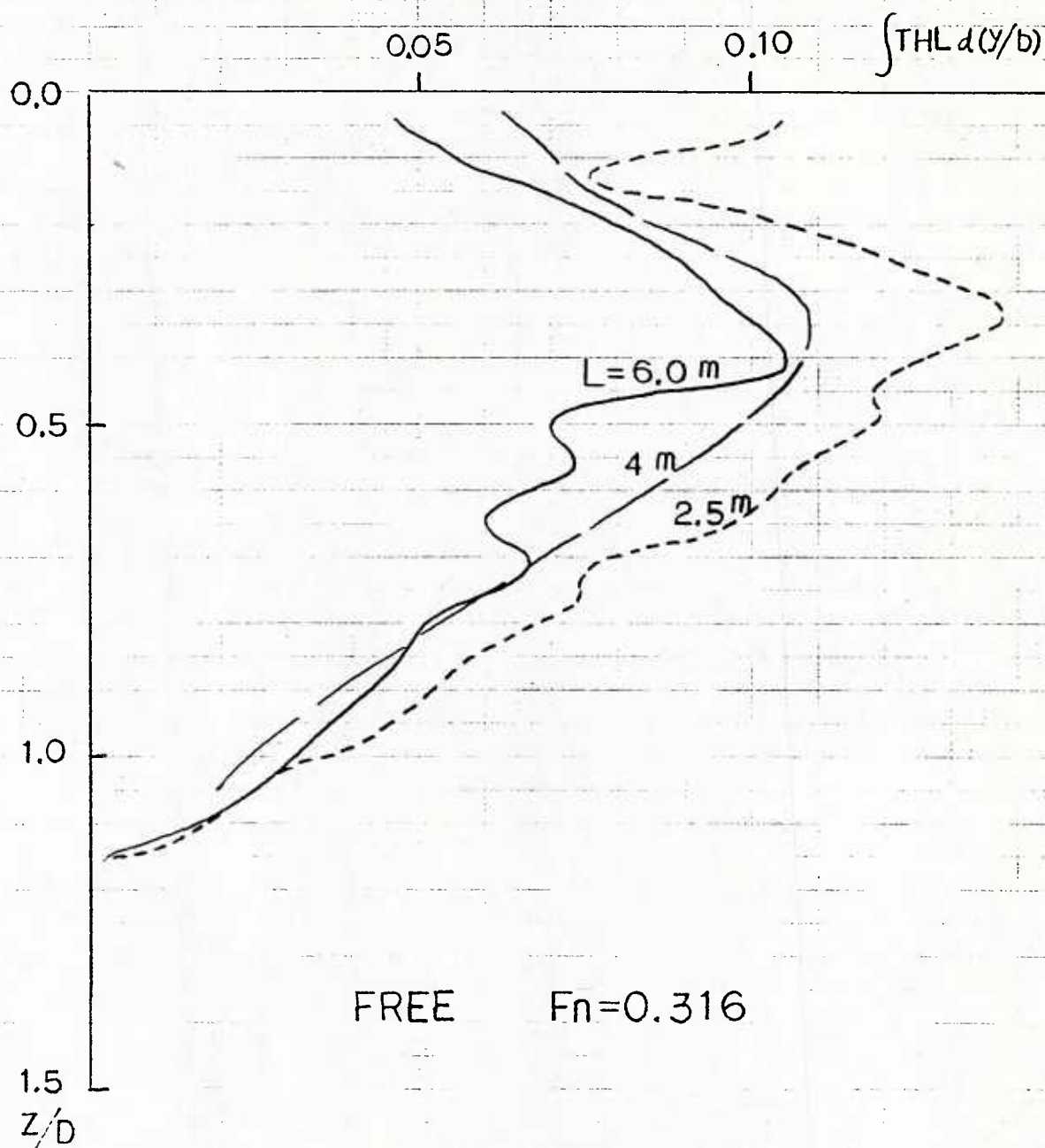


Fig.7 The comparison of horizontally integrated total head loss

4. Results of wave profile measurement on the hull

Condition of measurements

	Froude number
IHI (FR)	0.250 0.267 0.289 0.316
SRI (FR)	0.250 0.267 0.289 0.316
SRI (FX)	0.250 0.267 0.289 0.316
UT (FR)	0.250 0.267 0.287 0.316 0.354 0.408
UT (FX)	0.250 0.267 0.289 0.316 0.354 0.408
UT(S-FR.T-FX)	0.250 0.267 0.289 0.316 0.354 0.408

Figure 8 shows the comparison of wave profile on the hull on the condition of FR, where ξ is nondimensional wave elevation ($= g\zeta(x)/U^2$)

Table 1 gives nondimensional wave elevation for three models of 6.0m ,4.0m and 2.5m length.

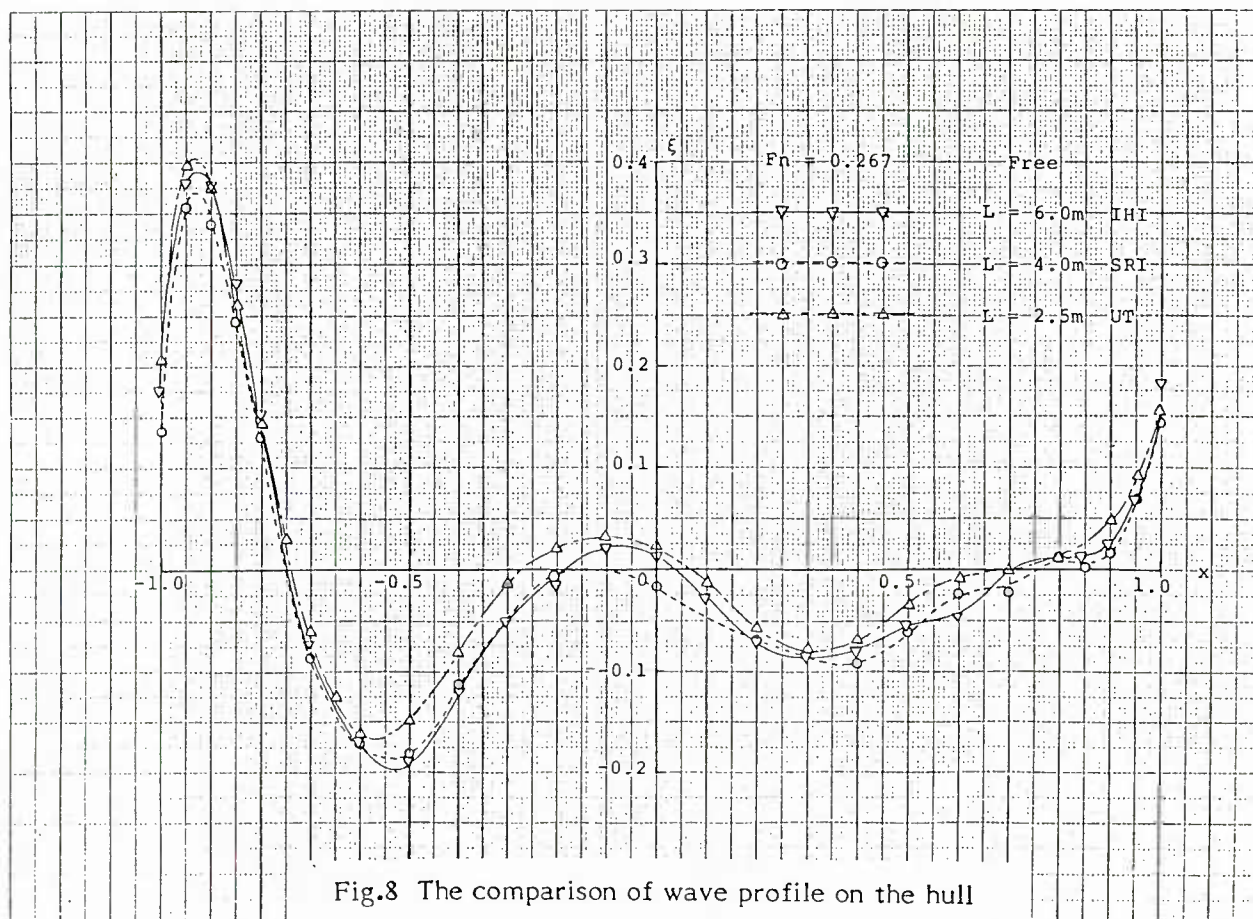
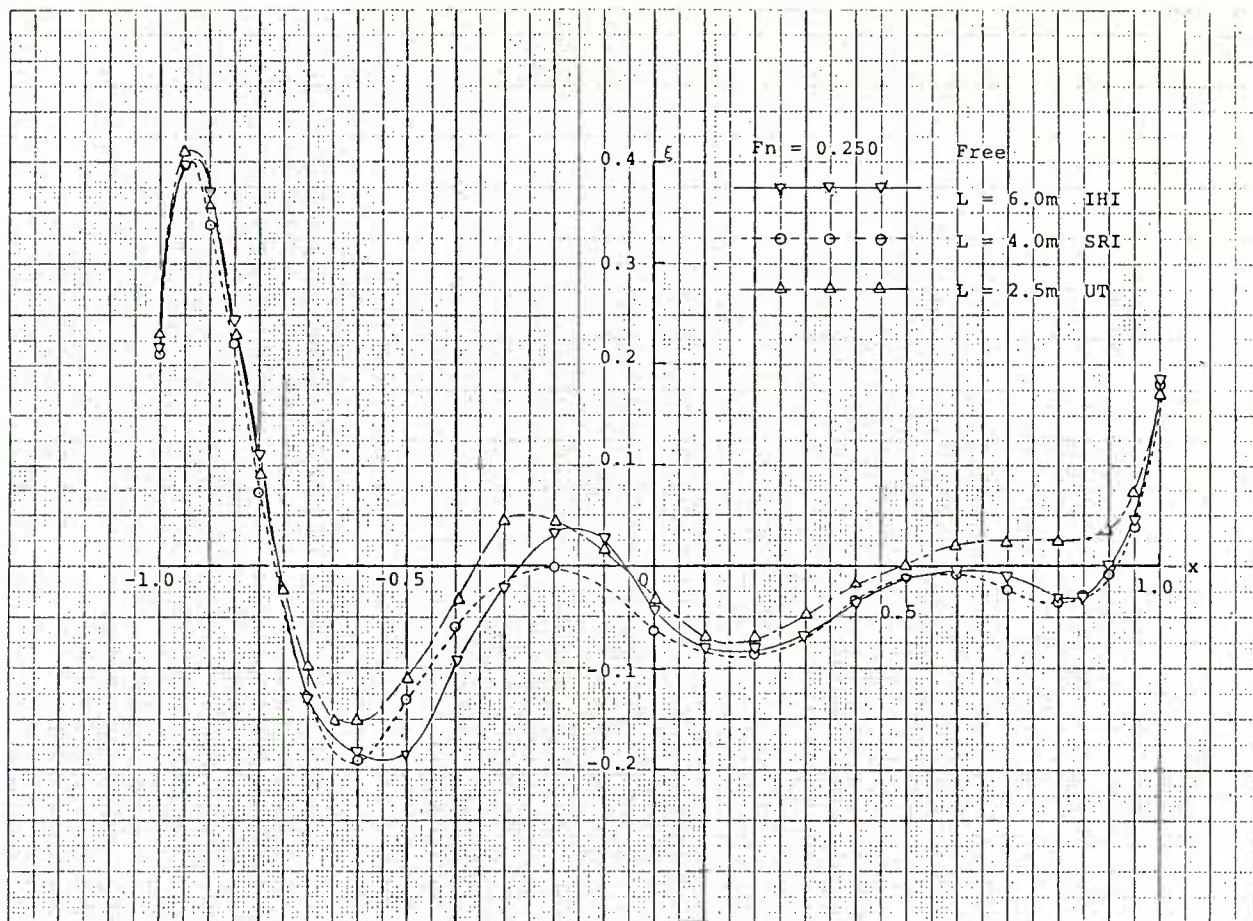


Fig.8 The comparison of wave profile on the hull

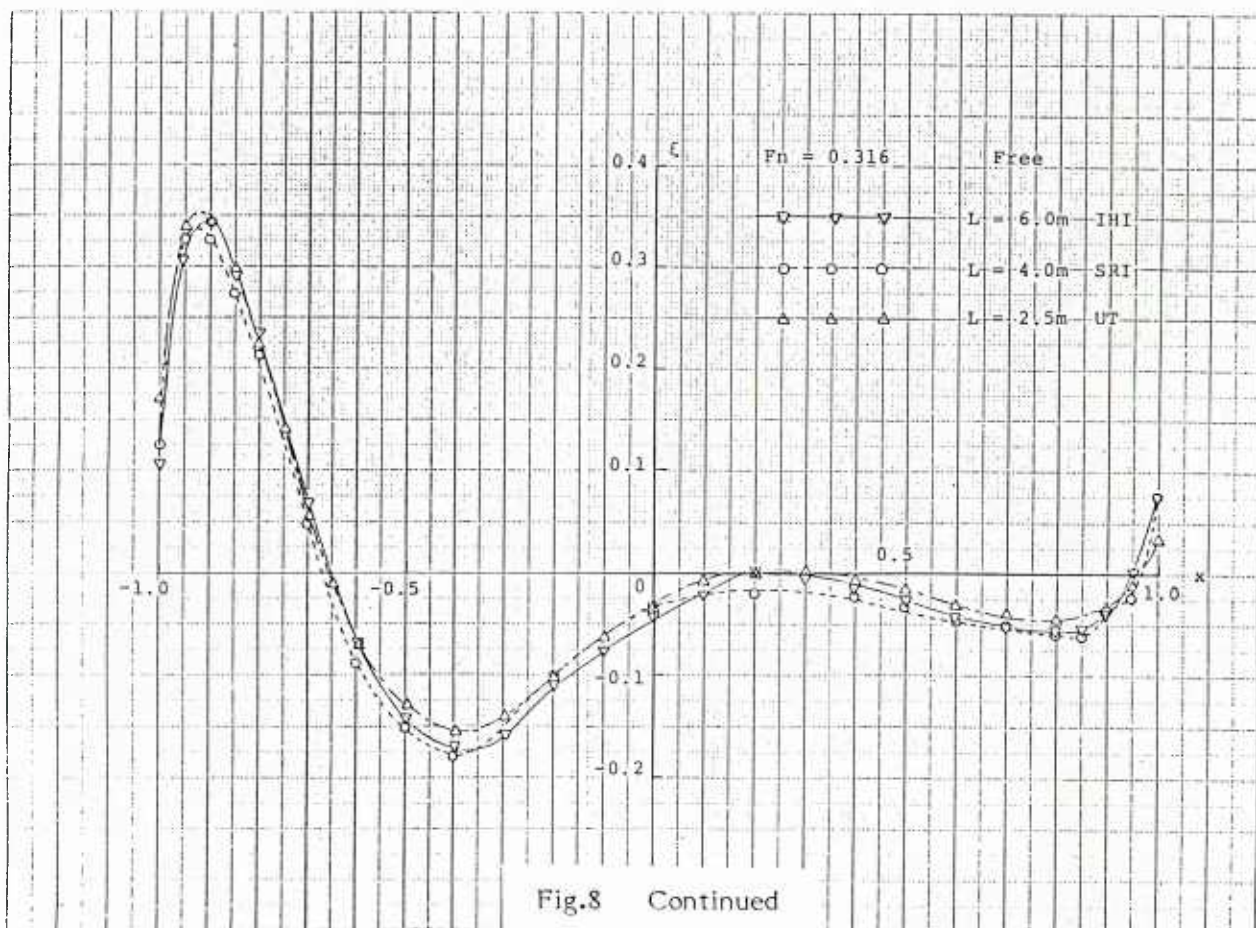
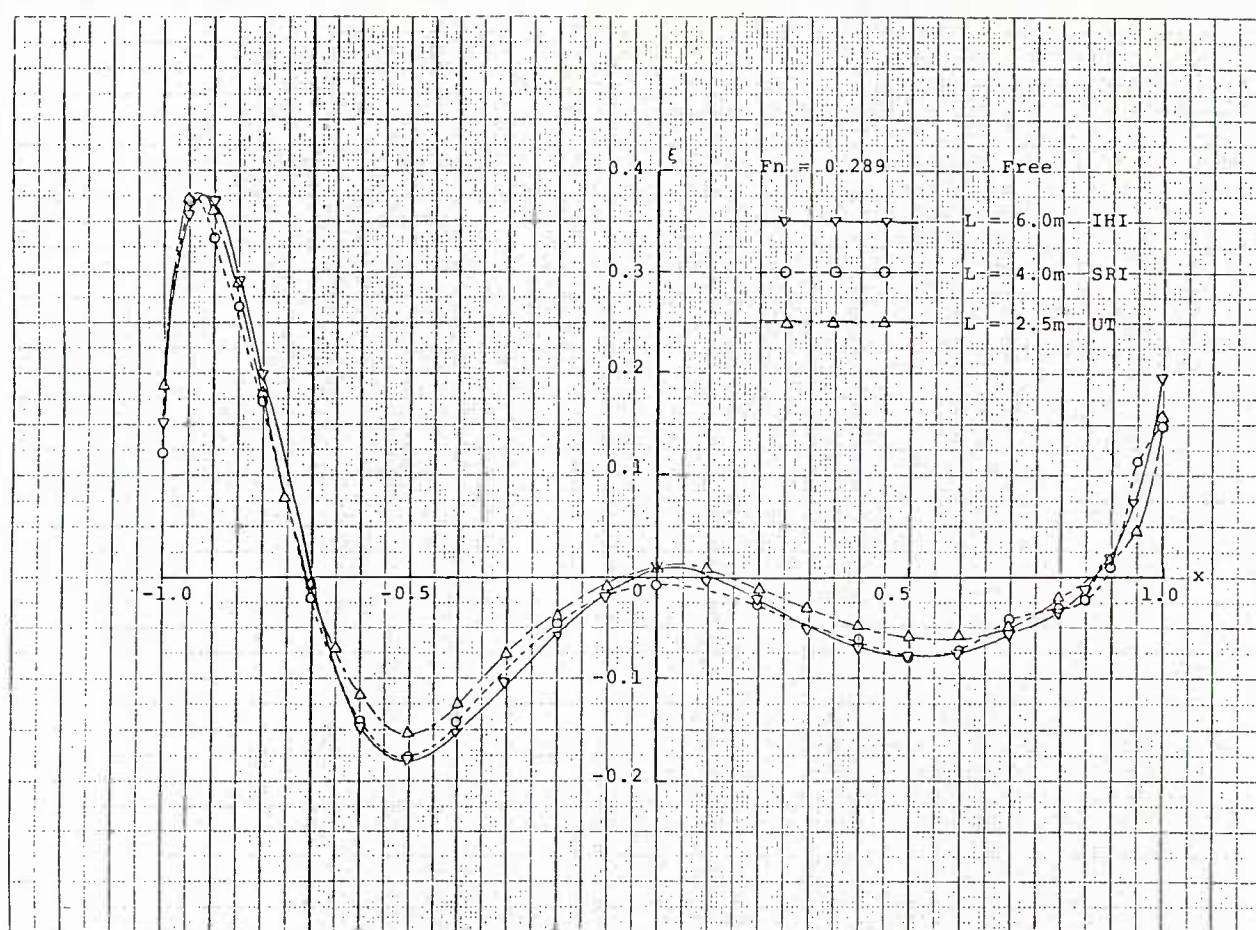


Fig.8 Continued

Table 1 The nondimensional wave elevation on the hull

2X/L	$g\zeta/U^2$ Free L=6.0m (IHI)			
	FN= .250	FN= .267	FN= .289	FN= .316
-1.000	.177	.218	.149	.109
-.950	.378	.400	.354	.306
-.900	.374	.373	.370	.343
-.850	.281	.246	.290	.294
-.800	.151	.113	.198	.237
-.700	-.077	-.131	-.010	.068
-.600	-.174	-.183	-.149	-.071
-.500	-.191	-.134	-.181	-.147
-.400	-.120	-.091	-.157	-.169
-.300	-.050	-.021	-.108	-.162
-.200	-.016	.034	-.056	-.111
-.100	.022	.024	-.020	-.080
.000	.014	-.044	.012	-.045
.100	-.027	-.081	-.003	-.021
.200	-.073	-.079	-.023	.003
.300	-.086	-.068	-.050	-.003
.400	-.080	-.035	-.070	-.015
.500	-.056	-.013	-.078	-.027
.600	-.046	-.004	-.078	-.043
.700	-.003	-.011	-.057	-.052
.800	.012	-.031	-.037	-.058
.850	.013	-.031	-.013	-.054
.900	.027	.002	.019	-.041
.950	.070	.045	.072	.000
1.000	.187	.184	.196	.077

2X/L	$g\zeta/U^2$ Free L=4.0m (SRI)			
	FN= .250	FN= .267	FN= .289	FN= .316
-1.000	.213	.137	.121	.120
-.950	.397	.355	.370	.327
-.900	.338	.340	.333	.325
-.850	.223	.245	.266	.275
-.800	.074	.130	.173	.212
-.700	-.127	-.085	-.021	.047
-.600	-.192	-.172	-.141	-.090
-.500	-.132	-.181	-.176	-.151
-.400	-.060	-.113	-.142	-.179
-.200	-.003	-.008	-.045	-.103
.000	-.064	-.017	-.038	-.032
.200	-.087	-.069	-.028	-.030
.400	-.034	-.094	-.061	-.023
.500	-.011	-.061	-.085	-.033
.600	-.008	-.023	-.074	-.049
.700	-.023	-.022	-.041	-.050
.800	-.035	.013	-.030	-.060
.850	-.029	.003	-.022	-.062
.900	-.009	.015	.011	-.035
.950	.037	.070	.113	-.023
1.000	.180	.143	.149	.076

2X/L	$g\zeta/U^2$ Fixed L=4.0m (SRI)			
	FN= .250	FN= .267	FN= .289	FN= .316
-1.000	.192	.175	.186	.155
-.950	.440	.392	.408	.340
-.900	.368	.329	.324	.330
-.850	.248	.252	.258	.275
-.800	.104	.133	.192	.205
-.700	-.136	-.070	-.006	.045
-.600	-.160	-.168	-.132	-.075
-.500	-.120	-.175	-.168	-.140
-.400	-.032	-.112	-.144	-.155
-.200	-.016	.000	-.048	-.100
.000	-.056	-.007	-.012	-.030
.200	-.080	-.070	-.024	-.005
.400	-.088	-.070	-.072	-.015
.500	-.072	-.063	-.084	-.035
.600	-.048	-.049	-.084	-.045
.700	.008	.014	-.054	-.050
.800	.016	.007	-.042	-.060
.850	.016	.007	-.024	-.050
.900	.024	.007	.006	-.045
.950	.080	.042	.084	-.030
1.000	.224	.154	.162	-.075

Table 1 Continued

2X/L	$g\zeta/U^2$ Free L=2.5 m (UT)					
	FN= .250	FN= .267	FN= .289	FN= .316	FN= .354	FN= .408
-1.000	.232	.208	.192	.170	.133	.091
-.950	.410	.399	.374	.338	.267	.232
-.900	.360	.377	.365	.346	.324	.282
-.850	.232	.265	.288	.298	.299	.274
-.800	.091	.142	.182	.227	.241	.237
-.750	-.024	.030	.077	.139	.184	.205
-.700	-.100	-.059	.000	.059	.120	.158
-.650	-.151	-.126	-.068	-.013	.062	.107
-.600	-.151	-.160	-.116	-.068	.004	.061
-.500	-.112	-.148	-.154	-.132	-.085	-.018
-.400	-.035	-.081	-.125	-.156	-.130	-.067
-.300	-.043	-.013	-.077	-.136	-.137	-.038
-.200	-.043	.021	-.039	-.107	-.130	-.123
-.100	-.018	.032	-.010	-.066	-.117	-.125
.000	-.032	.022	.009	-.034	-.098	-.126
.100	-.070	-.012	.009	-.009	-.073	-.119
.200	-.070	-.056	-.011	-.001	-.047	-.110
.300	-.044	-.078	-.030	.000	-.028	-.098
.400	-.017	-.067	-.049	-.008	-.015	-.080
.500	-.009	-.033	-.059	-.015	-.006	-.067
.600	-.022	-.010	-.059	-.031	-.002	-.059
.700	-.023	.002	-.050	-.038	-.002	-.056
.800	-.023	.013	-.021	-.046	-.009	-.048
.900	-.037	.047	.021	-.029	-.015	-.026
.950	-.075	.092	.046	-.013	.010	.000
1.000	.178	.160	.161	.036	.029	.025

2X/L	$g\zeta/U^2$ Fixed L=2.5 m (UT)					
	FN= .250	FN= .267	FN= .289	FN= .316	FN= .354	FN= .408
-1.000	.307	.246	.192	.160	.128	.086
-.950	.397	.358	.326	.312	.256	.236
-.900	.346	.336	.346	.328	.307	.288
-.850	.218	.224	.259	.264	.269	.274
-.800	.077	.101	.163	.192	.218	.230
-.750	-.064	-.011	.058	.104	.154	.187
-.700	-.141	-.090	-.019	.024	.090	.139
-.650	-.179	-.146	-.086	-.032	.032	.086
-.600	-.179	-.168	-.134	-.088	-.026	.043
-.500	-.128	-.157	-.163	-.144	-.102	-.029
-.400	-.051	-.112	-.144	-.160	-.141	-.086
-.300	-.026	-.045	-.096	-.136	-.141	-.106
-.200	.013	-.011	-.058	-.104	-.134	-.115
-.100	-.026	.000	-.019	-.072	-.115	-.120
.000	-.077	-.022	-.010	-.048	-.096	-.120
.100	-.102	-.056	-.010	-.028	-.077	-.110
.200	-.090	-.078	-.029	-.016	-.058	-.096
.300	-.064	-.090	-.048	-.012	-.038	-.082
.400	-.026	-.078	-.058	-.016	-.026	-.072
.500	-.013	-.056	-.067	-.032	-.013	-.062
.600	.000	-.034	-.058	-.048	-.013	-.053
.700	-.013	-.011	-.048	-.056	-.019	-.043
.800	-.013	.000	-.019	-.064	-.026	-.029
.900	.000	.011	.019	-.040	-.013	-.014
.950	.026	.056	.048	-.016	.000	-.005
1.000	.141	.157	.125	.024	.038	.034

2X/L	$g\zeta/U^2$ FR-sink, FX-trim L=2.5 m (UT)					
	FN= .250	FN= .267	FN= .289	FN= .316	FN= .354	FN= .408
-1.000	.236	.206	.168	.174	.132	.088
-.950	.415	.396	.351	.342	.266	.231
-.900	.364	.374	.351	.350	.324	.289
-.850	.223	.251	.275	.286	.292	.283
-.800	.082	.128	.169	.206	.241	.264
-.750	-.033	.016	.063	.126	.177	.220
-.700	-.110	-.063	-.013	.046	.113	.167
-.650	-.174	-.141	-.081	-.026	.055	.114
-.600	-.174	-.163	-.138	-.074	-.003	.070
-.500	-.123	-.152	-.157	-.138	-.086	-.012
-.400	-.033	-.096	-.138	-.154	-.137	-.076
-.300	.031	-.029	-.090	-.138	-.137	-.115
-.200	.044	.016	-.042	-.106	-.131	-.126
-.100	.018	.027	.006	-.066	-.118	-.131
.000	-.046	.016	.015	-.034	-.105	-.125
.100	-.085	-.029	.015	-.010	-.079	-.118
.200	-.085	-.074	.006	-.002	-.054	-.109
.300	-.046	-.074	-.004	-.002	-.035	-.096
.400	-.070	-.063	-.013	-.010	-.015	-.077
.500	.005	-.040	-.033	-.018	-.003	-.059
.600	.031	-.018	-.033	-.034	-.003	-.046
.700	.031	.004	-.023	-.042	.004	-.036
.800	.018	.016	-.004	-.042	-.003	-.027
.900	.031	.038	.025	-.034	.004	-.019
.950	.056	.072	.063	-.010	.017	.010
1.000	.184	.184	.159	.022	.055	.029

5. Results of pressure measurement on the hull surface

Condition of pressure measurements

	Froude number				
IHI (FR)	0.104	0.250	0.267	0.289	0.316
SRI (FR)		0.250	0.267	0.289	0.316
UT (FR)		0.250	0.267	0.289	0.316
UT (FX)		0.250	0.267	0.289	0.316

Pressure resistance coefficient

$$C_{PR} = R_p / \left(\frac{1}{2} \rho U^2 S \right)$$

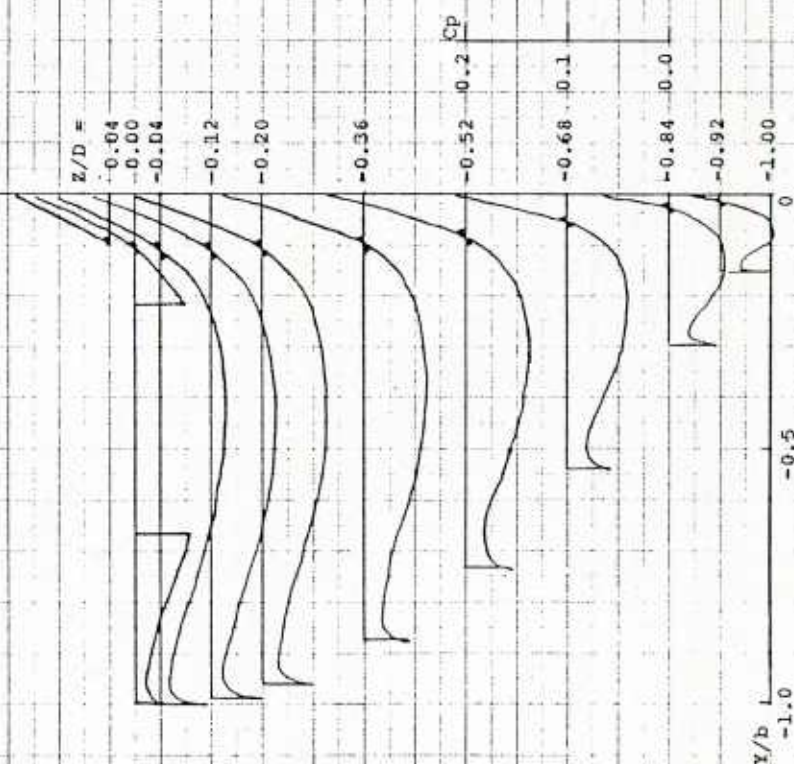
	IHI	SRI	UT	
Fn	FR	FR	FR	FX
0.250	0.891×10^{-3}	1.150×10^{-3}	0.878×10^{-3}	0.941 10
0.267	0.916	0.979	0.920	0.827
0.289	1.280	1.374	1.318	1.221
0.316	1.803	1.998	1.866	1.786

Figures 9 through 11 show examples of the pressure distributions on the hull surface projected on the midship section for three models of 6.0m, 4.0m and 2.5m length on the condition of FR.

Figure 12 shows the comparison of horizontally integrated pressure for three models of 6.0m, 4.0m, and 2.5m length on the condition of FR.

Tables 2 through 5 give the pressure coefficient on the hull surface.

IHI	Free
Wigley Hull	Aft Body
$L \times B \times D = 6.0 \times 0.6 \times 0.375 \text{ m}$	
$g_L/U^2 = 10.0$	$Fn = 0.316$



IHI	Free
Wigley Hull	Fore Body
$L \times B \times D = 6.0 \times 0.6 \times 0.375 \text{ m}$	
$g_L/U^2 = 10.0$	$Fn = 0.316$

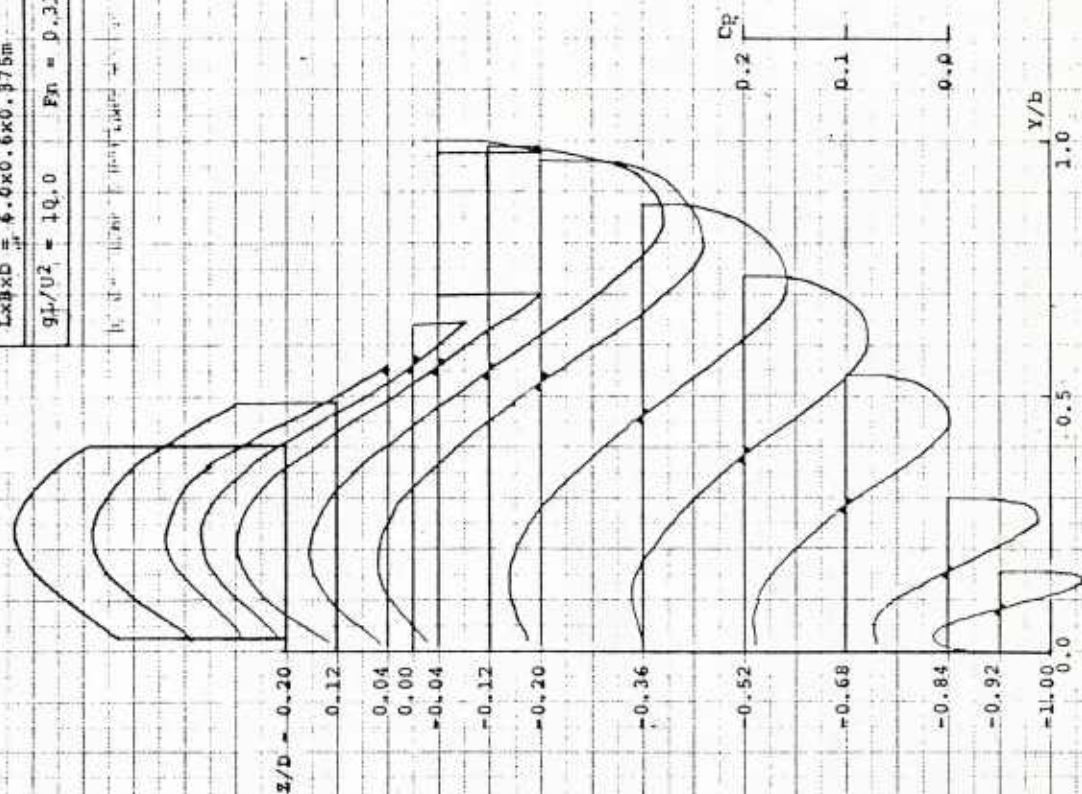
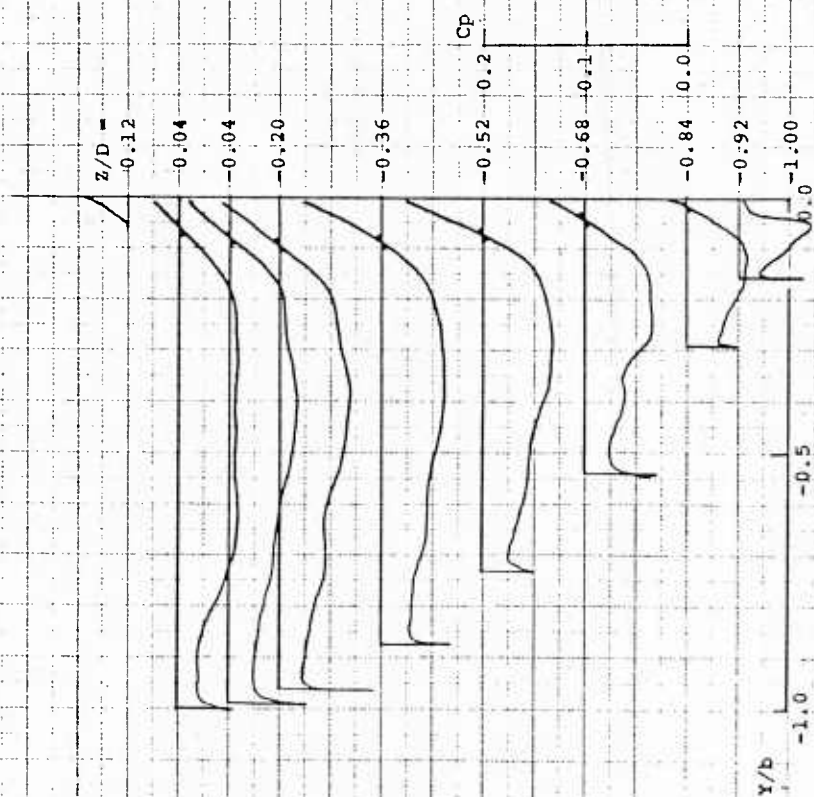


Fig.9 The pressure distribution on the hull of 6.0m model

SRI	Free
Wigley Hull	Aft Body
$LxBxD = 4.0 \times 0.4 \times 0.25m$	
$gU/U^2 = 10.0$	$Fn = 0.316$



SRI	Free
Wigley Hull	Fore Body
$LxBxD = 4.0 \times 0.4 \times 0.25m$	
$gU/U^2 = 10.0$	$Fn = 0.316$

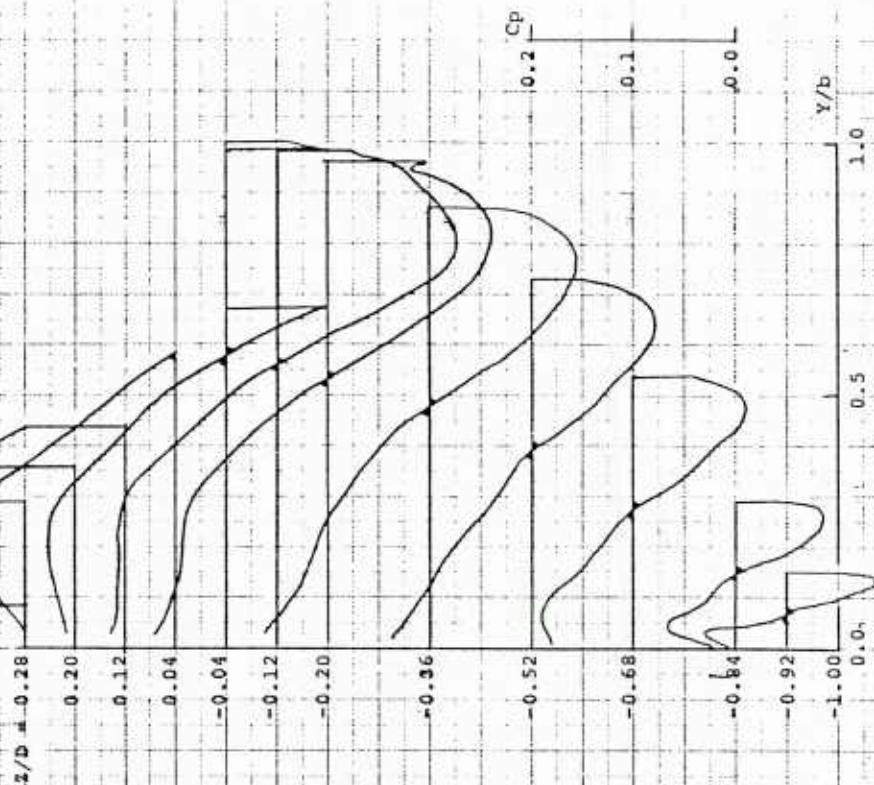
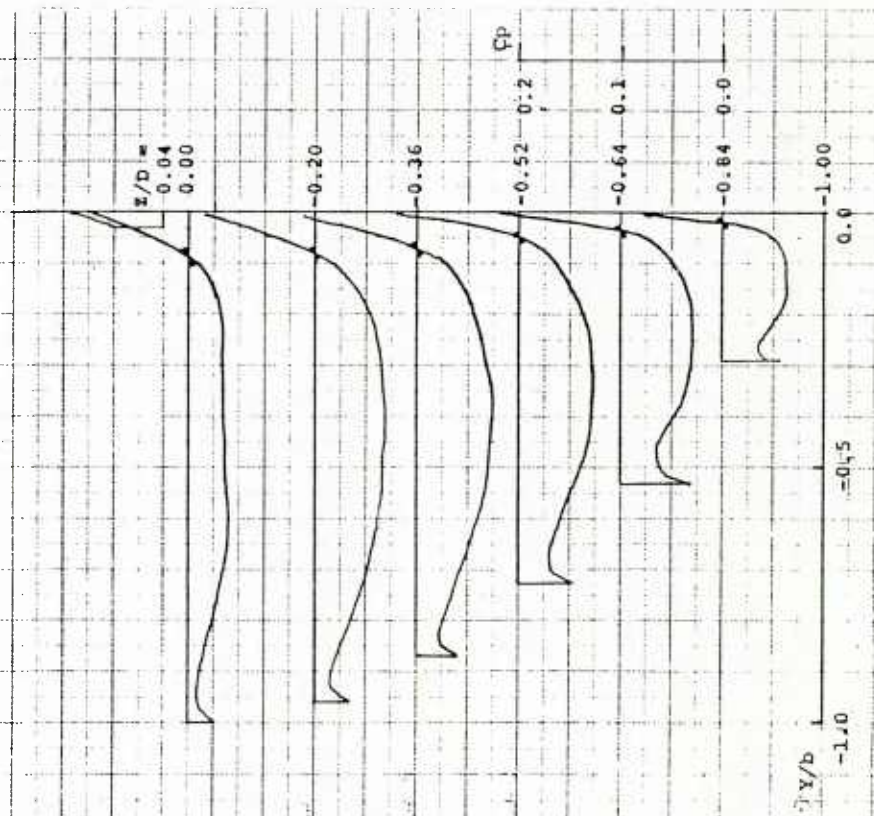


Fig.10 The pressure distribution on the hull of 4.0m model

Univ. of Tokyo	Free
Wigley Hull	Aft Body
$L \times B \times D = 2.5 \times 0.25 \times 0.156 \text{ m}$	
$gL/U^2 = 10.0$	$Fn = 0.316$
Univ. of Tokyo	



Univ. of Tokyo	Free
Wigley Hull	Pore Body
$L \times B \times D = 2.5 \times 0.25 \times 0.156 \text{ m}$	
$gL/U^2 = 10.0$	$Fn = 0.316$
Univ. of Tokyo	

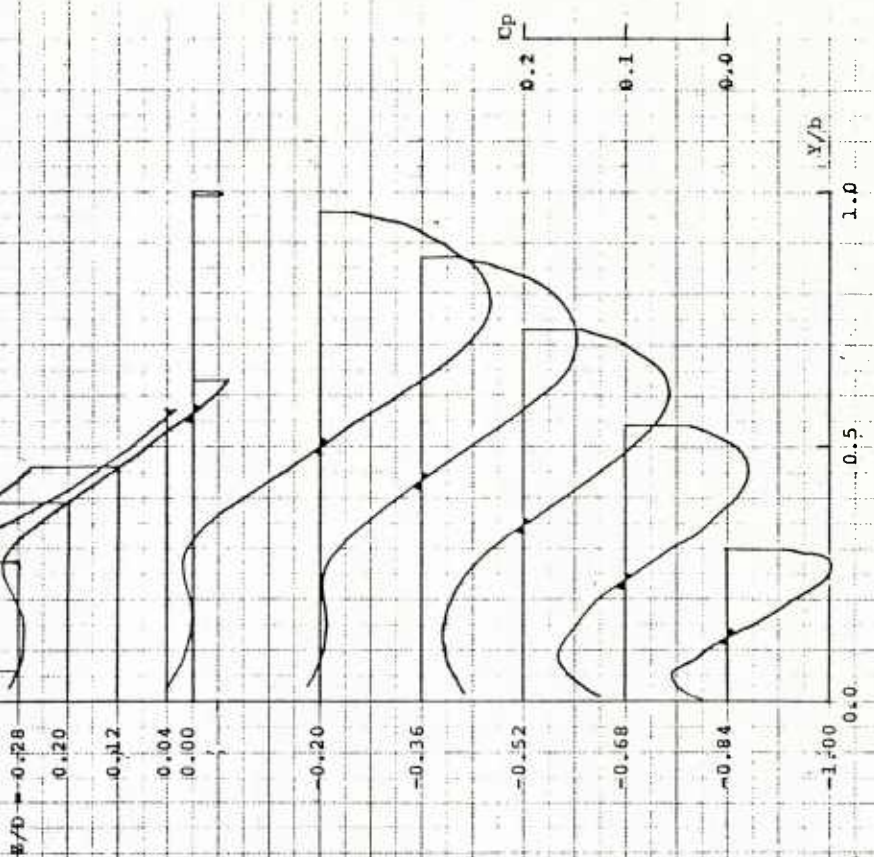


Fig.1.1 The pressure distribution on the hull of 2.5m model

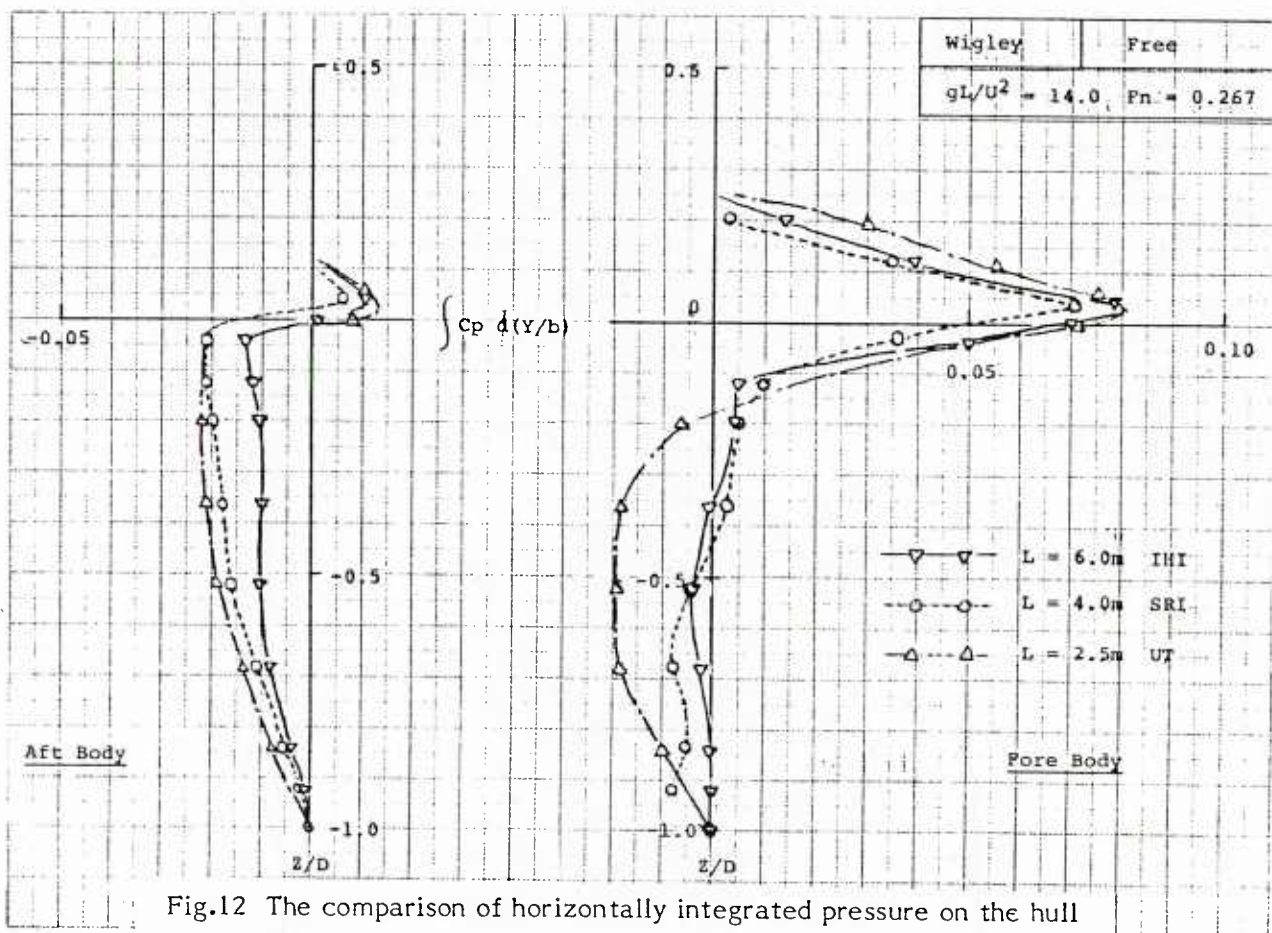
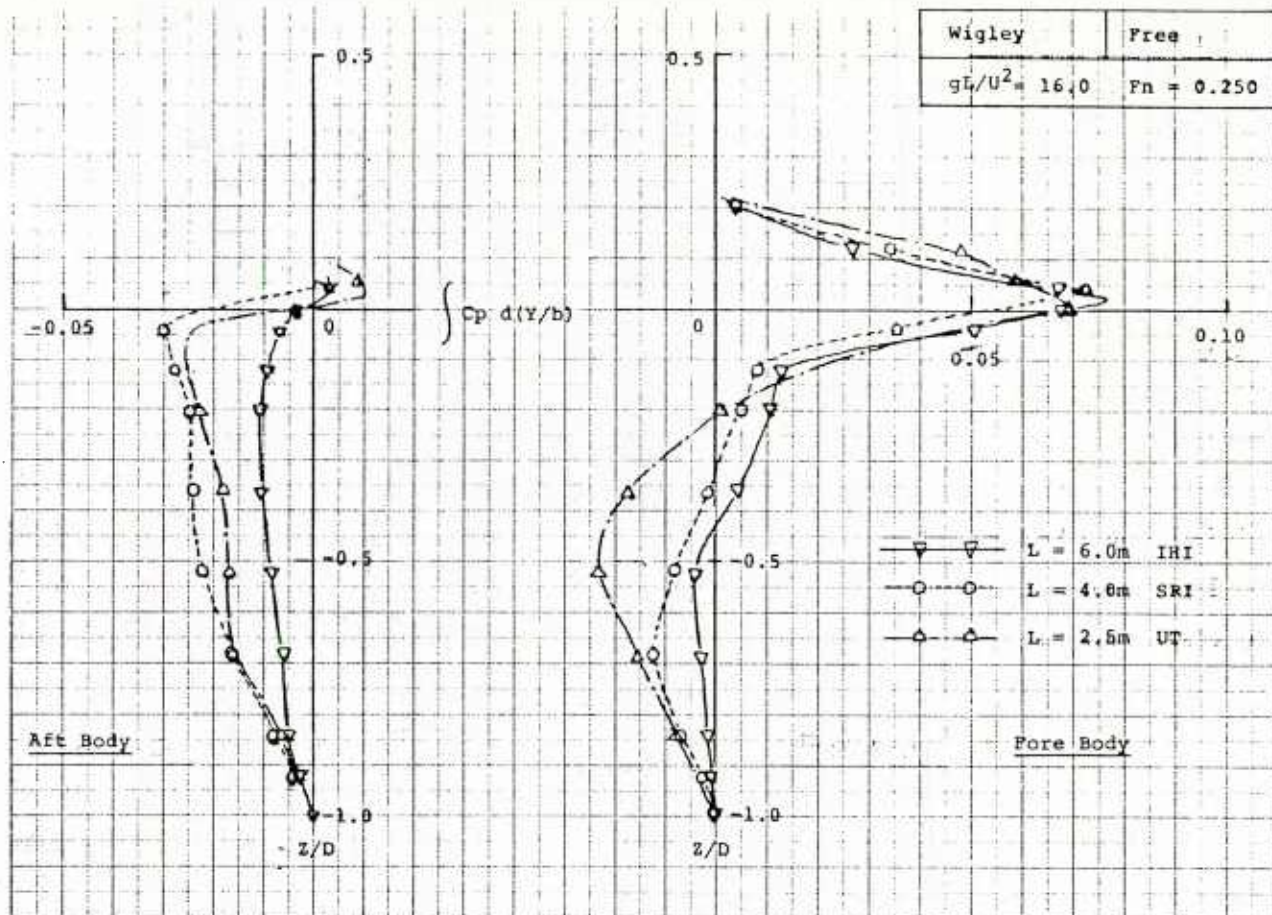


Fig.12 The comparison of horizontally integrated pressure on the hull

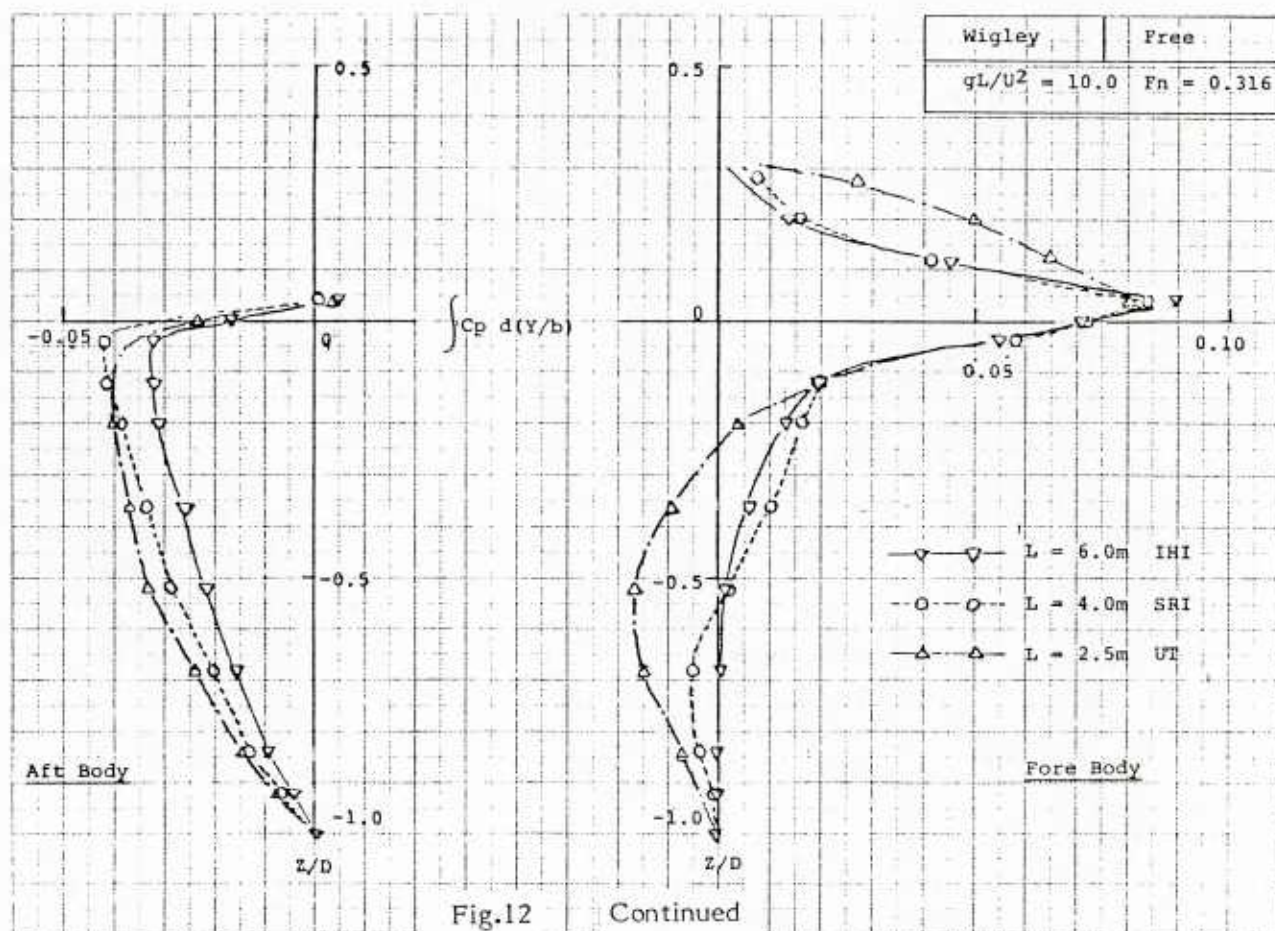
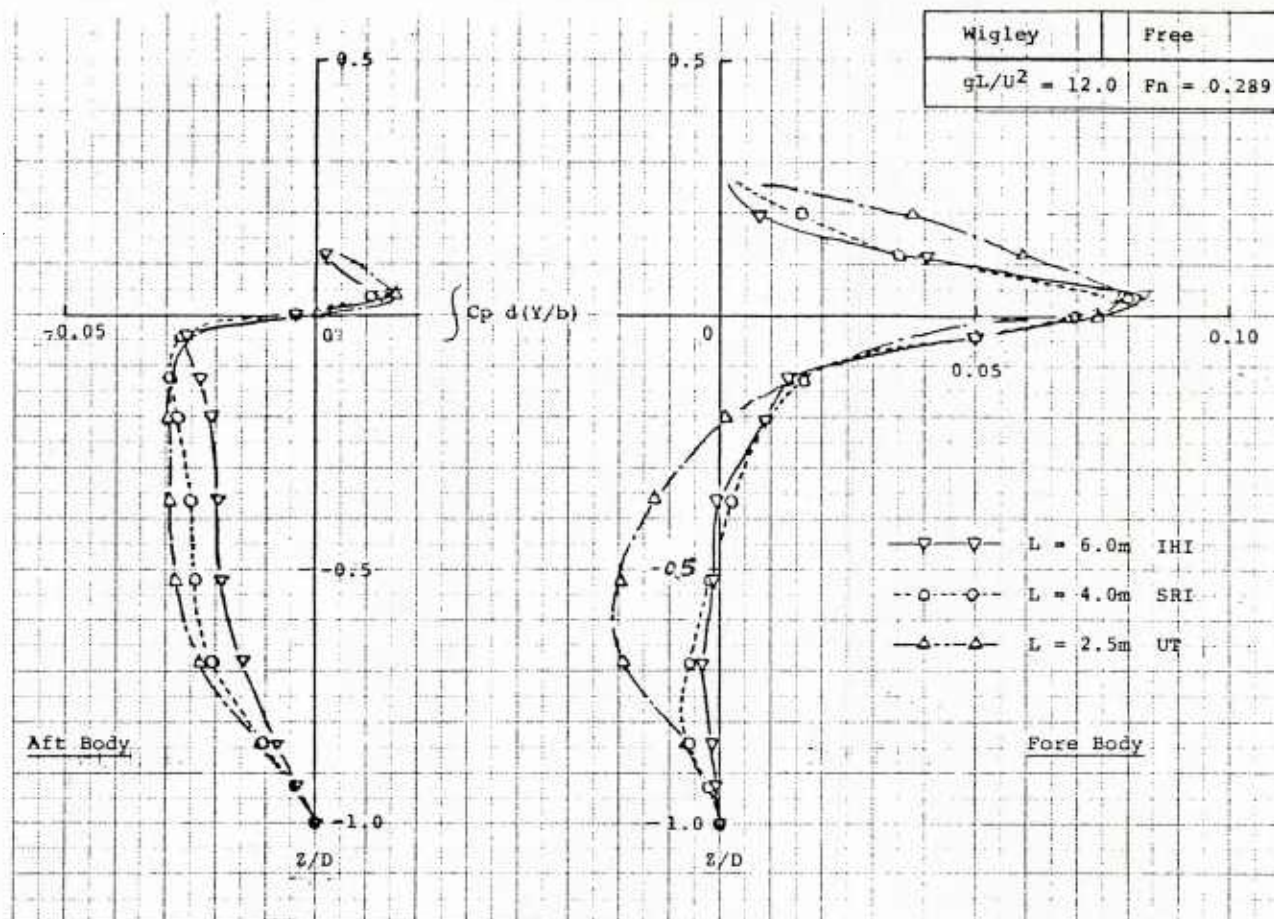


Fig.12 Continued

Table 2 The pressure coefficient on the hull of 6.0m model (FR)

Fn = 0.104 Free L=6.0 m (IHI)												
ST. 2X/L	10.000	9.750	9.500	9.250	9.000	8.500	8.000	7.500	7.000	6.000	5.500	5.000
Z/D	-1.000	-0.950	-0.900	-0.850	-0.800	-0.700	-0.600	-0.500	-0.400	-0.200	-0.100	0.000
.000	.000	.139	.113	.026	.000	-.014	-.009	-.046	.000	.000	.000	.000
-.040	.959	.135	.100	.022	-.046	-.017	-.014	-.046	-.084	-.046	-.052	-.054
-.120	.968	.126	.077	.014	-.034	-.023	-.024	-.047	-.063	-.046	-.054	-.060
-.200	.976	.117	.058	.008	-.026	-.029	-.033	-.048	-.051	-.046	-.053	-.063
-.360	.987	.098	.035	-.001	-.021	-.038	-.045	-.048	-.046	-.044	-.046	-.060
-.520	.992	.077	.026	-.003	-.022	-.042	-.048	-.047	-.044	-.041	-.040	-.052
-.680	.994	.061	.022	-.004	-.021	-.041	-.045	-.044	-.041	-.036	-.037	-.041
-.840	.994	.049	.020	-.005	-.018	-.035	-.039	-.039	-.036	-.033	-.034	-.038
-.920	.000	.044	.019	-.014	-.016	-.032	-.035	-.035	-.034	-.033	-.033	-.036
-1.000	.000	.040	.018	-.004	-.015	-.028	-.030	-.030	-.031	-.034	-.031	-.037
DIPPING	.0016	.0016	.0016	.0016	.0016	.0015	.0015	.0015	.0015	.0014	.0014	.0014

ST. 2X/L	5.000	4.500	4.000	3.000	2.500	2.000	1.500	1.000	.750	.500	.250	0.000
Z/D	.000	.100	.200	.400	.500	.600	.700	.800	.850	.900	.950	1.000
.000	.000	.000	.000	-.037	-.046	.000	.000	-.018	-.001	.030	.033	.159
-.040	-.054	-.055	-.056	-.039	-.045	-.044	-.039	-.017	.001	.031	.033	.157
-.120	-.060	-.057	-.056	-.044	-.044	-.043	-.034	-.015	.004	.035	.034	.155
-.200	-.063	-.058	-.055	-.048	-.045	-.043	-.033	-.013	.005	.036	.034	.153
-.360	-.060	-.057	-.048	-.053	-.048	-.044	-.033	-.012	.003	.030	.030	.151
-.520	-.052	-.054	-.044	-.053	-.052	-.046	-.035	-.018	-.007	.018	.070	.147
-.680	-.041	-.052	-.038	-.049	-.049	-.044	-.036	-.024	-.014	.007	.054	.127
-.840	-.038	-.047	-.034	-.043	-.044	-.041	-.034	-.023	-.012	.004	.034	.083
-.920	-.036	-.044	-.032	-.039	-.043	-.039	-.033	-.022	-.009	.004	.024	.054
-1.000	-.037	-.042	-.031	-.034	-.038	-.038	-.032	-.018	-.007	.006	.016	.021
DIPPING	.0014	.0014	.0013	.0013	.0013	.0012	.0012	.0012	.0012	.0012	.0012	.0011

Fn = 0.250 Free L=6.0 m (IHI)												
ST. 2X/L	10.000	9.750	9.500	9.250	9.000	8.500	8.000	7.500	7.000	6.000	5.500	5.000
Z/D	-1.000	-0.950	-0.900	-0.850	-0.800	-0.700	-0.600	-0.500	-0.400	-0.200	-0.100	0.000
.200	.000	.000	.372	.000	.000	.000	.000	.000	.000	.000	.000	.000
.120	.000	.266	.325	.239	.000	.000	.000	.000	.000	.000	.000	.000
.040	.000	.243	.283	.213	.097	.000	.000	.000	.000	.000	.000	.000
.000	.974	.233	.264	.200	.090	.000	.000	.000	.000	.012	-.007	.000
-.040	.979	.224	.246	.188	.083	-.097	.000	.000	-.080	.011	-.009	-.065
-.120	.986	.205	.216	.165	.071	-.091	-.168	-.153	-.057	.008	-.014	-.068
-.200	.991	.188	.189	.144	.059	-.086	-.158	-.144	-.059	.006	-.018	-.068
-.360	.997	.158	.147	.107	.039	-.077	-.139	-.124	-.055	.001	-.023	-.061
-.520	.998	.130	.116	.077	.024	-.068	-.119	-.101	-.051	-.005	-.026	-.052
-.680	.998	.105	.093	.054	.014	-.058	-.099	-.092	-.058	-.012	-.027	-.045
-.840	.999	.082	.076	.040	.009	-.046	-.079	-.071	-.052	-.019	-.027	-.041
-.920	.000	.071	.069	.036	.008	-.039	-.070	-.068	-.047	-.023	-.028	-.040
-1.000	.000	.061	.063	.034	.006	-.034	-.061	-.065	-.046	-.027	-.028	-.040
DIPPING	.0101	.0100	.0100	.0099	.0098	.0096	.0094	.0092	.0090	.0087	.0085	.0083

ST. 2X/L	5.000	4.500	4.000	3.000	2.500	2.000	1.500	1.000	.750	.500	.250	0.000
Z/D	.000	.100	.200	.400	.500	.600	.700	.800	.850	.900	.950	1.000
.200	.000	.000	.000	.000	.000	.000	.000	.000	.000	.000	.000	.000
.120	.000	.000	.000	.000	.000	.000	.000	.000	.000	.000	.000	.000
.040	.000	.000	.000	.000	.000	.000	.000	.000	.000	.000	.000	.176
.000	.000	.000	-.032	-.022	-.022	-.013	-.029	.000	-.029	-.011	.038	.174
-.040	-.065	-.100	-.034	-.027	-.020	-.012	-.026	-.035	-.026	-.008	.042	.173
-.120	-.068	-.095	-.037	-.034	-.019	-.013	-.022	-.029	-.023	-.005	.048	.173
-.200	-.068	-.090	-.040	-.040	-.020	-.016	-.021	-.026	-.022	-.004	.053	.174
-.360	-.061	-.079	-.045	-.046	-.028	-.024	-.026	-.027	-.023	-.006	.054	.177
-.520	-.052	-.067	-.048	-.047	-.033	-.030	-.031	-.030	-.024	-.007	.048	.170
-.680	-.045	-.058	-.049	-.046	-.035	-.034	-.033	-.028	-.023	-.005	.039	.147
-.840	-.041	-.052	-.050	-.041	-.033	-.034	-.032	-.025	-.020	-.002	.028	.099
-.920	-.040	-.052	-.049	-.038	-.031	-.032	-.030	-.023	-.016	.000	.022	.064
-1.000	-.040	-.051	-.049	-.034	-.029	-.030	-.029	-.020	-.011	.003	.016	.021
DIPPING	.0083	.0081	.0079	.0076	.0074	.0072	.0070	.0068	.0068	.0067	.0066	.0065

Table 2 Continued

Fn = 0.267 Free L=6.0 m (IHI)												
ST. 2X/L	10.000 -1.000	9.750 -.950	9.500 -.900	9.250 -.850	9.000 -.800	8.500 -.700	8.000 -.600	7.500 -.500	7.000 -.400	6.000 -.200	5.500 -.100	5.000 .000
Z/D												
.200	.000	.000	.350	.000	.000	.000	.000	.000	.000	.000	.000	.000
.120	.000	.250	.309	.259	.000	.000	.000	.000	.000	.000	.000	.000
.040	.000	.230	.271	.226	.136	.000	.000	.000	.000	.000	.000	.000
.000	.974	.221	.254	.211	.127	.000	.000	.000	.000	-.006	.011	-.009
-.040	.979	.212	.238	.197	.119	-.060	.000	.000	.000	-.007	.010	-.012
-.120	.986	.195	.208	.170	.102	-.058	-.159	-.173	-.123	-.008	.007	-.016
-.200	.991	.178	.183	.147	.087	-.056	-.146	-.163	-.112	-.010	.003	-.018
-.360	.997	.149	.142	.106	.058	-.052	-.131	-.141	-.103	-.012	-.005	-.019
-.520	.998	.124	.113	.075	.037	-.048	-.115	-.119	-.096	-.016	-.012	-.021
-.680	.998	.100	.091	.057	.023	-.043	-.097	-.100	-.081	-.021	-.017	-.024
-.840	.999	.080	.074	.044	.017	-.035	-.076	-.083	-.067	-.026	-.020	-.026
-.920	.000	.069	.067	.041	.016	-.030	-.065	-.075	-.063	-.029	-.020	-.026
-1.000	.000	.059	.061	.040	.016	-.024	-.053	-.068	-.061	-.032	-.021	-.025
DIPPING	.0120	.0119	.0118	.0117	.0116	.0114	.0112	.0110	.0108	.0104	.0102	.0100

ST. 2X/L	5.000 .000	4.500 .100	4.000 .200	3.000 .400	2.500 .500	2.000 .600	1.500 .700	1.000 .800	.750 .850	.500 .900	.250 .950	.000 1.000
Z/D												
.200	.000	.000	.000	.000	.000	.000	.000	.000	.000	.000	.000	.000
.120	.000	.000	.000	.000	.000	.000	.000	.000	.000	.000	.000	.185
.040	.000	.000	.000	.000	.000	.000	.000	.000	.000	.000	.064	.183
.000	-.009	.000	.000	.000	.000	.000	-.026	-.009	.007	.027	.067	.182
-.040	-.012	-.054	-.085	-.085	-.065	-.041	-.023	-.006	.008	.029	.070	.182
-.120	-.016	-.054	-.081	-.084	-.064	-.040	-.019	-.003	.008	.032	.074	.183
-.200	-.018	-.052	-.077	-.083	-.064	-.042	-.018	-.001	.009	.033	.076	.186
-.360	-.019	-.046	-.068	-.077	-.064	-.047	-.024	-.004	.008	.029	.076	.192
-.520	-.021	-.043	-.059	-.070	-.063	-.049	-.029	-.010	-.001	.016	.068	.185
-.680	-.024	-.040	-.052	-.064	-.060	-.051	-.030	-.012	-.008	.009	.056	.157
-.840	-.026	-.038	-.047	-.058	-.055	-.047	-.031	-.012	-.005	.012	.044	.106
-.920	-.026	-.036	-.044	-.054	-.051	-.044	-.030	-.010	.000	.015	.037	.071
-1.000	-.025	-.035	-.042	-.049	-.047	-.041	-.029	-.008	.006	.018	.027	.031
DIPPING	.0100	.0098	.0096	.0092	.0090	.0088	.0086	.0084	.0083	.0082	.0081	.0080

Fn = 0.289 Free L=6.0 m (IHI)												
ST. 2X/L	10.000 -1.000	9.750 -.950	9.500 -.900	9.250 -.850	9.000 -.800	8.500 -.700	8.000 -.600	7.500 -.500	7.000 -.400	6.000 -.200	5.500 -.100	5.000 .000
Z/D												
.200	.000	.000	.310	.291	.000	.000	.000	.000	.000	.000	.000	.000
.120	.000	.225	.279	.259	.187	.000	.000	.000	.000	.000	.000	.000
.040	.000	.205	.250	.229	.165	.000	.000	.000	.000	.000	.000	.000
.000	.968	.196	.236	.214	.154	-.020	.000	.000	.000	.000	-.014	.006
-.040	.972	.188	.222	.200	.144	-.020	.000	.000	.000	-.007	-.015	.002
-.120	.979	.173	.198	.175	.124	-.020	-.120	-.171	-.160	-.057	-.018	-.003
-.200	.985	.159	.176	.152	.106	-.020	-.113	-.165	-.150	-.057	-.020	-.009
-.360	.993	.137	.139	.113	.075	-.020	-.101	-.146	-.134	-.054	-.026	-.015
-.520	.997	.118	.111	.087	.054	-.019	-.089	-.121	-.117	-.049	-.028	-.018
-.680	.998	.098	.090	.068	.041	-.019	-.075	-.100	-.100	-.048	-.029	-.022
-.840	.998	.077	.074	.054	.032	-.017	-.060	-.079	-.084	-.050	-.031	-.022
-.920	.000	.066	.067	.049	.028	-.016	-.053	-.073	-.079	-.052	-.033	-.024
-1.000	.000	.056	.061	.045	.024	-.014	-.046	-.068	-.074	-.053	-.035	-.025
DIPPING	.0127	.0126	.0126	.0125	.0125	.0124	.0123	.0123	.0122	.0120	.0120	.0119

ST. 2X/L	5.000 .000	4.500 .100	4.000 .200	3.000 .400	2.500 .500	2.000 .600	1.500 .700	1.000 .800	.750 .850	.500 .900	.250 .950	.000 1.000
Z/D												
.200	.000	.000	.000	.000	.000	.000	.000	.000	.000	.000	.000	.000
.120	.000	.000	.000	.000	.000	.000	.000	.000	.000	.000	.000	.175
.040	.000	.000	.000	.000	.000	.000	.000	.000	.000	.000	.065	.178
.000	.006	-.003	-.025	.000	.000	.000	-.040	-.019	.010	.010	.069	.180
-.040	-.002	-.005	-.026	-.071	-.080	-.082	-.039	-.017	.013	.072	.182	
-.120	-.003	-.009	-.027	-.072	-.079	-.078	-.065	-.036	.014	.017	.076	.185
-.200	-.009	-.012	-.028	-.071	-.078	-.076	-.064	-.036	.016	.078	.191	
-.360	-.015	-.016	-.029	-.065	-.074	-.076	-.066	-.041	.020	.073	.198	
-.520	-.018	-.018	-.029	-.060	-.071	-.074	-.066	-.046	.028	.061	.191	
-.680	-.022	-.024	-.028	-.056	-.066	-.070	-.064	-.046	-.029	.049	.165	
-.840	-.022	-.024	-.028	-.051	-.059	-.064	-.060	-.041	-.024	.038	.112	
-.920	-.024	-.025	-.027	-.047	-.056	-.061	-.056	-.037	-.020	.031	.075	
-1.000	-.025	-.025	-.026	-.044	-.053	-.058	-.053	-.033	-.013	.027	.030	
DIPPING	.0119	.0118	.0117	.0116	.0115	.0114	.0113	.0113	.0112	.0112	.0111	.0111

Table 2 Continued

Fn = 0.316 Free L=6.0 m (IHI)												
ST. Z/L	10.000	9.750	9.500	9.250	9.000	8.500	8.000	7.500	7.000	6.000	5.500	5.000
Z/D	-1.000	-.950	-.900	-.850	-.800	-.700	-.600	-.500	-.400	-.200	-.100	.000
.200	.000	.213	.260	.261	.233	.000	.000	.000	.000	.000	.000	.000
.120	.000	.196	.238	.233	.203	.000	.000	.000	.000	.000	.000	.000
.040	.000	.181	.217	.208	.175	.038	.000	.000	.000	.000	.000	.000
.000	.000	.174	.206	.196	.162	.038	.000	.000	.000	.000	.000	.000
-.040	.000	.168	.197	.184	.150	.033	-.056	.000	.000	.000	.000	-.042
-.120	.000	.157	.177	.163	.128	.027	-.060	-.133	-.169	-.124	-.078	-.043
-.200	.000	.146	.159	.143	.110	.022	-.063	-.133	-.159	-.118	-.076	-.047
-.360	.000	.128	.130	.110	.083	.014	-.067	-.125	-.141	-.103	-.074	-.045
-.520	.000	.110	.106	.086	.065	.008	-.060	-.107	-.122	-.089	-.068	-.043
-.680	.000	.092	.086	.069	.050	.005	-.048	-.085	-.102	-.080	-.061	-.043
-.840	.000	.072	.069	.057	.040	.005	-.036	-.068	-.086	-.077	-.066	-.044
-.920	.000	.061	.062	.052	.038	.006	-.032	-.062	-.081	-.076	-.061	-.045
-1.000	.000	.050	.056	.048	.036	.008	-.027	-.059	-.077	-.077	-.063	-.045
DIPPING	.0173	.0172	.0171	.0169	.0168	.0165	.0162	.0160	.0157	.0152	.0149	.0146

ST. Z/L	5.000	4.500	4.000	3.000	2.500	2.000	1.500	1.000	.750	.500	.250	.000
Z/D	.000	.100	.200	.400	.500	.600	.700	.800	.850	.900	.950	1.000
.200	.000	.000	.000	.000	.000	.000	.000	.000	.000	.000	.000	.000
.120	.000	.000	.000	.000	.000	.000	.000	.000	.000	.000	.000	.000
.040	.000	.000	.000	.000	.000	.000	.000	.000	.000	.000	.000	.000
.000	-.042	-.016	-.009	-.022	-.039	.000	.000	.000	.000	.000	.000	.000
-.040	-.043	-.019	-.010	-.022	-.038	-.053	-.062	-.061	-.054	-.041	-.003	.008
-.120	-.046	-.023	-.011	-.023	-.035	-.052	-.061	-.058	-.052	-.037	.008	.117
-.200	-.047	-.025	-.013	-.023	-.035	-.051	-.059	-.057	-.051	-.037	.009	.127
-.360	-.045	-.026	-.017	-.022	-.036	-.051	-.059	-.058	-.052	-.039	.010	.140
-.520	-.043	-.028	-.021	-.023	-.038	-.050	-.059	-.059	-.055	-.040	.005	.138
-.680	-.043	-.030	-.022	-.026	-.038	-.050	-.057	-.057	-.054	-.039	.000	.116
-.840	-.044	-.032	-.023	-.026	-.036	-.047	-.053	-.050	-.046	-.032	-.004	.065
-.920	-.045	-.033	-.023	-.024	-.034	-.045	-.052	-.047	-.041	-.027	-.008	.030
-1.000	-.045	-.034	-.023	-.021	-.032	-.044	-.051	-.043	-.033	-.022	-.012	-.008
DIPPING	.0146	.0143	.0141	.0135	.0132	.0130	.0127	.0124	.0123	.0122	.0120	.0119

Table 3 The pressure coefficient on the hull of 4.0m model (FR)

Fn = 0.250 Free L=4.0 m (SRI)												
ST. 2X/L	10.000	9.750	9.500	9.250	9.000	8.500	8.000	7.500	7.000	6.000	5.500	5.000
Z/D	-1.000	-.950	-.900	-.850	-.800	-.700	-.600	-.500	-.400	-.200	-.100	.000
.200	.000	.000	.326	.000	.000	.000	.000	.000	.000	.000	.000	.000
.120	1.000	.278	.311	.216	.000	.000	.000	.000	.000	.000	.000	.000
.040	1.000	.246	.274	.194	.066	.000	.000	.000	.000	.000	.000	.000
-.040	1.000	.217	.204	.174	.053	-.109	.000	.000	-.068	.004	-.018	-.072
-.120	1.000	.197	.179	.154	.049	-.105	-.169	-.146	-.067	-.007	-.022	-.099
-.200	1.000	.182	.162	.132	.047	-.096	-.158	-.131	-.069	-.013	-.028	-.098
-.360	1.000	.154	.123	.090	.030	-.073	-.131	-.111	-.070	-.026	-.043	-.061
-.520	1.000	.124	.090	.058	.002	-.070	-.112	-.094	-.065	-.030	-.033	-.046
-.680	1.000	.060	.054	.013	-.005	-.054	-.086	-.077	-.054	-.035	-.035	-.052
-.840	1.000	.060	.054	.013	-.005	-.054	-.086	-.077	-.054	-.034	-.028	-.039
-.920	1.000	.057	.052	.011	-.015	-.051	-.078	-.078	-.056	-.036	-.025	-.046
-1.000	1.000	.063	.017	.023	.011	-.054	-.054	-.063	-.058	-.030	-.029	-.074
DIFFING	.0070	.0069	.0068	.0068	.0067	.0066	.0065	.0063	.0062	.0060	.0058	.0057

ST. 2X/L	5.000	4.500	4.000	3.000	2.500	2.000	1.500	1.000	.750	.500	.250	.000
Z/D	.000	.100	.200	.400	.500	.600	.700	.800	.850	.900	.950	1.000
.200	.000	.000	.000	.000	.000	.000	.000	.000	.000	.000	.000	.000
.120	.000	.000	.000	.000	.000	.000	.000	.000	.000	.000	.000	.000
.040	.000	.000	.000	.000	.000	.000	.000	.000	.000	.000	.045	.070
-.040	-.072	-.099	-.102	-.048	-.039	-.027	-.028	-.044	-.038	-.031	.029	.099
-.120	-.099	-.088	-.103	-.050	-.032	-.022	-.035	-.048	-.034	-.031	.037	.114
-.200	-.098	-.081	-.096	-.054	-.041	-.022	-.038	-.047	-.034	-.030	.042	.127
-.360	-.061	-.072	-.091	-.056	-.046	-.029	-.036	-.042	-.034	-.024	.042	.144
-.520	-.046	-.066	-.075	-.061	-.045	-.032	-.044	-.049	-.038	-.027	.035	.114
-.680	-.052	-.057	-.058	-.051	-.043	-.026	-.050	-.044	-.042	-.026	.022	.083
-.840	-.039	-.045	-.062	-.051	-.039	-.035	-.042	-.044	-.040	-.018	.014	.050
-.920	-.046	-.052	-.048	-.043	-.038	-.035	-.039	-.053	-.038	-.005	.010	.020
-1.000	-.074	-.062	-.061	-.074	-.036	-.063	-.033	-.038	-.006	-.030	-.018	.002
DIFFING	.0057	.0056	.0054	.0052	.0051	.0049	.0048	.0047	.0046	.0046	.0045	.0044

Fn = 0.267 Free L=4.0 m (SRI)												
ST. 2X/L	10.000	9.750	9.500	9.250	9.000	8.500	8.000	7.500	7.000	6.000	5.500	5.000
Z/D	-1.000	-.950	-.900	-.850	-.800	-.700	-.600	-.500	-.400	-.200	-.100	.000
.200	1.000	.312	.334	.000	.000	.000	.000	.000	.000	.000	.000	.000
.120	1.000	.259	.303	.232	.000	.000	.000	.000	.000	.000	.000	.000
.040	1.000	.226	.252	.213	.112	.000	.000	.000	.000	.000	.015	.022
-.040	1.000	.204	.203	.187	.090	-.049	.000	.000	-.114	-.012	.004	-.028
-.120	1.000	.189	.177	.165	.081	-.051	-.155	-.177	-.114	-.022	-.004	-.053
-.200	1.000	.175	.162	.144	.077	-.053	-.146	-.157	-.110	-.027	-.009	-.014
-.360	1.000	.153	.127	.102	.053	-.041	-.123	-.130	-.104	-.038	-.029	-.035
-.520	1.000	.125	.095	.070	.021	-.043	-.104	-.107	-.089	-.039	-.022	-.025
-.680	1.000	.095	.079	.043	.013	-.047	-.096	-.097	-.085	-.042	-.027	-.036
-.840	1.000	.063	.060	.023	.008	-.038	-.081	-.084	-.067	-.041	-.022	-.027
-.920	1.000	-.060	-.058	-.020	-.003	-.036	-.073	-.086	-.069	-.042	-.020	-.036
-1.000	1.000	.066	.022	.031	.022	-.039	-.048	-.069	-.072	-.036	-.024	-.062
DIFFING	.0079	.0078	.0077	.0077	.0076	.0075	.0074	.0073	.0072	.0070	.0069	.0068

ST. 2X/L	5.000	4.500	4.000	3.000	2.500	2.000	1.500	1.000	.750	.500	.250	.000
Z/D	.000	.100	.200	.400	.500	.600	.700	.800	.850	.900	.950	1.000
.200	.000	.000	.000	.000	.000	.000	.000	.000	.000	.000	.000	.000
.120	.000	.000	.000	.000	.000	.000	.000	.000	.000	.000	.014	.101
.040	.022	.000	.000	.000	.000	.000	.000	.000	.000	.000	.007	.116
-.040	-.028	-.054	-.084	-.084	-.075	-.043	-.014	-.010	.000	.007	.058	.123
-.120	-.053	-.046	-.088	-.088	-.069	-.039	-.022	-.013	.001	.006	.064	.128
-.200	-.014	-.043	-.081	-.088	-.075	-.038	-.025	-.015	.002	.006	.069	.128
-.360	-.035	-.041	-.077	-.082	-.074	-.045	-.025	-.014	-.001	.009	.067	.121
-.520	-.025	-.043	-.062	-.081	-.069	-.048	-.036	-.025	-.009	.001	.061	.137
-.680	-.036	-.039	-.053	-.067	-.064	-.040	-.043	-.022	-.016	.001	.046	.100
-.840	-.027	-.032	-.054	-.064	-.055	-.046	-.035	-.024	-.017	.006	.037	.069
-.920	-.036	-.040	-.042	-.057	-.053	-.046	-.030	-.033	-.025	.021	.035	.043
-1.000	-.062	-.050	-.054	-.088	-.049	-.076	-.024	-.020	.020	-.008	.004	.025
DIFFING	.0068	.0067	.0066	.0064	.0063	.0062	.0061	.0060	.0059	.0059	.0058	.0057

Table 3 Continued

Fn = 0.289 Free L=4.0 m (SRI)												
ST. 2X/L	10.000	9.750	9.500	9.250	9.000	8.500	8.000	7.500	7.000	6.000	5.500	5.000
Z/D	-1.000	-.950	-.900	-.850	-.800	-.700	-.600	-.500	-.400	-.200	-.100	.000
.200	1.000	.259	.321	.260	.000	.000	.000	.000	.000	.000	.000	.000
.120	1.000	.229	.269	.239	.161	.031	.000	.000	.000	.000	.000	.000
.040	1.000	.200	.228	.211	.142	.014	.000	.000	.000	.000	.011	.006
-.040	1.000	.186	.191	.186	.117	.007	-.092	-.125	.000	-.060	-.020	-.016
-.120	1.000	.174	.171	.166	.107	-.002	-.117	-.183	-.153	-.069	-.023	-.041
-.200	1.000	.165	.153	.146	.098	-.008	-.112	-.157	-.147	-.069	-.031	-.018
-.350	1.000	.146	.124	.103	.069	-.006	-.097	-.132	-.132	-.074	-.048	-.035
-.520	1.000	.120	.096	.074	.034	-.017	-.083	-.107	-.114	-.069	-.038	-.046
-.680	1.000	.093	.080	.047	.026	-.025	-.079	-.096	-.104	-.066	-.040	-.048
-.840	1.000	.062	.062	.026	.019	-.021	-.067	-.083	-.081	-.060	-.032	-.049
-.920	1.000	.059	.061	.025	.007	-.020	-.059	-.083	-.082	-.059	-.028	-.040
-1.000	1.000	.066	.023	.037	.032	-.025	-.037	-.067	-.083	-.051	-.032	-.060
DIPPING	.0087	.0087	.0087	.0087	.0086	.0086	.0086	.0085	.0085	.0084	.0084	.0083

ST. 2X/L	5.000	4.500	4.000	3.000	2.500	2.000	1.500	1.000	.750	.500	.250	.000
Z/D	.000	.100	.200	.400	.500	.600	.700	.800	.850	.900	.950	1.000
.200	.000	.000	.000	.000	.000	.000	.000	.000	.000	.000	.000	.000
.120	.000	.000	.000	.000	.000	.000	.000	.000	.000	.000	.000	.000
.040	.006	.000	.000	.000	.000	.000	.000	.000	.000	.001	.078	.170
-.040	-.016	-.013	-.032	-.068	-.088	-.076	-.056	-.043	-.026	-.003	.078	.166
-.120	-.041	-.008	-.040	-.074	-.081	-.072	-.064	-.047	-.022	-.004	.076	.167
-.200	-.018	-.008	-.035	-.072	-.085	-.071	-.066	-.053	-.022	-.004	.074	.168
-.350	-.035	-.013	-.038	-.068	-.081	-.068	-.063	-.045	-.026	.003	.066	.152
-.520	-.046	-.021	-.031	-.069	-.073	-.069	-.071	-.056	-.035	-.011	.057	.141
-.680	-.048	-.022	-.028	-.056	-.066	-.069	-.074	-.051	-.040	-.012	.039	.102
-.840	-.049	-.017	-.033	-.054	-.058	-.061	-.062	-.050	-.038	-.006	.028	.060
-.920	-.040	-.027	-.023	-.049	-.057	-.061	-.056	-.059	-.047	.010	.026	.037
-1.000	-.060	-.039	-.038	-.083	-.054	-.092	-.048	-.044	.004	-.016	-.007	.006
DIPPING	.0083	.0083	.0083	.0082	.0082	.0081	.0081	.0081	.0080	.0080	.0080	.0080

Fn = 0.316 Free L=4.0 m (SRI)												
ST. 2X/L	10.000	9.750	9.500	9.250	9.000	8.500	8.000	7.500	7.000	6.000	5.500	5.000
Z/D	-1.000	-.950	-.900	-.850	-.800	-.700	-.600	-.500	-.400	-.200	-.100	.000
.200	.000	.000	.319	.000	.000	.000	.000	.000	.000	.000	.000	.000
.120	1.000	.226	.284	.251	.000	.000	.000	.000	.000	.000	.000	.000
.040	1.000	.196	.242	.231	.180	.000	.000	.000	.000	.000	.000	.000
-.040	1.000	.178	.204	.199	.153	.065	.000	.000	.000	.000	.000	.000
-.120	1.000	.169	.178	.177	.133	.058	-.059	.000	.000	.000	-.075	-.053
-.200	1.000	.162	.159	.159	.120	.048	-.068	-.163	-.175	-.122	-.077	-.071
-.350	1.000	.155	.143	.141	.109	.035	-.070	-.139	-.161	-.120	-.081	-.094
-.520	1.000	.140	.117	.106	.079	.029	-.065	-.117	-.142	-.118	-.095	-.070
-.680	1.000	.117	.094	.076	.043	.013	-.057	-.096	-.121	-.104	-.075	-.046
-.840	1.000	.090	.080	.050	.035	-.001	-.058	-.085	-.110	-.095	-.071	-.062
-.920	1.000	.061	.064	.029	.026	-.003	-.051	-.074	-.086	-.085	-.060	-.045
-1.000	1.000	.060	.078	.030	.014	-.003	-.044	-.075	-.086	-.084	-.054	-.058
DIPPING	.0117	.0116	.0115	.0114	.0114	.0112	.0110	.0109	.0107	.0104	.0102	.0100

ST. 2X/L	5.000	4.500	4.000	3.000	2.500	2.000	1.500	1.000	.750	.500	.250	.000
Z/D	.000	.100	.200	.400	.500	.600	.700	.800	.850	.900	.950	1.000
.200	.000	.000	.000	.000	.000	.000	.000	.000	.000	.000	.000	.000
.120	.000	.000	.000	.000	.000	.000	.000	.000	.000	.000	.000	.000
.040	.000	.000	.000	.000	.000	.000	.000	.000	.000	.000	.000	.000
-.040	-.053	-.028	-.019	-.024	-.051	-.059	-.054	-.059	-.057	-.052	-.018	.027
-.120	-.071	-.027	-.024	-.028	-.043	-.047	-.063	-.067	-.054	-.054	-.008	.042
-.200	-.034	-.022	-.022	-.031	-.048	-.042	-.065	-.067	-.053	-.054	.001	.062
-.350	-.070	-.028	-.030	-.031	-.048	-.046	-.060	-.062	-.056	-.048	.004	.083
-.520	-.046	-.035	-.025	-.039	-.045	-.048	-.066	-.069	-.060	-.051	.004	.031
-.680	-.062	-.034	-.024	-.030	-.042	-.037	-.069	-.062	-.063	-.047	-.008	.037
-.840	-.045	-.029	-.032	-.034	-.039	-.047	-.057	-.059	-.059	-.034	-.012	.011
-.920	-.058	-.038	-.021	-.028	-.038	-.048	-.051	-.069	-.068	-.018	-.010	-.004
-1.000	-.068	-.050	-.036	-.063	-.037	-.079	-.047	-.055	-.021	-.049	-.043	-.035
DIPPING	.0100	.0098	.0097	.0094	.0092	.0091	.0088	.0088	.0087	.0086	.0085	.0084

Table 4 The pressure coefficient on the hull of 2.5m model (FR)

Fn = 0.289 Free L=2.5 m (UT)															
ST.	10.000	9.750	9.500	9.250	9.000	8.750	8.500	8.250	8.000	7.750	7.500	7.250	7.000	6.750	5.000
2x/L	-1.000	-0.950	-0.900	-0.850	-0.800	-0.750	-0.700	-0.650	-0.600	-0.550	-0.500	-0.450	-0.400	-0.350	1.000
Z/D	.000	.242	.304	.248	.242	.158	.120	.080	.040	.000	.000	.000	.000	.000	.000
	.000	.195	.213	.206	.137	.093	.053	.012	.000	.000	.000	.000	.000	.000	.000
	.000	.188	.203	.206	.132	.083	.043	.012	.000	.000	.000	.000	.000	.000	.000
	.000	.102	.138	.139	.065	.037	.017	.007	.000	.000	.000	.000	.000	.000	.000
	.000	.079	.083	.088	.030	.017	.007	.003	.000	.000	.000	.000	.000	.000	.000
	.000	.069	.067	.068	.012	.007	.003	.001	.000	.000	.000	.000	.000	.000	.000
	.000	.047	.053	.055	.007	.004	.002	.001	.000	.000	.000	.000	.000	.000	.000
	.000	.043	.049	.050	.006	.005	.003	.002	.000	.000	.000	.000	.000	.000	.000
DIPPING	.0050	.0050	.0050	.0050	.0050	.0050	.0050	.0050	.0050	.0050	.0050	.0050	.0050	.0050	.0051

Fn = 0.316 Free L=2.5 m (UT)															
ST.	10.000	9.750	9.500	9.250	9.000	8.750	8.500	8.250	8.000	7.750	7.500	7.250	7.000	6.750	5.000
2x/L	-1.000	-0.950	-0.900	-0.850	-0.800	-0.750	-0.700	-0.650	-0.600	-0.550	-0.500	-0.450	-0.400	-0.350	1.000
Z/D	.000	.249	.243	.245	.243	.159	.120	.080	.040	.000	.000	.000	.000	.000	.000
	.000	.175	.206	.213	.156	.093	.053	.012	.000	.000	.000	.000	.000	.000	.000
	.000	.171	.178	.217	.156	.093	.053	.012	.000	.000	.000	.000	.000	.000	.000
	.000	.131	.124	.135	.104	.074	.038	.016	.000	.000	.000	.000	.000	.000	.000
	.000	.100	.093	.098	.074	.049	.038	.016	.000	.000	.000	.000	.000	.000	.000
	.000	.073	.078	.088	.049	.038	.038	.016	.000	.000	.000	.000	.000	.000	.000
	.000	.055	.066	.066	.044	.038	.038	.016	.000	.000	.000	.000	.000	.000	.000
	.000	.045	.053	.055	.025	.025	.025	.016	.000	.000	.000	.000	.000	.000	.000
	.000	.043	.049	.050	.025	.025	.025	.016	.000	.000	.000	.000	.000	.000	.000
DIPPING	.0063	.0063	.0067	.0067	.0067	.0067	.0066	.0066	.0067	.0066	.0066	.0064	.0063	.0062	.0062

Fn = 0.250 Free L=2.5 m (UT)															
ST.	10.000	9.750	9.500	9.250	9.000	8.750	8.500	8.250	8.000	7.750	7.500	7.250	7.000	6.750	5.000
2x/L	-1.000	-0.950	-0.900	-0.850	-0.800	-0.750	-0.700	-0.650	-0.600	-0.550	-0.500	-0.450	-0.400	-0.350	1.000
Z/D	.000	.286	.296	.217	.000	.000	.000	.000	.000	.000	.000	.000	.000	.000	.000
	.000	.251	.239	.198	.055	.000	.000	.000	.000	.000	.000	.000	.000	.000	.000
	.000	.242	.224	.187	.056	.000	.000	.000	.000	.000	.000	.000	.000	.000	.000
	.000	.189	.149	.126	.045	.000	.000	.000	.000	.000	.000	.000	.000	.000	.000
	.000	.125	.113	.086	.027	.000	.000	.000	.000	.000	.000	.000	.000	.000	.000
	.000	.089	.089	.057	.011	.000	.000	.000	.000	.000	.000	.000	.000	.000	.000
	.000	.068	.068	.036	.002	.000	.000	.000	.000	.000	.000	.000	.000	.000	.000
	.000	.051	.049	.020	.001	.000	.000	.000	.000	.000	.000	.000	.000	.000	.000
	.000	.043	.049	.003	.001	.000	.000	.000	.000	.000	.000	.000	.000	.000	.000
DIPPING	.0040	.0039	.0039	.0039	.0039	.0038	.0038	.0037	.0036	.0035	.0035	.0035	.0035	.0035	.0035

Fn = 0.267 Free L=2.5 m (UT)															
ST.	10.000	9.750	9.500	9.250	9.000	8.750	8.500	8.250	8.000	7.750	7.500	7.250	7.000	6.750	5.000
2x/L	-1.000	-0.950	-0.900	-0.850	-0.800	-0.750	-0.700	-0.650	-0.600	-0.550	-0.500	-0.450	-0.400	-0.350	1.000
Z/D	.000	.279	.326	.238	.000	.000	.000	.000	.000	.000	.000	.000	.000	.000	.000
	.000	.247	.237	.228	.101	.000	.000	.000	.000	.000	.000	.000	.000	.000	.000
	.000	.218	.220	.206	.101	.000	.000	.000	.000	.000	.000	.000	.000	.000	.000
	.000	.209	.220	.206	.101	.000	.000	.000	.000	.000	.000	.000	.000	.000	.000
	.000	.157	.115	.098	.045	.000	.000	.000	.000	.000	.000	.000	.000	.000	.000
	.000	.116	.089	.068	.021	.000	.000	.000	.000	.000	.000	.000	.000	.000	.000
	.000	.085	.068	.044	.007	.000	.000	.000	.000	.000	.000	.000	.000	.000	.000
	.000	.064	.049	.025	.001	.000	.000	.000	.000	.000	.000	.000	.000	.000	.000
	.000	.043	.049	.006	.000	.000	.000	.000	.000	.000	.000	.000	.000	.000	.000
DIPPING	.0044	.0044	.0044	.0044	.0043	.0043	.0042	.0041	.0041	.0041	.0041	.0041	.0041	.0041	.0041

Fn = 0.250 Free L=2.5 m (UT)															
ST.	10.000	9.750	9.500	9.250	9.000	8.750	8.500	8.250	8.000	7.750	7.500	7.250	7.000	6.750	5.000
2x/L	-1.000	-0.950	-0.900	-0.850	-0.800	-0.750	-0.700	-0.650	-0.600	-0.550	-0.500	-0.450	-0.400	-0.350	1.000
Z/D	.000	.286	.296	.217	.000	.000	.000	.000	.000	.000	.000	.000	.000	.000	.000
	.000	.251	.239	.198	.055	.000	.000	.000	.000	.000	.000	.000	.000	.000	.000
	.000	.242	.224	.187	.056	.000	.000	.000	.000	.000	.000	.000	.000	.000	.000
	.000	.189	.149	.126	.045	.000	.000	.000	.000	.000	.000	.000	.000	.000	.000
	.000	.125	.113	.086	.027	.000	.000	.000	.000	.000	.000	.000	.000	.000	.000
	.000	.089	.089	.057	.011	.000	.000	.000	.000	.000	.000	.000	.000	.000	.000
	.000	.068	.068	.036	.002	.000	.000	.000	.000	.000	.000	.000	.000	.000	.000
	.000	.051	.049	.020	.001	.000	.000	.000	.000	.000	.000	.000	.000	.000	.000
	.000	.043	.049	.003	.001	.000	.000	.000	.000	.000	.000	.000	.000	.000	.000
DIPPING	.0041	.0040	.0039	.0039	.0039	.0038	.0038	.0038	.0038	.0038	.0038	.0038	.0038	.0038	.0038

Table 5 The pressure coefficient on the hull of 2.5m model (FX)

	F _n = 0.250	Fixed	I _s = 2.5 m	(UT)	
ST.	10.000	9.750	9.250	8.000	7.000
2X-L	-1.000	- .900	-1.650	- .800	- .400
Z-0	.000	.305	.000	.000	.000
.120	.000	.265	.218	.000	.000
.040	.000	.247	.213	.000	.000
- .000	.932	.246	.054	.000	.015
- .200	.934	.171	.137	.039	.065
- .300	.999	.124	.095	.017	.076
- .500	1.000	.091	.065	.001	.072
- .600	1.000	.068	.043	.010	.073
- .840	1.000	.052	.025	.011	.057
-1.000	1.000	.042	.016	.003	.037
DIPPING	.0000	.0000	.0000	.0000	.0000
ST.	5.000	4.000	2.000	1.000	.500
2X-L	.000	.200	.600	.800	.500
Z-0	.000	.000	.000	.000	.000
.120	.000	.000	.000	.000	.000
.040	.000	.000	.000	.000	.000
- .000	.000	.000	.000	.000	.000
- .500	.052	.093	.049	.035	.028
- .600	.055	.088	.047	.031	.024
- .800	.072	.077	.032	.044	.020
- .900	.077	.060	.034	.041	.018
- .930	.078	.065	.034	.038	.012
- .957	.077	.065	.041	.037	.036
-1.000	.055	.040	.020	.028	.007
DIPPING	.0000	.0000	.0000	.0000	.0000

[illegible][illegible][illegible]

STUDY OF TOTAL AND VISCOUS RESISTANCE FOR THE WIGLEY PARABOLIC SHIP FORM

Sangseon Ju

Iowa Institute of Hydraulic Research
The University of Iowa
Iowa City, Iowa 52242

INTRODUCTION

The Froude method was based on the assumption that the total resistance of both ship and model can be split into two components, one the frictional resistance and the other the residual resistance, which is essentially the wave resistance and the resistance due to eddies and vorticity.

It is now well known that the frictional-resistance coefficient C_f derived from a flat plate is not the same as that of the hull and, furthermore, that C_f is only a part of the viscous-resistance coefficient C_v . In order to improve the Froude method, it has been suggested that the ratio

$$1 + k = C_v/C_f \quad (1)$$

is independent of the Reynolds number Re and Froude number Fr , where k is the form factor and C_f may be represented by the Schoenherr flat-plate friction formula

$$\frac{0.242}{\sqrt{C_f}} = \log_{10} (Re \cdot C_f). \quad (2)$$

Except for interference effects, these two resistances obey the Reech-Froude law,

$$C_t(Fr, Re) = C_v(Re) + C_w(Fr) \quad (3)$$

where C_t , a function of Re and Fr , is the total-resistance coefficient and C_w the wave-resistance coefficient of the model. Applying the form-factor hypothesis, the total resistance of the model would then be given by

$$C_t = (1 + k) C_f + C_w \quad (4)$$

which is an important improvement over Froude's method.

When k is known, C_v is obtained from the definition (1), and then C_w is given by (3). One way of determining k utilizes experimental data at very low Froude numbers, where C_w is negligibly small in comparison with C_v . Unfortunately, the viscous resistance at low speeds is also small and the value of C_t at that speed may be inaccurate. Moreover, at low speeds, that is at low Reynolds numbers, the uncertain extent of laminar flow on the model may introduce another source of error. The form-factor procedure also involves the assumption that k is independent of Froude number, which is contradicted by many wake-survey measurements on models, even on models with a moderate block coefficient (0.6, for example) as can be seen in Tzou [1] and Tsai [2]. Nevertheless, in the present study, this form-factor procedure is one of the methods utilized, since it represents an important improvement over the Froude method.

In order to determine the functions representing the variation of viscous and wave resistance with Froude number, it is necessary to measure, in addition to the total resistance, either the viscous or wave-pattern resistance. Both are necessary, however, since wave resistance and the viscous resistance do not obey the same laws of similarity and there exist causes of systematic errors such that the sum of C_{vw} and C_{wp} is less than C_t , where C_{vw} denotes the viscous-resistance coefficient derived from wake-survey measurements, and C_{wp} the wave-resistance coefficient derived from a wave-pattern analysis.

In this study, the viscous resistances of the Wigley parabolic ship model were measured by the wake-survey method. Since no experimental data for the viscous resistance are available with this model restrained in both trim and sinkage, the differences between total and viscous resistances are compared with the wave resistance derived by wave-pattern analysis.

A formula for calculating the viscous resistance of a ship model from measurements in the wake, derived in [3], is

$$R_v = \frac{\rho/2}{2 - \frac{\bar{u}_e}{U_0}} \int_{\omega} [2g(H_0 - H_m) - (u_e - u_m)^2] dS \quad (5)$$

where H_m is measured total head in the wake
 H_0 is the undisturbed total head
 ρ is the mass density of water
 g is the acceleration of gravity
 ω is the area of the wake at the measurement section
 u_m is the measured longitudinal component of velocity in the wake
 u_e is the value of u_m at the edge of the wake
 \bar{u}_e is the mean of the values of u_e
 U_0 is the velocity of the uniform stream
 R_v is the viscous resistance.

In order to apply this formula, it is necessary to measure H_m and u_m .

EXPERIMENTAL EQUIPMENT AND PROCEDURE

All experiments were performed in the IIHR towing tank which is 91.44-m long, 3.048-m wide and 3.14-m deep. The ship model employed in this study was a Wigley parabolic ship model with 0.444 block coefficient, a length of 3.048 m and the wetted surface area of 1.381 m². For the selected form, the parametric values are $B/L = 0.1000$ and $H/L = 0.0625$. For turbulence stimulation along the hull, a row of studs of 3.2-mm diameter, 1.6-mm height and 9.5-mm spacing was fitted on the model 15.2 cm, 5 percent of the model length from the bow. With the towing arrangement used, the model was restrained in both trim and sinkage.

The pitot rake and the traversing-probe mechanism were set on the trailer 3.05 m behind the stern of the ship model.

The data acquisition system for the carriage speed, and the total head and pressure in the wake, consists of a 48-terminal scanivalve, a ± 0.021 -kg/cm² pressure transducer, a scanco CTRL2/S2 solenoid controller, IIHR

scanivalve positioning circuit, an Analog-to-Digital converter subsystem, and an HP-1000 E-series minicomputer, as shown in Figure 1. The carriage velocity and the pressure data are sampled simultaneously by this system. The computer is programmed so as to control the sequence of positions of the scanivalve and the duration of the stay at a particular opening in the course of a run. While at an opening, the computer program instructs the computer to delay sampling data until a transient has decayed, and then commands the A/D converter to take a desired number of samples in a given time.

To be sure that the water was at rest, dye was emitted at the measuring depth. A waiting time of 15 minutes was used in this experiment.

Reduction of sampling time is important in order to reduce the total number of runs. The voltage of the carriage speed is sampled easily because the signal does not change much. For the pressure measurement, two possible sequences were considered. The total pressure and the static pressure can be sampled alternately or separately. The separate sampling method was used in this experiment because the smaller transient time reduced the total number of runs.

Transient times, determined from preliminary experiments, are 0.2 sec between successive total-head tubes outside the wake region, 0.6 sec between successive total-head tubes in the wake region, 1.2 sec between total-head tubes and static-head tubes, and 0.2 sec between successive static-head tubes. The sampling time of 0.5 sec was used at each tube and it was increased to 1.0 sec in the wake region which gives the most contribution to viscous resistance calculation.

The calculation of the viscous resistance was carried out in the manner indicated by Tzou [1], with some slight differences. Although the model velocity was not exactly constant through a run, it was assumed that the flow in the wake behind stern is steady, but the measured wake characteristics correspond to the instantaneous model velocity due to the rigid connection between the pitot rake and the carriage. For this reason, the total head and the flow velocity were corrected to the mean carriage speed of a run. These corrected values were also corrected to the mean

carriage speed of a complete traverse of the wake section. The total-head readings were corrected as

$$H_m = \left(\frac{V_c}{V'_c}\right)^2 H'_m \quad (6)$$

where V'_c is the carriage speed corresponding to the measured value of H'_m , and V_c is the mean value of V'_c for the traverse over the measuring section. The flow velocity in the wake was corrected as

$$u_m = u'_m - (V'_c - V_c) \quad (7)$$

where u'_m is the uncorrected measured flow velocity. For this study, the total-head readings and the flow velocities were corrected at most 1.4 and 2.8 percent of their values respectively.

In order to know the variation of the viscous-resistance coefficient with Froude number, the obtained data were corrected to the standard temperature 18.3°C at which the total resistances were measured, under the Reech-Froude assumption that C_v is a function of Re . This temperature correction is essential since the kinematic viscosity ν varies with temperature, approximately 2.5 percent per degree C for water, and the viscous resistances are obtained at the different water-temperatures. For this study, the temperature coorection was at most 1 percent of the values of the viscous resistance.

DISCUSSION OF RESULTS

Total and viscous-resistance coefficients are shown against Reynolds number and compared with the Schoenherr line of the flat plate in Figure 2. The sinuous trend of the viscous-resistance coefficient with Reynolds number is seen to have much less amplitude than was found for the series-60 model by Tzou [1] and Tsai [2]. This suggests that the form-factor procedure may give good agreement with experimental results. This is probably a consequence of the slenderness of the Wigley ship model.

The total-resistance coefficients have been compared in Figure 3 with other experimental results; those for a 4-m model tested at the Ship Research Institute of Japan (SRI), and 2.5-m model tested at the University of Tokyo (U.T.). Here C_t from SRI and U.T. were corrected to a standard temperature of 18.3°C, and the C_t of Iowa was fitted by a smooth curve by comparing the experimental results from the three tanks. Then the residuary resistance C_w from the three tanks were calculated by using the form-factor formula (4) with $k = 0.100$ for Iowa, $k = 0.065$ for SRI and $k = 0.050$ for U.T. These were selected so as to obtain the best agreement between the C_w 's of the three tanks.

The viscous-resistance coefficients have been corrected to a standard temperature of 18.3°C, and then plotted against Froude number in Figure 4. The viscous-resistance coefficient shows a hump at Froude number of 0.24, and two hollows at Froude numbers of 0.22 and 0.32, in contrast with the monotonically decreasing trend assumed in the form-factor procedure. This suggests that the viscous resistance is affected by the wave resistance; thus its coefficient is a function of not only Reynolds number, but also Froude number, although this dependence seems to be small in this case.

The wave-resistance coefficients obtained by subtracting the viscous resistance of the wake-survey measurements from the total resistance, $C_t - C_{vw}$, are compared in Figure 5 and 6 with the residuary resistance C_w . $C_t - C_{vw}$ are seen to be in good agreement with C_w . The discrepancies between $C_t - C_{vw}$ and C_w of Iowa are less than 7 percent at Froude numbers greater than 0.23. The largest discrepancy of 20 percent occurs in the range of $0.21 < Fr < 0.22$ in which $C_t - C_{vw}$ has a hump. This is less than 3 percent of the total or viscous-resistance coefficients, that is about the same order as the experimental error. Generally speaking, $C_t - C_{vw}$ is greater than C_w at Froude numbers less than 0.23. $C_t - C_{vw}$ is also compared with the experimental results for C_{wp} from SRI and U.T., where C_{wp} was obtained by wave analysis of longitudinal-cut data. $C_t - C_{vw}$ and C_{wp} are in good agreement at Froude numbers in the range $0.24 < Fr < 0.34$, with discrepancies of less than 12 percent of C_w , or 3 percent of C_t or C_{vw} , which may be attributed partly to experimental error and partly to the

assumptions made in determining C_t , C_{vw} and C_{wp} . The large discrepancy of 35 percent occurs in the range $0.21 < Fr < 0.22$. This is 5 percent of the total or viscous-resistance coefficients. At Froude numbers less than 0.27, the viscous resistance is more than 80 percent of the total resistance, and its effect dominates the flow characteristics. One would expect that, in this range, $C_t - C_{vw}$ derived from wake-survey measurements would be more reliable than the C_{wp} derived from wave-pattern analysis, since C_{wp} is derived from measurements of small quantities, and the influence of the wake on the waves behind the ship may be significant. At low Froude numbers or Reynolds numbers, the wake is wider and the boundary layer is thicker than at higher Froude numbers, thus the effect of wake and boundary layer becomes relatively more important. At Froude numbers greater than 0.34, the discrepancies between $C_t - C_{vw}$ and C_{wp} become large again. C_{wp} is seen to be significantly smaller than $C_t - C_{vw}$ or C_w . This is believed to be due to the assumption made in the wave-pattern analysis of the linearized free-surface boundary condition.

The values of C_t , C_{vw} , $C_t - C_{vw}$ and C_w , read from the curves in Figs. 3, 4, 5 are tabulated against Froude number in Table 1.

ACKNOWLEDGEMENT

The author is indebted to Professor Louis Landweber for his continuous guidance and encouragement throughout the course of this study.

This study was sponsored by the Office of Naval Research, Department of the Navy under Contract No. N00014-82-K-0069 (NR-062-183).

REFERENCES

- [1] T.S. Tzou, "On the Determination of the Viscous Drag of a Ship Model", Ph.D. Dissertation, The University of Iowa, June 1969.
- [2] C.E. Tsai and L. Landweber, "Further Developments of a Procedure for Determination of Wave Resistance from Longitudinal-Cut Surface-Profile Measurements", Journal of Ship Research, Vol. 19, No. 2, June 1975.
- [3] L. Landweber, Appendix 2, Report of Resistance Committee, Proc. 14th ITTC, 1975.

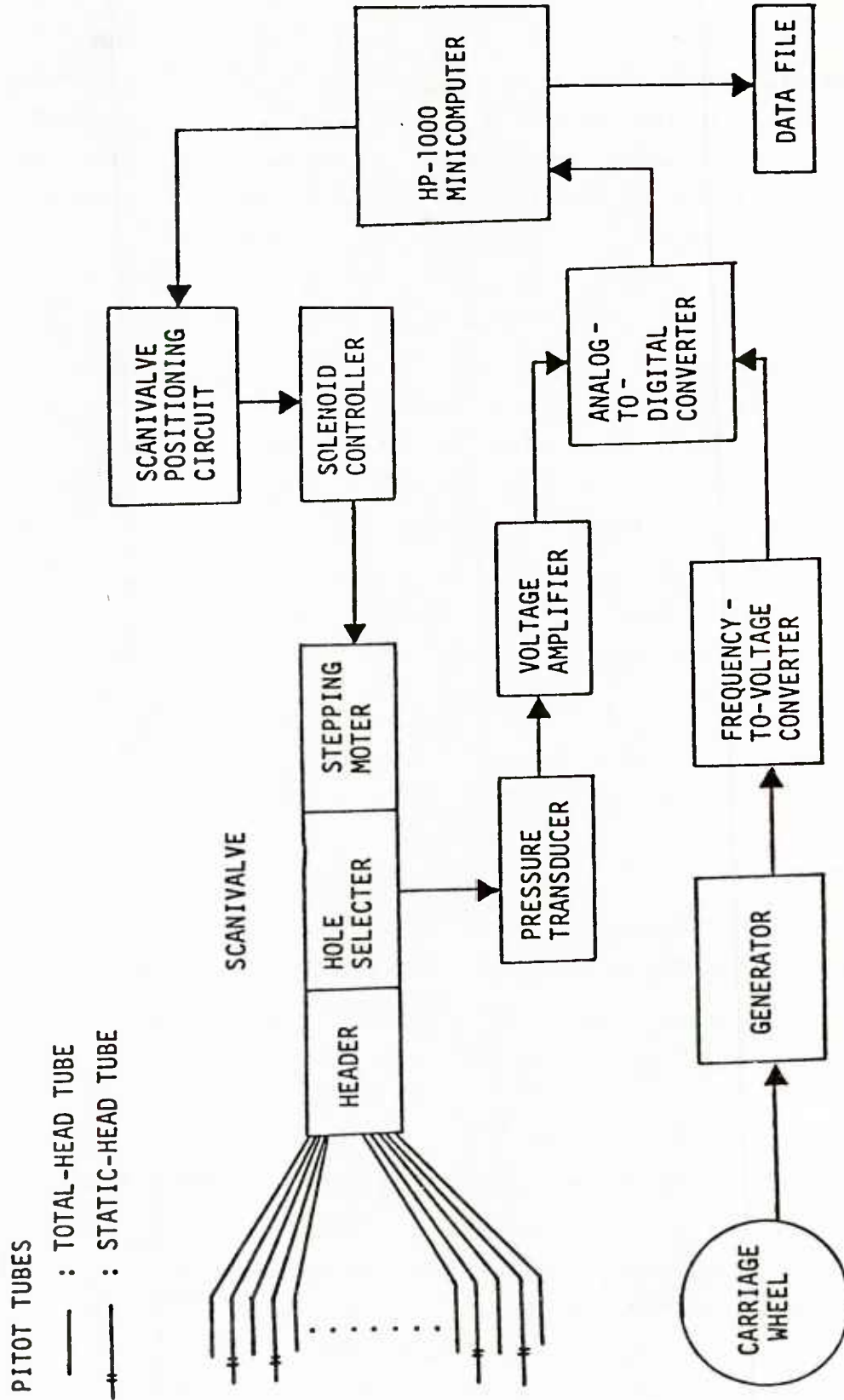


Figure 1 - Data-Acquisition System for the Carriage speed, Total Head and Static Head in the Wake.

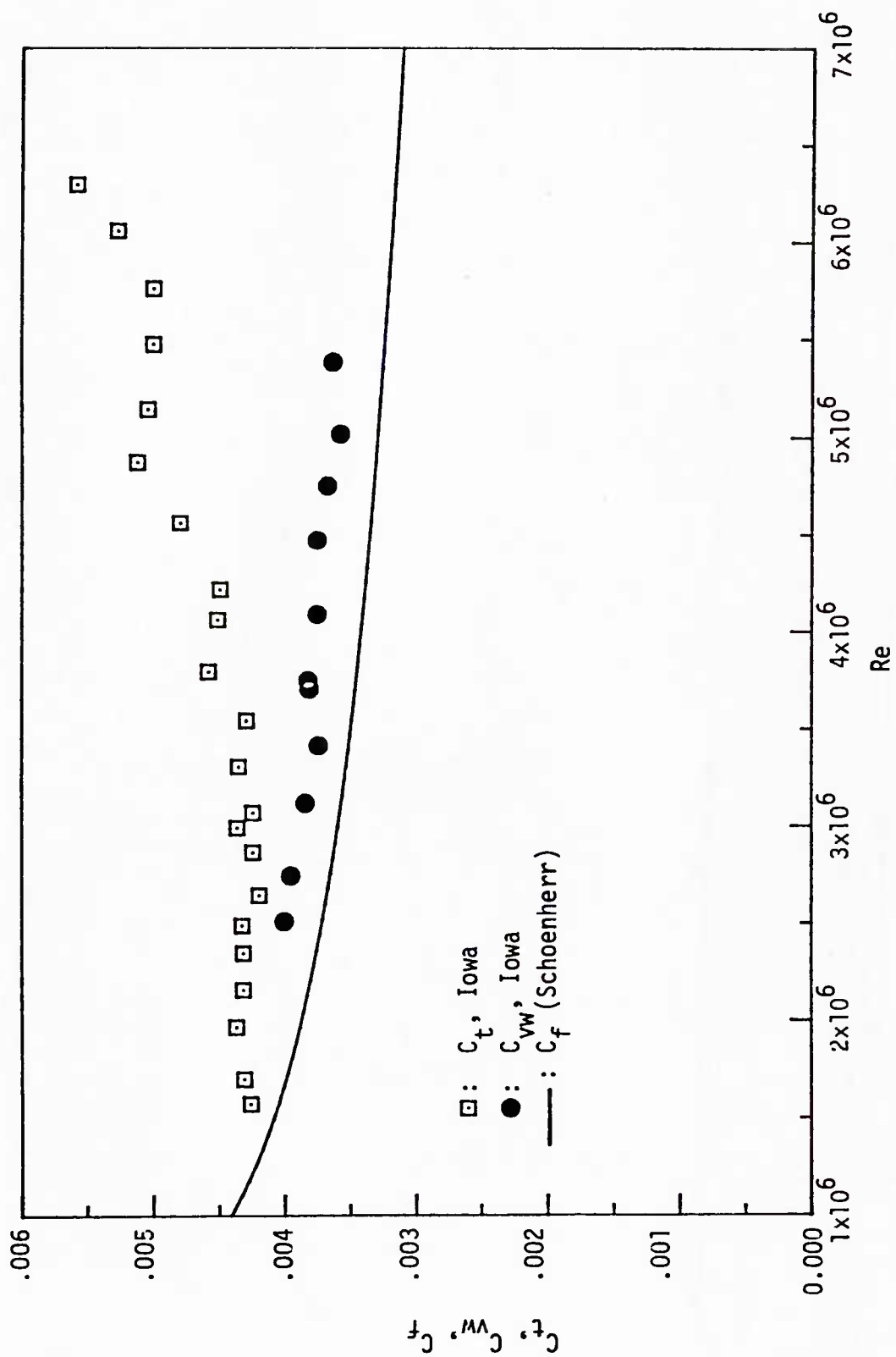


Figure 2 - Variation of Total and Viscous-Resistance Coefficients with Reynolds Number. (Fixed Condition).

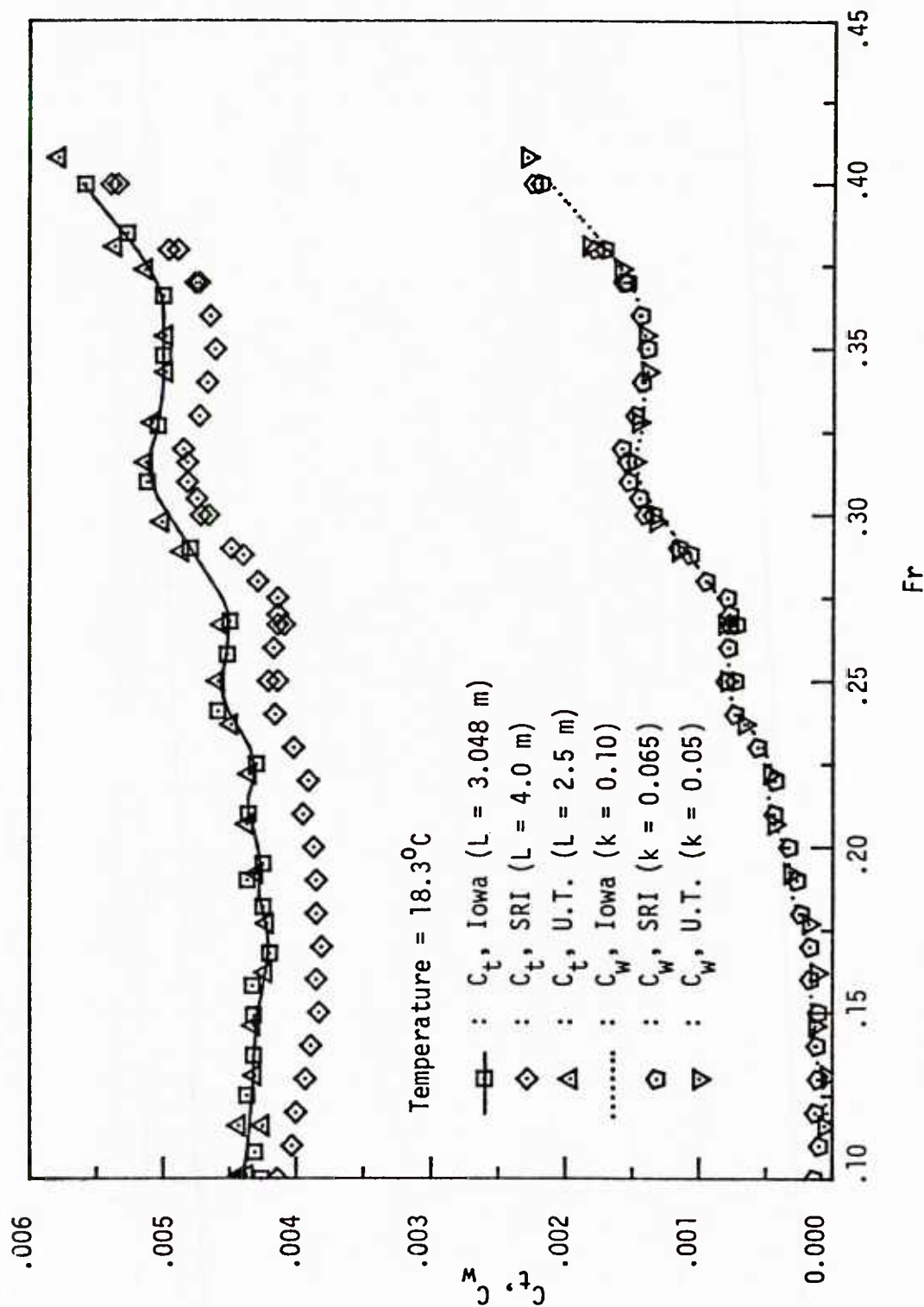


Figure 3 - Comparison of C_t 's and C_w 's vs. Froude Number. (Fixed Condition)

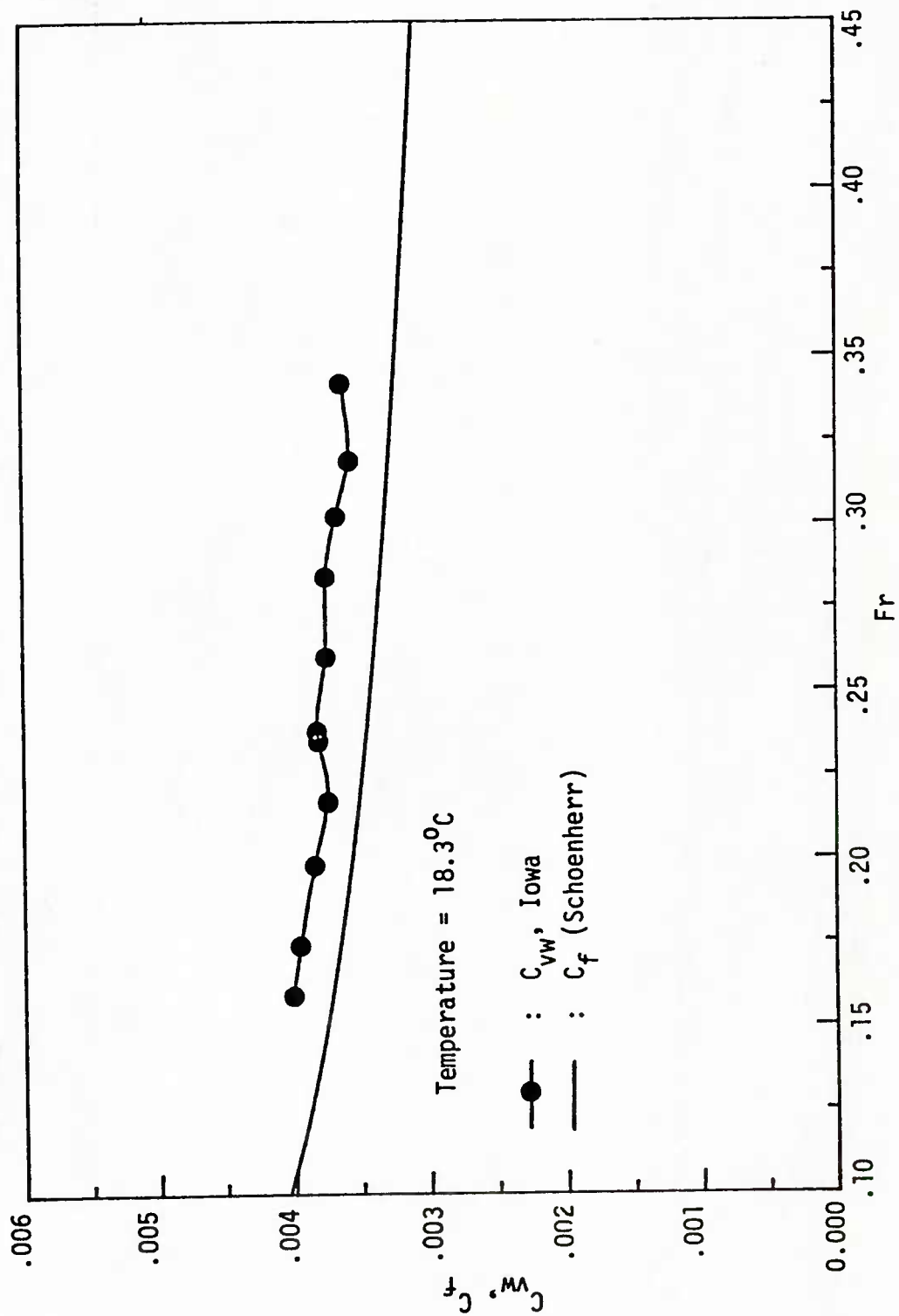


Figure 4 - Variation of Viscous-Resistance Coefficient with Froude Number.
(Fixed Condition)

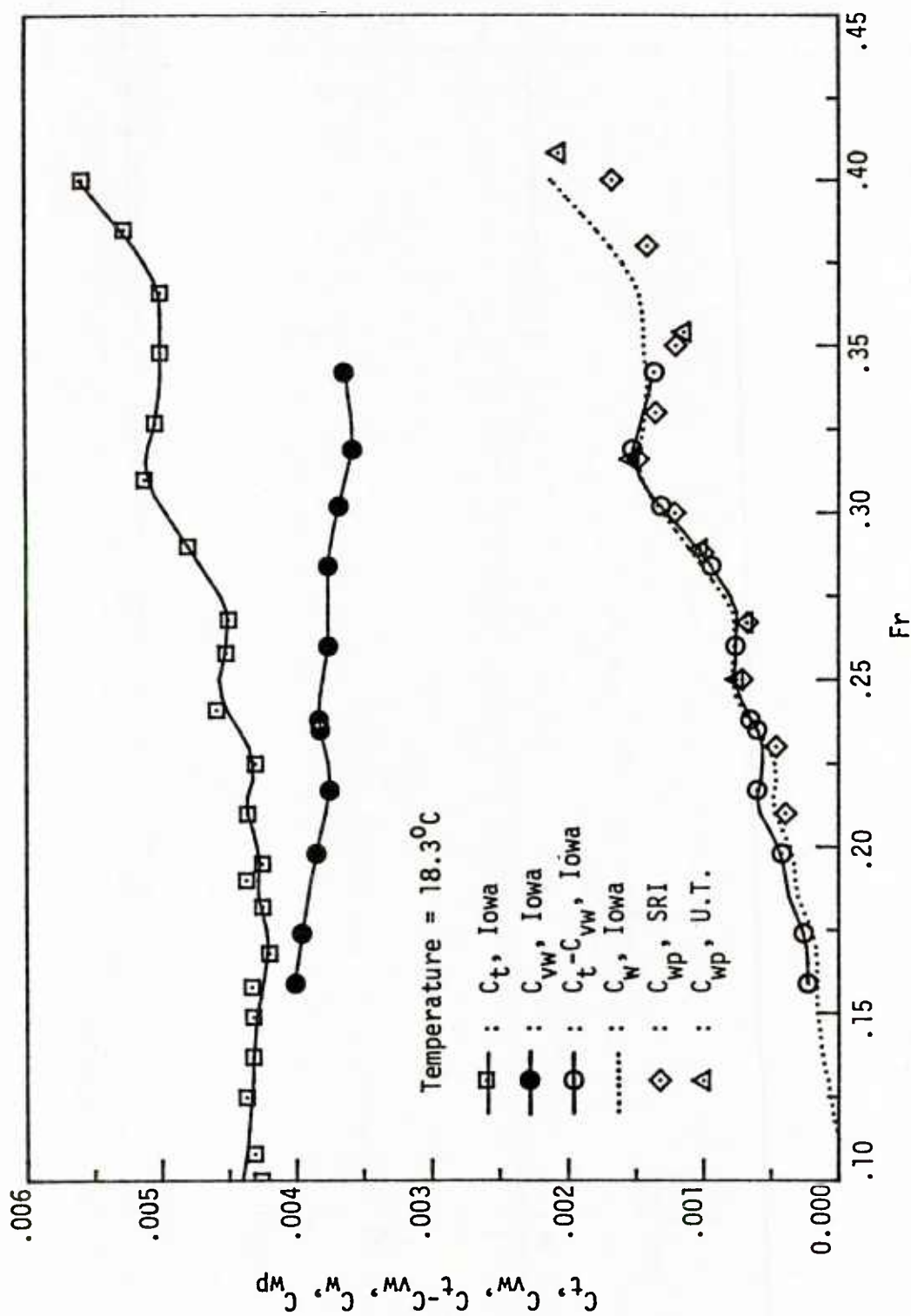


Figure 5 - Comparison of $C_t - C_{vw}$, C_w and C_{wp} vs. Froude Number. (Fixed Condition)

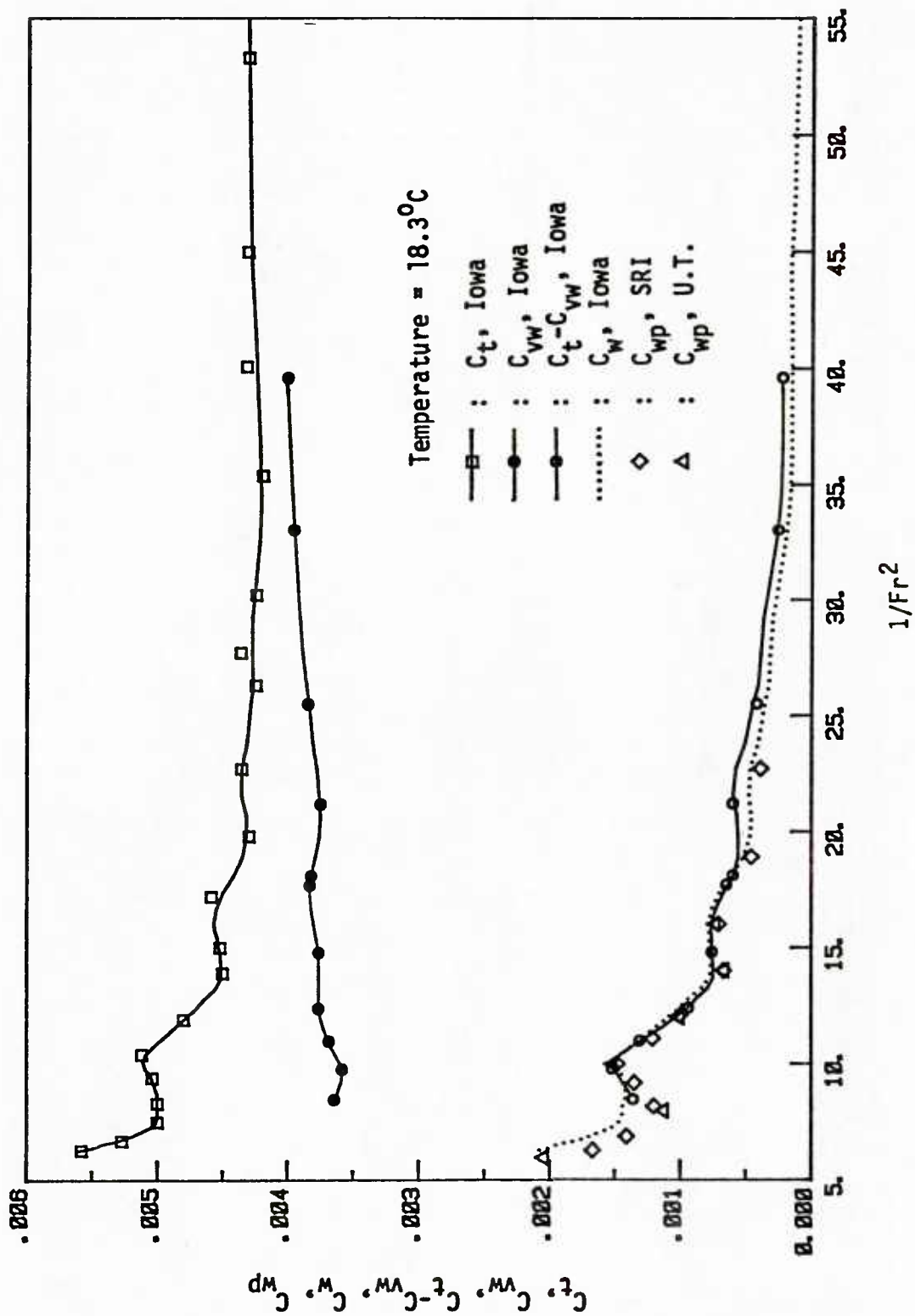


Figure 6 - Comparison of $C_t - C_w$, C_w and C_{wp} vs. $1/Fr^2$ (Fixed Condition)

Table 1. Values of C_t , C_{vw} , $C_t - C_{vw}$ and C_w with Froude Number.
(Fixed Condition, Temperature = 18.3°C)

Fr	C_t	C_{vw}	$C_t - C_{vw}$	C_w	Fr	C_t	C_{vw}	$C_t - C_{vw}$	C_w
.100	.00440	-	-	-.00005	.250	.00457	.00380	.00077	.00079
.105	.00438	-	-	-.00003	.255	.00454	.00378	.00076	.00078
.110	.00436	-	-	-.00001	.260	.00452	.00376	.00076	.00077
.115	.00435	-	-	.00001	.265	.00451	.00376	.00075	.00077
.120	.00434	-	-	.00004	.270	.00451	.00376	.00075	.00078
.125	.00433	-	-	.00006	.275	.00456	.00376	.00080	.00085
.130	.00432	-	-	.00008	.280	.00464	.00376	.00088	.00094
.135	.00432	-	-	.00011	.285	.00472	.00376	.00096	.00103
.140	.00431	-	-	.00013	.290	.00480	.00374	.00106	.00112
.145	.00430	-	-	.00014	.295	.00488	.00372	.00116	.00121
.150	.00429	-	-	.00017	.300	.00496	.00369	.00127	.00130
.155	.00426	-	-	.00016	.305	.00504	.00366	.00138	.00139
.160	.00424	.00401	.00023	.00016	.310	.00509	.00363	.00146	.00145
.165	.00422	.00399	.00023	.00016	.315	.00511	.00360	.00151	.00148
.170	.00421	.00397	.00024	.00017	.320	.00509	.00358	.00151	.00147
.175	.00422	.00395	.00027	.00020	.325	.00505	.00358	.00147	.00144
.180	.00425	.00393	.00032	.00025	.330	.00503	.00359	.00144	.00143
.185	.00428	.00391	.00037	.00030	.335	.00501	.00361	.00140	.00142
.190	.00428	.00389	.00039	.00032	.340	.00500	.00362	.00138	.00141
.195	.00427	.00386	.00041	.00033	.345	.00500	-	-	.00143
.200	.00429	.00384	.00045	.00036	.350	.00500	-	-	.00144
.205	.00432	.00381	.00051	.00041	.355	.00500	-	-	.00144
.210	.00436	.00378	.00058	.00047	.360	.00500	-	-	.00145
.215	.00436	.00376	.00060	.00048	.365	.00501	-	-	.00147
.220	.00432	.00375	.00057	.00046	.370	.00505	-	-	.00152
.225	.00432	.00376	.00056	.00047	.375	.00512	-	-	.00160
.230	.00435	.00379	.00056	.00052	.380	.00520	-	-	.00169
.235	.00442	.00382	.00060	.00060	.385	.00530	-	-	.00179
.240	.00450	.00383	.00067	.00070	.390	.00540	-	-	.00190
.245	.00455	.00382	.00073	.00076	.395	.00550	-	-	.00201
					.400	.00560	-	-	.00212

A GEOMETRICALLY CONSISTENT LINEARIZATION METHOD
FOR AN ELLIPTIC STRUT

DR. S. M. CALISAL
Department of Mechanical Engineering
University of British Columbia

ABSTRACT

The study of irrotational, incompressible flows about thin geometries can be carried out using the well known perturbation procedures. In two dimensional flows exact solutions based on mappings can be used to compare the accuracy of first order solutions. For most airfoil sections a first order perturbation solution is not sufficiently accurate in representing the pressure and velocity distribution, especially about the leading edge. For three-dimensional flows exact solutions are rare and for more complex problems such as ship wave resistance formulations an exact solution does not exist for comparison of results. In this last case second order solutions exist but are very difficult to calculate. Therefore, it would appear advantageous to improve first-order calculations. To this end a perturbation method that incorporates the geometric properties of the disturber is studied. This method is first applied to a symmetric Joukowski airfoil to an ellipse and an elliptic strut. This method, here called the "geometrically-consistent linearization method" predicts the leading edge pressure variations correctly for the two foils studied and appears to be superior to the classical first order solutions. An iterative solution following this procedure further improves the calculation. The method discussed and the following iteration procedure seem to form an efficient numerical solution to airfoil flow problems. The method is then applied to an elliptic strut wave resistance calculation.

INTRODUCTION

Perturbation methods provide powerful solution techniques for most engineering problems and for problems of fluid mechanics in particular. In the solution of problems by a perturbation method the boundary conditions and the general differential equation are expanded in series in increasing power of the perturbation parameter. The differential equation and the boundary conditions corresponding to the same power of the perturbation parameter are then solved to obtain the terms of the series representing the solution. This classical method is independent of the types of boundary conditions. The formulation presented here is based on the idea that "first order solutions, that is linearized solutions, may have the right form but not quite the right place" Van Dyke, [1]. The sample foils studied are classical problems and have exact close form solutions. They are reworked mainly to assess the value of the linearization method under study. The examples are symmetric about the axis corresponding to the major flow direction.

THEORY

A symmetric, thin, two dimensional disturbance in a uniform flow is shown in Figure 1. The Cartesian coordinates are chosen such that the x direction is aligned with the incoming flow. The function

$$y = \pm \epsilon \eta(x) \quad (1)$$

represents the impermeable boundary.

(a) Formal Classical Linearization

The linear potential flow solution about the above shape can be formulated in the following way. We assume that a potential solution of the form

$$\Phi = Ux + \epsilon \phi(x,y) + O(\epsilon^2)$$

exists where

$$\nabla^2 \Phi = 0 \quad .$$

The impermeable boundary condition to the first order in ϵ can be written as:

$$\begin{aligned}\vec{v} \cdot \vec{n} &= (U + \epsilon \phi_x(x,y), \epsilon \phi_y)(\epsilon \eta_x, -1) = 0 \\ &= U \eta_x - \phi_y = 0\end{aligned}\tag{3}$$

on the impermeable surface. The region of definition for ϕ is then extended to include the domain defined by the disturber. The potential function ϕ and its derivatives are then expressed by Taylor's series as follows:

$$\phi_y(x,\eta) = \epsilon \phi_y(x,0) + O(\epsilon^2) .\tag{4}$$

This simplifies the boundary condition (3) to the more manageable form

$$U \eta_x(x) - \phi_y = 0 \quad \text{at } y = 0 .\tag{5}$$

Various analytical or numerical methods and corrections are possible for the solution of (2) and (4) Van Dyke [1] and Lighthill [2]. The implied geometric criterion in equation (1) is that as the ϵ parameter is changed, the resulting geometry of the disturber is seen to change in the direction perpendicular to the incoming flow direction. This assumption is studied in some detail in the following paragraph.

(b) Geometrically Consistent Linearization (G.C.L.)

This linearization begins with assumptions identical to the classical solution, namely equations (1) and (2). We then study the meaning of the parameter ϵ . The perturbation theory requires that the disturbance and the disturber be treated together in a perturbation problem. Up to now this was interpreted to be the existence a parameter ϵ which describes a property of the disturber which is such that when $\epsilon \rightarrow 0$, the "disturbing character" of the disturber vanishes Wehausen [3]. The parameter ϵ is usually defined in terms of the magnitude of the disturber in the direction perpendicular to the uniform flow, as, for example, the maximum thickness divided by the chord length. Here we study directional effects, which can be important around the leading edge of an air foil and we show a "directional inconsistency" in the "thin airfoil" and by extension in "thin ship" theories.

Let us assume that the disturbance parameter ϵ in equations (1) and (2) is changed by an amount $d\epsilon$. Here we treat ϵ as a small quantity and $d\epsilon$ as an infinitesimal quantity. The new equation for the impermeable body from (1) will be

$$y = (\epsilon + d\epsilon)\eta(x) \quad (6)$$

while the corresponding potential will be:

$$\Phi = Ux + (\epsilon + d\epsilon) \phi(x,y) \quad \text{or}$$

or

$$\Phi = Ux + \epsilon\phi(x,y) + d\epsilon\phi(x,y) . \quad (7)$$

Equation (7) indicates that at any point b shown in Figure 1 there will be a change in the value of the potential function Φ by an amount $d\phi(x,y)$. We now express the function $d\Phi$ about point b on the disturbance using the normal and the tangential coordinates (n,τ) as shown in Figure 1. We obtain

$$d\Phi = \frac{\partial\Phi}{\partial n} dn + \frac{\partial\Phi}{\partial \tau} d\tau + d\epsilon\phi(x,y) . \quad (8)$$

For any point on the impermeable boundary $\frac{\partial\Phi}{\partial n} = 0$, if we select $d\tau = 0$ implying that we remain in a direction normal to a boundary, we obtain:

$$d\Phi = d\epsilon\phi(x,y) . \quad (9)$$

Equations (7 and 9) can be interpreted as follows: a change in Φ given by $d\epsilon\phi(x,y)$ has a directional quality. That is, this change is in the direction normal to the boundary. In fact all points in the direction normal to the boundary and on the boundary show a change $d\epsilon\phi(x,y)$ or $d\Phi$. A directional inconsistency can therefore be seen in the classical theory, as (6) implies a variation in the disturbance in the y direction, while the corresponding change in potential given by (9) and implied by (7) is in the direction normal to $y = \eta(x)$. As the perturbation theory requires that the disturbance and the disturber be treated together, our interpretation here is that the directional relationship shown above must be included in the formulation. We therefore add

the requirement that disturber and disturbance must change along the same direction. The validity of equations (1) and (2) with the directional compatibility will then be interpreted as follows. As the perturbation parameter ϵ changes the disturber maps into a new shape. During this mapping each point on the impermeable boundary moves along a path normal to the boundary. Equation (1) is therefore a rather simple description of the disturber and one must add that as $\epsilon \rightarrow 0$, the projection of the points on the disturber must be along the direction normal to the surface defining the disturber. The classical orthogonal projection along the y direction might therefore not be adequate. Whereas in one-dimensional perturbation problems such a directional requirement does not exist, in multi-directional problems it might be of certain importance. One possible result of this linearization technique is that the projection required by this method might give a region smaller, and different from the orthogonal projection.

APPLICATION FOR AN ELLIPTIC STRUT

The requirement that the geometry of the disturbance must change in the direction normal to the boundary as the disturbance parameter ϵ is changed by an amount $d\epsilon$ can be studied in various ways. The procedure used in this study is to approximate the mapping of a point on the boundary by a suitable polynomial. The general numerical procedure can be summarized as follows. Any point b in Figure 1 is assumed to map at point b' . The curve bb' is represented by a parabola normal to the boundary at b . This procedure maps the disturber on a segment on the x axis with a length less than the chord length. The leading edge is mapped at an interior point. The corresponding shift of singularities is equal to half of the local radius of curvature as given by Lighthill based on a different criterion. The resulting linearized problem

$$\nabla^2 \phi = 0 \tag{10a}$$

$$U \eta_{x_b} - \phi_{b'} = 0 \tag{10b}$$

is solved by the method of singularities. The application of G.C.L. to a symmetric elliptical foil and a Joukowski Airfoil were reported earlier in Calisal [4]. Here an application for a elliptic strut is defined as:

$$y = \pm \frac{b}{2} (1 - 4x^2)^{1/2} \quad \text{for} \quad -\frac{1}{2} \leq x \leq \frac{1}{2} \quad \text{is presented.}$$

The mapping of the points on the wetted surface to points on the centre-line of symmetry is accomplished as explained above. As the waterline slope remains constant at constant x values, the mapped region is divided in vertical strips. A source distribution based on thin ship theory is assumed to represent the model. 101 sources are used for this representation. The sources are located at the mid point of strips and at a vertical location

$$\bar{z} = -\frac{1}{k_0} \ln \frac{\int_0^d \sigma(x,z) e^{-k_0 z} dz}{\int_0^d \sigma(x,z) dz},$$

where d is the draft of the strut. The wave resistance is then calculated by the method described in Calisal [5] which uses a numerical far field wave survey data.

RESULTS AND DISCUSSION

Results obtained for the wave resistance is presented in a graphical form in Figure 2 and Figure 3. The resistance values given by G.C.L. are observed to be lower than the values predicted by Michell, Hegner methods, but higher in general than the zeroth order slender ship approximation method as reported by Nobless [1983]. The amplitude of oscillations in the resistance curve as given by G.C.L. method are seen to be less than the oscillations in the classical Michell curve, but the order of magnitude remains still high. Additional corrections or procedures seem to be necessary to include free surface boundary condition properly in the formulation. We are currently calculating the error in the ship boundary calculations, we will then proceed into the calculation of error in the free surface boundary condition at the calculated free surface.

ACKNOWLEDGEMENTS

The author would like to thank Mr. J. Chan for plotting the results and Natural Sciences and Engineering Research Council of Canada for computer time.

REFERENCES

1. VAN DYKE, M. Perturbation Methods in Fluid Mechanics, Academic Press, (1968).
2. Lighthill, M.J. "New Approach to Thin Aerofoil Theory," Aero. Quart. 8, pp.193-210 (1951).
3. WEHAUSEN, J.V. "Ship Wave Resistance," Class notes, University of California, Berkeley, (1966).
4. KOBUS, H.E. "Examination of Eggers' Relationship between Transverse Wave Profiles and Wave Resistance," Journal of Ship Research, p. 240, (1967).
5. MILNE THOMSON, L.M. Theoretical Hydrodynamics, 4th Edition, MacMillan, New York, (1960).
6. CALISAL, S.M. "A Geometrically Consistent Linearization Method," CANCAM, (1983).
7. CALISAL S.M. "Wave Resistance Computation by Numerical Far Field Wave Survey Data," Proceedings of the Workshop on Ship Wave Resistance Computations, (1979).
8. CHEN, C.Y., and NOBLESS, F. "Preliminary Numerical Study of a New Slender-Ship Theory of Wave Resistance," Journal of Ship Research, Vol. 27, No. 3, (September 1983).

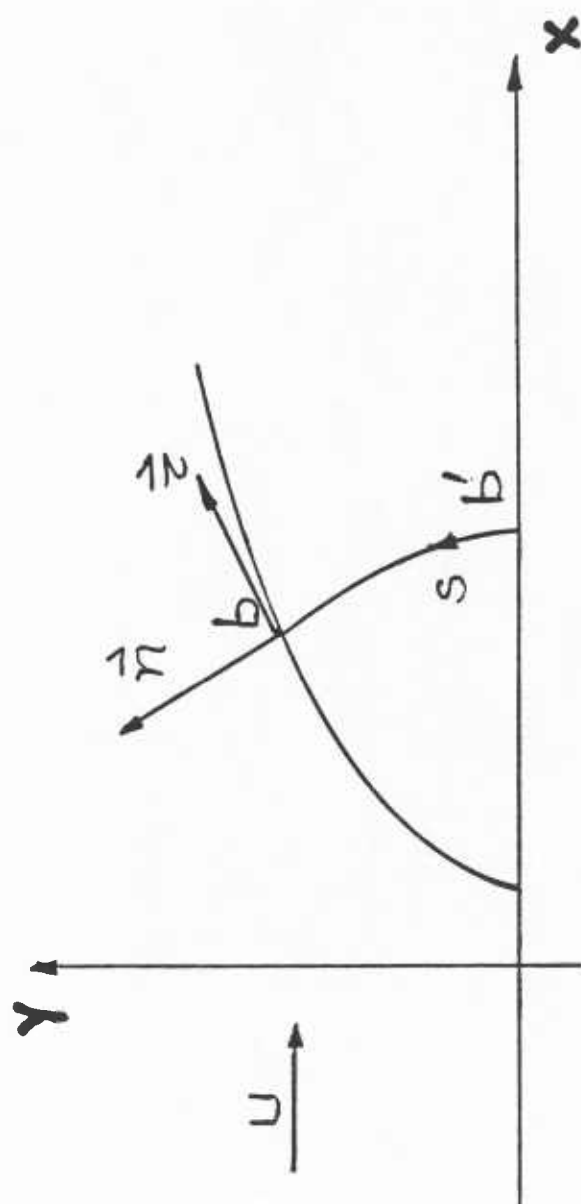


Fig. 1. Coordinate system

TABLE I
Wave Resistance Coefficient r as Defined by Nobless (1983)
for the Elliptic Strut

Froude number fr	$r \cdot 100 / fr$	$1 / (fr \cdot r)$
0.147400E+00	0.189203E+01	0.460036E+02
0.149100E+00	0.158557E+01	0.450002E+02
0.150800E+00	0.176772E+01	0.440004E+02
0.152500E+00	0.219637E+01	0.429982E+02
0.154300E+00	0.242609E+01	0.420026E+02
0.156200E+00	0.226656E+01	0.410020E+02
0.158100E+00	0.189138E+01	0.399988E+02
0.160100E+00	0.163529E+01	0.390016E+02
0.162200E+00	0.172480E+01	0.380001E+02
0.166700E+00	0.235049E+01	0.360017E+02
0.169000E+00	0.244843E+01	0.349990E+02
0.171500E+00	0.210253E+01	0.339979E+02
0.174100E+00	0.158858E+01	0.330014E+02
0.176800E+00	0.135956E+01	0.319983E+02
0.179600E+00	0.163402E+01	0.310015E+02
0.182600E+00	0.225168E+01	0.300012E+02
0.185700E+00	0.240478E+01	0.290018E+02
0.189000E+00	0.200902E+01	0.279996E+02
0.192500E+00	0.156770E+01	0.269995E+02
0.196100E+00	0.129467E+01	0.259989E+02
0.200000E+00	0.143686E+01	0.249999E+02
0.204100E+00	0.182522E+01	0.239986E+02
0.208500E+00	0.206899E+01	0.230011E+02
0.213200E+00	0.193519E+01	0.220000E+02
0.218200E+00	0.150495E+01	0.210003E+02
0.223600E+00	0.114434E+01	0.200001E+02
0.229400E+00	0.111886E+01	0.189992E+02
0.235700E+00	0.137615E+01	0.180009E+02
0.242500E+00	0.163844E+01	0.170003E+02
0.250000E+00	0.159521E+01	0.160007E+02
0.258200E+00	0.127107E+01	0.149994E+02
0.267300E+00	0.903490E+00	0.139999E+02
0.277400E+00	0.760326E+00	0.129995E+02
0.288700E+00	0.872974E+00	0.120003E+02
0.301500E+00	0.104371E+01	0.110001E+02
0.316200E+00	0.105128E+01	0.999969E+01
0.333300E+00	0.836377E+00	0.899975E+01
0.345000E+00	0.661211E+00	0.840203E+01
0.353600E+00	0.556739E+00	0.800014E+01
0.365000E+00	0.449469E+00	0.750595E+01
0.378000E+00	0.367151E+00	0.699991E+01
0.395000E+00	0.320641E+00	0.640890E+01
0.408200E+00	0.323401E+00	0.600001E+01
0.425000E+00	0.346680E+00	0.553591E+01
0.447200E+00	0.363874E+00	0.500003E+01
0.452000E+00	0.365413E+00	0.489487E+01
0.465000E+00	0.359688E+00	0.462498E+01
0.482000E+00	0.344646E+00	0.430394E+01
0.500000E+00	0.318482E+00	0.399999E+01
0.577400E+00	0.231584E+00	0.299994E+01
0.707100E+00	0.104317E+00	0.199996E+01

TABLE II

Wave Resistance Coefficient r as Defined by
Nobless (1983) for the Elliptic Strut

Froude number fr	$r*100/fr$	$1/(fr*fr)$
0.147400E+00	0.193308E+01	0.460036E+02
0.149100E+00	0.161143E+01	0.450002E+02
0.150800E+00	0.177702E+01	0.440004E+02
0.152500E+00	0.226687E+01	0.429982E+02
0.154300E+00	0.257673E+01	0.420026E+02
0.156200E+00	0.238371E+01	0.410020E+02
0.158100E+00	0.193704E+01	0.399988E+02
0.160100E+00	0.158281E+01	0.390016E+02
0.162200E+00	0.162232E+01	0.380001E+02
0.166700E+00	0.242206E+01	0.360017E+02
0.169000E+00	0.246066E+01	0.349990E+02
0.171500E+00	0.207913E+01	0.339979E+02
0.174100E+00	0.160146E+01	0.330014E+02
0.176800E+00	0.144292E+01	0.319983E+02
0.179600E+00	0.173739E+01	0.310015E+02
0.182600E+00	0.219860E+01	0.300012E+02
0.185700E+00	0.235871E+01	0.290018E+02
0.189000E+00	0.205065E+01	0.279996E+02
0.192500E+00	0.156572E+01	0.269995E+02
0.196100E+00	0.129776E+01	0.259989E+02
0.200000E+00	0.146337E+01	0.249999E+02
0.204100E+00	0.187614E+01	0.239986E+02
0.208500E+00	0.212214E+01	0.230011E+02
0.213200E+00	0.195480E+01	0.220000E+02
0.218200E+00	0.149997E+01	0.210003E+02
0.223600E+00	0.113714E+01	0.200001E+02
0.229400E+00	0.113804E+01	0.189992E+02
0.235700E+00	0.143132E+01	0.180009E+02
0.242500E+00	0.168481E+01	0.170003E+02
0.250000E+00	0.162162E+01	0.160007E+02
0.258200E+00	0.126778E+01	0.149994E+02
0.267300E+00	0.895294E+00	0.139999E+02
0.277400E+00	0.772620E+00	0.129995E+02
0.288700E+00	0.900219E+00	0.120003E+02
0.301500E+00	0.106834E+01	0.110001E+02
0.316200E+00	0.106877E+01	0.999969E+01
0.333300E+00	0.838333E+00	0.899975E+01
0.345000E+00	0.664020E+00	0.840203E+01
0.353600E+00	0.559935E+00	0.800014E+01
0.365000E+00	0.453870E+00	0.750595E+01
0.378000E+00	0.371703E+00	0.699991E+01
0.395000E+00	0.324632E+00	0.640890E+01
0.408200E+00	0.326426E+00	0.600001E+01
0.425000E+00	0.355234E+00	0.553591E+01
0.447200E+00	0.383898E+00	0.500003E+01
0.452000E+00	0.401857E+00	0.489487E+01
0.465000E+00	0.392260E+00	0.462498E+01
0.482000E+00	0.386090E+00	0.430394E+01
0.500000E+00	0.380765E+00	0.399999E+01
0.577400E+00	0.350545E+00	0.299994E+01
0.707100E+00	0.201808E+00	0.199996E+01

Wave slop method

Fig A. R_w for an Elliptic Strut [W.H.M.] ($b=.15, d=.05$)

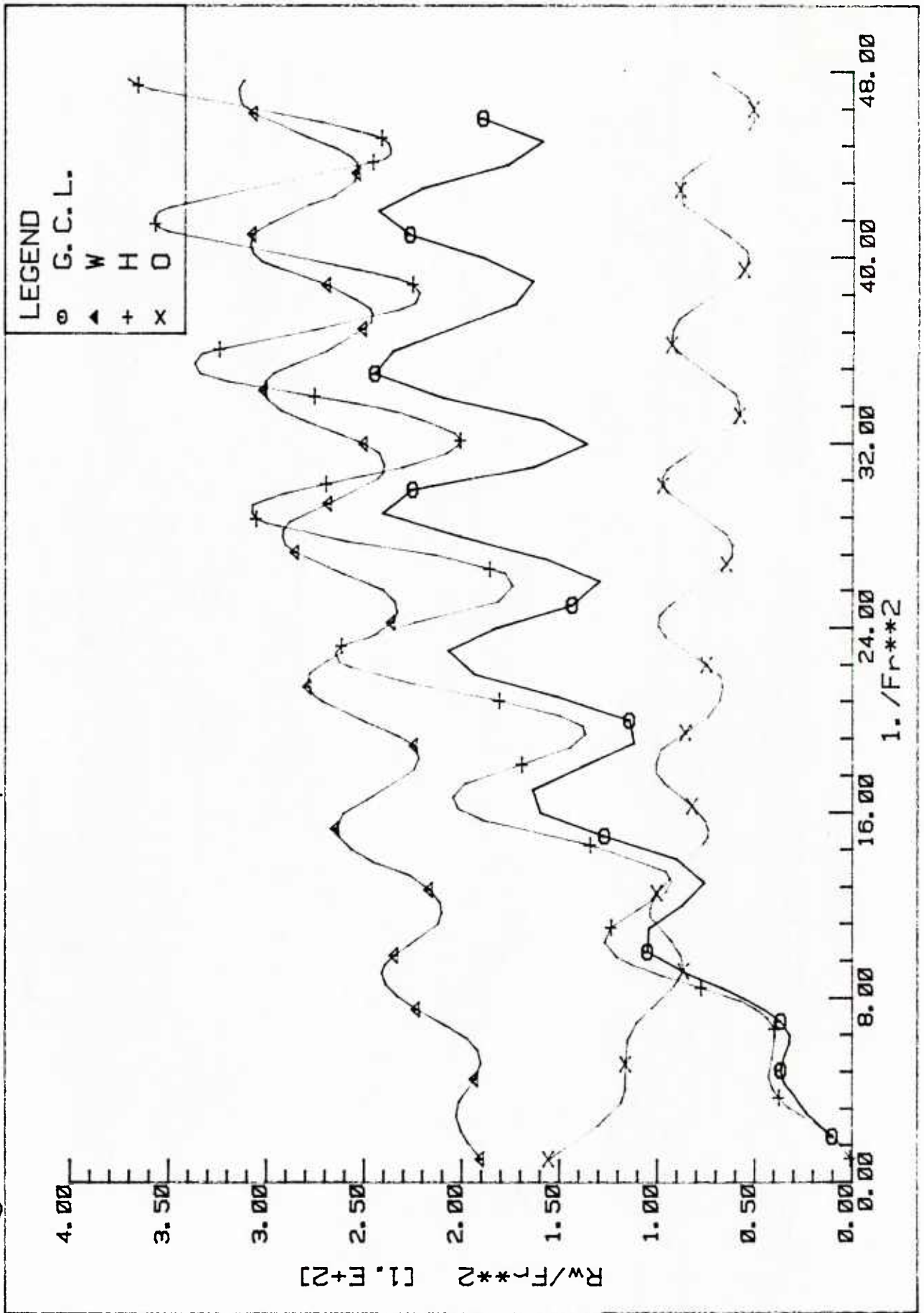
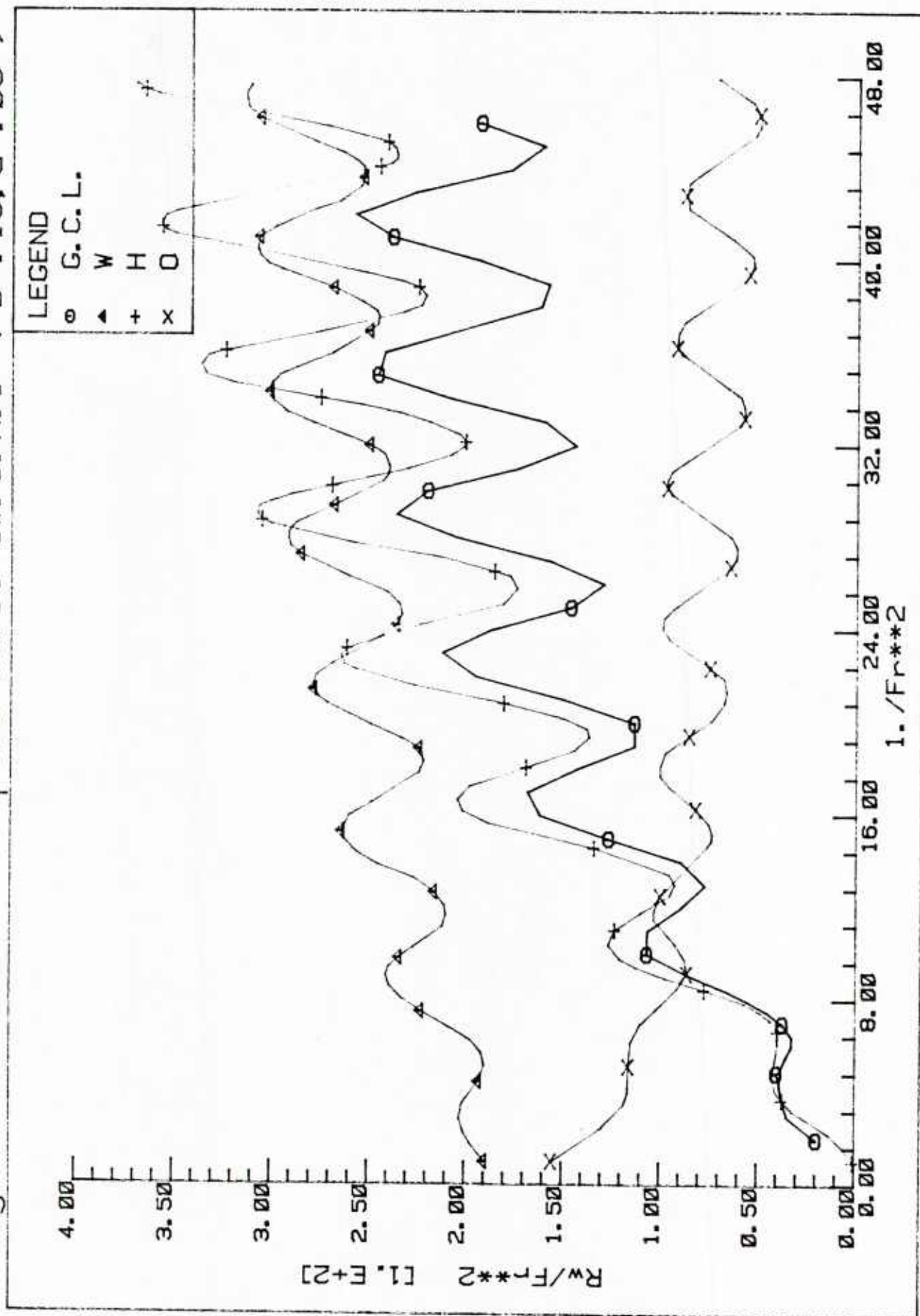


Fig B. R_w for an Elliptic Strut [W.S.M.] ($b=.15, d=.05$)



A SEMI-EMPIRICAL METHOD FOR WAVE RESISTANCE PREDICTION

by

A. Yucel Odabasi

The British Ship Research Association,
Wallsend, Tyne and Wear, NE28 6UY. England.

1 INTRODUCTION

While the studies on theoretical wave resistance have been continuing with the aim of producing more reliable formulations and efficient solution techniques, it appears that the current state of the art does not provide a sufficiently accurate and flexible method for design office use. To satisfy this need for the British Shipbuilding industry a study has been undertaken by BSRA to produce a semi-empirical method. The basis of the method has been taken from thin ship theory[1]. Certain modification has been made to overcome some inherent inaccuracies within the formulation. The resulting formulae have been further modified through a regression analysis based on a data base established from BSRA methodical series test results[2] and some Japanese and German data. Recently, a more homogeneous data base has been set up as a part of the (NSMB) Co-operative Research Activity which also led to some additional modifications in the formulations. This note describes the original BSRA method development since the latter is still in the process of being validated.

2 THE METHOD DEVELOPMENT

In a co-ordinate system shown in Fig.1 the wave resistance of a ship, according to the thin ship theory, may be expressed as:

$$R_w = 2g^2 \rho / (\pi V^2) \int_{-\pi/2}^{\pi/2} (P^2 + Q^2) \sec^3 \theta d\theta$$

where P and Q are, respectively, the cosine and sine components of the generated wave system, given by:

$$\left. \begin{matrix} P \\ Q \end{matrix} \right\} = \int_{-L/2}^{L/2} \int_{-T}^0 \frac{\partial y}{\partial x} \exp(kz \sec^2 \theta) \begin{matrix} \cos \\ \sin \end{matrix} (kx \sec \theta) dz dx,$$

and $k=g/V^2$ is the wave number, g is the gravitational acceleration, ρ is the density of water, V is the forward speed, L is the length, T is the draft of the ship, and $y=y(x,z)$ is the equation of ship surface.

When this expression is utilised in its original form it produces unrealistic waviness in low and medium speed ranges, and even if one attempts to smooth the results over a given speed range the magnitudes and slopes are not necessarily correct. In the past several attempts have been made to utilise thin ship theory to derive empirical or semi-empirical predictor formulae, cf. [3-5]. Within the approach adopted at BSRA the following basic assumptions have been employed:

- 1 Oscillatory nature of the wave resistance prediction stems from both the bow-stern wave interaction and the contribution of $\exp(kz \sec^2 \theta)$ term.
- 2 Tail ends of the wave spectra are generally inaccurate and sometimes misleading.
- 3 It is more preferable to apply a co-ordinate straining along x-direction.

As a result the wave making of fore-body and aft-end, in the low and medium speed range, were calculated separately and integration in P and Q were carried out through a special scheme which acts like a low-pass filter, i.e. deliberate introduction of numerical diffusion.

Computations carried out with these provisions indicated that the predicted wave resistance curves were smooth, provided that θ integration was carried out through a weighted summation.

The next task to be achieved was the correction of magnitude and gradients, which required the performance of a regression analysis. The data base was formed from the model test results of BSRA Methodical Series and published Japanese and West German data. Since the wave pattern data was practically non-existent, the

model wave resistance was derived through a form factor method from total resistance curves. Results obtained in this way were quite satisfactory for high and medium speed forms. In the low speed range the scatter was quite considerable and trend analyses indicated that this was partly due to the presence of wave breaking in some model tests. The data collected in that way was parted into two groups; commercial form range (covering low and medium speed data) and high speed form range. In each group a data screening exercise was undertaken to reduce bias as much as possible. Regression was performed on a log-log basis to obtain formulae. Trends showed that the computed wave resistance contributed in an exponential form in the commercial speed range. Figure 2 shows the predicted versus measured results for the commercial speed range data base.

3 APPLICATION OF THE METHOD

During the last four years this semi-empirical method has been used for both prediction and form improvement purposes. Within the context of this workshop three hulls were selected; Wigley form, Series-60 ($C_B=0.60$) hull and HSVA tanker form, representing all three speed ranges. Results are represented in Figs.3 to 5 and Table 1. In these figures the range of the measured data are also illustrated.

An inspection of the results indicate that for the Wigley form humps and hollows of the measured data are not well predicted although the computed results indicate flatnesses in these regions. This is partly due to the original intention in the derivation of the semi-empirical method which aimed at eliminating them. The result however is generally satisfactory.

For the Series-60 hull performance of the method is quite satisfactory and within the limits of measured data.

For the HSVA tanker form the trend is predicted correctly but the estimated magnitude is higher than measured values. This difference may be attributable to the presence of wave breaking resistance in some of the data employed in the regression analysis. Since, however, the wave making component of resistance for this type of hull, at the Froude numbers considered, is only a small fraction of the total resistance observed differences do not have any practical significance provided that the trend is predicted correctly.

CONCLUDING REMARKS

While the results presented here belong to a semi-empirical method, it was the intention that the use of theory would ensure:

- 1 Prediction of accurate results for the right reasons.
- 2 Provision of a more intimate relationship between the detailed hull geometry and the resistance characteristics.

Within the limitations, imposed by the data base, these objectives have generally been achieved. Current work on the extension of this technique, as a part of (NSMB) Co-operative Research activity, by the use of somewhat different methodology and more homogeneous data base is expected to improve the method performance.

ACKNOWLEDGEMENTS

The Author wishes to express his thanks to the Chairman and the Council of the British Ship Research Association for their permission to published this paper.

REFERENCES

- [1] Study on Wave-Making Resistance of Ships. INUI, T. 60th Anniversary Series, Soc. Naval Arch. Japan, Vol.2. (1967).
- [2] Methodical Series Experiments on Single Screw Ocean-Going Merchant Ship Forms. Extended and Revised Overall Analysis. PATTULLO, R.N.M. and WRIGHT, B.D.W. BSRA Report NS.333. (1971).
- [3] The Wave-Making Resistance of Ships. A Theoretical and Practical Analysis. HAVELOCK, T.H. Proc. Royal Soc. Ser.A., Vol.82. (1909).
- [4] A Power Prediction Method and Its Application to Small Ships. OORTMERSSEN, G. Int. Shipbldg. prog., Vol.18, No.207. (1971).
- [5] Prediction of Wave Resistance of Ships by Statistical Analysis. TAGANO, H. Mitsubishi Tech. Bull. No.90. (1974).

Table 1 Computed Results

Wigley Hull		Series-60 $C_B = 0.60$		HSVA Tanker	
Froude No.	Resistance Coeff. $\times 10^3$	Froude No.	Resistance Coeff. $\times 10^3$	Froude No.	Resistance Coeff. $\times 10^3$
0.23	0.5794	0.1417	0.1006	0.0975	0.0491
0.26	0.9899	0.1575	0.1286	0.1084	0.0793
0.2801	1.6166	0.1732	0.1645	0.1192	0.0858
0.3112	2.0679	0.1889	0.2099	0.1301	0.0974
0.3423	2.4005	0.2047	0.2666	0.1409	0.1612
0.3734	2.9714	0.2204	0.3321	0.1517	0.3041
0.4046	3.5757	0.2362	0.4143	0.1626	0.5743
0.4357	4.1241	0.2519	0.5354	0.1734	1.0404
0.4668	4.5921	0.2677	0.7205	0.1842	1.7618
0.4979	4.9609	0.2834	0.9975	0.1951	2.7530

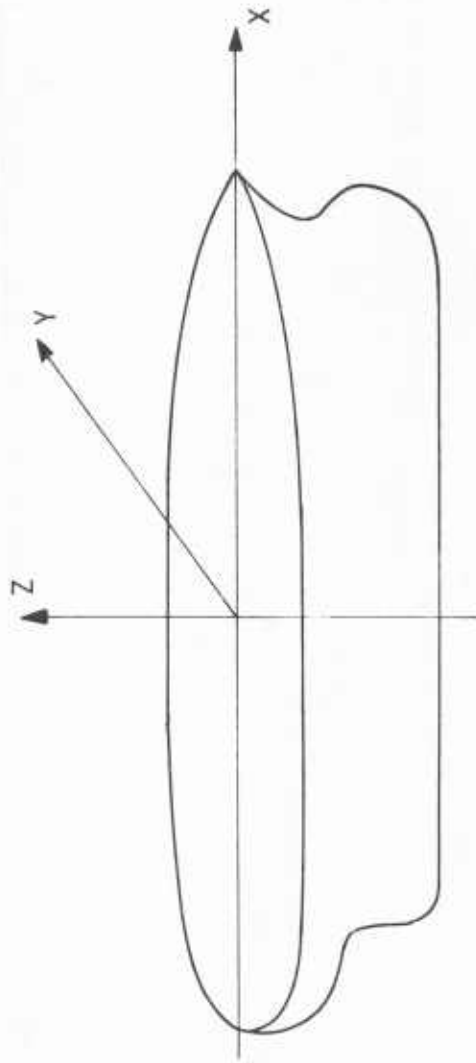


Figure 1 Co-ordinate Convention

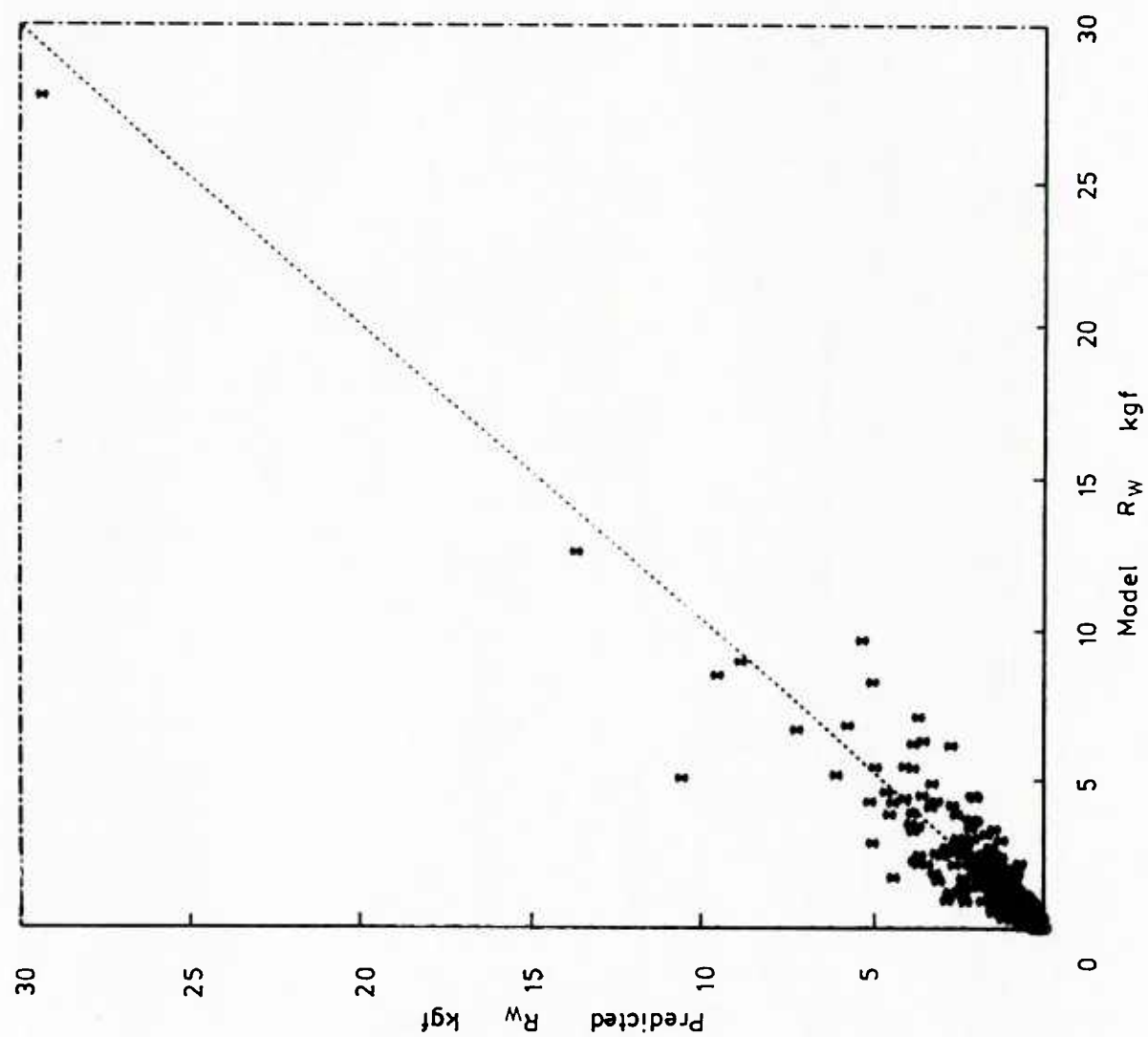


Figure 2 Predictor Low & Medium Speed data Combined

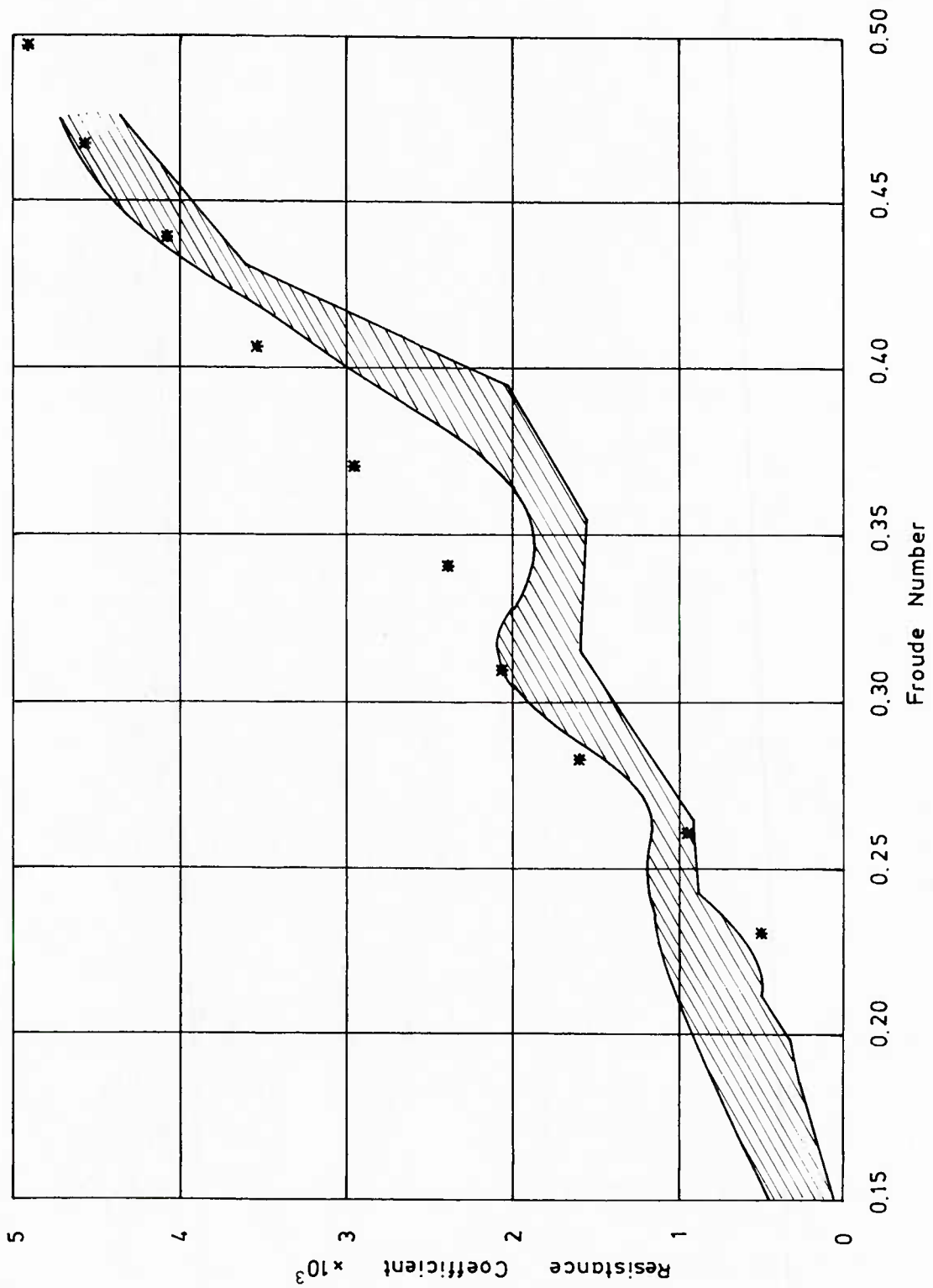


Figure 3 Wigley Hull

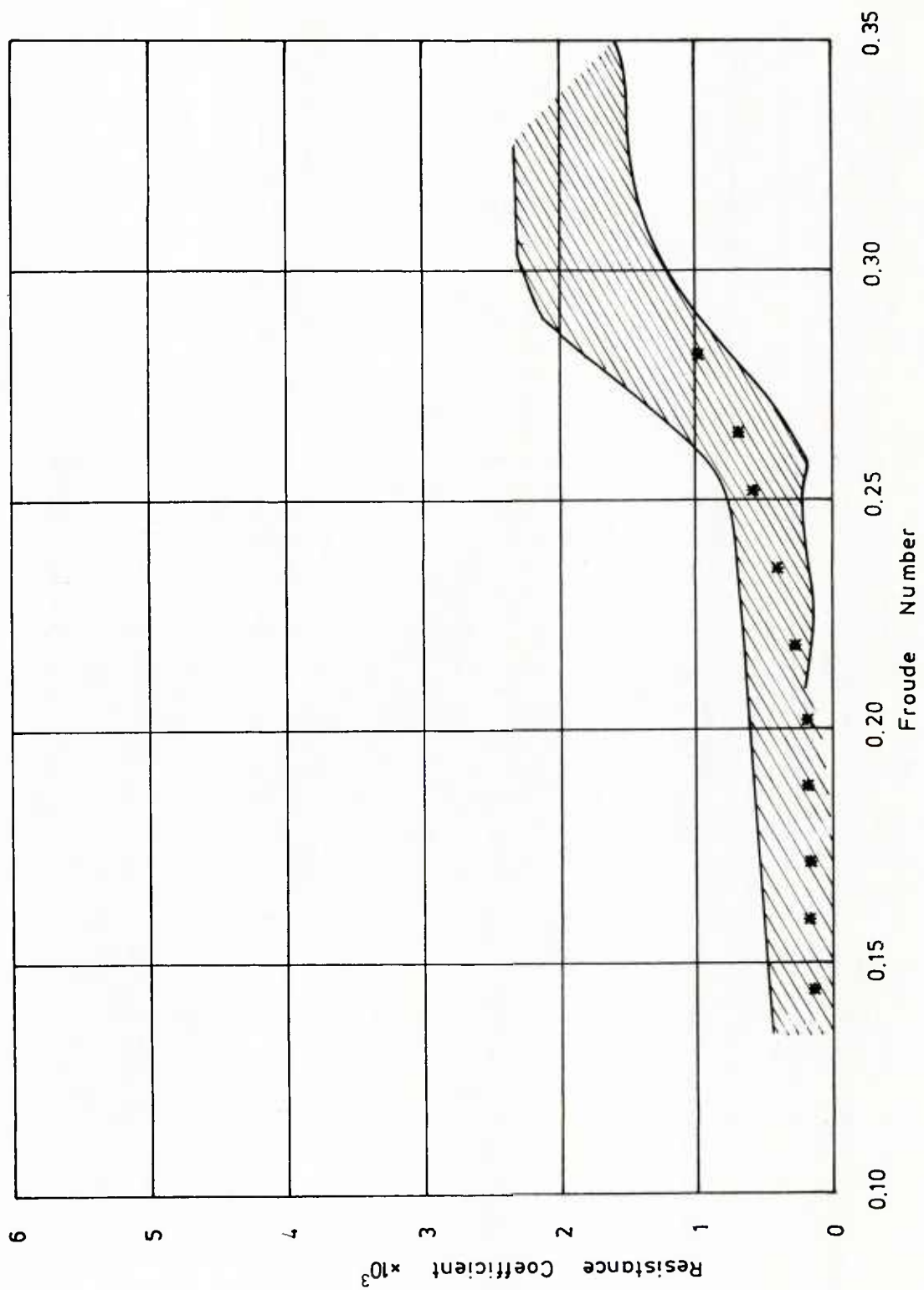


Figure 4 Series 60

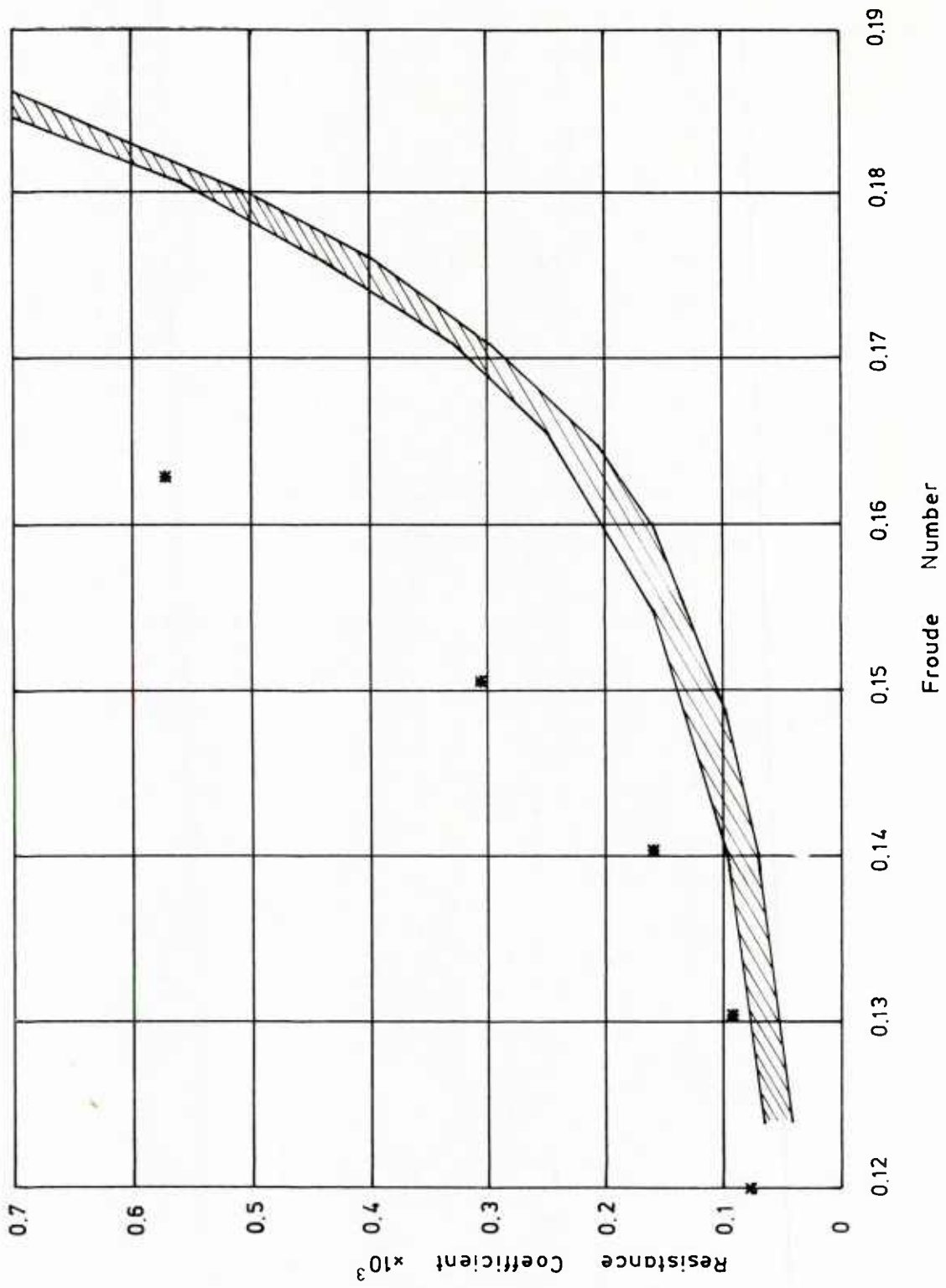


Figure 5 H.S.V.A. Tanker

COMPUTING WAVE RESISTANCE AND WAVE PROFILE
FOR SIX DIFFERENT HULL FORMS

by

Chi-Chao Hsiung¹

Ge Weizhen²

Jiunn-Ming Chuang¹

for

The Second Workshop on Ship Wave Resistance Computations
David W. Taylor Naval Ship Research and Development Centre
Washington, D.C., U.S.A.
16-17 November 1983

¹ Faculty of Engineering and Applied Science, Memorial University of
Newfoundland, St. John's, Newfoundland, Canada

² China Ship Scientific Research Centre, Wuxi, China

INTRODUCTION

Computations have been performed for six given hull forms specified by Reference [1]. In the wave resistance computations both the "tent" function method [2] and the thin-ship-panel method based on the thin-ship theory, and the Guilloton's method [3] have been employed for the Wigley hull and the Series 60 Block 60. The thin-ship theory has also been applied to the wave resistance computations for the strut-like hull form and the vertical cylinders. The wave resistance of the fully-submerged body was computed by the line-source-distribution method.

The wave profile computations were carried out only for the Wigley hull and the Series 60 Block 60. The thin-ship-panel method and the Guilloton's method were used in the above cases.

All above calculations were performed for the condition when neither sinkage nor trim is permitted.

COMPUTATIONAL METHODS

The "tent" function method has been described in details in a paper by Hsiung [2]. The Guilloton's method was basically followed the Gadd's interpretation [3]. To determine the source distribution in the Guilloton transformation, the source distribution on the centerplane obtained by the thin-ship theory was taken as the initial value. In our work, the iterative process was carried out until the value of the source strength in equation (3) of Reference [3] converging for a corresponding value of flow velocity in the longitudinal direction, rather than checking the convergence of the value of wave resistance.

The thin-ship-panel method is the by-product of the Guilloton's method. It is because one has to find the source distribution on the centerplane, and then carry out the Guilloton transformation. The centerplane of a ship is divided into 200 panels. It is assumed that the source strength is uniform over the panel, and that by the thin-ship theory the source strength is the local longitudinal slope of hull form at the centroid of the panel. Numerical integrations was conducted on the Havelock source function [4] to give the wave profile and wave resistance for a Froude number.

The wave resistance of the strut-like hull form and the vertical cylinders was computed by the thin-ship theory. In the case of the vertical cylinders, the draft was set to infinity. The resistance of the submerged spheroid was computed by the slender-body theory. The submerged body was represented by a source line along which the sources were distributed in steps [5].

COMPUTED RESULTS

Computed results for six hull forms are shown in Figs. 1 to 12. The corresponding numerical values are recorded in Tables 1.1 to 12.

The results computed by the "tent" function method and the thin-ship-panel method are almost identical as expected, since they are all based on the thin-ship theory. The Guilloton's method shows the improvement by reducing the unwanted peak near Froude number 0.3. The method of computation for the strut-like hull form and vertical cylinders was checked with the results calculated by Havelock [6]. But the computed results for the submerged spheroid are somewhat lower than Farell's data [7].

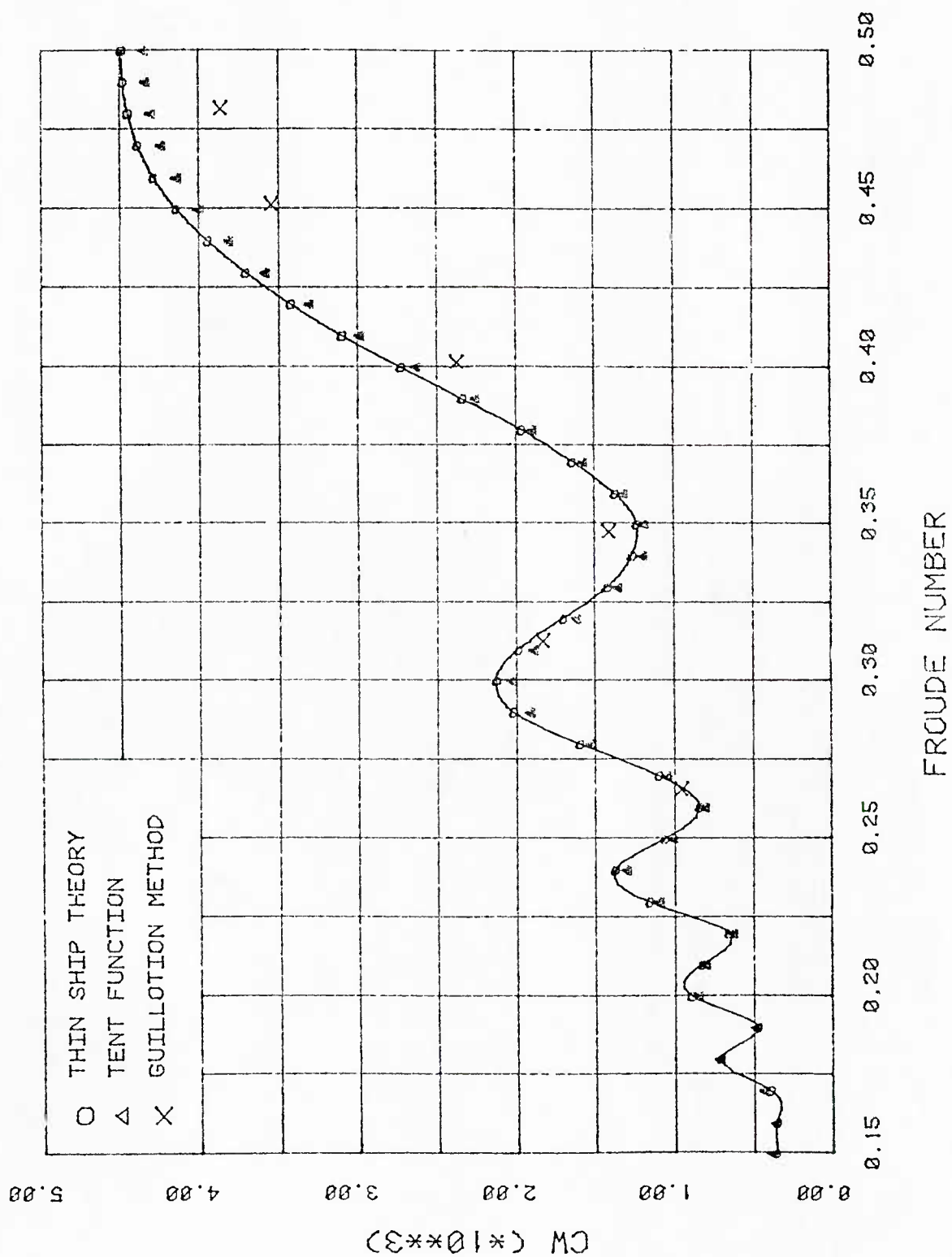
ACKNOWLEDGEMENTS

The authors are grateful for the support of the Natural Sciences and Engineering Research Council of Canada. The first author would like to acknowledge that a part of work presented in this paper is also a result of the contracted research with the Defense Research Establishment Atlantic, Canada.

REFERENCES

1. Letter from Dr. F. Noblesse, dated 25 May, 1982.
2. Hsiung, C.C., "Optimal Ship Forms for Minimum Wave Resistance", J. of Ship Research, Vol. 25, No. 2, June 1981.
3. Gadd, G.E., "Wave Resistance Calculations by Guilloton's Method", Trans. of RINA, Vol. 115, 1973.
4. Wehausen, J.V., "The Wave Resistance of Ships", Advances in Applied Mechanics, Vol. 13, 1973.
5. Ge, Weizhen and Cai, Yingchun, "Method of Estimating SWATH Resistance and Its Computer Program (Part I)", China Ship Scientific Research Center Publication, 1982.
6. Collected Papers on Hydrodynamics by T.H. Havelock, ONR, 1963.
7. Farell, C. and Guven, O., "On the Experimental Determination of the Resistance Components of a Submerged Spheroid", J. of Ship Research, Vol. 17, June 1973.

Fig 1 RESISTANCE COEFFICIENT OF WIGLEY HULL .



CW OF WIGLEY HULL BY THIN SHIP THEORY

FN	CW
0.1500000	3.6317663E-04
0.1600000	3.5415587E-04
0.1700000	3.9968794E-04
0.1800000	7.1220699E-04
0.1900000	4.7491590E-04
0.2000000	8.9110731E-04
0.2100000	8.2853116E-04
0.2200000	6.5658533E-04
0.2300000	1.1607442E-03
0.2400000	1.3790658E-03
0.2500000	1.0628403E-03
0.2600000	8.4262138E-04
0.2700000	1.0993102E-03
0.2800000	1.5959881E-03
0.2900000	2.0204654E-03
0.3000000	2.1317713E-03
0.3100000	1.9893907E-03
0.3200000	1.7003966E-03
0.3300000	1.4206440E-03
0.3400000	1.2642867E-03
0.3500000	1.2365050E-03
0.3600000	1.3740723E-03
0.3700000	1.6405915E-03
0.3800000	1.9673126E-03
0.3900000	2.3395636E-03
0.4000000	2.7323661E-03
0.4100000	3.1022218E-03
0.4200000	3.4275311E-03
0.4300000	3.7094147E-03
0.4400000	3.9501865E-03
0.4500000	4.1458397E-03
0.4600000	4.2924508E-03
0.4700000	4.3922588E-03
0.4800000	4.4531901E-03
0.4900000	4.4844835E-03
0.5000000	4.4929693E-03

TABLE 1.1

CW OF WIGLEY HULL BY TENT FUNCTION

FN	CW
0.1500000	3.8210987E-04
0.1600000	3.5766376E-04
0.1700000	4.3053465E-04
0.1800000	7.1058457E-04
0.1900000	4.7775963E-04
0.2000000	8.4927952E-04
0.2100000	7.9999410E-04
0.2200000	6.2549696E-04
0.2300000	1.0966132E-03
0.2400000	1.3033022E-03
0.2500000	1.0019189E-03
0.2600000	8.0146035E-04
0.2700000	1.0375907E-03
0.2800000	1.5195716E-03
0.2900000	1.9084768E-03
0.3000000	2.0225777E-03
0.3100000	1.8805618E-03
0.3200000	1.6097935E-03
0.3300000	1.3487736E-03
0.3400000	1.1929745E-03
0.3500000	1.1834357E-03
0.3600000	1.3177120E-03
0.3700000	1.5674091E-03
0.3800000	1.8939698E-03
0.3900000	2.2591520E-03
0.4000000	2.6307642E-03
0.4100000	2.9847163E-03
0.4200000	3.3049730E-03
0.4300000	3.5824007E-03
0.4400000	3.8132041E-03
0.4500000	3.9973864E-03
0.4600000	4.1374704E-03
0.4700000	4.2374516E-03
0.4800000	4.3020681E-03
0.4900000	4.3362156E-03
0.5000000	4.3446971E-03

TABLE 1.2

CW OF WIGLEY HULL BY GUILLOTON'S METHOD

FN	CW
0.2660000	9.5476204E-04
0.3130000	1.8351256E-03
0.3480000	1.4069616E-03
0.4020000	2.3733070E-03
0.4520000	3.5468070E-03
0.4820000	3.8627697E-03

TABLE 1.3

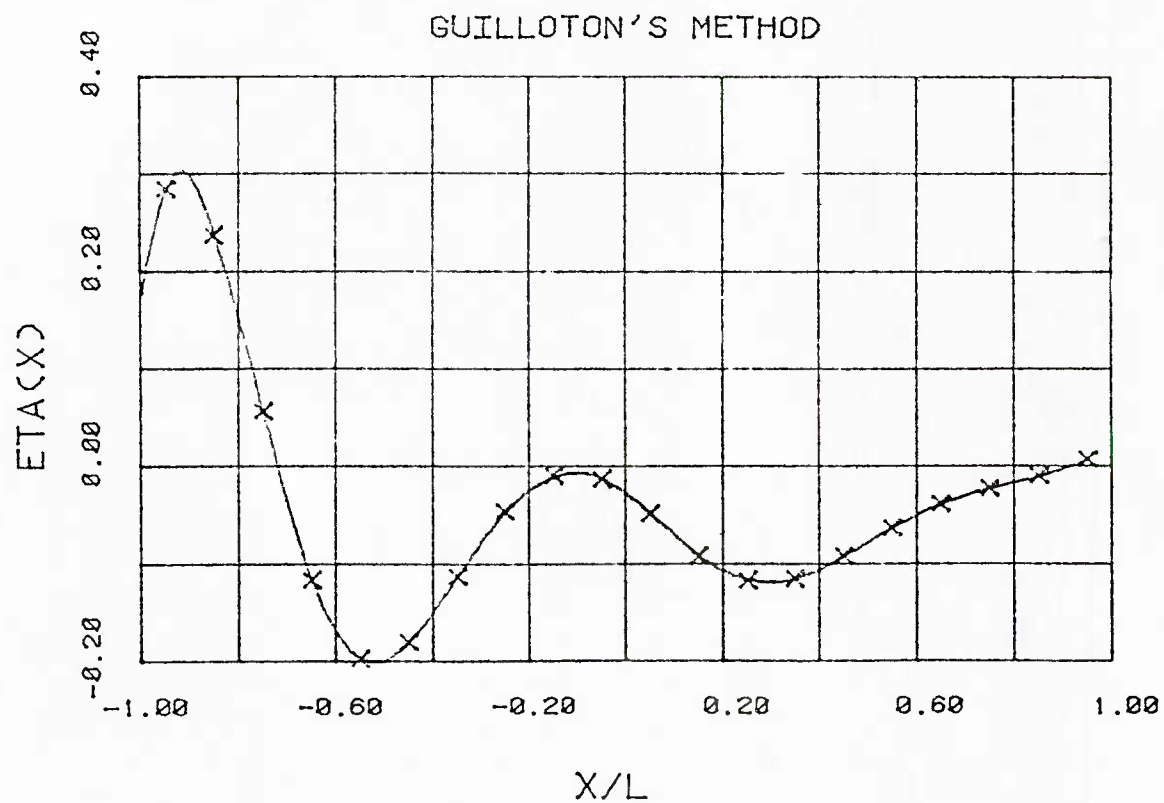
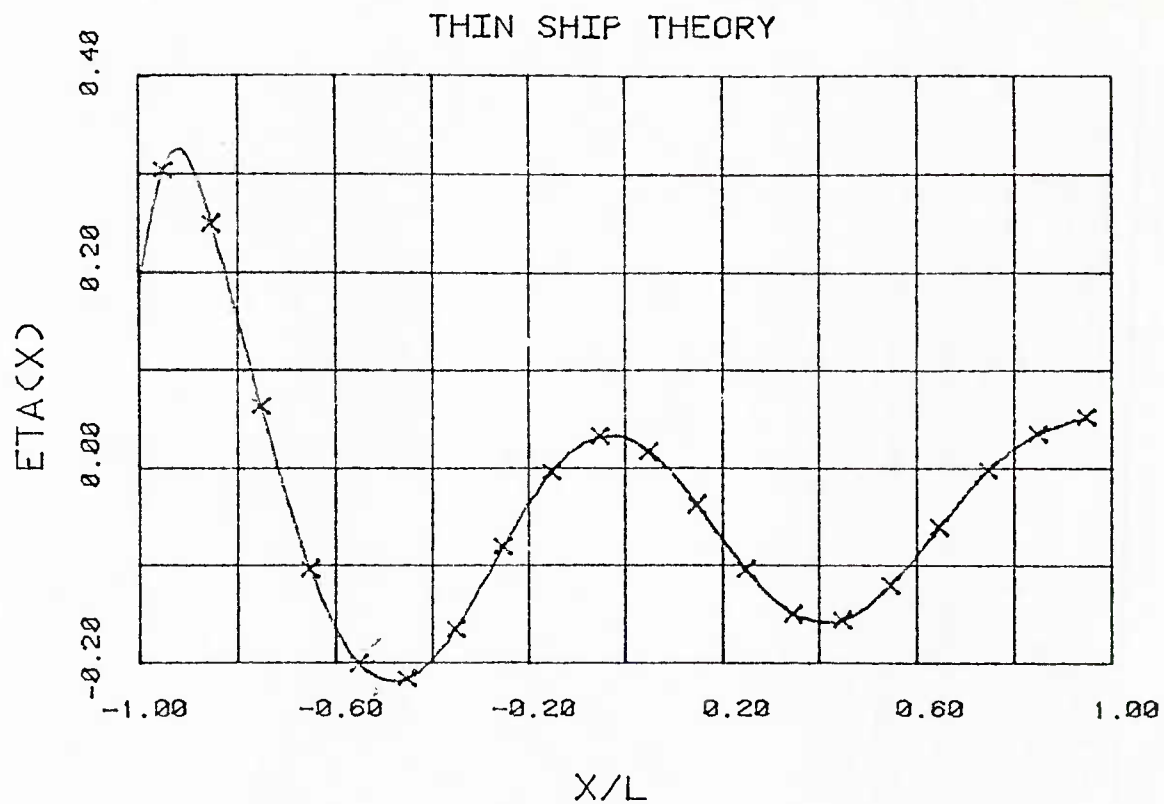


Fig 2 WIGLEY HULL-WAVE PROFILE FOR $FN=0.266$.

WIGLEY HULL - WAVE PROFILE FOR FN=0.266

X/L	ETA1 (THIN SHIP)	ETA2 (GUILLOTIN)
-0.9500000	0.3051215	0.2865334
-0.8500000	0.2499876	0.2392697
-0.7500000	6.3520233E-02	5.7668980E-02
-0.6500000	-0.1033109	-0.1147224
-0.5500000	-0.2001536	-0.1951490
-0.4500000	-0.2153220	-0.1774247
-0.3500000	-0.1635452	-0.1108241
-0.2500000	-7.8909069E-02	-4.4262219E-02
-0.1500000	-2.4032257E-03	-7.8960489E-03
-5.0000012E-02	3.3795640E-02	-1.1157164E-02
5.0000012E-02	1.8216740E-02	-4.6884794E-02
0.1500000	-3.6950212E-02	-9.0624034E-02
0.2500000	-0.1031819	-0.1157554
0.3500000	-0.1491808	-0.1134106
0.4500000	-0.1347591	-9.0288229E-02
0.5500000	-0.1189195	-6.0843173E-02
0.6500000	-5.8788463E-02	-3.6039152E-02
0.7500000	-2.1620700E-04	-1.9772587E-02
0.8500000	3.6240775E-02	-7.5415252E-03
0.9500000	5.3888038E-02	1.0045048E-02

TABLE 2

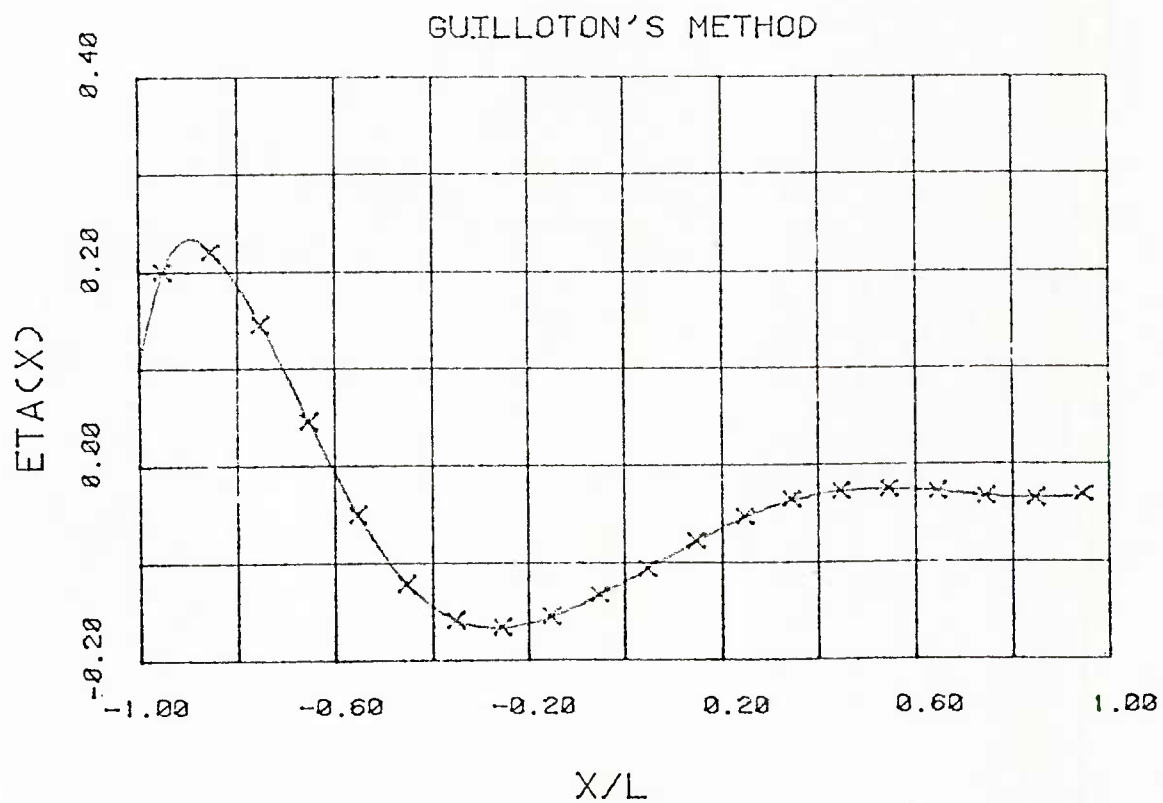
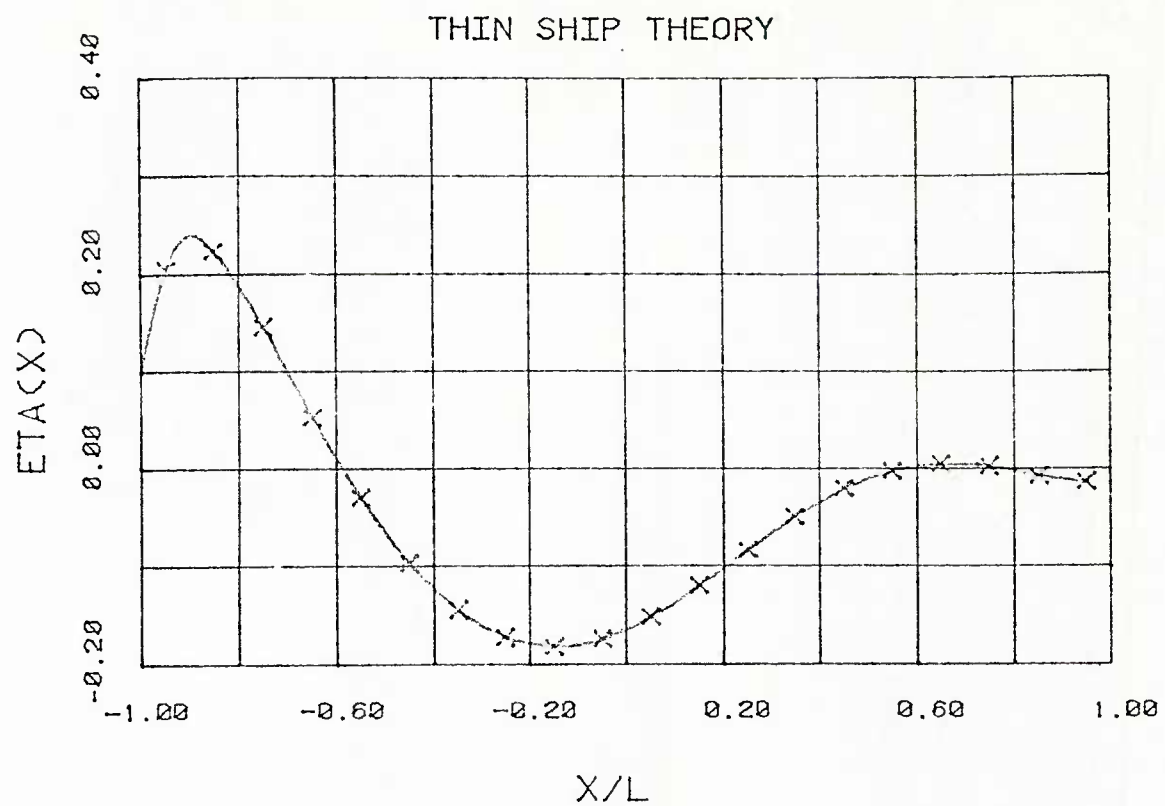


Fig 3 WIGLEY HULL-WAVE PROFILE FOR $FN=0.348$.

WIGLEY HULL - WAVE PROFILE FOR FN=0.348

X/L	ETA1 (THIN SHIP)	ETA2 (GUILLOTON)
-0.9500000	0.2054786	0.2002788
-0.8500000	0.2234954	0.2210384
-0.7500000	0.1463346	0.1457227
-0.6500000	5.3926069E-02	4.5555856E-02
-0.5500000	-2.9247411E-02	-5.0852876E-02
-0.4500000	-9.5797226E-02	-0.1216435
-0.3500000	-0.1435977	-0.1588560
-0.2500000	-0.1718958	-0.1662833
-0.1500000	-0.1809965	-0.1540801
-5.0000012E-02	-0.1726263	-0.1321347
5.0000012E-02	-0.1300055	-0.1051524
0.1500000	-0.1178961	-7.7106707E-02
0.2500000	-8.1765220E-02	-5.2341312E-02
0.3500000	-4.7128890E-02	-3.4759536E-02
0.4500000	-1.8844496E-02	-2.5969287E-02
0.5500000	-3.3867732E-04	-2.4283199E-02
0.6500000	6.8675121E-03	-2.7224386E-02
0.7500000	3.6001028E-03	-3.2151163E-02
0.8500000	-6.5173097E-03	-3.4747437E-02
0.9500000	-1.2836941E-02	-2.9948501E-02

TABLE 3

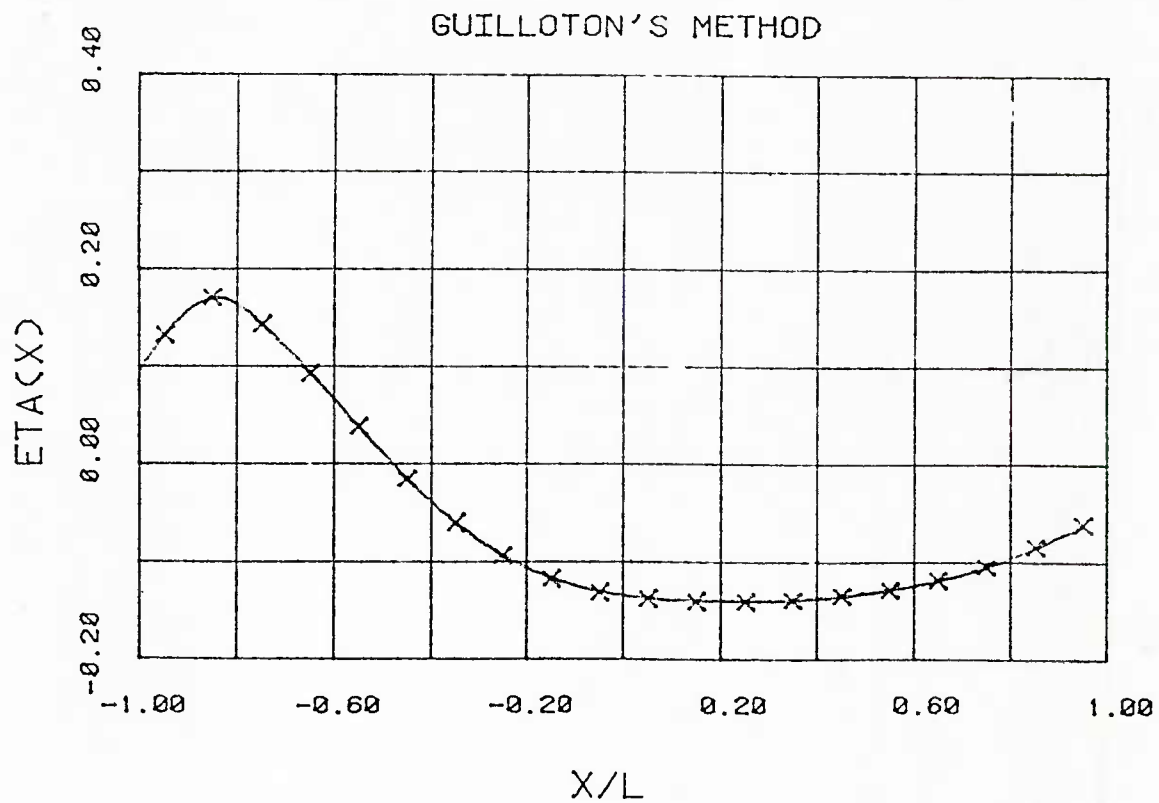
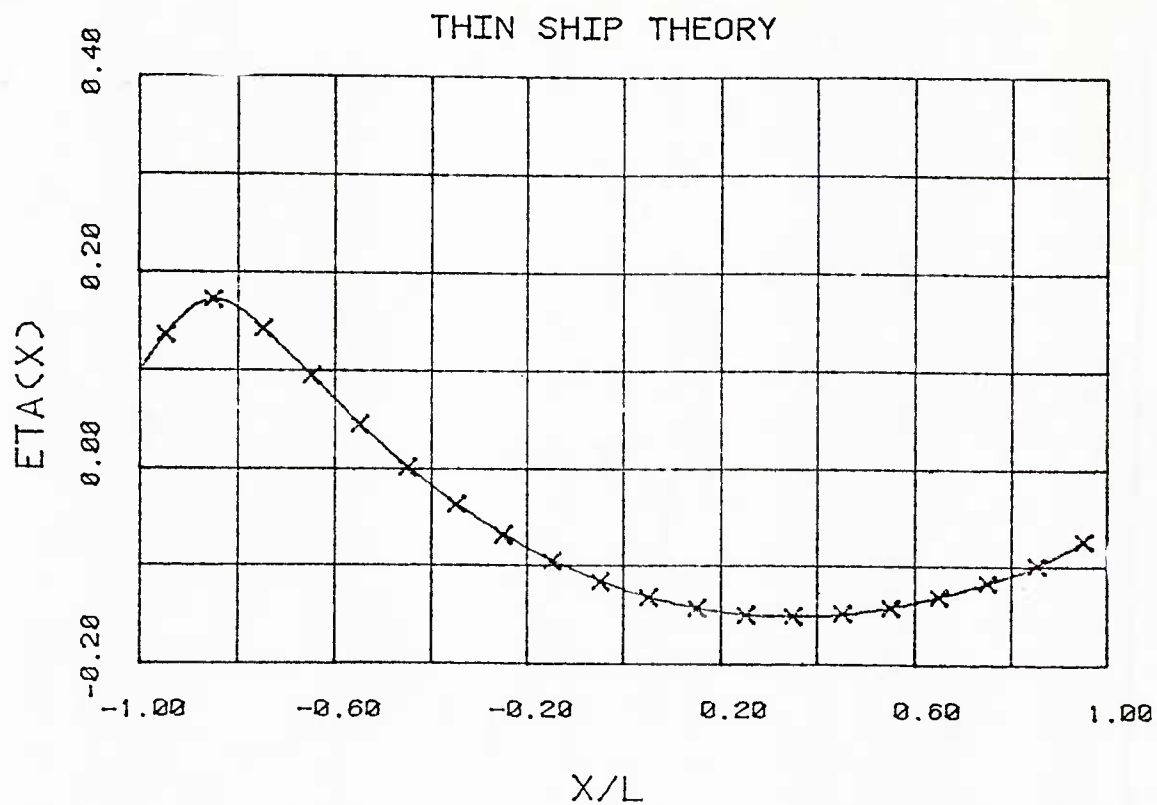


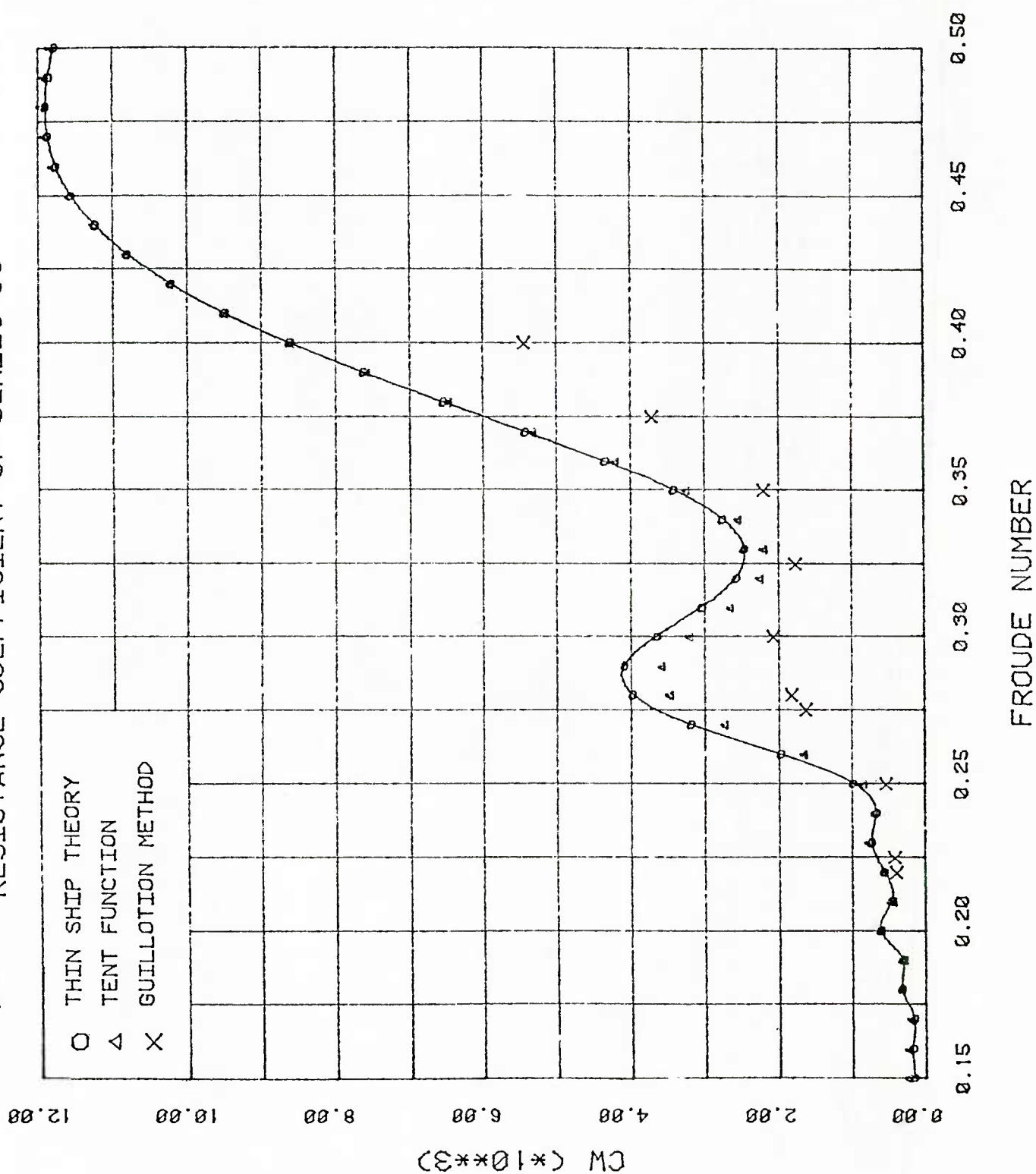
Fig 4 WIGLEY HULL-WAVE PROFILE FOR FN=0.452.

WIGLEY HULL - WAVE PROFILE FOR FN=0.452

X/L	ETA1 (THIN SHIP)	ETA2 (GUILLOTIN)
-0.9500000	0.1350566	0.1337907
-0.8500000	0.1710537	0.1718868
-0.7500000	0.1409574	0.1443545
-0.6500000	9.2776529E-02	9.4814062E-02
-0.5500000	4.3738030E-02	3.9319646E-02
-0.4500000	-2.3982115E-04	-1.3865666E-02
-0.3500000	-3.7936130E-02	-5.8809664E-02
-0.2500000	-6.9640309E-02	-9.2705108E-02
-0.1500000	-9.5853832E-02	-0.1156498
-5.0000012E-02	-0.1169232	-0.1293343
5.0000012E-02	-0.1330644	-0.1361684
0.1500000	-0.1443057	-0.1388636
0.2500000	-0.1507191	-0.1391374
0.3500000	-0.1523647	-0.1372155
0.4500000	-0.1495273	-0.1331300
0.5500000	-0.1424499	-0.1263099
0.6500000	-0.1315048	-0.1164574
0.7500000	-0.1170637	-0.1021766
0.8500000	-9.8998472E-02	-8.2395047E-02
0.9500000	-7.4016362E-02	-5.8869500E-02

TABLE 4

Fig 5 RESISTANCE COEFFICIENT OF SERIES 60



CW OF SERIES 60 BY THIN SHIP THEORY

FN	CW
0.1500000	1.5642904E-04
0.1600000	1.7877462E-04
0.1700000	1.5484815E-04
0.1800000	3.2726990E-04
0.1900000	3.1323647E-04
0.2000000	6.1639893E-04
0.2100000	4.6245803E-04
0.2200000	5.6330324E-04
0.2300000	7.3234888E-04
0.2400000	6.7022053E-04
0.2500000	9.7922562E-04
0.2600000	1.9687999E-03
0.2700000	3.1878450E-03
0.2800000	3.9789402E-03
0.2900000	4.0885573E-03
0.3000000	3.6507312E-03
0.3100000	3.0360848E-03
0.3200000	2.5685404E-03
0.3300000	2.4557943E-03
0.3400000	2.7579786E-03
0.3500000	3.4142092E-03
0.3600000	4.3464079E-03
0.3700000	5.4274281E-03
0.3800000	6.5443572E-03
0.3900000	7.6325741E-03
0.4000000	8.6329551E-03
0.4100000	9.5007615E-03
0.4200000	1.0223173E-02
0.4300000	1.0804974E-02
0.4400000	1.1252402E-02
0.4500000	1.1572327E-02
0.4600000	1.1776897E-02
0.4700000	1.1883665E-02
0.4800000	1.1911326E-02
0.4900000	1.1875643E-02
0.5000000	1.1788206E-02

TABLE 5.1

CW OF SERIES 60 BY TENT FUNCTION

FN	CW
0.1500000	2.4808920E-04
0.1600000	2.3140764E-04
0.1700000	2.0173048E-04
0.1800000	3.2943016E-04
0.1900000	2.9188229E-04
0.2000000	6.0311245E-04
0.2100000	4.3828145E-04
0.2200000	5.5791950E-04
0.2300000	7.7986822E-04
0.2400000	6.8394287E-04
0.2500000	8.4232009E-04
0.2600000	1.6542664E-03
0.2700000	2.7370204E-03
0.2800000	3.4766626E-03
0.2900000	3.5897854E-03
0.3000000	3.2035706E-03
0.3100000	2.6498660E-03
0.3200000	2.2480863E-03
0.3300000	2.1931238E-03
0.3400000	2.5413223E-03
0.3500000	3.2472506E-03
0.3600000	4.2115953E-03
0.3700000	5.3208461E-03
0.3800000	6.4718015E-03
0.3900000	7.5833821E-03
0.4000000	8.5993325E-03
0.4100000	9.4859647E-03
0.4200000	1.0227697E-02
0.4300000	1.0823034E-02
0.4400000	1.1278124E-02
0.4500000	1.1605371E-02
0.4600000	1.1819660E-02
0.4700000	1.1936721E-02
0.4800000	1.1972012E-02
0.4900000	1.1939375E-02
0.5000000	1.1853118E-02

TABLE 5.2

CW OF SERIES 60 BY GUILLOTON'S METHOD

FN	CW
0.2200000	3.9758420E-04
0.2250000	4.1717812E-04
0.2500000	5.3898746E-04
0.2750000	1.6149936E-03
0.2800000	1.8237114E-03
0.3000000	2.0692407E-03
0.3250000	1.7589367E-03
0.3500000	2.2010948E-03
0.3750000	3.7149263E-03
0.4000000	5.4445704E-03

TABLE 5.3

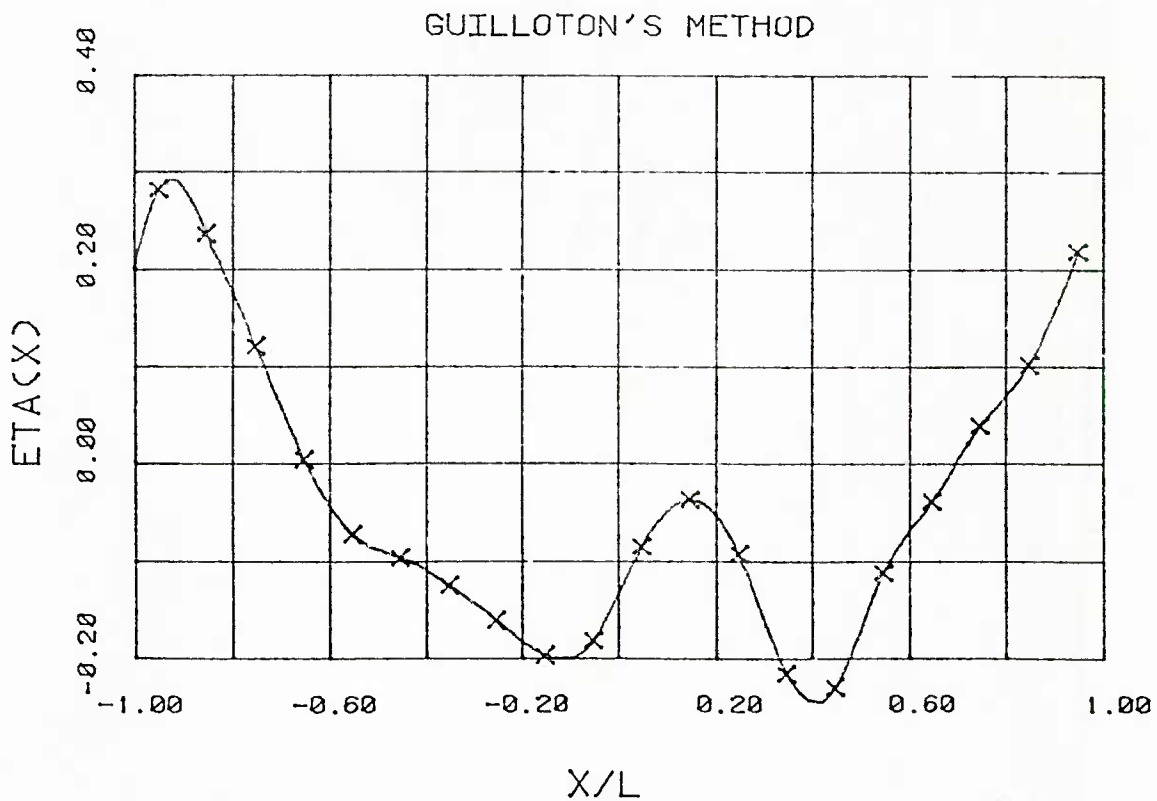
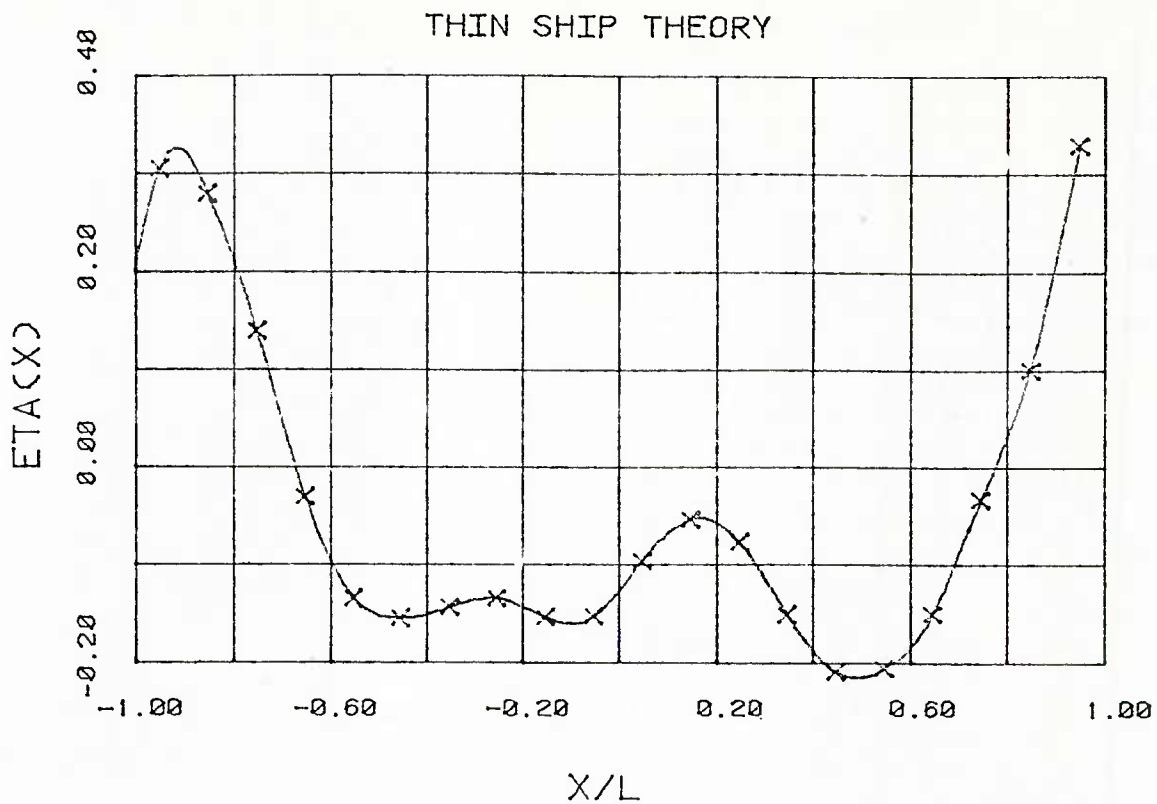


Fig 6 SERIES 60-WAVE PROFILE FOR $FN=0.22$

SERIES 60 - WAVE PROFILE FOR FN=0.22

X/L	ETA1 (THIN SHIP)	ETA2 (GUILLOTIN)
-0.9500000	0.3052846	0.2815694
-0.8500000	0.2790930	0.2355324
-0.7500000	0.1391348	0.1201823
-0.6500000	-3.0463187E-02	4.3013575E-03
-0.5500000	-0.1344233	-7.3074095E-02
-0.4500000	-0.1549724	-9.7014703E-02
-0.3500000	-0.1428066	-0.1259955
-0.2500000	-0.1341226	-0.1618298
-0.1500000	-0.1540230	-0.1976098
-5.0000012E-02	-0.1522811	-0.1813136
5.0000072E-02	-9.5033862E-02	-8.4873907E-02
0.1500000	-5.1881522E-02	-3.6006354E-02
0.2500000	-7.6246202E-02	-9.3320206E-02
0.3500000	-0.1506103	-0.2163067
0.4500000	-0.2100194	-0.2308198
0.5500001	-0.2064162	-0.1120181
0.6500000	-0.1501326	-3.8524017E-02
0.7500000	-3.2319311E-02	3.9135136E-02
0.8500000	0.1001317	0.1017799
0.9500000	0.3296069	0.2181877

TABLE 6

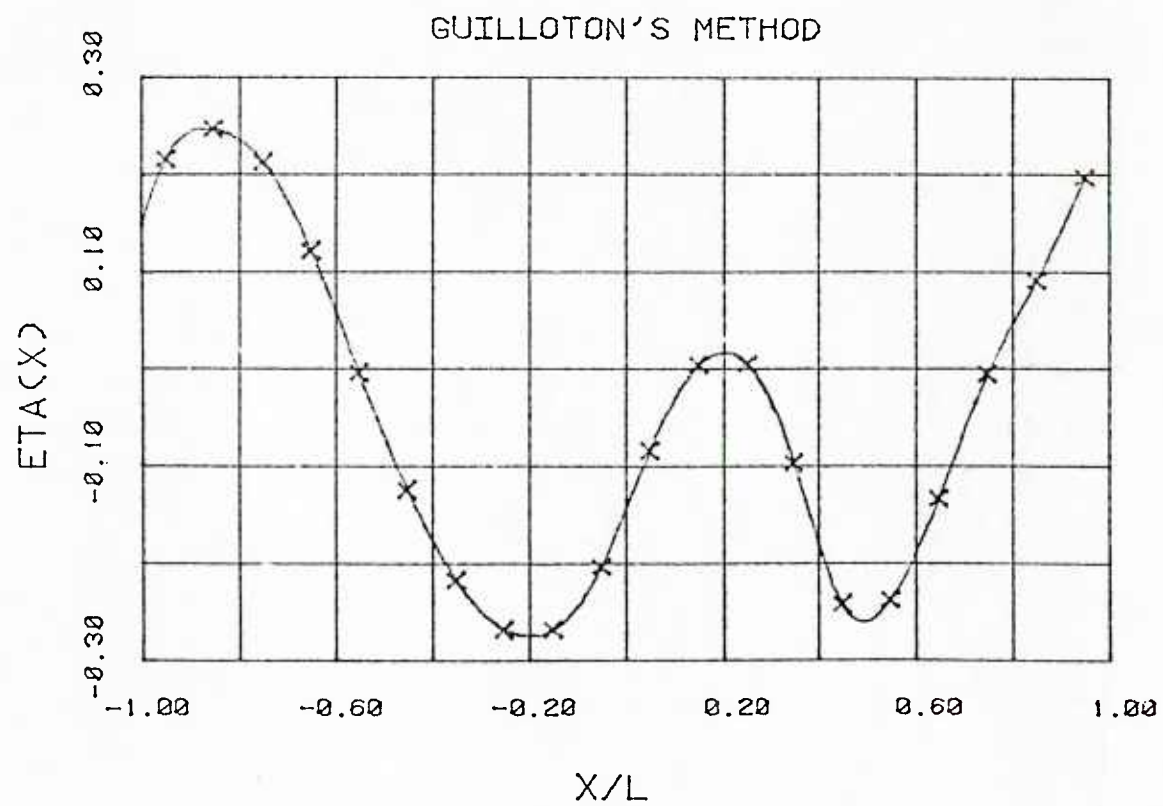
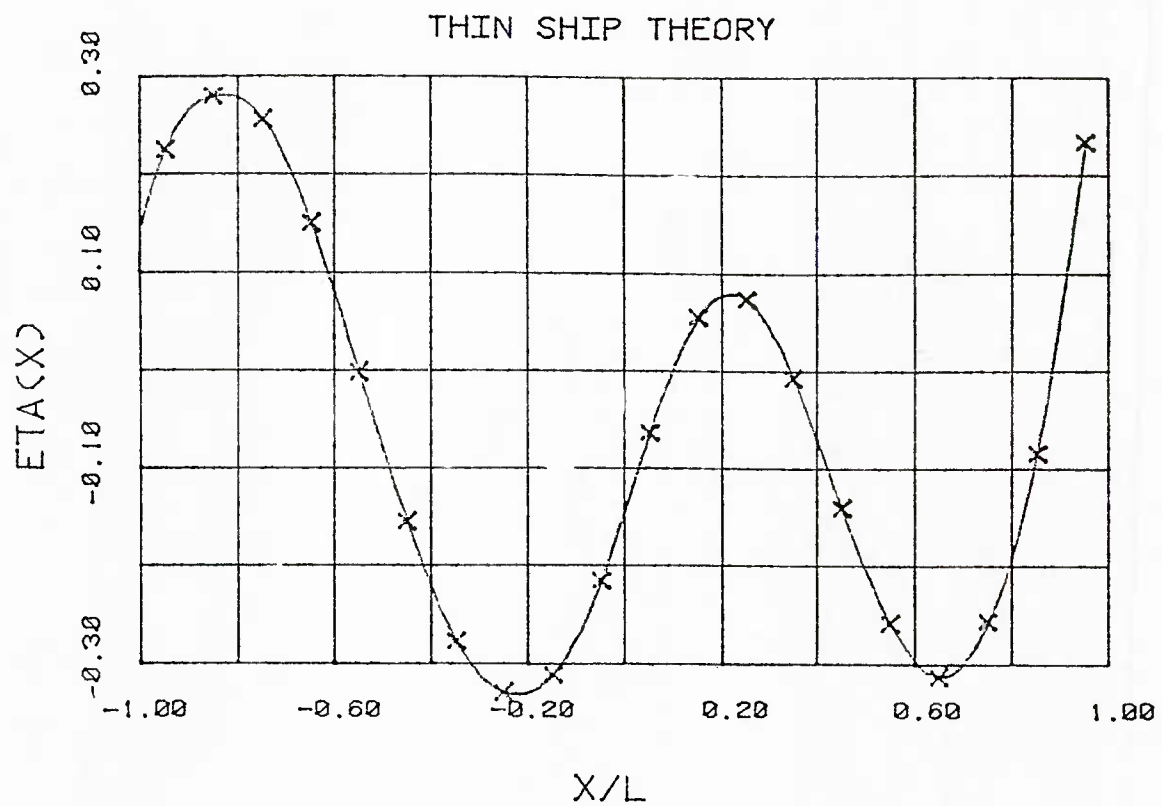


Fig 7 SERIES 60-WAVE PROFILE FOR $FN=0.28$.

SERIES 60 - WAVE PROFILE FOR FN=0.28

X/L	ETA1 (THIN SHIP)	ETA2 (GUILLOTIN)
-0.9500000	0.2238901	0.2162861
-0.8500000	0.2785840	0.2473029
-0.7500000	0.2543935	0.2128761
-0.6500000	0.1484109	0.1218956
-0.5500000	-3.1022455E-03	-4.0665506E-03
-0.4500000	-0.1564357	-0.1235684
-0.3500000	-0.2781956	-0.2168195
-0.2500000	-0.3320102	-0.2676115
-0.1500000	-0.3126584	-0.2665314
-5.0000012E-02	-0.2154710	-0.2022085
5.0000072E-02	-6.4463660E-02	-8.2536824E-02
0.1500000	5.3333588E-02	5.3125317E-03
0.2500000	7.1774252E-02	5.8623822E-03
0.3500000	-9.4510239E-03	-9.5667638E-02
0.4500000	-0.1414241	-0.2418211
0.5500001	-0.2593456	-0.2371797
0.6500000	-0.3152425	-0.1323687
0.7500000	-0.2571712	-4.7155460E-03
0.8500000	-8.6021617E-02	9.1400079E-02
0.9500000	0.2325647	0.1986911

TABLE 7

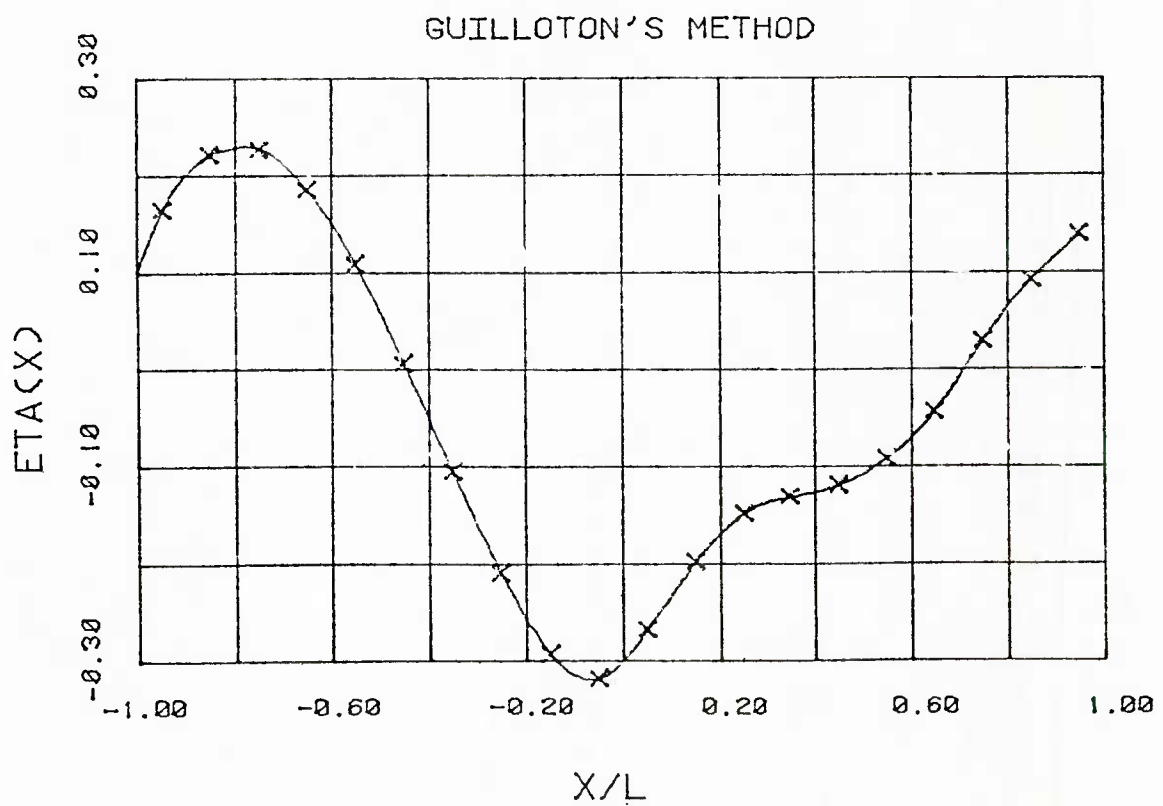
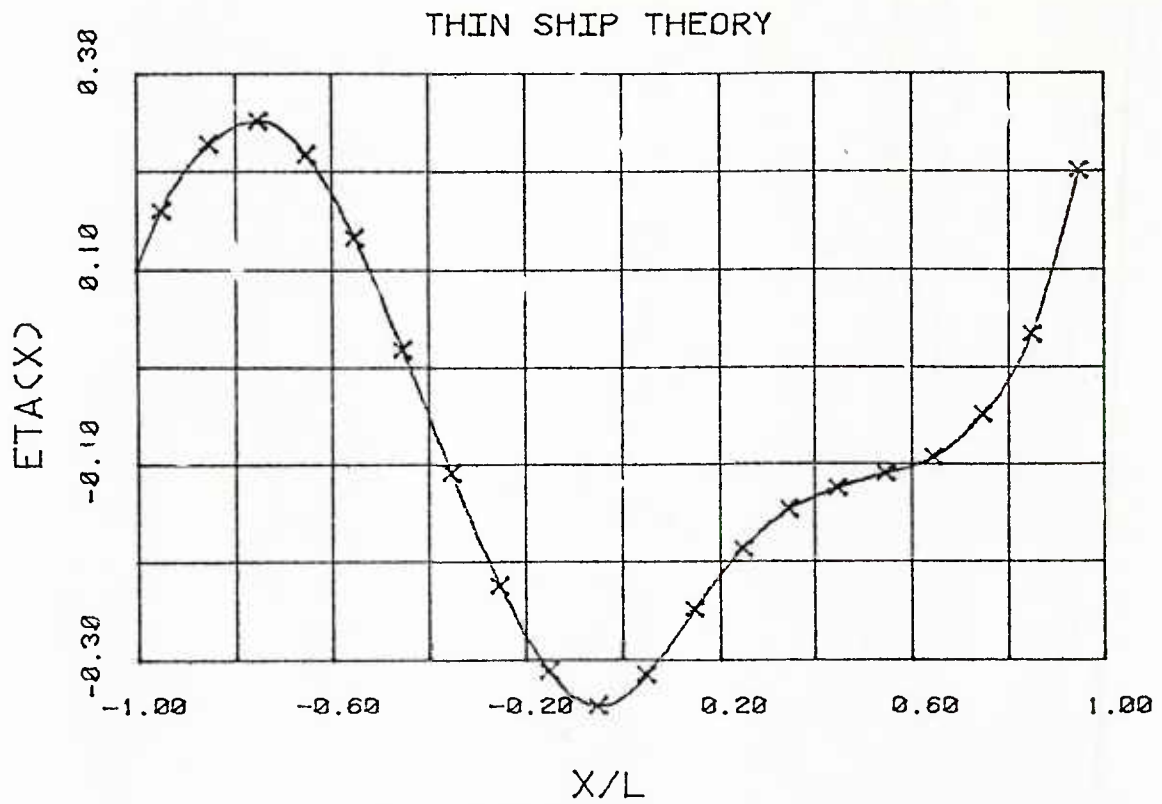


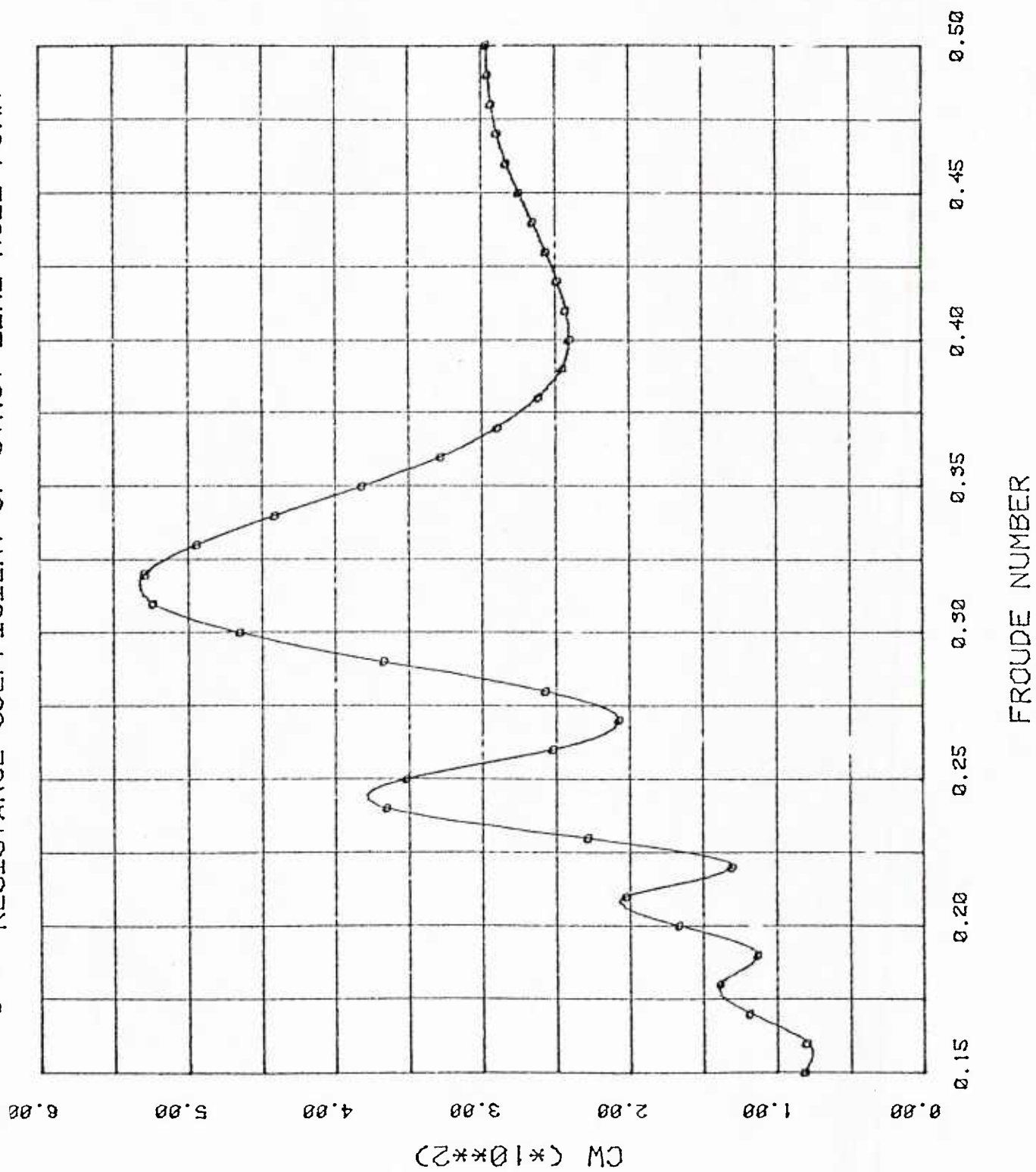
Fig 8 SERIES 60-WAVE PROFILE FOR $FN=0.35$.

SERIES 60 - WAVE PROFILE FOR FN=0.35

X/L	ETA1 (THIN SHIP)	ETA2 (GUILLON)
-0.9500000	0.1598329	0.1624244
-0.8500000	0.2286867	0.2191626
-0.7500000	0.2524406	0.2247555
-0.6500000	0.2171163	0.1832153
-0.5500000	0.1321755	0.1060407
-0.4500000	1.8033024E-02	3.1558215E-03
-0.3500000	-0.1085319	-0.1079524
-0.2500000	-0.2237432	-0.2123257
-0.1500000	-0.3122759	-0.2958371
-5.0000012E-02	-0.3478464	-0.3209364
5.0000072E-02	-0.3151497	-0.2697356
0.1500000	-0.2474189	-0.2003765
0.2500000	-0.1853730	-0.1501113
0.3500000	-0.1449856	-0.1328662
0.4500000	-0.1230086	-0.1208397
0.5500001	-0.1082036	-9.3354054E-02
0.6500000	-9.1433093E-02	-4.5507133E-02
0.7500000	-4.8124321E-02	2.7673233E-02
0.8500000	3.3734221E-02	9.0277351E-02
0.9500000	0.2016155	0.1374589

TABLE 8

Fig 9 RESISTANCE COEFFICIENT OF STRUT LIKE HULL FORM



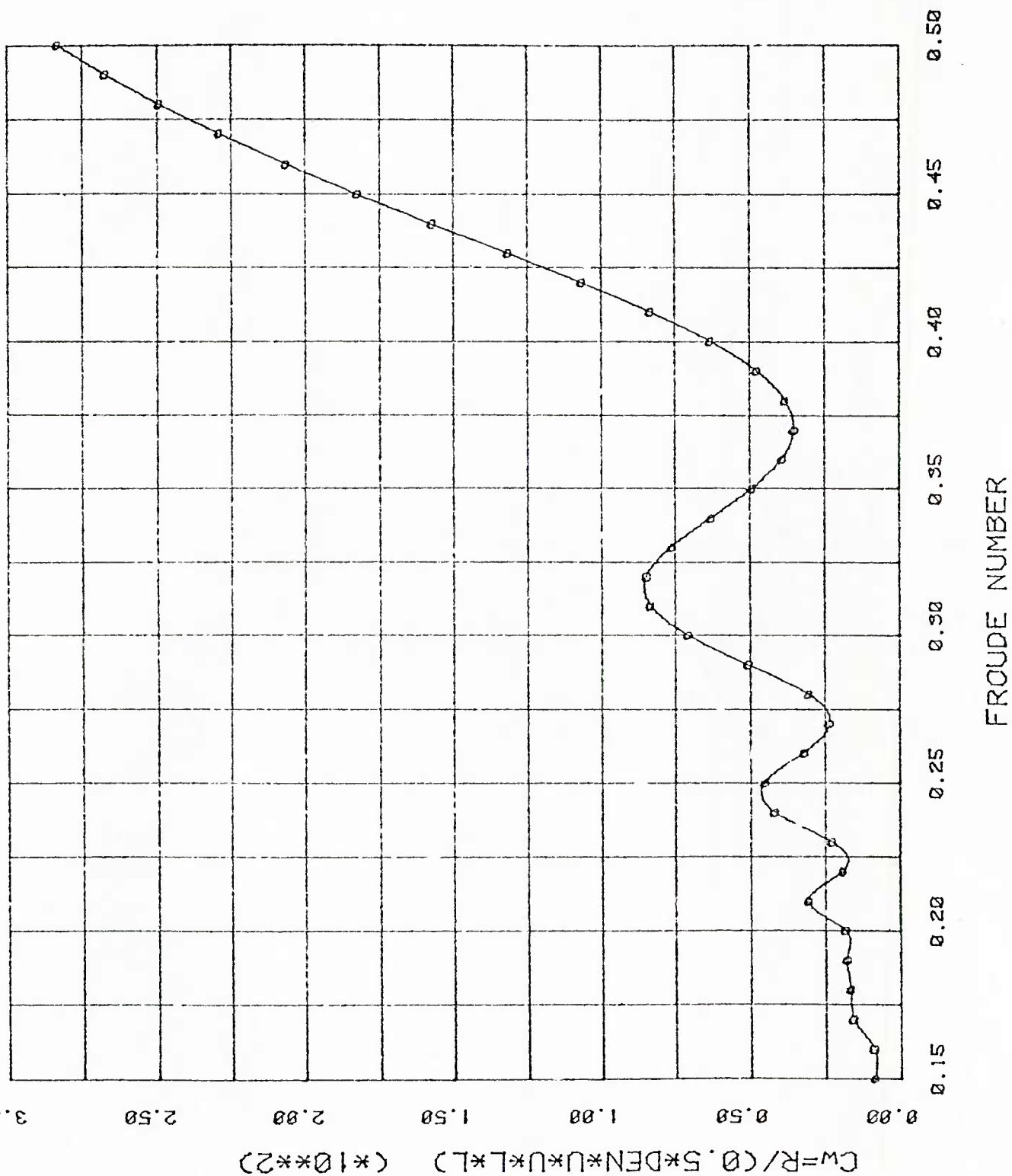
CW OF STRUT-LIKE HULL FORM

FN	CW
0.1500000	8.1065660E-03
0.1600000	7.9655498E-03
0.1700000	1.1834559E-02
0.1800000	1.3830028E-02
0.1900000	1.1278905E-02
0.2000000	1.6647350E-02
0.2100000	2.0269290E-02
0.2200000	1.3012456E-02
0.2300000	2.2861522E-02
0.2400000	3.6538150E-02
0.2500000	3.5184640E-02
0.2600000	2.5204040E-02
0.2700000	2.0714201E-02
0.2800000	2.5712179E-02
0.2900000	3.6714515E-02
0.3000000	4.6577137E-02
0.3100000	5.2388411E-02
0.3200000	5.2944589E-02
0.3300000	4.9453609E-02
0.3400000	4.4190176E-02
0.3500000	3.8187578E-02
0.3600000	3.2821029E-02
0.3700000	2.8930973E-02
0.3800000	2.6151875E-02
0.3900000	2.4505287E-02
0.4000000	2.4020765E-02
0.4100000	2.4277687E-02
0.4200000	2.4866298E-02
0.4300000	2.5642041E-02
0.4400000	2.6556471E-02
0.4500000	2.7502513E-02
0.4600000	2.8336283E-02
0.4700000	2.8961323E-02
0.4800000	2.9364111E-02
0.4900000	2.9586717E-02
0.5000000	2.9678321E-02

TABLE 9

RESISTANCE COEFFICIENT OF VERTICAL CYLINDER CELLIPTED

Fig 10

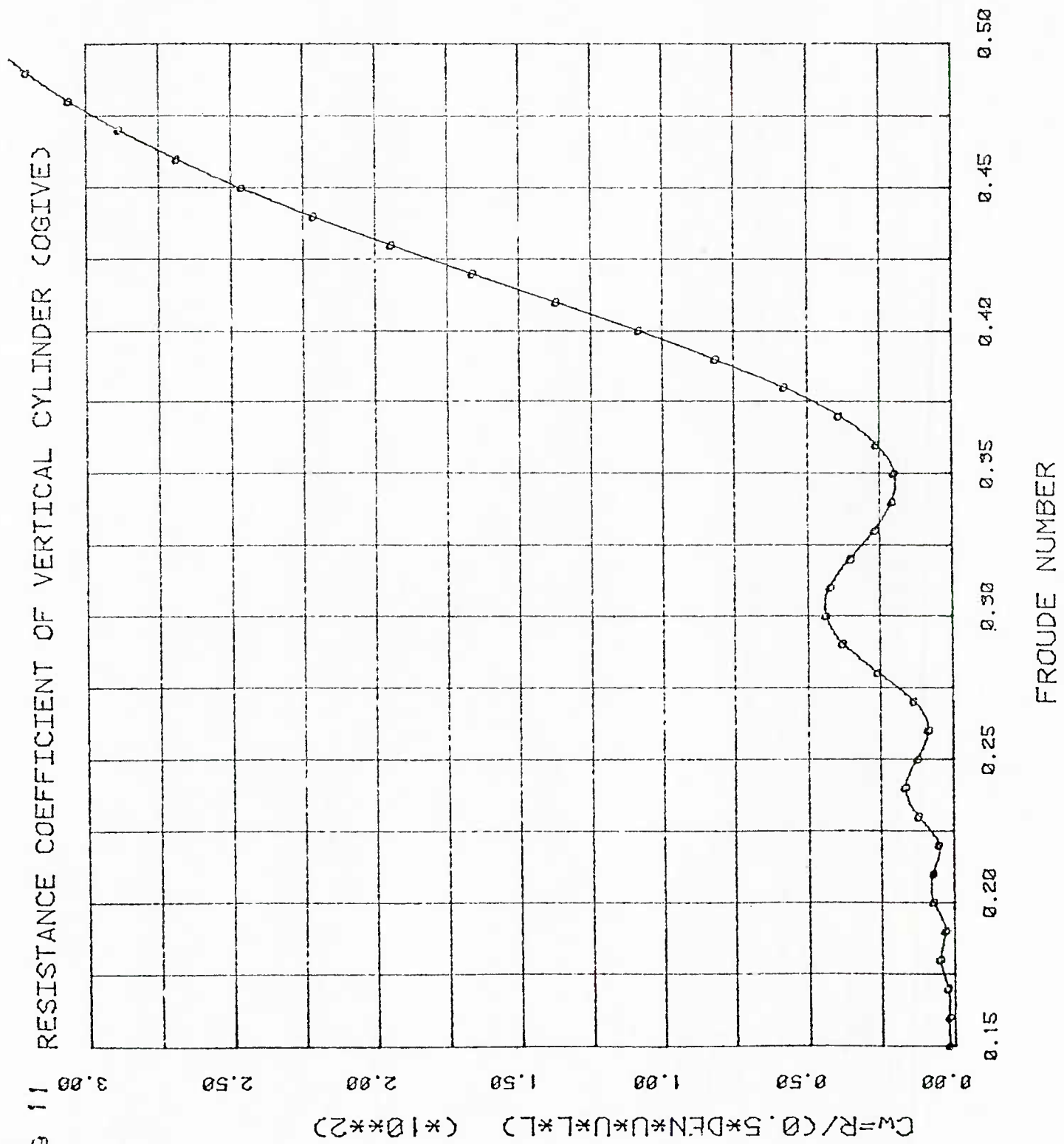


CW OF VERTICAL CYLINDER (ELLIPSE)

FN	CW
0.1500000	8.8575890E-04
0.1600000	9.1676132E-04
0.1700000	1.6006032E-03
0.1800000	1.6857819E-03
0.1900000	1.7954743E-03
0.2000000	1.8608503E-03
0.2100000	3.0832102E-03
0.2200000	1.9151616E-03
0.2300000	2.2872433E-03
0.2400000	4.1879127E-03
0.2500000	4.5148316E-03
0.2600000	3.2122706E-03
0.2700000	2.3391165E-03
0.2800000	3.0585299E-03
0.2900000	5.0576148E-03
0.3000000	7.0943723E-03
0.3100000	8.3628912E-03
0.3200000	8.4790550E-03
0.3300000	7.6176650E-03
0.3400000	6.2846607E-03
0.3500000	4.9132030E-03
0.3600000	3.8907451E-03
0.3700000	3.5135497E-03
0.3800000	3.8149050E-03
0.3900000	4.7721504E-03
0.4000000	6.3313493E-03
0.4100000	8.3550513E-03
0.4200000	1.0679820E-02
0.4300000	1.3172158E-02
0.4400000	1.5727531E-02
0.4500000	1.8254505E-02
0.4600000	2.0673146E-02
0.4700000	2.2922015E-02
0.4800000	2.4962451E-02
0.4900000	2.6775839E-02
0.5000000	2.8354995E-02

TABLE 10

Fig 11 RESISTANCE COEFFICIENT OF VERTICAL CYLINDER (OGIVE)

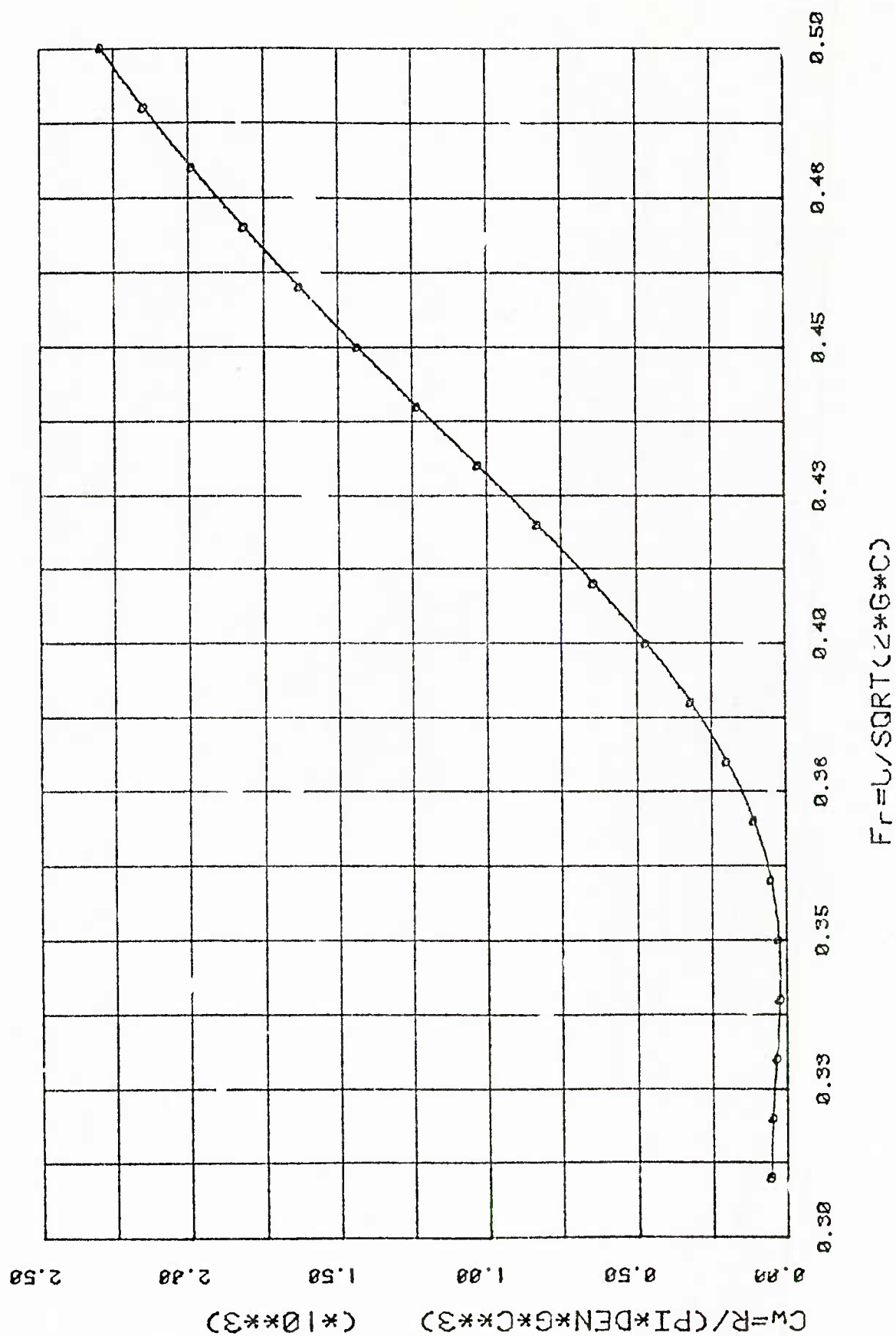


CW OF VERTICAL CYLINDER (OGIVE)

FN	CW
0.1500000	1.9842382E-04
0.1600000	1.9716229E-04
0.1700000	2.4710569E-04
0.1800000	5.0612568E-04
0.1900000	3.1890732E-04
0.2000000	7.3996390E-04
0.2100000	7.2802458E-04
0.2200000	5.3021929E-04
0.2300000	1.2436036E-03
0.2400000	1.6757681E-03
0.2500000	1.2394526E-03
0.2600000	8.6293794E-04
0.2700000	1.3696615E-03
0.2800000	2.5775360E-03
0.2900000	3.7854777E-03
0.3000000	4.3772473E-03
0.3100000	4.2124372E-03
0.3200000	3.5016793E-03
0.3300000	2.6498218E-03
0.3400000	2.0569409E-03
0.3500000	1.9877385E-03
0.3600000	2.5956957E-03
0.3700000	3.8906352E-03
0.3800000	5.7809562E-03
0.3900000	8.1459163E-03
0.4000000	1.0839794E-02
0.4100000	1.3707873E-02
0.4200000	1.6616650E-02
0.4300000	1.9462420E-02
0.4400000	2.2165034E-02
0.4500000	2.4663635E-02
0.4600000	2.6916677E-02
0.4700000	2.8901495E-02
0.4800000	3.0611161E-02
0.4900000	3.2049727E-02
0.5000000	3.3227872E-02

TABLE 11

Fig 12 RESISTANCE COEFFICIENT OF FULLY-SUBMERGED BODY



CW OF FULLY SUBMERGED BODY BY SLENDER THEORY

FN	CW
20	
0.3100000	5.6287299E-05
0.3200000	4.8942002E-05
0.3300000	3.4715700E-05
0.3400000	2.3403400E-05
0.3500000	2.6173600E-05
0.3600000	5.2705702E-05
0.3700000	1.0943770E-04
0.3800000	1.9898469E-04
0.3900000	3.2043361E-04
0.4000000	4.7013181E-04
0.4100000	6.4263988E-04
0.4200000	8.3163672E-04
0.4300000	1.0306530E-03
0.4400000	1.2335989E-03
0.4500000	1.4351032E-03
0.4600000	1.6304832E-03
0.4700000	1.8167931E-03
0.4800000	1.9907914E-03
0.4900000	2.1508590E-03
0.5000000	2.2958850E-03

TABLE 12

Computation of Non-linear Wave Resistance

by Young S. Hong

David Taylor Naval Ship Research and Development Center
Bethesda, Maryland U. S. A.

I. Introduction

In order to improve the predictions of the thin-ship theory, a non-linear wave making resistance equation has been developed. In this method, the body boundary condition is exact, and the free-surface condition is linearized. An iteration method is used to compute the wave resistance. The first iteration is the solution of the thin-ship theory. In this presentation, the number of iterations is ten for all models. The results of two models are compared with experimental data and show improved correlation.

II. Equations for the Non-linear Wave Resistance

The coordinate system, $oxyz$, is defined to be fixed to the ship. The oy -axis is directed vertically upward and the ox -axis is positive towards the stern. The oxz -plane is the undisturbed free surface. We assume the ship moves at a constant speed U in the negative x -direction. This is equivalent to keeping the ship fixed, but free to trim and sink, and letting the fluid flow in the positive x -direction with speed U . It is assumed that the fluid is incompressible and inviscid and the flow is irrotational. The velocity potential function $\phi(x,y,z)$ for the present problem is to solve the following conditions:

1. Laplace equation in the fluid domain

$$\frac{\partial^2 \phi}{\partial x^2} + \frac{\partial^2 \phi}{\partial y^2} + \frac{\partial^2 \phi}{\partial z^2} = 0 \quad (1)$$

2. the body boundary condition

$$f_x \phi_x + f_y \phi_y + \phi_z = U f_x, \text{ on } z = f(x,y) \quad (2)$$

3. the kinematic condition on the free surface

$$\eta_x \phi_x - \phi_y + \eta_z \phi_z = U \eta_x, \text{ on } y = \eta(x,z) \quad (3)$$

4. the radiation condition: the disturbance vanishes sufficiently fast far ahead of the ship

$$\lim_{x \rightarrow \infty} R(\phi_x^2 + \phi_y^2 + \phi_z^2) = 0, \quad R = (x^2 + z^2)^{1/2} \quad (4)$$

5. the bottom condition: the normal velocity to the bottom is zero

$$\phi_y(x,y,z) = 0, \text{ as } y \rightarrow -\infty \quad (5)$$

The boundary conditions, Equations (2) and (3) are exact. The numerical solution of Equation (1) with these exact boundary conditions is at present impossible. The thin-ship theory has been developed with linearization of these two boundary conditions^{1*}. In the process of the linearization, it is assumed that the derivatives of ϕ , f and η are small and their multiplications are neglected. Then the linearized body boundary condition becomes

$$\phi_z = Uf_x, \text{ on } z = 0 \quad (6)$$

and the linearized free-surface condition is given by

$$\phi_y = -U\eta_x, \text{ on } y = 0 \quad (7)$$

The solution of Equation (1) with these two boundary condition is called Michell's thin-ship theory.

In the process of the linearization of the body boundary condition, there are two points to be mentioned. The derivative of the hull function with respect to x , f_x , is usually small. However, when the ship has a parallel middle body, this derivative function is more concentrated at the bow and stern. The derivative of the hull function with respect to y , f_y , is far larger than f_x in proportion to the L/H ratio. Therefore, the simplification of the exact body boundary condition neglecting the multiplication of f_x and f_y with other terms is likely to include obvious misrepresentation of the hull function.

The exact body boundary condition, Equation (2), is applied in solving Equation (1) in order to include the effect of f_x and f_y . However, the linearized free-surface condition, Equation (7), is substituted for the exact condition. This is necessary since solution of the Green function for the exact free-surface condition is at present impossible. The present approach to compute the wave resistance is the numerical solution of Equation (1) with the partially linearized boundary condition

$$\phi_z = Uf_x - f_x\phi_x - f_y\phi_y, \text{ on } z = 0 \quad (8)$$

and the linearized free-surface condition, Equation (7). The other boundary conditions are given by Equations (4) and (5).

The solution can be written in integral form as

$$\phi(x,y,z) = \frac{1}{2\pi} \int \int_S G(x,y,z;x',y',z') \phi_z dx' dy' \quad (9)$$

and the wave resistance is given by

$$R = -2\rho U \int \int_S \phi_x f_x dx dy \quad (10)$$

The free-surface wave elevation is given from Equation (7) as

$$\eta = \frac{U}{g} \phi_x(x,0,z) \quad (11)$$

*Numbers in superscript designate references at the end of the paper.

The Green function in Equation (9) is given by Wehausen and Laitone² as

$$\begin{aligned}
 G(x,y,z;x',y',z') = & - [(x-x')^2 + (y-y')^2 + (z-z')^2]^{-1/2} \\
 & + [(x-x')^2 + (y+y')^2 + (z-z')^2]^{-1/2} \\
 & + \frac{4k_0}{\pi} \int_0^{\pi/2} d\theta \sec^2 \theta \oint_0^{\infty} dk \exp[k(y+y')] \frac{\cos[k(x-x')\cos\theta] \cos[k(z-z')\sin\theta]}{k - k_0 \sec^2 \theta} \\
 & + 4k_0 \int_0^{\pi/2} d\theta \sec^2 \theta \exp[k_0(y+y')\sec^2 \theta] \sin[k_0(x-x')\sec\theta] \cos[k_0(z-z')\sin\theta \sec^2 \theta] \quad (12)
 \end{aligned}$$

In the numerical computation, an iteration method has been applied. First, Equation (9) is computed with Equation (6) for ϕ_z (this is Michell's thin-ship or first-order solution). Then, ϕ_x and ϕ_y are numerically evaluated and Equation (9) is recomputed with Equation (8) for ϕ_z (this is called the non-linear solution). The result is compared with the previous result, and the process is repeated until a convergence test is satisfied. The numerical results converge after 5 - 10 iterations depending on the hull form.

III. Numerical Results

Numerical computations have been carried out for the hull forms whose principal dimensions are given in Table 1. The units of all dimensions are not indicated throughout this report since the final results are wave resistance coefficients. Except Series 60, $C_B=0.6$ hull, all hulls are idealized mathematical forms. The computed wave resistance coefficients are given in Tables 2 to 5 and in Figures 1 to 5. The non-dimensionalized wave elevations are given in Tables 7 to 9, and those for the Wigley and Series 60 hulls are plotted in Figures 10 and 11.

The results shown in this paper are for the tenth iteration. The number of iterations depends on the hull form. As a numerical test, for a strut-like hull (round end), the results of the fifteenth iteration have been compared with those of the tenth iteration and the agreement was very good. After this numerical test, the number of iterations was taken as ten for all other hulls.

The computed wave resistance coefficients are compared with the experimental data for the Wigley and Series 60, $C_B=0.6$, hulls. The results for the Wigley hull show moderate improvement compared with the experimental results given by Shearer and Cross³. The results of Series 60 show very good agreement with the experiment conducted by Kim and Jenkins⁴. Furthermore, the wave elevation calculated by the present method (non-linear) shows better agreement with the measured wave elevation than the first-order results.

For other hull forms, the experimental data are not available and therefore, it is difficult to say whether the results of the present method have been improved compared to the first order results. While Strut-like hull and Vertical cylinder do not have any draft-wise change of the beam, the derivative of hull function with respect to y , ϕ_y , is zero. Therefore, the last term in Equation (8) is zero and the

non-linear results are only due to the effect of the second term. In most cases, the influence of the third term is dominant in the non-linear results. Because of this fact, for the Strut-like hull and Vertical cylinder, the non-linear results are different from the first-order results, but the general tendency is similar.

In the computation of the wave resistance of the Vertical cylinder, there is one difficulty in handling the infinite draft. While the present computer program uses the precomputed master table for the Green function, Equation (12), to save the computer time, there is a limit set for the highest values of the draft. The details for the creation of the master table are given in References (6) and (7). In this table, the draft and Froude number are limited with $2H/(LF_n^2)=6.5$. For lower Froude number, the draft can be larger and for the higher Froude number, the draft becomes smaller. In the present numerical computation, for example when the Froude number is 0.375, the maximum draft will be 4.57. For this Froude number, the wave resistance coefficients for five different drafts (1.5, 2.25, 3.0, 3.75, and 4.5) are computed with $S=40.466$ which is the wetted surface area for $H=1.5$, and these results are plotted in Figure 6. From this figure the wave resistance for $H=\infty$ are extrapolated. The extrapolated wave resistance coefficient at this Froude number is 1.2 for the non-linear method and 1.05 for the first-order results.

The hull form of the submerged spheroid is somewhat different from the hull hull forms. While the program is organized to take the offset as input data, the centerplane of the hull should be rectangular. With the rectangular center-plane consisting of the major and minor axes of the centerplane of the spheroid, the grid points are generated in this rectangle shown in Figure 7 and the offset at these grid points are input data. When the grid point is outside of the centerplane of the spheroid, the hull function at this point is zero. Therefore, the input offsets taken with this procedure are not so accurate as the original spheroid offsets near the boundary of the centerplane of the spheroid. This inaccuracy causes some errors numerical computation of f_x and f_y . The computation of wave resistance of the spheroid is only to check whether the present computer program, which has been written for all general hull forms, is suitable for computation of wave resistance of a hull form like as submerged spheroid. The computed results show some discrepancies from the test conducted by Farell and Guven⁸ and from the calculation done by Farell⁹.

The changes in wave resistance coefficients for different number of iterations are shown in Figures 8 and 9. The interesting point is that the wave resistance of Series 60 hull becomes negative at the second and third iterations when the Froude number is 0.222 and later the resistance becomes positive.

The non-linear method improves the results of the thin-ship theory for two hull forms compared with the experimental data. The next step must be to apply this method to other hull forms such as naval and high speed commercial ships. Further improvements to the present method will include the effects of sinkage and trim on the computation.

IV. References

- 1 Wehausen, J. V., "Ship Hydrodynamics II - Wave Resistance," Lecture Note NA241, The Dept. of Naval Arch. and Offshore Engineering, Univ. of Cal. Berkeley, 1972
- 2 Wehausen, J. V. and E. V. Laitone, "Surface Waves," in Handbuch der Physik, vol. 9, pp 446-778, 1960
- 3 Shearer, J. R. and J. J. Cross, "The Experimental Determination of the Components of Ship Resistance for a Mathematical Model," Transaction of the Royal Institute of Naval Architects, vol. 107, pp 459-473, London, 1965
- 4 Kim, Y. H. and D. Jenkins, "Trim and Sinkage Effects on Wave Resistance with Series 60, $C_B=0.6$," DTNSRDC Report DTNSRDC/SPD-1013-01, Sept. 1981
- 5 Huang, T. T. and C. von Kerczek, "Shear Stress and Pressure Distribution on a Surface Ship Model; Theory and Experiments," 9th Symposium on Naval Hydrodynamics, Office of Naval Research, Paris, 1972
- 6 Yeung, R. W., "Sinkage and Trim in First-order Thin-ship Theory," Journal of Ship Research, vol. 16, No. 1, pp 47-59, March 1972
- 7 Hong, Y. S., "Numerical Calculation of Second-order Wave Resistance," Journal of Ship Research, vol. 21, No. 2, pp 94-106, June 1977
- 8 Farell, C. and O. Guven, "On the Experimental Determination of the Resistance Components of a Submerged Spheroid," Journal of Ship Research, vol. 17, pp 72-79, June 1973
- 9 Farell, C., "On the Wave Resistance of a Submerged Spheroid," Journal of Ship Research, vol. 17, pp 1-11, March 1973

Table: 1 Principal Dimensions

	Wigley	Series 60	Strut-like Hull Form		Vertical Cylinder		Submerged Spheroid
			Sharp End	Round End	Ellipse	Ogive	
Model No	111	222	3331	3332	4441	4442	555
LPP	20	400	10	10	10	10	10
B	2	53.3	1.5	1.5	1.5	1.5	1.98
H	1.25	21.33	0.75	0.75	∞	∞	2.574
B/L	0.1	0.133	0.15	0.15	0.15	0.15	0.198
H/L	0.625	0.0533	0.075	0.075	∞	∞	∞
S	59.277	27372.0	27.906	27.906	42.639*	40.466*	55.589
CB	0.444	0.6	0.86	0.86	0.783*	0.668*	
St. No	21	21	29	29	29	21	29
WL No	7	7	7	7	11	11	11
*These values are when H=1.5.							

Table: 2 Wave Resistances of Wigley and Series 60

Wigley Hull			Series 60		
F_n	1st order	non-linear	F_n	1st order	non-linear
0.266	0.0938	0.1098	0.222	0.0323	0.0190
0.313	0.1847	0.1724	0.252	0.0660	0.0428
0.350	0.1204	0.1456	0.282	0.3170	0.1233
0.402	0.2711	0.1739	0.302	0.2804	0.1659
0.452	0.4079	0.2332	0.323	0.1964	0.1561
0.482	0.4408	0.2649	0.353	0.3156	0.1626
	$\times 10^{-2}$	$\times 10^{-2}$		$\times 10^{-2}$	$\times 10^{-2}$

Table: 3 Wave Resistances of Strut-like Hull Form

F_n	Sharp End		Round End	
	1st order	non-linear	1st order	non-linear
0.200	0.1712	0.0702	0.1093	0.1325
0.212	0.1945	0.0961	0.1443	0.1570
0.225	0.1526	0.0387	0.0964	0.1248
0.238	0.2692	0.1652	0.2142	0.2281
0.250	0.2786	0.1774	0.2296	0.2474
0.262	0.2004	0.0929	0.1532	0.1907
0.275	0.1794	0.0680	0.1290	0.1834
0.288	0.2504	0.1377	0.1995	0.2533
0.300	0.3299	0.2162	0.2797	0.3286
0.325	0.3666	0.2487	0.3177	0.3683
0.350	0.2808	0.1615	0.2325	0.2953
	$\times 10^{-1}$	$\times 10^{-1}$	$\times 10^{-1}$	$\times 10^{-1}$

Table 4: Wave Resistance of Vertical Cylinder

F_n	Ellipse ¹		Ogive ²	
	1st order	non-linear	1st order	non-linear
0.225	0.0964	0.0725	0.2211	0.1519
0.238	0.1695	0.1362		
0.250	0.2119	0.1702	0.3305	0.2558
0.262	0.1533	0.1168		
0.275	0.1116	0.0865	0.4539	0.3457
0.288	0.1615	0.1330	0.7790	0.6287
0.300	0.2316	0.1969	0.9196	0.7623
0.312	0.2742	0.2319	0.8376	0.6897
0.325	0.2750	0.2300	0.6450	0.5300
0.338			0.4752	0.3672
0.350	0.1860	0.1480	0.4490	0.3380
0.360			0.5517	0.4387
0.370			0.7403	0.6118
0.375	0.1280	0.1000	1.2000	1.0500
	$\times 10^{-1}$	$\times 10^{-1}$	$\times 10^{-2}$	$\times 10^{-2}$
1 S=42.639 when L=10 and H=1.5				
2 S=40.466 when L=10 and H=1.5				

Table 5: Wave Resistance of Submerged Spheroid

F_n	1st order	non-linear	F_r
0.29695	0.0989		0.300
0.32170	0.0644		0.325
0.34645	0.0415	0.0278	0.350
0.37119	0.0187	0.0078	0.375
0.39594	0.0513	0.0241	0.400
0.42068	0.8199		0.425
0.44543	1.1108		0.450
0.47018	1.2935		0.475
0.49492	1.4658		0.500
	$\times 10^{-2}$	$\times 10^{-2}$	

Table 6: Wave Elevation ($2gn/U^2$) of Wigley Hull

$2x/L$	$F_n = 0.266$		$F_n = 0.482$	
	1st order	non-linear	1st order	non-linear
-1.0	0.314	0.276	0.101	0.094
-0.9	0.266	0.218	0.136	0.124
-0.8	0.152	0.099	0.143	0.123
-0.7	-0.021	-0.060	0.113	0.081
-0.6	-0.150	-0.151	0.072	0.030
-0.5	-0.205	-0.156	0.031	-0.016
-0.4	-0.187	-0.106	0.006	-0.050
-0.3	-0.121	-0.043	-0.038	-0.070
-0.2	-0.042	-0.002	-0.064	-0.078
-0.1	0.013	0.006	-0.087	-0.081
0.0	0.022	-0.014	-0.105	-0.079
0.1	-0.012	-0.044	-0.124	-0.078
0.2	-0.071	-0.069	-0.133	-0.074
0.3	-0.126	-0.079	-0.140	-0.076
0.4	-0.151	-0.076	-0.143	-0.082
0.5	-0.136	-0.065	-0.144	-0.076
0.6	-0.089	-0.052	-0.142	-0.072
0.7	-0.031	-0.046	-0.136	-0.078
0.8	0.016	-0.044	-0.127	-0.089
0.9	0.052	-0.030	-0.109	-0.089
1.0	0.089	0.0	-0.085	-0.077

Table 7: Wave Elevation ($2g\eta/U^2$) of Series 60

$2x/L$	$F_n = 0.222$		$F_n = 0.302$	
	1st order	non-linear	1st order	non-linear
-1.0	0.295	0.255	0.158	0.142
-0.9	0.292	0.231	0.231	0.190
-0.8	0.215	0.143	0.261	0.193
-0.7	0.057	0.0	0.215	0.123
-0.6	-0.081	-0.092	0.113	0.020
-0.5	-0.150	-0.104	-0.022	-0.077
-0.4	-0.156	-0.078	-0.161	-0.143
-0.3	-0.139	-0.069	-0.273	-0.180
-0.2	-0.135	-0.094	-0.330	-0.185
-0.1	-0.141	-0.122	-0.318	-0.157
0.0	-0.129	-0.111	-0.240	-0.107
0.1	-0.102	-0.067	-0.128	-0.048
0.2	-0.092	-0.041	-0.031	-0.010
0.3	-0.117	-0.065	0.012	-0.018
0.4	-0.161	-0.114	-0.006	-0.064
0.5	-0.191	-0.135	-0.066	-0.118
0.6	-0.176	-0.108	-0.134	-0.138
0.7	-0.098	-0.056	-0.171	-0.112
0.8	0.045	-0.025	-0.137	-0.046
0.9	0.223	0.140	-0.009	0.050
1.0	0.404	0.263	0.162	0.154

Table 8: Wave Elevation ($2\eta/U^2$) of Strut-like Hull Form (Sharp End)

$2x/L$	$F_n = 0.250$		$F_n = 0.350$	
	1st order	non-linear	1st order	non-linear
-1.0	0.637	0.482	0.384	0.322
-0.975	0.943	0.672	0.553	0.431
-0.95	1.144	0.804	0.701	0.531
-0.925	1.196	0.852	0.802	0.606
-0.9	1.132	0.835	0.829	0.638
-0.85	0.804	0.683	0.767	0.619
-0.8	0.355	0.424	0.626	0.534
-0.7	-0.553	-0.231	0.213	0.239
-0.6	-1.066	-0.762	-0.201	-0.100
-0.5	-1.005	-0.904	-0.518	-0.397
-0.4	-0.482	-0.588	-0.671	-0.554
-0.3	0.157	-0.046	-0.669	-0.587
-0.2	0.547	0.376	-0.563	-0.515
-0.1	0.524	0.469	-0.401	-0.369
0.0	0.174	0.244	-0.218	-0.216
0.1	-0.260	-0.116	-0.038	-0.059
0.2	-0.518	-0.391	0.120	0.079
0.3	-0.474	-0.440	0.232	0.183
0.4	-0.200	-0.271	0.286	0.232
0.5	0.088	-0.042	0.259	0.209
0.6	0.173	0.049	0.138	0.097
0.7	-0.018	-0.106	-0.059	-0.106
0.8	-0.386	-0.456	-0.301	-0.376
0.85	-0.624	-0.726	-0.449	-0.556
0.9	-0.880	-1.049	-0.621	-0.771
0.925	-1.037	-1.276	-0.736	-0.920
0.95	-1.326	-1.750	-0.921	-1.163
0.975	-1.804	-2.603	-1.264	-1.631
1.0	-2.374	-3.658	-1.718	-2.268

Table 9: Wave Elevation ($2gn/U^2$) of Strut-like Hull
Form (Round End)

$2x/L$	$F_n = 0.250$		$F_n = 0.350$	
	1st order	non-linear	1st order	non-linear
-1.0	1.658	0.968	1.242	0.808
-0.975	1.966	1.030	1.178	0.726
-0.95	1.918	1.508	1.161	0.685
-0.925	1.515	0.981	1.178	0.719
-0.9	1.091	0.825	1.055	0.719
-0.85	0.267	0.467	0.674	0.564
-0.8	-0.404	0.075	0.389	0.387
-0.7	-1.210	-0.588	-0.121	0.030
-0.6	-1.265	-0.887	-0.478	-0.273
-0.5	-0.727	-0.728	-0.680	-0.480
-0.4	0.019	-0.246	-0.740	-0.524
-0.3	0.574	0.233	-0.639	-0.497
-0.2	0.673	0.462	-0.466	-0.436
-0.1	0.351	0.359	-0.298	-0.285
0.0	-0.154	0.022	-0.107	-0.127
0.1	-0.553	-0.297	0.071	0.012
0.2	-0.612	-0.428	0.220	0.126
0.3	-0.329	-0.347	0.293	0.201
0.4	0.060	-0.135	0.306	0.220
0.5	0.261	0.025	0.237	0.137
0.6	0.099	-0.070	0.017	-0.066
0.7	-0.313	-0.399	-0.262	-0.337
0.8	-0.709	-0.694	-0.517	-0.643
0.85	-0.830	-0.765	-0.630	-0.768
0.9	-0.849	-0.691	-0.712	-0.827
0.925	-0.818	-0.603	-0.739	-0.848
0.95	-0.740	-0.458	-0.755	-0.839
0.975	-0.583	-0.193	-0.737	-0.769
1.0	-0.382	0.131	-0.691	-0.672

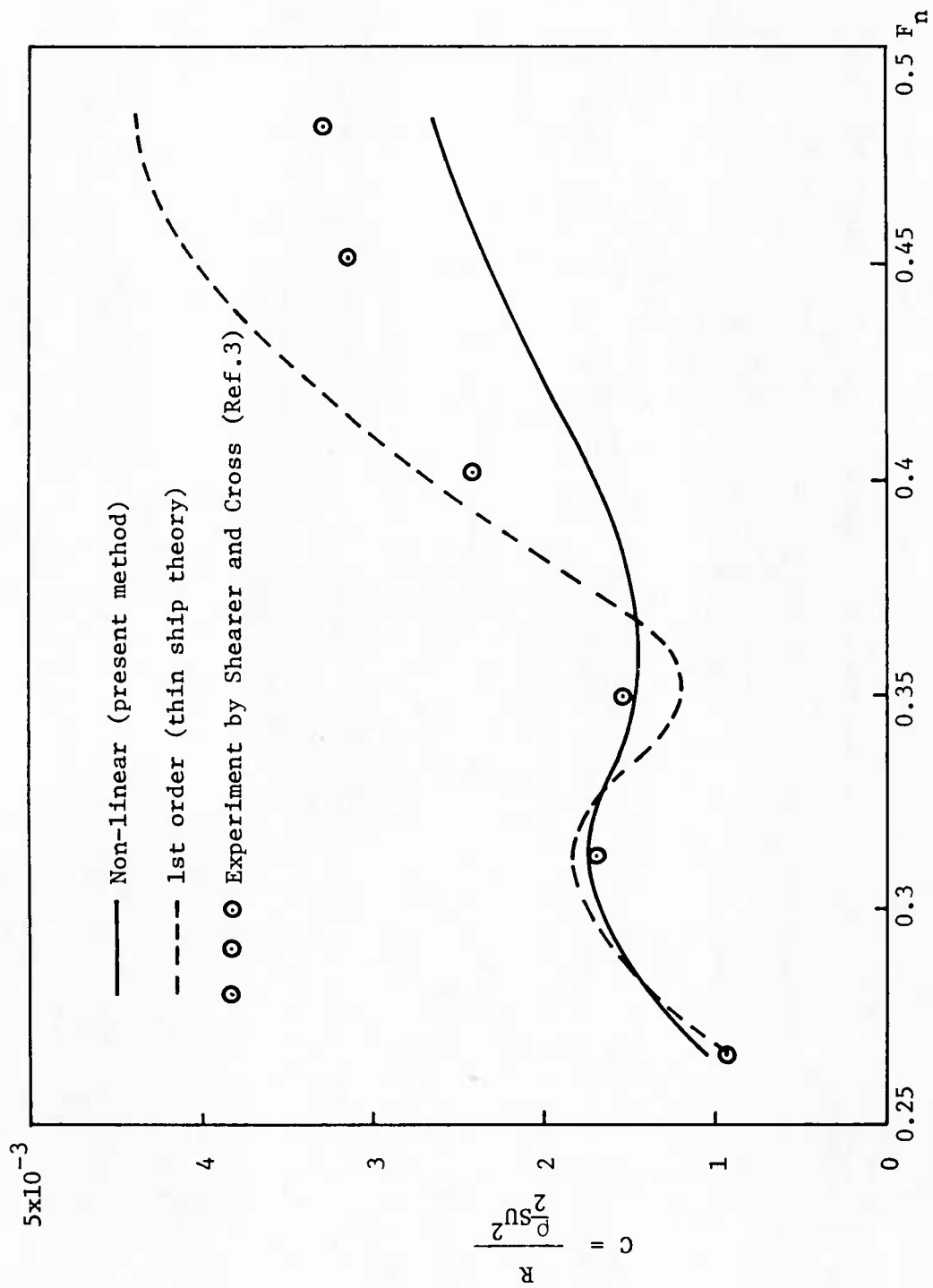


Figure 1 - Wave Resistance Coefficients of Wigley Hull

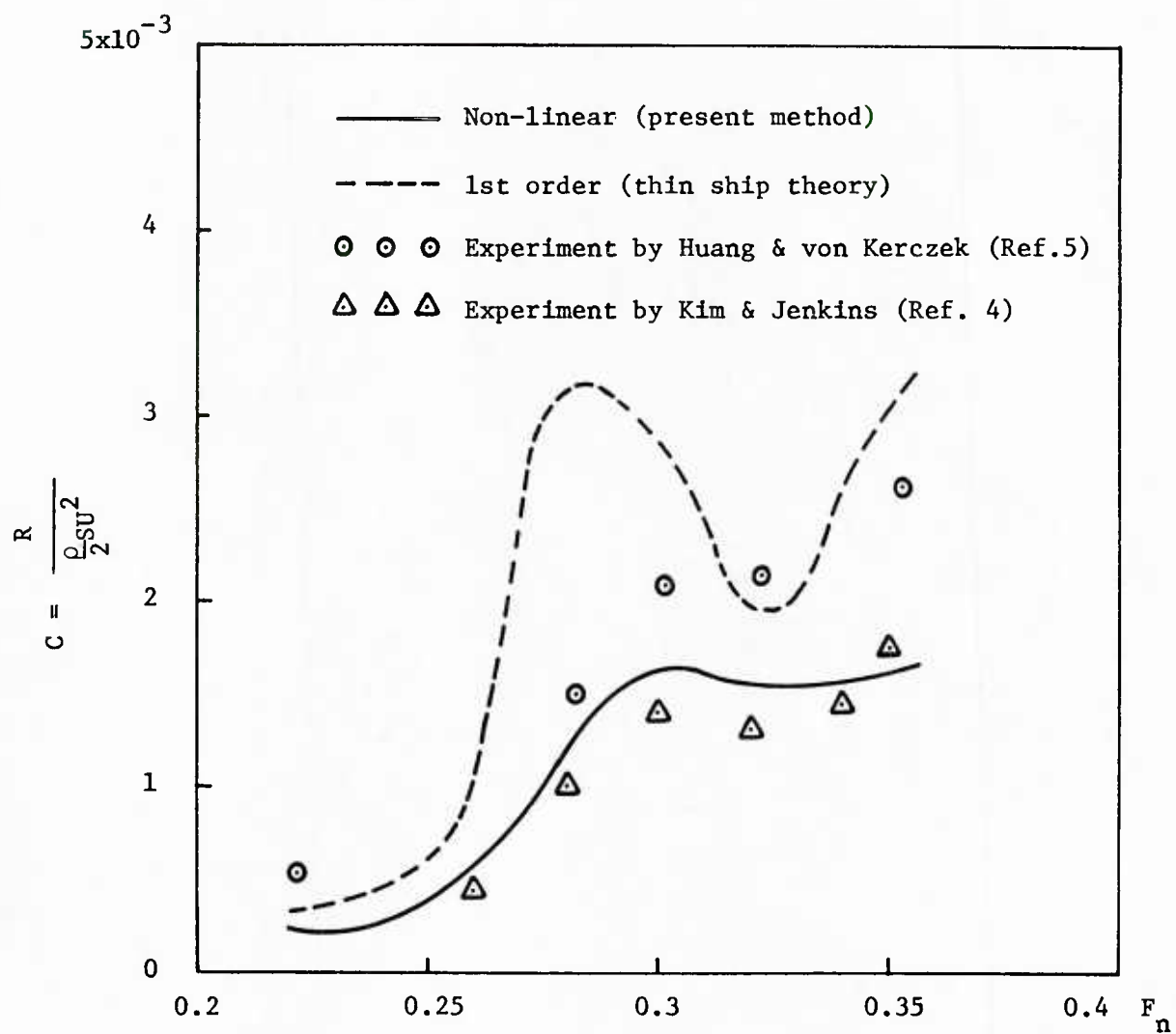


Figure 2 - Wave Resistance Coefficients of Series 60, $C_B=0.6$

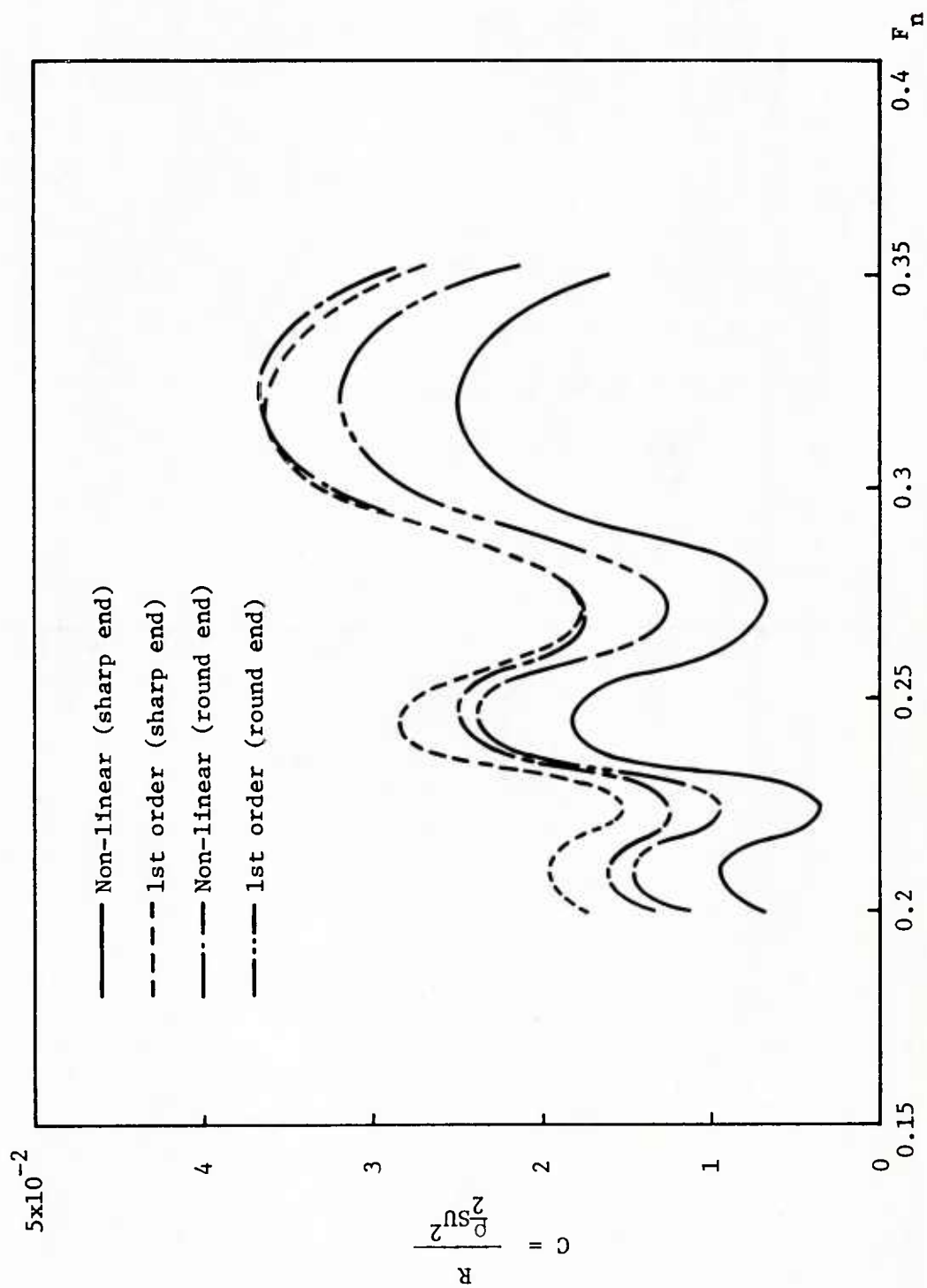


Figure 3 - Wave Resistance Coefficients of Strut-like Hull

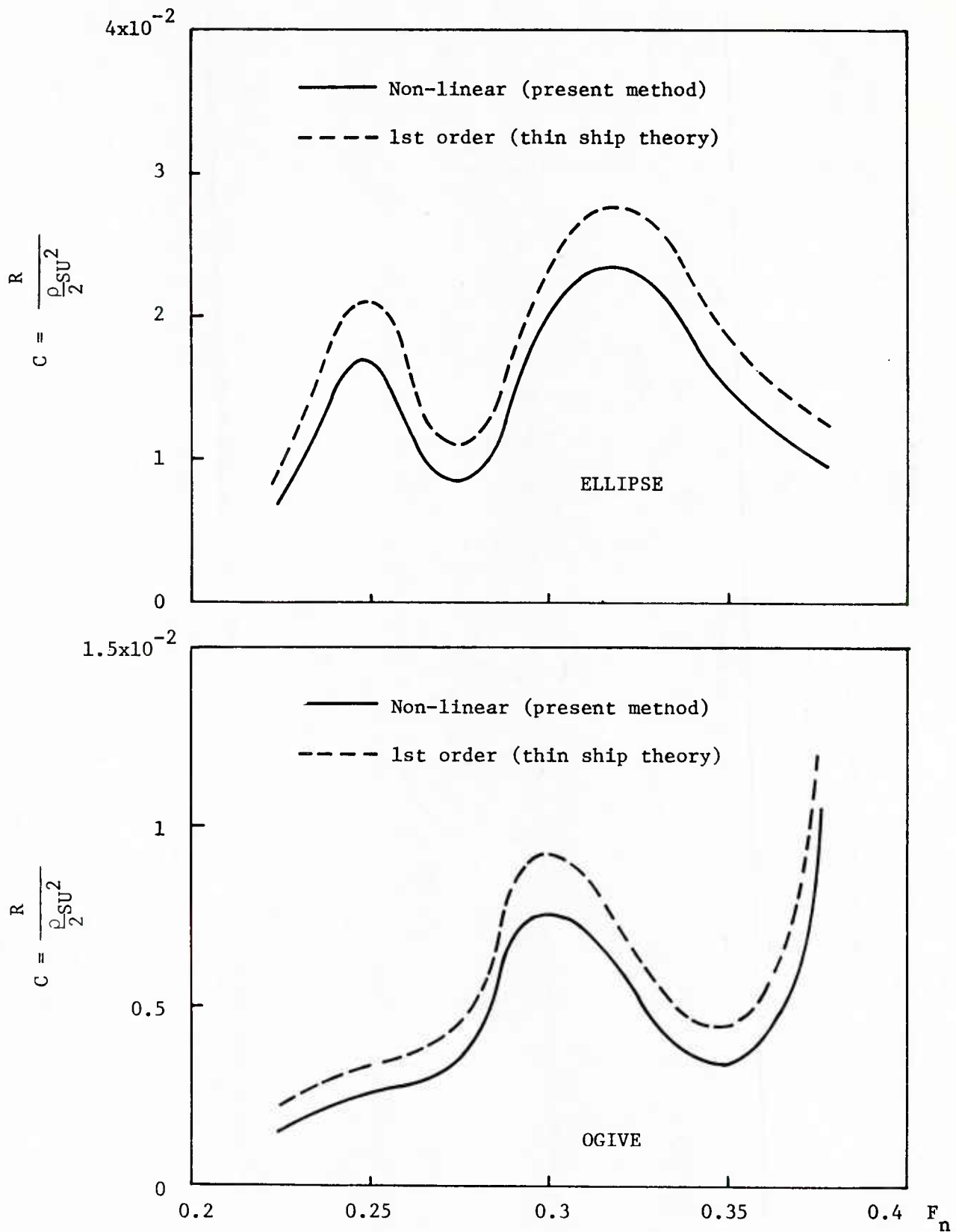


Figure 4 - Wave Resistance Coefficients of Vertical Cylinder

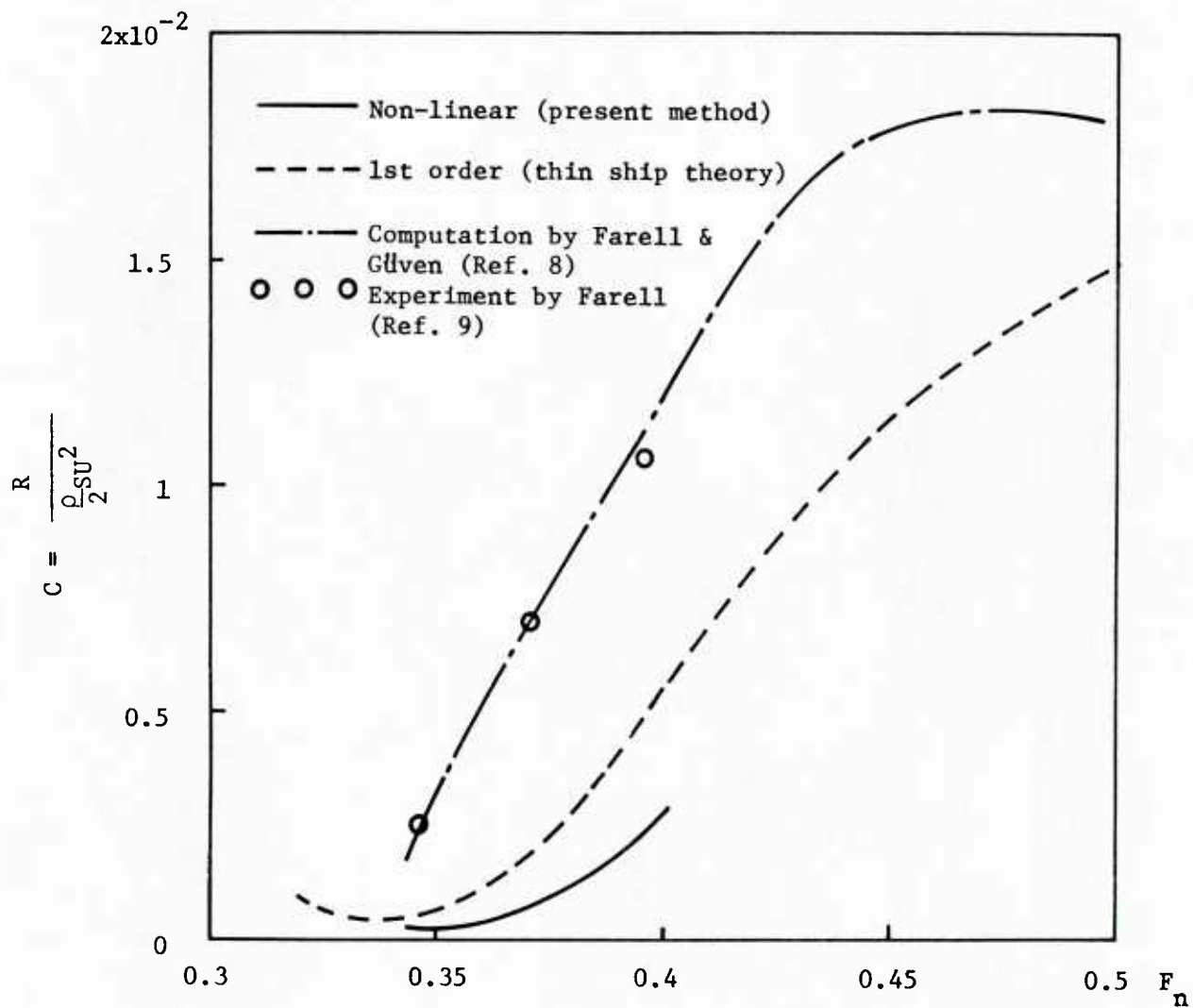


Figure 5 - Wave Resistance Coefficients of Submerged Spheroid

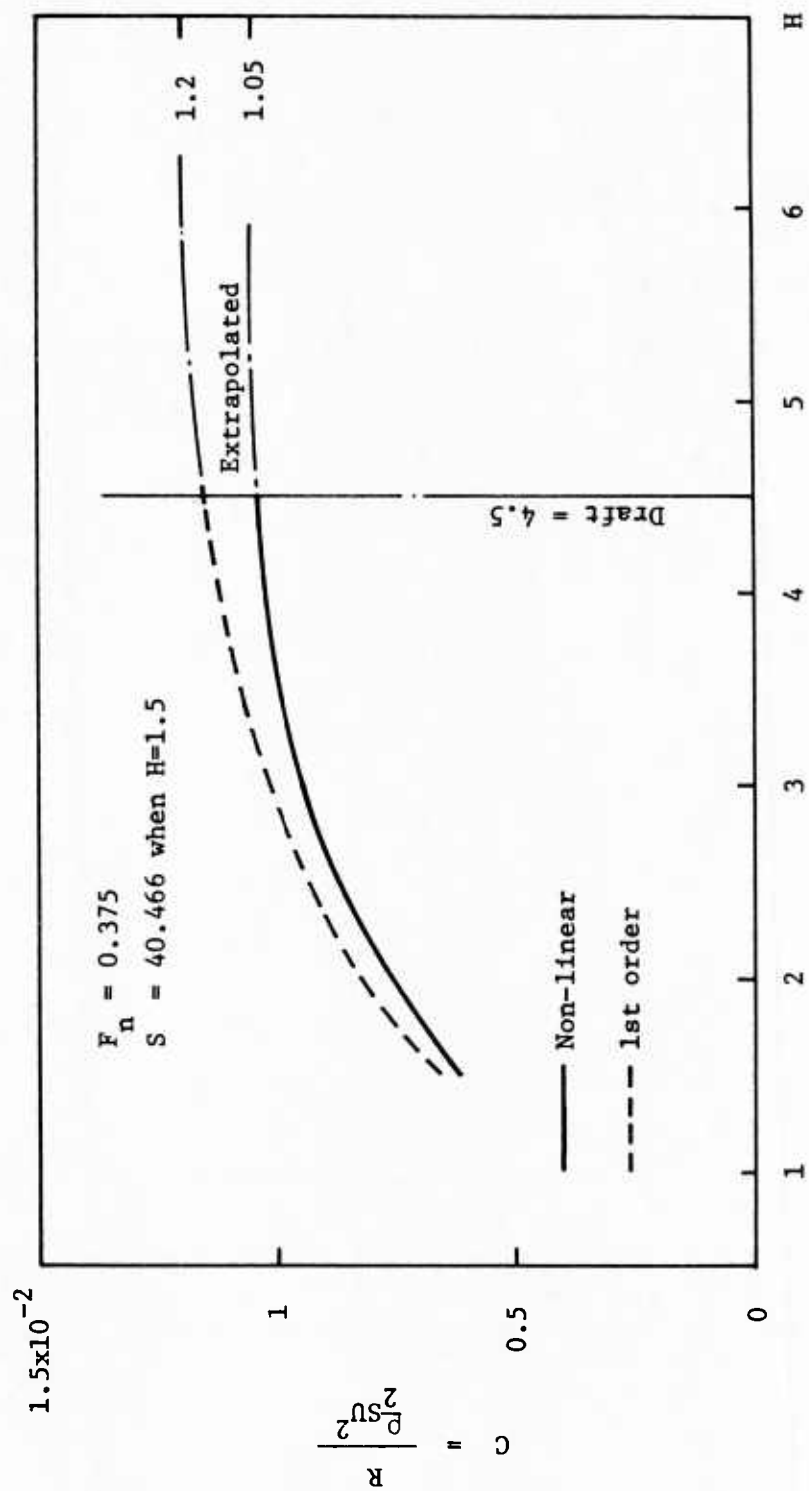


Figure 6 - Wave Resistance Coefficients of Vertical Cylinder (Ogive) as a Function of Draft

Free surface

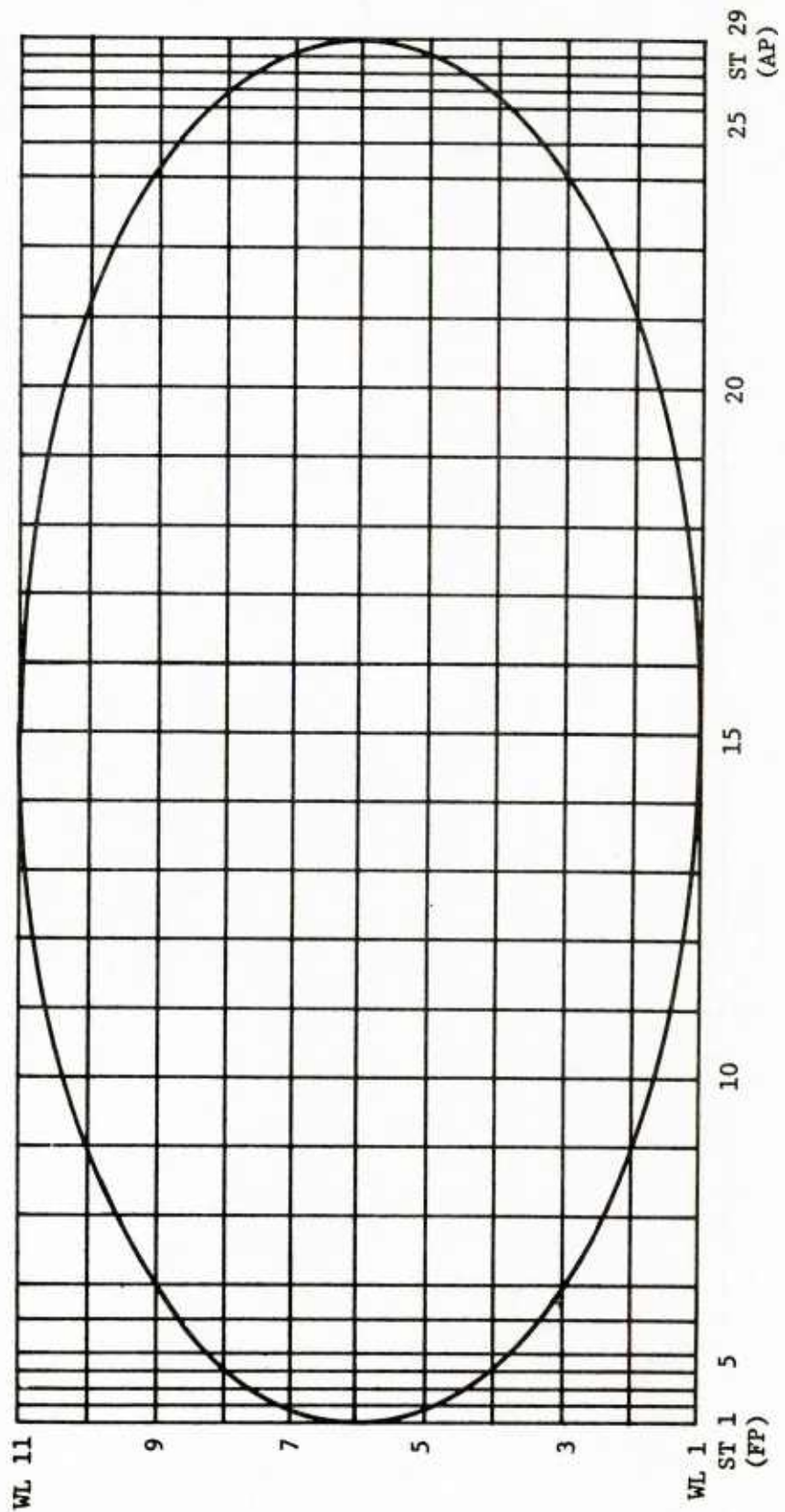


Figure 7 - Center Plane of the Submerged Spheroid

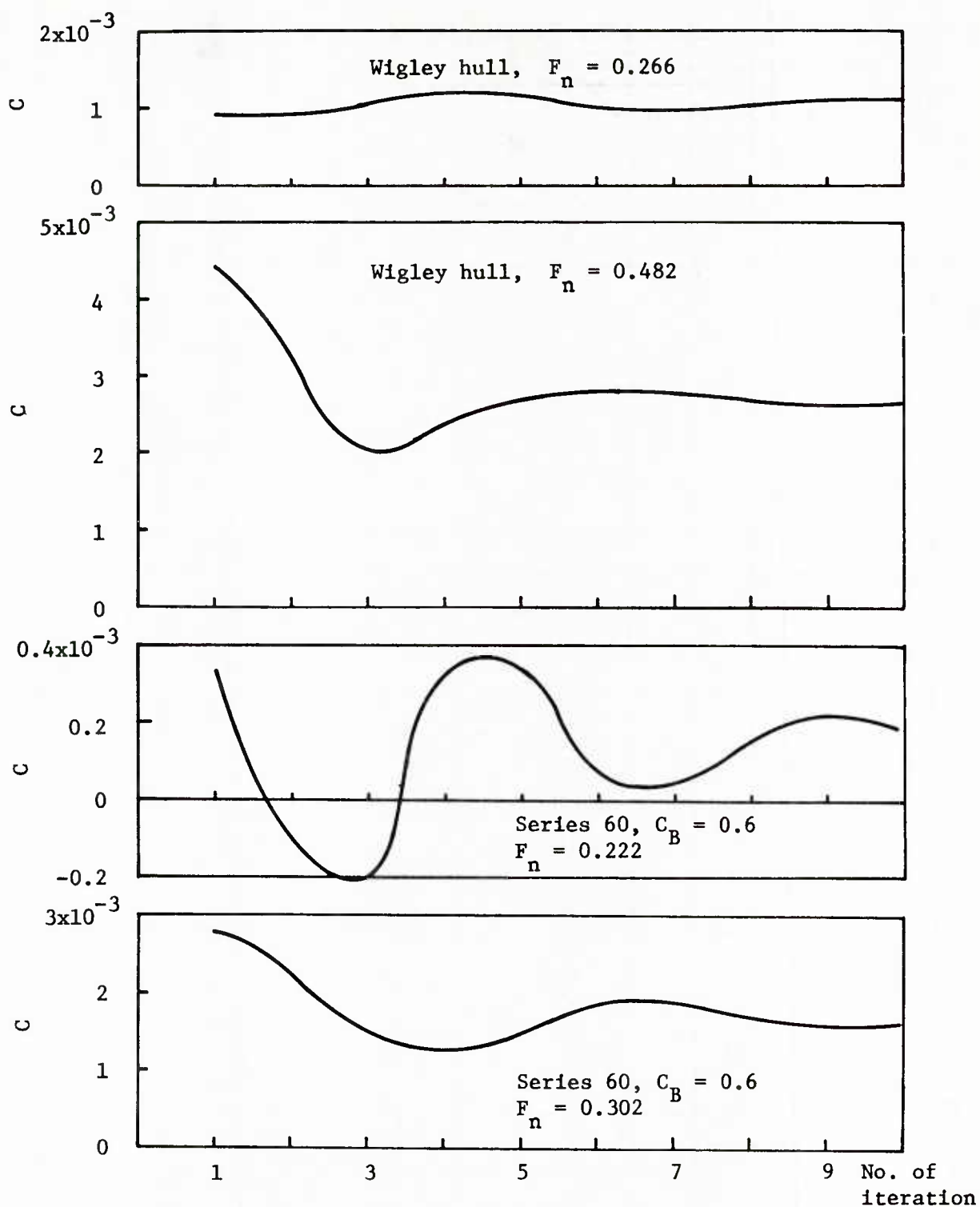


Figure 8 - Wave Resistance Coefficients of Wigley Hull and Series 60, $C_B=0.6$ Hull as a Function of Number of Iteration

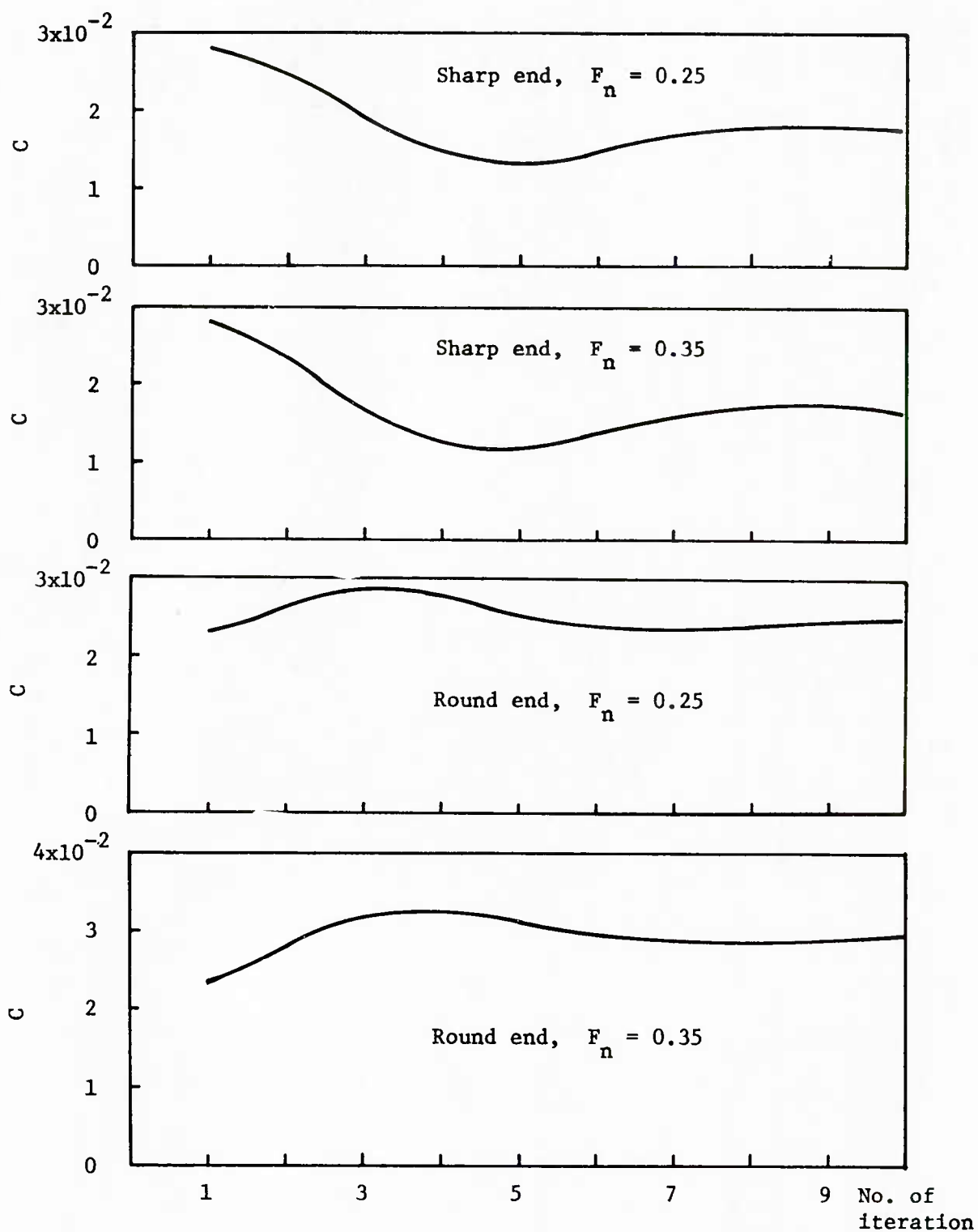


Figure 9 - Wave Resistance Coefficients of Strut-like Hull as a Function of Number of Iteration

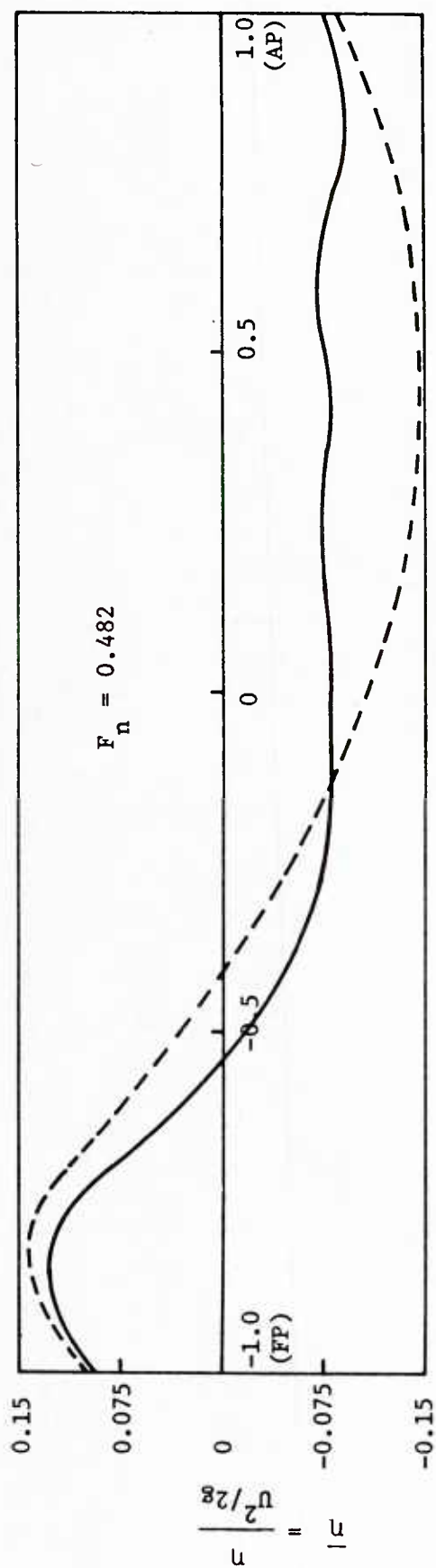
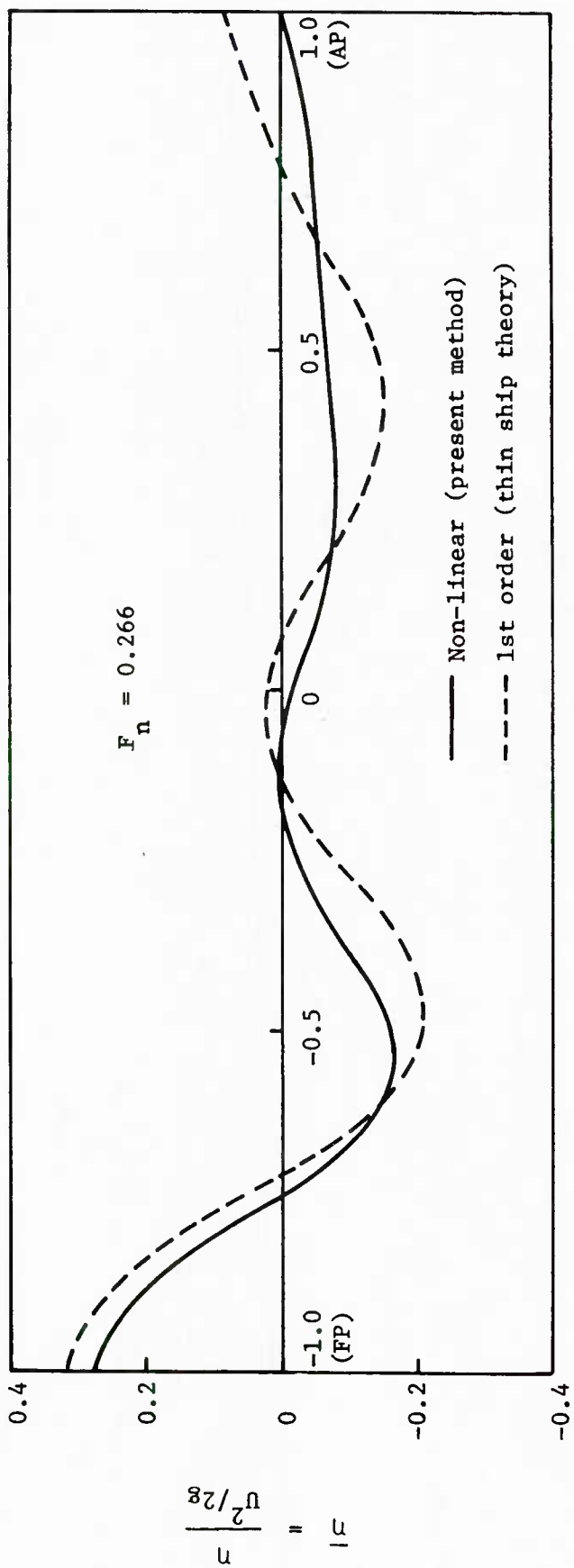


Figure 10 - Wave Elevation of Wigley Hull

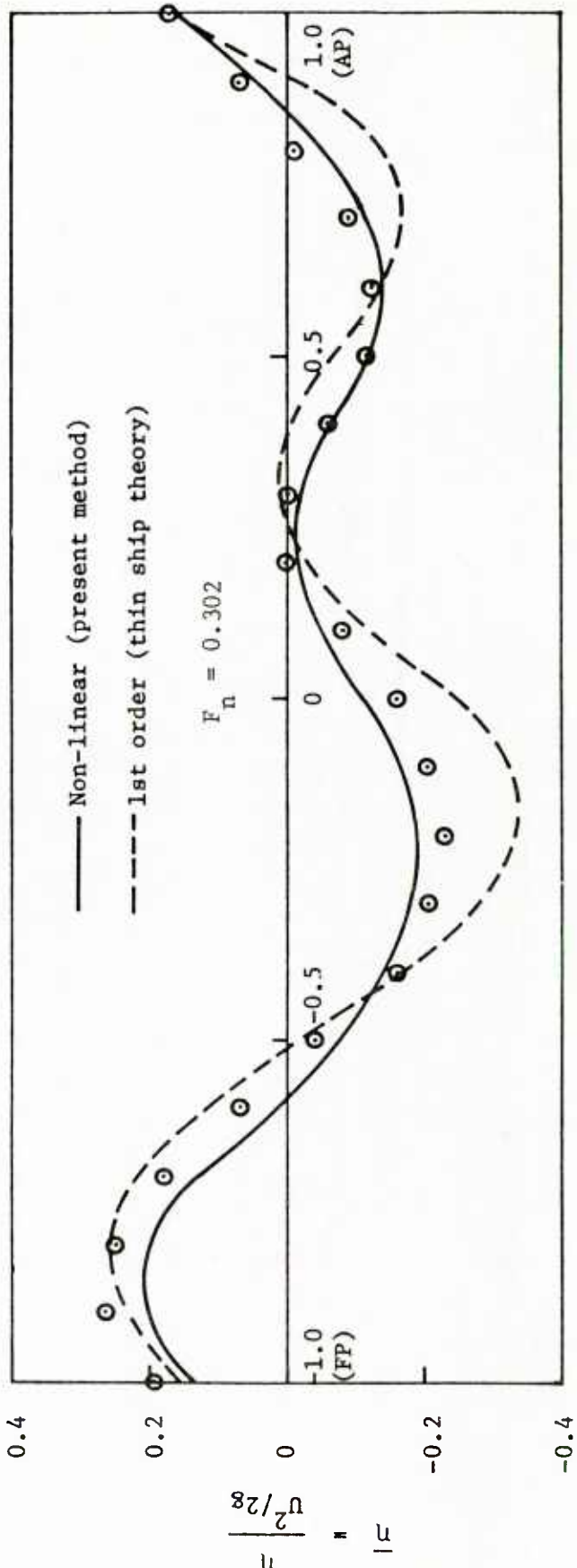
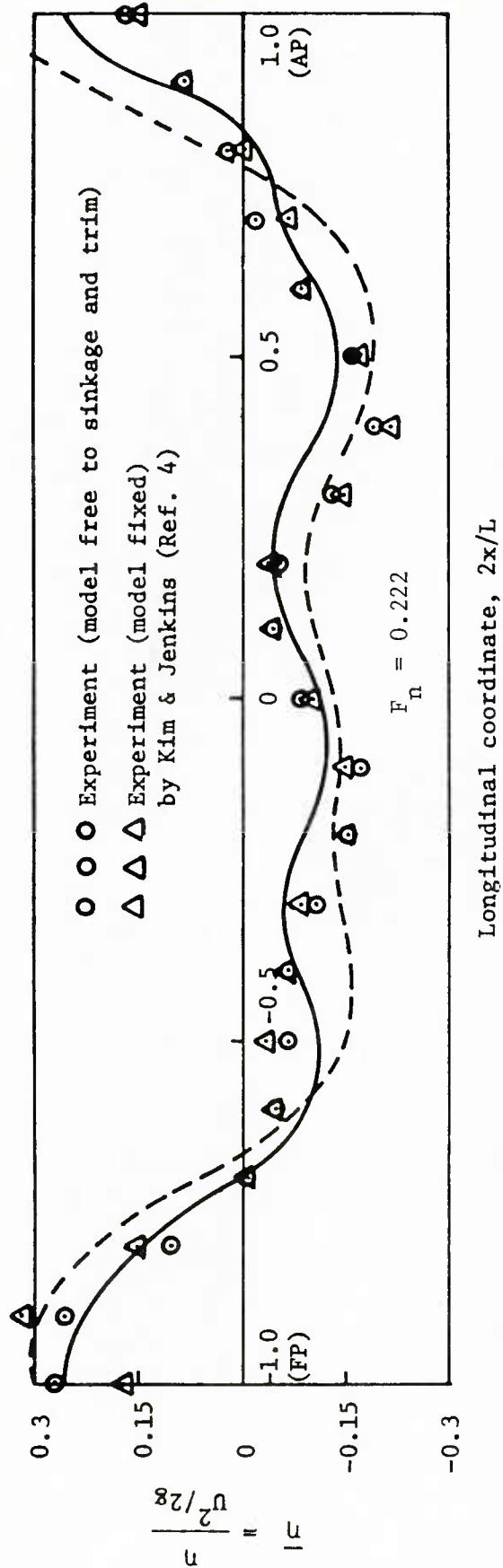


Figure 11 - Wave Elevation of Series 60, $C_B = 0.6$

A Slender-Body Solution for the Centerplane Distribution for the Wigley Ship Form

by

L. Landweber and Sangseon Ju
Iowa Institute of Hydraulic Research
The University of Iowa

Introduction

The Wigley ship form which is being considered in the present Workshop, has the equation

$$|y_p| = f(x,t) = \frac{b}{h^2} (1 - t^2)(h^2 - x^2); \quad |t| \leq 1, \quad |x| \leq h \quad (1)$$

with $b = 0.100$ and $h = 0.125$. This form is slender except near the bow and stern where it becomes thin. Here t , y , and x denote longitudinal, lateral, and vertical coordinates. This unusual notation was chosen so as to reserve $z = x + iy$ as a complex variable. Solutions for the irrotational flow about this double body in a uniform, unbounded stream in the t -direction can be obtained in terms of distributions of sources or the velocity potential on the hull surface. On the other hand, there is no assurance that a solution expressed in terms of a centerplane distribution exists.

If it exists, a centerplane distribution would yield two important advantages. The first is that, in performing subsequent wave-resistance calculations, the difficult evaluation of a singular line integral around the hull contour at $x = 0$ would be avoided. The second is that a procedure for including effects of viscosity on wavemaking resistance [1] could then be directly applied. For these reasons, and because the hydrodynamic problem of proving the existence of a centerplane distribution and developing an algorithm for its calculation is an interesting classical problem, the present investigation was undertaken.

In the present work, we shall present a procedure for determining whether a slender-body solution in terms of a centerplane distribution exists and apply it to the case of the Wigley form (1).

Conformal Mappings of Transverse Sections

The exterior mapping of ogivelike sections into a unit circle will be performed in two stages, of which the first is the transformation which maps the exterior of the ogive, having the same edge angles at $x = \pm h$, into the exterior of the unit circle in a W -plane,

$$\frac{W-1}{W+1} = \left(\frac{z-h}{z+h}\right)^\lambda, \quad \lambda = \frac{\pi/2}{\pi-\alpha}, \quad \tan \alpha = \left|\frac{dy}{dx}\right|_{x=h} \quad (2)$$

This yields a profile without corners, resembling an ellipse, with nearly equal major and minor axes, in the W -plane; see Fig. 1. The exterior of this profile could then be mapped into the exterior of the unit circle by the infinite series $W = \sum_{n=0}^{\infty} a_{2n-1} \zeta^{1-2n}$, but it was found that, for the forms of present interest, a very good approximation could be obtained by truncating the series at $n = 2$, i.e. by

$$W = a_{-1}\zeta + \frac{a_1}{\zeta} + \frac{a_3}{\zeta^3}; \quad \zeta = \rho e^{i\phi}, \quad W = R e^{i\theta} \quad (3)$$

The coefficients of (3) are selected so as to satisfy the conditions

$$W(1) = 1, \quad W(i) = iH, \quad \int \overline{W} dW = 2iS_1$$

where H is obtained from (2) and S_1 is the area of the profile in the W -plane. These yield the equations

$$a_{-1} + a_1 + a_3 = 1, \quad a_{-1} - a_1 + a_3 = H, \quad a_{-1}^2 - a_1^2 - 3a_3^2 = S_1/\pi \quad (4)$$

which can be readily solved for a_{-1} , a_1 and a_3 . Here H is given by

$$H = \cot(\lambda \arctan h/c), \quad c = b(1 - t^2) \quad (5)$$

The transformation (3) has four branch points, obtained from $dW/d\zeta = 0$, at

$$\zeta_B^2 = \frac{1}{2a_{-1}} [a_1 \pm (a_1^2 + 12a_{-1}a_3)^{1/2}] \quad (6)$$

Also the origin 0 in the W-plane maps into the two pairs of conjugate points given by

$$\zeta_0^2 = \frac{1}{2a_{-1}} [-a_1 \pm (a_1^2 - 4a_{-1} a_3)^{1/2}] \quad (7)$$

and shown as O_1, O_2, O_3, O_4 in Fig. 2. The cut in the W-plane given by the path $B_1OB_2OB_3OB_4OB_1$ yields the closed curved path $B_1O_1B_2O_2B_3O_3B_4O_4B_1$ in the ζ -plane which demarcates the region of regularity where the mapping is one-to-one. The curves in the ζ -plane are given by

$$\rho^2 = \frac{1}{2a_{-1}} \{a_1 + [a_1^2 + 4a_{-1}a_3(2 \cos 2\phi + 1)]^{1/2}\}, \quad 0 \leq \phi \leq \phi_{01} \quad (8)$$

$$\rho^2 = \frac{1}{2a_{-1}} \{-a_1 + [a_1^2 - 4a_{-1}a_3(2 \cos 2\phi - 1)]^{1/2}\}, \quad \phi_{01} \leq \phi \leq \frac{\pi}{2} \quad (9)$$

where ϕ_{01} is the argument of ζ_0 in the first quadrant.

The axis ACB of the parabolic section in the z-plane becomes the circular arc ACB (and its mirror image in the real axis) in the W-plane, and then the curve ACB or the pair of curves AC_2 and C_1B according as $\overline{OC} >$ or $< \overline{OB}_2$ in the W-plane. The equation of the circular arc is

$$R = [1 + \tan^2 \beta \sin^2 \theta]^{1/2} - \tan \beta \sin \theta, \quad \beta = \lambda \alpha \quad (10)$$

which gives, when $\theta = \pi/2$,

$$\overline{OC} = \sec \beta - \tan \beta = \cot \frac{\pi^2/4}{\pi - \alpha} \quad (11)$$

Also, putting $\zeta_{B_2} = i\eta_2$, we obtain, by (3) and (4),

$$\overline{OB}_2 = a_{-1}\eta_2 - \frac{a_1}{\eta_2} + \frac{a_3}{\eta_2^2} = \frac{2}{3} (2a_{-1} \eta_2 - \frac{a_1}{\eta_2}) \quad (12)$$

The foregoing condition then becomes

$$\cot \frac{\pi^2/4}{\pi - \alpha} > \text{or} < \frac{2}{3} (2a_{-1} \eta_2 - \frac{a_1}{\eta_2}) \quad (13)$$

We shall see that, when $\overline{OC} < \overline{OB}_2$, it will not be possible to find a solution in terms of an axial distribution alone, although slightly modified sections with the same value of c/h , may have such solutions. This was found to be the case for the parabolic sections of the Wigley form (1) for $|t| < 0.63$. On the assumption that the wavemaking resistance would be insensitive to these slight changes in section shape in the midship part of the form, if the draft and the contour at the free surface were preserved, it was decided, for the midrange, to use the modified forms

$$y = \frac{2y_p}{[(1+\gamma)^2 - 4\gamma x'^2]^{1/2} + 1 - \gamma}, \quad x' = x/h \quad (14)$$

where, by (1), $y_p = c(1-x'^2)$, $c = b(1-t^2)$. This form coincides with y_p when $\gamma = 0$ and becomes the ogive with the same values of c and h when $\gamma = \gamma_0 = c^2/h^2$. For the ogive, however, the transformation from the W to the ζ -plane is $W = z$, which yields no branch points; i.e. $\overline{OB}_2 = 0$. This suggests that, by varying the parameter γ continuously from 0 at the junction with the last parabolic section to c^2/h^2 at the midsection $t = 0$, the condition $\overline{OC} > \overline{OB}_2$ could be satisfied at all the sections, and an exact slender-body centerplane source distribution may be obtained for a slightly modified ship form. The selected relation is

$$\gamma = \frac{b^2}{2h^2} (1 - \tau^2)^2 (2 + \tau^2), \quad \tau = t/t_j \quad (15)$$

where $t = t_j$ at the junction of the parabolic and modified section. This satisfies the continuity conditions that $dy/dt = 0$ at $t = 0$ and t_j and that $\gamma = b^2/h^2$ at $t = 0$ and $\gamma = 0$ at $t = t_j$.

Formulation of Slender-Body Approximation and Its Solution

Let u , v , w and Φ denote the components of the disturbance velocity and the disturbance velocity potential for the ship form in a stream of unit velocity in the t -direction. The boundary condition on the hull surface is then

$$\frac{\partial \Phi}{\partial n} = - \frac{\partial t}{\partial n} = f_t (1 + f_x^2 + f_t^2)^{-1/2}$$

where n denotes distance in the direction of the outward normal to the hull surface. In the direction n' normal to a transverse section (at a fixed value of t), we find

$$\frac{\partial \phi}{\partial n'} = f_t (1 + w)(1 + f_x^2)^{-1/2} \approx f_t (1 + f_x^2)^{-1/2} \quad (16)$$

assuming that $w \ll 1$. If also $\phi_{tt} \ll \phi_{xx}$ and ϕ_{yy} , then we have

$$\phi_{xx} + \phi_{yy} \approx 0 \quad (17)$$

Equations (16) and (17) pose an exterior, two-dimensional Neumann problem. For the Wigley form, (16) becomes

$$(\partial \phi / \partial n')_p = -2bt (1 - x'^2)(1 + 4\gamma_0 x'^2)^{-1/2} \quad (18)$$

and, for the modified form (14), we have

$$f_t = -\frac{4bt (1 - x'^2)}{Q + 1 - \gamma} + \frac{2\gamma' x'^2 y_p}{Q(1 + \gamma - 2\gamma x'^2 + Q)}, \quad f_x = -\frac{2cx'}{hQ}, \quad \gamma' = \frac{d\gamma}{dt} \quad (19)$$

We shall solve this problem for the unit circle in the ζ -plane, where the boundary condition

$$\frac{\partial \phi}{\partial \rho} = \frac{\partial \phi}{\partial n'}, \quad \left| \frac{dz}{dW} \frac{dW}{d\zeta} \right| = F(\phi), \quad \rho = 1 \quad (20)$$

is given by (2) and (3). One can then show that the solution for a source distribution $\sigma(\phi)$ on the contour of the unit circle, obtaining by solving the Fredholm integral equation of the second kind for this exterior Neumann problem, is

$$\sigma = \frac{1}{\pi} [F(\phi) - \frac{M}{2}] = G(\phi, t) / \pi \quad (21)$$

where $2\pi M$ is the total flux through the section. This is the same as the flux through the unit circle, and hence, by (16), the total source strength M is given by

$$M = \frac{1}{\pi} \int_{-h}^h \frac{\partial \phi}{\partial n'} (1 + f_x^2)^{1/2} dx = \frac{1}{\pi} \int_{-h}^h f_t dx = \frac{1}{2\pi} \frac{dS}{dt} \quad (22)$$

where S is the section area. Thus the complex potential $\Omega = \phi + i\psi$ is given by

$$\Omega(\zeta, t) = \frac{1}{\pi} \int_0^{2\pi} G(\phi', t) \ln(\zeta - e^{i\phi'}) d\phi', \quad \rho \geq 1 \quad (23)$$

For the parabolic and modified sections, we find for M

$$M_p = -\frac{8bht}{3\pi} \quad (24)$$

$$M = -\frac{bht}{\pi\gamma} \left[\frac{(1+\gamma)^2}{2\sqrt{\gamma}} \arcsin \frac{2\sqrt{\gamma}}{1+\gamma} - 1 + \gamma \right] + \frac{ch\gamma'}{4\pi\gamma^2} \left[\frac{\gamma^2 - 2\gamma - 3}{2\sqrt{\gamma}} \arcsin \frac{2\sqrt{\gamma}}{1+\gamma} + \gamma + 3 \right] \quad (25)$$

As is well known [2], solutions of the two-dimensional slender-body problem, such as (21), do not satisfy the condition that the potential vanish at infinity. This anomaly is overcome by treating the solution as an inner one which is matched with a three-dimensional outer solution in the method of asymptotic expansions. Here we shall take a different approach. At each transverse section, (23) will be applied to find an equivalent axial distribution of sources, i.e. a distribution along the x-axis, if it exists. Each two-dimensional source element, $m_2 dx$, will then be replaced by its equivalent three-dimensional source element, $m dx dt$, where $m = m_2/2$. This would yield a centerplane distribution of three-dimensional sources, the potential of which vanishes at infinity.

If an axial distribution $m_2(x)$ exists, it is given by

$$m_2 = \frac{1}{\pi} v(x, 0) = -\frac{1}{\pi} \operatorname{Im} \left(\frac{d\Omega}{d\zeta} \frac{d\zeta}{dW} \frac{dW}{dz} \right)_{ACB} \quad (26)$$

where

$$\frac{d\Omega}{d\zeta} = \frac{1}{\pi} \int_{-\pi}^{\pi} G(\phi, t) (\zeta - e^{i\phi'})^{-1} d\phi', \quad \rho \geq 1 \quad (27)$$

Thus, in order to evaluate (26), we must be able to continue the function of a complex variable (27), analytically, into the unit circle to the arc ACB, or the pair of arcs AC_2 and C_1B . In the latter case, the normal component of $d\Omega/d\zeta$ would, by symmetry, have a discontinuity (equal but opposite magnitudes) of the real component along CB_2 in the W-plane, indicating the presence of a source distribution along CB_2 . In the Wigley form, this would yield a distribution on the horizontal centerplane bounded by the internal contour generated by the branch points B_2 and B_4 .

The foregoing result, that the slender-body singularity system is given by a pair of distributions on orthogonal centerplanes, is interesting, but not useful for application to wavemaking calculations, since the Havelock Green function would be singular at the horizontal centerplane. In order to avoid this complication, the section shapes of the Wigley form in its midrange were gradually modified so that the branch points B_2 and B_4 were excluded from the interior of the original section in the z -plane, as was discussed in the previous section.

In order to continue $d\Omega/d\zeta$ into the unit circle, consider the Taylor expansion of the function about an exterior point ζ_0 ,

$$\frac{d\Omega}{d\zeta} = \sum_{n=0}^{\infty} A_n (\zeta - \zeta_0)^n, \quad (28)$$

where, by (27),

$$A_n = \frac{1}{n!} \frac{\partial^{n+1} \Omega(\zeta_0)}{\partial \zeta_0^n} = -\frac{1}{\pi} \int_{-\pi}^{\pi} \frac{G(\phi', t) d\phi'}{(\ell i\phi' - \zeta_0)^{n+1}}, \quad n = 0, 1, 2, \dots \quad (29)$$

The circle of convergence of the series (28) extends until a singularity of the function is encountered. These occur at the branch points, A, B, B_1, B_2, B_3, B_4 . Also, because the imaginary parts of $d\Omega/d\zeta$ at opposite sides of the diameter AB are equal in magnitude but have opposite signs, singularities will be distributed along AB unless this quantity is zero. Substitution into (26) then yields

$$m_2(x, t) = \frac{1}{\pi^2} \sum_{n=0}^{\infty} \int_{-\pi}^{\pi} G(\phi', t) \operatorname{Im} \frac{(d\zeta/dz)(\zeta - \zeta_0)^n}{(\ell i\phi' - \zeta_0)^{n+1}} d\phi' \quad (30)$$

for points ζ on ACB . If the series (30) converges, it can be truncated at a sufficiently large value of $n = N-1$ with negligible error. We then have

$$m_2(x, t) = \frac{\operatorname{Im}}{\pi^2} \left\{ \frac{d\zeta}{dW} \frac{dW}{dz} \int_{-\pi}^{\pi} \frac{G(\phi', t)}{\ell i\phi' - \zeta} \left[1 - \left(\frac{\zeta - \zeta_0}{\ell i\phi' - \zeta_0} \right)^N \right] d\phi' \right\} \quad (31)$$

The resulting value of m_2 must be independent of both ζ_0 and N .

Numerical Evaluation

In order to evaluate m (or $m = \frac{1}{2} m_2$), the various factors of (31) were first expressed in polar form and combined to yield the imaginary part. The result, for large values of N , was a real, oscillatory integrand of very large amplitude for $E = |(\zeta - \zeta_0)/(e^{i\phi} - \zeta_0)| > 1$.

At each value of t , the integral was computed by Simpson's rule with 1000 points for five different points ζ_0 . With each ζ_0 , values of the integral were obtained for a succession of values of N , beginning with $N = 20$. Eventually, for $N > 100$, some values of E became so large that, even with double precision, the differences between the ordinates of the quadrature formula were meaningless. It was found, however, that, for most points of the arc ACB, the integral yielded a consistent value of m_2 , independent of ζ_0 and N , before the limitation of computer accuracy had been reached. Least accurate results were obtained near the keel point B. These were corrected by smoothing the values of m_2 , using a least-squares cubic-spline fit. The smoothed set of values of $m(x,t)$ are given in Table 1 and graphed in Figs. 3 and 4.

The accuracy of the values of m_2 was verified by computing the corresponding values of $\partial\phi/\partial n'$ from the axial distribution and comparing the results with the exact slender-body boundary condition. The agreement was greatly improved by the smoothing, which gave an error of less than 0.02 percent.

Graphs of the centerplane distribution at various horizontal sections are shown in Fig. 4. The nonzero values of $m(x',1)$ shown in the figure are a consequence of the smoothing procedure. Actually, $m(x,t)$ must approach zero as $t \rightarrow 1$, but with an infinite slope at $t = 1$, a sharp approach to zero occurring for t very close to 1.

Near the extremities of the body, where the transverse sections are thin, and near the keel, the slender-body distribution agrees well with the second-order thinship solution. Closer to the free-surface level, $x' = 0$, the results by the two methods are seen to differ greatly.

In the continuation of this work, the present slender-body distribution will be substituted into an iteration formula for solving the integral equation [1] for the modified Wigley form to obtain, at least, a second approximation.

References

1. T. Miloh and L. Landweber, "Ship Centerplane Source Distribution", Journal of Ship Research, Vol. 24, No. 1, Mar. 1980.
2. J.N. Neuman, Marine Hydrodynamics, The MIT Press, Cambridge, Massachusetts, 1977.

Acknowledgement

This work was supported by the Office of Naval Research under Contract Nos. N00014-82-K-0069 (NR-062-183) and N00014-83-K-0136.

Table 1 - Slender Body Centerplane Source Distribution for
Wigley Model with $b/h = 0.8$ and $l/b = 10$.

x'	$t = 0.05$	$t = 0.15$	$t = 0.25$	$t = 0.35$	$t = 0.45$	$t = 0.55$	$t = 0.65$	$t = 0.75$	$t = 0.85$
0.00000	-0.02601	-0.07155	-0.10231	-0.11269	-0.10970	-0.09308	-0.07237	-0.05374	-0.04060
0.02500	-0.02541	-0.06962	-0.09909	-0.10913	-0.10639	-0.09094	-0.07146	-0.05347	-0.04052
0.05000	-0.02372	-0.06445	-0.09063	-0.09986	-0.09779	-0.08533	-0.06900	-0.05271	-0.04031
0.07500	-0.02121	-0.05696	-0.07876	-0.08699	-0.08592	-0.07745	-0.06538	-0.05150	-0.03994
0.10001	-0.01810	-0.04805	-0.06532	-0.07263	-0.07280	-0.06851	-0.06098	-0.04990	-0.03944
0.12500	-0.01464	-0.03866	-0.05213	-0.05890	-0.06042	-0.05968	-0.05621	-0.04796	-0.03880
0.15000	-0.01105	-0.02957	-0.04067	-0.04748	-0.05038	-0.05196	-0.05139	-0.04574	-0.03802
0.17500	-0.00752	-0.02107	-0.03099	-0.03824	-0.04249	-0.04535	-0.04664	-0.04328	-0.03711
0.20000	-0.00420	-0.01335	-0.02274	-0.03067	-0.03617	-0.03963	-0.04202	-0.04067	-0.03608
0.22500	-0.00126	-0.00656	-0.01562	-0.02420	-0.03079	-0.03456	-0.03758	-0.03796	-0.03495
0.25000	0.00112	-0.00087	-0.00931	-0.01831	-0.02575	-0.02992	-0.03340	-0.03520	-0.03373
0.27500	0.00285	0.00360	-0.00355	-0.01255	-0.02059	-0.02553	-0.02953	-0.03246	-0.03242
0.30000	0.00397	0.00695	0.00161	-0.00702	-0.01536	-0.02137	-0.02592	-0.02975	-0.03104
0.32500	0.00462	0.00936	0.00608	-0.00188	-0.01029	-0.01745	-0.02257	-0.02708	-0.02959
0.35000	0.00492	0.01098	0.00974	0.00268	-0.00560	-0.01376	-0.01943	-0.02448	-0.02807
0.37500	0.00499	0.01198	0.01250	0.00645	-0.00148	-0.01035	-0.01649	-0.02193	-0.02648
0.40000	0.00493	0.01251	0.01430	0.00931	0.00189	-0.00721	-0.01371	-0.01946	-0.02485
0.42500	0.00479	0.01265	0.01528	0.01137	0.00459	-0.00435	-0.01109	-0.01709	-0.02318
0.45000	0.00459	0.01250	0.01566	0.01279	0.00673	-0.00176	-0.00863	-0.01481	-0.02148
0.47500	0.00436	0.01213	0.01565	0.01375	0.00843	0.00056	-0.00635	-0.01265	-0.01978
0.50000	0.00410	0.01162	0.01546	0.01438	0.00981	0.00262	-0.00424	-0.01061	-0.01810
0.52500	0.00386	0.01104	0.01524	0.01485	0.01096	0.00441	-0.00229	-0.00871	-0.01644
0.55000	0.00362	0.01042	0.01499	0.01517	0.01190	0.00597	-0.00051	-0.00693	-0.01482
0.57500	0.00340	0.00976	0.01465	0.01532	0.01265	0.00730	0.00112	-0.00525	-0.01320
0.60000	0.00317	0.00908	0.01418	0.01529	0.01318	0.00842	0.00260	-0.00367	-0.01158
0.62500	0.00293	0.00841	0.01352	0.01506	0.01351	0.00936	0.00396	-0.00214	-0.00994
0.65000	0.00269	0.00774	0.01266	0.01464	0.01365	0.01014	0.00518	-0.00068	-0.00829
0.67500	0.00245	0.00709	0.01164	0.01404	0.01358	0.01075	0.00627	0.00070	-0.00666
0.70000	0.00222	0.00648	0.01056	0.01332	0.01334	0.01118	0.00718	0.00196	-0.00510
0.72500	0.00200	0.00591	0.00951	0.01251	0.01293	0.01142	0.00791	0.00305	-0.00365
0.75000	0.00179	0.00539	0.00857	0.01165	0.01235	0.01148	0.00841	0.00393	-0.00234
0.77500	0.00161	0.00494	0.00780	0.01078	0.01163	0.01134	0.00869	0.00462	-0.00123
0.80000	0.00143	0.00451	0.00715	0.00990	0.01083	0.01103	0.00879	0.00513	-0.00022
0.82500	0.00127	0.00407	0.00653	0.00898	0.00998	0.01058	0.00877	0.00556	0.00074
0.85000	0.00111	0.00359	0.00587	0.00804	0.00918	0.01004	0.00870	0.00600	0.00176
0.87500	0.00095	0.00302	0.00507	0.00704	0.00846	0.00942	0.00866	0.00651	0.00291
0.90000	0.00077	0.00236	0.00410	0.00600	0.00784	0.00874	0.00861	0.00709	0.00419
0.92500	0.00059	0.00165	0.00301	0.00486	0.00708	0.00779	0.00826	0.00740	0.00522
0.95000	0.00040	0.00096	0.00192	0.00358	0.00587	0.00635	0.00723	0.00703	0.00558
0.97500	0.00020	0.00035	0.00092	0.00212	0.00391	0.00419	0.00510	0.00556	0.00480
1.00000	0.00000	0.00000	0.00000	0.00000	0.00000	0.00000	0.00000	0.00000	0.00000

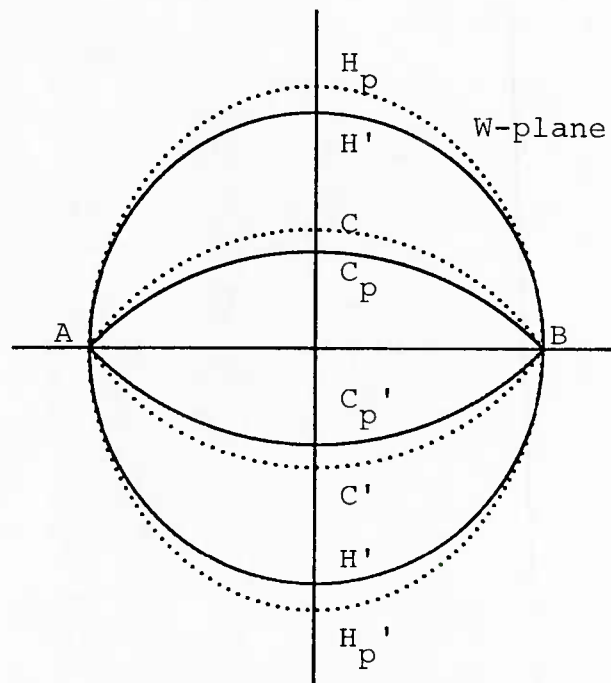
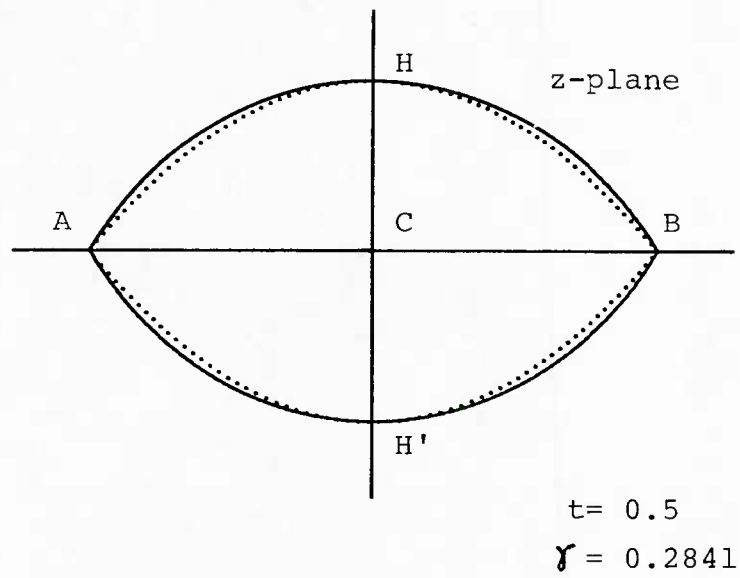


Figure 1 - Mapping of Parabolic and Modified Sections by Ogive Transformation.

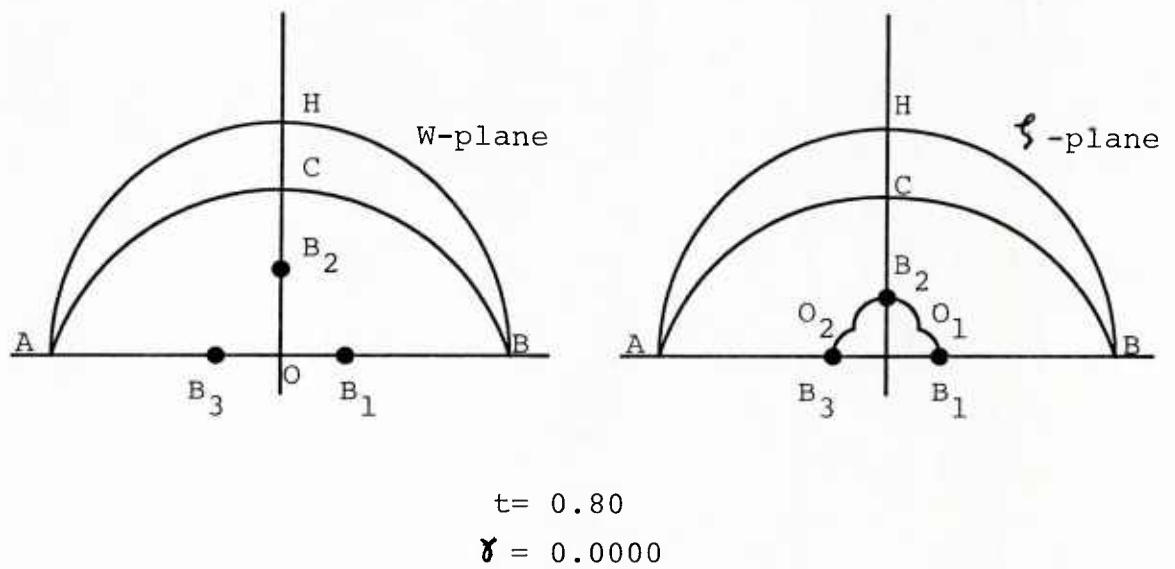
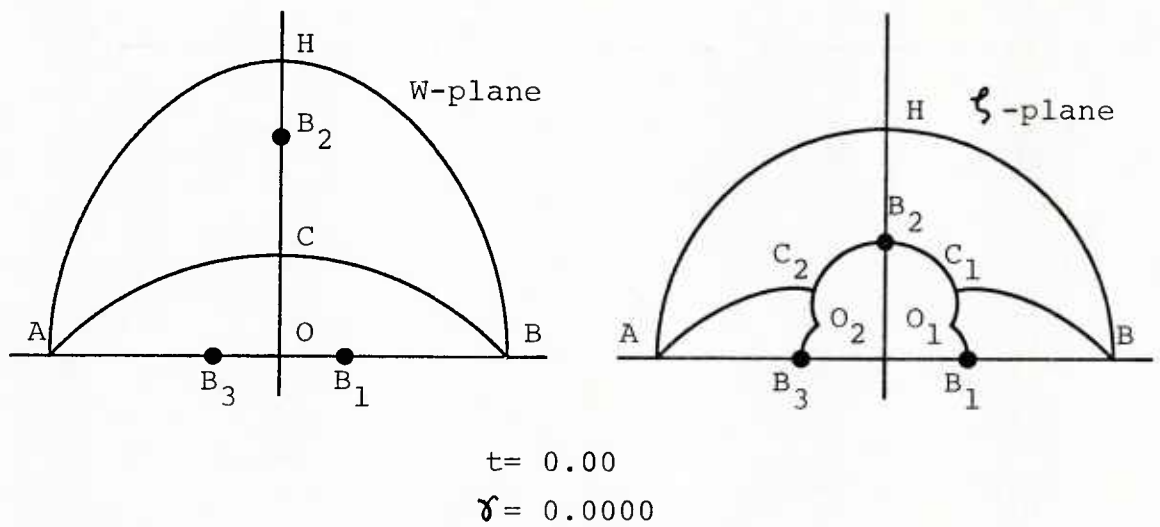


Figure 2 - Transformation of Section in W-plane into a Unit Circle, Showing Mappings of Cuts between Branch Points.

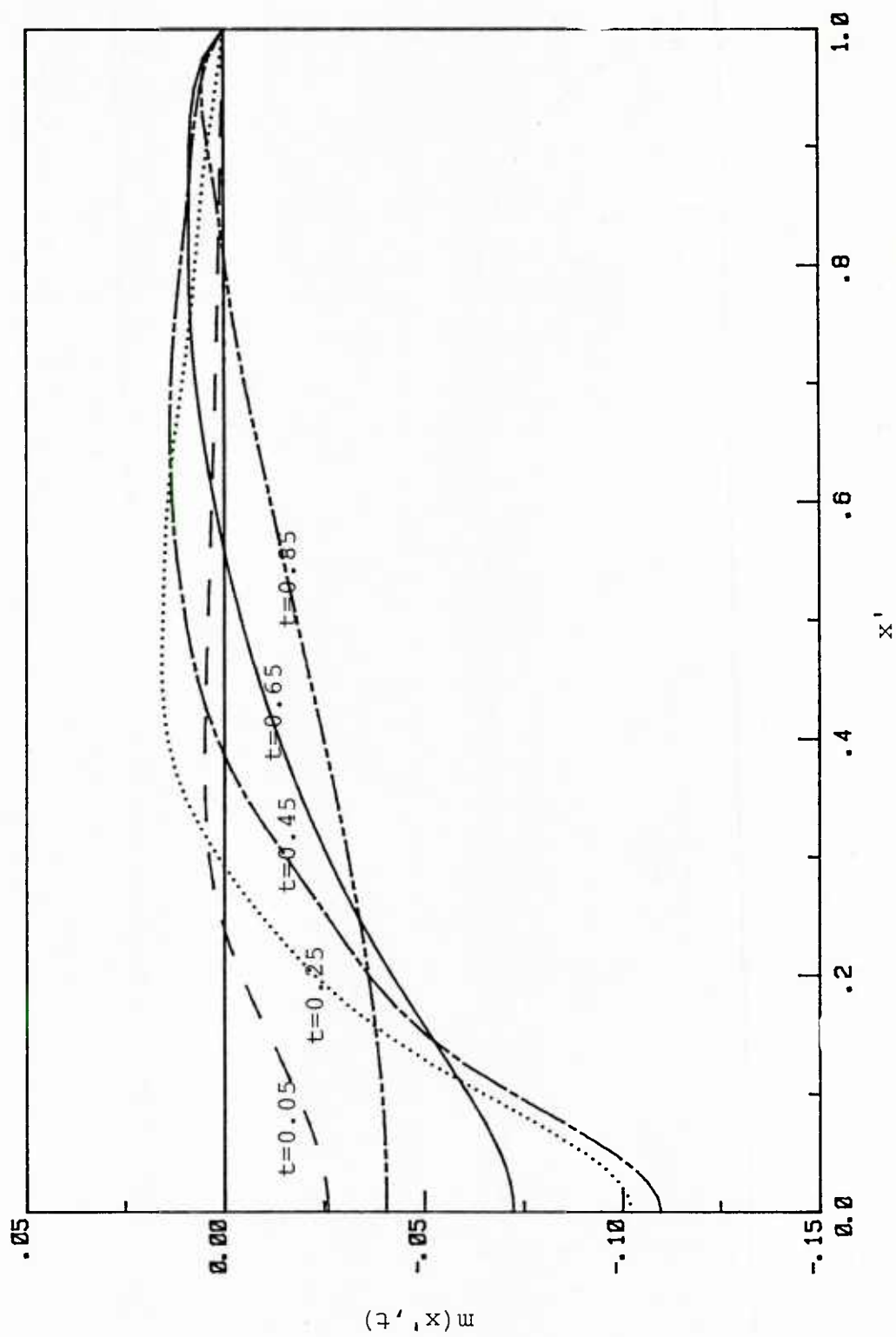


Figure 3 - Centerplane Source Distributions at Various Transverse Sections.

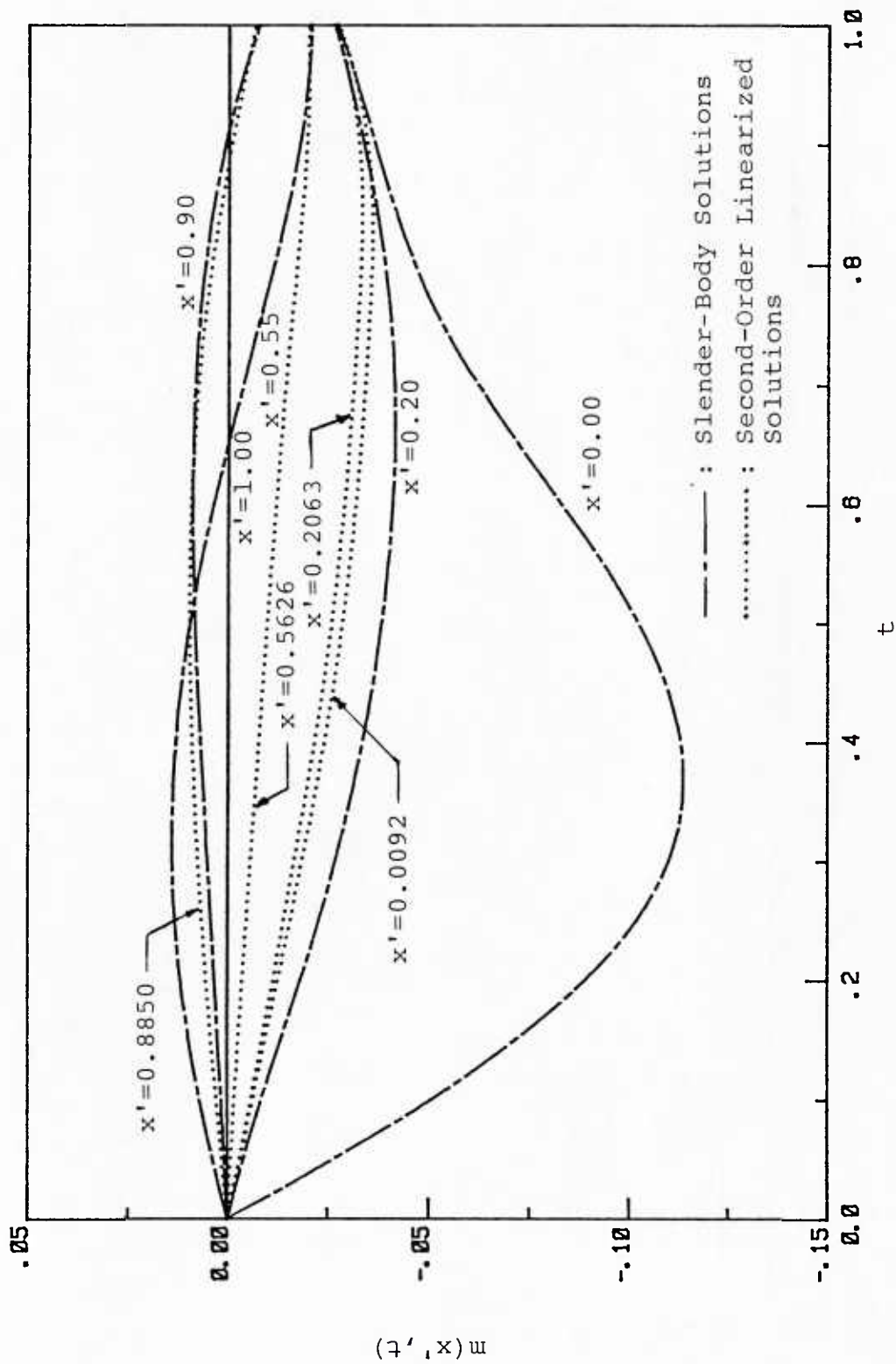


Figure 4 - Centerplane Source Distributions at Various Horizontal Sections Compared with Second-Order Linearized Solutions.

The Second Workshop on Ship Wave Resistance Computations

An Application of New Slender Ship Theory to Series 60, $C_b = 0.60$.

by

H. Maruo and M. Ikehata

I. Introduction

A new approach to solve the flow around a slender ship with forward velocity was presented and wave resistance was formulated newly by one of the authors in 1982¹⁾. This new slender ship theory is based on the asymptotic expression of the Kelvin-source, that is the kernel function of the Neumann-Kelvin problem, around its track. The solution of the boundary value problem is equivalent to an approximation to the Neumann-Kelvin problem. The normal velocity on the hull surface is determined by an integral equation of the second kind of the Volterra type instead of one of the Fredholm type of the Neumann-Kelvin problem. It is solvable numerically by the marching procedure without great time-consuming matrix calculations. This method is expected to enable the numerical computation of the flow field around the hull of a ship to be more accurate even with the limited capacity of today's computers.

Some numerical results for Series 60, $C_b = 0.6$, hull are presented in this paper. The wave pattern and wave resistance are computed at two Froude numbers, 0.267 and 0.304. These results are better than those of Michell's theory in comparison with measured results. However, it costs much time to compute not only wave resistance but also wave pattern over some range of Froude numbers. More improvements are strongly desired in the numerical procedure.

Let us begin with the digest of this new slender ship theory for the convenience of explanation.

2. Digest of the New Slender Ship Theory¹⁾

2.1 Asymptotic expression of the Kelvin-source around its track

Consider a uniform flow of velocity U in the positive direction of x axis with the origin on the still water surface, y axis horizontally perpendicular to the x axis and the z axis vertically downwards. As is well known, the velocity potential of a source at the point $x = x'$, $y = y'$, $z = z'$, under the free surface for the linearized condition, the Kelvin-source, is given by

$$G = -\frac{1}{r} + \frac{1}{r'} + G' \quad (1)$$

where

$$r = \sqrt{(x - x')^2 + (y - y')^2 + (z - z')^2} \quad (2)$$

$$r' = \sqrt{(x - x')^2 + (y - y')^2 + (z + z')^2}$$

$$G' = \frac{2k_0}{\pi} \int_{-\pi/2}^{\pi/2} \sec^2 \theta \, d\theta \int_0^\infty \frac{t \cos t\bar{z} - k_0 \sec^2 \theta \sin t\bar{z}}{t^2 + k_0^2 \sec^4 \theta} \exp[-t|\bar{x} \cos \theta + \bar{y} \sin \theta|] dt \quad (3)$$

$$-4 k_0 \int_{\theta_1}^{\pi/2} e^{-k_0 \bar{z} \sec^2 \theta} \sin(k_0 \bar{x} \sec \theta + k_0 \bar{y} \sec \theta \tan \theta) \sec^2 \theta \, d\theta, \text{ for } \bar{y} > 0$$

where $k_0 = g/U^2$

$$\bar{x} = x - x', \bar{y} = y - y', \bar{z} = z + z' \quad (4)$$

$$\theta_1 = \tan^{-1}(-\bar{x} / \bar{y}), -\pi/2 < \theta_1 < \pi/2 \quad (5)$$

In order to derive the asymptotic expression of G' around the \bar{x} axis, let $|\bar{y}|$ and $|\bar{z}|$ tend to zero. The double integral term of (3) becomes

$$\begin{aligned} & \frac{2k_0}{\pi} \int_{-\pi/2}^{\pi/2} \sec^2 \theta \, d\theta \int_0^\infty \frac{t \exp(-t|\bar{x}| \cos \theta)}{t^2 + k_0^2 \sec^4 \theta} dt \\ &= -\frac{2}{|\bar{x}|} + \pi k_0 \{H_1(k_0 |\bar{x}|) - Y_1(k_0 |\bar{x}|) - \frac{2}{\pi}\} \end{aligned} \quad (6)$$

where H_1 is the Struve function and Y_1 is the Bessel function. The single integral term of (3) approaches

$$\begin{aligned}
 & -4k_0 \int_{-\pi/2}^{\pi/2} e^{-k_0 \bar{z} \sec^2 \theta} \sin(k_0 \bar{x} \sec \theta + k_0 \bar{y} \sec \theta \tan \theta) \sec^2 \theta d\theta \\
 & = -8k_0 \int_1^\infty e^{-k_0 \bar{z} u^2} \sin(k_0 \bar{x} u) \cos(k_0 \bar{y} u \sqrt{u^2 - 1}) \frac{u}{\sqrt{u^2 - 1}} du \\
 & \approx -8\sqrt{k_0} \int_0^\infty e^{-\bar{z} v^2} \sin(\bar{x} \sqrt{k_0} v) \cos(\bar{y} v^2) dv + \frac{8}{\bar{x}} + 4\pi k_0 Y_1(k_0 \bar{x}) \quad (7)
 \end{aligned}$$

for $\bar{x} > 0$ and vanishes for $\bar{x} < 0$. Hence, the asymptotic expression of G' may be written in the form

$$\begin{aligned}
 G' \approx & \pi k_0 H_1(k_0 |x - x'|) + \{\pi k_0 Y_1(k_0 |x - x'|) + 2|x - x'|^{-1}\} \{1 + 2 \operatorname{sgn}(x - x')\} \\
 & - 2k_0 - 4\sqrt{k_0} E(\bar{x}, \bar{y}, \bar{z}) \{1 + \operatorname{sgn}(x - x')\} \quad (8)
 \end{aligned}$$

where

$$E(\bar{x}, \bar{y}, \bar{z}) = \int_0^\infty e^{-\bar{z} v^2} \sin(\bar{x} \sqrt{k_0} v) \cos(\bar{y} v^2) dv \quad (9)$$

The term of E represents the diverging wave, while the transverse wave is represented by $4\pi k_0 Y_1(k_0 \bar{x})$. Other terms are symmetric in \bar{x} and represent local disturbances.

2.2 Velocity potential for the slender ship

Put a slender ship in the uniform stream, with the origin of the coordinate system at the intersection of the bow with the free surface and the x axis in the center plane of the ship, positive astern. We assume the irrotational motion of an inviscid incompressible fluid.

With the velocity potential in the form $Ux + \phi$, the disturbance velocity potential ϕ can be given the following expression according to the Green's third formula, under the condition of the linearized free surface.

$$\phi = \frac{1}{4\pi} \int \int_S \left(\frac{\partial \phi}{\partial n} G - \phi \frac{\partial G}{\partial n} \right) dS \quad (10)$$

where S is the hull surface below the still water, n is the outward normal on the surface and G is of course the Kelvin-source given by (1).

Put $\phi = \phi_1 + \phi_2$ corresponding to $G = (-1/\gamma + 1/\gamma') + G'$. On account of the assumption of a slender ship, introducing the asymptotic expression (8) of G' , the expressions for ϕ_1 and ϕ_2 near the hull can be written as follows:

$$\phi_1 = \frac{1}{4\pi} \int_{C(x)} \left(\frac{\partial \phi_1}{\partial \nu} - \phi_1 \frac{\partial}{\partial \nu} \right) \ln \frac{(y - y')^2 + (z - z')^2}{(y - y')^2 + (z + z')^2} ds(y', z') \quad (11)$$

$$\begin{aligned} \phi_2 = & \frac{1}{4\pi} \int_0^L dx' [\pi k_0 H_1(k_0 |x - x'|) - 2k_0 \\ & + \{\pi k_0 Y_1(k_0 |x - x'|) + 2|x - x'|^{-1}\} \{1 + 2 \operatorname{sgn}(x - x')\}] \int_{C(x')} V_n ds \\ & - \frac{\sqrt{k_0}}{\pi} \int_0^x dx' \int_{C(x')} \left(\frac{\partial \phi_1}{\partial \nu} - \phi_1 \frac{\partial}{\partial \nu} \right) E(\bar{x}, \bar{y}, \bar{z}) ds \end{aligned} \quad (12)$$

where $C(x)$ is the contour of the hull surface at each transverse section at x , $ds(y', z')$ is the length element on $C(x)$, ν is the normal drawn outwards to $C(x)$, and

$$\partial \phi_1 / \partial \nu = V_n \quad (13)$$

The potential ϕ_1 diminishes at infinity in the fashion like a dipole and vanishes at $z = 0$, while $E(\bar{x}, \bar{y}, \bar{z})$ is a plane harmonic function in the lower half space vanishing at infinity. By Green's reciprocal theorem,

$$\begin{aligned} & \int_{C(x')} \left(\frac{\partial \phi_1}{\partial \nu} - \phi_1 \frac{\partial}{\partial \nu} \right) E(\bar{x}, \bar{y}, \bar{z}) ds \\ & = -2 \int_{b(x')}^{\infty} V_z(x', y') E(\bar{x}, \bar{y}, z) dy' \end{aligned} \quad (14)$$

where $b(x') =$ the half breadth of waterline,

$$V_z(x, y) = \frac{\partial \phi_1}{\partial z} \Big|_{z=0} \quad (15)$$

Therefore, ϕ_2 becomes

$$\begin{aligned}\phi_2 = & \frac{1}{4\pi} \int_0^L dx' [\pi k_0 H_1(k_0 |x - x'|) - 2k_0 \\ & + \{\pi k_0 Y_1(k_0 |x - x'|) + 2|x - x'|^{-1}\} \{1 + 2\text{sgn}(x - x')\}] \int_{C(x')} v_n ds \\ & + \frac{2\sqrt{k_0}}{\pi} \int_0^x dx' \int_{b(x')}^{\infty} V_z(x', y') E(x - x', y - y', z) dy' \quad (16)\end{aligned}$$

Next we consider the boundary value problem. The boundary condition on the hull surface is given by

$$\frac{\partial \phi_1}{\partial v} = -Un_x - \frac{\partial \phi_2}{\partial v} \quad (17)$$

for a slender ship. n_x is the x-component of the outward normal unit vector on the hull surface.

If we put

$$V_n = -Un_x - \frac{\partial \phi_2}{\partial v} \quad (18)$$

(17) coincides with (13). The second term $\partial \phi_2 / \partial v$ denotes the effect of the free surface.

To solve this boundary value problem by the conformal mapping, let us define the complex number $Z = y + iz$ and $\zeta = \xi + i\eta$. We consider a mapping function $Z = f(\zeta)$ which maps the lower half region $z \geq 0$ and exterior to $C(x)$ onto the lower half region $\eta \geq 0$ and exterior to a unit circle in the ζ -plane, as shown in Fig. 1.

The normal velocity V_n on $C(x)$ in Z -plane is transformed to v_n on the unit circle in the ζ -plane.

$$v_n(\psi) = V_n \left| \frac{dZ}{d\zeta} \right|_{\zeta = e^{i\psi}} = V_n |f'(e^{i\psi})| \quad (19)$$

Considering antisymmetry of ϕ_1 with respect to z and ψ , ϕ_1 can be expressed in terms of $v_n(\psi)$ as

$$\phi_1 = \frac{1}{\pi} \int_0^\pi v_n(\psi') \ln \left| \frac{\zeta - e^{i\psi'}}{\zeta - e^{-i\psi'}} \right| d\psi' \quad (20)$$

The vertical velocity V_z can then be derived from (20) and (15) as

$$V_z = \frac{-2}{\pi |f'(\xi)|} \int_0^\pi v_n(\psi') \frac{\sin \psi'}{\xi^2 + 1 - 2\xi \cos \psi'} d\psi' \quad (21)$$

Substituting (21) into (16) and taking the normal derivative, we obtain the normal velocity due to ϕ_2 .

$$\frac{\partial \phi_2}{\partial v} = -I_m \frac{2\sqrt{k_0}}{\pi} \int_0^x dx' \int_1^\infty V_z \frac{E_Z^* \{x - x', f(e^{i\psi}) - f(\xi)\} e^{i\psi}}{|f'(e^{i\psi})|} f'(\xi) d\xi \quad (22)$$

where I_m means the imaginary part, E_Z^* is $\partial E^* / \partial Z$ and

$$E^*(\bar{x}, Z) = -i \int_0^\infty e^{iv^2 Z} \sin(\sqrt{k_0} \bar{x}) dv \quad (23)$$

From (18), (19), (21) and (22), the boundary condition may be written in the form

$$v_n = -\ln_x |f'(e^{i\psi})| + I_m \frac{2\sqrt{k_0}}{\pi} \int_0^x dx' \int_1^\infty E_Z^* \{x - x', f(e^{i\psi}) - f(\xi)\} f'(\xi) d\xi \\ \times \left\{ \frac{-2}{\pi |f'(\xi)|} \int_0^\pi v_n(\psi') \frac{\sin \psi'}{\xi^2 + 1 - 2\xi \cos \psi'} d\psi' \right\} \quad (24)$$

This is an integral equation for v_n as a function of x and ψ . Since it is of the Volterra type with respect to x , the marching procedure can be effectively applied to the numerical solution.

2.3 Wave profile and wave resistance

The free surface elevation is determined by Bernoulli's theorem and the condition of constant pressure.

$$H = -\frac{1}{g} \left\{ U \frac{\partial \phi}{\partial x} + \frac{1}{2} \left\{ \left(\frac{\partial \phi}{\partial y} \right)^2 + \left(\frac{\partial \phi}{\partial z} \right)^2 \right\} \right\}_{z=0} \quad (25)$$

The formulas (20) for ϕ_1 and (16) for ϕ_2 show that the quadratic terms in (25) concern only the singular part of the potential.

The wave resistance can be determined by the Havelock's formula

$$R_w = 16 \pi \rho k_0^2 \int_1^\infty |H(u)|^2 \frac{u^2}{\sqrt{u^2 - 1}} du \quad (26)$$

where $H(u)$ is the Kochin function defined by

$$H(u) = \frac{1}{4\pi} \iint_S \left(\frac{\partial \phi_1}{\partial n} - \phi_1 \frac{\partial}{\partial n} \right) \exp(-k_0 z u^2 + i k_0 x u + i k_0 y \sqrt{u^2 - 1}) dS \quad (27)$$

Employing similar relations to (7) and (14) then the wave resistance is given by the following

$$\begin{aligned} R_w = & \frac{2}{\pi} \rho k_0^2 \int_0^\infty \left| \int_0^L dx \int_{b(x)}^\infty V_z(x, y) \exp(i k_0 x \sqrt{v} + i k_0 y v) dy \right|^2 dv \\ & + \frac{1}{\pi} \rho \int_0^L dx \int_{C(x)} V_n ds \int_0^L dx' \int_{C(x')} V_n ds \left[\frac{1}{(x - x')^2} - \frac{\pi}{2} k_0^2 Y_0 \{k_0(x - x')\} \right] \\ & + \frac{\pi k_0}{2(x - x')} Y_1 \{k_0(x - x')\} \end{aligned} \quad (28)$$

The first term on the right hand side is the resistance due to the diverging wave and the second term is that due to the transverse wave.

3. Numerical Results of Application to Series 60

The numerical procedure is shown in the flow chart, Fig. 2. First of all, the mapping function $f(\zeta)$ must be determined at each section of the ship. Next, the solution of the integral equation (24) yields $v_n(\psi)$. Once $v_n(\psi)$ is solved, V_z , V_n , ϕ_1 and ϕ_2 are derived successively. These enable the wave profile H and the wave resistance R_w to be calculated.

We take the length of the ship to be a unit and use the well-known three parameter form²⁾ as the function $f(\zeta)$.

$$f(\zeta) = p(\zeta + a_1 \zeta^{-1} + a_3 \zeta^{-3} + a_5 \zeta^{-5}) \quad (29)$$

The coefficients p , a_1 , a_3 and a_5 which were selected by Ogiwara and the authors³⁾ are available. These are shown in Fig. 3, together with the body plans of the

original hull form and of the three-parameter form. The calculations of $v_n(\psi, x)$ and $V_z(x, y)$ have been carried out for forty one sections shown in Fig. 3. At the bow, $V_n(\psi, 0)$ can easily be shown to be

$$v_n(\psi, 0) = - U n_x |f'(e^{i\psi})| \quad (30)$$

At the second section, the contribution due to $v_n(\psi, 0)$ in the second term of equation (24) should be added to $- U n_x |f'(e^{i\psi})|$. At the subsequent sections, all contributions due to $v_n(\psi, x')$, $x' < x$, should be added in a similar procedure.

We have chosen three Froude numbers, 0.00, 0.267 and 0.304, for the first examples because of the limitation of cost and time. The longitudinal distributions of $v_n(\psi, x)$ along the curve of $\psi = 9^\circ$ are shown in Fig. 4, and the sectional distributions at the two sections are given in Fig. 5. The results for $F_n = 0.267$ deviate more than those for $F_n = 0.304$ from those for zero Froude number.

The normal velocity V_n on the frame line and the vertical velocity V_z on the load water-line are both easily calculated from v_n . The wave resistance has been obtained by integration of (28), with V_z and V_n substituted at two Froude numbers only. These are given in the first column in Table 1. There are three other wave resistance coefficients referred to in Table 1 for comparison. One is a computation of the Michell integral by Suzuki-Kanagawa. The others are towing-test and wave analysis results with a 3-m ship model at the Yokohama National University Ship Model Basin. Fig. 6 shows the comparison. Both points of the present theory are closer to the curve of towing test results than the Michell integral; but they are still too high.

If we take into account a correction for a finite draft of the Kelvin-source in calculating the transverse wave term by

$$\left(\frac{1}{T} \int_0^T e^{-k_0 z} dz \right)^2 \approx \left(1 - \frac{1}{2} k_0 T \right)^2 \quad (31)$$

the coefficients of wave resistance computed are reduced to 1.60×10^{-3} at $F_n = 0.304$ and to 1.35×10^{-3} at $F_n = 0.267$. This is an improvement.

The wave profile alongside the hull is shown in Figs. 7 and 8, and the wave pattern in Figs. 9 and 10. The agreement with measurement is seen to be fairly good

in comparison of the wave profiles in Figs. 7 and 8. If the transverse wave were corrected by the effect of a finite draft of the Kelvin-source, we would get better agreement. In the present computation, the free-surface elevation was calculated directly by numerical differentiation of the total velocity potential ϕ in three directions, so that we could not separate the transverse wave for correction.

It is seen in the wave-pattern comparisons of Figs. 9 and 10, that the computed heights of all crests exceed twice of the measured ones. Apart from this, the two wave patterns resemble each other well.

4. Concluding Remarks

We have obtained promising results by applying a new slender-ship theory. Another merit of this theory is that it avoids the inconsistent treatment of the Neumann-Kelvin approximation. It is necessary to improve the numerical procedure for time saving in order to collect more results of application.

References

1. Maruo, H.: New approach to the theory of slender ships with forward velocity, Bulletin of the Faculty of Engineering Yokohama National University, Vol. 31, March 1982.
2. Landweber, L. and Macagno, M.: Added mass of a three-parameter family of two dimensional forms oscillating in a free surface, Journal of Ship Research, Vol. 2, No. 4, March 1959.
3. Ogiwara, S., Maruo, H. and Ikehata, M.: On the method for calculating the approximate solution of source distribution over the hull surface, Journal of the Society of Naval Architects of Japan, Vol. 126, December 1969.

Table 1 Wave Resistance Coefficients of Series 60, $C_b = 0.60$

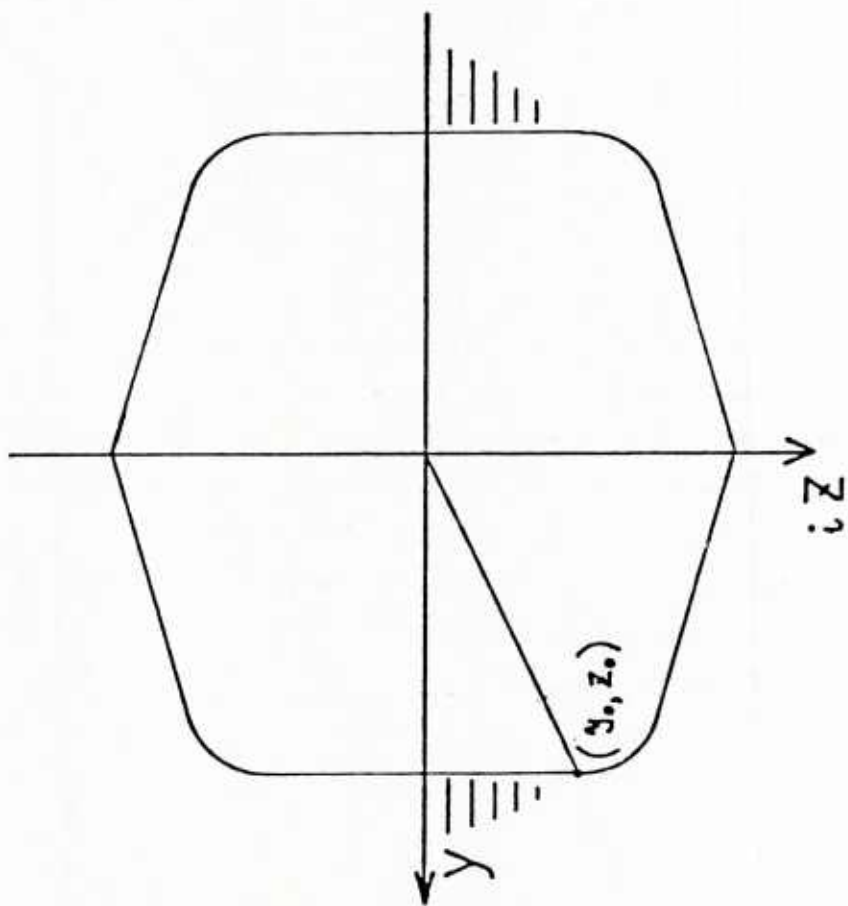
$$C_w \times 10^3 = \frac{R_w}{\frac{1}{2} \rho V^2 S} \times 10^3$$

Froude Number	Computation		Experiment	
	Maruo's NSST(2)	Michell Integral(3)	Towing Test(4)	Wave Analysis(5)
0.22		0.56		
0.23		0.74		
0.234		0.72	0.30	
0.244		0.67	0.39	
0.253		1.06	0.39	0.15
0.259		1.70	0.56	
0.267	2.29	2.57		
0.271		2.99	0.75	0.31
0.280		3.69	0.97	0.52
0.290		3.93	1.38	
0.299		3.62	1.62	0.79
0.304	2.46	3.34		
0.308		3.11	1.86	0.77
0.318		2.58	1.78	
0.327		2.32	1.73	0.79
0.336		2.42	1.77	
0.345		2.84	2.01	
0.354			2.26	1.14

Remarks:

- (1) Measured by Model, of which particulars are
 $L_{pp} = 3\text{m}$, $B = 0.400\text{ m}$, $d = 0.16\text{m}$, $\nabla = 0.11632\text{ m}^3$, $S = 1.535\text{ m}^2$.
- (2) New Slender Ship Theory developed by Maruo, 1982.
- (3) Interpolated values at testing Froude Numbers from Suzuki-Kanagawa's calculation.
- (4) $C_w = C_T - (1+k) C_{f0}$, where C_T is total resistance coefficient, k is form factor (0.27 determined) and C_{f0} is Schoenherr's frictional resistance coefficient.
- (5) By longitudinal cut at $y/L_{pp} = 1.33$.

Z - plane



ξ - plane

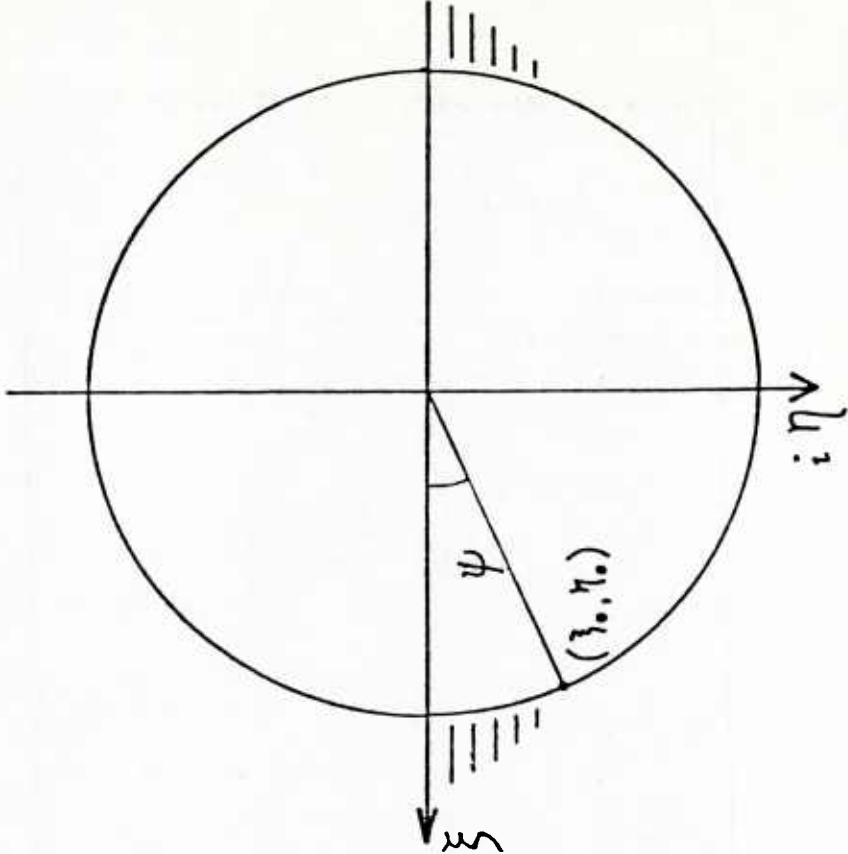


Fig. 1 Correspondence between Z and ξ Planes

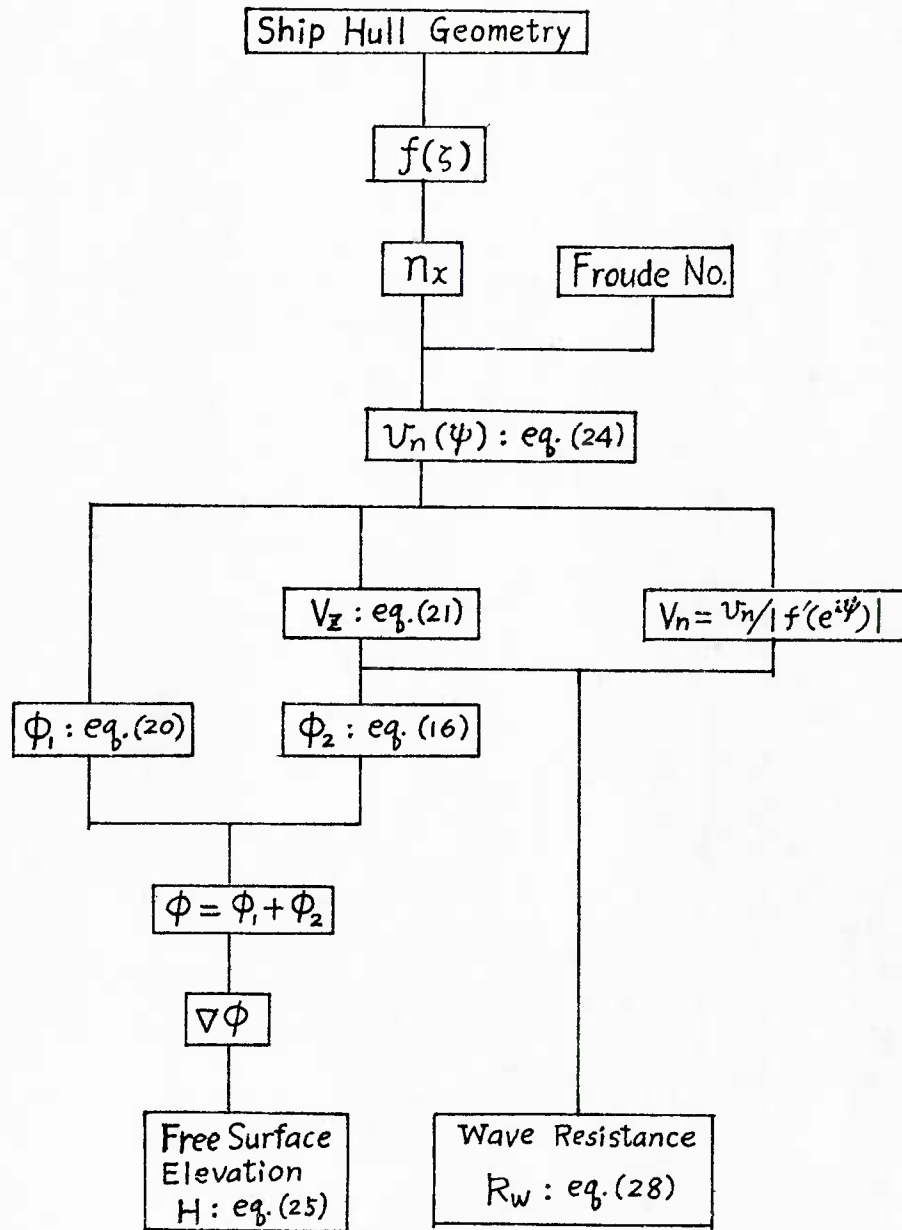


Fig. 2 Flow Chart of Numerical Procedure of New Slender Ship Theory (NSST)

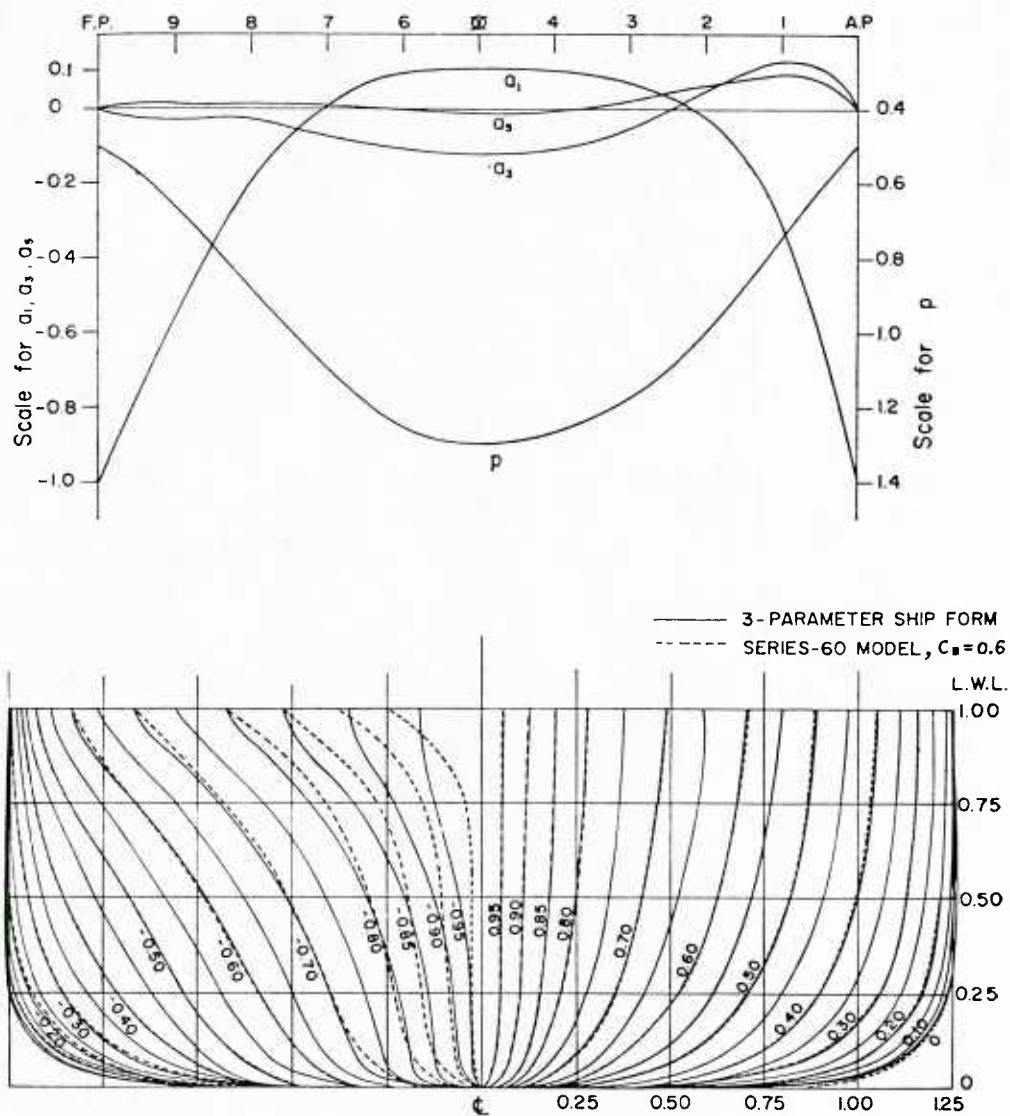


Fig. 3 Parameters and Body Plans of Three Parameter Hull Form

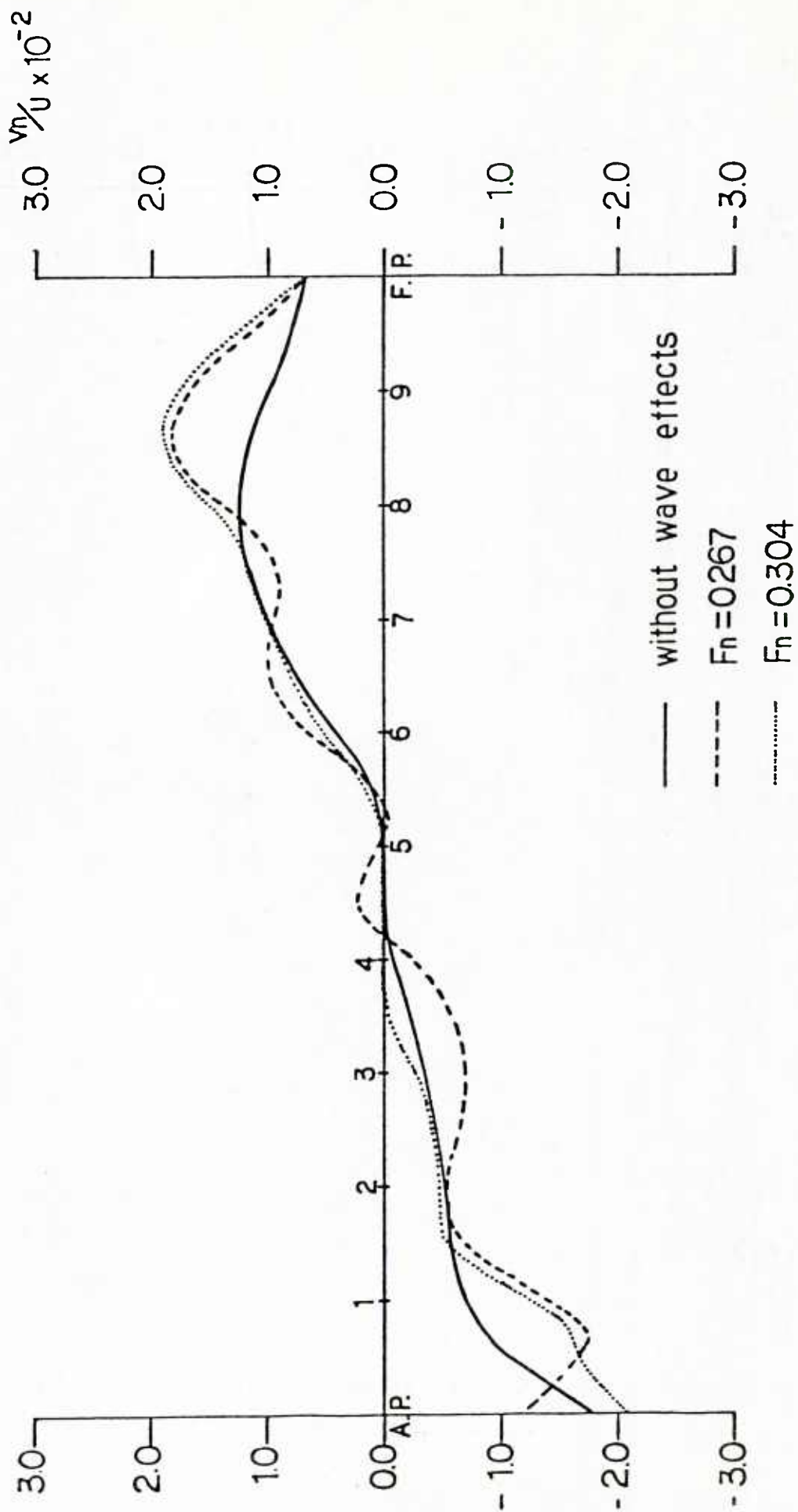


Fig. 4 Normal Velocity in ζ -Plane at $\psi = 9^\circ$, $v_n(\psi; x)$

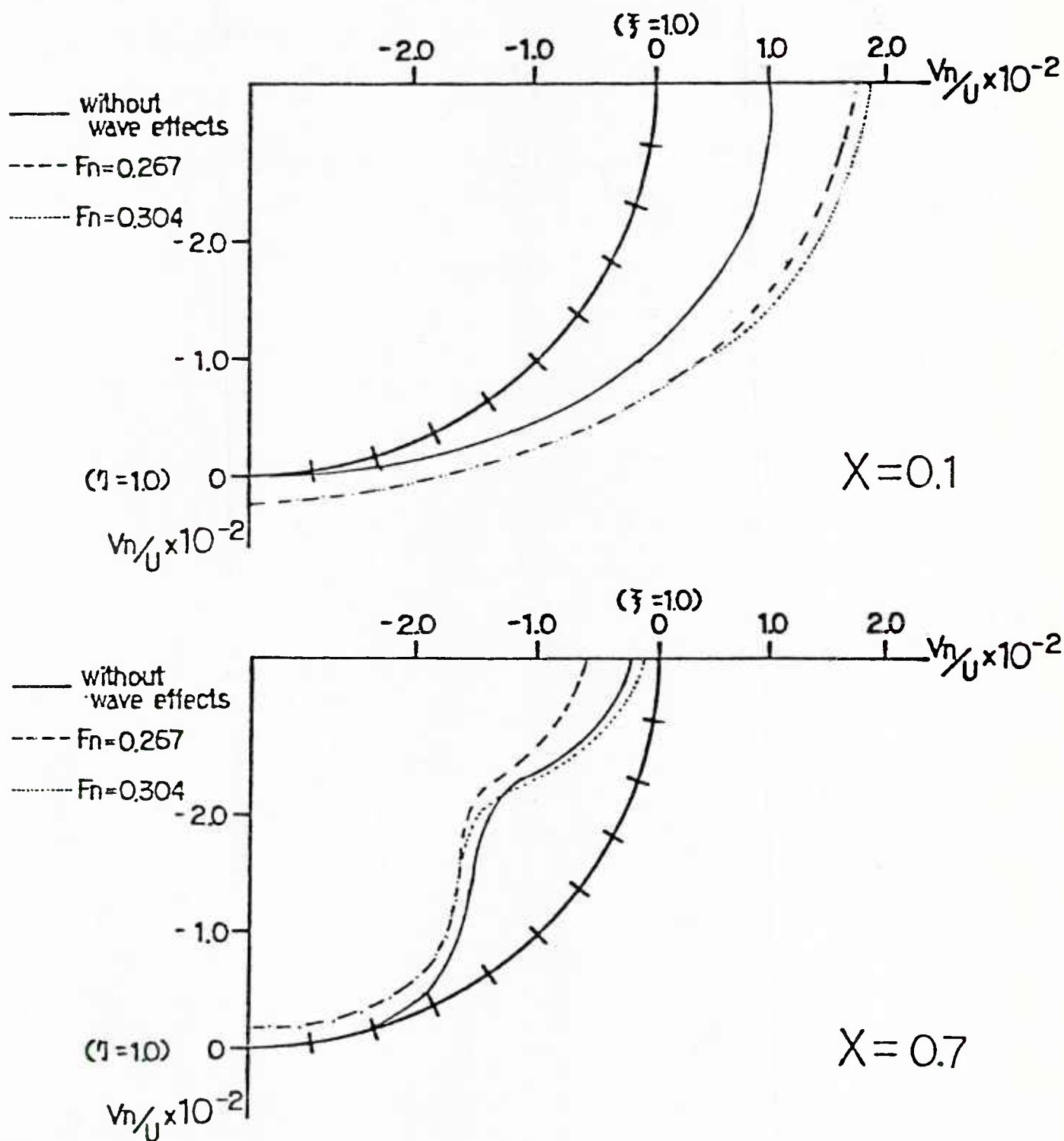


Fig. 5 Normal Velocity in ζ -Plane, $v_n(\psi; x)$
at $x=0.1$ and $x=0.7$

Wave Resistance Coefficients of Series 60, $C_b = 0.6$

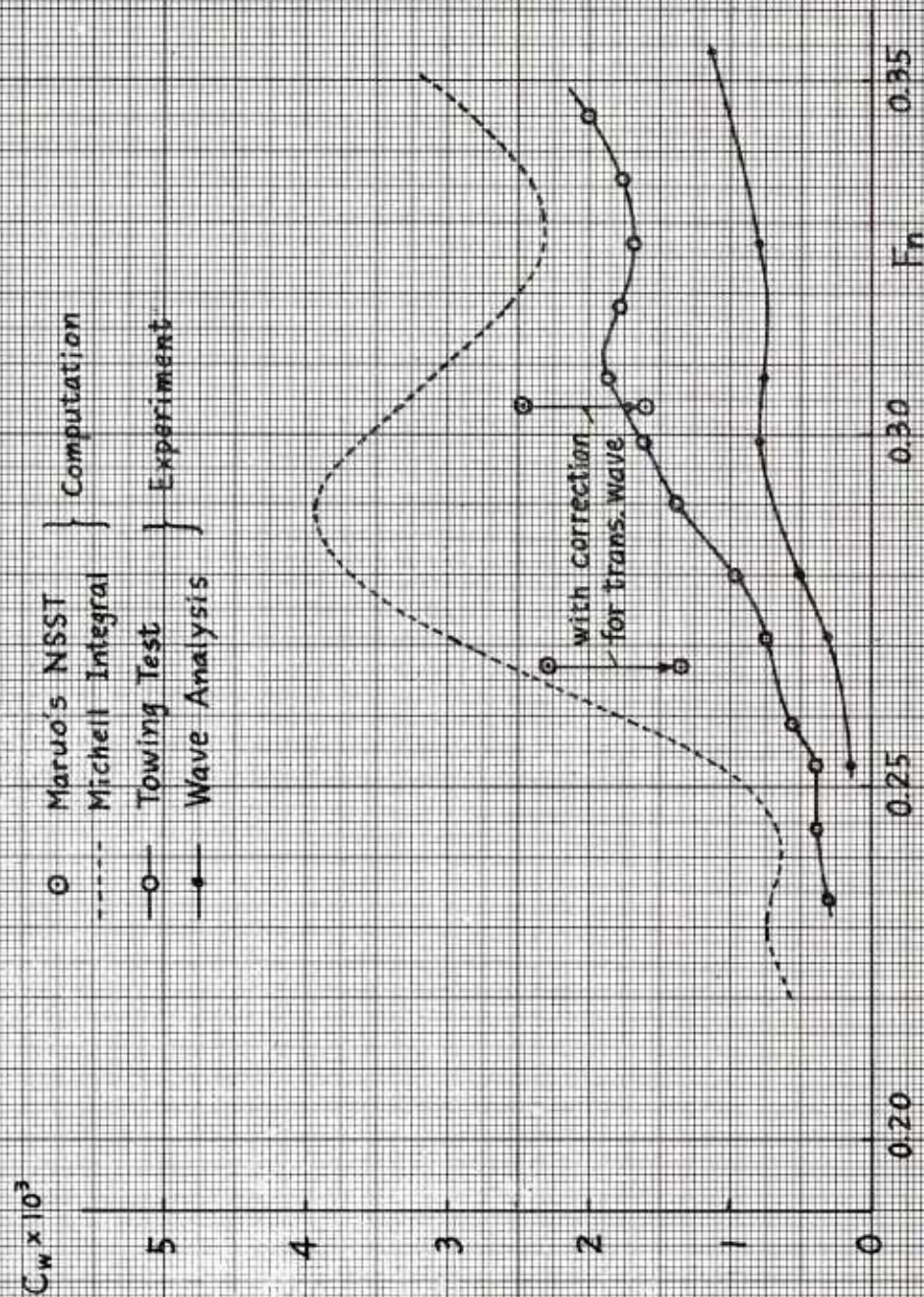


Fig. 6 Wave Resistance Coefficients of Series 60, $C_b = 0.60$

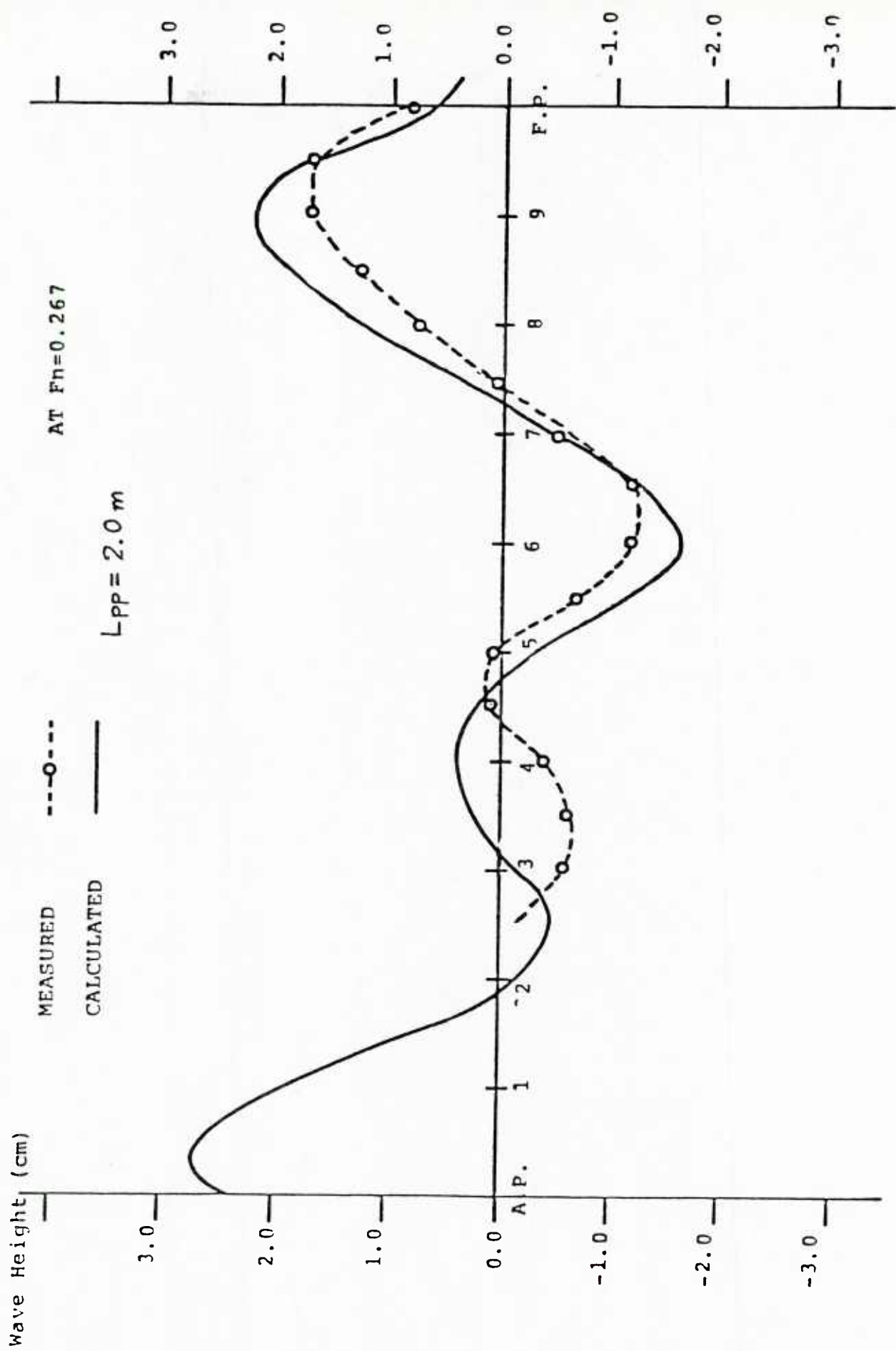


Fig. 7 Wave Profiles at $F_n = 0.267$

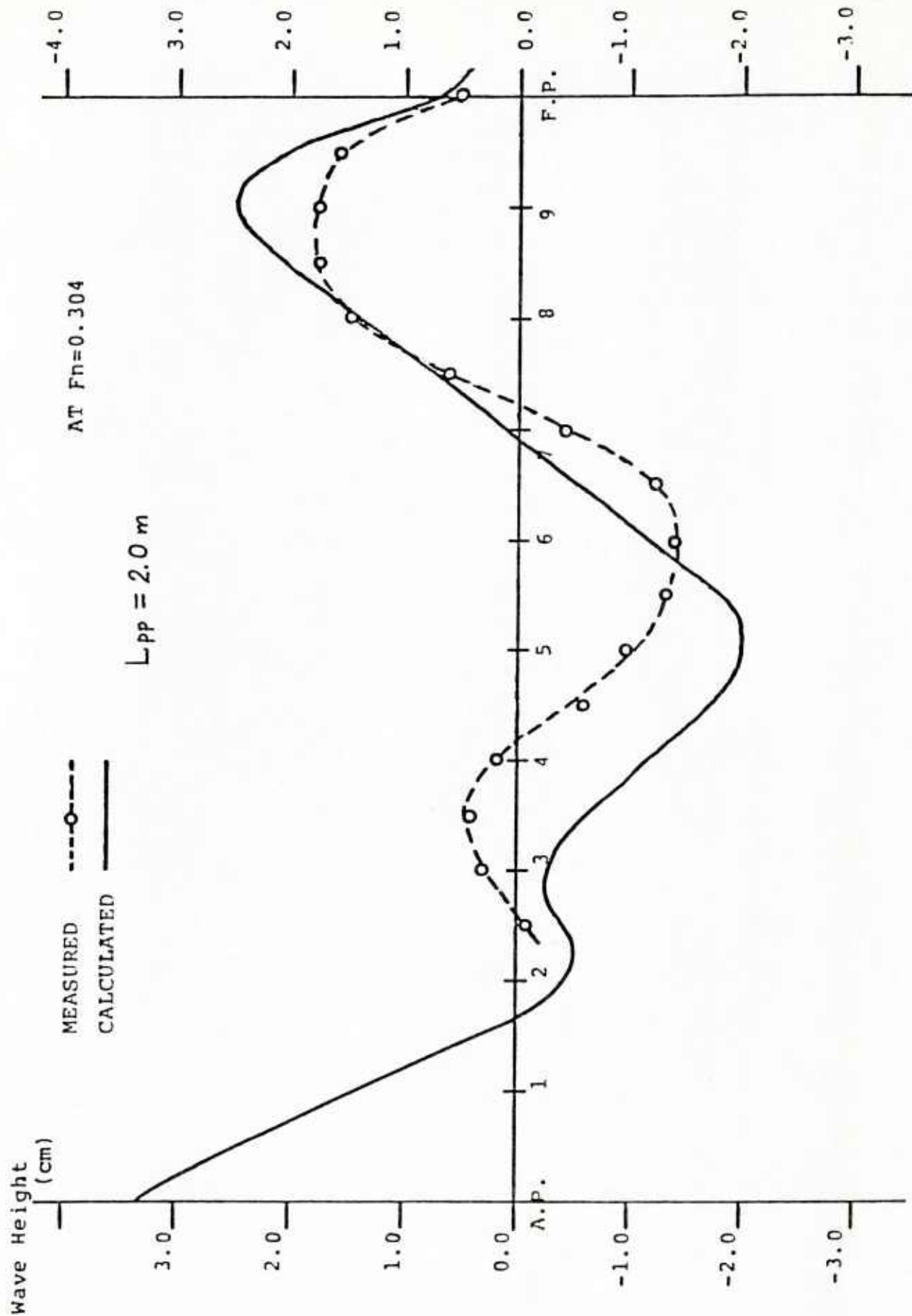


Fig. 8 Wave Profiles at $F_n = 0.304$

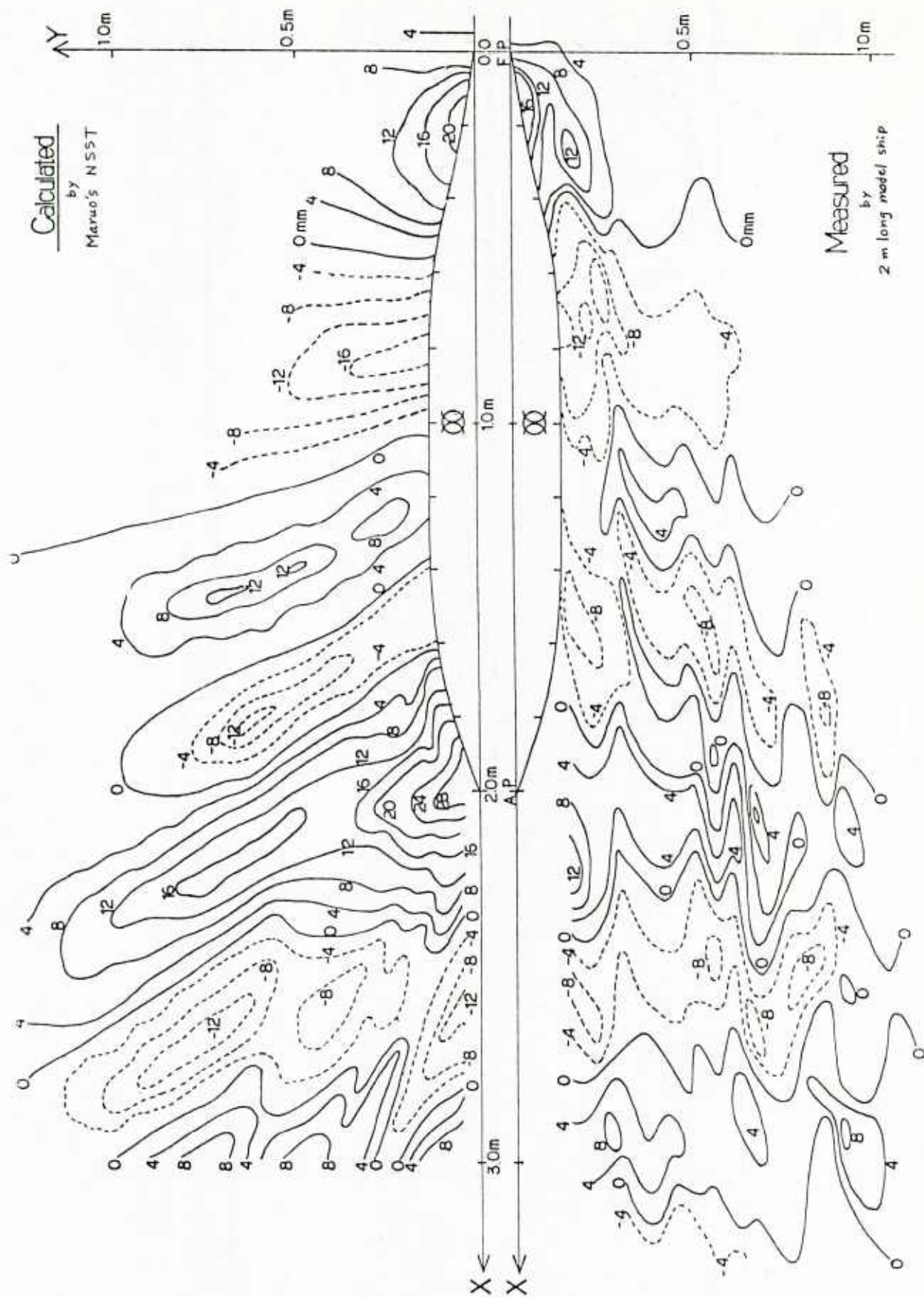


Fig. 9 Wave Patterns at $F_n = 0.267$

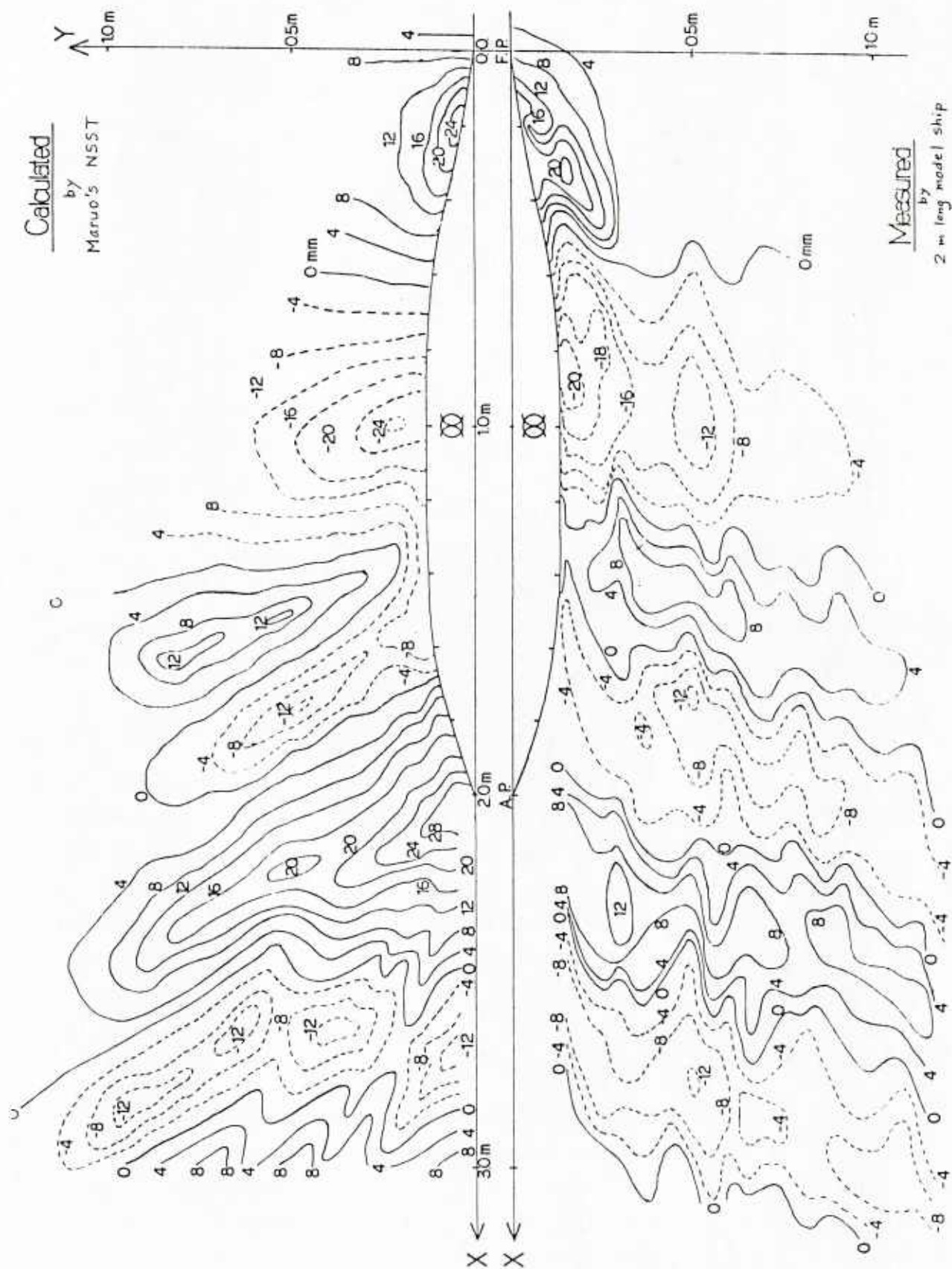


Fig. 10 Wave Patterns at $F_n = 0.304$

A NUMERICAL INVESTIGATION OF THE SLENDER-SHIP WAVE RESISTANCE APPROXIMATION

Carl A. Scragg
Science Applications, Inc.

Introduction

In a recent program funded by the Naval Sea Systems Command, SAI performed numerical calculations of the total resistance of some representative destroyer hull forms [1]. For the calculation of the wave resistance, we developed a computer code which employs Noblesse's zeroth-order slender-ship wave resistance approximation [2]. That particular approximation was chosen because it allows one to perform wave resistance calculations which are only slightly more complicated than the evaluation of Michell's integral, and yet the results of Koch and Noblesse [3] suggest that, at least for some hull forms, the slender-ship approximation can lead to results which approach the generally good agreement with experimental values obtained by some of the more complex computer codes (e.g. see Dawson [3] and M. S. Chang [3]).

The agreement which we obtained between the measured and calculated wave resistance for those destroyer hull forms was quite encouraging. In the present investigation we have used that same computer program to calculate the wave resistance of all of the hull forms suggested by the organizers of the workshop plus one high-speed transom-stern hull (the ATHENA). It is hoped that, through the efforts of the participants in this Second Workshop on Ship Wave Resistance Calculations, we will begin to understand the range of hull forms for which the zeroth-order slender-ship approximation leads to results which are in good agreement with higher-order theories and/or experimental results.

The theoretical development of the slender-ship approximation can be found in [2] and our own numerical approach to the evaluation of the wave resistance is discussed in [1]. We use a Green function approach in which singularities (Havelock sources) are distributed over the hull surface S and along the waterline C . The velocity potential ϕ can be written as

$$\phi = \int_S ds \sigma G + \int_C dl n_x \tau_y \sigma G \quad ,$$

where σ = source density,

G = Green function,

n_x = longitudinal component of the hull normal vector,

and τ_y = lateral component of the waterline tangent vector.

In the zeroth-order slender-ship approximation, the source density is proportional to n_x and direct computation of the velocity potential is possible. We use a panelization technique in which we assume that the hull surface can be approximated by a collection of flat panels over which the source density is constant. Over each flat panel, the singularity distribution can be integrated analytically.

Results for High-Speed Transom Stern Ships

Our initial results were for the two destroyer hull forms discussed in [1]. Each hull was panelized with 158 triangular panels on the half-body (port-starboard symmetry is assumed) as shown in Figure 1. These hulls have large bulbous bows and transom sterns. As suggested by Gadd [3] during the last workshop, the transom sterns were left open. A hydrostatic resistance component was included to account for the first-order effect of unwetting the transom, as suggested by both Gadd and Chang [3]. The results are compared to the experimentally determined residuary resistance in Figure 2. We are in general, quite pleased with the agreement both qualitatively and quantitatively. We are especially pleased that both experimental results and numerical predictions indicate a similar low Froude number region in which one hull has the lower wave resistance and a high Froude number region in which the other hull has the lower wave resistance.

Encouraged by these results, the wave resistance of the ATHENA was calculated. The hull was panelized with 240 triangular panels on each half body and the results are presented in Figure 3. In the last workshop, this particular hull proved to be most troublesome, but two participants (Dawson and Chang) did present results

which were banded by the experimentally determined residuary resistance and the wave pattern resistance, at least for the fixed sinkage and trim case. The present results are not in as good agreement as those presented by Dawson or Chang, exhibiting too great a hump in the resistance curve near a Froude number of 0.45. We note that the results for the destroyer hulls were also too high relative to experimental values at this Froude number, but the discrepancy was not as great.

Wigley Hull Results

For the Wigley hull, we used 100 triangular panels to model this smoothly curving surface. In Figure 4, the results of our calculations are compared with earlier published results calculated by Koch and Noblesse [3]. The experimental values shown here are Lackenby's 1965 results [4] which have been corrected for sinkage and trim effects using calculations by Dawson [3]. The agreement with Koch and Noblesse's results is an indication of the adequacy of the number of panels which were used. In fact, we found that doubling the number of panels would change the results by less than one percent. As a check on our code, we have also calculated a few values of the wave resistance using thin-ship theory and a few more using Hogner's approximation (the waterline integral is ignored). The agreement with Koch and Noblesse's results is very good.

Series 60, $C_B = 0.60$, Results

The Series 60 hull was modeled by 241 triangular panels, using the provided table of offsets to determine the corners of the panels. The results of our calculations are shown in Figure 5. The experimental results all include the effects of sinkage and trim while the calculations do not. The agreement between the predicted and the measured values is unacceptable and we can not expect that the inclusion of sinkage and trim in the calculations would improve the situation. In examining the results of the last workshop, it was noticed that Hong's [3] results using thin-ship theory were qualitatively similar and quantitatively only slightly higher than these results. Interestingly, the significant differences found between the thin-ship results and the slender-ship results for the Wigley hull ($\sim 20\%$ at $F_n = 0.30$), are much smaller for the Series 60 hull ($\sim 5\%$ at $F_n = 0.28$).

Results for a Strut-Like Hull Form

A simple strut with vertical sides and a constant draft (0.075) was considered. The waterline is defined by

$$y = \pm 0.075 \cdot 8x(1 - 2x) \quad \frac{1}{4} \leq x \leq \frac{1}{2} ,$$

$$y = \pm 0.075 \quad -\frac{1}{4} \leq x \leq \frac{1}{4} ,$$

$$y = \pm 0.075 \left[1 - 16(x + 0.25)^2 \right]^{\frac{1}{2}} \quad -\frac{1}{2} \leq x \leq -\frac{1}{4} .$$

The sharp end of the strut presents no particular difficulties in panelization, and it was represented by 10 quadrilateral panels. For the elliptical end, we must be much more careful since the slope of the waterline curve becomes infinite at the stern. Since we are approximating the continuously varying source strength by a constant over the dimensions of one panel, it is important that the panel size be small enough for this approximation to be valid. The criterion which we used here (determined by limited numerical experimentation) was that the panel dimensions must be so small that the continuous source strength will always be within 10 percent of the constant value by which it is being approximated. This leads to panel lengths near the elliptical end of 0.5 percent of the strut length. In total, the elliptical end was modeled with 15 quadrilateral panels of varying lengths. The predicted wave resistance is shown in Figure 6.

Results for Two Vertical Cylinders

Calculations of the wave resistance of two vertical cylinders were performed and the results are presented in Figures 7 and 8. In all cases, the depth was taken to be so large that the cylinder was approximately two dimensional. The waterplane area was used to non-dimensionalize the wave resistance:

$$\text{waterplane area} = 0.1178 \text{ for the ellipse,}$$

$$\text{waterplane area} = 0.10045 \text{ for the ogive.}$$

The panelization of the ellipse required the same criterion on panel length which was used for the elliptical end of the strut-like hull form. This resulted in 48 panels of varying length, whereas the ogive was paneled with only 20 panels.

The Fully-Submerged Body

The prolate spheroid was panelized with 192 surface panels, again using the criterion that the source density should be within 10 percent of its mean value over the dimensions of the panel. A submerged body such as this can also be approximated by a series of line sources along its centerline (i.e. thin-ship approximation). The cost of such a line-source calculation is an order of magnitude less than the corresponding surface panel calculation required by the slender-body approach. The small differences between the numerical results shown in Figure 9, indicate that this is perhaps not a cost-effective application of slender-body theory. However, if the body were not a body-of-revolution, then surface panelization might be indicated.

Since Farell and Güven [5] give experimental results which indicate a wave resistance coefficient which is significantly above the first-order approximation, this would appear to be a situation in which the thin-ship approximation yields better agreement with experimental values than does the slender-ship approximation.

Costs

All of these calculations were performed on a VAX 11/780 computer. The calculation of the wave resistance at a single Froude number requires approximately 1 minute of CPU for each 100 triangular panels on the body. At current rates ($\sim \$100/\text{hour}$), a typical calculation might cost \$2.50 per Froude number.

Conclusions

It would appear that the slender-ship approximation offers some promise for the economical approximation of the wave resistance for some hull forms. We do not expect it to be as accurate as some of the more sophisticated numerical approaches, but its speed and simplicity can make it a valuable tool in the design process.

For the two destroyer hulls, this approach led to results which were in good agreement with experimental results, although we note that the wave resistance is slightly over predicted near the large hump in the curve at high Froude numbers (~ 0.45). For the ATHENA, the agreement was not as good, especially near the wave

resistance hump ($F_n \sim 0.45$). These results, although not as good as those obtained by Dawson or Chang [3], did agree reasonably well with experimental values at Froude numbers both below and above this Froude number.

For the Wigley hull, the slender-ship approximation appears to yield significantly better agreement with experimentally determined values than were obtained by the thin-ship approximation, especially for high Froude numbers. As was the case with the ATHENA [3], the slender-ship results were somewhat lower than the thin-ship results at all Froude numbers. For the series 60 hull, the reduction in predicted wave resistance obtained by using the slender-ship approximation was very slight and the results did not agree with the experimentally determined values to an acceptable degree. The submerged hull was the only case examined thus far in which thin-ship results agreed with experiment better than the slender-ship results. It was also the only case in which both theories under predicted the wave resistance.

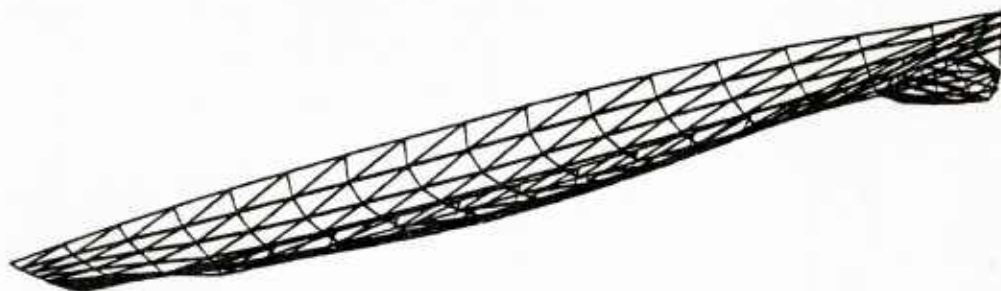


Figure 1. Panelized destroyer hull form.

REFERENCES

1. von Kerczek, C. H., F. Stern, C. A. Scragg, and W. Sandberg. "Total Resistance Calculations of Appended Destroyer Hull Forms," to be presented at Chesapeake Section Meeting of SNAME, 7 Dec 1983.
2. Noblesse, Francis. "A Slender-Ship Theory of Wave Resistance," Journal of Ship Research, Vol. 27, No. 1, March 1983.
3. Proceedings of the Workshop on Ship Wave-Resistance Computations, 13-14 November 1979, NSRDC, Bethesda, Maryland.
4. Lackenby, H. "An Investigation Into the Nature and Interdependence of the Components of Ship Resistance," Trans. of the Royal Institute of Naval Architects, Vol. 107, London, 1965.
5. Farrell, C. and Güven, O. "On the Experimental Determination of the Resistance Components of a Submerged Spheroid," Journal of Ship Research, Vol. 17, No. 2, June 1973.

WAVE RESISTANCE COEFFICIENT

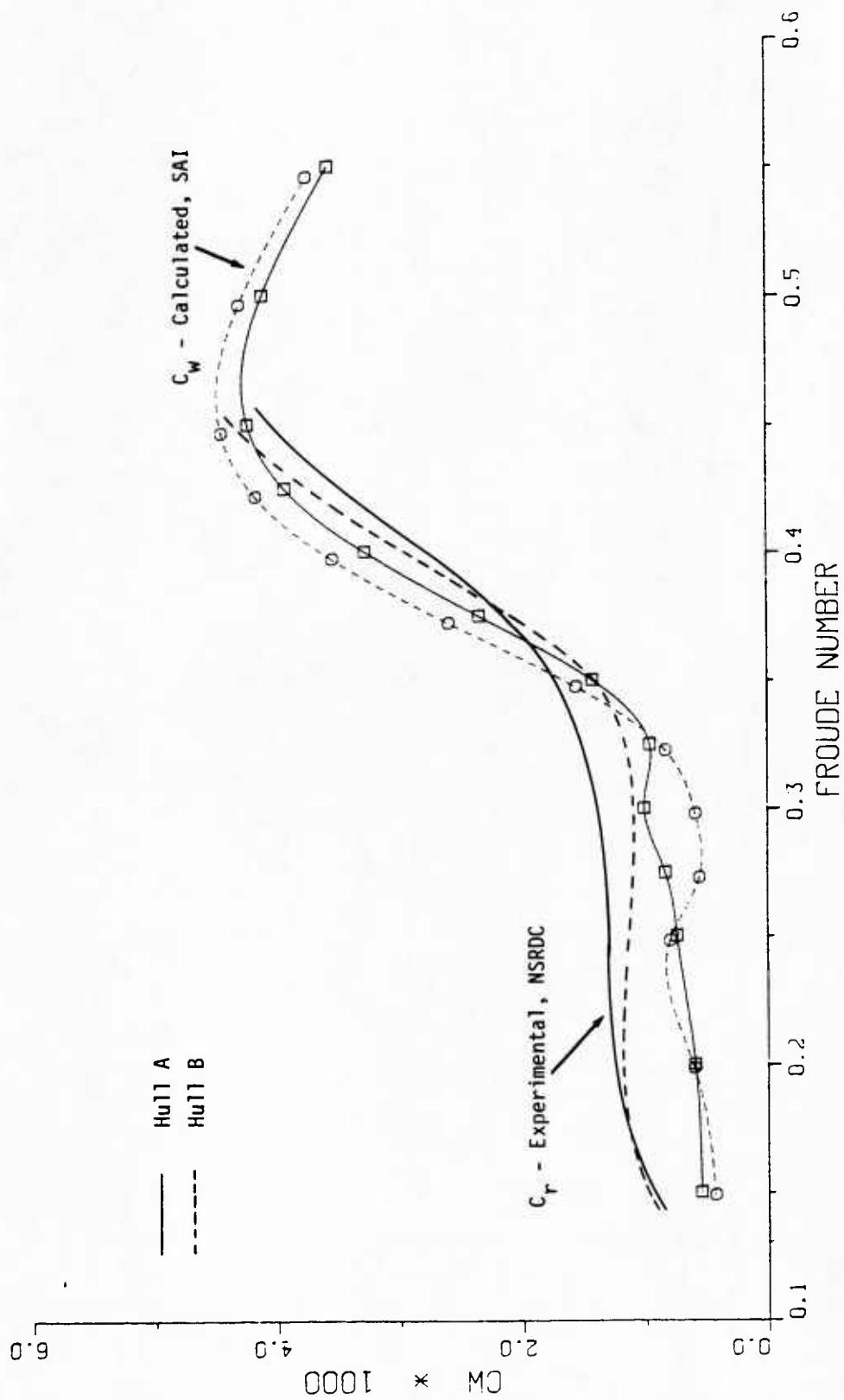


Figure 2. Measured and predicted wave resistance for two destroyer hull forms (free to sink and trim).

WAVE RESISTANCE COEFFICIENT

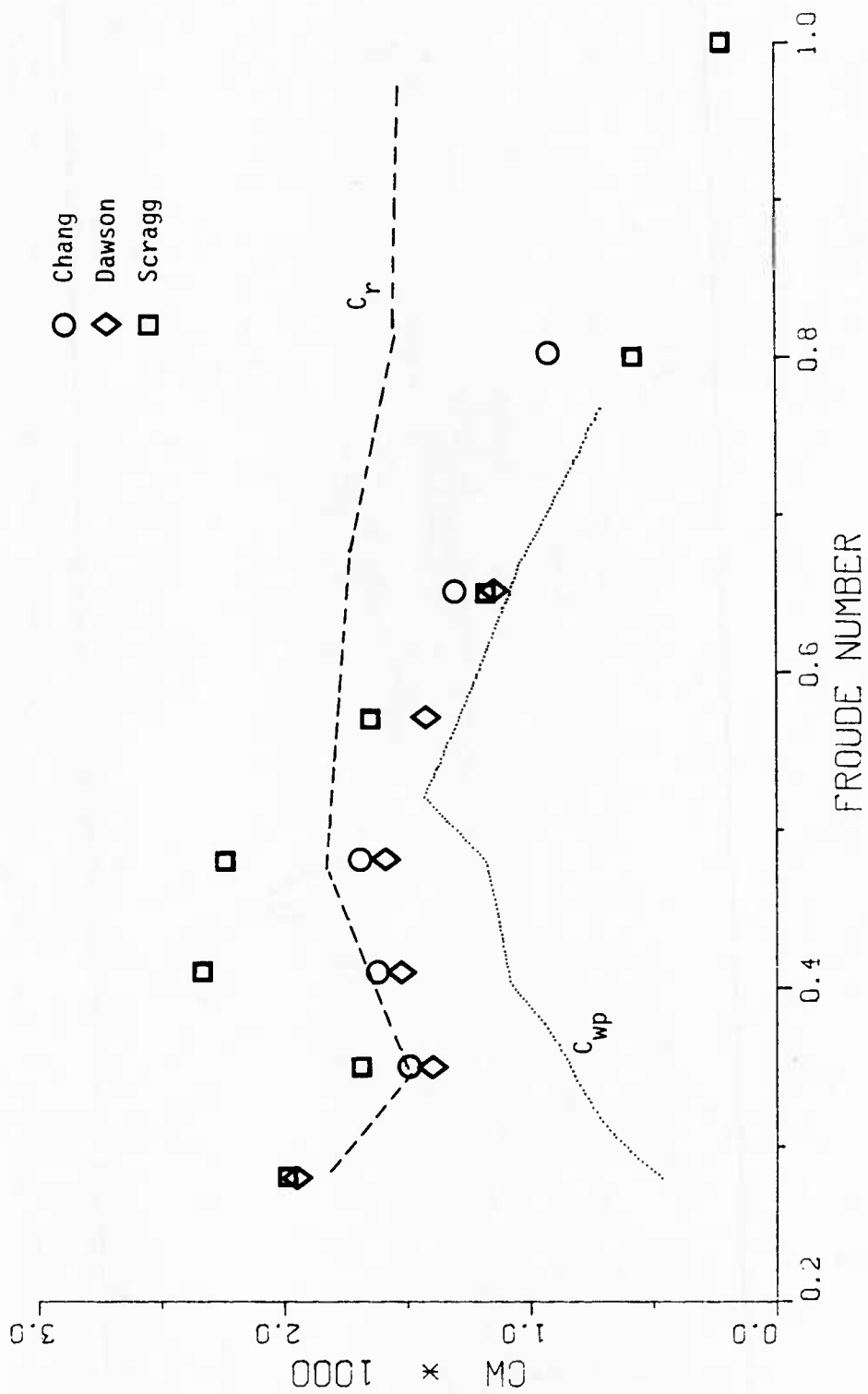


Figure 3. Measured and predicted wave resistance for the ATHENA (fixed sinkage and trim). Experimental results and computations by Dawson and Chang are taken from [3].

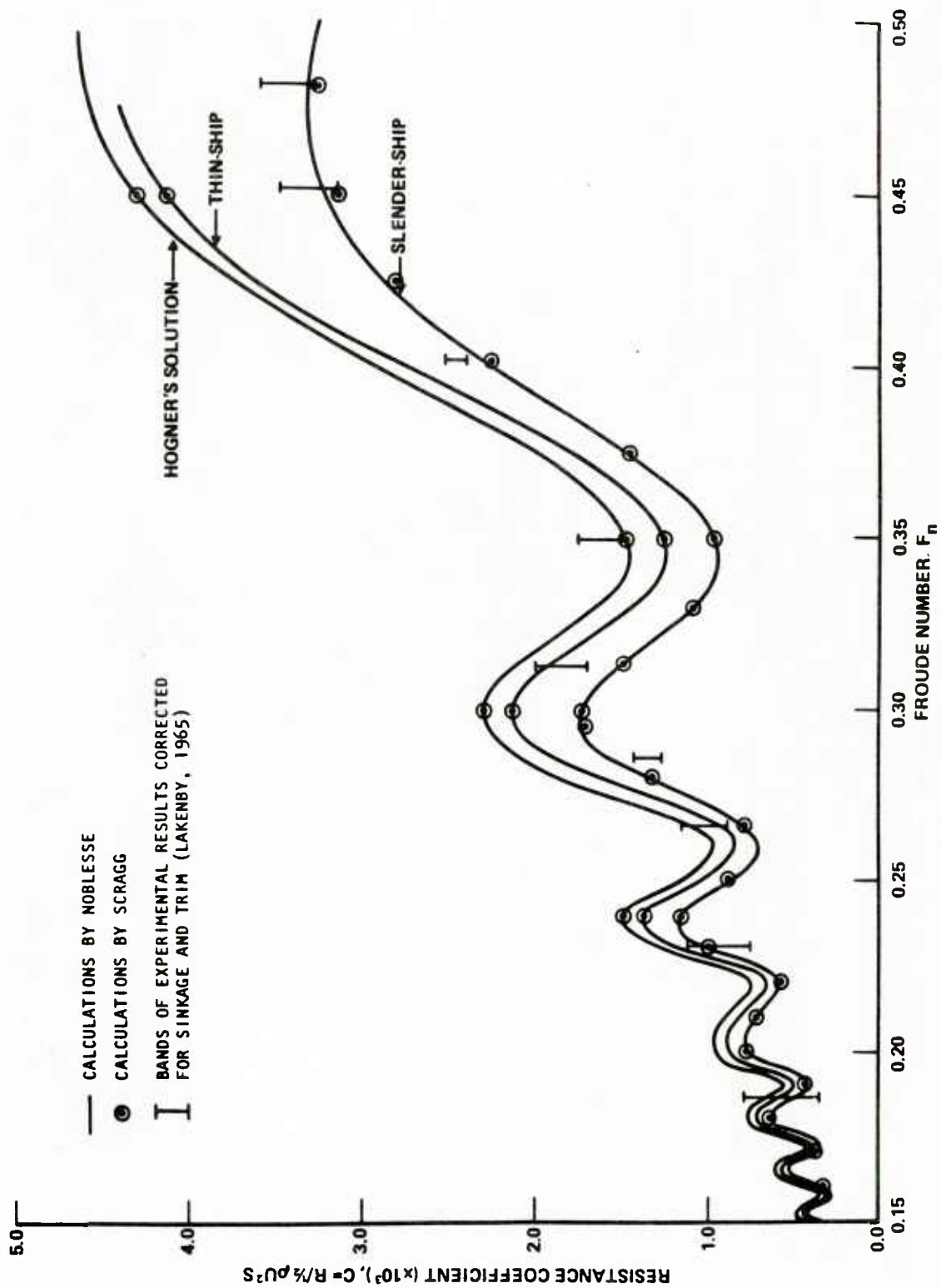


Figure 4. Measured and predicted wave resistance for the Wigley hull (fixed sinkage and trim).
 Noblesse's computations taken from [3].

WAVE RESISTANCE COEFFICIENT

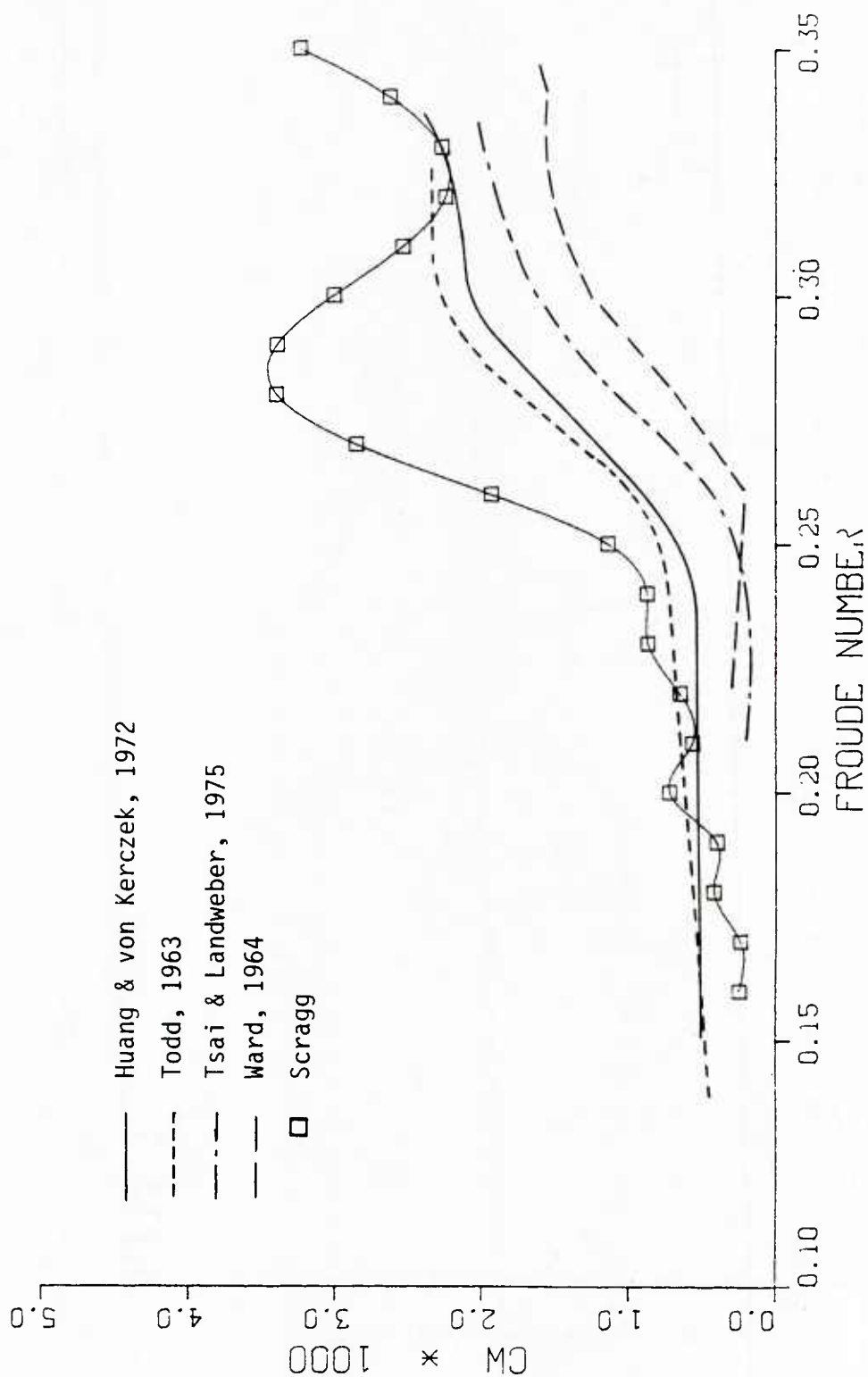


Figure 5. Measured (free to sink and trim) and predicted (fixed sinkage and trim) wave resistance for the Series 60, $C_B = 0.60$. Experimental results are taken from [3].

WAVE RESISTANCE COEFFICIENT

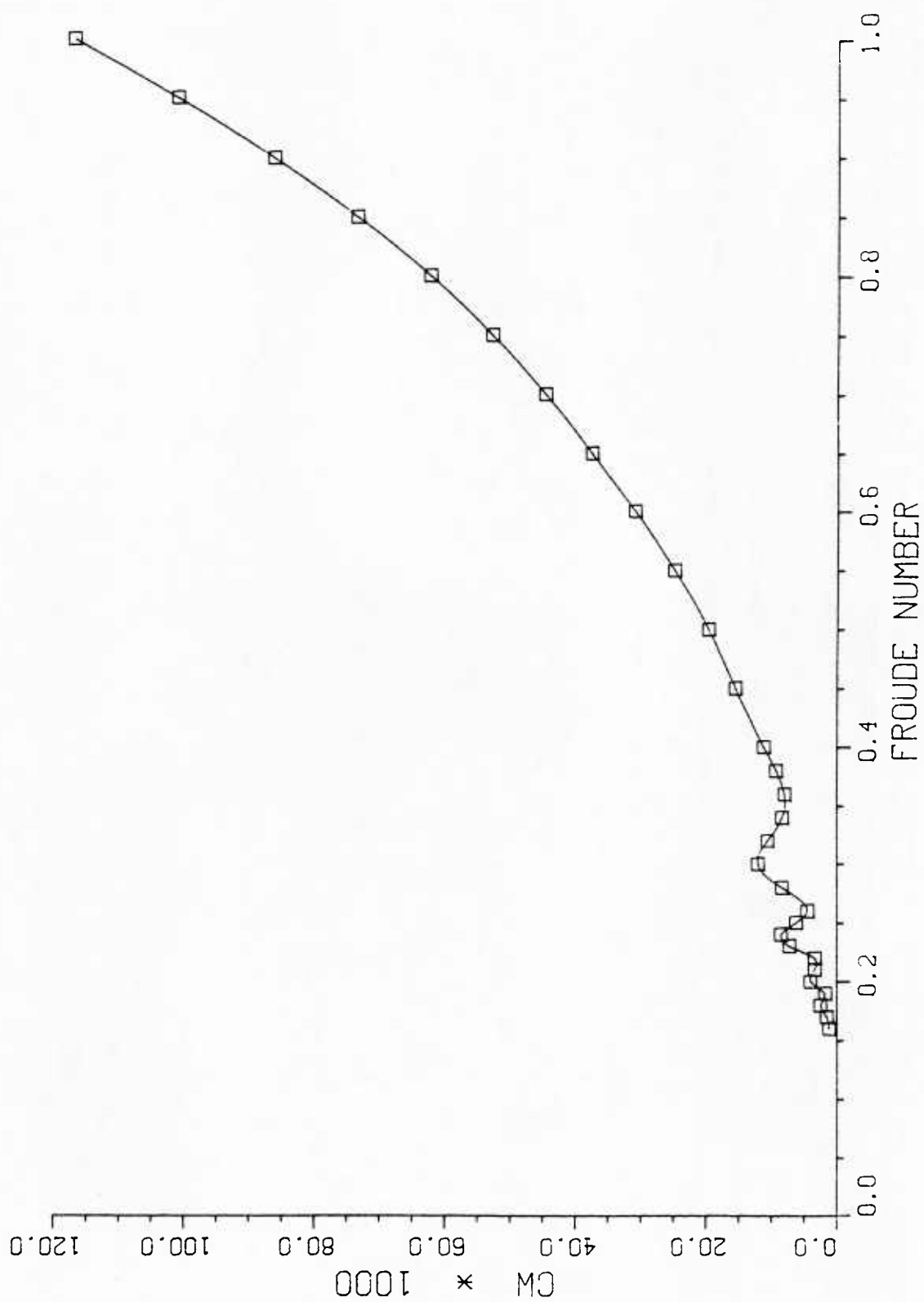


Figure 6. Predicted wave resistance of a strut-like hull form.

WAVE RESISTANCE COEFFICIENT

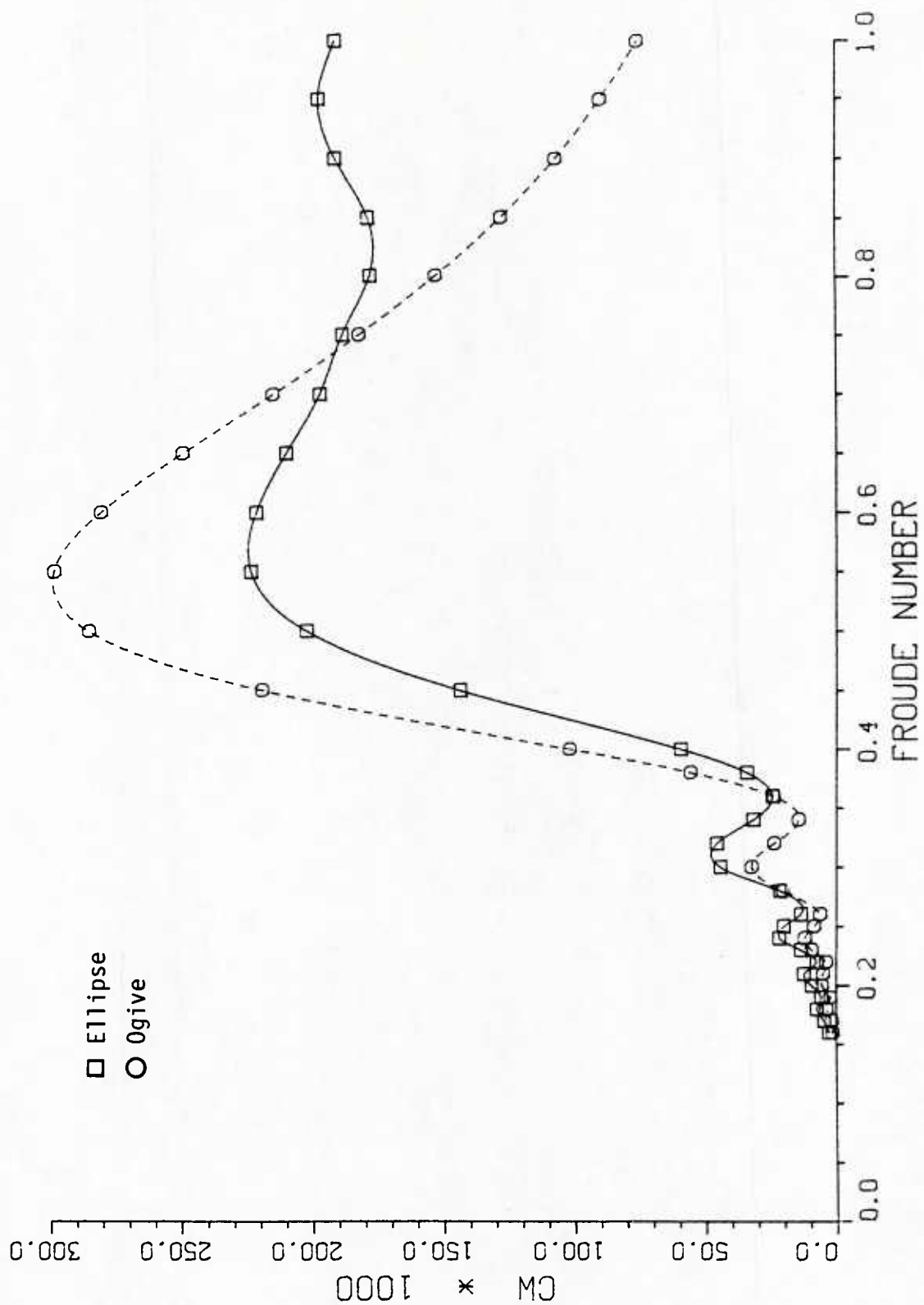


Figure 7. Predicted wave resistance for the vertical cylinders.

WAVE RESISTANCE COEFFICIENT

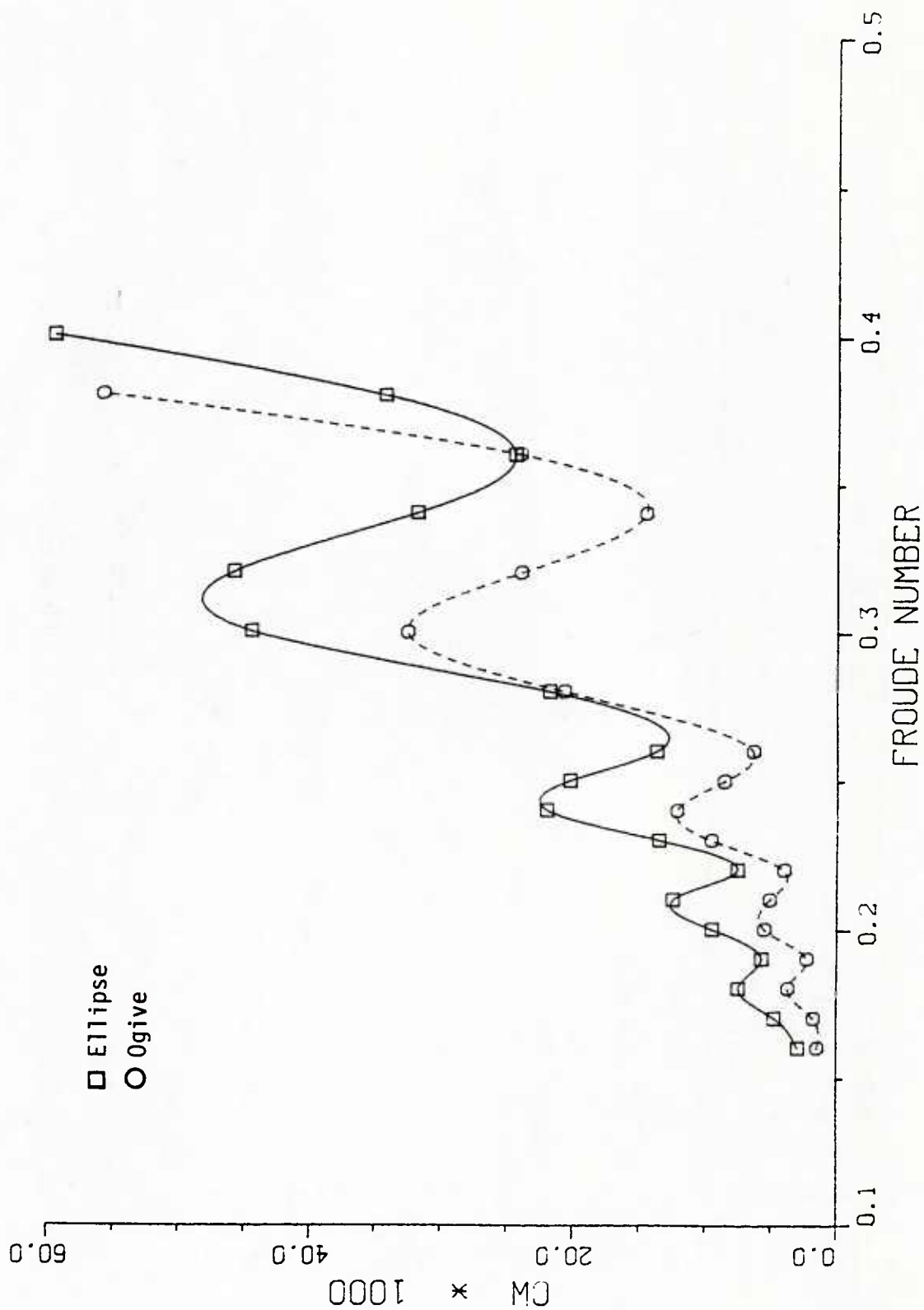


Figure 8. Predicted wave resistance for two vertical cylinders at low Froude number.

WAVE RESISTANCE COEFFICIENT

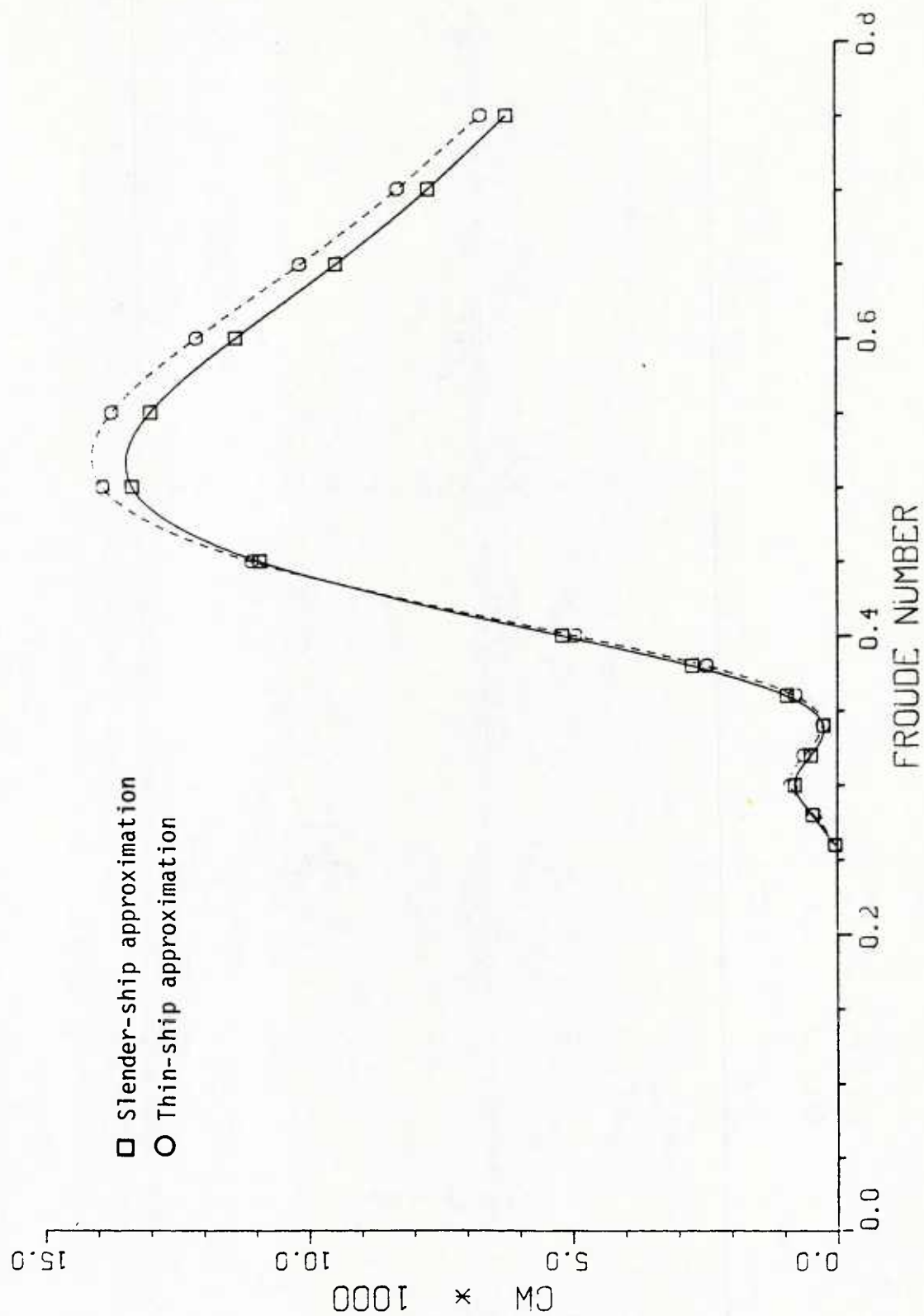


Figure 9. Predicted wave resistance for a fully submerged body.

WIGLEY HULL

Fn	Cw·1000
.16	.320
.17	.368
.18	.638
.19	.421
.20	.774
.21	.714
.22	.560
.23	.988
.24	1.158
.250	.875
.266	.779
.280	1.319
.295	1.701
.313	1.482
.330	1.077
.350	.957
.375	1.440
.402	2.241
.425	2.797
.452	3.160
.482	3.242

NOTE: S = 0.1487

SERIES 60

CB = 0.60

Fn	Cw·1000
.16	0.248
.17	0.239
.18	0.419
.19	0.399
.20	0.723
.21	0.566
.22	0.650
.23	0.871
.24	0.877
.25	1.144
.26	1.930
.27	2.849
.28	3.394
.29	3.389
.30	3.000
.31	2.530
.32	2.240
.33	2.264
.34	2.617
.35	3.231

NOTE: S = 0.170329

STRUT-LIKE HULL FORM

Fn	Cw·1000
.16	1.19
.17	1.53
.18	2.52
.19	1.78
.20	4.01
.21	3.38
.22	3.39
.23	7.22
.24	8.53
.25	6.22
.26	4.48
.28	8.41
.30	12.06
.32	10.58
.34	8.34
.36	7.99
.38	9.28
.40	11.18
.45	15.50
.50	19.61
.55	24.82
.60	30.90
.65	37.42
.70	44.52
.75	52.66
.80	62.15
.85	73.29
.90	86.16
.95	100.81
1.00	116.61

NOTE: S = 0.2852

ELLIPTICAL CYLINDER

Fn	Cw·1000
.16	2.93
.17	4.72
.18	7.48
.19	5.70
.20	9.46
.21	12.43
.22	7.50
.23	13.48
.24	21.93
.25	20.19
.26	13.66
.28	21.74
.30	44.43
.32	45.78
.34	31.81
.36	24.41
.38	34.23
.40	59.40
.45	143.38
.50	201.75
.55	222.86
.60	220.65
.65	209.15
.70	196.43
.75	187.80
.80	177.33
.85	178.11
.90	190.41
.95	196.68
1.00	190.35

NOTE: $C_w = \frac{R_w}{\frac{1}{2} \rho V^2 S}$

Where S was taken as the
waterplane area, S = 0.1178

OGIVE CYLINDER

Fn	Cw·1000
.16	1.46
.17	1.75
.18	3.71
.19	2.27
.20	5.50
.21	5.09
.22	3.98
.23	9.48
.24	12.12
.25	8.54
.26	6.35
.28	20.64
.30	32.52
.32	23.93
.34	14.48
.36	24.03
.38	55.74
.40	101.78
.45	218.91
.50	284.56
.55	297.69
.60	279.89
.65	248.70
.70	214.27
.75	181.50
.80	152.47
.85	127.56
.90	106.71
.95	89.62
1.00	75.60

NOTE: $C_w = \frac{R_w}{\frac{1}{2} \rho V^2 S}$

Where S was taken as the
waterplane area, S = 0.10045

SUBMERGED BODY		ATHENA	
Fn	Cw.1000	Fn	Cw.1000
.16	.00005	0.28	1.988
.17	.00005	0.35	1.688
.18	.00100	0.41	2.331
.19	.00053	0.48	2.239
.20	.00732		
.21	.0049	0.57	1.647
.22	.0114	0.65	1.177
.23	.0575	0.80	0.580
.24	.0763	1.00	0.221
.25	.0374		
.26	.0436		
.28	.467		
.30	.804		
.32	.500		
.34	.260		
.36	.953		
.38	2.736		
.40	5.189		
.45	10.907		
.50	13.319		
.55	12.966		
.60	11.358		
.65	9.461		
.70	7.704		
.75	6.222		

NOTE: S = 0.1304

NOTE: S = .50192

NUMERICAL STUDY OF EIGHT WAVE-RESISTANCE APPROXIMATIONS

by Francis Noblesse

David W. Taylor Naval Ship Research and Development Center

Abstract

This study presents results of ship wave-resistance calculations, for several simple hull forms, based on 8 wave-resistance approximations that are compared with one another and with existing experimental data for 2 thin hull forms.

Introduction

The wave-resistance calculations for simple hull forms reported in this study were performed in preparation for the task of developing a general computer code for calculating the wave resistance of an arbitrary ship form on the basis of the slender-ship theory presented in Noblesse [1]. More precisely, the present preliminary calculations were performed for two main purposes. First, it was necessary to perform a number of systematic calculations for completing the previous numerical study of Chen and Noblesse [2]. Specifically, this previous study contains a fairly extensive set of calculations, for both sharp- and round-ended hull forms, based on the zeroth-order slender-ship approximation $r^{(0)}$, that is compared with the approximations of Michell [3] and Hogner [4], and on the first-order slender-ship low-Froude-number approximation $r_{LF}^{(1)}$, that is shown to be practically identical to the low-speed approximation r_{LF} advocated by Guevel, Vaussy, and Kobus [5], Baba [6], Maruo [7], and Kayo [8]. However, only a preliminary numerical study of the more interesting and potentially more useful first-order slender-ship approximation $r^{(1)}$ is included in [2]. Indeed, calculations were performed for only one hull form: the Wigley hull. Furthermore, the nonoscillatory near-field term ϕ_N in the velocity potential $\phi = \phi_N + \phi_W$, where ϕ_W represents the wave term, was simply approximated by its zero-Froude-number limit ϕ_N^0 in [2]. The effect of the near-field potential ϕ_N is evaluated in the present numerical study, and results of fairly extensive calculations, for both sharp- and round-ended hull forms, are reported. The second major motivation for the present preliminary wave-resistance calculations for simple hull forms was the need for studying various numerical aspects of ship wave-resistance calculations in the framework of simple mathematically-defined hull forms for which numerical inaccuracies can be controlled more effectively than for arbitrary ship forms. The need for this preliminary study of numerical aspects of wave-resistance calculations stems from the fact that calculations of wave resistance are known to be

somewhat "difficult", as is attested by the significant discrepancies that sometimes occur among sets of numerical results obtained by different investigators on the basis of identical or closely-related methods [9].

As was mentioned previously, 8 wave-resistance approximations are considered in this study. These wave-resistance approximations correspond to the 8 approximations to the velocity potential ϕ defined below by Equations (1a,b,c,d) and (2a,b,c,d). More precisely, the wave-resistance approximations are given by the Havelock integral, as is [1], in which the Kochin free-wave amplitude function is determined by using the following approximations to the velocity potential:

$$\phi = 0, \quad \phi = \phi_N^0, \quad \phi = \phi_N^\infty, \quad \phi = \phi_N \quad (1a,b,c,d)$$

$$\phi = \phi_W, \quad \phi = \phi_N^0 + \phi_W, \quad \phi = \phi_N^\infty + \phi_W, \quad \phi = \phi_N + \phi_W \quad (2a,b,c,d)$$

In these equations, the potential $\phi = \phi_N + \phi_W$ is the first-order slender-ship approximation to the Neumann-Kelvin velocity potential given in [1], specifically by Equation (24a). The potential ϕ_W is the wave potential given by Equation (53b) in [1], and the potential ϕ_N corresponds to the nonoscillatory near-field potential associated with both the singular term $(-1/R)$ and the near-field term N in expression (8) in [1] for the Green function. The potentials ϕ_N^0 and ϕ_N^∞ are the zero- and infinite-Froude-number limits of the near-field potential ϕ_N associated with the simple sea-surface boundary conditions $\partial\phi_N^0/\partial z = 0$ and $\phi_N^\infty = 0$ on the mean sea plane $z = 0$. Specifically, the potential ϕ_N^0 is given by Equation (49) in [1], and the potential ϕ_N^∞ is given by the same equation in which the image source is replaced by an image sink. The approximation to the wave resistance, r , corresponding to the trivial slender-ship approximation (1a) to the velocity potential ϕ is the zeroth-order slender-ship approximation $r^{(0)}$, that can be regarded as a generalization of the classical wave-resistance approximations of Michell [3] and Hogner [4], as is shown in [1]. The wave-resistance approximation corresponding to the approximation $\phi = \phi_N^0$ defined by Equation (1b) is the first-order slender-ship low-Froude-number approximation $r_{LF}^{(1)}$ that was shown in [2] to be practically identical to the Guevel, Baba, Maruo, Kayo low-speed approximation r_{LF} . The wave potential ϕ_W is ignored in the approximations (1a,b,c,d); comparison of the wave-resistance curves corresponding to these approximations with one another will indicate whether the near-field potential ϕ_N might be neglected or approximated by one or the other of the computationally-simpler potentials ϕ_N^0 or ϕ_N^∞ . The wave potential ϕ_W is included in the approximations (2a,b,c,d), and the effect of this potential can be judged by comparing the wave-resistance curves

associated with the approximations (2a,b,c,d) and (1a,b,c,d). The wave-resistance approximation corresponding to the approximation (2d) is the first-order slender-ship approximation $r^{(1)}$. The simplified approximation (2b) was used in [2] in place of the approximation (2d). Comparison of these 2 wave-resistance curves, and of the curves associated with the approximations (2c) and (2a), will indicate whether a simple approximation to the near-field potential ϕ_N might be used. The wave-resistance curves associated with the above-defined approximations to the velocity potential are compared with one another for 3 simple sharp- and round-ended hull forms, and with existing experimental data for 2 thin sharp-ended hull forms in the following 2 sections.

Systematic Wave-Resistance Calculations for Three Simple Strut-Like Hull Forms

Calculations have been performed for 3 simple strut-like hull forms having constant draft and rectangular framelines, and beam/length and draft/length ratios equal to $B/L = 0.15$ and $D/L = 0.075$. The 3 hull forms are a sharp-ended "parabolic strut", a round-ended "elliptic strut", and a "parabolic/elliptic strut" having a sharp bow (or stern) and a round stern (or bow); for the parabolic/elliptic strut, results are presented for both cases when the sharp end is taken as the bow and as the stern (hull moving forward and backward). More precisely, the waterlines of the parabolic and elliptic struts are defined by the equations $y = \pm 0.075(1-4x^2)$ and $y = \pm 0.075(1-4x^2)^{1/2}$ where $-1/2 < x < 1/2$, respectively, and the waterlines of the parabolic/elliptic strut are defined by the equations $y = \pm 0.075(1-2x)(1-4a+2x)/(1-2a)^2$ for $a < x < 1/2$ and $y = \pm 0.075[1-4(x-a)^2/(1+2a)^2]^{1/2}$ for $-1/2 < x < a$, where a is taken as $a = 2^{1/2}-3/2 \approx -0.086$ so that there is no discontinuity in curvature at the junction between the parabolic and elliptic arcs at $x = a$. The results of wave-resistance calculations are depicted in the form of wave-resistance curves showing the nondimensional wave resistance $r \equiv R/\rho U^2 L^2$ (where ρ = density of water, U = ship speed, L = ship length) divided by the square of the Froude number $F \equiv U/(gL)^{1/2}$, that is r/F^2 , as a function of $1/F^2$ for $1 < 1/F^2 < 31$, which corresponds to the Froude-number range $1 > F > 0.18$. The wave-resistance curves were drawn by using cubic-spline fits of the numerical results obtained for 18, 26, and 17 values of the Froude number, in the range $1 < 1/F^2 < 32$, for the parabolic, elliptic, and parabolic/elliptic struts, respectively. The numerical results are listed in Tables 1, 2, and 3.

Figures 1a and 1b show the zeroth-order approximation $r^{(0)}$, the low-speed approximation $r_{LF}^{(1)}$, and the first-order approximation $r^{(1)}$ corresponding to the

approximations $\phi = 0$, ϕ_N° , and $\phi_N + \phi_W$, respectively, for the parabolic and elliptic struts. These figures show that differences between the curves corresponding to $\phi = 0$ and $\phi = \phi_N^{\circ}$, while appreciable, are much less important than differences between any one of these 2 curves and the curve $\phi = \phi_N + \phi_W$. In particular, there are no appreciable phase shifts between the curves $\phi = 0$ and $\phi = \phi_N^{\circ}$; the curve $\phi = \phi_N^{\circ}$ lying mostly below, and above, the zeroth approximation $\phi = 0$ for the parabolic, and elliptic, strut. Differences between these 2 curves, on the one hand, and the curve $\phi_N + \phi_W$, on the other hand, are important, including appreciable phase shifts. In particular, Fig. 1a for the parabolic strut shows that the curve $\phi_N + \phi_W$ is significantly lower than the curves $\phi = 0$ and ϕ_N° for small values of F , and the amplitudes of its oscillations, which are quickly damped as $F \rightarrow 0$, are greatly reduced. Fig. 1b for the elliptic strut shows even more striking differences, especially for large values of F for which the curve $\phi_N + \phi_W$ is considerably higher than the curves $\phi = 0$ and ϕ_N° . The curve $\phi_N + \phi_W$ also has an additional oscillation in the vicinity of $1/F^2 = 7$ that is not present for the other 2 curves.

The above-noted large differences between the curve $\phi_N + \phi_W$ and the curves $\phi = 0$ and ϕ_N° are mostly caused by the wave potential ϕ_W , rather than the near-field potential ϕ_N , as can be seen from Figs. 2a and 2b showing the wave-resistance curves associated with the approximations $\phi = 0$, $\phi = \phi_N$, and $\phi = \phi_W$ for the parabolic and elliptic struts, respectively. Differences between the curves $\phi = 0$ and ϕ_N can be seen to be relatively small. As a matter of fact, comparison of Figs. 1a and 2a, and of Figs. 1b and 2b, show that differences between the curves $\phi = \phi_N$ and $\phi = 0$ are smaller than differences between the curves $\phi = \phi_N^{\circ}$ and $\phi = 0$. The curves corresponding to the approximation $\phi = \phi_W$, on the other hand, are quite different from the curves $\phi = 0$ and ϕ_N , and clearly are similar to - although appreciably higher than - the curves $\phi_N + \phi_W$ in Figs. 1a and 1b. The wave potential ϕ_W thus has a very pronounced effect, and indeed is relatively more important than the near-field potential ϕ_N . Nevertheless, the near-field potential ϕ_N also has an appreciable, although less drastic, effect. More precisely, comparison of Figs. 1a and 2a, and of Figs. 1b and 2b, show appreciable differences between the curves $\phi_N + \phi_W$ and ϕ_W , and it is interesting that these differences are considerably larger than those that can be observed in Figs. 2a and 2b between the curves $\phi = \phi_N$ and $\phi = 0$.

Figures 3a and 3b show the wave-resistance curves corresponding to the

approximations $\phi = \phi_N^0$, ϕ_N^∞ , and ϕ_N for the parabolic and elliptic struts, respectively. The infinite-Froude-number-limit curve ϕ_N^∞ can be seen to provide a fairly good approximation to the curve ϕ_N for values of $1/F^2$ less than about 14, that is for F greater than about 0.27. For smaller values of F , discrepancies between the curves ϕ_N^∞ and ϕ_N increase, and the curve ϕ_N becomes more nearly in phase with and closer to the zero-Froude-number-limit curve ϕ_N^0 . However, differences between the curves ϕ_N^0 and ϕ_N are appreciable, especially in Fig. 3b for the elliptic strut, for the Froude-number range considered in Figs. 3a and 3b.

Figures 4a and 4b show the wave-resistance curves associated with the approximations $\phi = \phi_N^0 + \phi_W$, $\phi_N^\infty + \phi_W$, and $\phi_N + \phi_W$ for the parabolic and elliptic struts, respectively. Differences among the curves $\phi_N^0 + \phi_W$, $\phi_N^\infty + \phi_W$, and $\phi_N + \phi_W$ are qualitatively similar to, although generally larger than, the previously-noted differences among the curves ϕ_N^0 , ϕ_N^∞ , and ϕ_N . In particular, the curve $\phi_N^\infty + \phi_W$ is fairly close to the curve $\phi_N + \phi_W$, especially for the elliptic strut, for values of $1/F^2$ less than about 14, that is for F greater than about 0.27. For smaller values of F , a significant difference in phase develops between these 2 curves, notably for the parabolic strut. Although there are only minor differences in phase between the curves $\phi_N^0 + \phi_W$ and $\phi_N + \phi_W$, the former curve is well above the latter and discrepancies are fairly large, especially for the elliptic strut. Comparison of Figs. 4a and 3a, and of Figs. 4b and 3b, clearly demonstrate the very-large effect of the wave potential ϕ_W that was already noted in Figs. 2a and 2b.

Figure 5 shows 3 wave-resistance approximations, namely the zeroth-order approximation $r^{(0)}$, the low-speed approximation $r_{LF}^{(1)}$, and the first-order approximation $r^{(1)}$ corresponding to the approximations $\phi = 0$, ϕ_N^0 , and $\phi_N + \phi_W$, respectively, for the previously-defined parabolic/elliptic strut, in both cases when the sharp end is taken as the bow and as the stern (hull moving forward and backward). The approximations $\phi = 0$ and ϕ_N^0 yield identical wave-resistance curves for both cases when the hull is moving forward and backward, and differences between these 2 approximations are relatively minor. Specifically, the curve ϕ_N^0 lies above the curve $\phi = 0$, without apparent difference of phase. The approximation $\phi_N + \phi_W$, on the other hand, yields different wave-resistance curves for the cases when the hull moves forward and backward. These differences stem from the wave potential ϕ_W , that is different in the forward- and backward-motion cases, unlike the near-field potential ϕ_N and its zero- and infinite-Froude-number limits ϕ_N^0 and ϕ_N^∞ that merely undergo a change in sign. Figure 5 shows

that differences between the curves $\phi_N + \phi_W$ for the forward- and backward-motion cases and between any one of these 2 curves and the curves $\phi = 0$ and ϕ_N^0 are important, including notable phase shifts. In particular, the curve $\phi_N + \phi_W$ for the round-bow/sharp-stern strut lies much above the other 3 curves for large values of F , and the oscillations of the curve $\phi_N + \phi_W$ for the sharp-bow/round-stern strut are greatly reduced for small values of F , especially in the range $19 < 1/F^2 < 31$ ($0.23 > F > 0.18$) where the curve is almost flat.

Comparison of Theoretical and Experimental Wave-Resistance Values for the Sharma Strut and the Wigley Hull

Experimental values of wave resistance have been determined by Sharma [10] for a sharp-ended parabolic strut of the kind considered in the previous section, with beam/length and draft/length ratios equal to 0.05 and 0.15, respectively. Experiments were performed under conditions when neither sinkage nor trim of the model was allowed. Both experimental values determined by analysis of measured wave profiles and use of Froude's method of subtracting an estimated viscous resistance from the measured total resistance are given in [10]. These experimental values are indicated in Fig. 6 together with the zeroth-order approximation $r^{(0)}$, the low-speed approximation $r_{LF}^{(1)}$, and the first-order approximation $r^{(1)}$ corresponding to the approximations $\phi = 0$, ϕ_N^0 , and $\phi_N + \phi_W$, respectively. These 3 theoretical wave-resistance curves are depicted for $1 < 1/F^2 < 25$, corresponding to $1 > F > 0.2$. The curves were plotted by using cubic-spline fits of 14 numerical results obtained for $1 < 1/F^2 < 26$; these numerical results are listed in Table 4. Figure 6, and all subsequent figures in this section, represent the nondimensional resistance $r \equiv R/\rho U^2 L^2$, which is proportional to the wave-resistance coefficient $C_w \equiv R/1/2 \rho U^2 S$ where $S \equiv$ wetted-hull surface, rather than r/F^2 that was represented in Figs. 1 through 5 in the previous section. Differences among the approximations $\phi = 0$, ϕ_N^0 , and $\phi_N + \phi_W$ are very-much smaller for the extremely thin ($B/L = 0.05$) and deep ($D/L = 0.15$) Sharma strut considered in Fig. 6 than for the thicker ($B/L = 0.15$) and shallower ($D/L = 0.075$) strut considered in Fig. 1a. As a matter of fact, the first-order approximation $r^{(1)}$ and the low-speed approximation $r_{LF}^{(1)}$ are not noticeably different from the zeroth-order approximation $r^{(0)}$, which is practically identical to the Michell thin-ship approximation (not shown in Fig. 6), for the thin and deep Sharma strut. Furthermore, Fig. 6 shows that these theoretical approximations are in excellent agreement with both sets of experimental data points for values of $1/F^2$ less than

about 8, that is for $F > 0.35$, and lie between the 2 sets of experimental data for smaller values of the Froude number.

Figure 7 shows the numerical results obtained in Chen and Noblesse [2] for the Wigley hull, that has parabolic waterlines and framelines, beam/length and draft/length ratios equal to 0.1 and 0.0625, respectively, and more precisely, is defined by the equation $y = \pm 0.05(1-4x^2)(1-256z^2)$ where $-0.5 < x < 0.5$ and $0 > z > -0.0625$. Four theoretical wave-resistance curves are depicted in Fig. 7. These are the Michell thin-ship approximation, and the wave-resistance approximations corresponding to the velocity-potential approximations $\phi = 0$, ϕ_N° , and $\phi_N^{\circ} + \phi_W$. The wave-resistance curves were plotted by using cubic-spline fits of 31 numerical results obtained for $2 < 1/F^2 < 32$; these numerical results are listed in Table 5. Also shown in Fig. 7 are the ranges of variation of experimental data, for 10 values of the Froude number, obtained in the manner that is explained in Chen and Noblesse [11]. Briefly, these experimental data consist of 11 sets of data, determined by using both wave analysis and the usual Froude method, for the Wigley hull in unrestrained conditions (hull free to assume its natural sinkage and trim), to which theoretical corrections for sinkage- and-trim effects, based on 4 sets of theoretical results, were applied. A detailed comparison of the theoretical results and experimental data represented in Fig. 7 is given in [2]. The most interesting feature of the results depicted in Fig. 7 resides in the fairly-large phase shift between the curve $\phi_N^{\circ} + \phi_W$ and the other 3 wave-resistance curves, resulting in improved agreement with the experimental data.

No new numerical calculations were performed for the Wigley hull form in the framework of the present numerical study, that is limited to strut-like hull forms having constant drafts and rectangular framelines. However, calculations have been performed for a parabolic strut having beam/length ratio equal to that of the Wigley hull, namely $B/L = 0.1$, and draft/length ratio equal to 0.04, so that this strut, with rectangular framelines, has approximately the same cross-sectional area as the Wigley hull, with parabolic framelines and draft/length ratio equal to 0.0625. The results of these calculations are listed in Table 6 and depicted in Fig. 8. Specifically, the wave-resistance curves corresponding to the approximations $\phi = 0$, ϕ_N° , $\phi_N^{\circ} + \phi_W$, and $\phi_N + \phi_W$ are shown for $2 < 1/F^2 < 32$. The 4 wave-resistance curves shown in Fig. 8, and differences among them, are qualitatively much alike those considered previously in connection with Fig. 7 and Figs. 1a and 4a. In particular, the curves $\phi_N^{\circ} + \phi_W$ and $\phi_N + \phi_W$ are clearly out of phase

with the curves $\phi = 0$ and ϕ_N^0 , due to the wave potential ϕ_W as was mentioned previously. Both Figs. 8 and 4a also show that the oscillations of the curves $\phi_N^0 + \phi_W$ and $\phi_N + \phi_W$ are roughly in phase. This result and the close similarity between the comparable wave-resistance curves represented in Figs. 8 and 7 may be used to determine a rough estimate of the wave-resistance curve corresponding to the approximation $\phi_N + \phi_W$ for the Wigley hull. Specifically, if $r^{(1)}$ and $r_0^{(1)}$ are the wave-resistance approximations associated with the approximations $\phi_N + \phi_W$ and $\phi_N^0 + \phi_W$, respectively, a rough estimate of $r^{(1)}$ for the Wigley hull can be determined by assuming that the ratio $r^{(1)}/r_0^{(1)}$ takes the same value for the Wigley hull and the related strut considered in Fig. 8.

The values of the first-order approximation $r^{(1)}$ for the Wigley hull estimated in the foregoing manner are listed in Table 5, and the corresponding curve is depicted, together with the Michell wave-resistance curve and experimental data, in Figs. 9a,b,c. More precisely, the experimental data points shown in Figs. 9a, b,c are the data obtained recently at the Ship Research Institute (SRI), the University of Tokyo (UT), and Yokohama National University (YNU) in Japan [12] and at the University of Iowa (UI) in the USA [13] for the Wigley hull under conditions when neither sinkage nor trim was allowed. Experimental data obtained by using 3 different experimental techniques are indicated in Figs. 9a,b,c. Specifically, Fig. 9a shows the experimental data obtained at SRI and at UT by using the method of wave-pattern analysis; Fig. 9b presents the experimental results obtained by Sangseon Ju at UI by subtracting from the measured total resistance the viscous resistance determined experimentally by using the wake-survey method; finally, Fig. 9c shows the experimental values of residuary resistance obtained at SRI, UT, YNU, and UI by using the usual Froude method. The wave-pattern-analysis results of SRI and UT shown in Fig. 9a are in good agreement with one another for the 4 values of the Froude number for which there are experimental data from both SRI and UT, and are fairly close to the first-order approximation $r^{(1)}$ for values of $1/F^2$ smaller than 14, that is for $F > 0.27$. The viscous-wake-analysis results of UI depicted in Fig. 9b also are in fairly good agreement with the first-order approximation $r^{(1)}$ for $F > 0.27$, but are much less oscillatory than $r^{(1)}$ for smaller values of F . Comparison of Figs. 9a and 9b indicates that the UI wake-survey results and the wave-analysis results of SRI and UT are in fairly good agreement with one another. There are notable differences among the 4 sets of residuary resistance shown in Fig. 9c for values of $1/F^2$ greater than about 14, that is for

F smaller than about 0.27. Furthermore, differences between the residuary-resistance values of Fig. 9c and both the wave-analysis data of Fig. 9a and the first-order approximation $r^{(1)}$ are appreciable for values of $1/F^2$ smaller than about 9, that is for F greater than about 0.33. It will be interesting to compare the experimental data shown in Figs. 9a,b,c with a more accurate evaluation of the first-order approximation $r^{(1)}$, including the nonlinear terms in the sea-surface boundary condition in particular, and with the second-order approximation $r^{(2)}$.

Conclusions

. Differences between the first- and zeroth-order slender-ship approximations $r^{(1)}$ and $r^{(0)}$ were found to be important for all the hull forms considered in this study, except the extremely thin and deep Sharma strut for which the terms involving the velocity potential in the expression for the Kochin free-wave amplitude function thus appear to have no appreciable effect.

. The numerical results for the Wigley hull obtained previously in [2] had shown that the wave potential ϕ_W has a very pronounced effect upon the wave resistance, causing a large phase shift in particular. This finding is confirmed by the more extensive numerical results obtained in the present study. The low-speed approximation advocated by Guevel et al. [5], Baba [6], Maruo [7], and Kayo [8], in which the wave potential is neglected and the potential is approximated by the zero-Froude-number potential, therefore does not seem justified, except possibly for extremely small values of the Froude number, as was previously concluded in [1,2].

. The nonoscillatory near-field potential ϕ_N has less drastic effects upon the wave resistance than the wave potential ϕ_W . In particular, ϕ_N affects the phase of the wave-resistance curve to a lesser degree than ϕ_W . Nevertheless, ϕ_N has appreciable effects upon the wave resistance, and cannot simply be neglected. Neither can ϕ_N be approximated by its zero-Froude-number limit ϕ_N^0 , except perhaps for very small values of the Froude number. However, use of the infinite-Froude-number approximation ϕ_N^∞ might be justified for values of F greater than about 0.27. This finding and the relatively-small importance of ϕ_N by comparison with ϕ_W suggest that it may be sufficient, for practical calculations, to use the following simple algebraic approximation for the near-field term N in expression (8) in [1] for the Green function:

$$N \approx 1/r' - [2/(F^2 + r')] \{ [1 - F^2(z + \zeta)] / (F^2 + r') (r' + |x - \xi|) \}$$

where r' is the distance between the field point (x,y,z) and the mean-sea-surface

mirror image $(\xi, \eta, -\zeta)$ of the singular point (ξ, η, ζ) . The foregoing simple algebraic approximation has the property that it yields the first 2 terms in the ascending series [14] and in the asymptotic expansion [15] of N , and thus provides a good approximation to N for both small and large values of r'/F^2 . A substantial part of the computing time required for evaluating the first-order approximation $r^{(1)}$ is spent for calculating the near-field potential ϕ_N , so that a significant reduction in computing time can be achieved by using the foregoing algebraic approximation to the near-field term N in the Green function.

. The first-order wave-resistance approximation $r^{(1)}$ appears to be in fairly-good agreement with experimental data for the Sharma strut and the Wigley hull for values of the Froude number greater than about 0.27. However, numerical results must obviously be obtained and compared with experimental data for other hull forms. This task will be performed in the near future, after a computer code for arbitrary ship forms is developed.

. Finally, 2 important non-conclusions ought to be mentioned. (i) The nonlinear terms in the sea-surface condition appear in the form of a sea-surface integral in the expression for the Kochin free-wave amplitude function [1]. This sea-surface integral was neglected for simplicity in the calculations reported in this study, but should be evaluated for assessing the effects of free-surface nonlinearities. (ii) It would also be necessary to evaluate the second-order slender-ship approximation $r^{(2)}$ for verifying if $r^{(2)}$ does not differ significantly from $r^{(1)}$ as is suggested, but by no means firmly established, by the restricted proof of convergence given in Noblesse [16]. It is hoped that these 2 important tasks can be performed in the not-too-distant future.

Acknowledgments

The work reported in this study was performed under the David W. Taylor Naval Ship Research and Development Center's General Hydromechanics Research Program. I also wish to thank Dr. Timothy F. Hogan for helping me become familiar with DTNSRDC's computer system, and Dr. Thomas T. Huang and Mr. Justin H. McCarthy for their support of this work.

References

1. Noblesse, F., "A Slender-Ship Theory of Wave Resistance," Journal of Ship Research, Vol. 27, No. 1, pp. 13-33 (1983).
2. Chen, C.Y. and F. Noblesse, "Preliminary Numerical Study of a New Slender-Ship Theory of Wave Resistance," Journal of Ship Research, Vol. 27, No. 3,

pp. 172-186 (1983).

3. Michell, J.H., "The Wave Resistance of a Ship," Philosophical Magazine, Series 5, Vol. 45, pp. 106-123 (1898).
4. Hogner, E., "Eine Interpolationsformel für den Wellenwiderstand von Schiffen," Jahrbuch der Schiffbautechnischen Gesellschaft, Vol. 33, pp. 452-456 (1932).
5. Guevel, P., P. Vaussy and J.M. Kobus, "The Distribution of Singularities Kinematically Equivalent to a Moving Hull in the Presence of a Free Surface," International Shipbuilding Progress, Vol. 21, pp. 311-324 (1974).
6. Baba, E., "Wave Resistance of Ships in Low Speed," Mitsubishi Technical Bulletin No. 109, Nagasaki, Japan (1976).
7. Maruo, H., "Wave Resistance of a Ship with Finite Beam at Low Froude Numbers," Bulletin of the Faculty of Engineering, Yokohama National University, Japan, Vol. 26, pp. 59-75 (1977).
8. Kayo, Y., "A Note on the Uniqueness of Wave-Making Resistance when the Double-Body Potential is Used as the Zero-Order Approximation," Trans. West-Japan Society of Naval Architects, No. 55, pp. 1-11 (1978).
9. Proceedings, Workshop on Ship Wave-Resistance Computations, David W. Taylor Naval Ship Research and Development Center, Bethesda, Maryland (1979).
10. Sharma, S.D., "Some Results Concerning the Wavemaking of a Thin Ship," Journal of Ship Research, Vol. 13, pp. 72-81 (1969).
11. Chen, C.Y. and F. Noblesse, "Comparison Between Theoretical Predictions of Wave Resistance and Experimental Data for the Wigley Hull," Journal of Ship Research, to appear.
12. "Cooperative Experiments on Wigley Parabolic Models in Japan," Prepared for the 17th ITTC Resistance Committee (1983).
13. Sangseon Ju, "Study of Total and Viscous Resistance for the Wigley Parabolic Ship Form," Iowa Institute of Hydraulic Research Report No. 261, The University of Iowa, Iowa City, Iowa (1983).
14. Noblesse, F., "Alternative Integral Representations for the Green Function of the Theory of Ship Wave Resistance," Journal of Engineering Mathematics, Vol. 15, No. 4, pp. 241-265 (1981).
15. Noblesse, F., "The Near-Field Disturbance in the Centerplane Havelock Source Potential," Proceedings First International Conference on Numerical Ship Hydrodynamics, David W. Taylor Naval Ship Research and Development Center, Bethesda, Maryland, pp. 481-501 (1975).
16. Noblesse, F., "Convergence of a Sequence of Slender-Ship Low-Froude-Number Wave-Resistance Approximations," Journal of Ship Research, to appear.

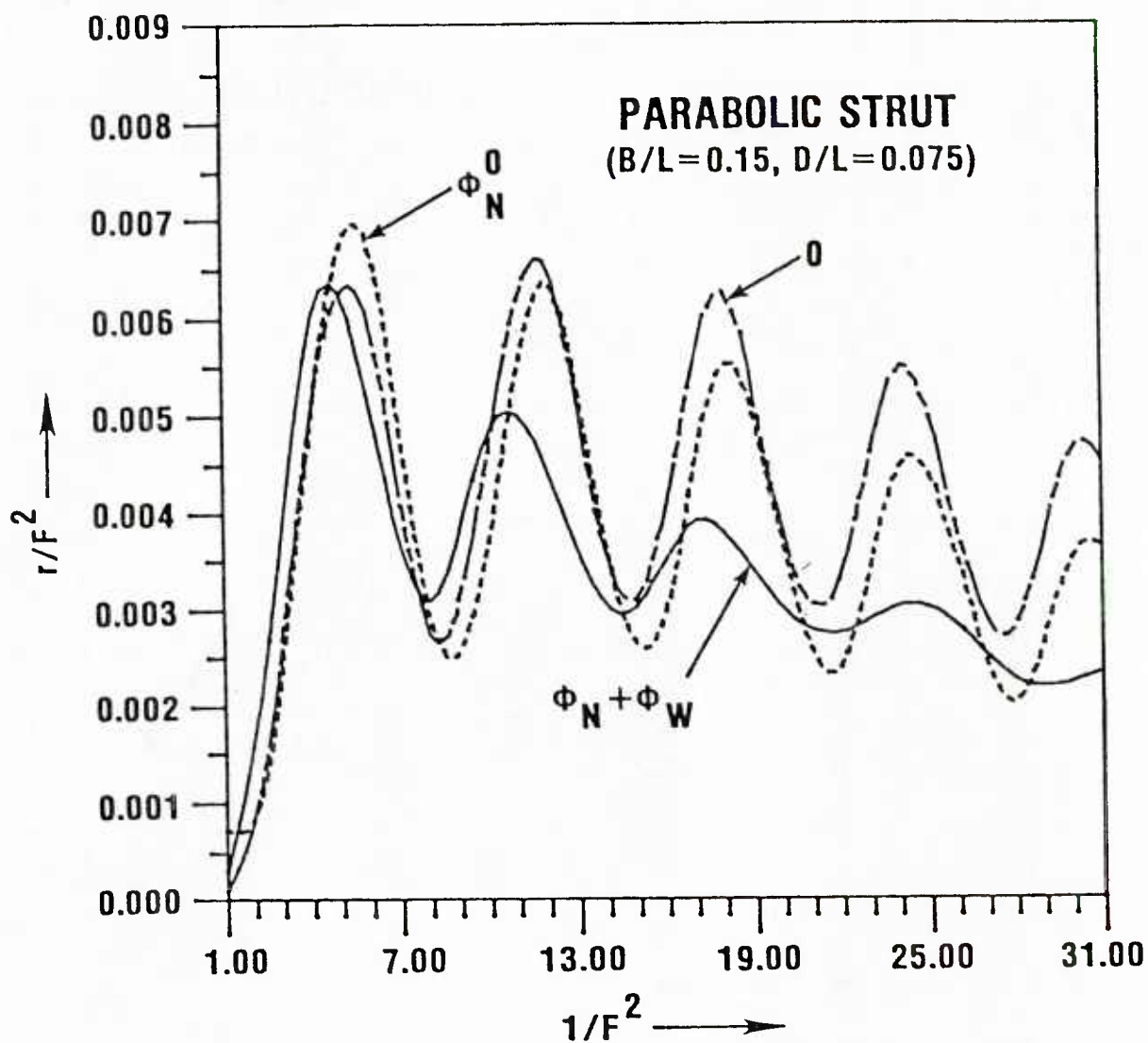


Fig. 1a - Wave-resistance approximations associated with the velocity-potential approximations $\phi = 0$, ϕ_N^0 , and $\phi_N + \phi_W$ for the parabolic strut

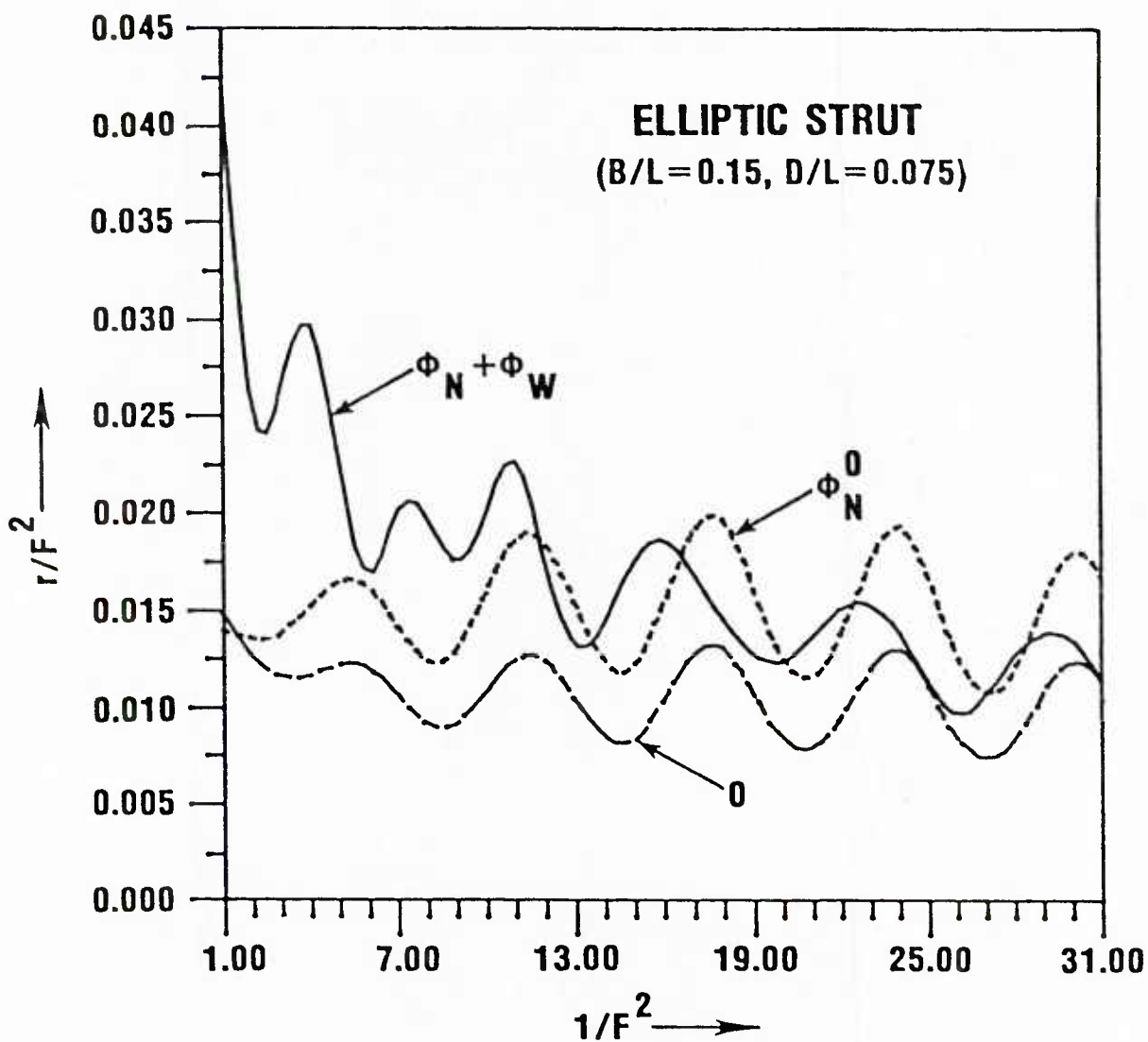


Fig. 1b - Wave-resistance approximations associated with the velocity-potential approximations $\phi = 0$, ϕ_N^0 , and $\phi_N + \phi_W$ for the elliptic strut

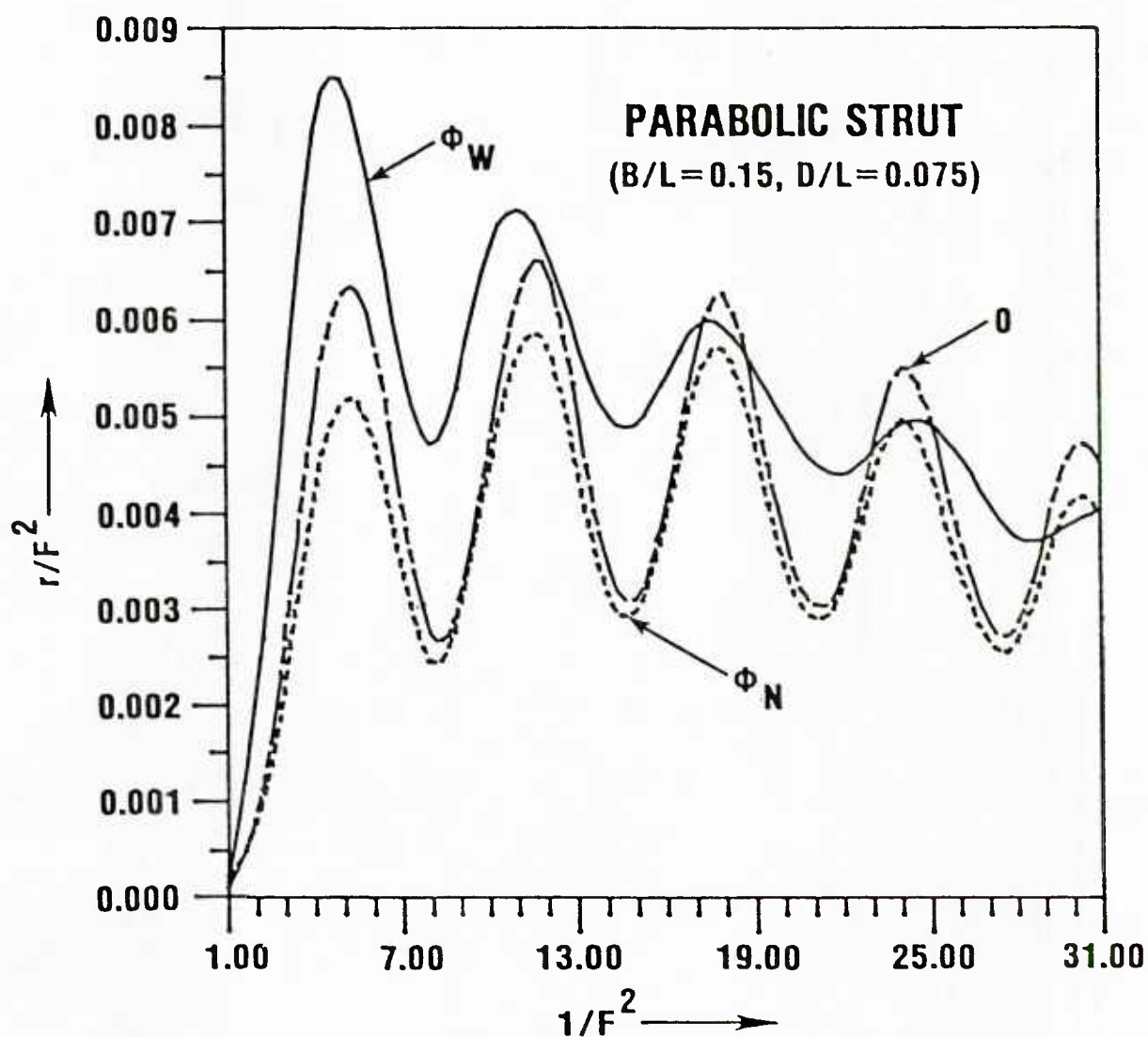


Fig. 2a - Wave-resistance approximations associated with the velocity-potential approximations $\phi = 0$, ϕ_N , and ϕ_W for the parabolic strut

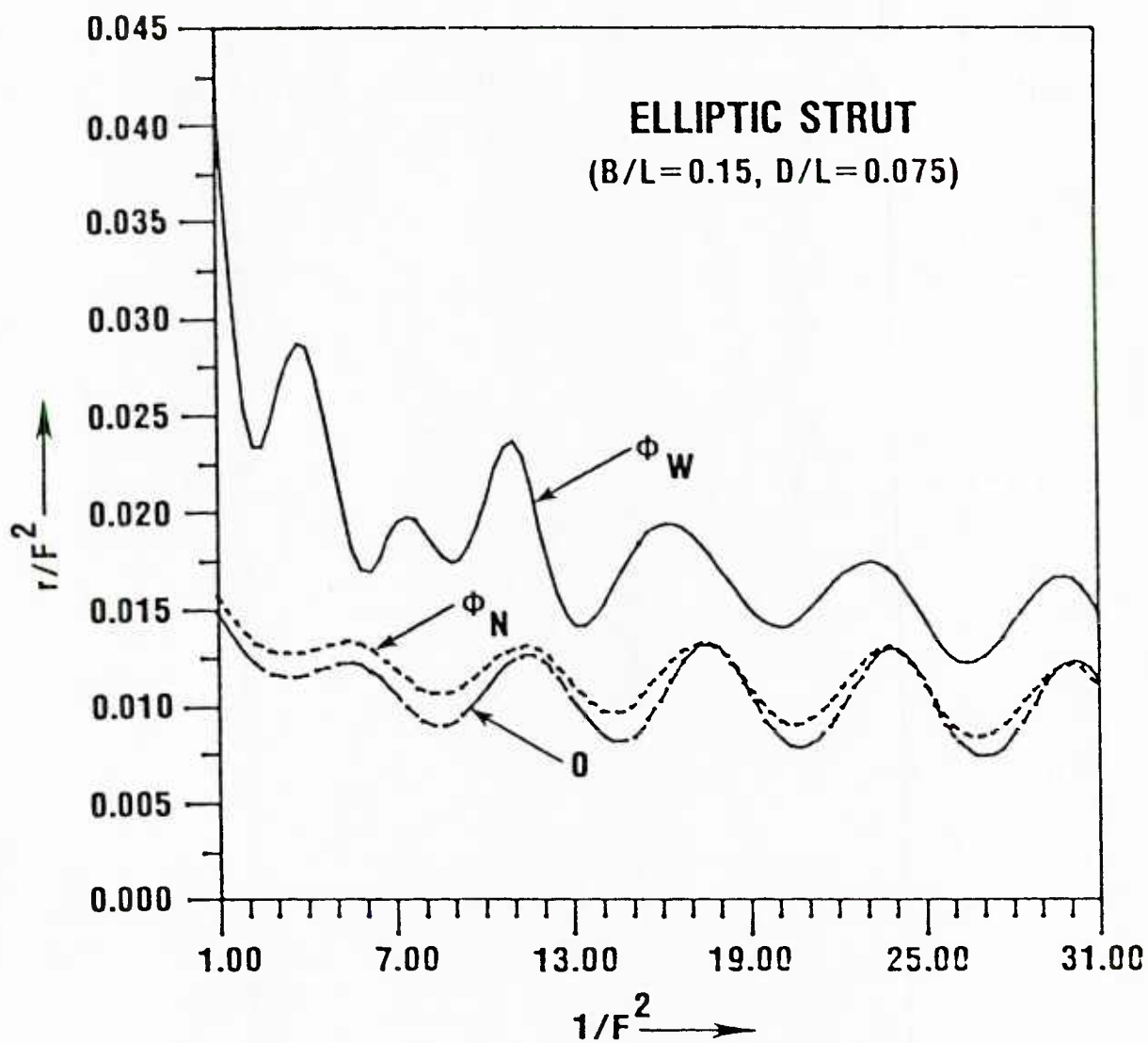


Fig. 2b - Wave-resistance approximations associated with the velocity-potential approximations $\phi = 0$, ϕ_N , and ϕ_W for the elliptic strut

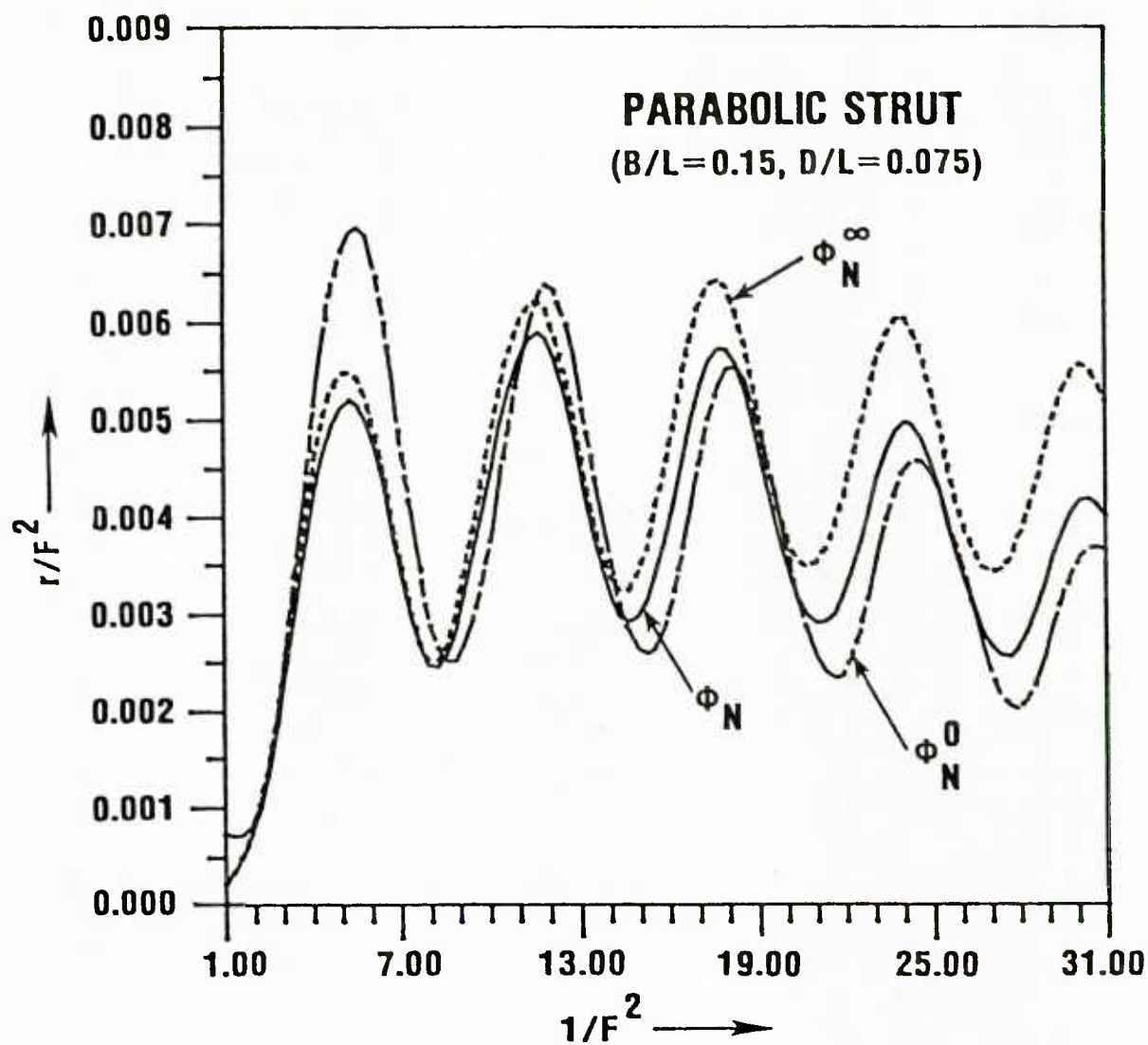


Fig. 3a - Wave-resistance approximations associated with the velocity-potential approximations $\phi = \phi_N^0$, ϕ_N^∞ , and ϕ_N for the parabolic strut

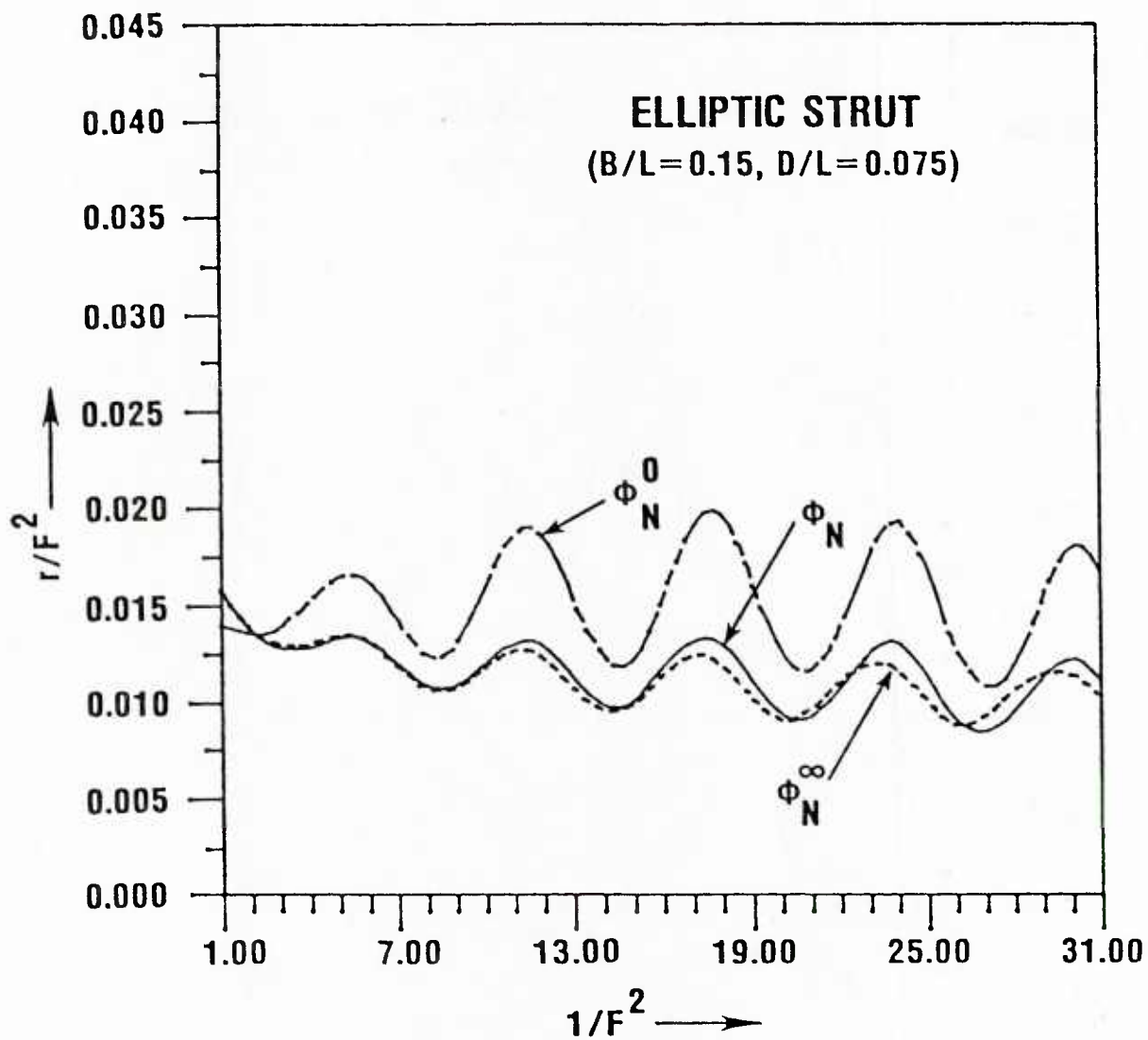


Fig. 3b - Wave-resistance approximations associated with the velocity-potential approximations $\phi = \phi_N^0$, ϕ_N^∞ , and ϕ_N for the elliptic strut

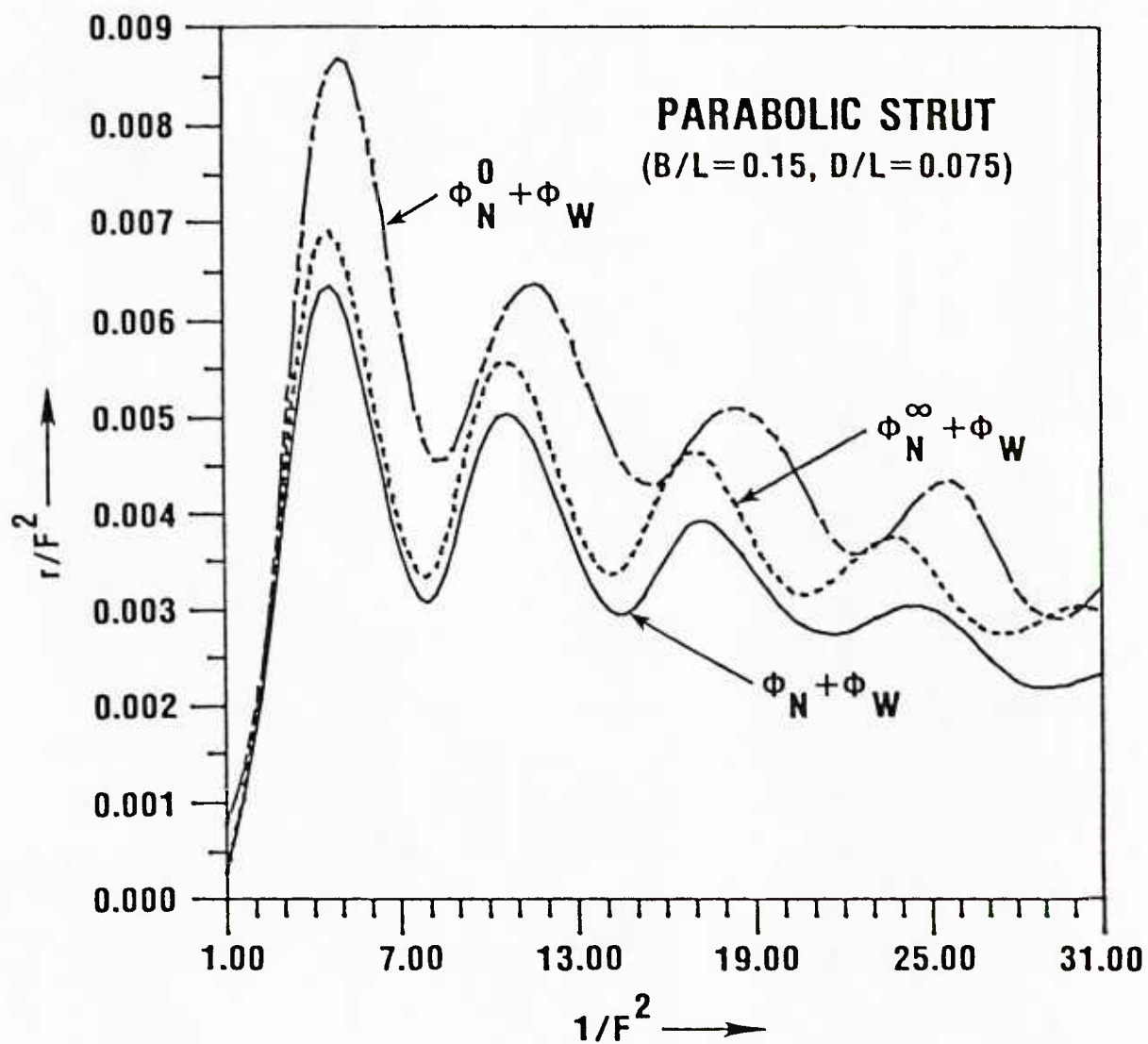


Fig. 4a - Wave-resistance approximations associated with the velocity-potential approximations $\phi = \phi_N^0 + \phi_W$, $\phi_N^\infty + \phi_W$, and $\phi_N + \phi_W$ for the parabolic strut

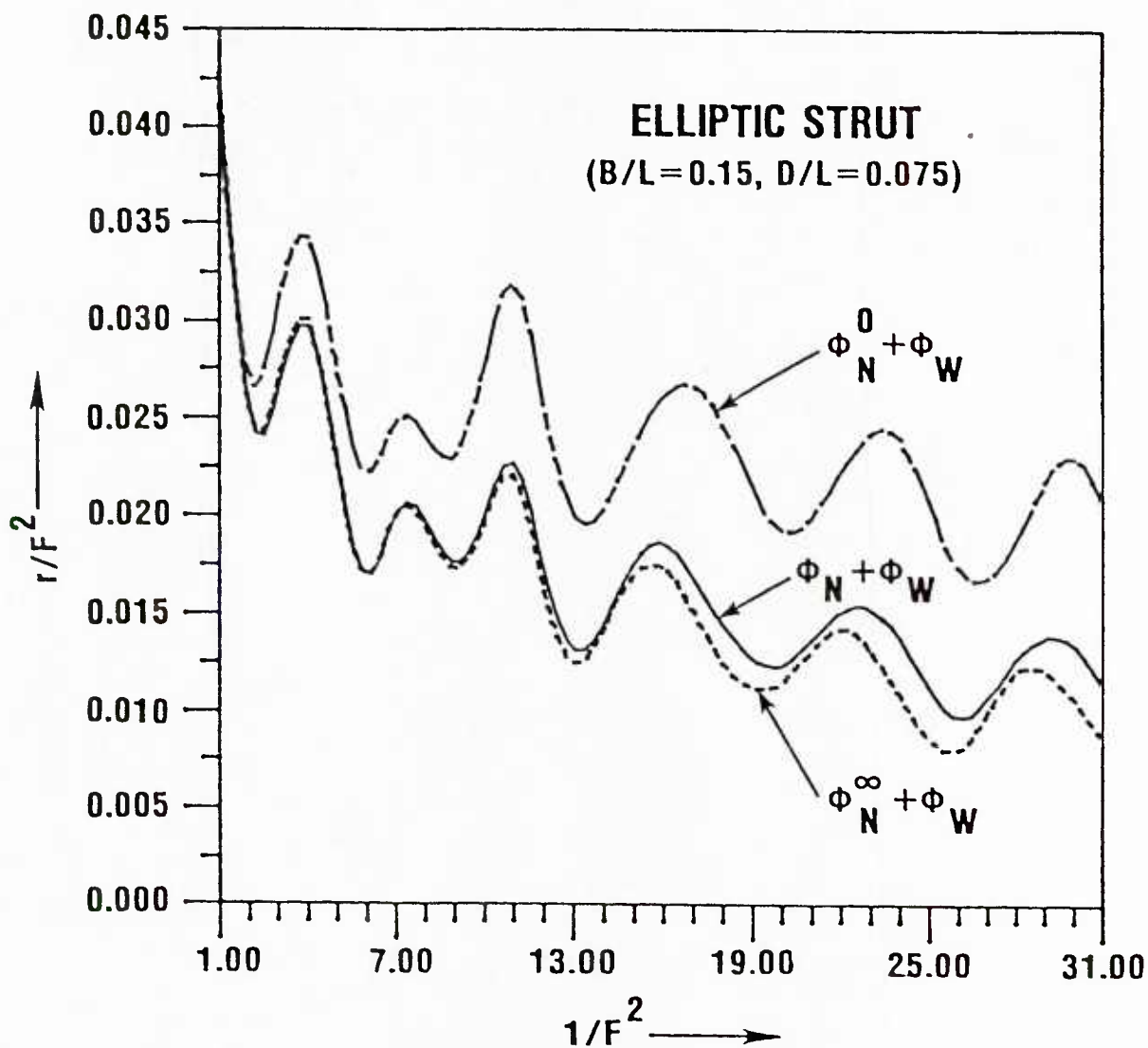


Fig. 4b - Wave-resistance approximations associated with the velocity-potential approximations $\phi = \phi_N^0 + \phi_W$, $\phi_N^\infty + \phi_W$, and $\phi_N + \phi_W$ for the elliptic strut

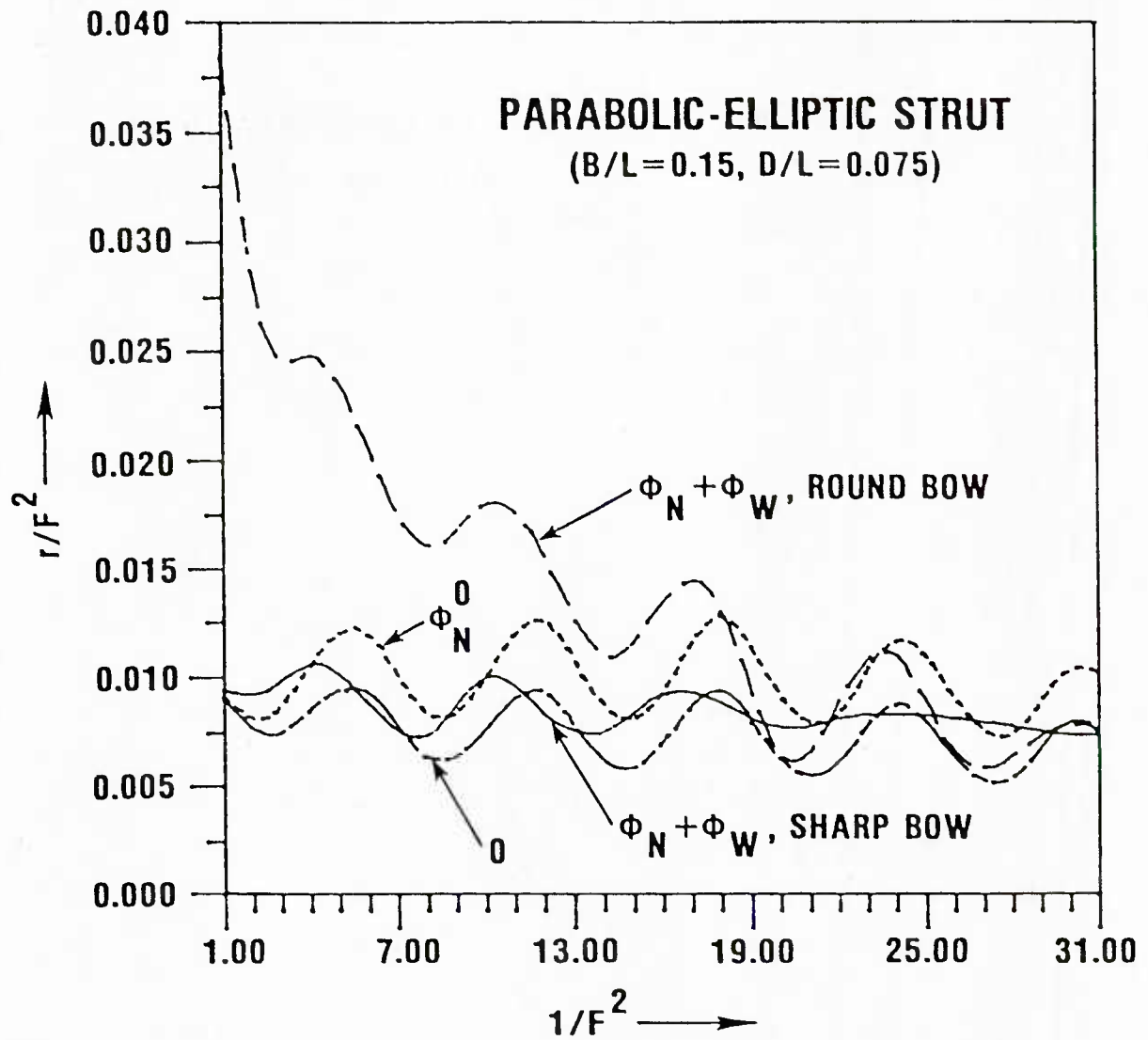


Fig. 5 - Wave-resistance approximations associated with the velocity-potential approximations $\phi = 0$, ϕ_N^0 , and $\phi_N + \phi_W$ for the parabolic/elliptic strut in forward and backward motion

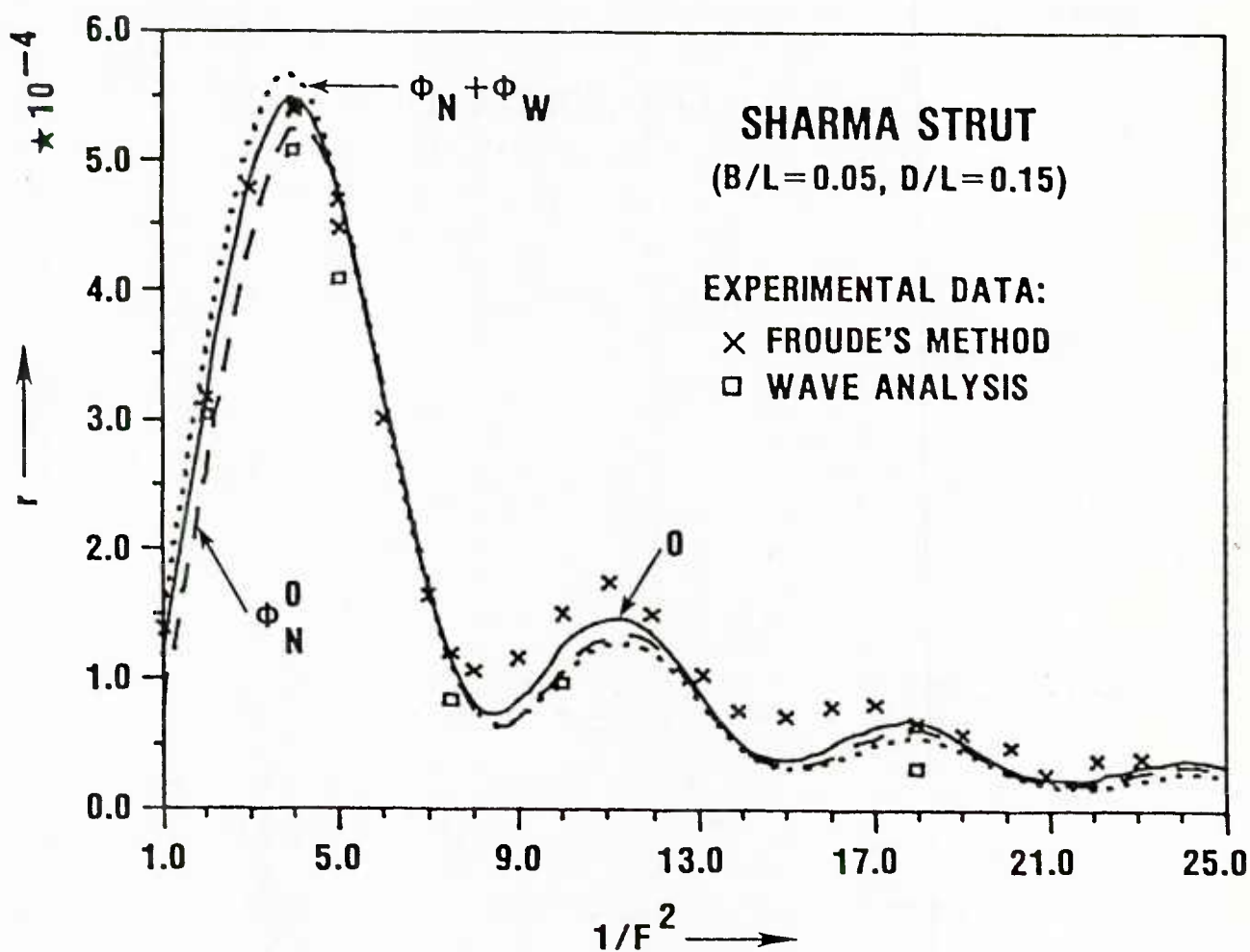


Fig. 6 - Experimental data and wave-resistance approximations associated with the velocity-potential approximations $\phi = 0$, ϕ_N^0 , and $\phi_N + \phi_W$ for the Sharma parabolic strut

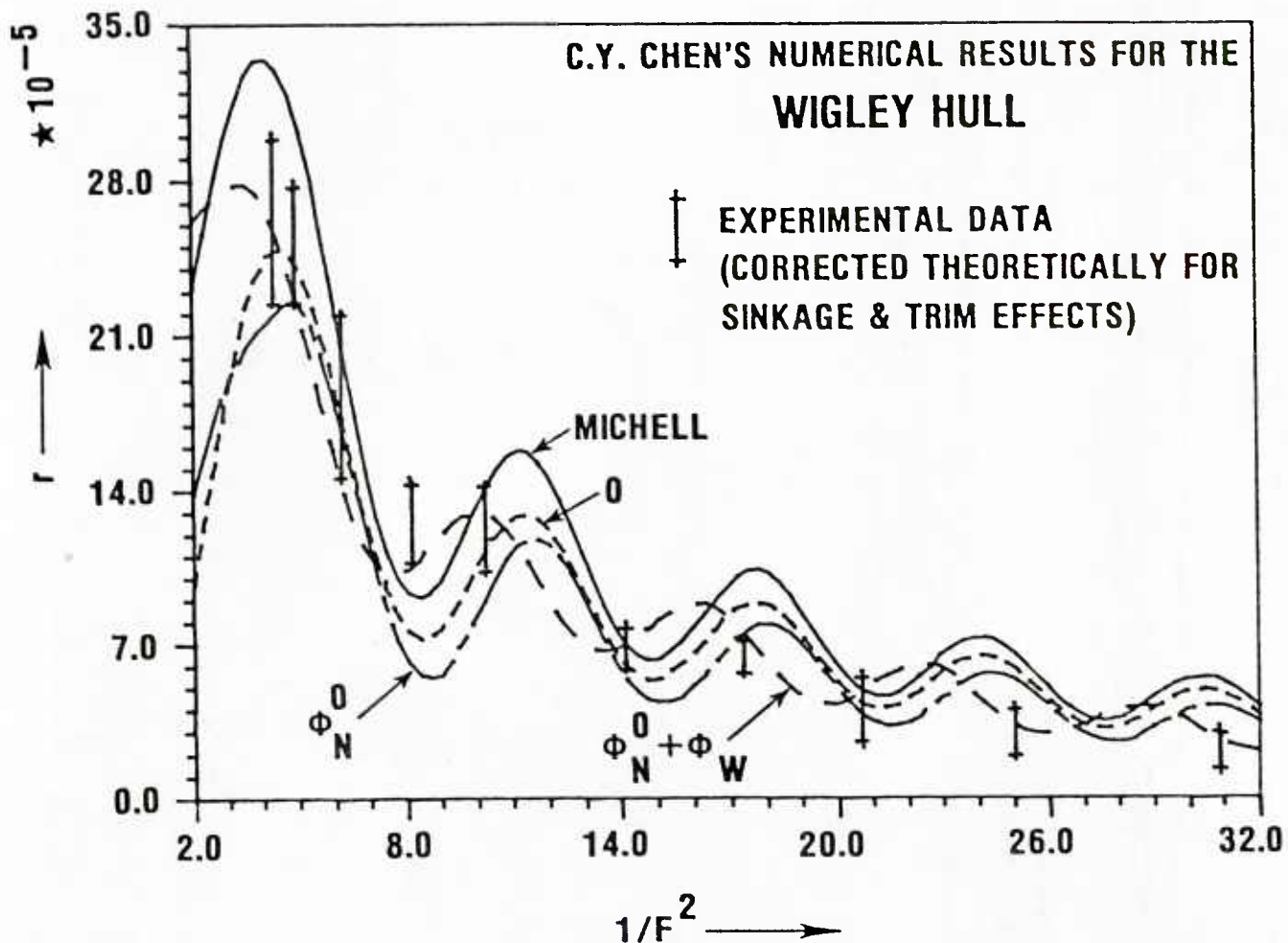


Fig. 7 - Experimental data and wave-resistance approximations associated with the Michell theory and the velocity-potential approximations $\phi = 0$, ϕ_N^0 , and $\phi_N^0 + \phi_W$ for the Wigley hull

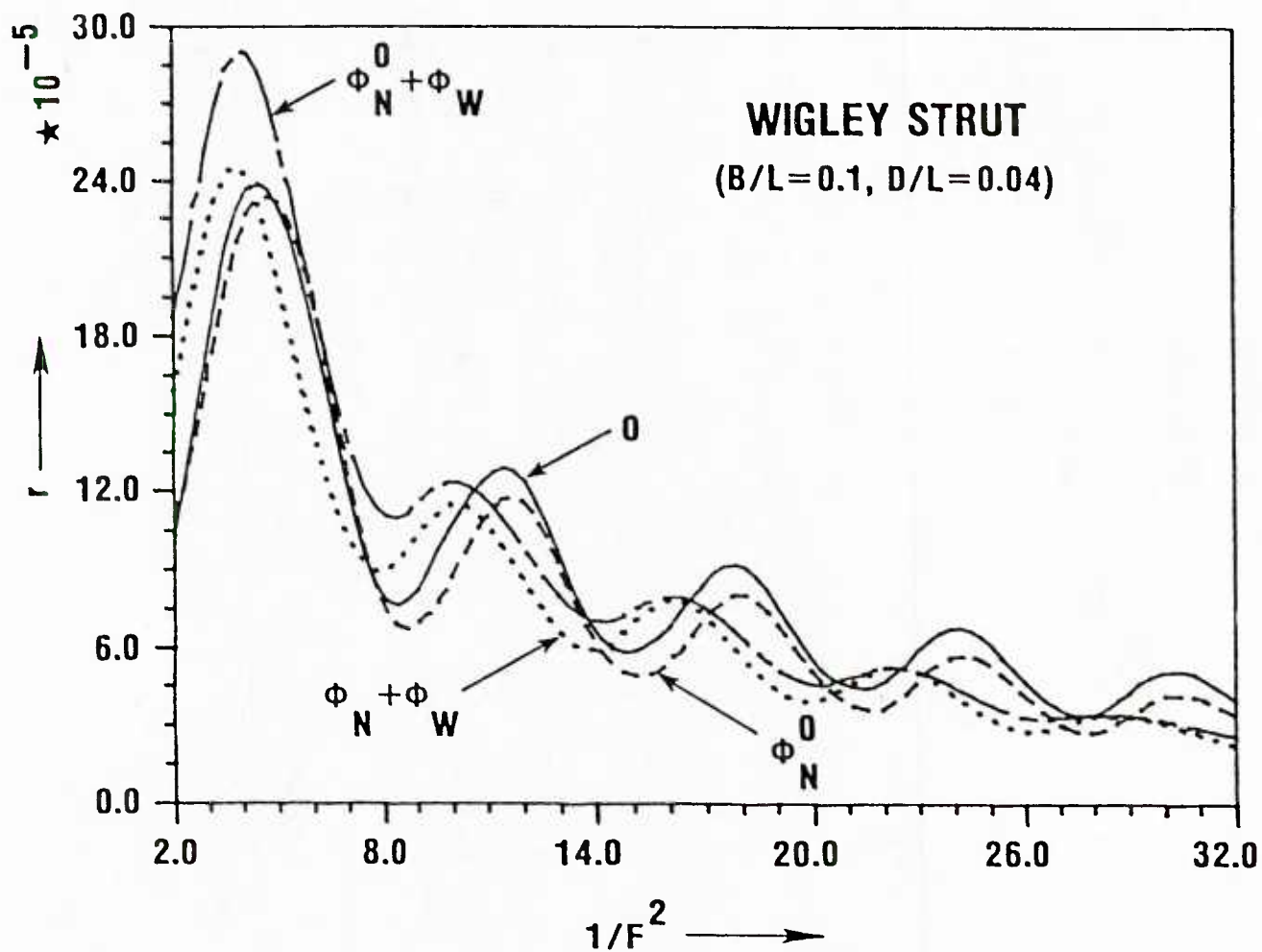


Fig. 8 - Wave-resistance approximations associated with the velocity-potential approximations $\phi = 0$, ϕ_N^0 , $\phi_N^0 + \phi_W$, and $\phi_N + \phi_W$ for the Wigley strut

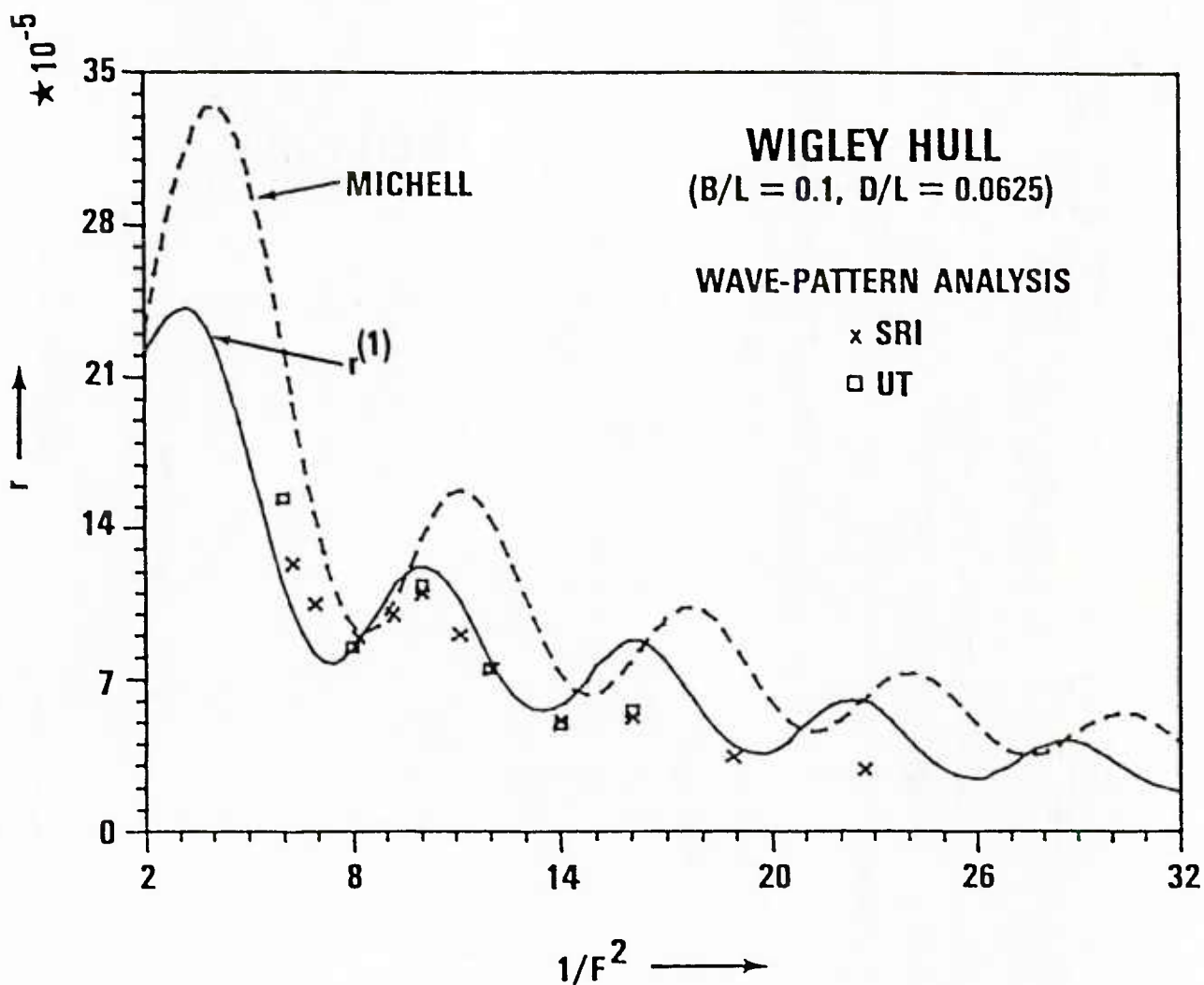


Fig. 9a - Experimental data based on the method of wave-pattern analysis and wave-resistance curves associated with the Michell theory and the first-order slender-ship approximation

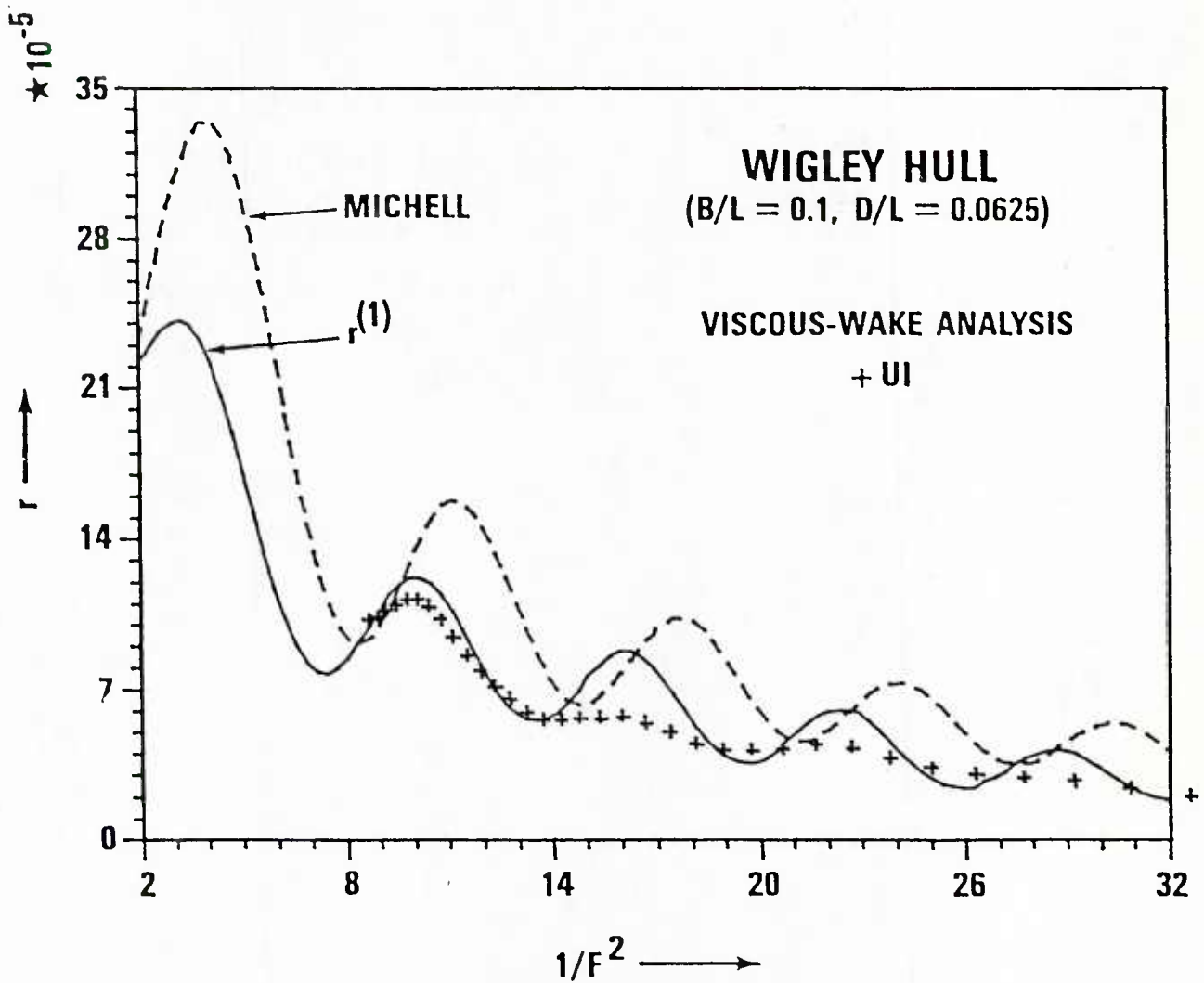


Fig. 9b - Experimental data based on the method of viscous-wake survey and wave-resistance curves associated with the Michell theory and the first-order slender-ship approximation

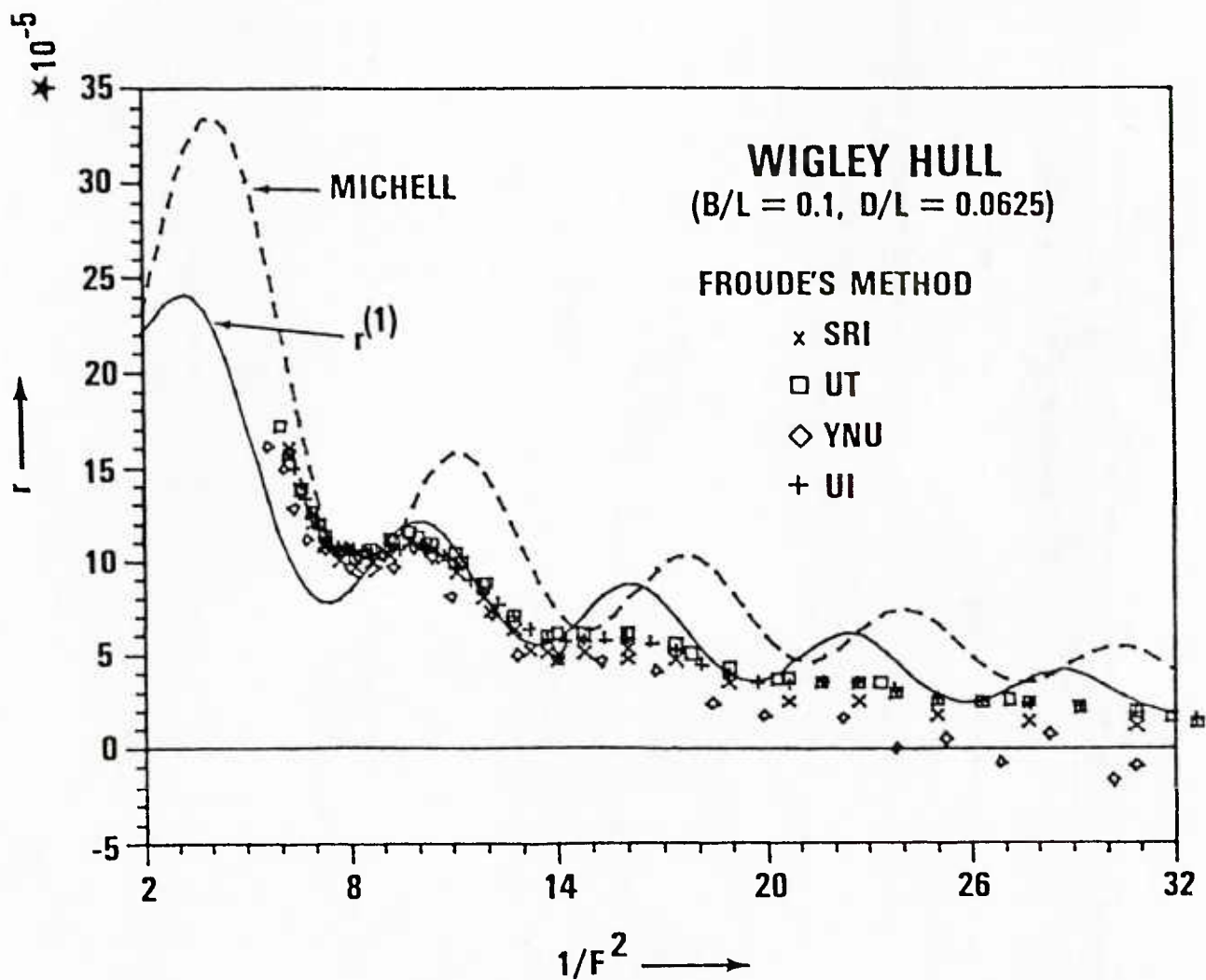


Fig. 9c - Experimental data based on the Froude method and wave-resistance curves associated with the Michell theory and the first-order slender-ship approximation

TABLE 1 - Values of the Nondimensional Wave Resistance $r = R/\rho U^2 L^2$ for the Parabolic Strut

$1/F^2$	$\phi = 0$	ϕ_N^0	ϕ_N^∞	ϕ_N	ϕ_W	$\phi_N^0 + \phi_W$	$\phi_N^\infty + \phi_W$	$\phi_N + \phi_W$
1	.894E-04	.709E-03	.206E-03	.224E-03	.159E-03	.765E-03	.264E-03	.281E-03
2.5	.646E-03	.561E-03	.584E-03	.542E-03	.139E-02	.118E-02	.112E-02	.106E-02
4	.126E-02	.125E-02	.112E-02	.104E-02	.197E-02	.190E-02	.163E-02	.150E-02
6	.983E-03	.112E-02	.842E-03	.805E-03	.121E-02	.131E-02	.907E-03	.837E-03
8	.339E-03	.364E-03	.312E-03	.304E-03	.588E-03	.584E-03	.417E-03	.383E-03
10	.463E-03	.366E-03	.473E-03	.439E-03	.666E-03	.560E-03	.535E-03	.482E-03
12	.545E-03	.531E-03	.504E-03	.480E-03	.560E-03	.525E-03	.406E-03	.370E-03
14	.248E-03	.253E-03	.240E-03	.225E-03	.357E-03	.347E-03	.239E-03	.214E-03
16	.254E-03	.187E-03	.294E-03	.246E-03	.337E-03	.273E-03	.269E-03	.219E-03
17	.331E-03	.265E-03	.360E-03	.311E-03	.348E-03	.282E-03	.274E-03	.231E-03
18	.347E-03	.307E-03	.351E-03	.316E-03	.328E-03	.282E-03	.241E-03	.210E-03
20	.188E-03	.183E-03	.189E-03	.173E-03	.247E-03	.234E-03	.162E-03	.149E-03
22	.153E-03	.109E-03	.194E-03	.147E-03	.200E-03	.165E-03	.154E-03	.125E-03
24	.229E-03	.186E-03	.252E-03	.207E-03	.205E-03	.164E-03	.156E-03	.126E-03
26	.146E-03	.135E-03	.153E-03	.132E-03	.177E-03	.165E-03	.116E-03	.108E-03
28	.999E-04	.716E-04	.135E-03	.942E-04	.134E-03	.115E-03	.986E-04	.802E-04
30	.155E-03	.118E-03	.185E-03	.138E-03	.130E-03	.983E-04	.101E-03	.745E-04
32	.115E-03	.101E-03	.127E-03	.102E-03	.129E-03	.114E-03	.871E-04	.771E-04

TABLE 2 - Values of the Nondimensional Wave Resistance $r = R/\rho U^2 L^2$ for the Elliptic Strut

$1/F^2$	$\phi = 0$	ϕ_N^0	ϕ_N^∞	ϕ_N	ϕ_W	$\phi_N^0 + \phi_W$	$\phi_N^\infty + \phi_W$	$\phi_N + \phi_W$
1	.148E-01	.139E-01	.157E-01	.156E-01	.414E-01	.410E-01	.427E-01	.425E-01
2	.623E-02	.674E-02	.686E-02	.679E-02	.122E-01	.135E-01	.128E-01	.127E-01
2.5	.473E-02	.540E-02	.527E-02	.521E-02	.932E-02	.109E-01	.970E-02	.958E-02
3	.384E-02	.462E-02	.431E-02	.425E-02	.859E-02	.102E-01	.890E-02	.878E-02
4	.291E-02	.379E-02	.326E-02	.320E-02	.712E-02	.856E-02	.751E-02	.741E-02
5	.244E-02	.329E-02	.269E-02	.266E-02	.435E-02	.548E-02	.456E-02	.451E-02
6	.199E-02	.269E-02	.219E-02	.218E-02	.280E-02	.369E-02	.282E-02	.280E-02
7	.151E-02	.203E-02	.169E-02	.170E-02	.277E-02	.354E-02	.285E-02	.286E-02
8	.114E-02	.155E-02	.134E-02	.135E-02	.237E-02	.301E-02	.245E-02	.247E-02
9	.102E-02	.144E-02	.119E-02	.120E-02	.193E-02	.255E-02	.191E-02	.194E-02
10	.108E-02	.159E-02	.118E-02	.120E-02	.203E-02	.274E-02	.195E-02	.199E-02
11	.113E-02	.169E-02	.115E-02	.118E-02	.215E-02	.290E-02	.201E-02	.206E-02
12	.103E-02	.154E-02	.102E-02	.107E-02	.155E-02	.217E-02	.138E-02	.146E-02
13	.798E-03	.118E-02	.821E-03	.862E-03	.109E-02	.155E-02	.956E-03	.101E-02

TABLE 2 - Continued

$1/F^2$	$\phi = 0$	ϕ_N^0	ϕ_N^∞	ϕ_N	ϕ_W	$\phi_N^0 + \phi_W$	$\phi_N^\infty + \phi_W$	$\phi_N + \phi_W$
14	.600E-03	.878E-03	.682E-03	.695E-03	.108E-02	.145E-02	.101E-02	.103E-02
15	.557E-03	.810E-03	.661E-03	.670E-03	.119E-02	.157E-02	.113E-02	.117E-02
16	.652E-03	.959E-03	.711E-03	.738E-03	.121E-02	.163E-02	.108E-02	.116E-02
17	.748E-03	.112E-02	.729E-03	.771E-03	.111E-02	.157E-02	.897E-03	.986E-03
18	.720E-03	.109E-02	.657E-03	.717E-03	.949E-03	.138E-02	.698E-03	.797E-03
20	.416E-03	.624E-03	.452E-03	.463E-03	.700E-03	.962E-03	.574E-03	.617E-03
22	.433E-03	.625E-03	.501E-03	.486E-03	.752E-03	.101E-02	.646E-03	.687E-03
24	.541E-03	.805E-03	.483E-03	.541E-03	.696E-03	.999E-03	.453E-03	.571E-03
26	.325E-03	.490E-03	.338E-03	.345E-03	.476E-03	.670E-03	.308E-03	.371E-03
28	.297E-03	.422E-03	.378E-03	.338E-03	.506E-03	.666E-03	.427E-03	.450E-03
30	.411E-03	.599E-03	.378E-03	.405E-03	.553E-03	.767E-03	.356E-03	.445E-03
32	.270E-03	.403E-03	.271E-03	.270E-03	.360E-03	.508E-03	.202E-03	.263E-03

TABLE 3 - Values of the Nondimensional Wave Resistance $r = R/\rho U^2 L^2$
for the Parabolic/Elliptic Strut

1/F ²	$\phi = 0$	ϕ_N^0	$\phi_N + \phi_W$	
			Sharp bow	Round bow
1	.894E-02	.906E-02	.932E-02	.384E-01
2.5	.293E-02	.326E-02	.376E-02	.103E-01
4	.213E-02	.264E-02	.265E-02	.619E-02
6	.154E-02	.200E-02	.145E-02	.345E-02
8	.784E-03	.104E-02	.918E-03	.200E-02
10	.763E-03	.996E-03	.100E-02	.180E-02
12	.776E-03	.105E-02	.689E-03	.131E-02
14	.433E-03	.618E-03	.536E-03	.781E-03
16	.439E-03	.584E-03	.577E-03	.841E-03
18	.520E-03	.712E-03	.487E-03	.734E-03
20	.309E-03	.459E-03	.382E-03	.319E-03
22	.280E-03	.379E-03	.368E-03	.402E-03
24	.366E-03	.488E-03	.346E-03	.458E-03
26	.241E-03	.351E-03	.310E-03	.251E-03
28	.192E-03	.263E-03	.275E-03	.228E-03
30	.265E-03	.345E-03	.244E-03	.262E-03
32	.195E-03	.277E-03	.237E-03	.206E-03

TABLE 4 - Values of the Nondimensional Wave Resistance $r = R/\rho U^2 L^2$
for the Sharma Strut

$1/F^2$	$\phi = 0$	ϕ_N^0	$\phi_N + \phi_W$
1	.118E-03	.807E-04	.150E-03
2.5	.409E-03	.352E-03	.444E-03
4	.548E-03	.526E-03	.566E-03
6	.321E-03	.328E-03	.319E-03
8	.808E-04	.762E-04	.768E-04
10	.125E-03	.108E-03	.105E-03
12	.134E-03	.127E-03	.120E-03
14	.488E-04	.465E-04	.450E-04
16	.495E-04	.416E-04	.369E-04
18	.674E-04	.613E-04	.553E-04
20	.322E-04	.301E-04	.285E-04
22	.249E-04	.208E-04	.172E-04
24	.382E-04	.337E-04	.289E-04
26	.227E-04	.208E-04	.190E-04

TABLE 5 - Values of the Nondimensional Wave Resistance $r = R/\rho U^2 L^2$
for the Wigley Hull

$1/F^2$	Michell	$\phi = 0$	ϕ_N^0	$\phi_N^0 + \phi_W$	$\phi_N + \phi_W$
2	.232E-03	.974E-04	.139E-03	.261E-03	.221E-03
3	.304E-03	.188E-03	.190E-03	.277E-03	.241E-03
4	.335E-03	.243E-03	.214E-03	.269E-03	.226E-03
5	.304E-03	.240E-03	.224E-03	.221E-03	.173E-03
6	.224E-03	.187E-03	.180E-03	.155E-03	.114E-03
7	.139E-03	.119E-03	.113E-03	.109E-03	.798E-04
8	.942E-04	.770E-04	.633E-04	.103E-03	.831E-04
9	.100E-03	.778E-03	.571E-04	.120E-03	.108E-03
10	.134E-03	.106E-03	.843E-04	.130E-03	.122E-03
11	.158E-03	.128E-03	.113E-03	.118E-03	.109E-03
12	.145E-03	.122E-03	.115E-03	.895E-04	.784E-04
13	.108E-03	.925E-04	.897E-04	.691E-04	.575E-04
14	.725E-04	.627E-04	.577E-04	.686E-04	.579E-04
15	.628E-04	.536E-04	.427E-04	.807E-04	.754E-04
16	.786E-04	.667E-04	.515E-04	.891E-04	.879E-04
17	.984E-04	.841E-04	.703E-04	.809E-04	.773E-04
18	.102E-03	.880E-04	.792E-04	.616E-04	.546E-04

TABLE 5 - Continued

$1/F^2$	Michell	$\phi = 0$	ϕ_N^0	$\phi_N^0 + \phi_W$	$\phi_N + \phi_W$
19	.835E-04	.732E-04	.693E-04	.456E-04	.382E-04
20	.590E-04	.521E-04	.488E-04	.427E-04	.367E-04
21	.460E-04	.406E-04	.341E-04	.516E-04	.488E-04
22	.513E-04	.450E-04	.348E-04	.598E-04	.598E-04
23	.658E-04	.578E-04	.463E-04	.582E-04	.575E-04
24	.732E-04	.647E-04	.557E-04	.448E-04	.418E-04
25	.656E-04	.584E-04	.533E-04	.326E-04	.281E-04
26	.489E-04	.438E-04	.408E-04	.289E-04	.242E-04
27	.363E-04	.325E-04	.284E-04	.337E-04	.304E-04
28	.363E-04	.324E-04	.253E-04	.405E-04	.396E-04
29	.458E-04	.408E-04	.318E-04	.411E-04	.408E-04
30	.538E-04	.481E-04	.399E-04	.338E-04	.327E-04
31	.519E-04	.467E-04	.411E-04	.248E-04	.229E-04
32	.412E-04	.372E-04	.339E-04	.208E-04	.180E-04

TABLE 6 - Values of the Nondimensional Wave Resistance $r = R/\rho U^2 L^2$
for the Wigley Strut

$1/F^2$	$\phi = 0$	ϕ_N^0	$\phi_N^0 + \phi_W$	$\phi_N + \phi_W$
1	.150E-04	.977E-04	.985E-04	.379E-04
2.5	.140E-03	.134E-03	.221E-03	.193E-03
4	.234E-03	.223E-03	.291E-03	.244E-03
6	.184E-03	.194E-03	.195E-03	.143E-03
8	.789E-04	.758E-04	.111E-03	.896E-04
10	.108E-03	.884E-04	.124E-03	.116E-03
12	.124E-03	.116E-03	.979E-04	.858E-04
14	.652E-04	.611E-04	.699E-04	.590E-04
16	.694E-04	.552E-04	.799E-04	.788E-04
18	.913E-04	.805E-04	.632E-04	.560E-04
20	.547E-04	.501E-04	.456E-04	.392E-04
22	.478E-04	.375E-04	.524E-04	.524E-04
24	.682E-04	.572E-04	.445E-04	.415E-04
26	.465E-04	.412E-04	.331E-04	.277E-04
28	.348E-04	.274E-04	.344E-04	.336E-04
30	.511E-04	.415E-04	.316E-04	.306E-04
32	.396E-04	.340E-04	.258E-04	.223E-04

LINEAR AND NON-LINEAR CALCULATIONS
FOR THE WAVE-RESISTANCE OF SUBMERGED BODIES

by M. LENOIR, J. CAHOUE, C. GUTTMANN

E.N.S.T.A. - Groupe Hydrodynamique Navale -
Centre de l'Yvette - Chemin de la Hunière - 91120 PALAISEAU (France)

I. INTRODUCTION

The computation of the wave-resistance of ships, is one of the most challenging problem in the field of naval hydrodynamics. The first trouble is related to the turbulent character of the flow, whose Reynolds number is high. Only few attempts have been made in this direction, and from now on we shall consider the fluid as perfect and the flow as irrotational.

Other difficulties are more specific and concern the boundaries of the fluid domain, which is unbounded and unknown, for the location of the free surface is one of the very unknowns of the problem. The purpose of the second part of this paper is to exhibit an algorithm for the solution of such a problem.

An other procedure consists in linearizing the free-surface conditions ; one is thus led to the so-called "Neumann-Kelvin problem" which involves the Laplace equation together with a linearized free-surface condition with a second-order tangential derivative. This highly unusual feature makes the consideration of surface-piercing bodies specially difficult.

Finally, one must mention that the problem itself is ill-conditioned, for the quantity of interest is the wave-resistance, i.e. the integral of the pressure on the body. The wave-resistance is small as compared with other quantities, such as the velocity potential and the free-surface elevation ; it is thus difficult to compute it accurately.

In the sequel, we shall only deal with some of these difficulties. We consider only the case of a submerged body, for which two methods are presented. In the first part we show some results related to the solution of the 3-D Neumann-Kelvin problem ; the method of solution is the coupling between Finite Elements and Integral Representation (F.E.I.R.) devised by JAMI and LENOIR [1]. The high order of approximation allows good results with only few degrees of freedom. In the second part, we exhibit a procedure for the solution of the non-linear 2-D free-surface problem. We use a combination of BAI's [2] localized finite element method, which accounts for the behaviour of the solution at infinity, and of a fixed point algorithm for seeking the location of the free surface. We need only small calculation domains and few iterations for obtaining results which are significantly different to those deriving from the linearized theory.

II. NUMERICAL SOLUTION OF THE 3-D NEUMANN-KELVIN PROBLEM, FOR A SUBMERGED BODY

This situation is presently one of the best known, especially concerning the conditions at infinity, which are properly taken into account by a Green's function of the Laplacian satisfying the linearized free surface condition and the upstream decay condition. The classical singularity distribution method leads however to poor accuracy, for it is limited to low-order approximations ; the purpose of the F.E.I.R. coupling method is precisely to remove this drawback.

The problem under consideration

The mean position of the free surface is denoted by $\check{\Gamma}S = \{M | z_M = 0\}$, Γ is the surface of the body and $\check{\Omega}$ the linearized fluid domain ; the depth is assumed infinite. The body is fixed in the coordinate system and the components of the incoming velocity are following : $(-V_\infty, 0, 0)$.

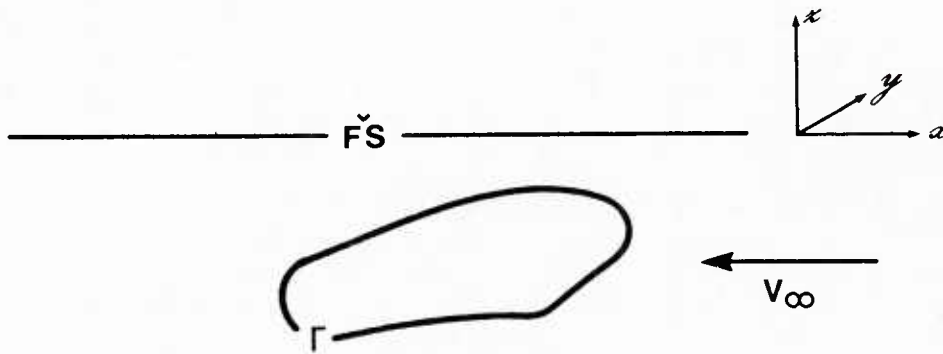


Figure 1

By $\phi_w = -V_\infty x$, we denote the incoming velocity potential, and by $\check{\phi}$ the perturbation potential, which satisfies

$$\begin{aligned}
 & \Delta \check{\phi} = 0 \text{ in } \check{\Omega}, \\
 (P) \quad & \frac{\partial^2 \check{\phi}}{\partial x^2} + k_0 \frac{\partial \check{\phi}}{\partial z} = 0 \text{ on } \check{\Gamma}S, \\
 & \frac{\partial \check{\phi}}{\partial n} = -V_\infty (\vec{n}, \vec{i}_x) \text{ on } \Gamma, \text{ and} \\
 (C_\infty) \quad & \phi, \frac{\partial \phi}{\partial x} \rightarrow 0 \text{ when } x \rightarrow +\infty ; \phi, \frac{\partial \phi}{\partial z} \rightarrow 0 \text{ when } z \rightarrow -\infty,
 \end{aligned}$$

where \vec{i}_x denotes the unit vector along the \vec{ox} axis, and where $k_0 = g/V_\infty^2$, and g is the acceleration of gravity.

A brief description of the F.E.I.R. coupling method

Just as in the singularity distribution method, our main tool is a Green's function $G_M(P)$ of problem (P) , satisfying

$$\left\{ \begin{array}{l} \Delta_P G_M(P) = \delta_M \text{ in } R_-^3, \\ \frac{\partial^2 G_M(P)}{\partial x_P^2} + k_0 \frac{\partial G_M(P)}{\partial z_P} = 0 \text{ on } \check{F}\check{S}, \text{ and} \\ \text{the decay conditions } (C_\infty). \end{array} \right.$$

One can prove in fact, see GUTTMANN [3], that this problem has one and only solution in the space $S'(R_-^3)$ of tempered distributions. This solution is known, and several analytical expressions can be found in Noblesse [4]. As a consequence, GUTTMANN [3], shows that any solution ϕ of P satisfies the following integral representation formula :

$$(I.R.) \quad \check{\phi}(M) = \int_{\Gamma} \{ \phi(P) \frac{\partial}{\partial M_P} G_M(P) - \frac{\partial \check{\phi}}{\partial n}(P) G_M(P) \} ds_P, \quad \forall M \in \check{\Omega}.$$

Let's now draw a fictitious boundary Σ around the body, which does not intersect Γ . Relation (I.R.) leads us to a boundary condition along Σ and makes $\phi = (\check{\phi}|_{\Omega})$ a solution of problem (P) , set in the bounded domain Ω :

$$(P) \quad \left\{ \begin{array}{l} \Delta \phi = 0 \text{ in } \Omega, \\ \frac{\partial \phi}{\partial n} = -V_\infty (\vec{n} | \vec{i}_x) \text{ on } \Gamma, \text{ and} \\ \phi(M) = \int_{\Gamma} \{ \phi(P) \frac{\partial}{\partial M_P} G_M(P) + V_\infty (\vec{n} | \vec{i}_x)(P) G_M(P) \} ds_P. \end{array} \right.$$

$\check{F}\check{S}$

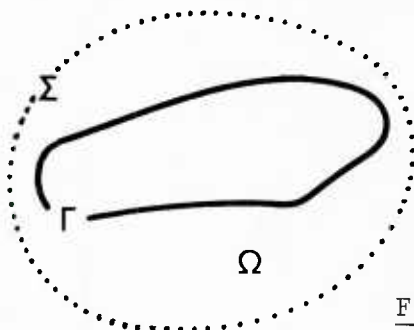


Figure 2

Conversely, assuming that (\check{P}) is well-posed, one can prove, see LENOIR [5], that (P) is well-posed and that its solution is nothing but the restriction of $\check{\phi}$ to Ω .

The variational formulation of problem (P) is then approximated via finite elements. It is worth noticing that the conditions at infinity and on the free surface do not appear explicitly and that the location of Σ is essentially arbitrary; one can thus restrict Ω to one or two layers of elements around the body. The most important feature of this method is that no integral involves a singular kernel, for M and P belong respectively to Σ and Γ , which do not intersect. The usual techniques of finite elements procedures, such as high order isoparametric elements and numerical integration, are thus available and lead to good accuracy with restricted number of unknowns.

An analytical formula for the Green's function

A detailed analytical study of the Green's function $G_M(P)$ is available in EUVRARD [6], from which we extract the following set of formulas :

$$G_M(P) = D(M,P) + \phi_F(M,P) + \phi_N(M,P),$$

where ϕ_F is referred to as the far-field and ϕ_N as the near-field.

$$D(M,P) = -\frac{1}{4M} \left\{ \frac{1}{|MP|} - \frac{1}{|M'P|} \right\},$$

where M' is symmetrical to M with respect to \check{FS} .

Put then $X = (X_P - X_M)/k_0$, $Y = (Y_P - Y_M)/k_0$, and $Z = (Z_P + Z_M)/k_0$;
we have

$$\phi_F(M,P) = 0 \text{ if } X \leq 0, \text{ and otherwise}$$

$$\phi_F(M,P) = -\sqrt{2} k_0 \int_{-\infty}^{+\infty} e^{-2i\pi u|Y|} \frac{m(u)}{\ell(u)} \sin(X \frac{m(u)}{\sqrt{2}}) e^{\frac{Zm^2(u)}{2}} du,$$

where $\ell(u) = (1 + 16\pi^2 u^2)^{1/2}$ and $m(u) = (1 + \ell(u))^{1/2}$, and

$$\phi_N(M,P) = \frac{k_0}{2\pi^2} \operatorname{Im} \int_0^{\pi/2} \sin \theta \{ e^{a(\theta)} E_1(a(\theta)) + e^{b(\theta)} E_1(b(\theta)) \} d\theta, \text{ where}$$

$$a(\theta) = \sin \theta \{ i|X| + Y \cos \theta + Z \sin \theta \}, \text{ and } b(\theta) = \sin \theta \{ i|X| - Y \cos \theta + Z \sin \theta \}.$$

Numerical calculation of the Green's function

The estimation of integral (I.R.) requires numerous calculations of $G_M(P)$: one for each pair (M,P), where M and P run respectively over the respective sets of degrees of freedom of Σ and Γ . It is thus of prime interest to devise efficient approximation procedures for $G_M(P)$.

Our procedure for the calculation of the near-field potential is rather crude, and we believe it could be substantially improved : the integrand is approximated by splines of order 2 and degree 3, with equidistant interpolation abscissas, the number of which varies from 15 to 40 according to the values of X, Y and Z.

The calculation of the far field potential is more sophisticated and relies on WEBER's [7] method, for the calculation of Fourier transforms. We put

$$\phi_L(M, P) = \int_{-\infty}^{+\infty} e^{-2i\pi u|Y|} h(u, X, Z) du,$$

and develop ϕ_L on the basis of the $\psi_n(Y) = e^{-Y/2} L_n(Y)$, $n \geq 0$, where L_n is the Laguerre polynomial of order n :

$$\phi_L(M, P) = \sum_{n \geq 0} C_n^T(X, Z) \psi_n\left(\frac{Y}{T}\right).$$

Coefficients C_n^T are given by the following formula :

$$C_n^T(X, Z) = \frac{1}{4\pi T} \int_0^{2\pi} (1 + i \cotg \frac{\theta}{2}) h\left(-\frac{1}{4\pi T} \cotg \frac{\theta}{2}, X, Z\right) e^{-in\theta} d\theta,$$

and are calculated via Fast Fourier Transform. Parameter T is chosen in such a way to reduce the number of coefficients C_n^T significantly different from 0.

Some results

We present here some preliminary results. The case under consideration is that of a submerged ellipsoid of respective big and small axis 2a and 2b. The depth of the center, denoted by H, is equal to 2b.

The meshes are made up of one layer of second order prismatic and cubic finite elements ; the symmetry of the problem with respect to the (x, z) plane is taken into account. The accuracy of the method has been checked in the case where the exact solution is nothing then the Green's function $G_M(P_0)$ associated with a point P_0 inside the body.

The tables show the variation of the non-dimensional wave-resistance R_H versus the Froude number F_R , with

$$F_R = \frac{V_\infty}{\sqrt{gH}}, \text{ and } R_H = \frac{R_w}{\pi \rho g b^3},$$

where R_w is the horizontal component of the resulting force on the body, and ρ the mass per unit fluid volume.

Comparisons have been carried out with the numerical results of DELHOMMEAU [8] and with the (semi-)analytical results of HAVELOCK [9].

The first table is devoted to the case of a sphere ($a = b = 1$), and the second to that of an ellipsoid ($a = 2.5$, $b = 1$). The agreement with Havelock's results is quite satisfactory for the sphere ; the (small) discrepancy which can be noticed on the second table is presently under consideration : does it follow from a lack of accuracy in Havelock's result or in the calculation of the Green's function ?

III. NUMERICAL SOLUTION OF THE 2-D NON LINEAR FREE-SURFACE PROBLEM, FOR A BUMP ON THE BOTTOM

Within the scope of the linear theory, some trouble occurs when the obstacle runs through the free surface. The computation of the integral representation itself is not an easy matter, but primarily the 2-D results of SUZUKI [10] and LENOIR [5] show the existence of values of the Froude number which make the problem ill-posed. We consider the linearization as faulty in the vicinity of the water-line ; we are thus led to the solution of the non-linear free surface problem.

The first stage of this work will be described below : it is related to the case of a 2-D immersed body ; for the sake of simplicity we shall restrict ourselves to a bump on the bottom.

The problem

We study the perturbation of an uniform free-surface flow by a fixed bump on the bottom. The fluid is assumed perfect and incompressible, the flow irrotational and stationary. The flow depends on the shape of the body, and the Froude number $F = V_\infty (gH)^{-1/2}$, where V_∞ and H denote respectively the speed and the depth at infinity, and g the acceleration of gravity. The flow is accounted for as supercritical if $F > 1$, and subcritical otherwise.

The fluid domain is denoted by Ω ; the respective equations of the free-surface Γ and of the bottom \bar{B} are given by $y = 1 + \eta$, and $y = f$, where f is compactly supported. The non-dimensional equations satisfied by the perturbation stream-function ψ and the perturbation η of the free-surface elevation are following :

- (1) $\Delta\psi = 0$ in $\check{\Omega}$,
- (2) $\psi + f = 0$ on \check{B} ,
- (3) $\psi + \eta = 0$, and (P)
- (4) $2(F^{-2} \eta + \partial\psi/\partial y) + |\nabla\psi|^2 = 0$ on \check{FS} ,
- (5) ψ and $|\nabla\psi|$ are bounded and vanish upstream.

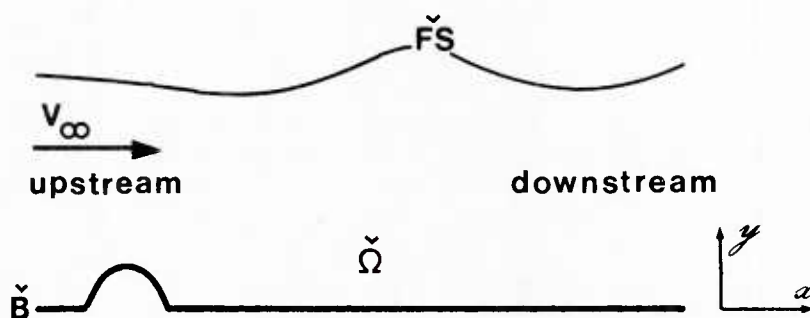


Figure 3

The numerical methods which are accounted for in the literature faced two major difficulties. On the one hand, the solution depends highly on the size of the computation domain (HESS [11]), it is the result of a lack of accuracy regarding the conditions at infinity ; on the other hand, the usual fixed point algorithms, are only satisfactory in the supercritical case (see LIU [12], VON KERCKZEK and SALVESEN [13], KORVING and HERMANS [14]).

The essential features of our algorithm are following : it is a fixed point-procedure, which implementation is quite easy, and the conditions at infinity are taken into account by a localized finite element method (BAI [2]). Indeed, we consider that the non-linearity is only significant in the vicinity of the body ; on the other hand the linear approximation allows an accurate account of the behaviour of the flow at infinity.

A localized finite element method

We shall give here only some brief informations about the use of the localized finite element method for the stream function equations.

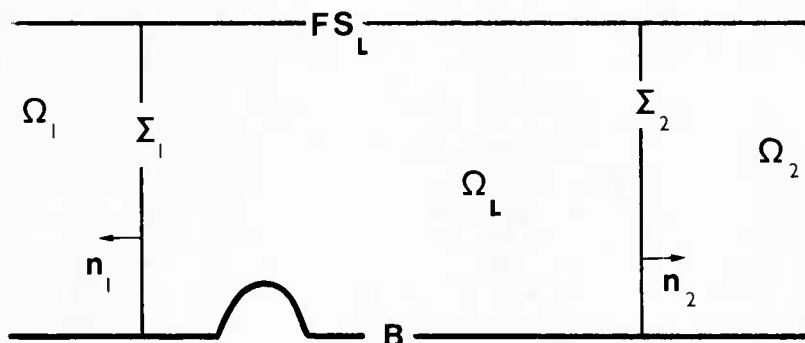


Figure 4

Assume η and $|\nabla\psi|$ are small with respect to 1. The elimination of η between the linear approximations of equations (3) and (4) leads to

$$(6) \quad \partial\psi/\partial y = F^{-2} \psi \text{ on } FS_L^V, \text{ defined by the equation } y = 1.$$

In the super-critical case, the solution in Ω_R^V , $k = 1, 2$ is approximated by a linear combination of the following functions :

$$(7) \quad \phi_i^k(x, y) = e^{(3-2k)\omega_i x} \sin \omega_i y, \text{ with}$$

$$\operatorname{tg} \omega_i = F^2 \omega_i, \quad \omega_i > 0, \quad 1 \leq i \leq N_k, \quad k = 1, 2.$$

We are thus led to the following variational formulation.

$$(P_{N_1, N_2}) \quad \left| \begin{array}{l} \text{Find } (\psi, \wedge_1, \wedge_2) \in V \times R^{N_1} \times R^{N_2} \text{ such that, } \forall (\phi, M_1, M_2) \in V' \times R^{N_1} \times R^{N_2}, \\ \int_{\Omega_L} (\nabla\psi | \nabla\phi) dx dy - F^{-2} \int_{FS_L} \psi \phi dx - \sum_{k=1}^2 \int_{\Sigma_k} \frac{\partial\psi^k}{\partial n_k} \phi dy = 0, \\ \int_{\Sigma_k} (\psi - \psi^k) \phi_i^k dy = 0, \quad 1 \leq i \leq N_k, \quad k = 1, 2, \text{ where} \end{array} \right.$$

$$V = \{\psi \in H^1(\Omega_L) | \psi|_B = -f\}, \quad V' = \{\psi \in H^1(\Omega_L) | \psi|_B = 0\}, \text{ and}$$

$$\psi^k = \sum_{i=1}^{N_k} \lambda_i^k \phi_i^k, \text{ with } \wedge_k = (\lambda_1^k, \dots, \lambda_{N_k}^k), \quad k = 1, 2.$$

In the subcritical case the basis (7) must be complemented downstream by

$$(8) \quad \phi_\ell(x, y) = \sin(\omega_0 + (\ell-1)\pi/2) \operatorname{sh} \omega_0 y, \quad \ell = 1, 2, \text{ with } \operatorname{th} \omega_0 = F^2 \omega_0, \quad \omega_0 > 0.$$

As a consequence, Λ_2 is complemented by the components λ_1 and λ_2 , and we put

$$\psi^2 = \sum_{i=1}^{N_2} \lambda_i^2 \phi_i^2 + \sum_{\ell=1}^2 \lambda_\ell \phi_\ell$$

Problem (P_{N_1, N_2}) is then complemented by the two following equations

$$(9^k) \quad \int_{\Sigma_k} (\psi - \psi^k) \operatorname{sh} \omega_0 y dy = 0, \quad k = 1, 2.$$

Solution of the non-linear problem

From now on, we shall take into account the exact non linear equations on the free surface. In terms of the total stream function $\psi_T = \psi + y$, equation (4) expresses as

$$\partial \psi_T / \partial n = (1 - 2\eta F^{-2})^{1/2}, \text{ from which we deduce}$$

$$\begin{aligned} \partial \psi / \partial n &= (1 - 2\eta F^{-2})^{1/2} - (1 + (d\eta/dx)^2)^{-1/2}, \\ &= 2F^{-2} \eta (1 + (1 - 2\eta F^{-2})^{1/2})^{-1} + 1 - (1 + (d\eta/dx)^2)^{-1/2} \end{aligned}$$

Equations (3) and (4) can thus be replaced by (3) and

$$(10) \quad \partial \psi / \partial n = v(\eta) \psi + \xi(\eta), \text{ where}$$

$$(11) \quad v(\eta) = 2F^{-2} (1 + (1 - 2F^{-2} \eta)^{1/2})^{-1}, \text{ and } \xi(\eta) = 1 - (1 + (d\eta/dx)^2)^{-1/2}.$$

At the beginning of iteration number $n + 1$, we assume the height, $1 + \eta^n$, of the free surface known ; the computation domain Ω^n follows, it is limited by the vertical boundaries Σ_1^n and Σ_2^n . Then, we solve problem

$$(P^{n+1}) \quad \left\{ \begin{array}{l} \Delta \psi^{n+1} = 0 \text{ in } \Omega^n, \text{ and} \\ \partial \psi^{n+1} / \partial n = v(\eta^n) \psi^{n+1} + \xi(\eta^n) \text{ on } y = 1 + \eta^n, \end{array} \right.$$

together with the slip condition (2) on the bottom, and the boundary conditions on Σ_1^n and Σ_2^n which follow from the localized finite element method. From (3) we deduce then

$$\eta^{n+1}(x) = -\psi^{n+1}(x, 1 + \eta^n)$$

Note that equation (10) has been devised in such a way to reduce to equation (6) when η vanishes.

Some preliminary results

Each problem (P^n) is approximated by first order quadrangular finite elements, and the successive meshes derive from affinities. Similar results to those of FORBES and SCHWARTZ [15] have been obtained with much smaller computation domains.

Table 3 is related to the case of a supercritical flow and shows the dependence of the solution on the computation domain Ω_L , for a Neumann condition on Σ_k^n . Table 4 is related to the subcritical case and allows the estimation of the discrepancy between the linear and non-linear solutions.

It is worth noticing that our method leads to a solution which does not depend on the size of the computation domain ; we are thus led to assume that the non-linearity above all affects the phase and the amplitude of the downstream wave, in the subcritical case. Let us also mention that the procedure does not converge when the global Froude number is close to 1, i.e. when breaking occurs.

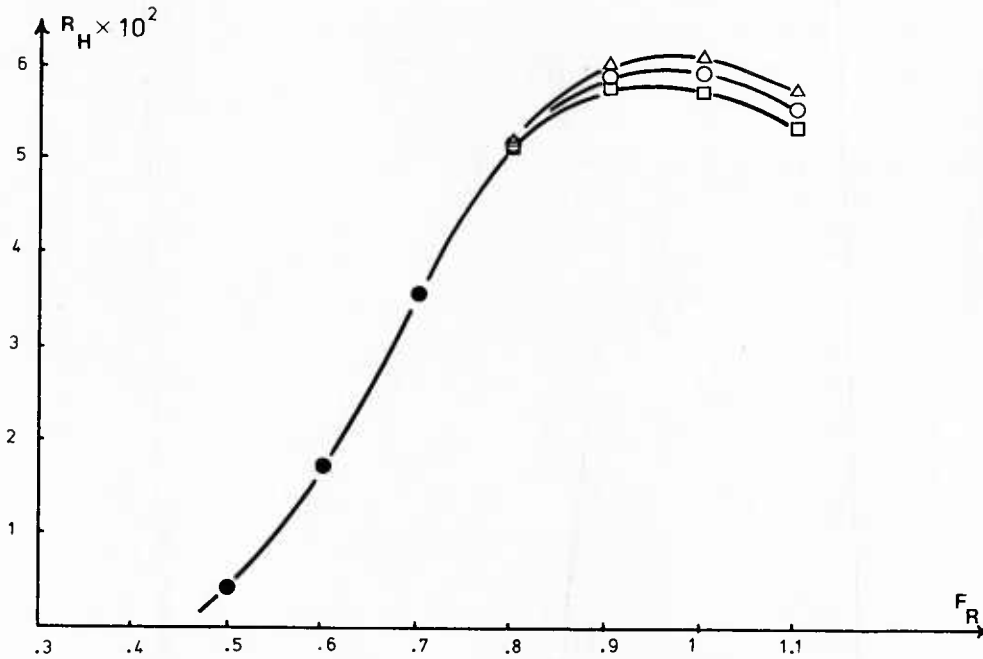
Aknowledgments

This study has been partly supported by the D.R.E.T. under contract number 81/1001.

IV. REFERENCES

- [1] M. LENOIR, A. JAMI : *"A variational formulation for exterior problems in linear hydrodynamics"*. Comp. Meth. in Appl. Mech. Eng., 1978, 16, p. 341.
- [2] K.J. BAI : *"A localized finite element method for steady two-dimensional free-surface flows"*. First Int. Conf. on Num. Hydrodynamics, Berkeley, 1977, p. 278.
- [3] C. GUTTMANN : *"Etude théorique et numérique du problème de Neumann-Kelvin tridimensionnel pour un corps totalement immergé"*. Thesis, 1983, E.N.S.T.A. Paris.
- [4] F. NOBLESSE : *"Alternative expressions for the Green function of the theory of ship wave resistance"*. Report MITSG 79-23, 1979, M.I.T., Cambridge.
- [5] M. LENOIR : *"Méthodes de couplage en hydrodynamique navale, et application à la résistance de vagues bidimensionnelle"*. Thesis, Rapport 164, 1982, E.N.S.T.A., Paris.
- [6] D. EUVRARD : *"Les mille et une facettes de la fonction de Green du problème de la résistance de vagues"*. Rapport 144, E.N.S.T.A., Paris.
- [7] WEBER : *"Numerical computation of the Fourier transform using Laguerre functions and the fast Fourier transform"*. Num. Math. 36, 1981, p. 197.
- [8] G. DELHOMMEAU : *"Contribution à l'étude théorique et à la résolution numérique du problème de la résistance de vagues"*. Thesis, 1978, E.N.S.M., Nantes.
- [9] T.H. HAVELOCK : *"The wave resistance of a spheroid"*. Proc. Roy. Soc. A. 131, 1931, p. 275.
- [10] K. SUZUKI : *"Numerical studies of the Neumann-Kelvin problem for a two-dimensional semi-submerged body"*. Proc. Third Int. Conf. on Num. Ship Hydrodynamics, 1981, Paris.
- [11] J.L. HESS : *"Progress in the calculation of non-linear free-surface problems by surface-singularity techniques"*. Proc. Second Int. Conf. on Num. Ship Hydrodynamics, 1977, Berkeley, p. 278.
- [12] P.L.F. LIU : *"Boundary integral equation method applied to free surface flow problems"*. Innovative Num. Anal. for the Appl. Eng. Sci., 1980, Montréal, p. 179.
- [13] C.H. VON KERCZEK, N. SALVESEN : *"Numerical solutions of two-dimensional non-linear wave problems"*. O.N.R. Tenth Naval Hydrodynamics Symposium, 1974, Cambridge, p. 649.

- [14] C. KORVING, A. HERMANS : *"The wave resistance for flow problems with a free surface"*. Proc. Second Int. Conf. on Num. Ship Hydrodynamics, 1977, Berkeley, p. 285.
- [15] L.K. FORBES, L. SCHWARTZ : *"Free-surface flow over a semicircular obstruction"*. J. Fluid Mech., 114, 1982, p. 299



□ $N_B = 49$

○ $N_B = 89$

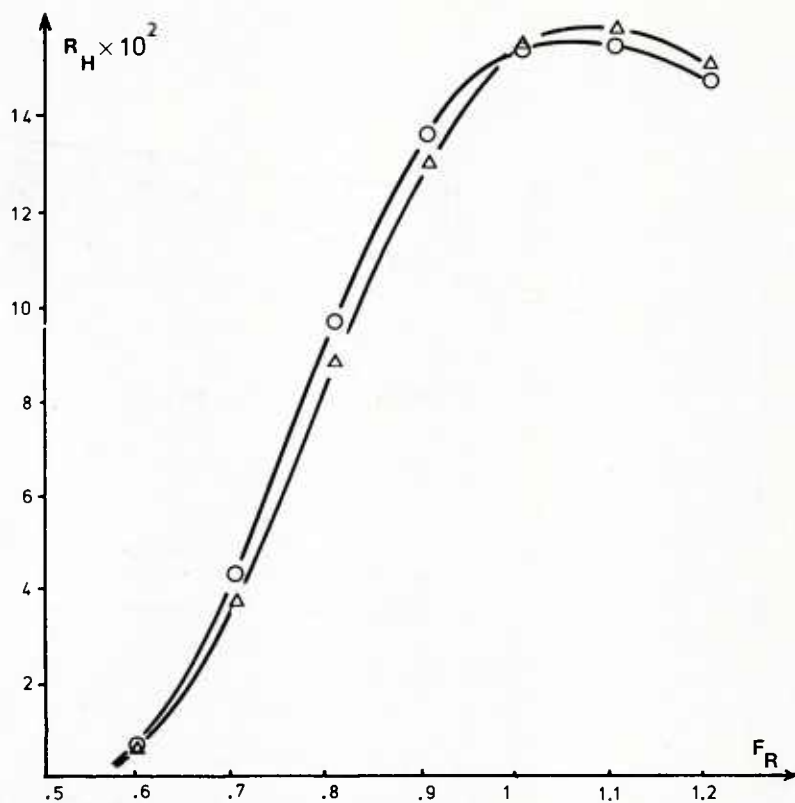
△ Havelock

Variations of R_H versus F_R and N_B

N_B : Number of unknowns on the body

$N_B \backslash F_R$.5	.6	.7	.8	.9	1.	1.1
49	$.32 \cdot 10^{-2}$	$1.72 \cdot 10^{-2}$	$3.55 \cdot 10^{-2}$	$5.09 \cdot 10^{-2}$	$5.71 \cdot 10^{-2}$	$5.69 \cdot 10^{-2}$	$5.32 \cdot 10^{-2}$
89	$.35 \cdot 10^{-2}$	$1.74 \cdot 10^{-2}$	$3.65 \cdot 10^{-2}$	$5.33 \cdot 10^{-2}$	$5.9 \cdot 10^{-2}$	$5.95 \cdot 10^{-2}$	$5.5 \cdot 10^{-2}$

Table 1 - The sphere



○ Present method

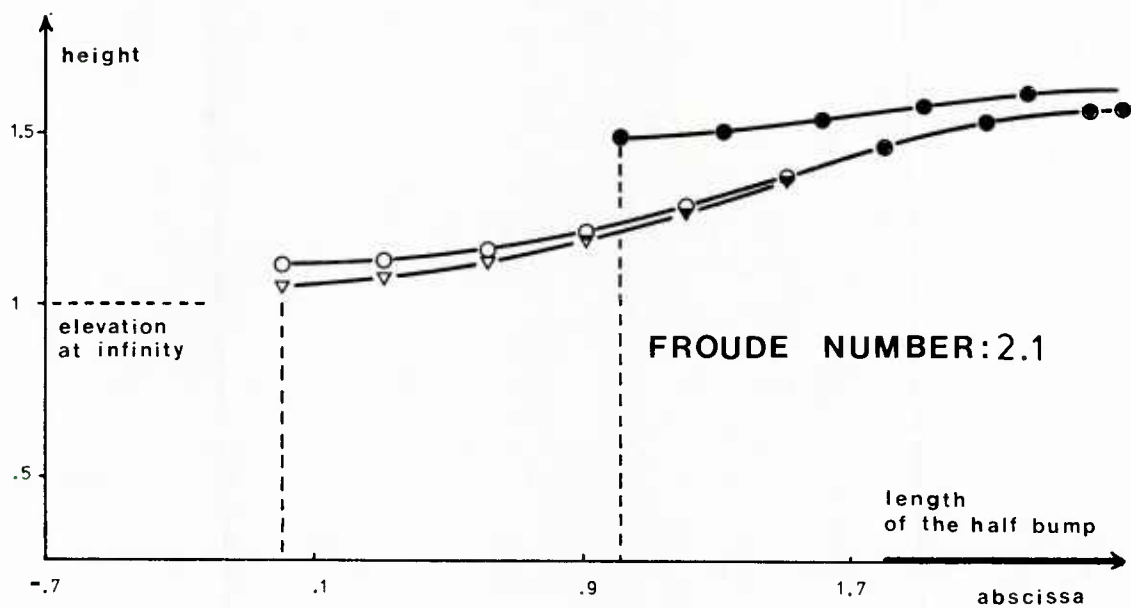
△ Havelock

Variations of R_H versus F_R

Number of unknowns on the body : 85

FR	.6	.7	.8	.9	1.	1.1	1.2
R_H	$.61 \cdot 10^{-2}$	$4.32 \cdot 10^{-2}$	$9.72 \cdot 10^{-2}$	$13.73 \cdot 10^{-2}$	$15.54 \cdot 10^{-2}$	$15.71 \cdot 10^{-2}$	$14.88 \cdot 10^{-2}$

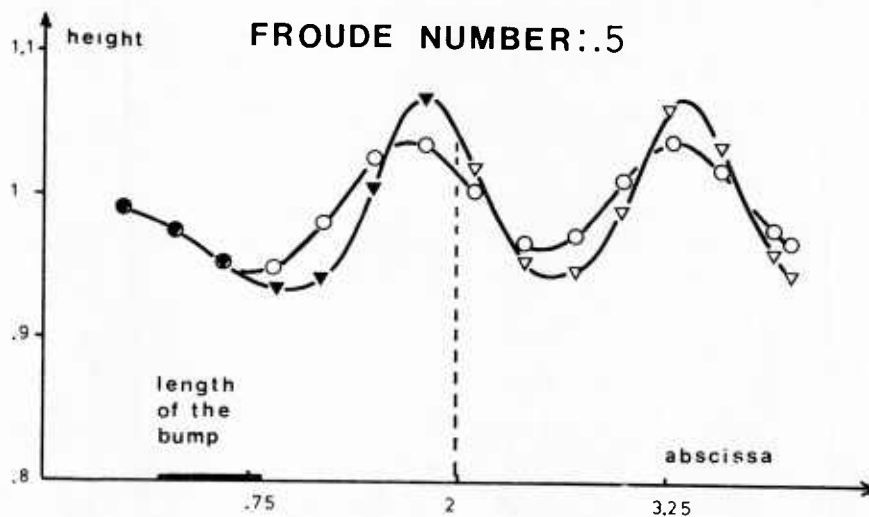
Table 2 - The ellipsoid of ratio 2.5



▽ Present method

○ Neumann condition on Σ_k^n

Table 3 - Free surface - The supercritical case



▽ Non-linear problem

○ Linearized problem

Table 4 - Free surface - The subcritical case

A COMPUTATION OF FLOW AROUND A SHIP

Allen V. Hershey

Naval Postgraduate School
Monterey, California 93943

ABSTRACT

A computation system is under development for the determination of velocity in the wave trains of submarines and ships. The first order linear approximation is used for the free boundary, while full accuracy is used for the body boundary. The body shape is simulated geometrically by a radical representation, and is simulated hydrodynamically by continuous distributions of source density. A point source is centered in a parallelepiped, which is large enough to bracket the ship. Velocities at grid points in the parallelepiped have been computed by Fourier integration, and have been converted into coefficients for interpolation by the fast Fourier transform. The velocity at each point on the surface of the ship is computed for unit source density at each other point. Then a matrix of flux is inverted to obtain the source density. The square of the velocity is integrated in accordance with the Bernoulli equation to obtain the wave resistance.

INTRODUCTION

For a number of years a computation system¹ was under development at the Dahlgren Laboratory of the Naval Surface Weapons Center. Currently the computation system is under further development as part of the research program at the Naval Postgraduate School. The function of the system is the computation of wave trains behind submarines and ships. Work on the system has led to a general library of subroutines which are useful for many applications. Included in the library are subroutines for exponential integrals, Fresnel integrals, Bessel functions, polynomial approximations, and matrix arithmetic.

In November 1979 there was a Workshop on Ship Wave Resistance Computations². A number of workers were invited to compute flows around a set of ships. The results were so discordant that a second workshop was scheduled for November 1983. Especially out of line was a result which had been obtained with the previous version of the current system. However, it was discovered later that the computer's arctangent routine was bad, and this could have contributed to the discrepancy. The objective of current work is to do numerical analysis for improved accuracy. The computer is asked to give as much accuracy as possible with double precision.

The method of computation consists of three stages. In the first stage the surface of the ship is expressed mathematically. Surface coordinates and surface components are computed for grid points on the surface. In the second stage the velocity at each grid point is computed for a unit point source at each other grid point. The velocity is derived from the Havelock integral for a linearized free-boundary condition. In the third stage the surface of the ship is represented by a continuous distribution of source density over the surface. The velocity at each point is derived from the source densities at other points after the inversion of a matrix of flux.

A new method for the simulation of the offsets of a ship has been presented in a previous report³. It uses radicals to represent the offsets of waterlines and section lines. On hand are the official offset data for a Series 60 Block 60 commercial ship, a DD963 destroyer, a CVN68 aircraft carrier, a T10-S tanker, and a former 12-meter yacht. Only the first of the ships on this list has been simulated on the computer. The scope of the present report is limited to the radical representation at a Froude number of one third.

Analysis of the flow around a point source has been presented in a previous report⁴. The potential and the velocity are given by double Fourier integrals. It is fashionable to express the integrals as the sum of a monotonic part and an oscillatory part. However, it was recognized long ago that these are parts of a single analytic integral. The integrand is cyclic and the trapezoidal rule is the high-accuracy rule of quadrature. However, there are so many wiggles in the range of interest that the trapezoidal rule requires too many intervals. A breakthrough has been achieved. An integration by parts makes possible the integration through many wiggles in a single interval. The integration by parts is provided by a chain of subroutines.

Experiments on the computer have compared the accuracy of interpolations by splines, Lagrange polynomials, orthonormal polynomials, and trigonometric polynomials. The most satisfactory interpolations were by trigonometric polynomials.

PARALLELEPIPED

Interpolation in a table is less expensive than random access to subroutines if the table is small enough. The point source is bracketed by a parallelepiped which is just large enough to contain the ships on the list. The length and the depth of the parallelepiped are divided by equally spaced section planes and waterline planes, while the width is divided into Chebyshev spacing. The subroutines were used to compute the velocity at each grid point in the parallelepiped. The data for each position in length and depth were transformed into the coefficients for trigonometric interpolation by the fast Fourier transform. The coefficients provide one-dimensional interpolation at each position in length and depth.

SOURCE DENSITY

The reference plane for coordinates in the fluid is the free surface of the undisturbed fluid. The unit of length is the distance between perpendiculars of the ship. The unit of velocity is the ship length per unit time.

The length of the ship is divided into 64 intervals. A section line is situated at the midpoint of each interval of length. The depth of the fluid is divided into 14 intervals. A waterline is situated at the midpoint of each interval of depth. The spacing between waterlines is $\frac{1}{256}$ and the bottom does not coincide with the edge of an interval.

The velocity at each grid point on the surface of the ship for a unit source density at each other grid point was computed by interpolation to give a matrix of velocity. The flux through each grid point for unit source density at each other grid point was computed from the scalar product between the normal to the surface and the velocity at the surface to give a matrix of flux. The matrix was partitioned with the data for one pair of waterlines in each partition. The matrix was inverted with a unique partitioned matrix subroutine to obtain the source density.

WAVE RESISTANCE

The current system integrates the pressure downward from the reference plane. The computed value of the coefficient of wave resistance is given in the following table.

DIMENSIONS AND RESISTANCE

(Simulation)

Series 60 Block 60

Length	1
Beam	$\frac{2}{15}$
Draft	$\frac{4}{75}$
Area	0.1723
Volume	0.004221
Froude Number	$\frac{1}{3}$
Wave Resistance Coefficient	0.002440

This value is indicated by the letter H in the figure, which is from reference 2. It agrees well with other values of the wave resistance coefficient.

The pressure on the hull is partly hydrostatic and partly hydrodynamic. Along the wave profile the pressure is zero. Only the fluid below the wave profile touches the body. The integration of pressure should be limited to the surface below the wave profile.

The computation of source density is based upon the assumption that the product of source density and velocity per unit source can be expressed as a trigonometric polynomial. This may not be adequate near the stem or the stern where opposite sides are close together, or near the reference plane where source and image are close together. Accuracy could be improved by an increase in the number of intervals. However, the fashionable solution is to replace point sources with panel sources. This might well be done with the aid of a subroutine which computes the potential of a rectangular plate when the source density is expressible as a power polynomial in the coordinates of the plate.

There are many experiments yet to be done. Full documentation will be presented in a forthcoming report from the Naval Postgraduate School.

CONCLUSION

A good value for the wave resistance coefficient has been obtained with the current system, but further refinements should be explored on the computer.

BIBLIOGRAPHY

1. *Computation System for Surface Wave Trains.*
A. V. Hershey, Proceedings First International Conference on Numerical Ship Hydrodynamics, J. W. Schot, and N. Salvesen, editors,
(Naval Ship Research and Development Center, Bethesda, Maryland, October 1975)
2. *Proceedings of the Workshop on Ship Wave-Resistance Computations.*
K. J. Bai, and J. H. McCarthy, editors,
(Naval Ship Research and Development Center, Bethesda, Maryland, October 1975)
3. *Radical Representations of Ship Simulations.*
A. V. Hershey, Naval Surface Weapons Center, Dahlgren, Virginia, Report No. NSWC/DL TR-3687 (July 1977)
4. *Computation of Velocity in the Wave Train of a Point Source.*
A. V. Hershey, Naval Surface Weapons Center, Dahlgren, Virginia, Report No. NSWC/DL TR-3720 (September 1977)

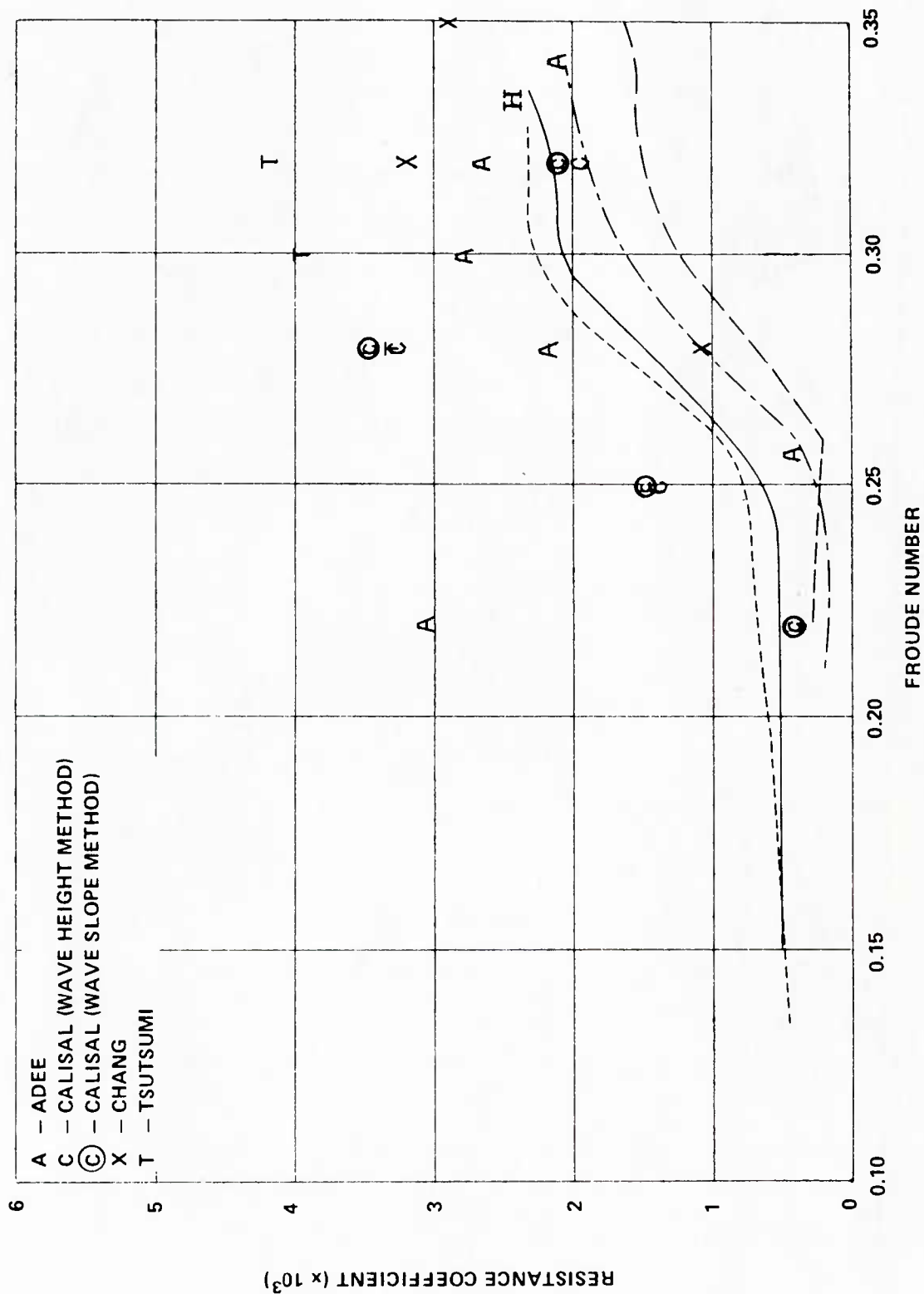


Figure 18 — Series 60 - Neumann-Kelvin Problem

NUMERICAL SOLUTION OF THE NEUMANN-KELVIN PROBLEM AND ITS APPLICATION TO SHIP WAVE-RESISTANCE COMPUTATIONS

Wu-ting Tsai^{*}, Yeun-junn Lin^{*} and Ching-chao Liao^{**}

ABSTRACT

Numerical solution of the Neumann-Kelvin problem by the Green's function method is accomplished for the computations of ship wave-resistance. To make the load of computation reasonable, some numerical experimental results are introduced in the present analysis. A computer program based on such mathematical model and numerical simplifications is developed. Two examples calculated for the Wigley model and Series 60 ($C_b=0.6$), show that the results are satisfactory.

INTEGRAL EQUATION TO BE SOLVED

In this study, the ship is considered to be in steady uniform motion on the free surface of an otherwise calm water of infinite extent. The Cartesian coordinate system $o-xyz$, moving with steady velocity $-U$ with the ship, is taken as shown in Fig. 1, where the xy -plane coincides with the undisturbed free surface. An irrotational motion of an incompressible, homogeneous and inviscid fluid is assumed. Then the velocity potential $\Phi(x,y,z)$ of a fluid domain V can be written as

$$\Phi(x,y,z) = Ux + \phi(x,y,z) \quad (1)$$

* Department of Naval Architecture, National Taiwan University

** Engineering School, Chung Cheng Institute of Technology

where $\varphi(x,y,z)$ is the potential of the perturbation due to the ship. When some suitable restrictions are imposed on the geometry and/or the velocity of the ship such that the free-surface boundary conditions are linearized, the perturbation potential φ shall be the solution of the following boundary value problem,

$$\nabla^2 \varphi = 0 \quad \text{in fluid domain } V \quad (2)$$

$$\frac{\partial \varphi}{\partial n} = -U \vec{n} \cdot \vec{i} \quad \text{on hull surface } S \quad (3)$$

$$\frac{\partial^2 \varphi}{\partial x^2} + k_0 \frac{\partial \varphi}{\partial z} = 0 \quad k_0 = \frac{g}{U^2} \quad \text{on calm free surface } z=0 \quad (4)$$

$$\lim_{R \rightarrow \infty} \varphi = \begin{cases} o(1/R) & x < 0 \\ O(1/R) & x > 0 \end{cases} \quad R = (x^2 + y^2 + z^2)^{1/2} \quad (5)$$

This is the so-called Neumann-Kelvin problem, which Brard (1971, 1972) dealt with, in the steady wave resistance theory and plays an important role between the linear theory and the exact problem.

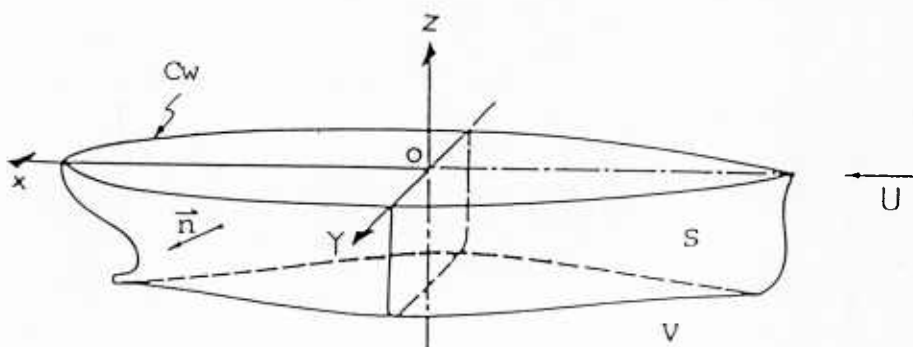


Fig. 1 Coordinate System

The above specific problem may be solved by means of an appropriate Green's function relating to the boundary conditions. The desired function $G(P;Q)$, often known as the Havelock source function or Kelvin source function, is a harmonic function in the fluid domain except having a singularity at Q , and satisfied the linearized free-surface condition and the radiation condition as follows,

$$G(P;Q) = \delta(P;Q) \quad P, Q \in V \quad (6)$$

$$\frac{\partial^2 G}{\partial x^2} + k_0 \frac{\partial G}{\partial z} = 0, \quad \text{on } z=0 \quad (7)$$

$$\lim_{R \rightarrow \infty} G(P; Q) = \begin{cases} o(1/R) & x < 0 \\ O(1/R) & x > 0. \end{cases} \quad R = |P - Q| \quad (8)$$

This yields the expression,

$$G(P; Q) = -\frac{1}{4\pi} \left[\frac{1}{r} \pm \frac{1}{r^*} - I^\pm(P; Q) \right], \quad (9)$$

where

$$\left\{ \begin{aligned} Y &= [(x-\xi)^2 + (y-\eta)^2 + (z-\zeta)^2]^{\frac{1}{2}}, \\ r^* &= [(x-\xi)^2 + (y-\eta)^2 + (z+\zeta)^2]^{\frac{1}{2}}, \\ I^+ &= -4k_0 \int_0^{\frac{\pi}{2}} d\theta \sec\theta e^{k_0(z+\zeta)\sec\theta} \cdot \sin[k_0(x-\xi)\cos\theta] \cdot \cos[k_0(y-\eta)\sin\theta \sec\theta] \\ &\quad + \operatorname{Re} \left\{ \frac{2}{\pi} \int_{-\frac{\pi}{2}}^{\frac{\pi}{2}} d\theta \operatorname{P.V.} \int_0^\infty k \frac{\exp[k(z+\zeta) + i k \tilde{\omega}]}{k - k_0 \sec\theta} dk \right\}, \\ I^- &= -4k_0 \int_0^{\frac{\pi}{2}} d\theta \sec\theta e^{k_0(z+\zeta)\sec\theta} \cdot \sin[k_0(x-\xi)\cos\theta] \cdot \cos[k_0(y-\eta)\sin\theta \sec\theta] \\ &\quad + \operatorname{Re} \left\{ \frac{2k_0}{\pi} \int_{-\frac{\pi}{2}}^{\frac{\pi}{2}} d\theta \sec\theta \operatorname{P.V.} \int_0^\infty \frac{\exp[k(z+\zeta) + i k \tilde{\omega}]}{k - k_0 \sec\theta} dk \right\}, \\ \tilde{\omega} &= (x-\xi)\cos\theta + (y-\eta)\sin\theta. \end{aligned} \right. \quad (10)$$

By use of such a source function, the Green's second identity gives the perturbation potential φ into the form,

$$\varphi(P) = \iint_S \sigma(Q) G(P; Q) dS(Q) - \frac{1}{4\pi k_0} \oint_{C_w} \sigma(Q) I^-(P; Q) \vec{n}_Q \cdot \vec{i} d\gamma, \quad (11)$$

where $\sigma(Q)$ is the density of the source distribution to be determined to represent an equivalent flow field. Meanwhile, the Neumann-Kelvin problem can be replaced by the following equation,

$$\begin{aligned} \frac{1}{2} \sigma(P) + \iint_S \sigma(Q) \frac{\partial G}{\partial n_P}(P; Q) dS(Q) \\ - \frac{1}{4\pi k_0} \oint_{C_w} \sigma(Q) \frac{\partial I^-}{\partial n_P}(P; Q) \vec{n}_Q \cdot \vec{i} d\gamma = -U \vec{n}_P \cdot \vec{i}, \quad (P \in S \cup C_w) \end{aligned} \quad (12)$$

which is a Fredholm integral equation of the second kind for the unknown function $\sigma(Q)$ defined over the hull surface S and waterline C_w .

Though other types of integral equation had been derived, e.g., Liao (1973), only the form given by equation (12), i.e., the representation by an equivalent source distribution, will be considered in the present study.

NUMERICAL TREATMENT OF THE INTEGRAL EQUATION

Numerical solution of the integral equation (12) requires an approximate representation of the hull surface S and waterline C_w , and an approximate evaluation of the relevant integration over S and C_w , to discretize the integral equation (12). In the present numerical computations, the hull surface and waterline are approximated by a large number of plane quadrilaterals and line segments respectively. Over each of the elements the source density is assumed to be constant. Thus the integral equation (12) is replaced by a set of linear algebraic equations for those unknown values of source density over the plane and line elements. The source density of the waterline element is assumed to have the same value as that of the plane element adjacent to such line element. With the hull-surface boundary condition being satisfied at the centroid of each plane element, the discrete form of the integral (12) is

$$\frac{1}{2} m_i + \sum_{\substack{j=1 \\ (j \neq i)}}^N m_j A_{ij} + \sum_{j=1}^M m_j B_{ij} = -\vec{n}_i \cdot \vec{c} \quad (i=1, 2, \dots, N) \quad (13)$$

where $m_i (= \sigma_i/U)$ is the nondimensional source density on the i -th element,

\vec{n}_i is the normal vector of the i -th plane element directed

toward the fluid domain V , and

N is the number of plane elements which approximate the whole hull surface S with the first M elements ending at the waterline.

A_{ij} and B_{ij} are called the influenced coefficient matrices,

$$A_{ij} = \iint_{S_j} \vec{n}_i \cdot \nabla_i G(x_i, y_i, z_i; \xi_j, \tau_j, \zeta_j) dS, \quad (14)$$

$$B_{ij} = -\frac{1}{4\pi\kappa_0} \int_{C_{wj}} \vec{n}_i \cdot \nabla_i I(x_i, y_i, z_i; \xi_j, \tau_j, 0) \vec{n}_j \cdot \vec{e} d\gamma, \quad (15)$$

where S_j is the region of the j -th plane element, and

C_{wj} is the region of the j -th line element.

Construction of the influence coefficient matrices A_{ij} and B_{ij} is quite a great numerical work due to the tedious integrations of the kernel function all over the elements representing the hull surface and the waterline. To reduce the extremely long computer time and make the computations practical, one may adopt the numerical experimental results obtained by Lin (1980), and the integration of each kernel function is simplified by the approximations,

$$A_{ij} \cong \frac{\vec{n}_i}{4\pi} \left[-\iint_{S_j} \nabla_i \left(\frac{1}{r} \pm \frac{1}{r^*} \right) dS + a_j \nabla_i I^{\pm}(x_i, y_i, z_i; \xi_{oj}, \tau_{oj}, \zeta_{oj}) \right], \quad (16)$$

$$B_{ij} \cong -\frac{\vec{n}_i}{4\pi\kappa_0} \left[l_j (\vec{n}_j \cdot \vec{e})^2 \cdot \nabla_i I(x_i, y_i, z_i; \xi_{oj}, \tau_{oj}, 0) \right], \quad (17)$$

where a_j is the area of the j -th plane element,

l_j is the arc length of the j -th line element,

$(\xi_{oj}, \tau_{oj}, \zeta_{oj})$ is the centroid of the j -th plane element, and

$(\xi_{oj}, \tau_{oj}, 0)$ is the midpoint of the j -th line element.

Formulas developed by Hess and Smith (1962, 1964) are used for integrating the kernel of Rankine-source term kernels $\nabla_i(\frac{1}{r} \pm \frac{1}{r^*})$. Concentration of constant source density panel as a point source is assumed for the integration of the wavy term kernels $\nabla_i I^\pm$.

CALCULATION OF THE DERIVATIVES OF THE HAVELOCK SOURCE FUNCTION

To compute the derivatives of the Havelock source function ∇I^\pm in equations (16) and (17) numerically, the integration contours in complex $k\cos\theta$ plane, as suggested by Noblesse (1977, 1978, 1979) are used to evaluate the principal value double integrals. Fig. 2 is an illustration of the integration contours, which have two poles at $\pm\alpha_0$ and a branch point at $|\beta|$ or $-|\beta|$, where $\alpha = k\cos\theta$, $\beta = k\sin\theta$, and

$$\alpha_0 = \sqrt{\frac{1 + (1 + 4\beta^2)^{1/2}}{2}}$$

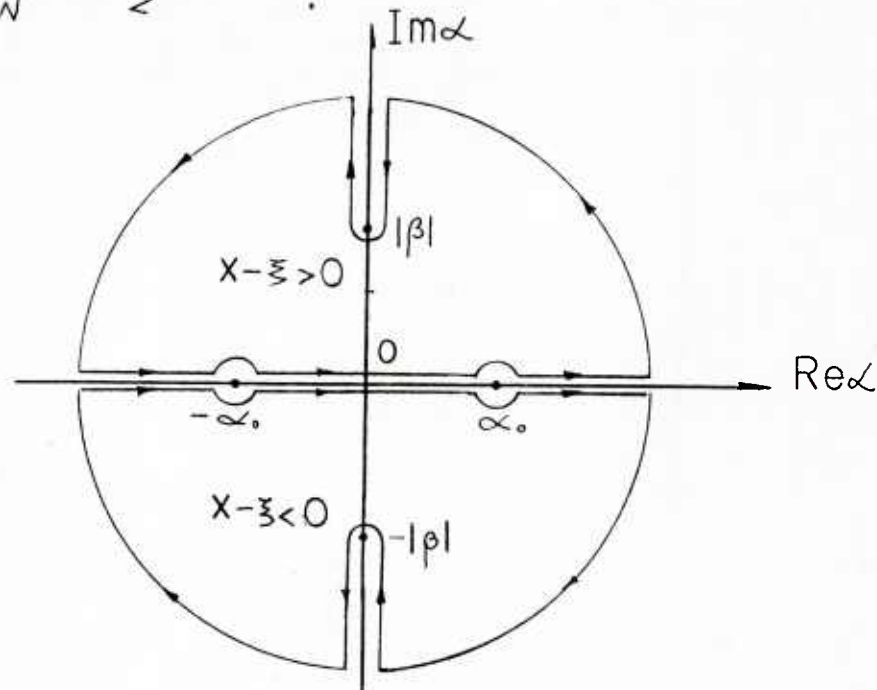


Fig. 2 Integration Contours in Complex α Plane

Via the above scheme, the ∇I^\pm have the following expressions,

$$\left\{ \begin{aligned} \frac{\partial I^+}{\partial x} &= -H(x-\xi) 4k_0^2 \int_{-\pi/2}^{\pi/2} d\theta \sec^2 \theta \cdot \exp[k_0(\beta+\xi) \sec \theta] \cdot \cos[k_0 \tilde{\omega} \sec \theta] \\ &\quad + \operatorname{sgn}(x-\xi) \frac{2k_0^2}{\pi} \int_{-1}^1 dt \sqrt{1-t^2} \operatorname{Re}[e^z E_1(z) - \frac{1}{z} + \frac{1}{z^2}], \\ \frac{\partial I^+}{\partial y} &= -H(x-\xi) 4k_0^2 \int_{-\pi/2}^{\pi/2} d\theta \sec^4 \theta \cdot \sin \theta \exp[k_0(\beta+\xi) \sec \theta] \cdot \cos[k_0 \tilde{\omega} \sec \theta] \\ &\quad + \frac{2k_0^2}{\pi} \int_{-1}^1 dt \cdot t \sqrt{1-t^2} \operatorname{Im}[e^z E_1(z) - \frac{1}{z} + \frac{1}{z^2}], \\ \frac{\partial I^+}{\partial \beta} &= -H(x-\xi) 4k_0^2 \int_{-\pi/2}^{\pi/2} d\theta \sec^2 \theta \cdot \exp[k_0(\beta+\xi) \sec \theta] \sin[k_0 \tilde{\omega} \sec \theta] \\ &\quad + \frac{2k_0^2}{\pi} \int_{-1}^1 dt (1-t^2) \operatorname{Im}[e^z E_1(z) - \frac{1}{z} + \frac{1}{z^2}], \end{aligned} \right. \quad (18)$$

and

$$\left\{ \begin{aligned} \frac{\partial I^-}{\partial x} &= -H(x-\xi) 4k_0^2 \int_{-\pi/2}^{\pi/2} d\theta \sec^2 \theta \cdot \exp[k_0(\beta+\xi) \sec \theta] \cdot \cos[k_0 \tilde{\omega} \sec \theta] \\ &\quad + \operatorname{sgn}(x-\xi) \frac{2k_0^2}{\pi} \int_{-1}^1 dt \sqrt{1-t^2} \operatorname{Re}[e^z E_1(z) - \frac{1}{z}], \\ \frac{\partial I^-}{\partial y} &= -H(x-\xi) 4k_0^2 \int_{-\pi/2}^{\pi/2} d\theta \sec^4 \theta \sin \theta \exp[k_0(\beta+\xi) \sec \theta] \cdot \cos[k_0 \tilde{\omega} \sec \theta] \\ &\quad + \frac{2k_0^2}{\pi} \int_{-1}^1 dt t \sqrt{1-t^2} \operatorname{Im}[e^z E_1(z) - \frac{1}{z}], \\ \frac{\partial I^-}{\partial \beta} &= -H(x-\xi) 4k_0^2 \int_{-\pi/2}^{\pi/2} d\theta \sec^2 \theta \cdot \exp[k_0(\beta+\xi) \sec \theta] \cdot \sin[k_0 \tilde{\omega} \sec \theta] \\ &\quad + \frac{2k_0^2}{\pi} \int_{-1}^1 dt (1-t^2) \operatorname{Im}[e^z E_1(z) - \frac{1}{z}]. \end{aligned} \right. \quad (19)$$

where $H(x-\xi)$ is the Heavside step function,

$$E_1(z) = \int_z^\infty \frac{e^{-t}}{t} dt \quad \text{is the complex exponential integral, and}$$

$$Z = k_0 \sqrt{1-t^2} [(\beta+\xi) \sqrt{1-t^2} + (\gamma-\eta)t + i|\alpha-\xi|] \quad (20)$$

The principal value double integral has been transformed into a one-fold integral whose integrand contains a complex exponential integral.

Fig. 3.a and Fig. 3.b show the integrands of the first integrals in equations (19) for a particular set of nondimensional variables $k_0(x-\xi)$, $k_0(y-\eta)$ and $k_0(z+\xi)$. The Simpson's rule is used for such numerical integration. For the integrands of the second integrals in equations (19), Fig. 4.a and Fig. 4.b indicate that the integrands are smooth functions in the integration interval. Gauss-Chebyshev quadrature (using Chebyshev polynomials of the second kind) is used for doing these numerical integrations.

The evaluation of the complex exponential integral $E_1(z)$, $z=u+iv$ is carried out as follows, for $u^2+v^2 < 5$, the series expansion provided by Abramowitz and Stegun (1964) is used,

$$E_1(z) = -\gamma - \ln z - \sum_{n=1}^{\infty} \frac{(-1)^n z^n}{n \cdot n!} \quad |\arg z| < \pi \quad (21)$$

where $\gamma=0.57721566\dots$ is the Euler's constant, for $u^2+v^2 \geq 5$,

$$e^z E_1(z) = e^z \int_z^\infty \frac{e^{-t}}{t} dt$$

$$= \int_0^\infty e^{-t} \left[\frac{t+u}{(t+u)^2 + v^2} \right] dt + i \int_0^\infty e^{-t} \left[\frac{-v}{(t+u)^2 + v^2} \right] dt \quad (22)$$

Gauss-Laguerre quadrature is used to do the numerical integrations of the infinite integrals in equation (22). The computation of complex exponential integral was verified by comparing the results with the tables listed in Abramowitz and Stegun (1964) PP. 249-251.

COMPUTATIONS OF THE WAVE RESISTANCE

After solving the linear simultaneous equations for the unknown source density, the velocity and the pressure coefficient at the hull surface can be obtained by

$$\nabla \phi(x_i, y_i, z_i) \cong -\frac{U}{4\pi} \sum_{j=1}^N m_j \left[\iint_{S_j} \nabla_i \left(\frac{1}{r} \pm \frac{1}{r^*} \right) ds + a_i \nabla_i I^\pm(x_i, y_i, z_i; \xi_{oj}, \tau_{oj}, \xi_{oj}) \right]$$

$$+ \frac{U}{4\pi k_0} \sum_{j=1}^M m_j \left[l_j \cdot (\vec{n}_j \cdot \vec{e}) \cdot \nabla_i I^-(x_i, y_i, z_i; \xi_{oj}, \tau_{oj}, 0) \right], \quad (23)$$

and

$$C_p = 1 - \frac{|U \vec{e} + \nabla \phi|^2}{U^2}. \quad (24)$$

Free surface elevation $f(x, y, 0)$ is given by

$$f(x, y, 0) = -\frac{g}{U} \frac{\partial \phi}{\partial x}(x, y, 0). \quad (25)$$

As for the computations of ship wave-resistance, the suggestion of Breslin and King Eng (1963) is adopted. By numerical experimentations, they found that the point sources can replace the panels to give sufficiently accurate calculation of wave resistance. The wave resistance acting upon the ship can be computed most directly by integrating the x-component of the pressure acting on the hull surface,

$$C_p = \frac{R_p}{\frac{1}{2} \rho U^2 S} \cong \sum_{i=1}^N q_i (\vec{n}_i \cdot \vec{i}). \quad (26)$$

An alternative expression of wave resistance can also be derived from the conservation of momentum, and the wave resistance coefficient C_w can be expressed as

$$\begin{aligned} C_w &= \frac{R_w}{\frac{1}{2} \rho U^2 S} = \frac{2\pi}{S} L^2 \int_0^{\pi/2} [C^*(\theta)^2 + S^*(\theta)^2] d\theta. \\ &= \frac{2\pi}{S} L^2 \int_0^{\pi/2} A^*(\theta)^2 d\theta \end{aligned} \quad (27)$$

where $A^*(\theta)$ is called the weighted amplitude function, and

$$\begin{aligned} \left. \begin{matrix} C^*(\theta) \\ S^*(\theta) \end{matrix} \right\} &= \frac{k_0}{\pi L} \sec^{\frac{3}{2}} \theta \left\{ \iint_S m(\xi, \eta, \zeta) \exp(k_0 \xi \sec \theta) \frac{\cos}{\sin} (k_0 \xi \sec \theta) \cos(k_0 \eta \sec \theta \sin \theta) dS \right. \\ &\quad \left. - \frac{1}{k_0} \oint_{C_w} m(\xi, \eta, 0) \frac{\cos}{\sin} (k_0 \xi \sec \theta) \cos(k_0 \eta \sec \theta \sin \theta) \vec{n} \cdot \vec{i} d\eta \right\} \\ &\cong \frac{k_0}{\pi L} \sec^{\frac{3}{2}} \theta \left\{ \sum_{i=1}^N m_i a_i \exp(k_0 \xi_{0i} \sec \theta) \frac{\cos}{\sin} (k_0 \xi_{0i} \sec \theta) \cdot \cos(k_0 \eta_{0i} \sec \theta \sin \theta) \right. \\ &\quad \left. - \frac{1}{k_0} \sum_{i=1}^M m_i b_i (\vec{n}_i \cdot \vec{i}) \frac{\cos}{\sin} (k_0 \xi_{0i} \sec \theta) \cdot \cos(k_0 \eta_{0i} \sec \theta \sin \theta) \right\} \end{aligned} \quad (28)$$

NUMERICAL RESULTS

Two ship hull forms, the Wigley model and the Series 60, $C_b=0.6$, are used for numerical solution of the Neumann-Kelvin problem and for the computations of ship wave-resistance. The numerical results include wave resistance coefficients, wave elevations on ship hull side, and weighted amplitude functions. The computations were carried out on the UNIVAC 1100 computer system at the National Taiwan University. Wave resistance coefficients and wave elevations are compared with experimental data and other numerical results which also solve the Neumann-Kelvin problem. Both the experimental data and the numerical results were presented to the "PROCEEDING OF THE WORKSHOP ON SHIP WAVE RESISTANCE COMPUTATIONS, 1979".

Wigley Model For the reason of symmetry, the starboard side of the Wigley model is approximated by 252 plane quadrilateral elements. The results of computation are shown in Table 1 and Fig. 5 to Fig. 15,

- Table 1 List of Wave-Resistance Coefficients for Wigley Model,
- Fig. 5 Arrangement of Surface Elements for Wigley Model,
- Fig. 6 Comparison of Wave-Resistance Coefficients (C_p) with
Experimental and Other Numerical Results for Wigley
Model,
- Fig. 7 Comparison of Wave-Resistance Coefficients (C_w) with
Experimental and Other Numerical Results for Wigley
Model,
- Fig. 8 Comparison of Wave Profile with Experimental and Other
Numerical Results for Wigley Model at $Fn=0.266$,

- Fig. 9 Comparison of Wave Profile with Experimental and Other Numerical Results for Wigley Model at $Fn=0.348$,
- Fig. 10 Comparison of Wave Profile with Experimental and Other Numerical Results for Wigley Model at $Fn=0.452$,
- Fig. 11 Amplitude Function of Wigley Model at $Fn=0.266$,
- Fig. 12 Amplitude Function of Wigley Model at $Fn=0.313$,
- Fig. 13 Amplitude Function of Wigley Model at $Fn=0.348$,
- Fig. 14 Amplitude Function of Wigley Model at $Fn=0.402$,
- Fig. 15 Amplitude Function of Wigley Model at $Fn=0.452$.

Series 60, $C_b=0.6$ The starboard side hull surface is meshed into 325 plane elements and the numerical results are illustrated in Table 2 and Fig. 16 to Fig. 31,

Table 2 List of Wave-Resistance Coefficients for Series 60, $C_b=0.6$,

Fig. 16 Arrangement of Surface Elements of Fore Body for Series 60, $C_b=0.6$,

Fig. 17 Arrangement of Surface Elements of Aft Body for Series 60, $C_b=0.6$,

Fig. 18 Comparison of Wave-Resistance Coefficients (C_p) with Experimental and Other Numerical Results for Series 60, $C_b=0.6$,

Fig. 19 Comparison of Wave-Resistance Coefficients (C_w) with Experimental and Other Numerical Results for Series 60, $C_b=0.6$,

Fig. 20 Comparison of Wave Profile with Experimental and Other Numerical Results for Series 60, $C_b=0.6$ at $Fn=0.22$,

Fig. 21 Comparison of Wave Profile with Experimental Results for Series 60, $C_b=0.6$ at $Fn=0.25$,

- Fig. 22 Comparison of Wave Profile with Experimental and Other Numerical Results for Series 60, $C_b=0.6$ at $Fn=0.28$,
Fig. 23 Comparison of Wave Profile with Experimental and Other Numerical Results for Series 60, $C_b=0.6$ at $Fn=0.30$,
Fig. 24 Comparison of Wave Profile with Experimental and Other Numerical Results for Series 60, $C_b=0.6$ at $Fn=0.32$,
Fig. 25 Comparison of Wave Profile with Experimental and Other Numerical Results for Series 60, $C_b=0.6$ at $Fn=0.35$,
Fig. 26 Amplitude Function of Series 60, $C_b=0.6$ at $Fn=0.22$,
Fig. 27 Amplitude Function of Series 60, $C_b=0.6$ at $Fn=0.25$,
Fig. 28 Amplitude Function of Series 60, $C_b=0.6$ at $Fn=0.28$,
Fig. 29 Amplitude Function of Series 60, $C_b=0.6$ at $Fn=0.30$,
Fig. 30 Amplitude Function of Series 60, $C_b=0.6$ at $Fn=0.32$,
Fig. 31 Amplitude Function of Series 60, $C_b=0.6$ at $Fn=0.35$.

CONCLUDING REMARKS

"Neumann-Kelvin problem approach" is used as the mathematical model in the present computations. Two essential points can be concluded for the numerical scheme:

- 1) Concentration of the source panels as point sources is applied for the approximate integration of the wavy term kernels, and for the computations of the wave resistance.
- 2) The source density of each waterline element is assumed to be identical with that of the plane element ending at such line element.

Two ship hull forms, the Wigley Model and Series 60, $C_b=0.6$, are used for the numerical calculation. The numerical results are satisfactory for both two ship hull forms. The following conclusions can be obtained from the numerical results :

1) By use of both wave resistance coefficients and wave profiles, one cannot judge that whether the waterline integral terms plays an important role for the numerical analysis of the Neumann-Kelvin problem or not.

2) For both of the two methods for computing the wave resistance, pressure integration, and amplitude function approach, the results show no significant difference, yet the pressure integration scheme has less hump-hollow phenomenon.

ACKNOWLEDGMENTS

The authors wish to express their sincere gratitude to Professor Wei-yuan Hwang for reviewing the manuscript and useful comments.

REFERENCES

Abramowitz, M. and Stegun, I. A., "HANDBOOK OF MATHEMATICAL FUNCTIONS," Dover Publications, New York, 1964.

Brard, R., "The Neumann-Kelvin Problem for Surface Ships," Report 11 CST., Bassin d'Essais des Carenes, Paris, Jan. 1971.

Brard, R., "The Representation of a Given Ship Form by Singularity Distributions When the Boundary Condition on the Free Surface is Linearized," Journal of Ship Research, Vol. 16, March 1972, pp. 79-92.

Breslin, J. P. and King Eng, "Calculation of the Wave Resistance," Proc. Int. Seminar on Theoretical Wave Resistance, Ann Arbor, Michign, 1963, pp.1083-1110.

Guevel, P. , Delhommeau, G. and Cordonnier, J. P., "Numerical Solution of Neumann-Kelvin Problem by the Method of Singularities," Proc. Second Int. Conf. Numerical Ship Hydrodynamics, Berkeley, Calif., pp.107-123.

Hess, J. L. and Smith, A. M. O., "Calculation of Non-lifting Potential Flow About Arbitry Three-Dimensional Bodies," Douglas Aircraft Co., Inc. , Report No. E.S. 40622, March 1962.

Hess, J. L. and Smith, A. M. O., "Calculation of Potential Flow About Arbitrary Three-Dimensional Bodies," Journal of Ship Research, Vol. 8, No. 2, 1964, pp.22-44.

Liao, C. C., "On the Potential Theory Applied to the Steady Ship Wave Problem," Doctoral Thesis, Department of Naval Architecture, The University of Tokoy, Dec. 1973.

Lin, Y. J., "Evaluation of Resistance Increment Due to Propeller and Its Application to Aft-Part Hull Form Design," Doctoral Thesis, Department of Naval Architecture, The University of Tokoy, June 1980.

Noblesse, F., "The Fundamental Solution in the Theory of Steady Motion of a Ship," Journal of Ship Research, Vol. 21, No. 2 , June 1977. pp.82-88.

Noblesse, F., "On the Fundamental Function in the Theory of Steady Motion of Ships," Journal of Ship Research, Vol. 22, No. 4, Dec. 1978, pp. 212-215.

Noblesse, F., "Alternative Expressions for the Green Function of the Theory of Ship Wave Resistance," MIT Sea Grant College Program, Report No. MITSG 79-23, Sept. 1979.

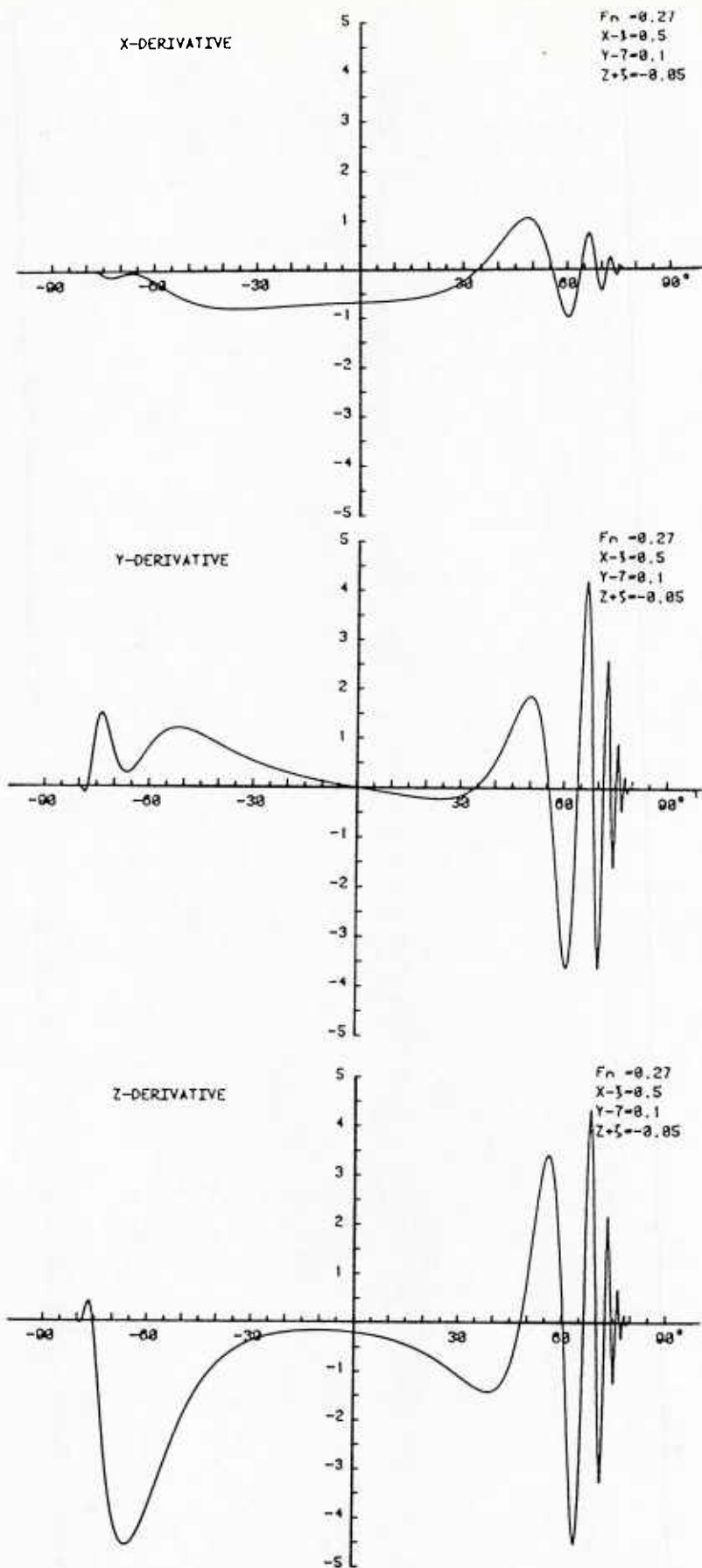


Fig. 3.a Integrands of the First Integrals
in Equations (19)

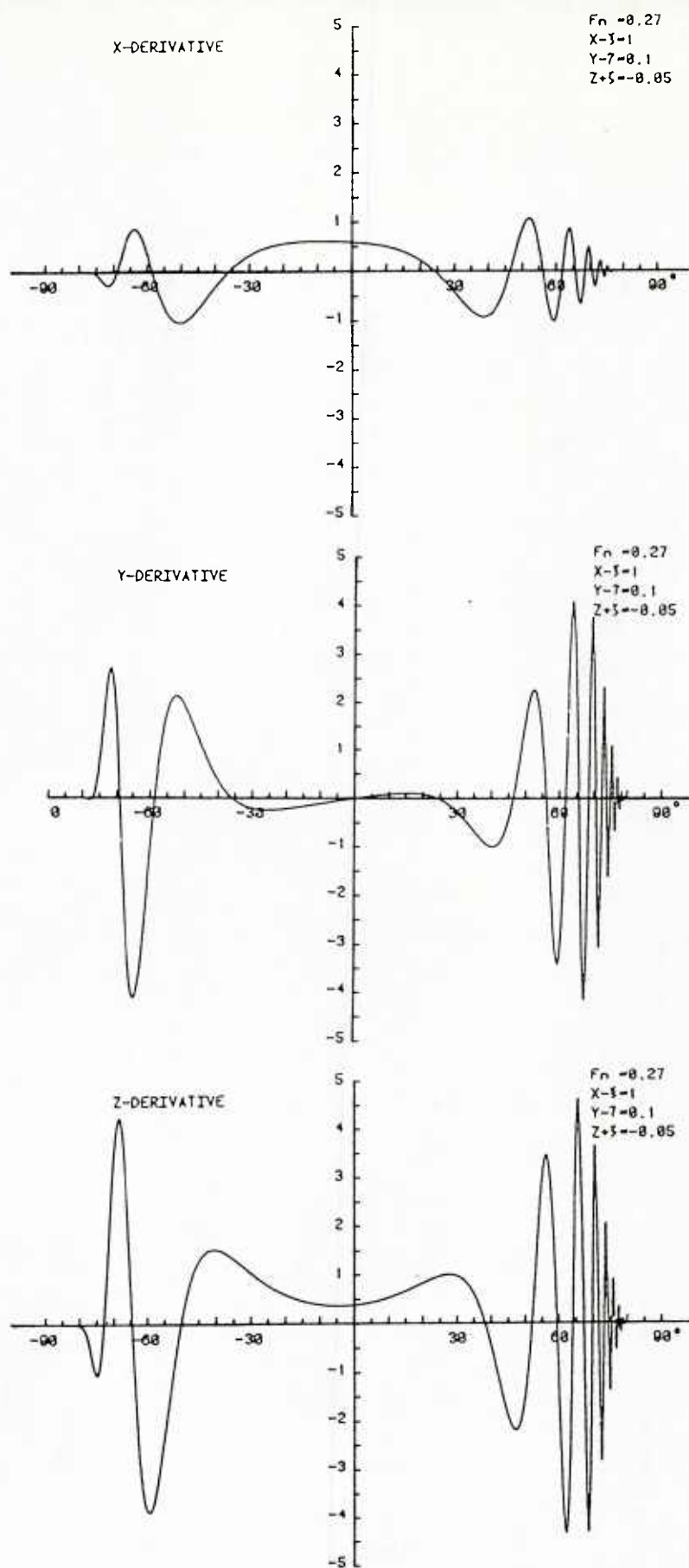


Fig. 3.b Integrands of the First Integrals
in Equations (19)

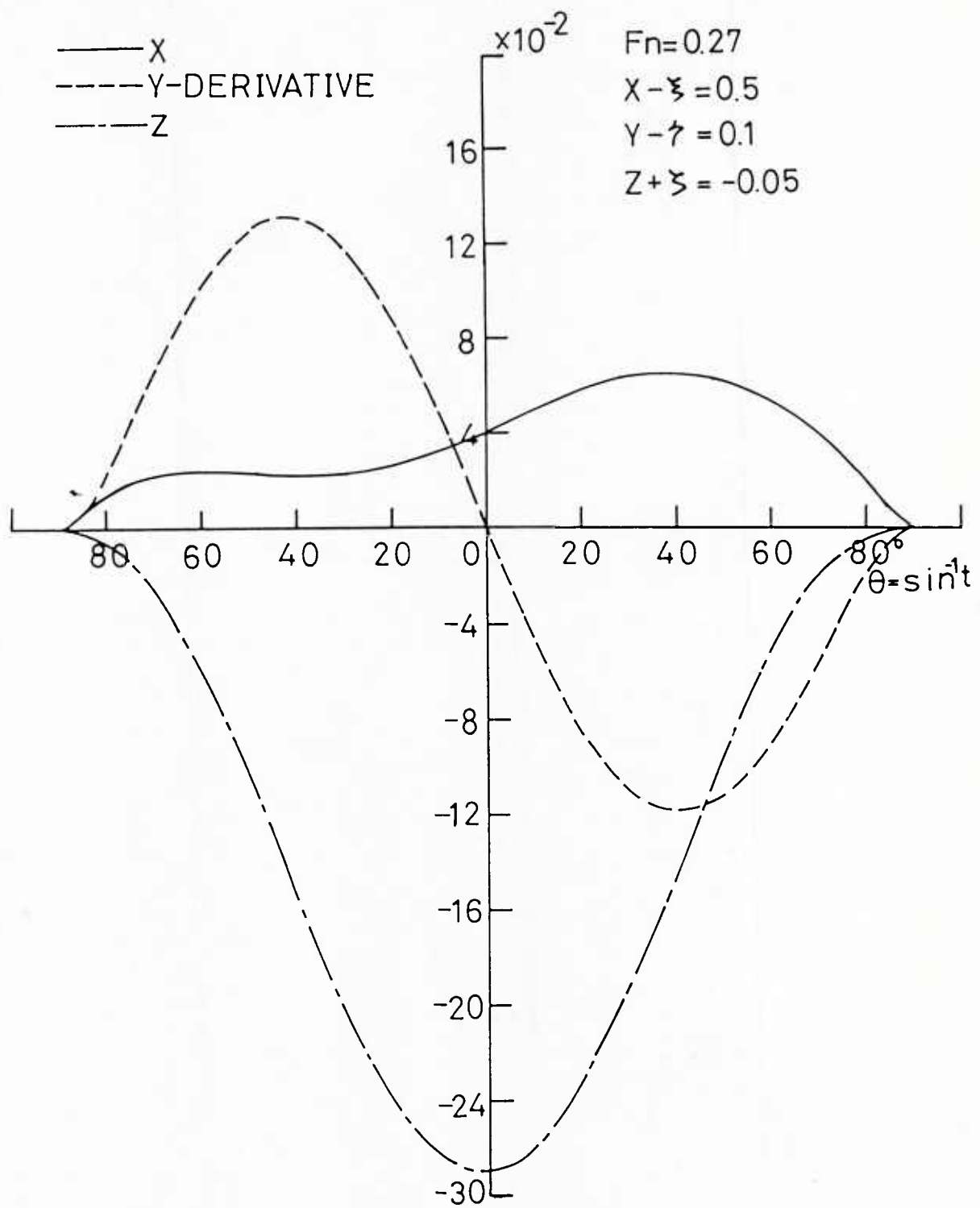


Fig. 4.a Integrands of the Second Integrals
in Equations (19)

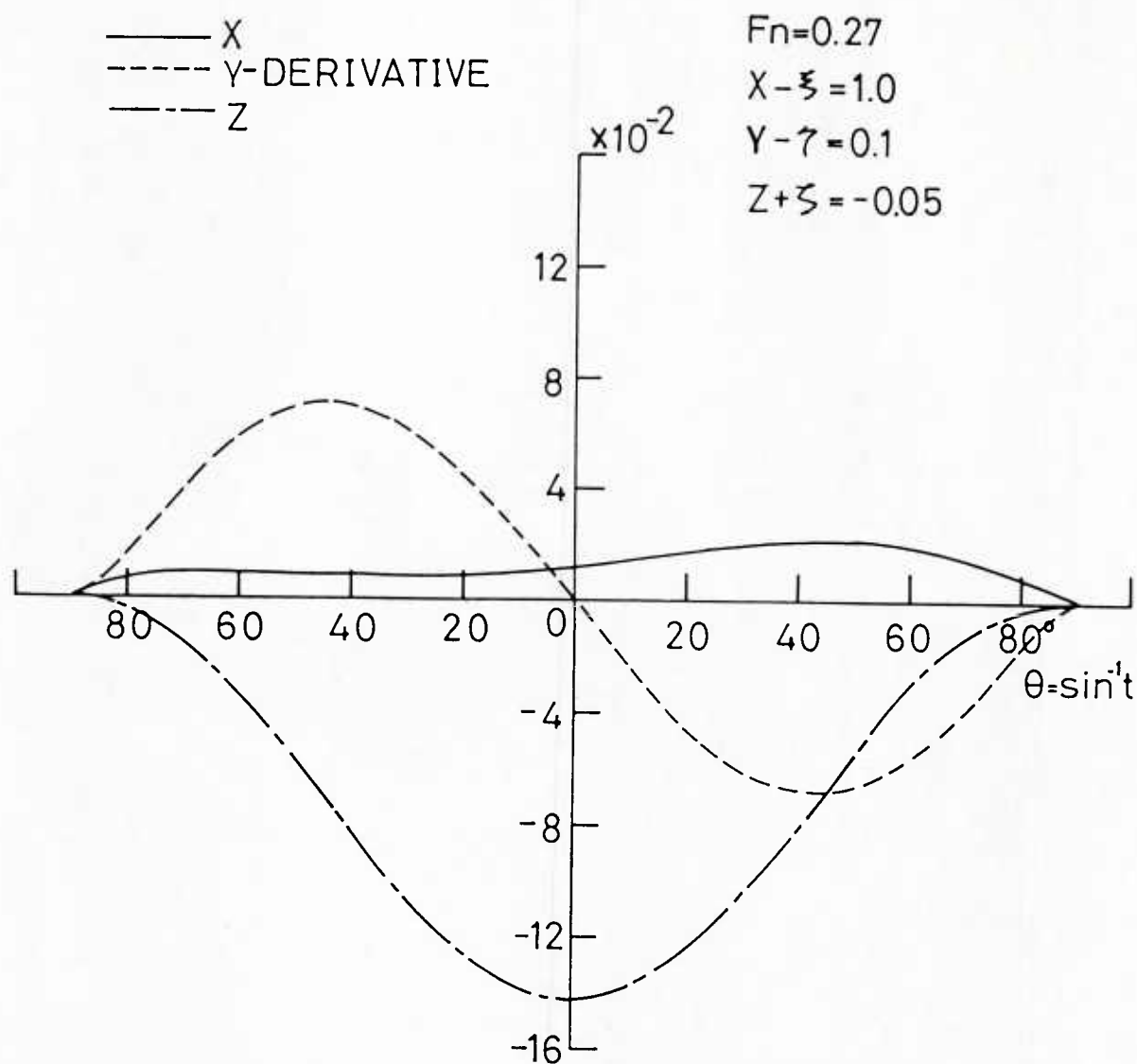


Fig. 4.b Integrands of the Second Integrals
in Equations (19)

Fn	Cw X 10 ³			Cp X 10 ³		
	Thin Ship Theory	Double Model	Not Consider WL. Int.	Consider WL. Int.	Not Consider WL. Int.	Consider WL. Int.
0.22	0.6534	0.8166	0.6147	0.5106	0.8584	0.5406
0.25	1.0641	1.2643	0.7942	0.9539	1.1591	0.9470
* 0.266	0.9458	1.2533	0.7663	0.9319	1.1282	0.9922
0.27	1.0881	1.4582	0.8216	0.9850	1.1964	1.0427
0.28	1.6056	2.0936	1.0601	1.2793	1.4450	1.2600
0.30	2.1441	2.7003	1.3841	1.9181	1.7825	1.7238
* 0.313	1.9133	2.4161	1.3594	2.0893	1.7326	1.7659
0.32	1.7136	2.1873	1.3128	2.0328	1.6659	1.7222
0.348	1.2396	1.7033	1.1224	1.4550	1.5119	1.3972
* 0.35	1.2475	1.7230	1.1234	1.4342	1.5170	1.3879
0.36	1.3738	1.9118	1.1937	1.3976	1.5977	1.3680
0.40	2.7273	3.5226	1.9042	2.0685	2.2509	1.8269
* 0.452	4.1797	5.1244	2.9703	2.9320	3.1947	2.8368

(* is the recommended Froude number for computations
by 1979 WORKSHOP ON SHIP WAVE-RESISTANCE COMPUTATIONS)

Table 1 List of Wave-Resistance Coefficients for Wigley Model

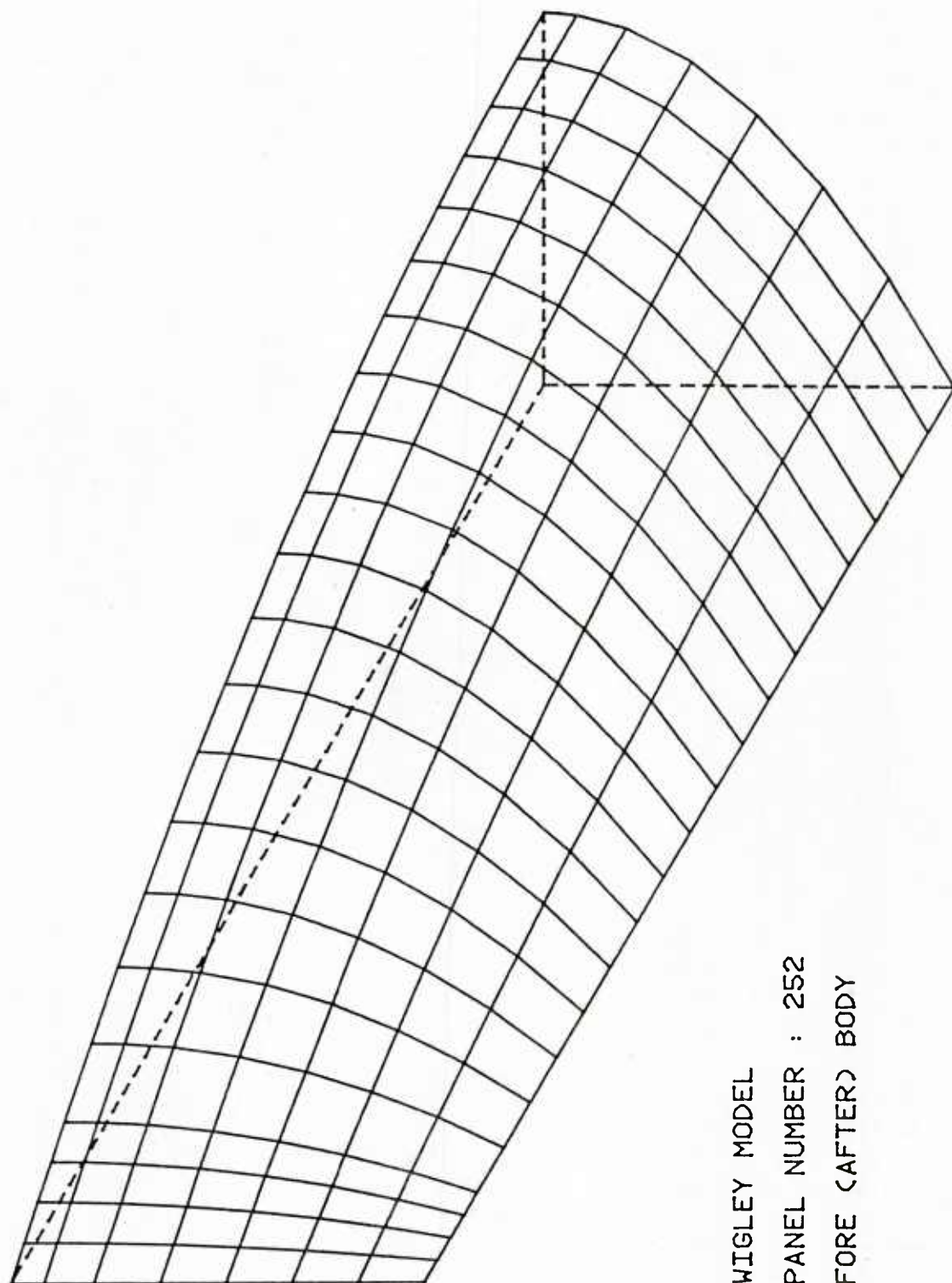


Fig. 5 Arrangement of Surface Elements for Wigley Model

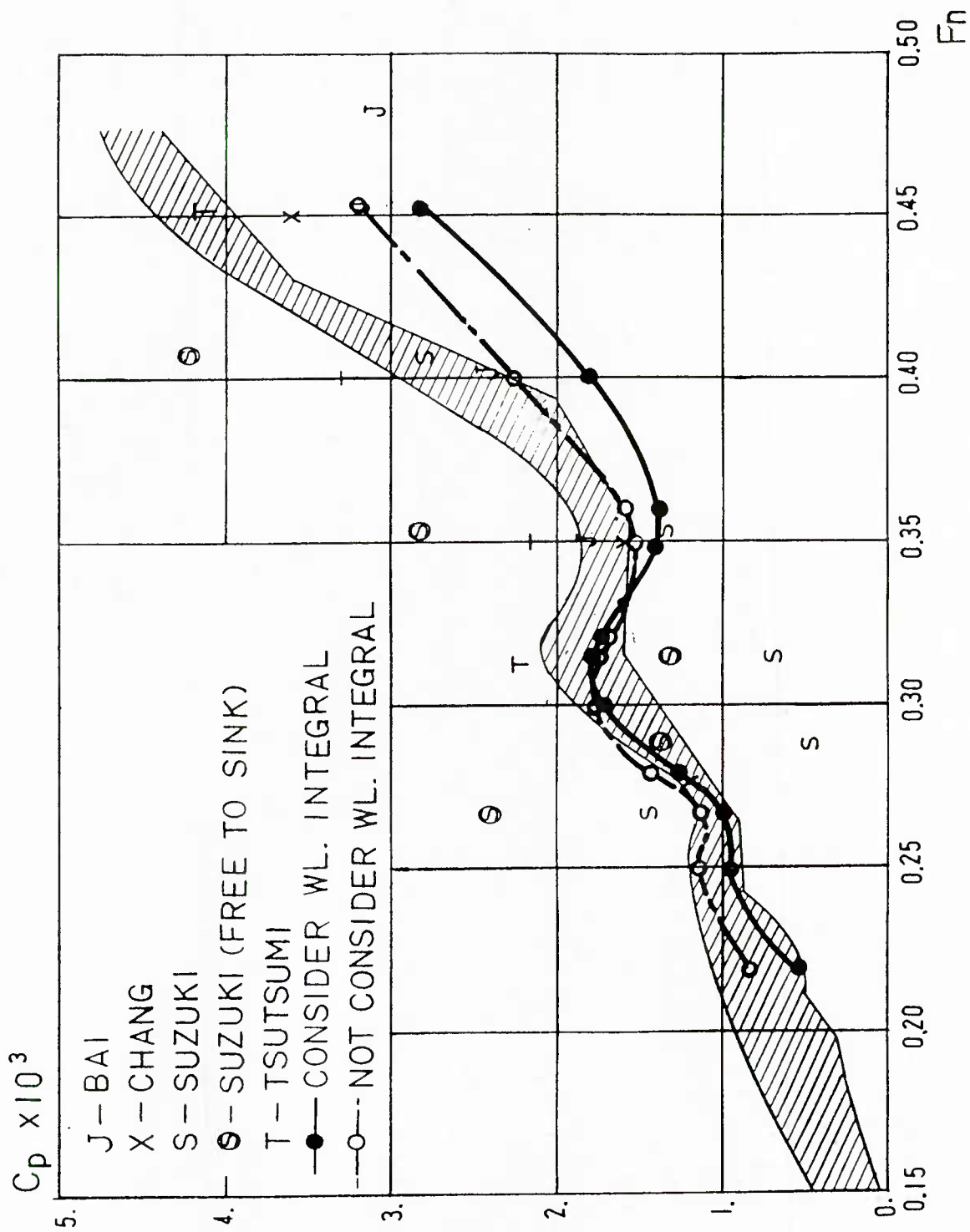


Fig. 6 Comparison of Wave-Resistances (C_p) with Experimental and Other Numerical Results for Wigley

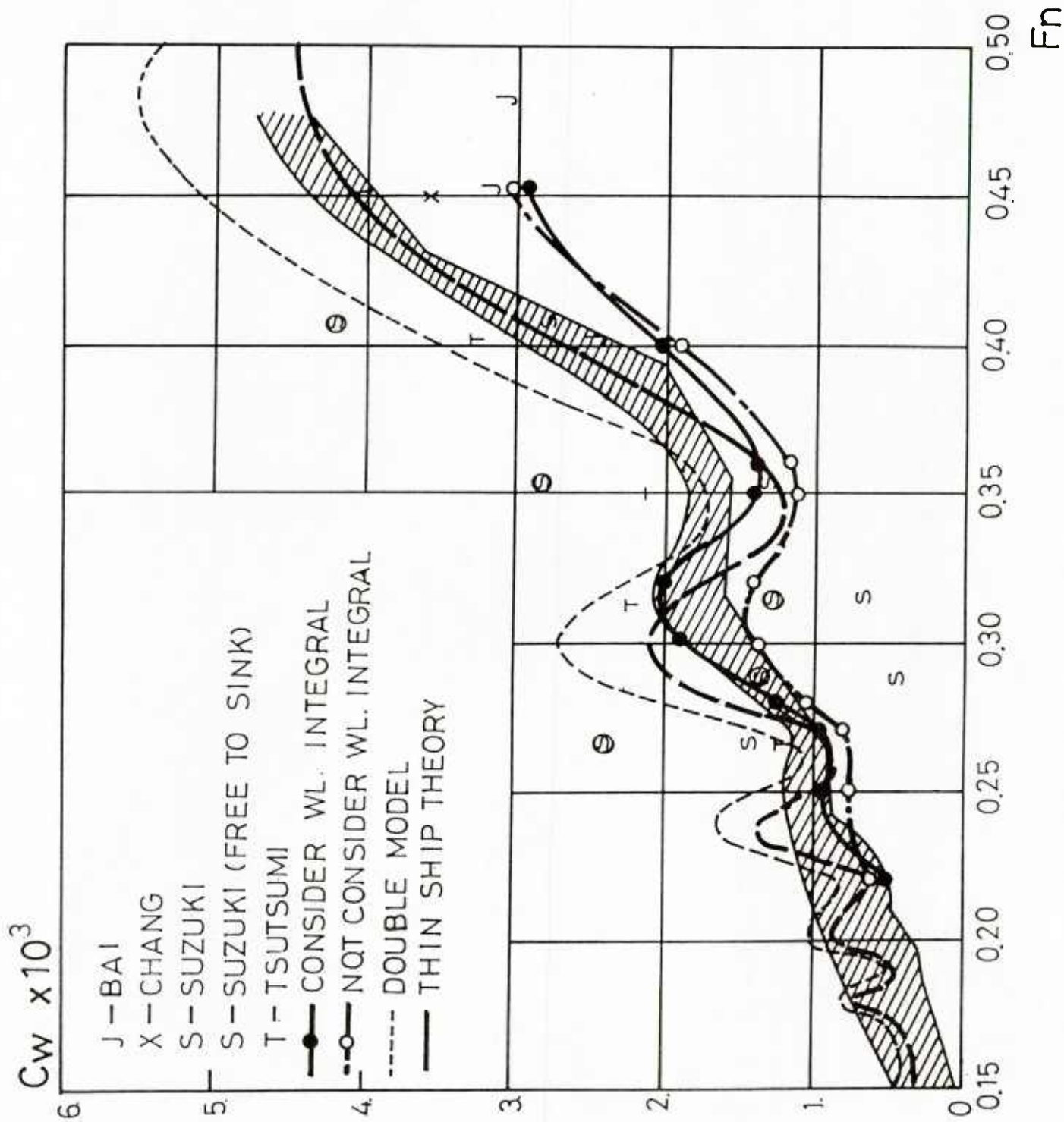


Fig. 7 Comparison of Wave-Resistance Coefficients (C_w) with Experimental and Other Numerical Results for Wigley Model

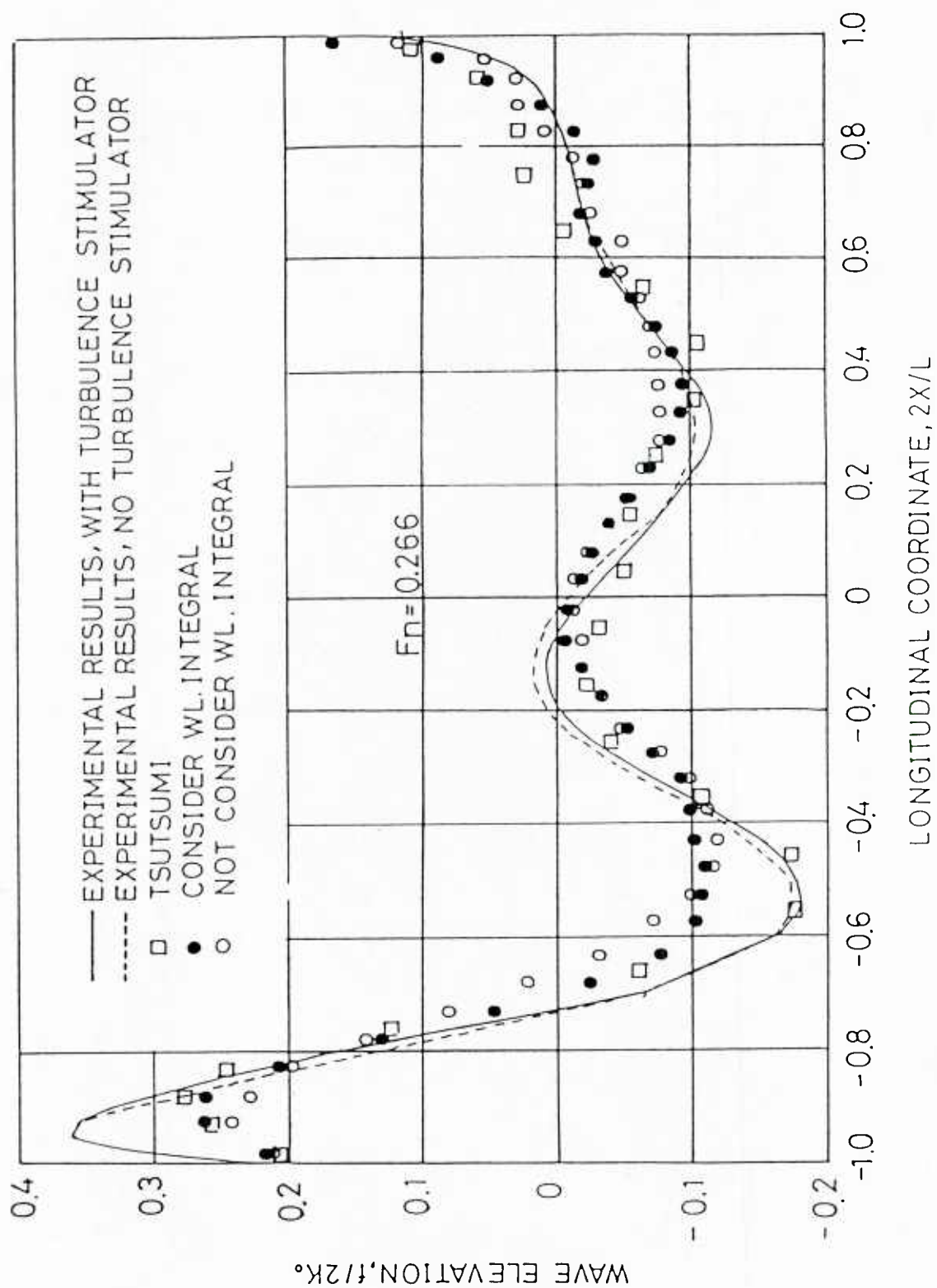


Fig. 8 Comparison of wave profile with Experimental and Other Numerical Results for Wigley Model at $F_n=0.266$

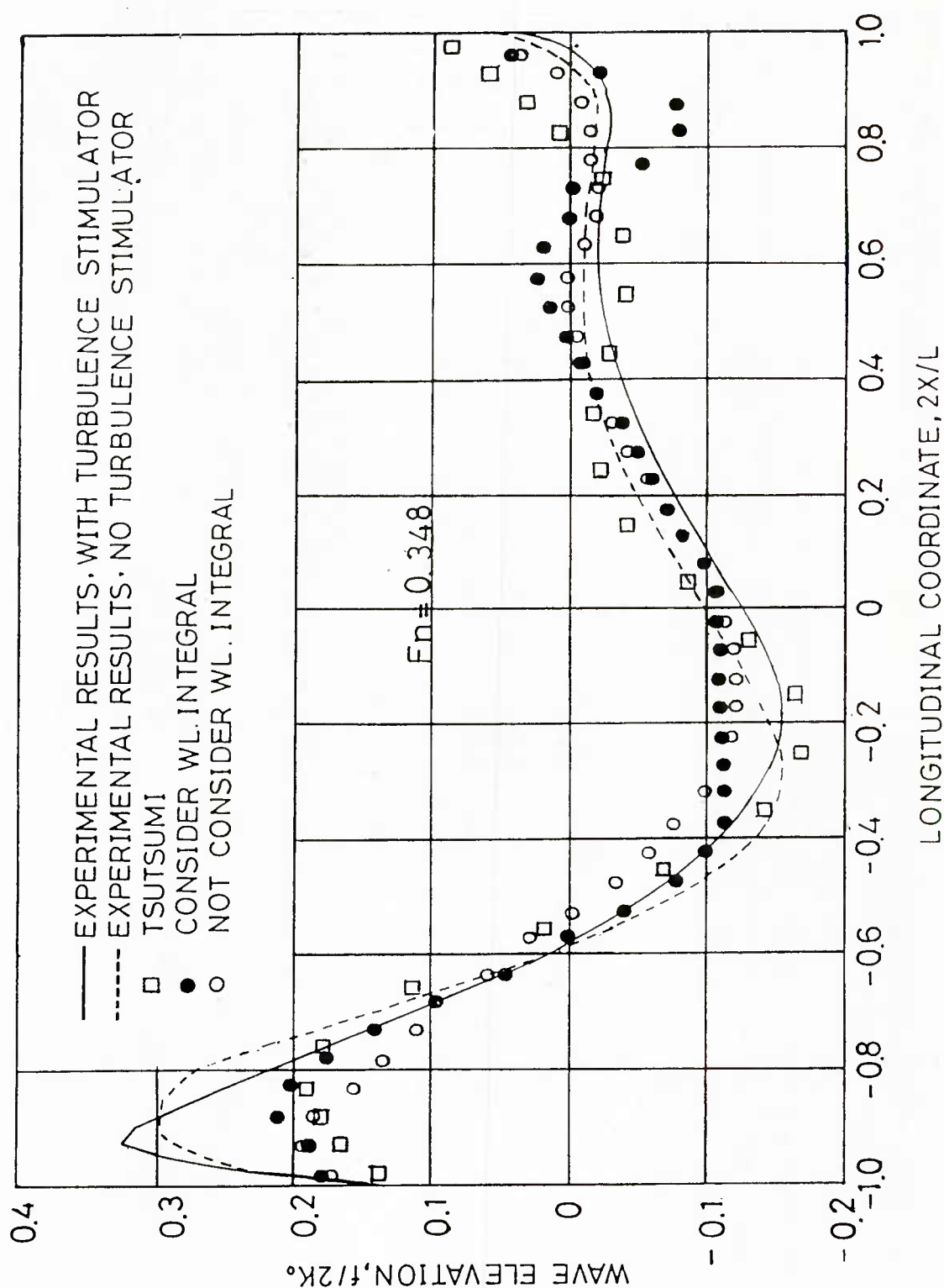


Fig. 9 Comparison of Wave Profile with Experimental and Other Numerical Results for Wigley Model at $F_n = 0.348$

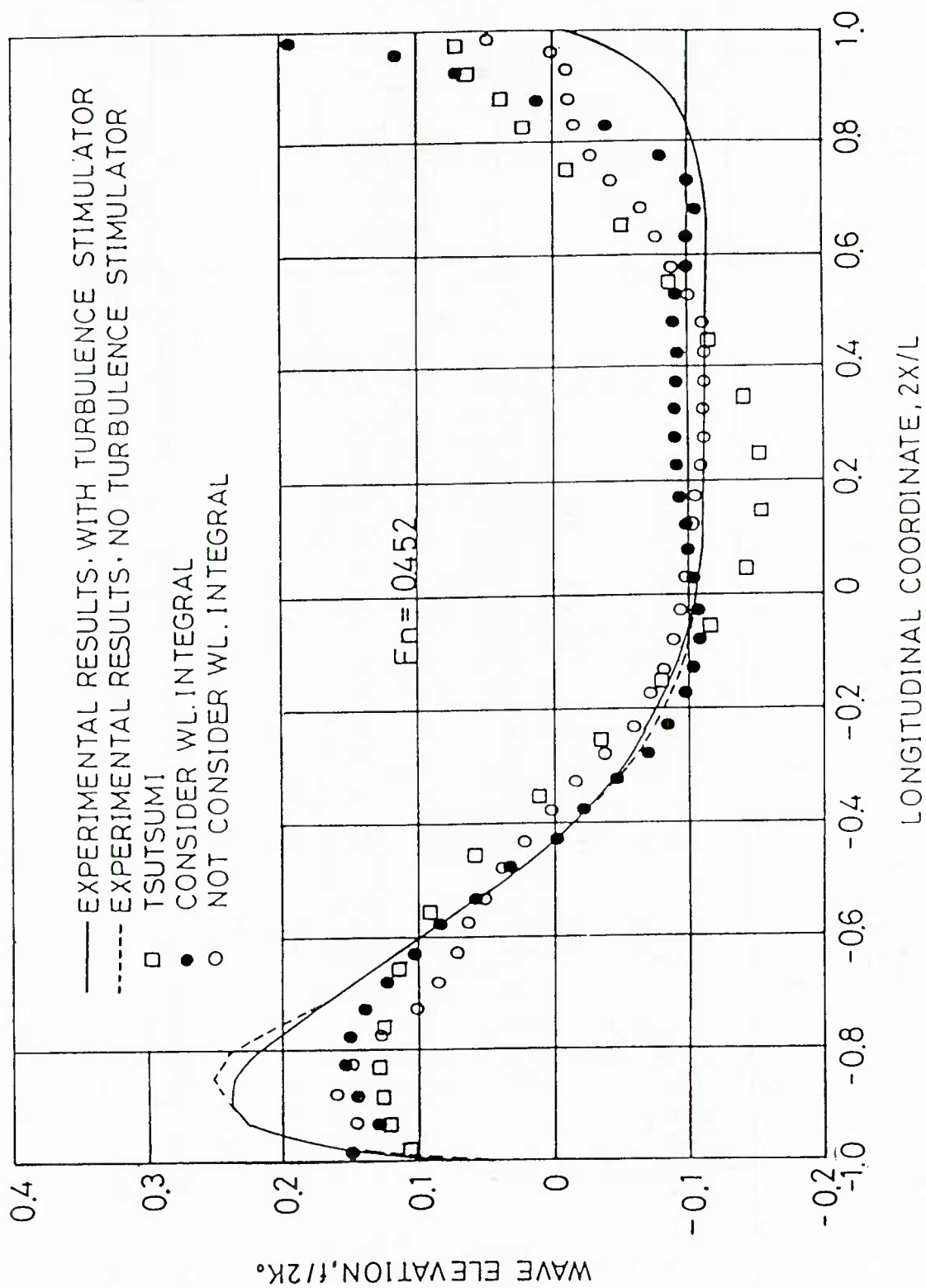


Fig. 10 Compariso of Wave Profile with Experimental and Other Numerical Results for Wigley Model at $Fn=0.452$

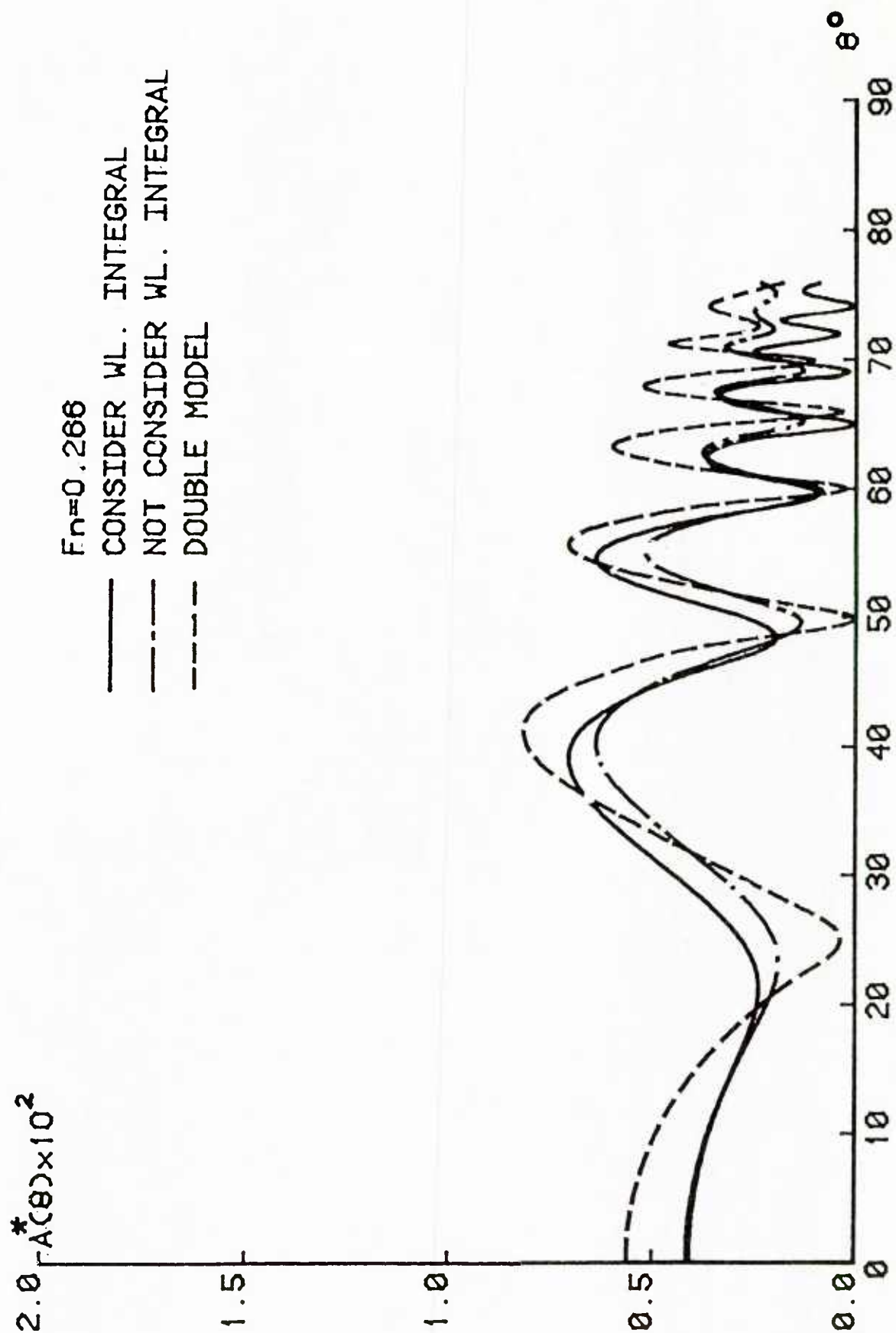


Fig. 11 Amplitude Function of Wigley Model at $Fn=0.266$

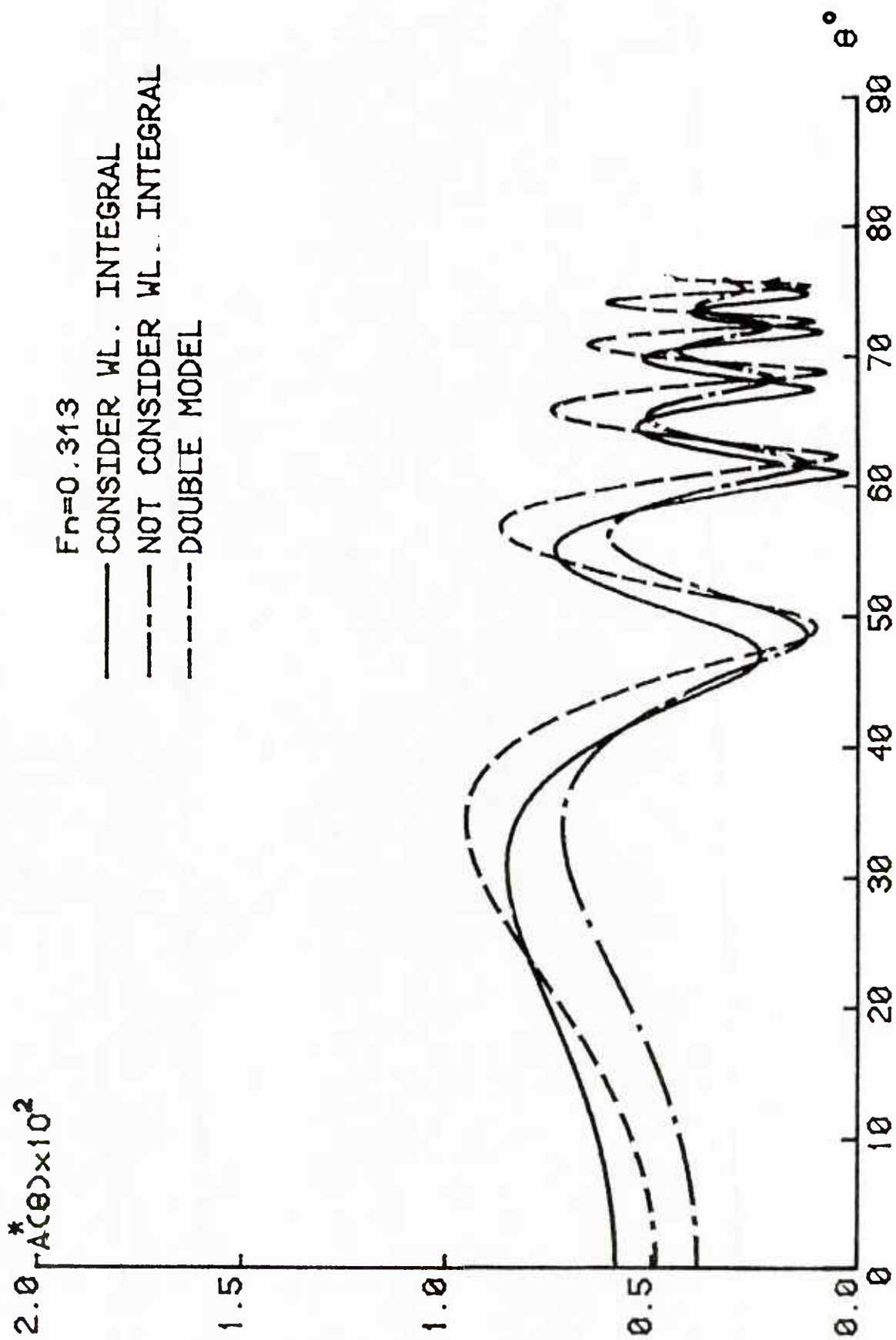


Fig. 12 Amplitude Function of wigley Model at $Fn=0.313$

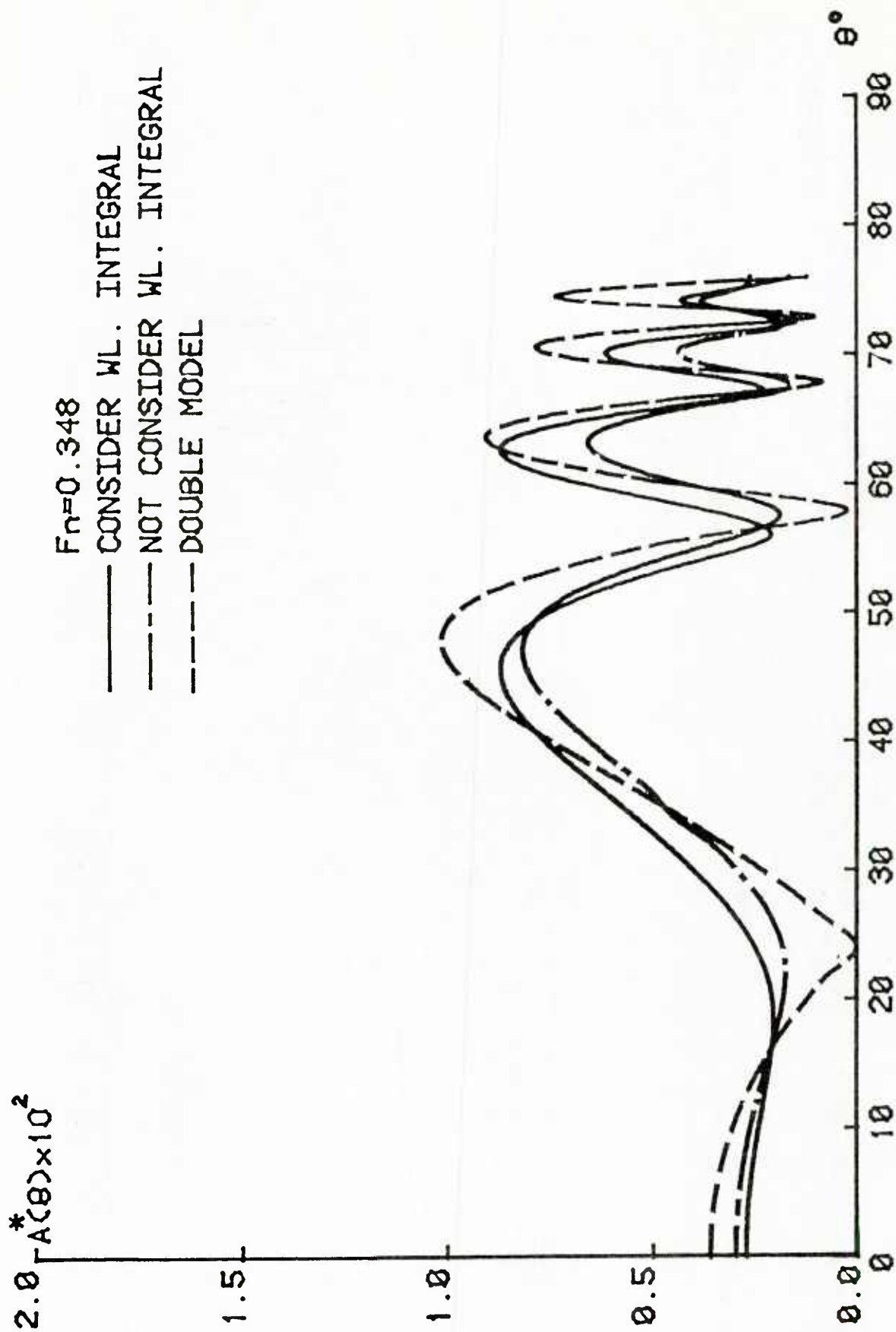


Fig. 13 Amplitude Function of Wigley Model at $Fn=0.348$

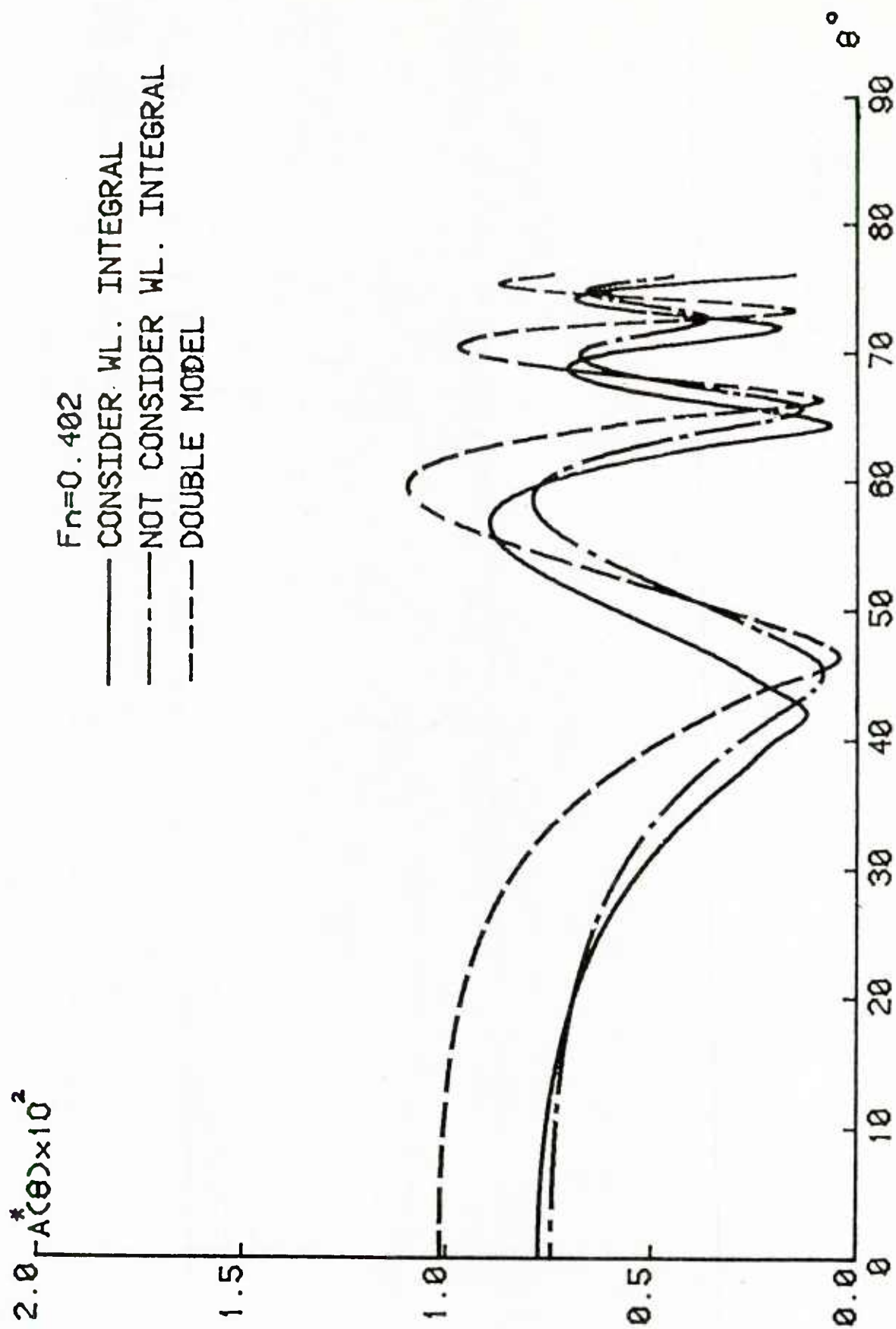


Fig. 14 Amplitude Function of Wigley Model at $Fn=0.402$

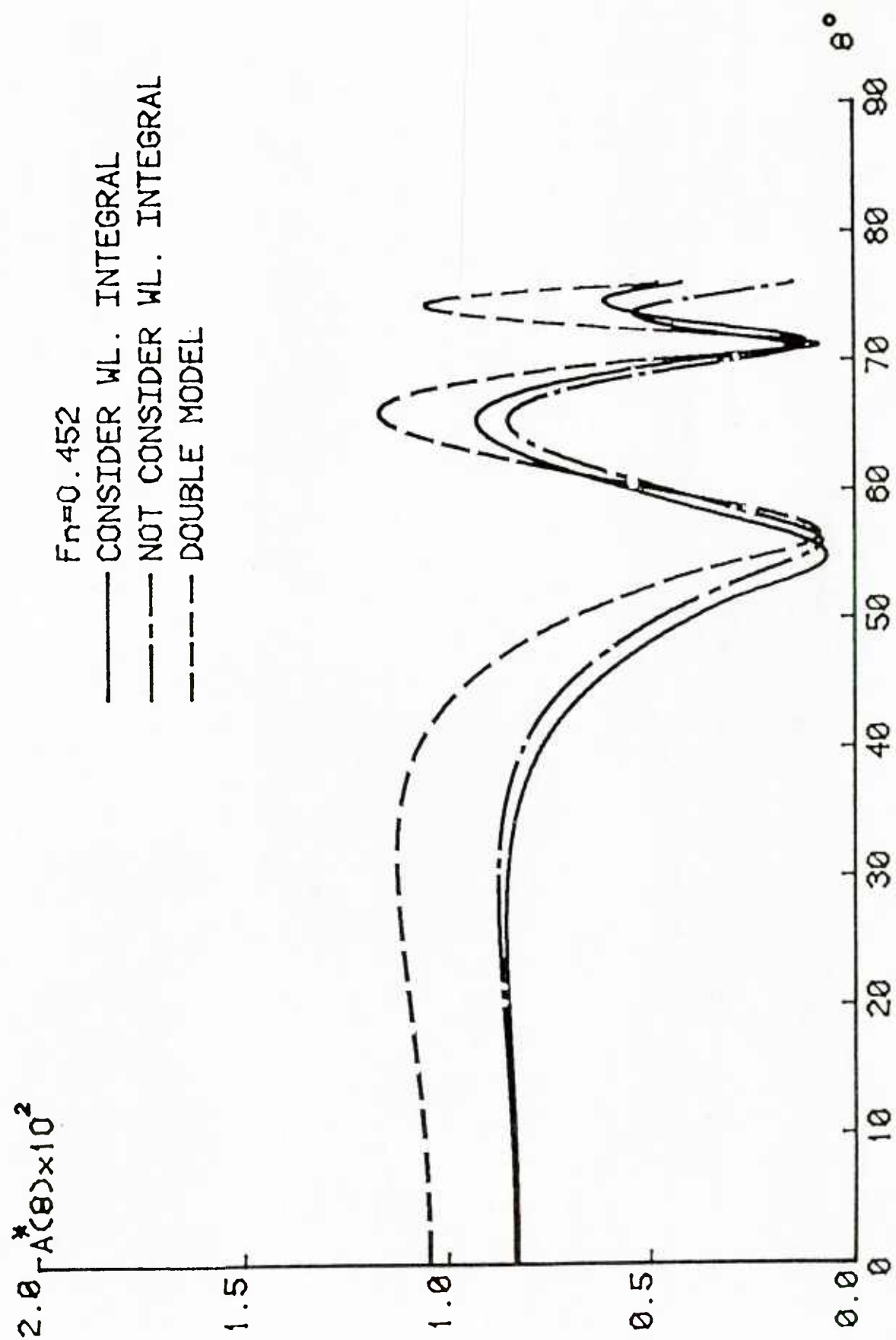


Fig. 15 Amplitude Function of wigley Model at $Fn=0.452$

Fn	Cw x 10 ³		Cp x 10 ³	
	Double Model	Not Consider WL. Int.	Not Consider WL. Int.	Consider WL. Int.
* 0.22	0.8082	0.4589	0.6564	0.3832
* 0.25	1.9467	0.7746	0.8499	0.8256
0.27	5.2291	1.5946	1.7144	1.8095
* 0.28	6.1652	1.8988	2.3190	2.1439
0.30	5.6534	2.0969	2.4007	2.4694
* 0.32	4.4869	2.1081	2.1400	2.3681
0.35	5.9109	2.6239	2.5661	2.9302
0.36	7.1298	3.0550	3.0553	3.4592
				3.4263

(* is the recommended Froude number for computations

by 1979 WORKSHOP ON SHIP WAVE-RESISTANCE COMPUTATIONS)

Table 2 List of Wave-Resistance Coefficients for Series 60, Cb=0.6

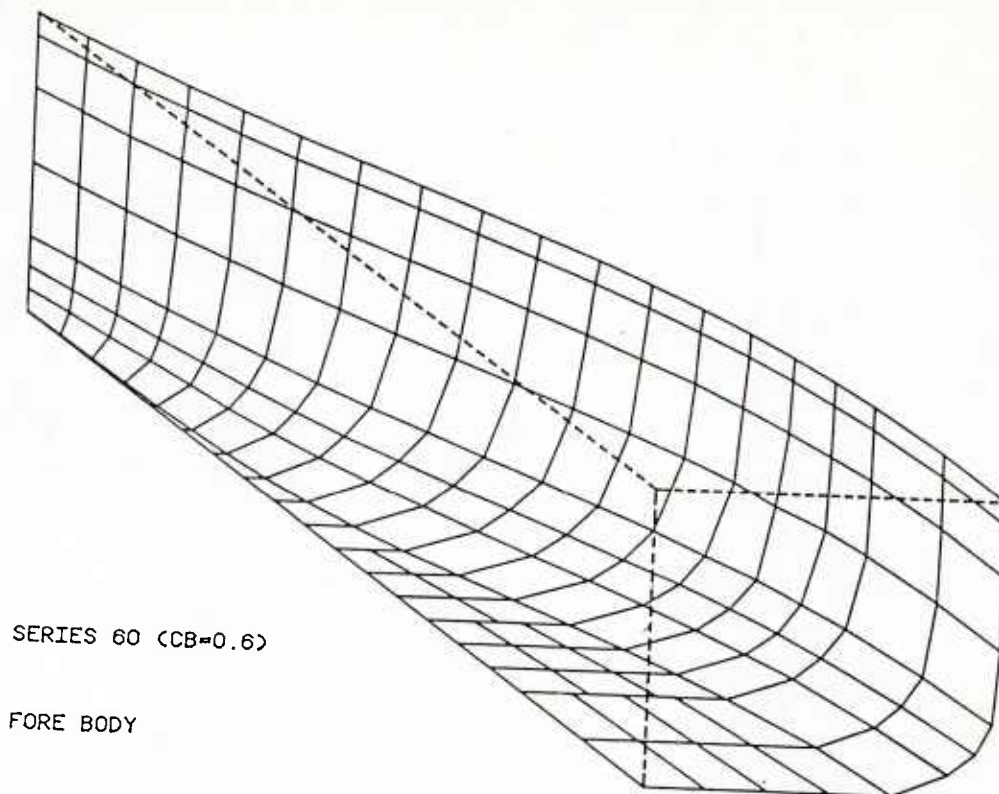


Fig. 16 Arrangement of Surface Elements of Fore Body
for Series 60, $C_B=0.6$

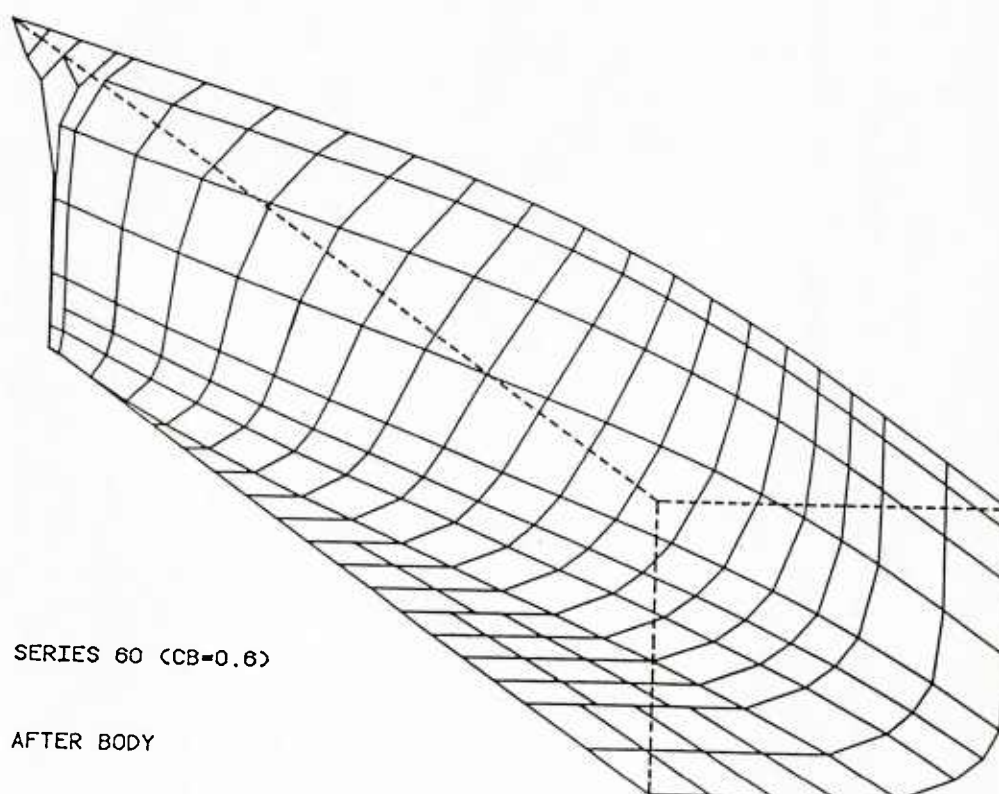


Fig. 17 Arrangement of Surface Elements of Aft Body
for Series 60, $C_B=0.6$

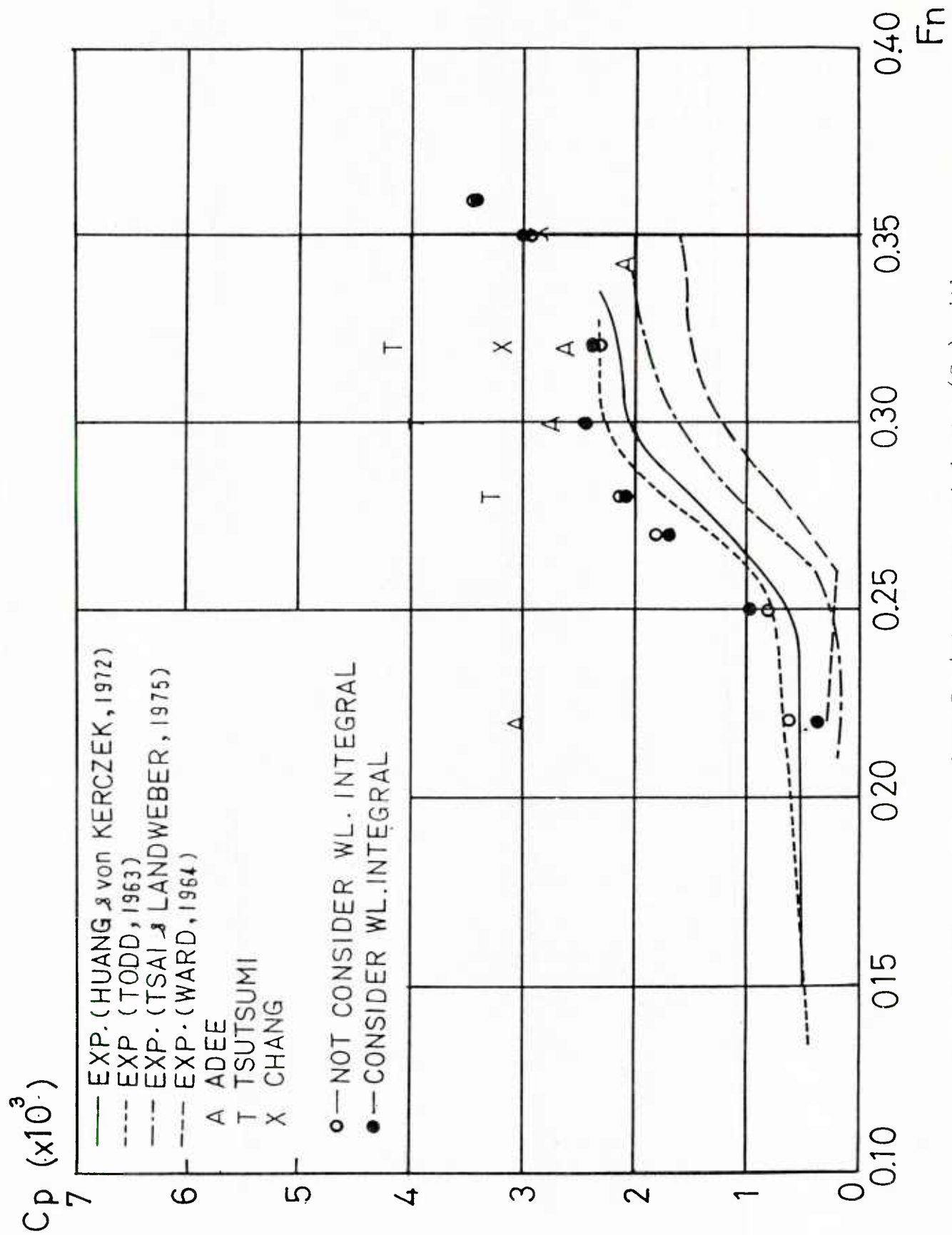


Fig. 18 Comparison of Wave-Resistance Coefficients (C_p) with Experimental and Other Numerical Results for Series 60, $C_b=0.6$,

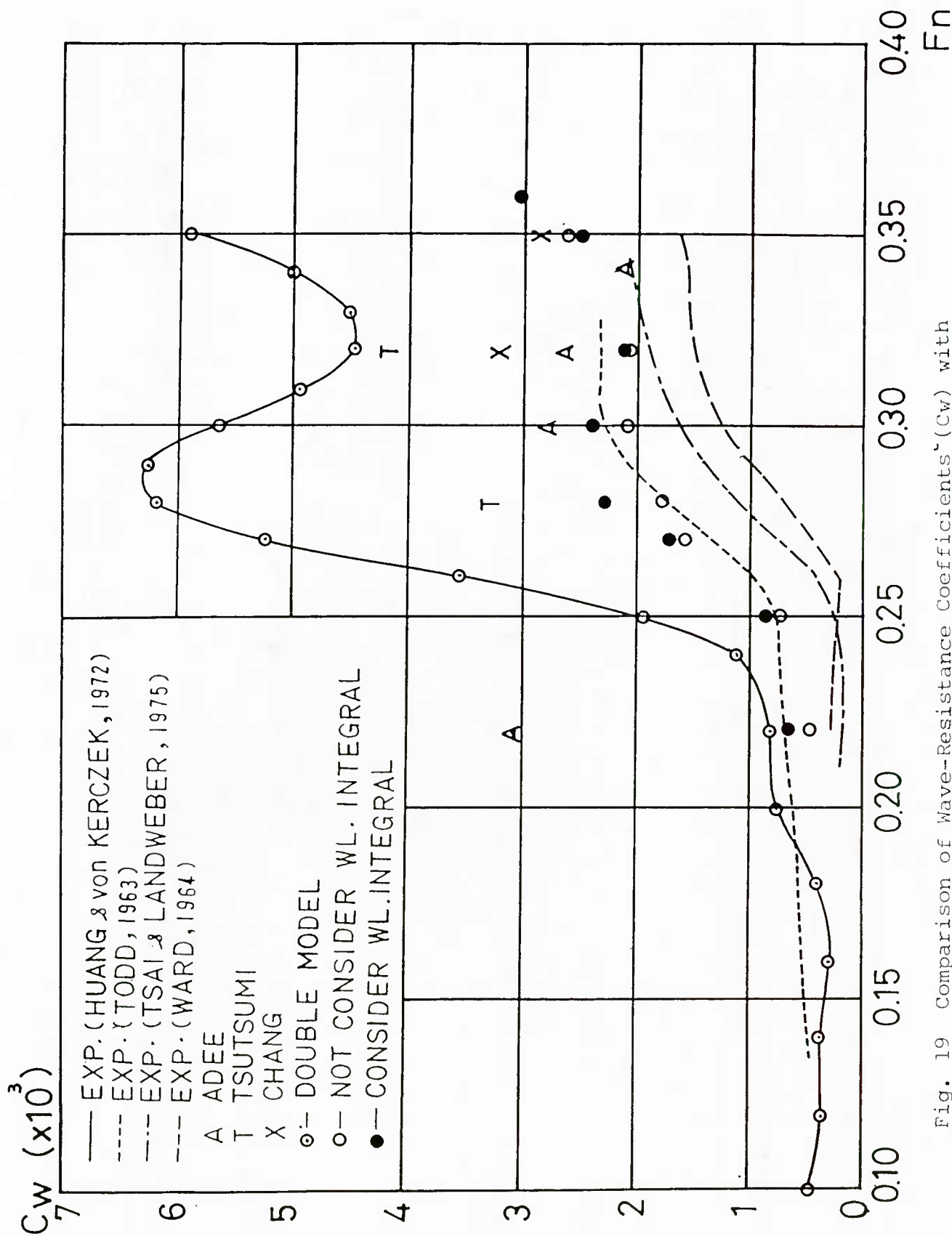


Fig. 19 Comparison of Wave-Resistance Coefficients^{*} (C_w) with Experimental and Other Numerical Results for Series 60, $C_b=0.6$,

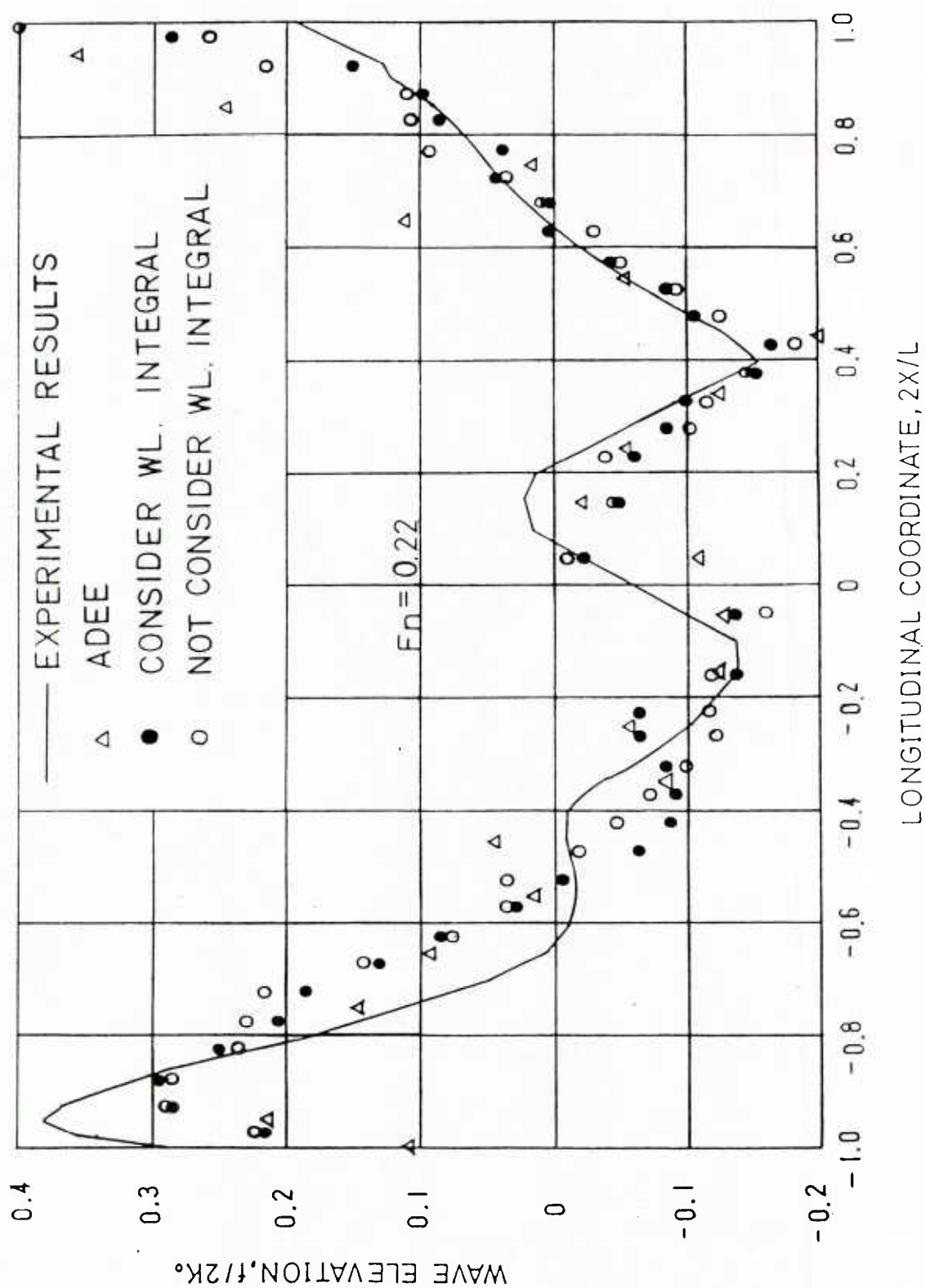


Fig. 20 Comparison of Wave Profile with Experimental and Other Numerical Results for Series 60, $C_D=0.6$ at $Fn=0.22$

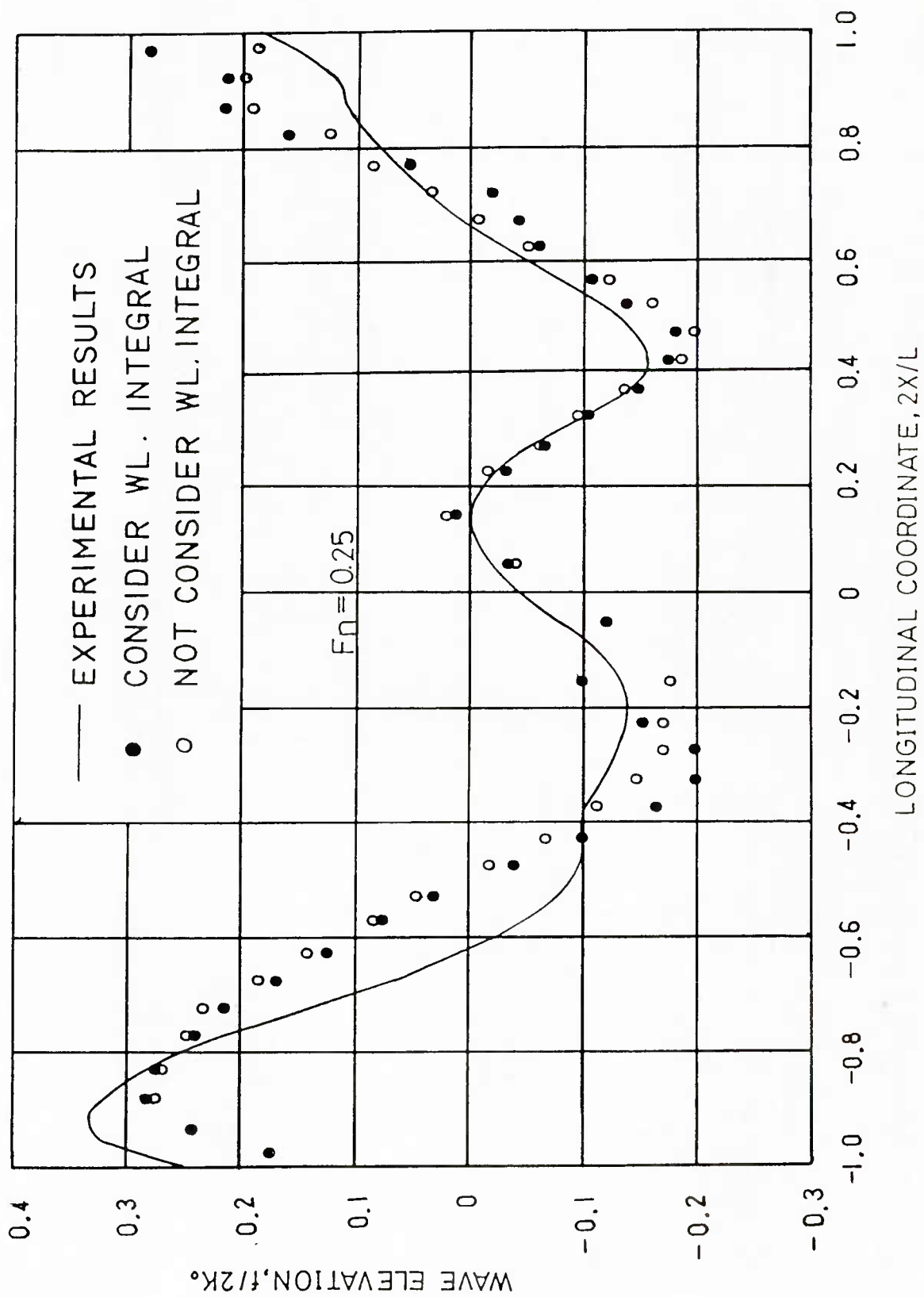


Fig. 21 Comparison of Wave Profile with Experimental Results for Series 60, $C_b = 0.6$ at $Fn = 0.25$

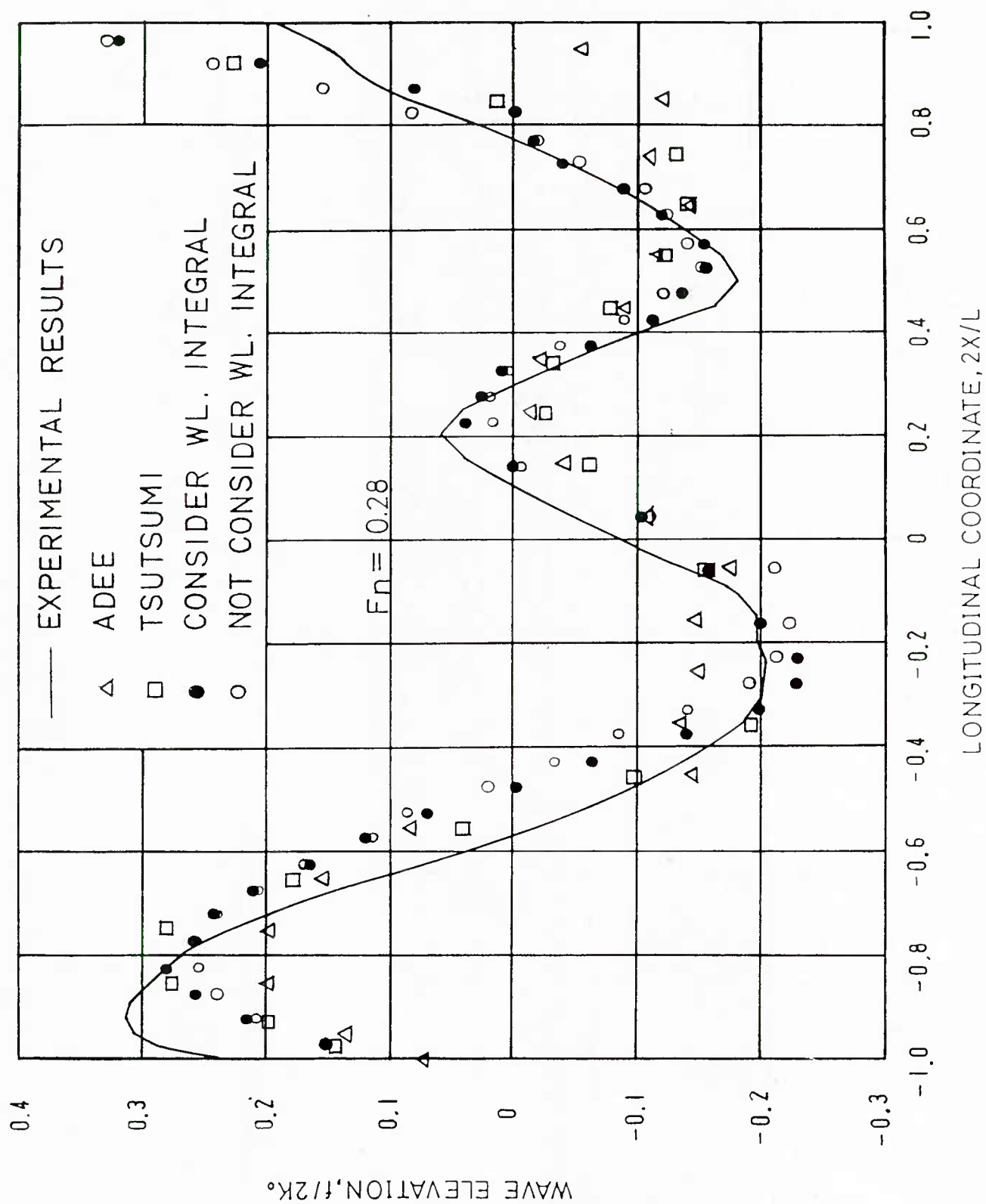


Fig. 22 Comparison of Wave Profile with Experimental and Other Numerical Results for Series 60, $C_b=0.6$ at $F_n=0.28$

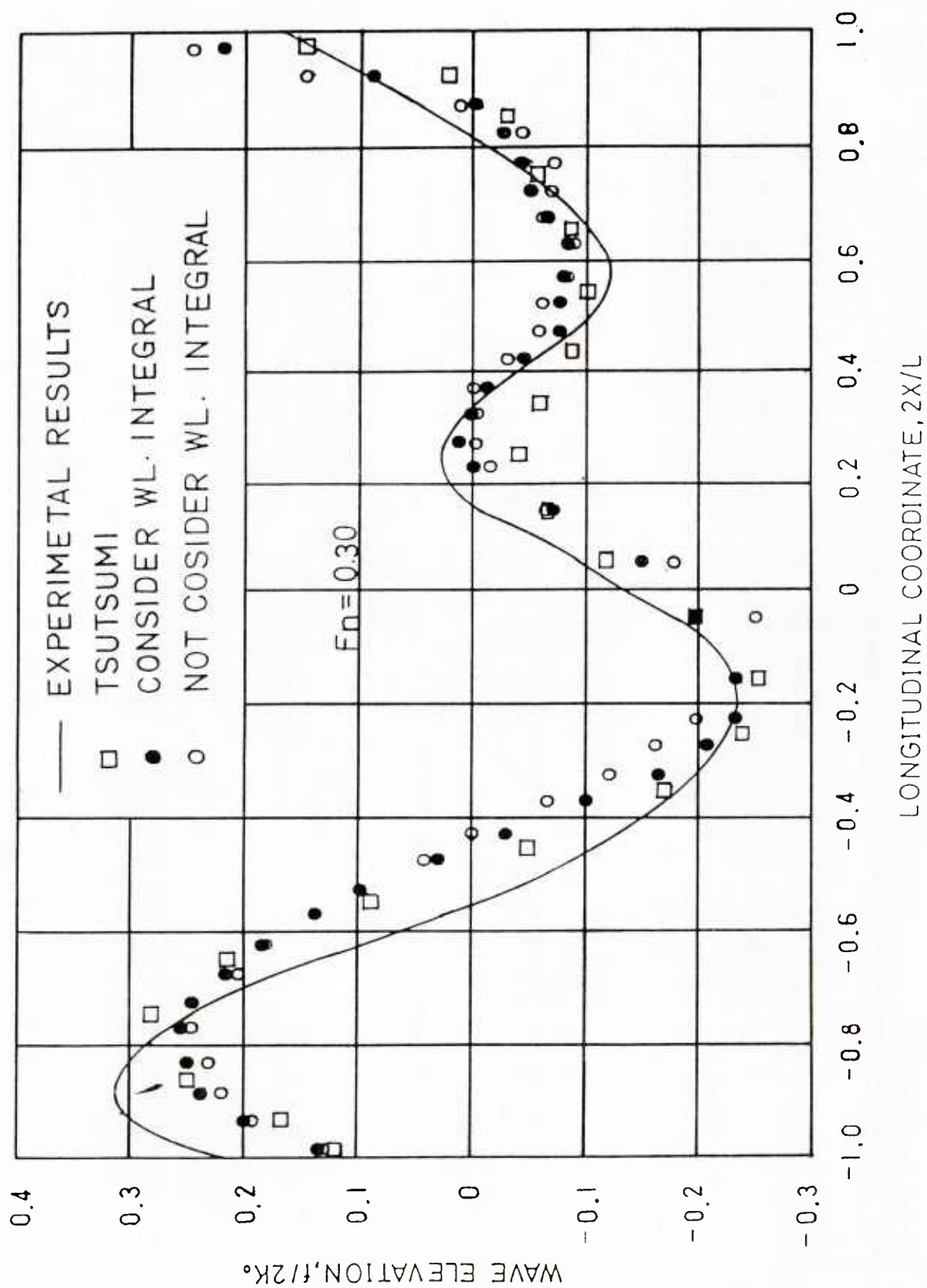


Fig. 23 Comparison of Wave Profile with Experimental and Other Numerical Results for Series 60, $C_p=0.6$ at $Fn=0.30$

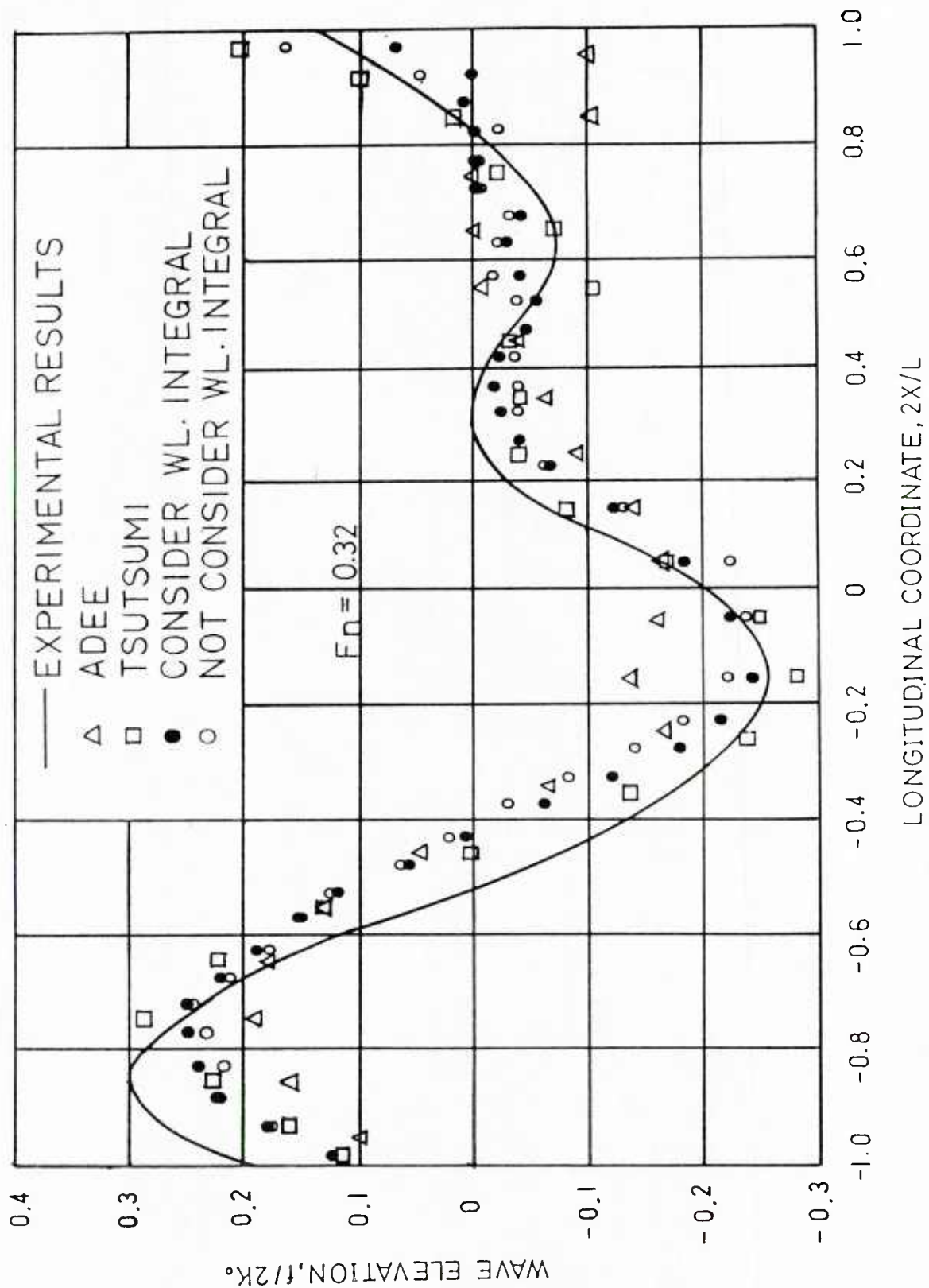


Fig. 24 Comparison of Wave Profile with Experimental and Other Numerical Results for Series 60, $C_b=0.6$ at $Fn=0.32$

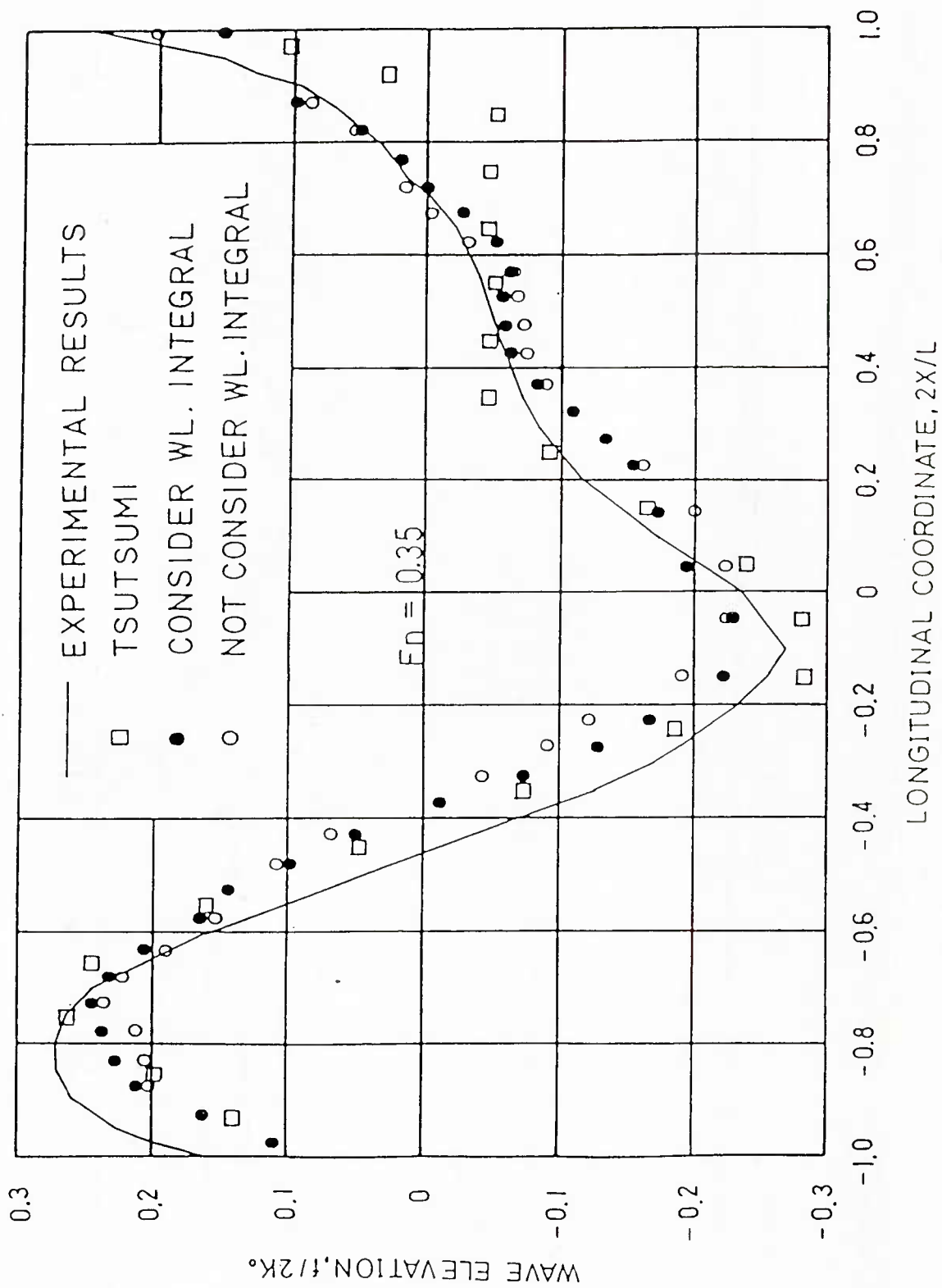


Fig. 25 Comparison of Wave Profile with Experimental and Other Numerical Results for Series 60, $C_b=0.6$ at $Fn=0.35$

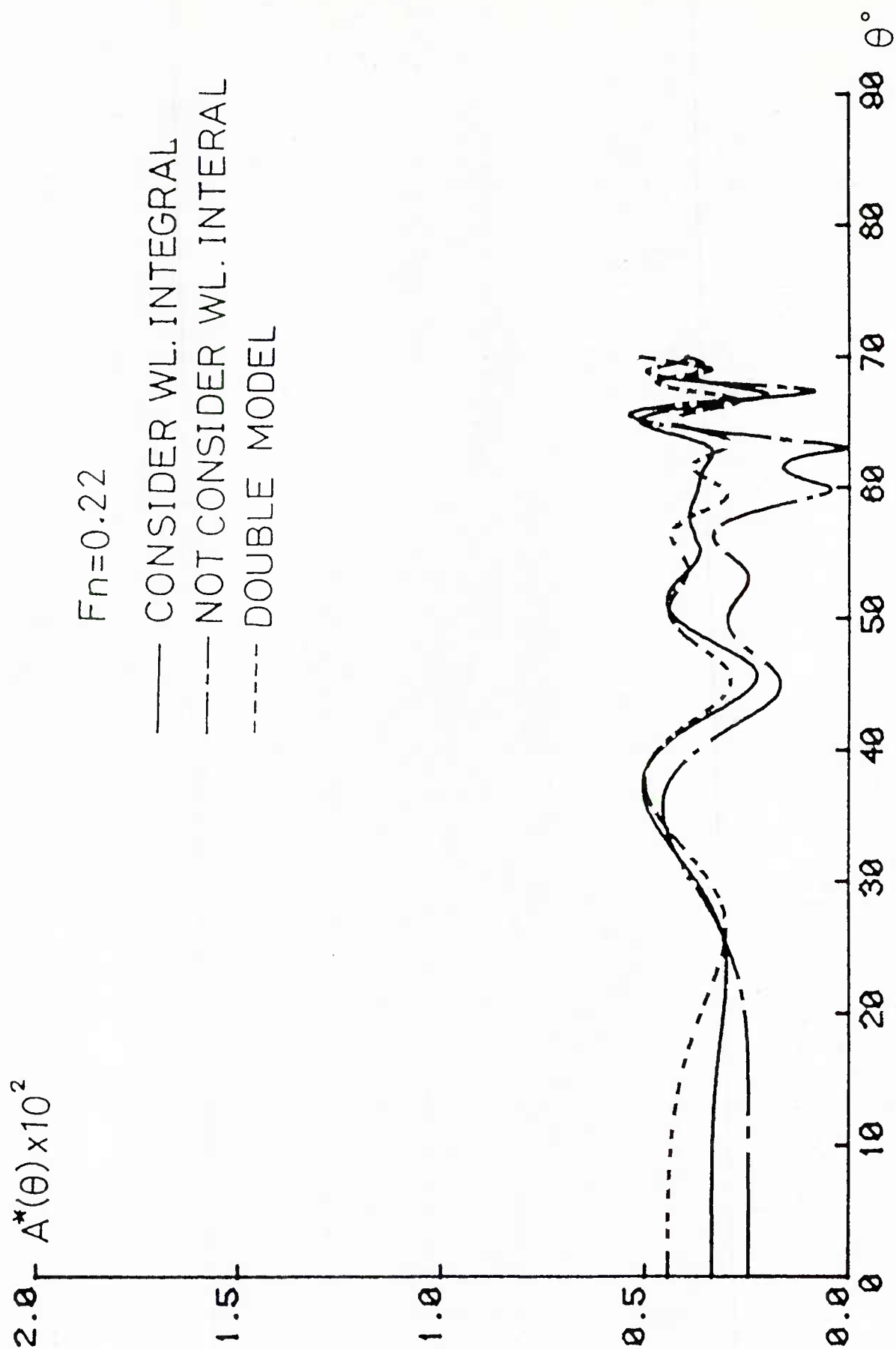


Fig. 26 Amplitude Function of Series 60, $C_b=0.6$ at $Fn=0.22$

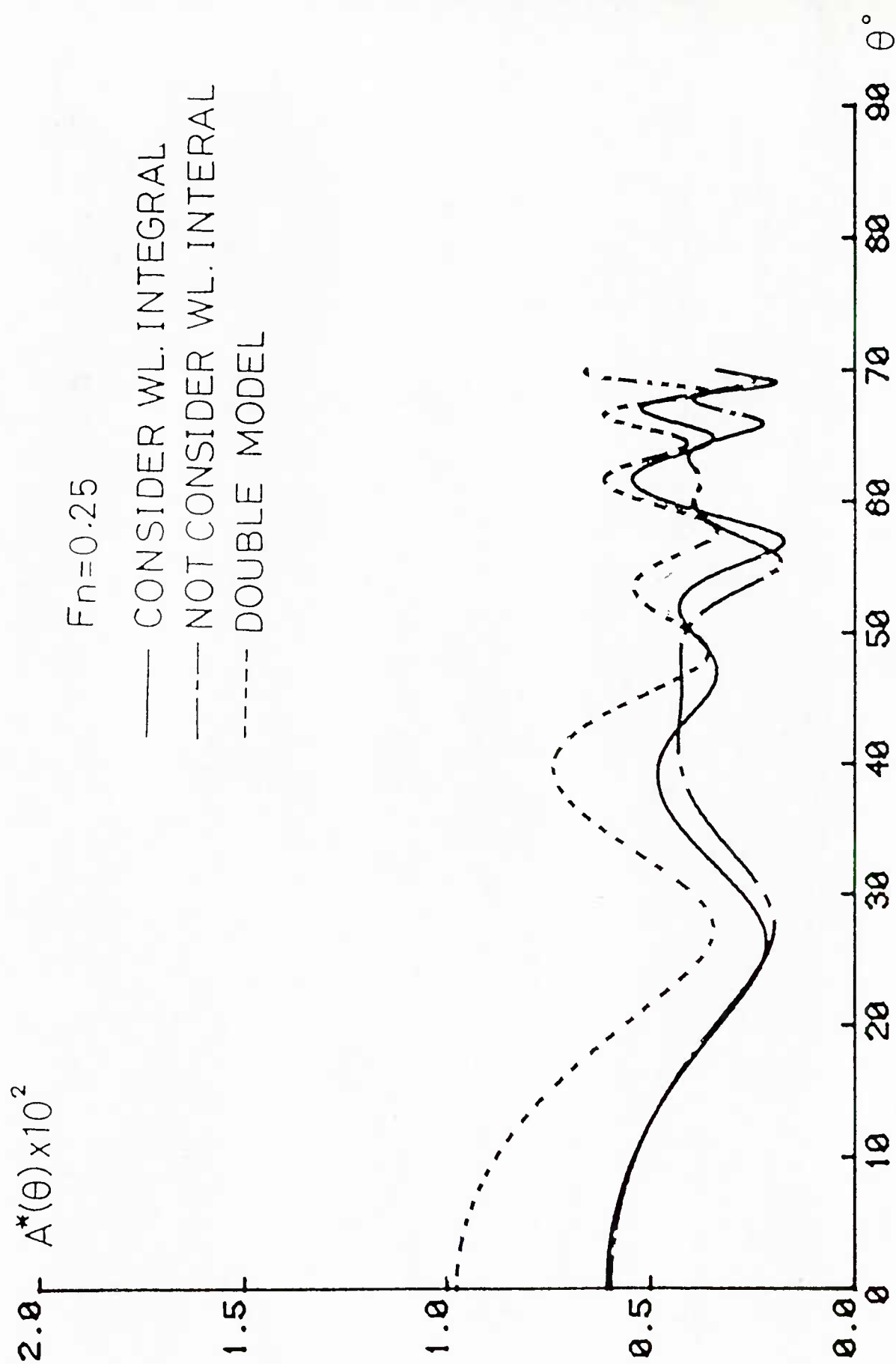


Fig. 27 Amplitude Function of Series 60, $C_b=0.6$ at $Fn=0.25$

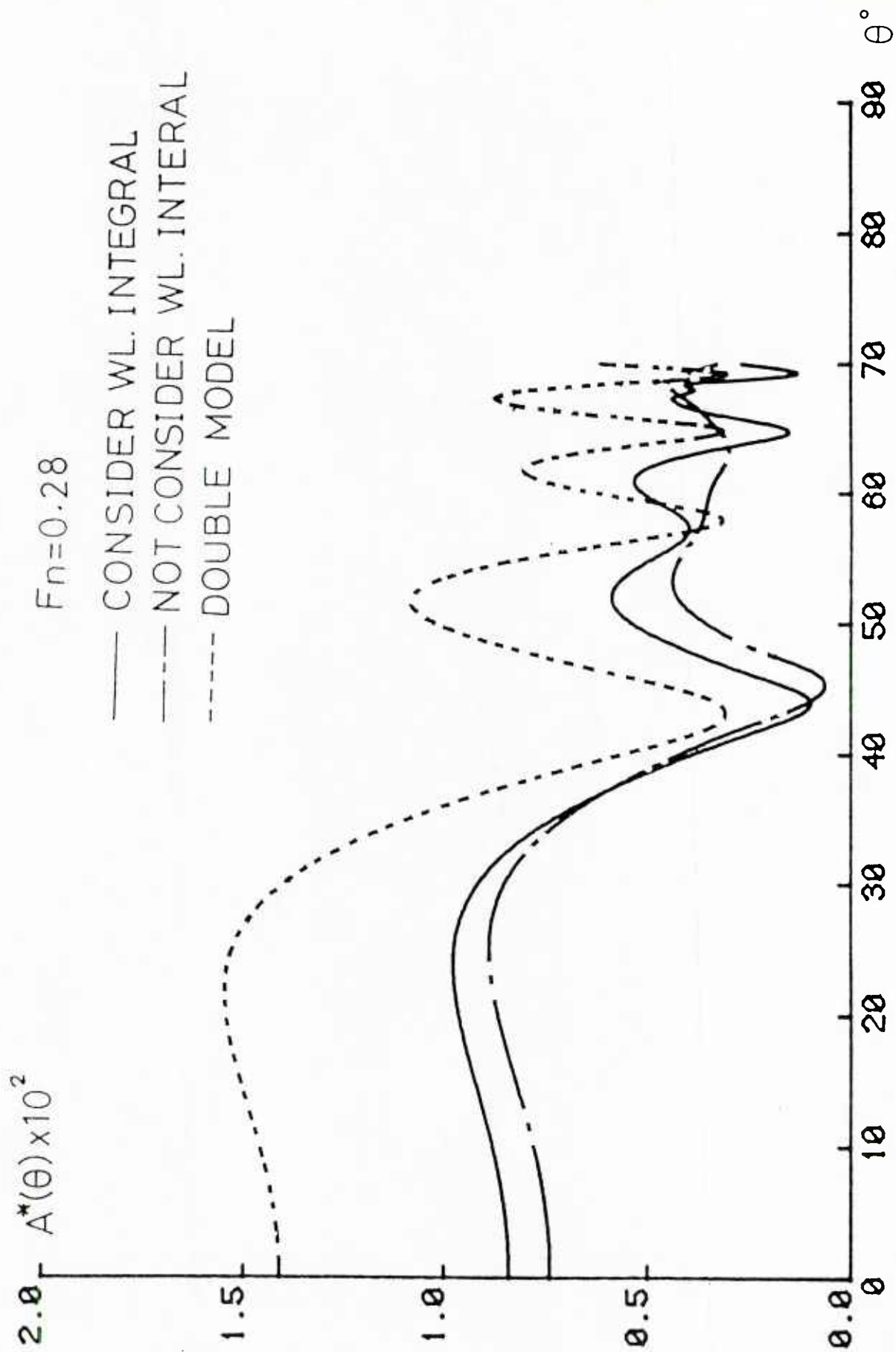


Fig. 28 Amplitude Function of Series 60, $C_b=0.6$ at $Fn=0.28$

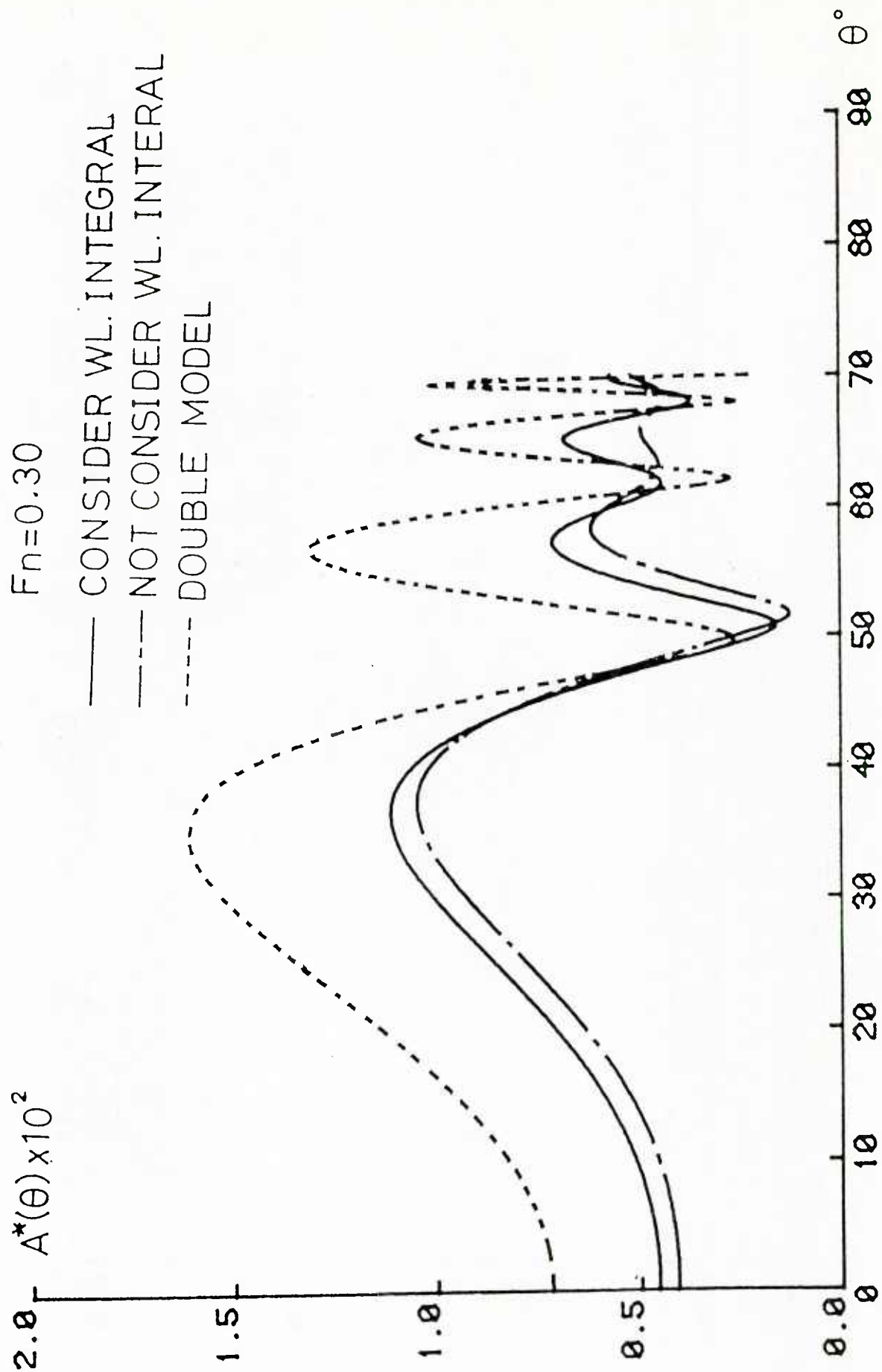


Fig. 29 Amplitude Function of Series 60, $C_p=0.6$ at $Fn=0.30$

$Fn=0.32$

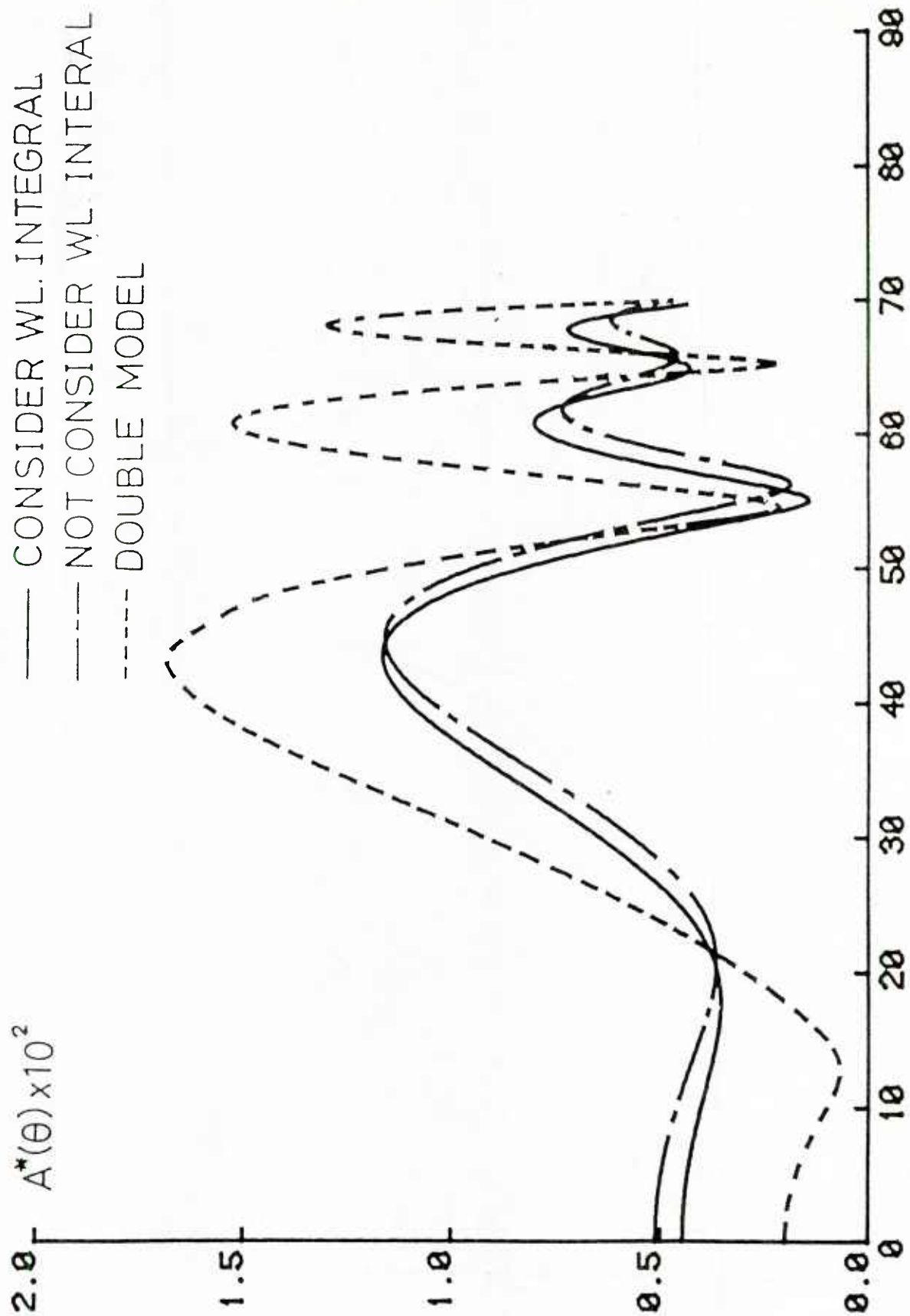


Fig. 30 Amplitude Function of Series 60, $C_p=0.6$ at $Fn=0.32$

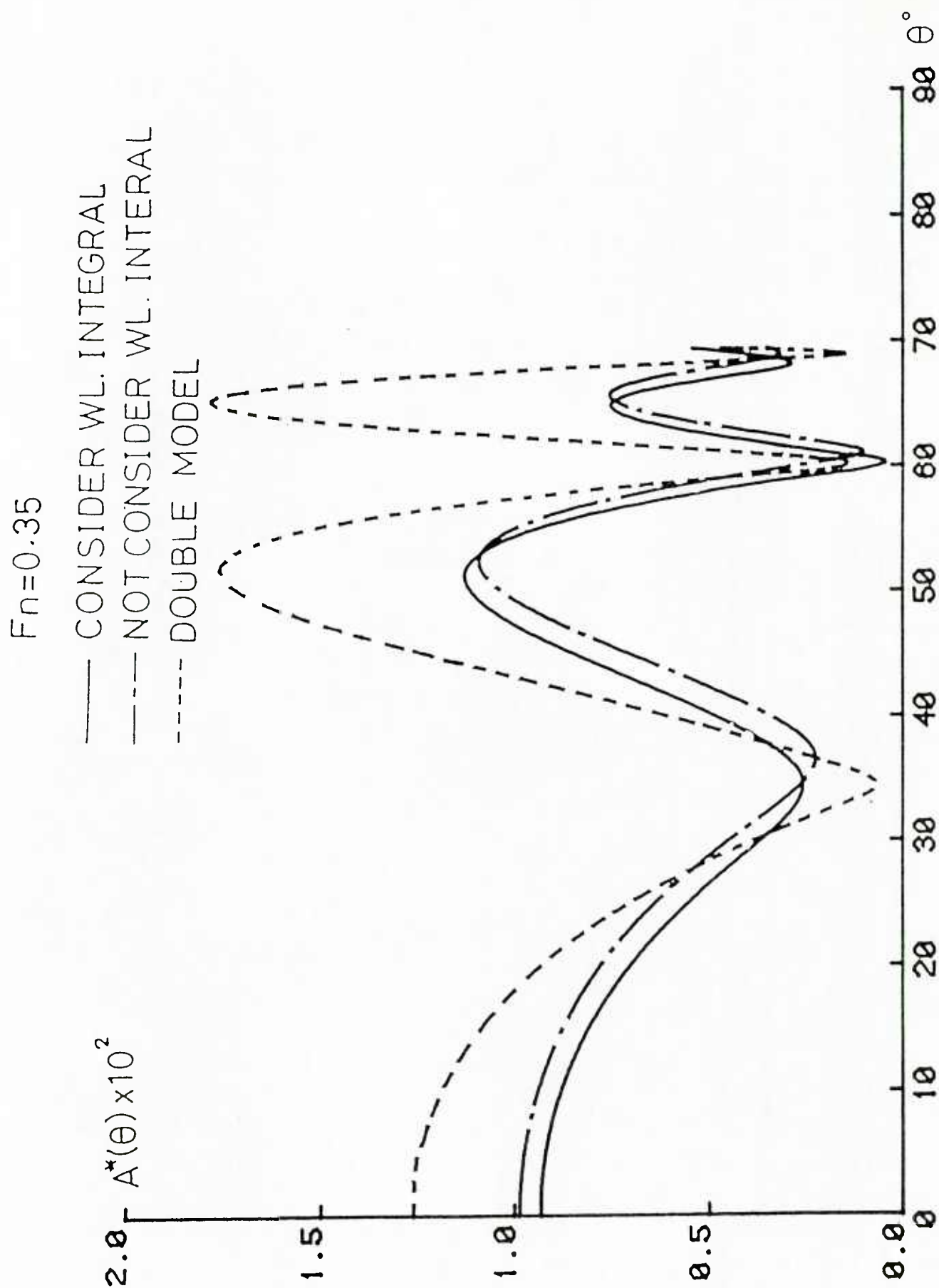


Fig. 31 Amplitude Function of Series 60, $C_b=0.6$ at $Fn=0.35$

Neumann-Kelvin Problem Solved by the Iterative Procedure Using Hess & Smith Solver Program

H. Adachi and H. Takeshi
Ship Research Institute

Abstract

The analysis of the low speed theory by the iterative method will introduce the Neumann-Kelvin problem as the basic fundamental problem. This fact will provide an additional importance of the N-K problem in the wave making resistance calculation.

In order to calculate the N-K problem, a method making use of the Hess & Smith program as a fundamental one is devised. The method is found to be useful to treat the line integral and give the lucid explanation for the N-K problem.

1. Neumann-Kelvin Problem in the Low Speed Theory

The admittedly basic form of the velocity potential in the low speed theory of the steady wave making resistance theory seems to be given by the following form, ^{1),2)}

$$\phi = x + \phi = x + \phi^R + \phi^W, \quad (1)$$

where ϕ^R is the velocity potential of the basic flow satisfying,

$$\left. \begin{array}{ll} \text{(L)} & \nabla^2 \phi^R(P) = 0 & P \in De \\ \text{(F)} & \frac{\partial \phi^R}{\partial z} = 0 & P \in Fe \\ \text{(H)} & \frac{\partial \phi^R}{\partial n} = - \frac{\partial x}{\partial n} & P \in S_B \\ \text{(R)} & |\nabla \phi^R| \rightarrow 0 \text{ as } |P| \rightarrow \infty, \end{array} \right\} \quad (2)$$

where De is the fluid region outside of hull S_B bounded by the free surface Fe ($z=0$) and the surrounding surface S_R , and \vec{n} is the inward normal vector in the fluid region De . (See Fig. 1) And ϕ^W is the velocity potential with wavy property superposed on the basic flow which satisfies the following conditions.

$$\left. \begin{aligned}
 (L) \quad \nabla^2 \phi^W &= 0 & P \in De \\
 (F) \quad \left\{ (1 + \phi_x^R) \frac{\partial}{\partial x} + \phi_y^R \frac{\partial}{\partial y} \right\}^2 \phi^W + v \frac{\partial \phi^W}{\partial z} &= D(x, y) & P \in Fe \\
 (H) \quad \frac{\partial \phi^W}{\partial n} &= 0 & P \in S_B \\
 (R) \quad \text{Radiation condition,} & &
 \end{aligned} \right\} \quad (3)$$

where

$$D(x, y) = -\phi_{xx}^R + N(x, y), \quad (4)$$

with

$$\begin{aligned}
 N(x, y) = -\frac{1}{2} \{ & (2 \frac{\partial}{\partial x} + \phi_x^R \frac{\partial}{\partial x} + \phi_y^R \frac{\partial}{\partial y}) (\phi_x^{R^2} + \phi_y^{R^2}) \\
 & - \phi_{zz}^R (2\phi_x^R + \phi_x^{R^2} + \phi_y^{R^2}) \}_{z=0}. \quad (5)
 \end{aligned}$$

The free surface condition for the wavy potential can be rewritten as follows,

$$(F) \quad F \phi^W = D(x, y) + E(x, y) \quad P \in Fe, \quad (6)$$

where

$$F = \frac{\partial^2}{\partial x^2} + v \frac{\partial}{\partial z} \quad \text{with } v = g/U^2.$$

And

$$E(x, y) = -\left\{ (1 + \phi_x^R) \frac{\partial}{\partial x} + \phi_y^R \frac{\partial}{\partial y} \right\}^2 \phi^W + \phi_{xx}^W.$$

The boundary value problem (3) may be treated iteratively assuming the condition,

$$E(x, y) = o(\phi_{xx}^W).$$

Thus, the free surface condition for the j th iteration problem writes,

$$(F) \quad F \phi_j^W = E_j(x, y) \quad P \in Fe, \quad (7)$$

where

$$E_1 = D, \quad E_j = E(\phi_{j-1}^W) \quad j \geq 2. \quad (8)$$

Therefore j th problem will take the following general form.

$$\left. \begin{aligned}
 (L) \quad \nabla^2 \phi_j^W &= 0 & P \in De \\
 (F) \quad F \phi_j^W &= E_j(x, y) & P \in Fe \\
 (H) \quad \frac{\partial \phi_j^W}{\partial n} &= 0 & P \in S_B \\
 (R) \quad \text{Radiation condition.} & &
 \end{aligned} \right\} \quad (9)$$

Making use of the Green's theorem, the j th wavy potential will be written into,

$$\phi_j^W(P) = \frac{1}{4\pi} \iint_S dS \left\{ G(P, Q) \frac{\partial}{\partial n} \phi_j^W - \phi_j^W \frac{\partial G}{\partial n_Q} \right\}, \quad (10)$$

where the Green function must satisfy the following conditions.

$$\left. \begin{array}{ll} (L) & \nabla^2 G(P, Q) = 4\pi\delta(P-Q) \quad z < 0 \\ (F) & FG(P, Q) = 0 \quad z = 0 \\ (R) & \text{Radiation condition.} \end{array} \right\} \quad (11)$$

Then ϕ_j^W can be transformed as follows,

$$\begin{aligned} \phi_j^W = & -\frac{1}{4\pi} \iint_{S_B} dS \phi_j^W \frac{\partial G}{\partial n_Q} - \frac{1}{4\pi v} \iint_{F_e} dS E_j G \\ & - \frac{1}{4\pi v} \oint_L d\eta \left\{ G \frac{\partial}{\partial \xi} \phi_j^W - \phi_j^W \frac{\partial G}{\partial \xi} \right\} \quad P \in D_e. \end{aligned} \quad (12)$$

Since E_j is a known function over F_e , an integral equation for ϕ_j^W can be derived as $P \rightarrow Q \in S_B$. The iteration scheme mentioned here is equivalent to that proposed by Kitazawa³⁾.

Therefore, the boundary value problem (9) is the fundamental one in the iterative scheme for the low speed wave making theory. However, no attempts have been existed to solve it numerically. For one reason, the problem involves the N-K problem as the fundamental solution. Thus, without the numerical procedure for the N-K problem, we will not be able to go further into the investigation of the low speed theory. However, there may be many other tools of attacking the low speed theory than the iterative method mentioned here.

Now we will derive the N-K problem from (9). Let's decompose ϕ^W into two components,

$$\phi^W = \underbrace{\phi^{WP}}_{\text{Pressure potential component}} + \underbrace{\phi^{WD}}_{\text{Diffraction potential component}} \quad (13)$$

They satisfy the following conditions, respectively,

$$\begin{array}{lll}
 (L) & \nabla^2 \phi^{WP} = 0 & P \in De \\
 (F) & F \phi^{WP} = E & P \in Fe \\
 (R) & \text{Radiation condition,} &
 \end{array} \left. \vphantom{\begin{array}{l} (L) \\ (F) \\ (R) \end{array}} \right\} \quad (14)$$

and

$$\begin{array}{lll}
 (L) & \nabla^2 \phi^{WD} = 0 & P \in De \\
 (F) & F \phi^{WD} = 0 & P \in Fe \\
 (H) & \frac{\partial \phi^{WD}}{\partial n} = - \frac{\partial \phi^{WP}}{\partial n} & P \in S_B \\
 (R) & \text{Radiation condition.} &
 \end{array} \left. \vphantom{\begin{array}{l} (L) \\ (F) \\ (H) \end{array}} \right\} \quad (15)$$

The problem for the diffraction component apparently defines the N-K problem recurringly. Since the pressure potential problem can be given explicitly, if E function were known, it remains to solve the diffraction potential problem that is the N-K problem.

Let's consider the first iteration problem which is the most important step in the low speed theory. Then,

$$E(x,y) = D(x,y) = - \phi_{xx}^R + N(x,y).$$

So the pressure potential will be decomposed into two components.

$$\phi^{WP} = \underbrace{\phi_L^{WP}}_{\text{Linear term,}} + \underbrace{\phi_N^{WP}}_{\text{Non linear correction term}} \quad (16)$$

where each potential satisfies the following free surface conditions,

$$(F) \quad F \phi_L^{WP} = -\phi_{xx}^R \quad P \in Fe, \quad (17)$$

and

$$(F) \quad F \phi_N^{WP} = N(x,y) \quad P \in Fe, \text{ respectively.} \quad (18)$$

According to this decomposition of the pressure potential, the diffraction potential is similarly divided into two components, such that,

$$\phi^{WD} = \phi_L^{WD} + \phi_N^{WD}, \quad (19)$$

where each potential satisfies the following hull surface conditions,

$$(H) \quad \frac{\partial \phi_L^{WD}}{\partial n} = - \frac{\partial \phi_L^{WP}}{\partial n} \quad P \in S_B, \quad (20)$$

and

$$(H) \quad \frac{\partial}{\partial n} \phi_N^{WD} = - \frac{\partial}{\partial n} \phi_N^{WP} \quad P \in S_B, \text{ respectively.} \quad (21)$$

It is easily seen that the higher order iteration includes terms only corresponding to the nonlinear correction term. If we collect the linear terms, the original N-K problem recovers. Thus,

$$\phi^{NK} = \phi^R + \phi_L^{WP} + \phi_L^{WD}. \quad (22)$$

This potential satisfies (15), in which ϕ^{WP} must be replaced by x . Then the total potential at the first step of the iteration becomes,

$$\phi_1 = x + \phi^{NK} + \phi_{1N}^{WP} + \phi_{1N}^{WD}. \quad (23)$$

With these decomposition of the potentials, we can classify the calculation methods of the low speed theory. As for the original N-K problem, it plays main role as the linear term in the low speed theory. And moreover the nonlinear correction term will lead to the general N-K problem. Therefore the N-K problem is indispensable in the low speed theory.

2. Solution Method of the N-K Problem

So far, we have observed that the N-K problem is vital to the low speed theory. And the general form of the N-K problem is defined as follows,

$$\left. \begin{array}{ll} (L) \quad \nabla^2 \phi = 0 & P \in D_e \\ (F) \quad F \phi = 0 & P \in F_e \\ (H) \quad \frac{\partial \phi}{\partial n} = -v(P) & P \in S_B \\ (R) \quad \text{Radiation condition.} \end{array} \right\} \quad (24)$$

In order to derive the solution of the problem, we use similar decomposition to (22), and derive the successive potential which are summed up to the N-K solution. Thus let

$$\phi = \phi_0^R + \phi_0^P + \phi_0^D. \quad (25)$$

The rigid wall potential satisfies (2), the pressure potential does (14) with the free surface condition (17). And the diffraction potential defines again the N-K problem with the hull surface condition,

$$(H) \quad \frac{\partial}{\partial n} \phi_0^D = -v_1(P) = -\frac{\partial}{\partial n} \phi_0^P \quad P \in S_B. \quad (26)$$

Thus repeating this procedure, we have for the N-K potential,

$$\phi = \sum_0^\infty \{ \phi_i^R + \phi_i^P \}, \quad (27)$$

where ϕ_i^R and ϕ_i^P satisfy the following conditions respectively.

$$\left. \begin{array}{ll} (L) & \nabla^2 \phi_i^R = 0 \quad P \in D_e \\ (F) & \frac{\partial}{\partial z} \phi_i^R = 0 \quad P \in F_e \\ (H) & \frac{\partial}{\partial n} \phi_i^R = -v_i(P) \quad P \in S_B \\ (R) & |\nabla \phi_i^R| \rightarrow 0 \text{ as } P \rightarrow \infty \end{array} \right\} \quad (28)$$

and

$$\left. \begin{array}{ll} (L) & \nabla^2 \phi_i^P = 0 \quad P \in D_e \\ (F) & F \phi_i^P = -\frac{\partial^2}{\partial x^2} \phi_i^R \quad P \in F_e \\ (R) & \text{Radiation condition} \end{array} \right\} \quad (29)$$

The rigid wall potential problem (28) is a well posed one. And the pressure potential problem (29) can be solved when the rigid wall potential is known over F_e .

For simplicity, we want to solve the N-K problem by only the source singularity distribution method. Then let's define the interior potentials corresponding to ϕ_i^R and ϕ_i^P as follows,

$$\left. \begin{array}{ll} (L) & \nabla^2 \psi_i^R = 0 \quad P \in D_i \\ (F) & \frac{\partial}{\partial z} \psi_i^R = 0 \quad P \in F_i \\ (H) & \psi_i^R = \phi_i^R \quad P \in S_B \end{array} \right\} \quad (30)$$

and

$$\left. \begin{array}{ll} (L) & \nabla^2 \phi_i^P = 0 \quad P \in D_i \\ (F) & F \phi_i^P = -\frac{\partial^2}{\partial x^2} \psi_i^R \quad P \in F_i \end{array} \right\} \quad (31)$$

Here it must be said that as the free surface condition on F_i is arbitrary, so other forms of the condition are possible.

Now it is easily shown that the rigid wall potential can be given by the source distribution over S_B .

$$\phi_i^R(P) = \frac{1}{4\pi} \iint_{S_B} dS(Q) \sigma_i(Q) G_R(P, Q) , \quad (32)$$

where

$$\sigma_i = \frac{\partial}{\partial n} \phi_i^R - \frac{\partial}{\partial n} \psi_i^R \quad Q \in S_B . \quad (33)$$

And the Green function is

$$G_R(P, Q) = -1/r - 1/r' . \quad (34)$$

Therefore $\sigma_i(Q)$ can be calculated by the Hess & Smith program with slight modifications.

For the pressure potential, applying the Green's theorem, we have,

$$\begin{aligned} \phi_i^P(P) &= -\frac{1}{4\pi} \iint_{Fe+Fi} dS \{ \phi_i^P \frac{\partial}{\partial n_Q} G - G \frac{\partial}{\partial n} \phi_i^P \} \\ &= -\frac{1}{4\pi} \{ \frac{1}{v} \oint_L d\eta (\phi_{i\xi}^R - \psi_{i\xi}^R) G + \iint_{Fe} dS \phi_i^R G_\zeta + \iint_{Fi} dS \psi_i^R G_\zeta \} \end{aligned} \quad (35)$$

Let's define such function G_W by analytical continuation on $Fe+Fi$ that

$$\frac{\partial}{\partial \zeta} G_W = \frac{\partial}{\partial \zeta} G \text{ and analytic in } z < 0.$$

We can have for G_W ,

$$G_W(P, Q) = \frac{1}{\pi} \operatorname{Re} \int_{-\pi}^{\pi} d\theta \int_0^{\infty} dk \frac{k \exp\{k(z+\zeta) + ik(x-\xi)\cos\theta + ik(y-\eta)\sin\theta\}}{k - v \sec^2 \theta} . \quad (36)$$

Thus $G_R + G_W$ satisfies (11). Applying the Green's theorem with G_W to the surface integral terms in (35), and considering the Dirichlet condition on S_B of the rigid wall potentials, (35) will be deformed as follows,

$$\begin{aligned} \phi_i^P(P) &= -\frac{1}{4\pi v} \oint_L d\eta \cos(x, n) \{ \frac{\partial}{\partial n} \phi_i^R - \frac{\partial}{\partial n} \psi_i^R \} G(P, Q) \\ &\quad + \frac{1}{4\pi} \iint_{S_B} dS \{ \frac{\partial}{\partial n} \phi_i^R - \frac{\partial}{\partial n} \psi_i^R \} G_W(P, Q) . \end{aligned} \quad (37)$$

Therefore, we can write with (32) and (37),

$$\phi(P) = (27) = -\frac{1}{4\pi v} \oint_L d\ell \sigma(Q) \cos^2(x, n) G + \frac{1}{4\pi} \iint_{S_B} dS \sigma(Q) G(P, Q) , \quad (38)$$

with source distribution,

$$\sigma = \sum_0^{\infty} \sigma_i . \quad (39)$$

Since the Kochin function derived from (38) becomes,

$$H(\theta, v \sec^2 \theta) = H(\theta, v \sec^2 \theta) + \frac{1}{4\pi v} \oint_L d\ell \cos^2(x, n) \sigma e^{-iv \sec^2 \theta (\xi \cos \theta + \eta \sin \theta)} \quad (40)$$

where H function is the usual Kochin function. (40) is identical with the modified Kochin function of Guével et al.⁴⁾. Then the wave making resistance is given by

$$R_W = 8\pi \rho v^2 \int_{-\frac{1}{2}\pi}^{\frac{1}{2}\pi} d\theta \sec^3 \theta |H(\theta, v \sec^2 \theta)|^2 . \quad (41)$$

3. Singular Solution of the N-K Problem

It is shown that the source distribution of the N-K problem does not have singular behavior because it is derived from well posed problem (28). Therefore we may call the solution (38) as the least singular solution after Ursell⁵⁾. And it will be possible to introduce a singular solution ϕ_s which satisfies the conditions,

$$\left. \begin{array}{ll} (L) & \nabla^2 \phi_s = 0 & P \in De \\ (F) & F \phi_s = 0 & P \in Fe \\ (H) & \frac{\partial}{\partial n} \phi_s = 0 & P \in S_B \\ (R) & \text{Radiation condition} \end{array} \right\} \quad (42)$$

Apparently ϕ_s is thought to be a solution which might be included in the N-K solution. A possible solution for (42) will take the following form,

$$\phi_s^P(P) = -\frac{1}{4\pi v} \oint_L d\ell \cos^2(x, n) \sigma_s(Q) G(P, Q) , \quad (43)$$

which inherits the properties from the pressure potential. This potential satisfies the conditions,

$$\begin{array}{ll}
 \text{(L)} & \nabla^2 \phi_s^P = 0 \\
 \text{(F)} & F \phi_s^P = 0 \\
 \text{(R)} & \text{Radiation condition}
 \end{array}
 \left. \begin{array}{l} P \in De \\ P \in Fe \end{array} \right\} \quad (44)$$

In order for ϕ_s to satisfy (42), one more potential ϕ_s^D should be introduced which is the solution of (15), that is the N-K problem. Therefore the singular solution can be obtained if the line source distribution σ_s is determined. This source is very similar to that in (37) and arbitrary. Since σ_s in (43) is a line sources on L, then if σ_s is added to σ of the least singular solution, the total source distribution becomes discontinuous at L. As far as the source distribution is concerned, we observe that the least singular N-K source (39) is continuous on S_B while the singular N-K source $\sigma + \sigma_s$ is discontinuous at L. Moreover we have to impose the condition to determine the density of singular source. Two choices are possible for such condition. One is the request that the N-K solution should be least singular as advocated by Ursell, in this case $\sigma_s = 0$. Another one is to use σ_s as one of the tools for the corrections for the nonlinear free surface condition. An attempt for the latter case has been made by Suzuki⁶⁾, advocating σ_s should be related to the sinkage correction.

4. Numerical Calculation of the N-K Problem

In order to calculate the source distribution σ_i in (32) by the Hess & Smith solver program, it is necessary to evaluate $v_i(P)$ in (28) at the control points of the element meshes on the hull. This can be performed by evaluating the products between the directinal derivatives of the pressure potential and the direction cosines of the element meshes. Green functions G_R and G_W are calculated from (34) and (36), respectively.

The results of the iteration are shown in Fig.2 for both wave resistance and source distribution along upper most elements. The zero th order sources coincide with the original Hess & Smith sources. Therefore the sources in Fig. 2 are for the wavy terms. It is obvious from C_w in the figure that the iteration converges at several steps of the iteration. The rather rapid fluctuation is noticeable in the

sources around the midship. This comes from the coarse division of mesh panels near midship and the rapid fluctuation of the potential as seen in Fig. 3.

The wave resistance is shown in Fig.4 compared with the results of the wave analysis conducted in the S.R.I.. The level of the calculation is about the same as that of the experiments which is usually lower than the residual resistance. As proved in the preceding section, the least singular N-K solution is a part of the solution of the low speed theory. Therefore we may not expect that the least singular N-K solution gives good results over wide range of Froude number.

References

- 1) Baba, E., and Hara, M., "Numerical Evaluation of A Wave-Resistance Theory for Slow Ships", 2nd Internat. Conference on Numer. Ship Hydrodyn., Berkley, (1977)
- 2) Maruo, H., "Wave Resistance of a Ship with Finite Beam at Low Froude Numbers", Bulletin of the Faculty of Eng., Yokohama National Univ., Vol.26, (1977)
- 3) Kitazawa, T., and Kajitani, H., "Computations of Wave-Resistance by the Low Speed Theory Imposing Accurate Hull Surface Condition", Proc. Workshop on Ship Wave Resistance Computations, Bethesda, (1979)
- 4) Guével, P., Vaussy, P., and Kobus, J.M., "The Distribution of Singularities Kinematically Equivalent to a Moving Hull in the Presence of a Free Surface", I.S.P., Vol.21, (1974)
- 5) Ursell, F., "Mathematical Notes on the Two-Dimensional Kelvin-Neumann Problem", Proc. 13th Symp. on Naval Hydrodyn., Tokyo, (1980)
- 6) Suzuki, K., "Calculation of Ship Wave Resistance with Special Reference to Sinkage", Proc. Workshop on Ship Wave Resistance Computations, Bethesda, (1979)

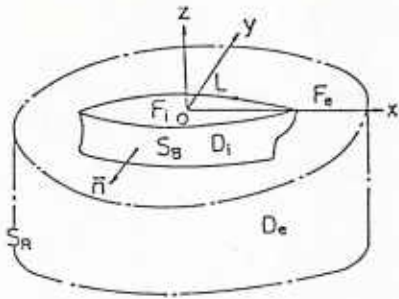


Fig. 1 Coordinate System

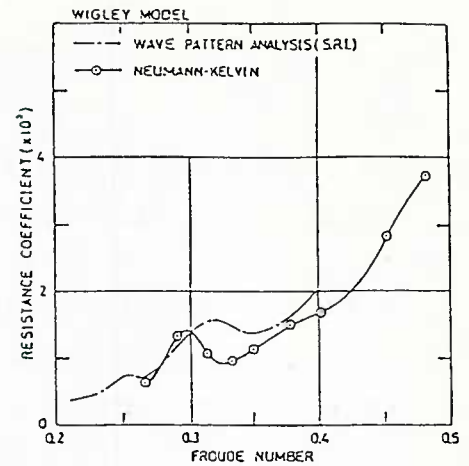


Fig. 4 Wave Resistance Coefficient for Wigley's Hull

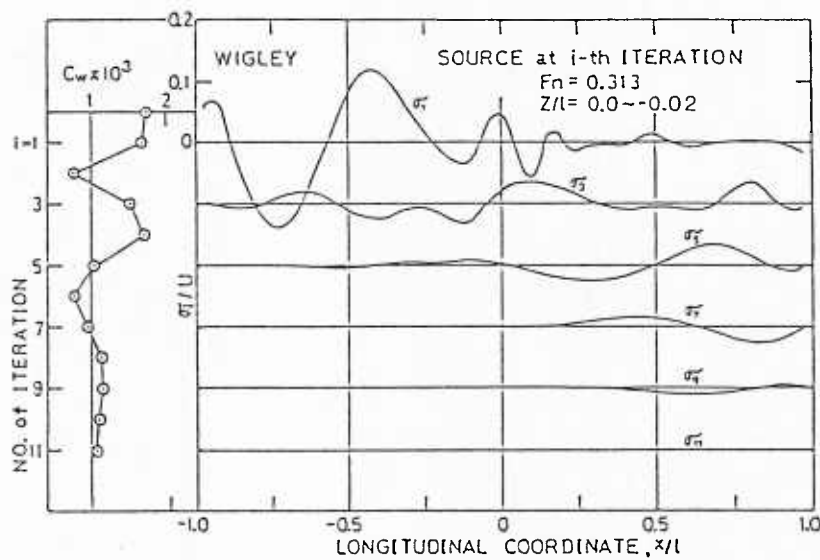


Fig. 2 Wavy Sources and C_w at each Iteration for Wigley's Hull

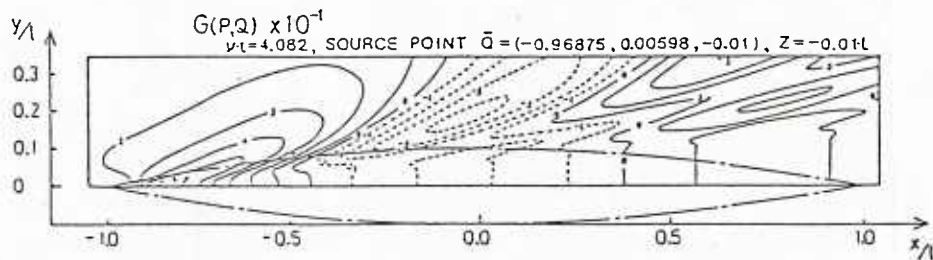


Fig. 3 Contour of Green Function, $G(\bar{x}, \bar{y}, \bar{z})$ at $Fn=0.35$

TABLE 1 WAVE RESISTANCE COEFFICIENT

H. Adachi & H. Takeshi / Neumann - Kelvin

WIGLEY	
Fn	$C_w \times 10^3$
0.266	0.630
0.289	1.313
0.313	1.072
0.333	0.962
0.350	1.134
0.378	1.497
0.402	1.672
0.452	2.841
0.482	3.728

TABLE 2 WAVE ELEVATIONS ALONG WIGLEY'S HULL

(Fore Part)

H. Adachi & H. Takeshi / Neumann - Kelvin Problem

$\begin{matrix} \text{Fn} \\ x/\ell \end{matrix}$	0.266	0.313	0.350	0.402	0.452	0.482
-1.0	Bow					
-0.9687	0.151	0.123	0.108	0.092	0.081	0.075
-0.9062	0.205	0.168	0.145	0.121	0.102	0.093
-0.8437	0.182	0.170	0.153	0.130	0.111	0.101
-0.7812	0.114	0.141	0.138	0.124	0.108	0.099
-0.7187	0.028	0.093	0.110	0.109	0.100	0.094
-0.6562	-0.051	0.037	0.072	0.087	0.086	0.083
-0.5937	-0.106	-0.018	0.029	0.060	0.069	0.070
-0.5312	-0.133	-0.063	-0.013	0.031	0.049	0.053
-0.4687	-0.137	-0.096	-0.050	0.001	0.027	0.035
-0.4062	-0.127	-0.115	-0.078	-0.028	0.004	0.016
-0.3437	-0.107	-0.123	-0.098	-0.053	-0.018	-0.004
-0.2812	-0.081	-0.123	-0.110	-0.072	-0.039	-0.023
-0.2187	-0.056	-0.116	-0.115	-0.087	-0.056	-0.040
-0.1562	-0.041	-0.101	-0.116	-0.098	-0.070	-0.055
-0.0937	-0.021	-0.088	-0.108	-0.105	-0.082	-0.067
-0.0312	-0.008	-0.085	-0.098	-0.107	-0.092	-0.079

TABLE 2 WAVE ELEVATIONS ALONG WIGLEY'S HULL
(Aft Part)

H. Adachi & H. Takeshi / Neumann - Kelvin Problem

$\begin{matrix} \text{Fn} \\ x/\ell \end{matrix}$	0.266	0.313	0.350	0.402	0.452	0.482
0.0312	-0.003	-0.062	-0.102	-0.098	-0.099	-0.089
0.0937	-0.016	-0.033	-0.100	-0.093	-0.094	-0.095
0.1562	-0.037	-0.034	-0.072	-0.104	-0.082	-0.088
0.2187	-0.054	-0.014	-0.051	-0.112	-0.080	-0.072
0.2812	-0.060	0.0	-0.053	-0.087	-0.102	-0.073
0.3437	-0.064	0.003	-0.028	-0.076	-0.105	-0.098
0.4062	-0.051	0.001	-0.012	-0.080	-0.086	-0.096
0.4687	-0.031	-0.013	0.0	-0.066	-0.093	-0.083
0.5312	-0.009	-0.016	0.019	-0.048	-0.093	-0.090
0.5937	0.006	-0.020	0.026	-0.029	-0.085	-0.095
0.6562	0.011	-0.018	0.020	-0.010	-0.087	-0.093
0.7187	0.013	-0.008	0.011	0.019	-0.075	-0.092
0.7812	0.030	0.017	-0.001	0.042	-0.050	-0.097
0.8437	0.065	0.022	-0.009	0.055	-0.022	-0.087
0.9062	0.119	0.042	0.017	0.048	0.019	-0.065
0.9687	0.163	0.049	0.101	0.038	0.082	-0.001
1.0	Stern					

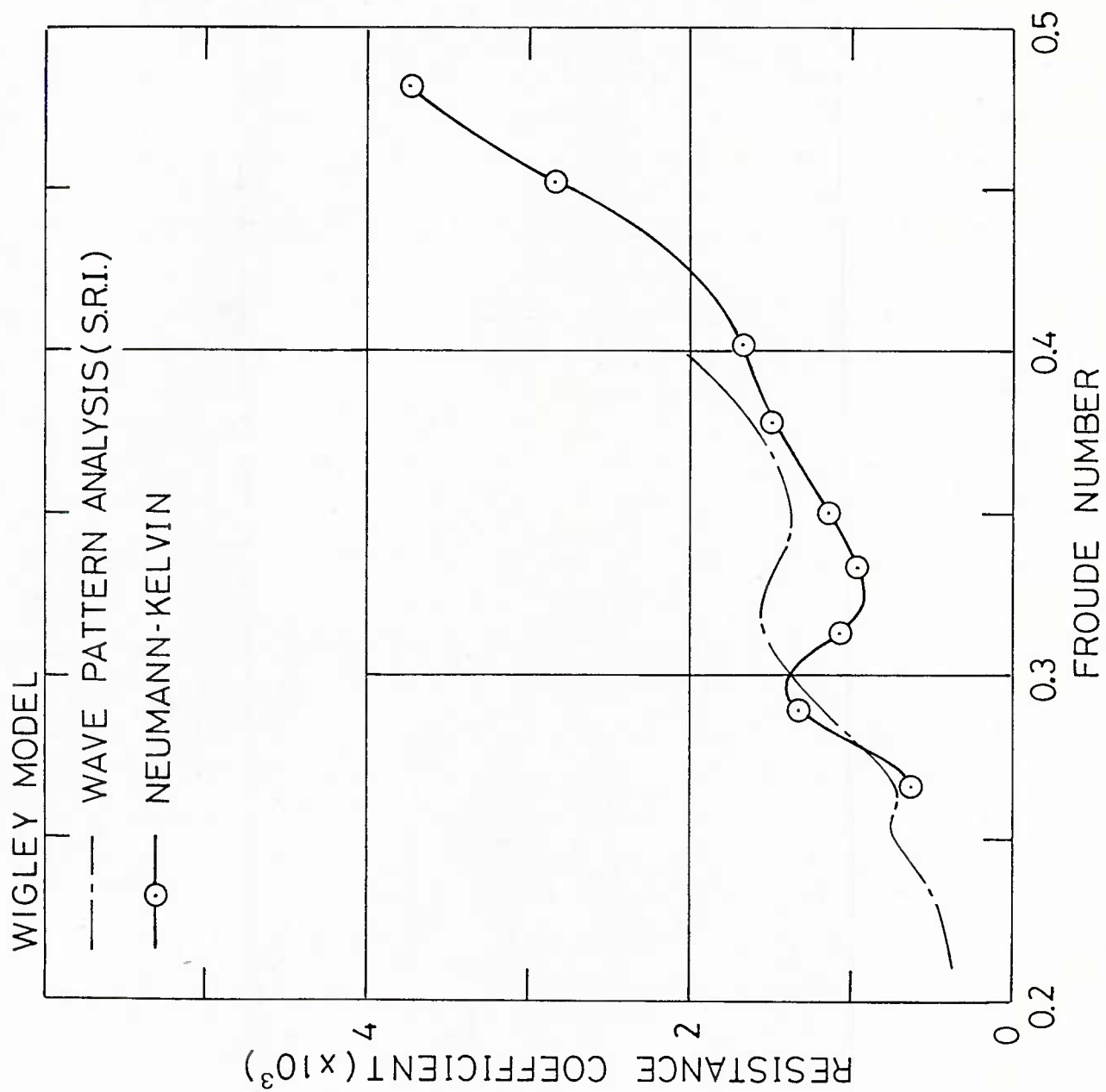


Fig. 4 Wave Resistance Coefficient for Wigley's Hull

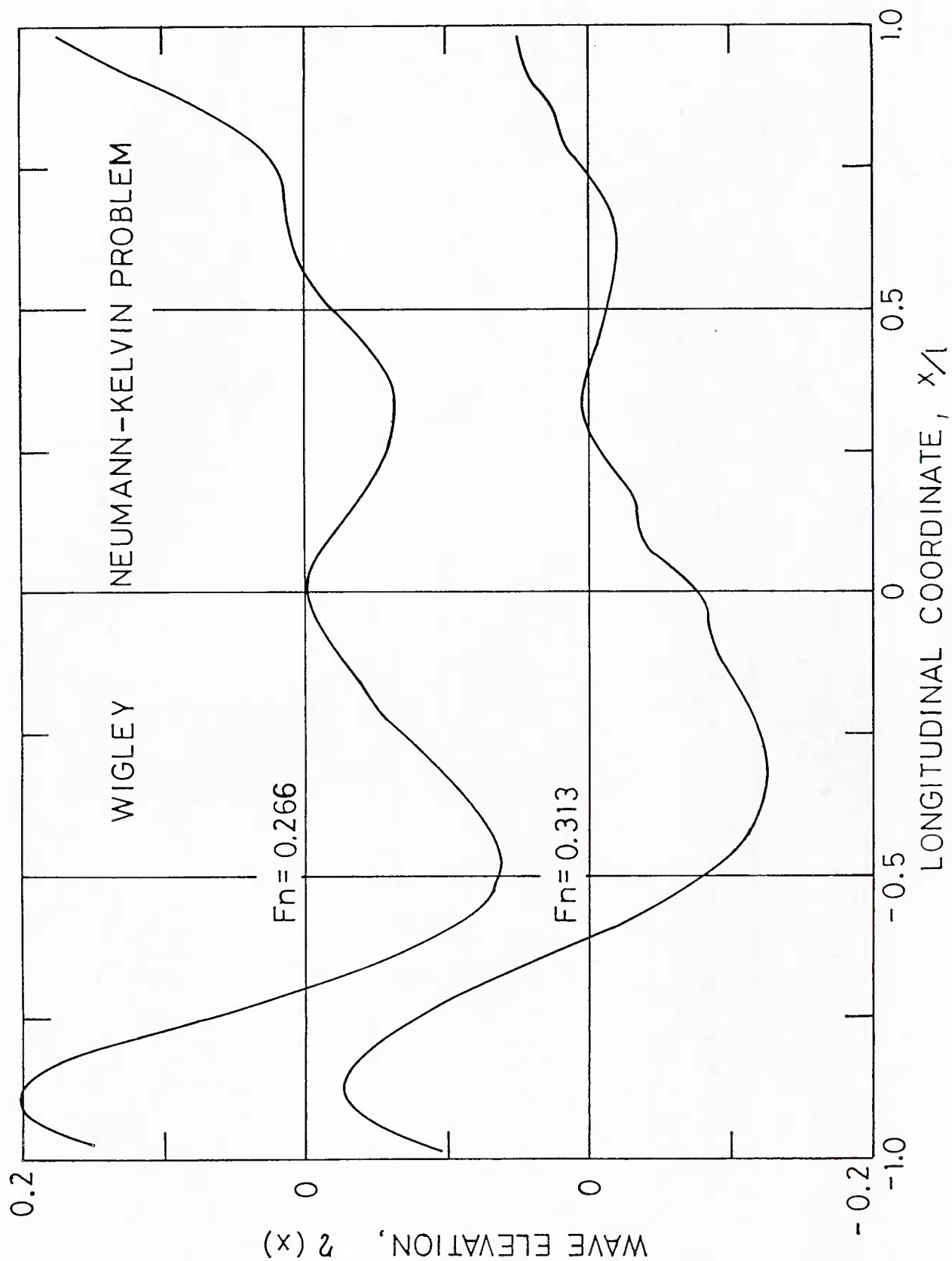


Fig. 5-a Wave Elevation along Wigley's Hull, $Fn=0.266, 0.313$

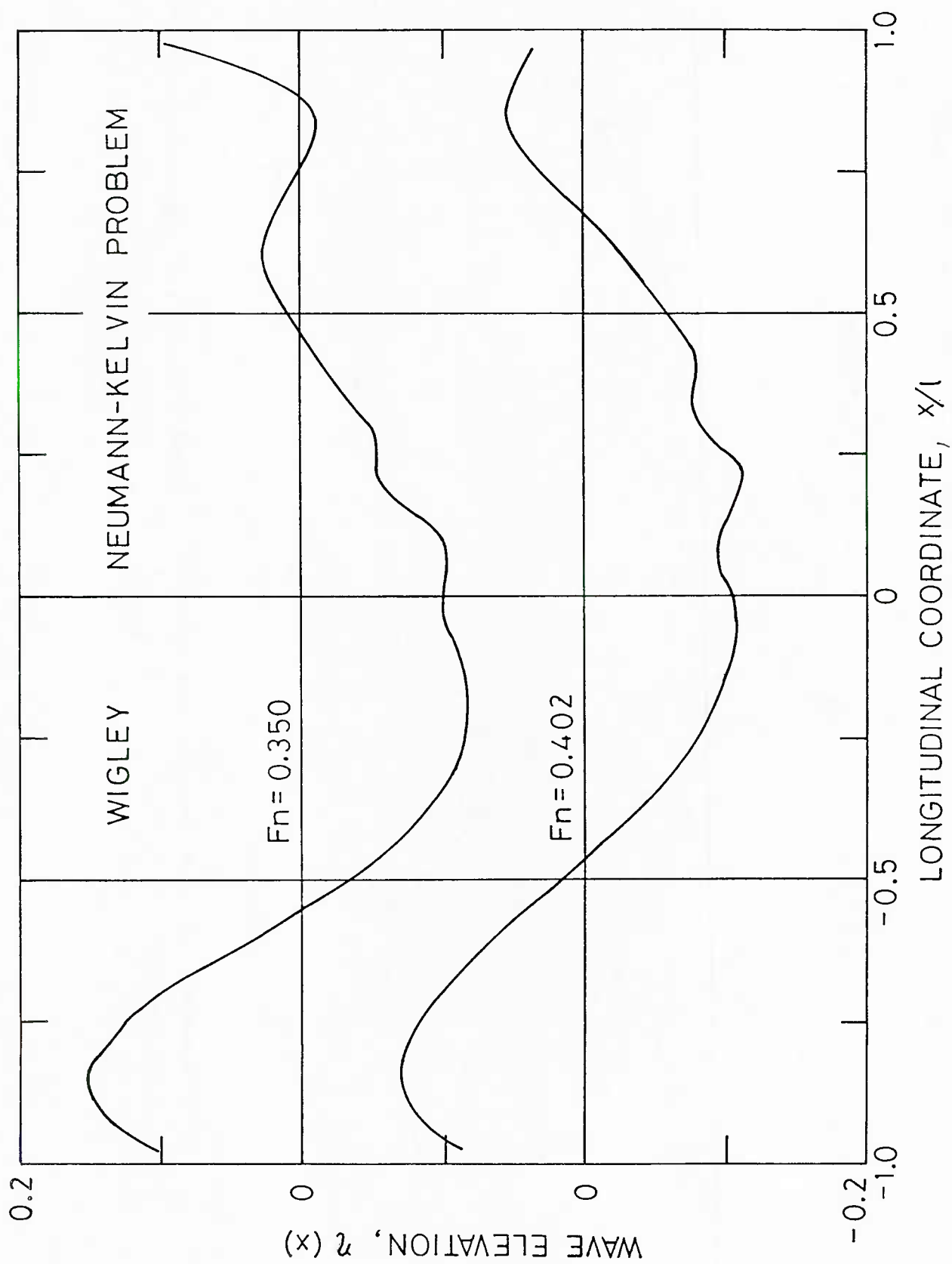


Fig. 5-b Wave Elevation along Wigley's Hull, $Fn=0.350, 0.402$

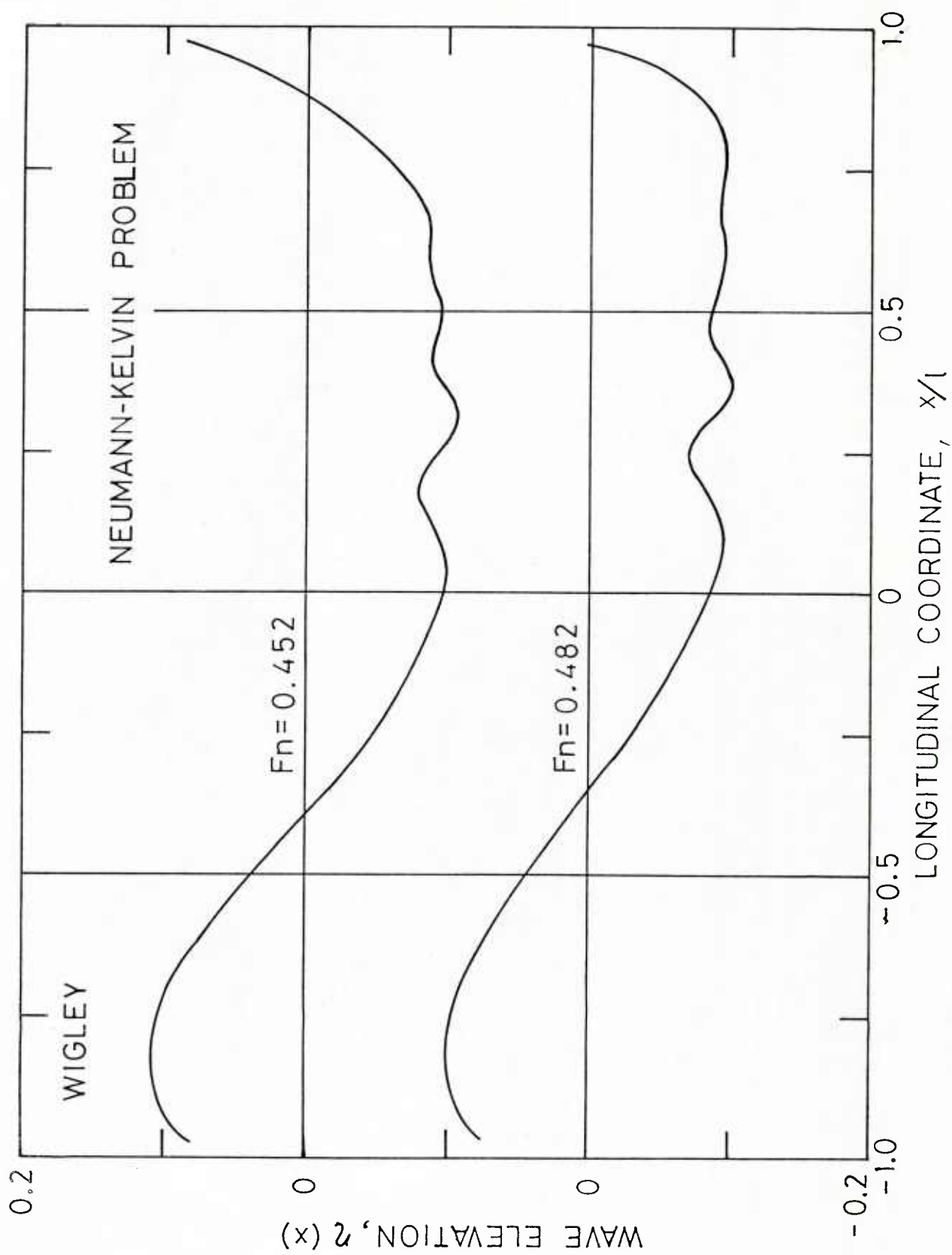


Fig. 5-c Wave Elevation along Wigley's Hull, $Fn=0.452, 0.482$

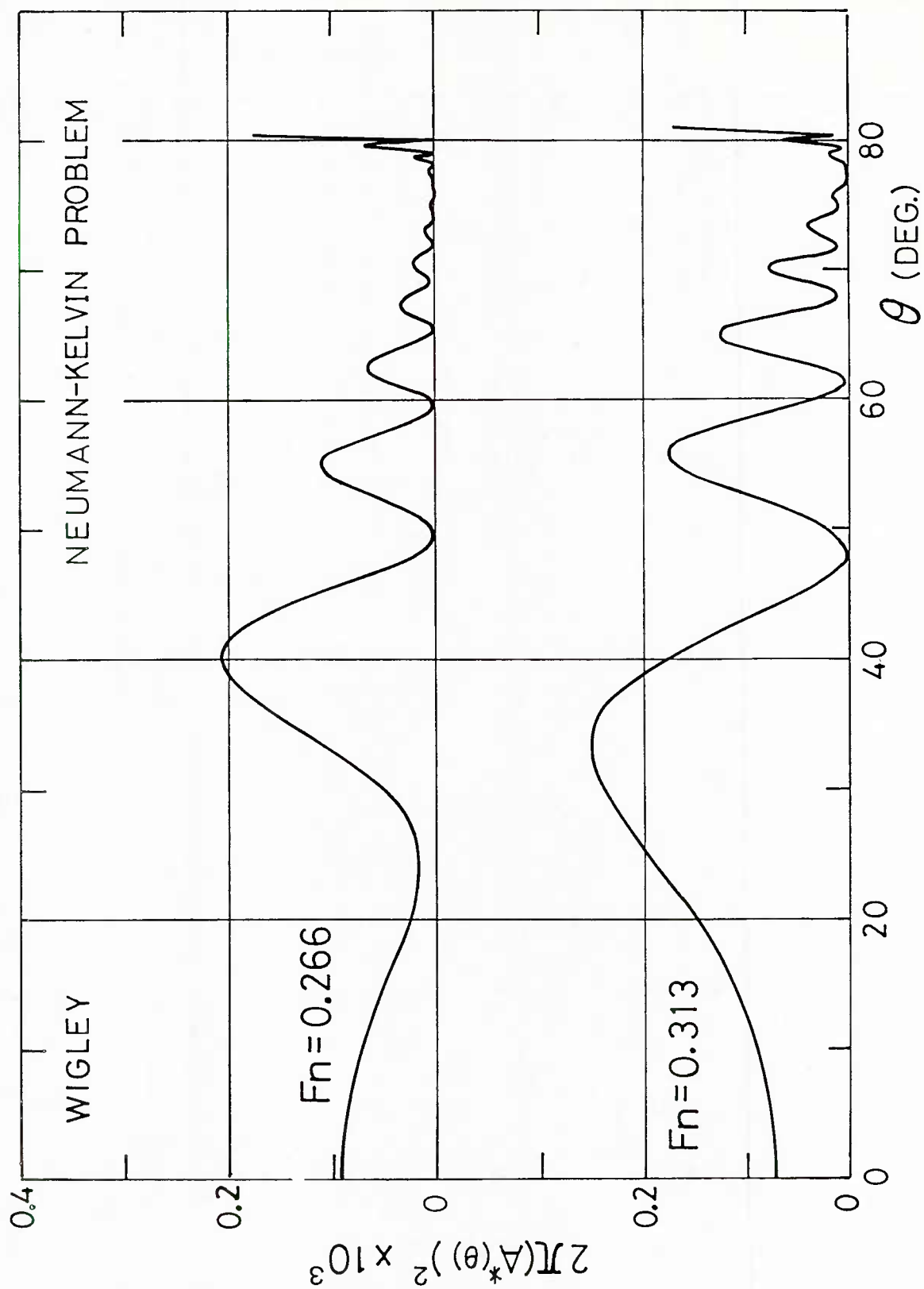


Fig. 6-a Wave Amplitude Function for Wigley's Hull, $Fn=0.266, 0.313$

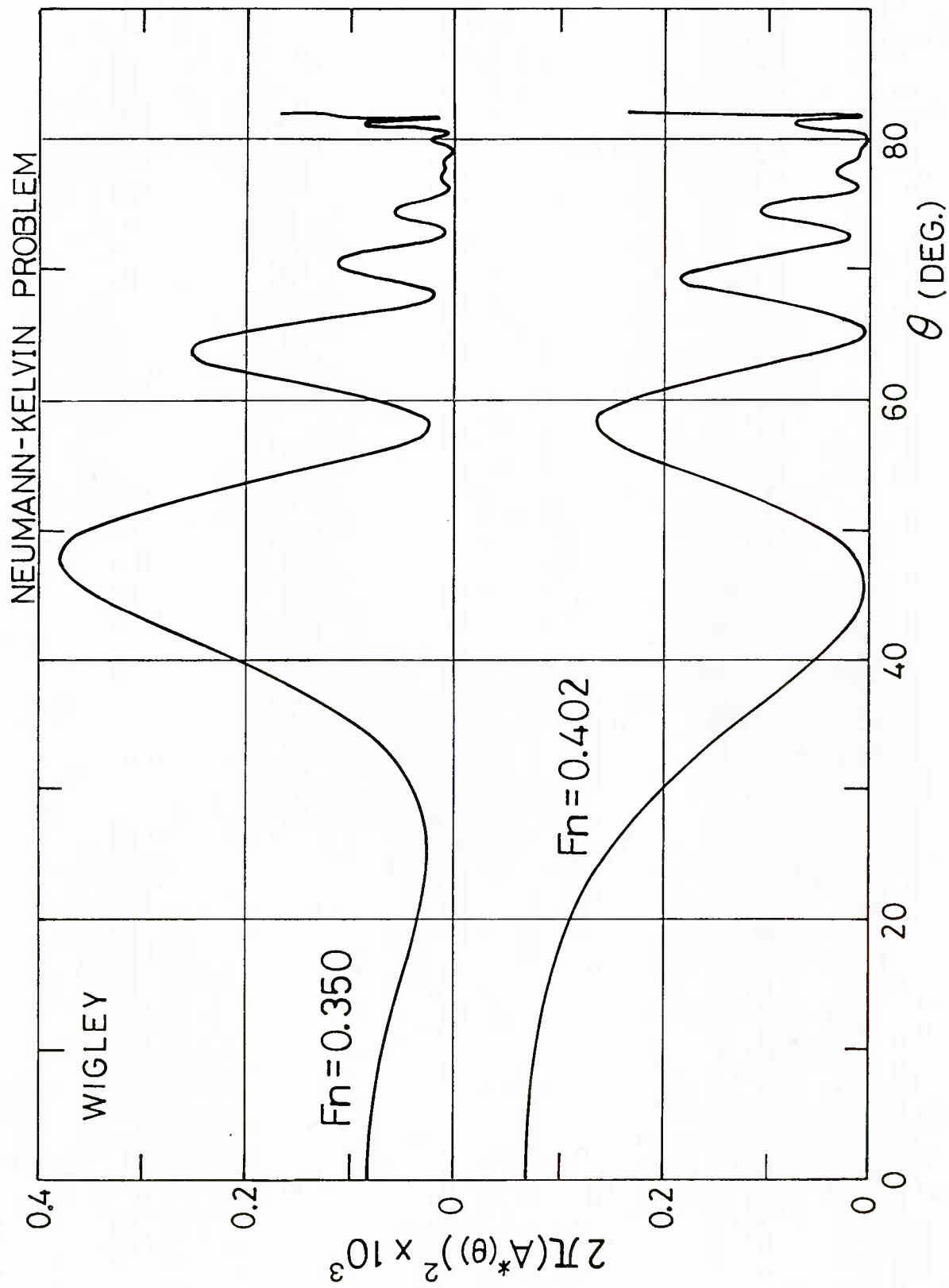


Fig. 6-b Wave Amplitude Function for Wigley's Hull, $Fn=0.350, 0.402$

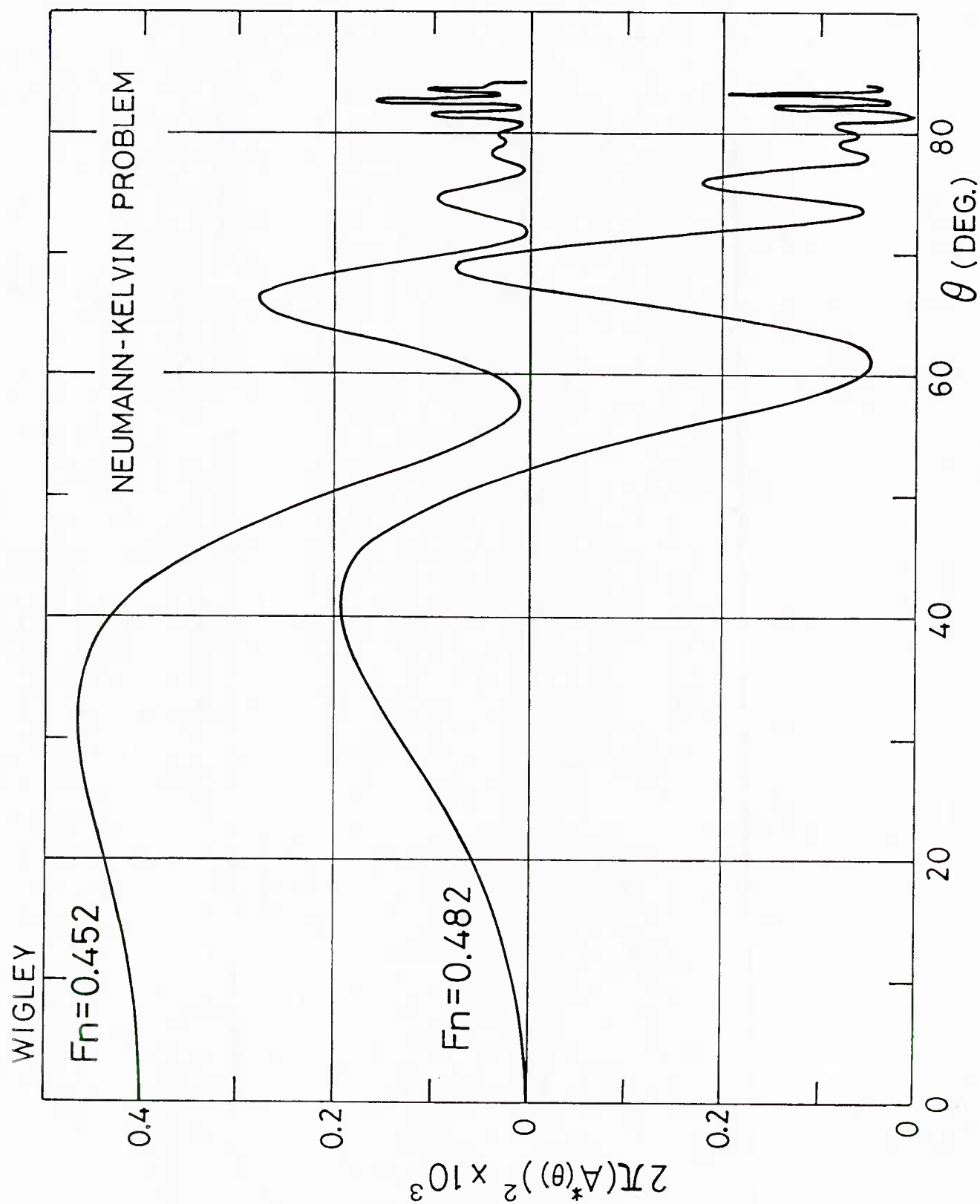


Fig. 6-c Wave Amplitude Function for Wigley's Hull, $Fn=0.452, 0.482$

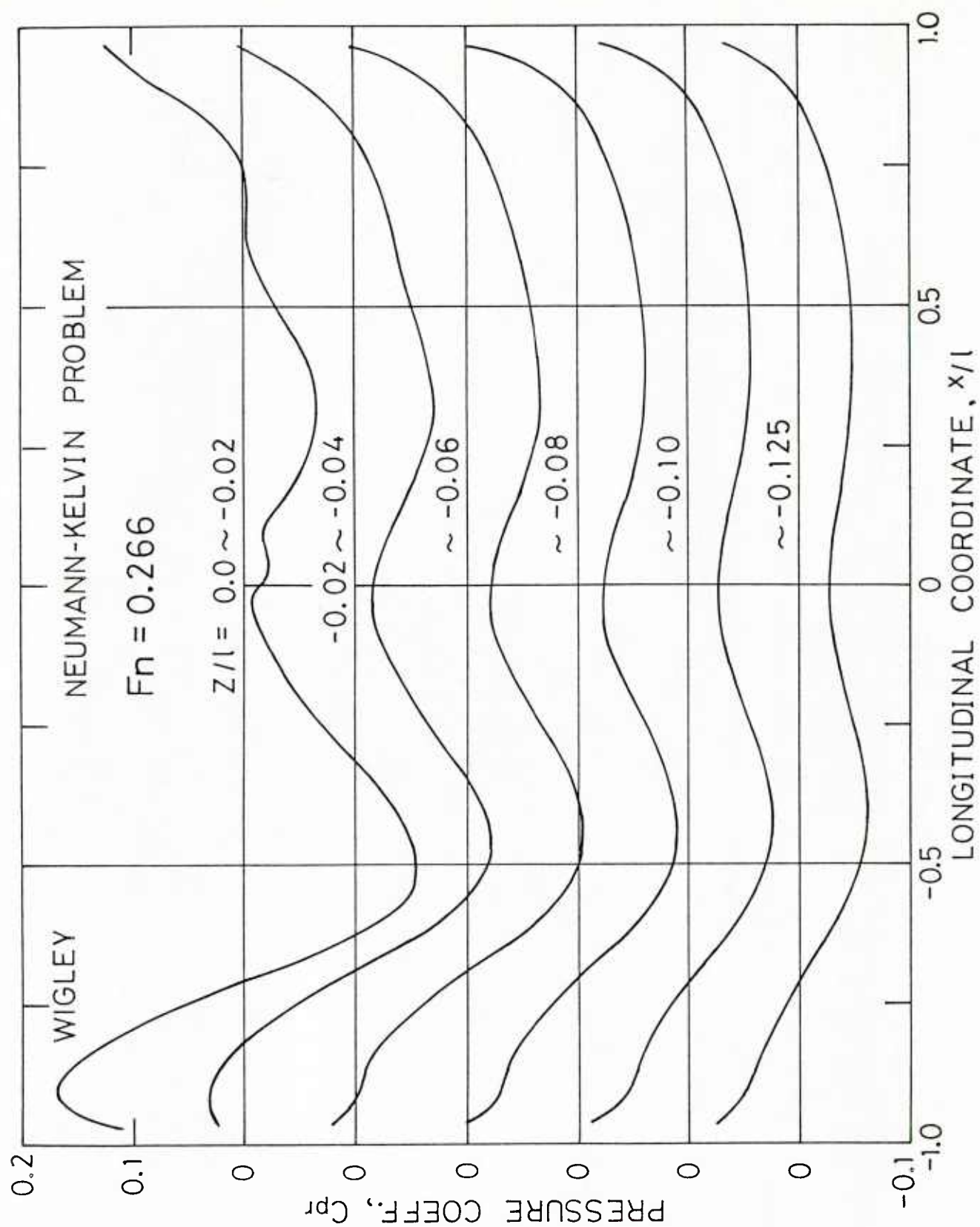


Fig. 7-a Pressure Distribution on Wigley's Hull, $F_n=0.266$

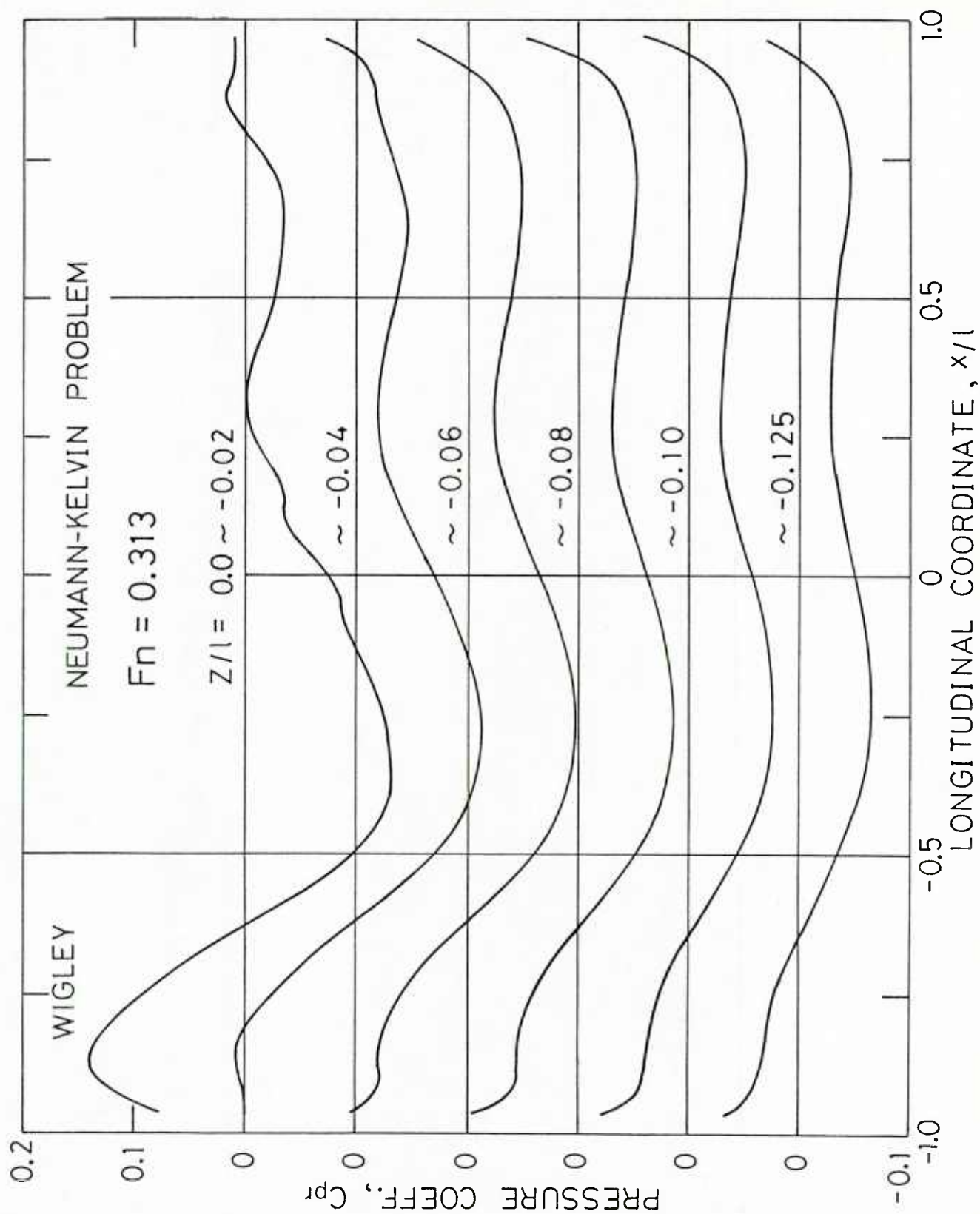


Fig. 7-b Pressure Distribution on Wigley's Hull, $Fn=0.313$

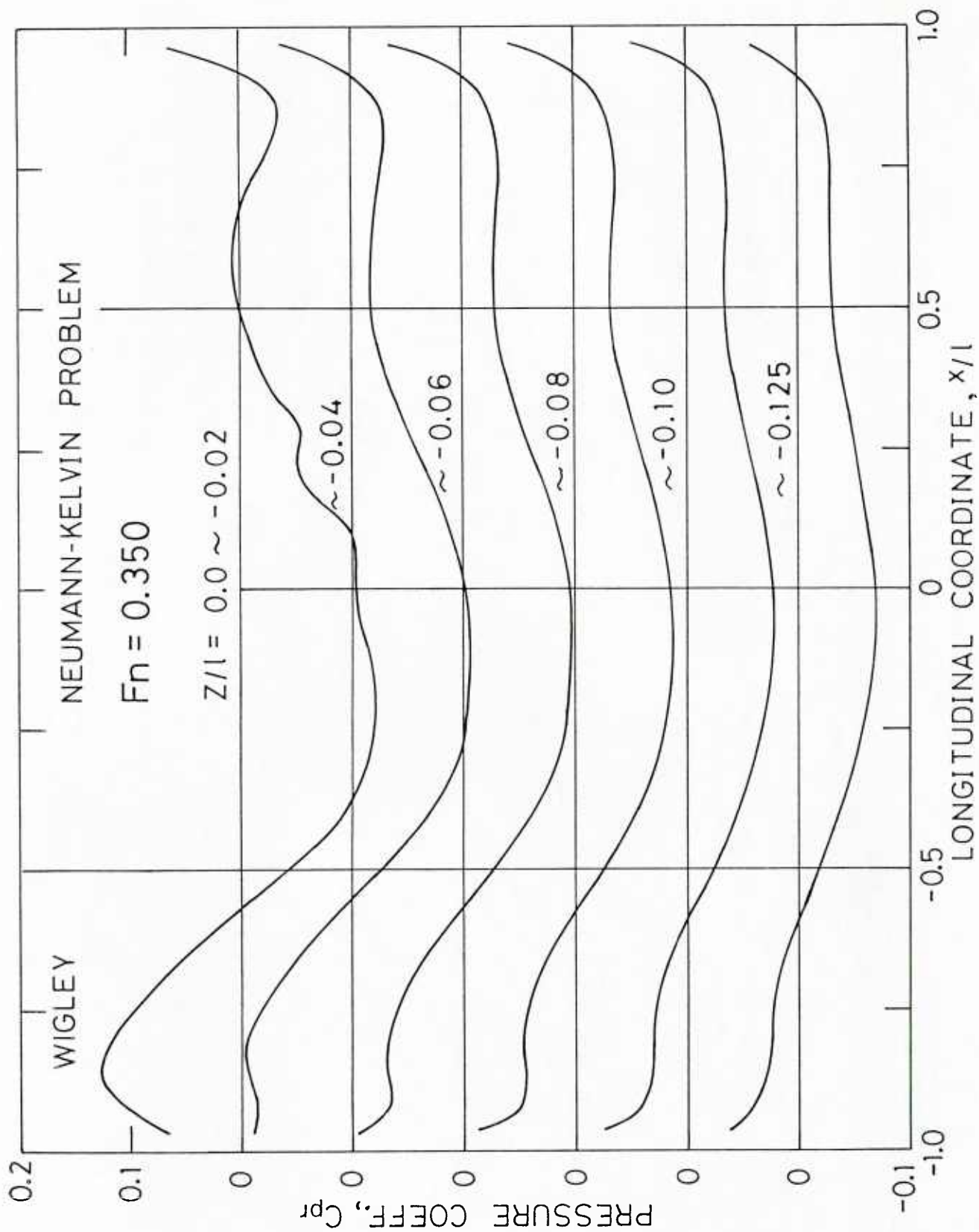


Fig. 7-c Pressure Distribution on Wigley's Hull, $F_n=0.350$

TABLE 3 WAVE RESISTANCE COEFFICIENT

H. Adachi & H. Takeshi / Neumann - Kelvin

SERIES 60	
Fn	C _w * x 10 ³
0.220	0.648
0.250	0.478
0.280	2.253
0.300	-
0.320	2.141
0.350	2.736

$$* C_w = 2\pi \int_0^{70^\circ} [A^*(\theta)]^2 d\theta$$

TABLE 4 WAVE ELEVATIONS^{**} ALONG THE HULL OF SERIES 60

H. Adachi & H. Takeshi / Neumann - Kelvin Problem

$\begin{array}{c} \text{Fn} \\ \text{x/l} \end{array}$	0.220	0.250	0.280	0.320	0.350
-1.0	Bow				
-0.9738	0.162	0.142	0.126	0.109	0.100
-0.9250	0.216	0.189	0.165	0.139	0.123
-0.8750	0.227	0.219	0.201	0.176	0.160
-0.8250	0.200	0.216	0.212	0.194	0.180
-0.7499	0.081	0.142	0.171	0.178	0.172
-0.6499	-0.030	0.047	0.107	0.147	0.157
-0.5500	-0.103	-0.051	0.020	0.089	0.117
-0.4502	-0.141	-0.129	-0.075	0.007	0.052
-0.3501	-0.172	-0.184	-0.162	-0.090	-0.035
-0.2500	-0.179	-0.210	-0.216	-0.177	-0.127
-0.1500	-0.140	-0.181	-0.236	-0.228	-0.197
-0.0500	-0.125	-0.100	-0.165	-0.233	-0.227
0.0500	-0.065	-0.048	-0.108	-0.168	-0.196
0.1500	-0.034	-0.014	-0.009	-0.140	-0.163
0.2500	-0.081	-0.026	-0.004	-0.060	-0.150
0.3503	-0.107	-0.108	-0.011	-0.032	-0.090
0.4517	-0.089	-0.131	-0.070	-0.025	-0.071
0.5525	-0.020	-0.074	-0.089	-0.014	-0.044
0.6530	0.099	0.018	-0.060	0.012	-0.016
0.7516	0.147	0.114	-0.017	0.024	0.022
0.8249	0.058	0.236	0.058	0.010	0.036
0.8748	0.126	0.323	0.157	0.013	0.088
0.9246	0.173	0.321	0.317	0.055	0.106
0.9730	0.360	0.311	0.495	0.213	0.187
1.0	Stern				

^{**} $\eta(x/l) = -\frac{2}{U} \frac{\partial}{\partial x} \phi$ at the null point of upper
most elements ($z/l = 0.0 \sim -0.02665$)

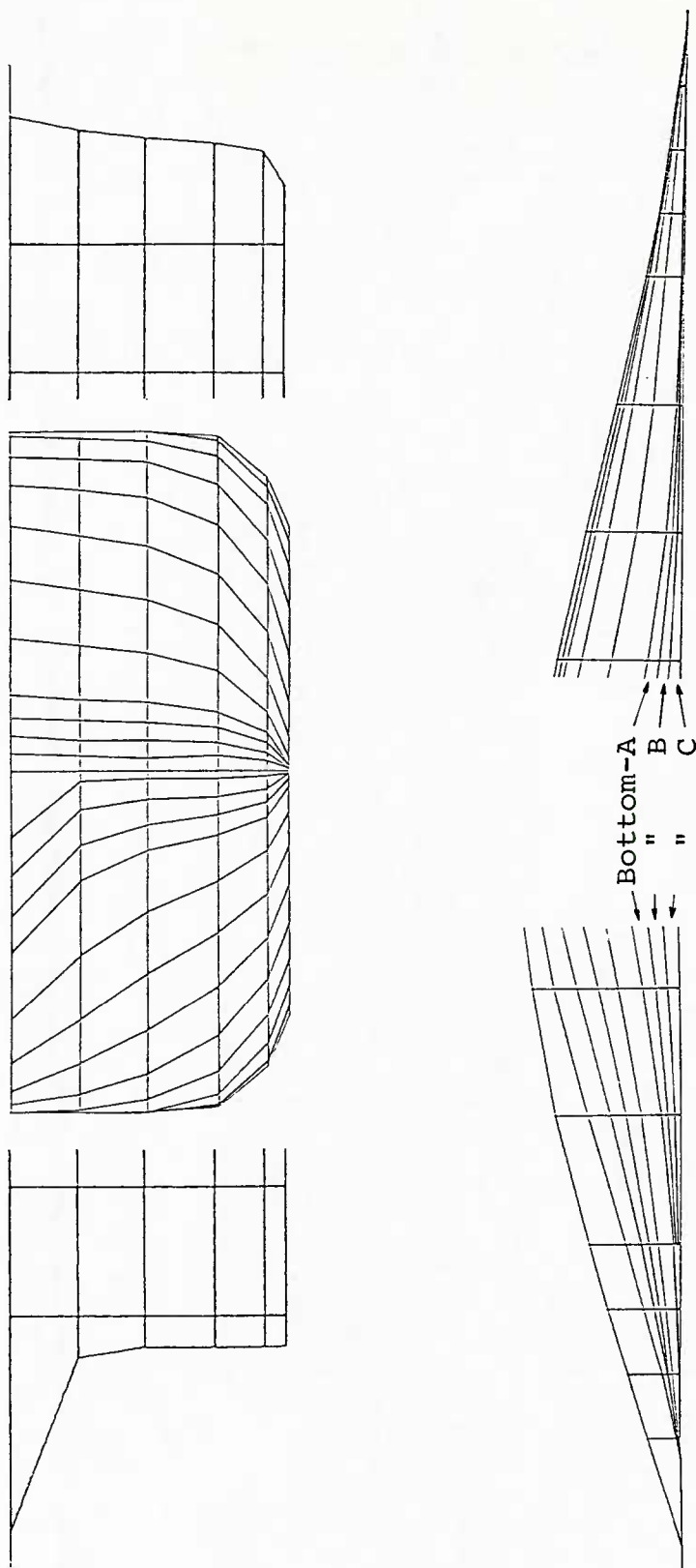


Fig. 8 Hull Surface Panel Arrangement for Series 60

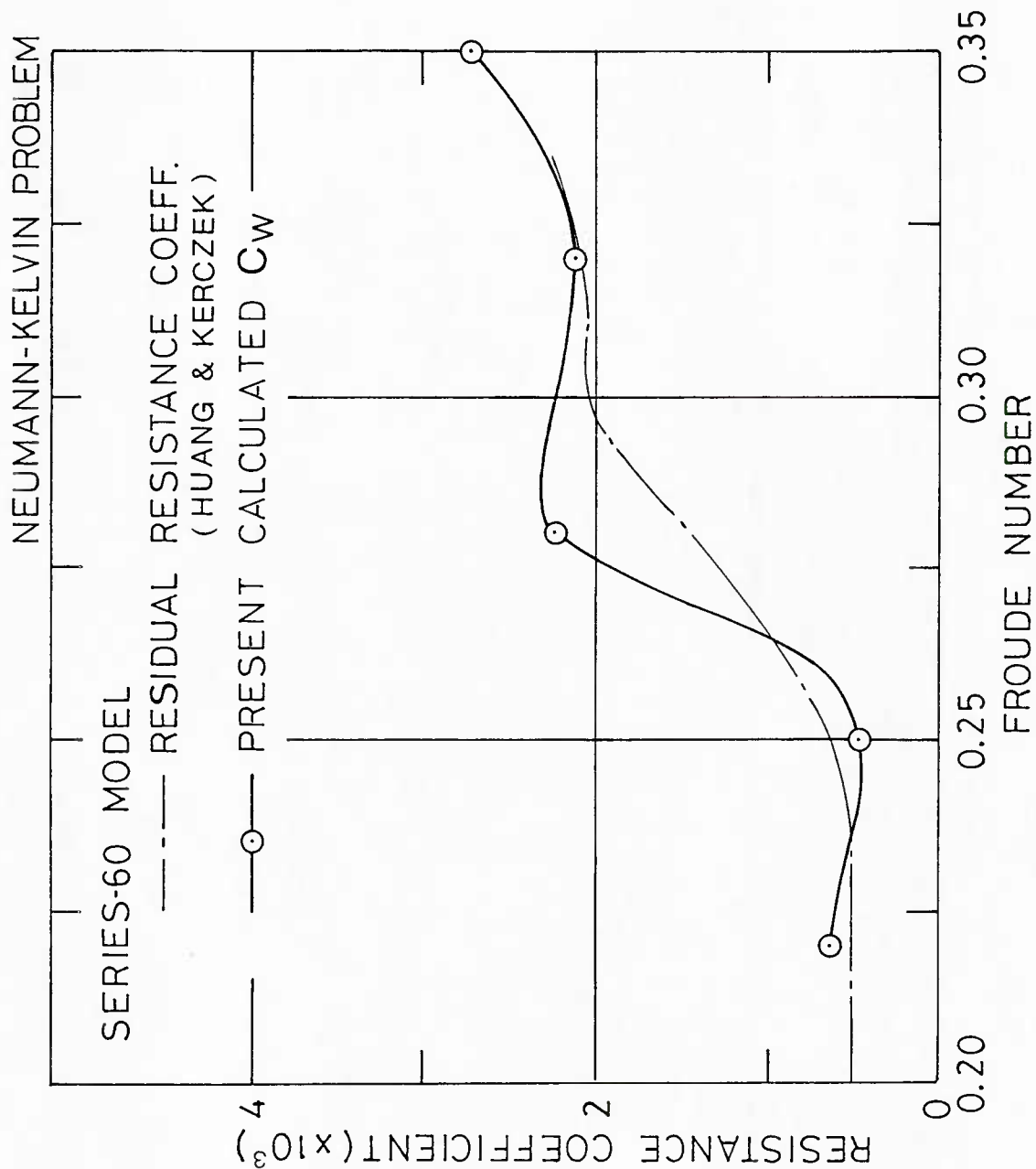


Fig. 9 Wave Resistance Coefficient for Series 60

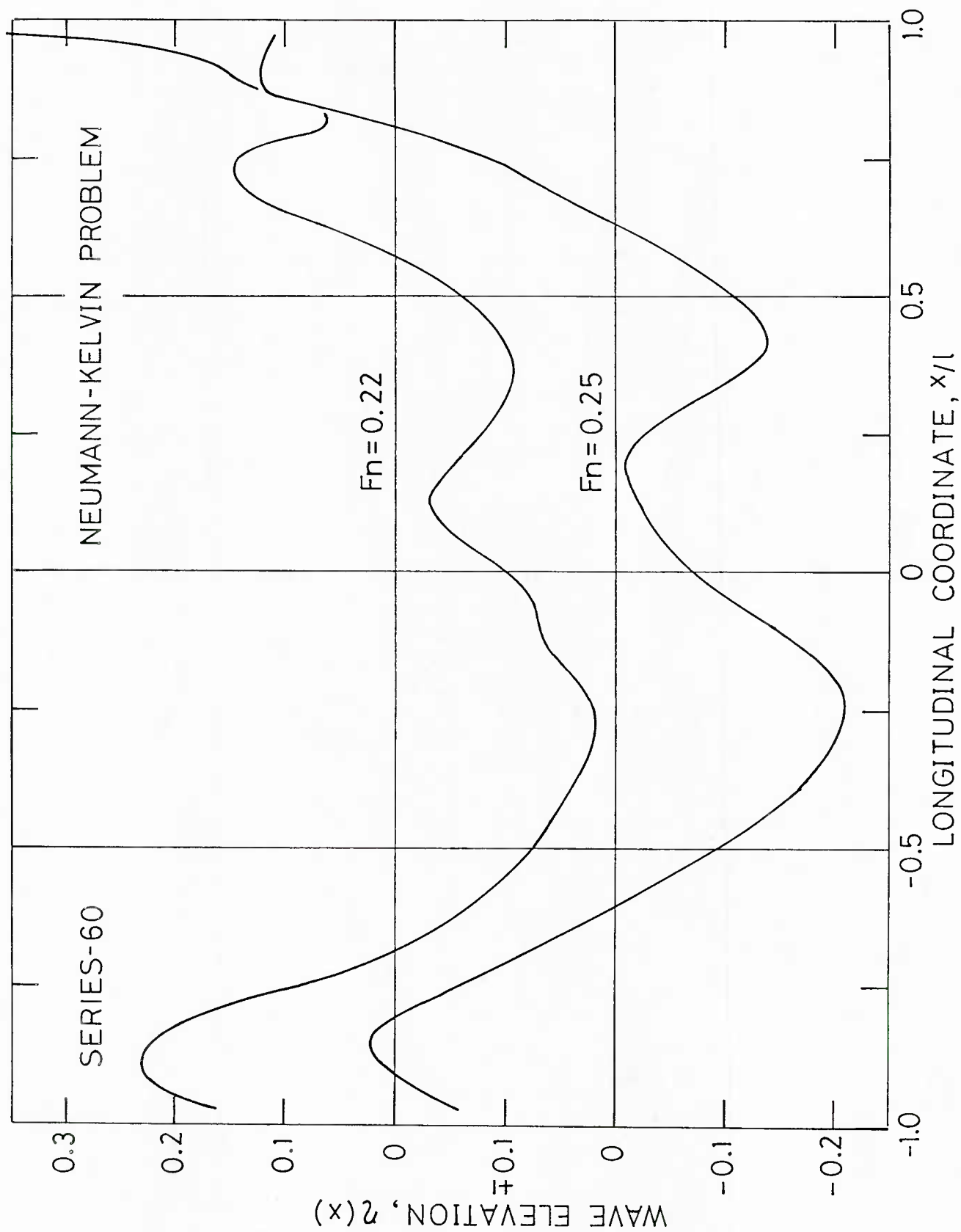


Fig. 10-a Wave Elevation along the Hull of Series 60, $Fn=0.22, 0.25$

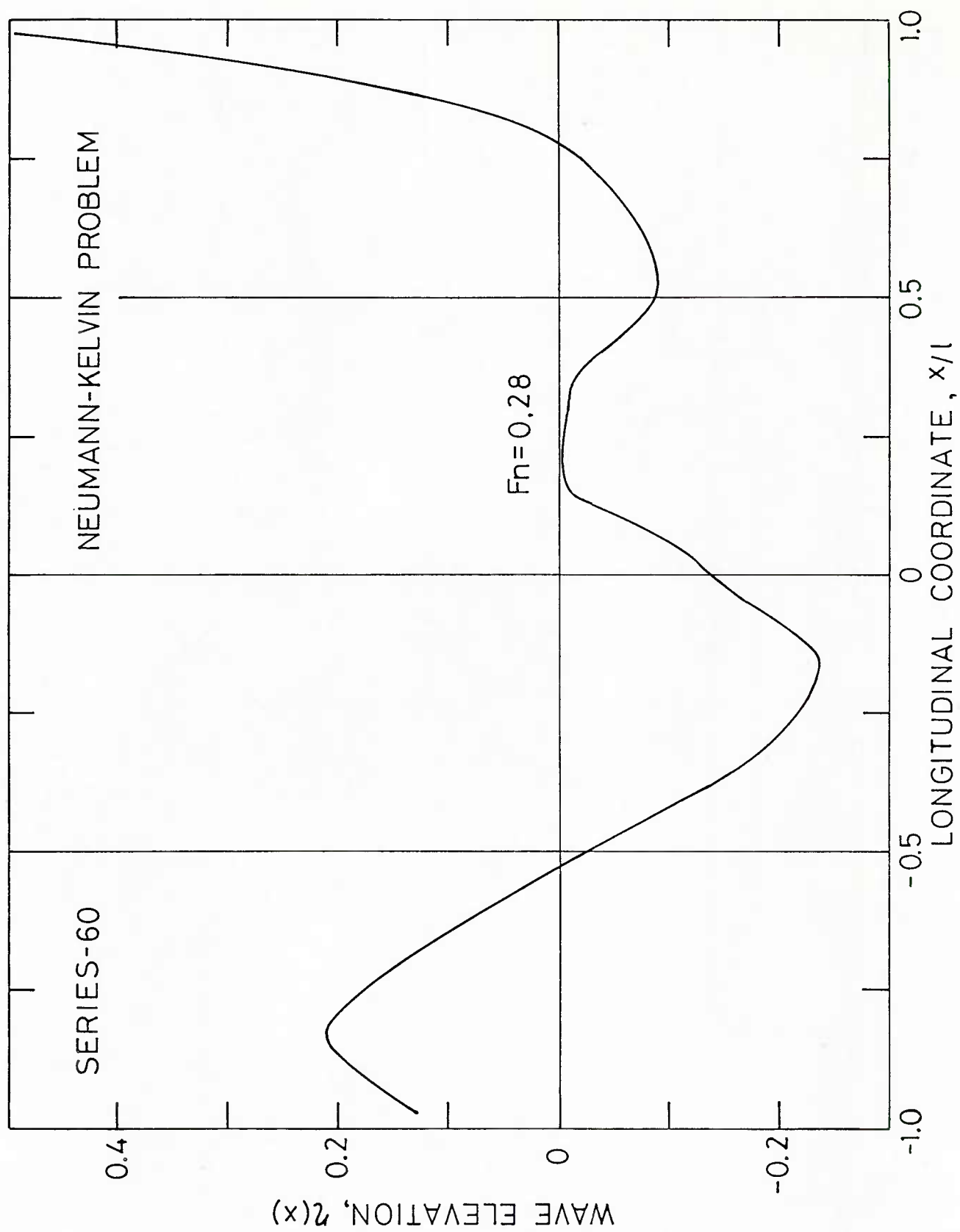


Fig. 10-b Wave Elevation along the Hull of Series 60, $Fn=0.28$

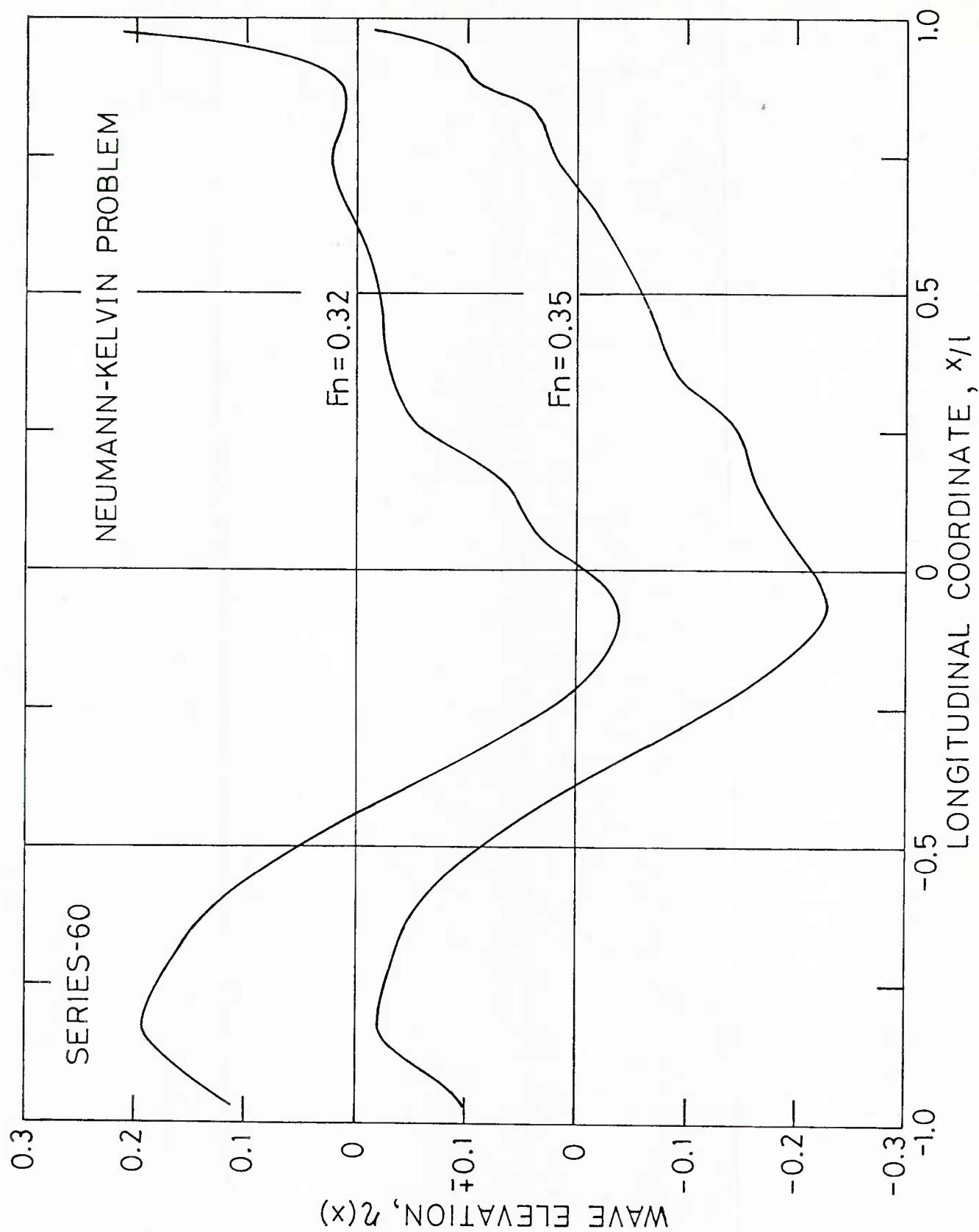


Fig. 10-c Wave Elevation along the Hull of Series 60, $F_n=0.32, 0.35$

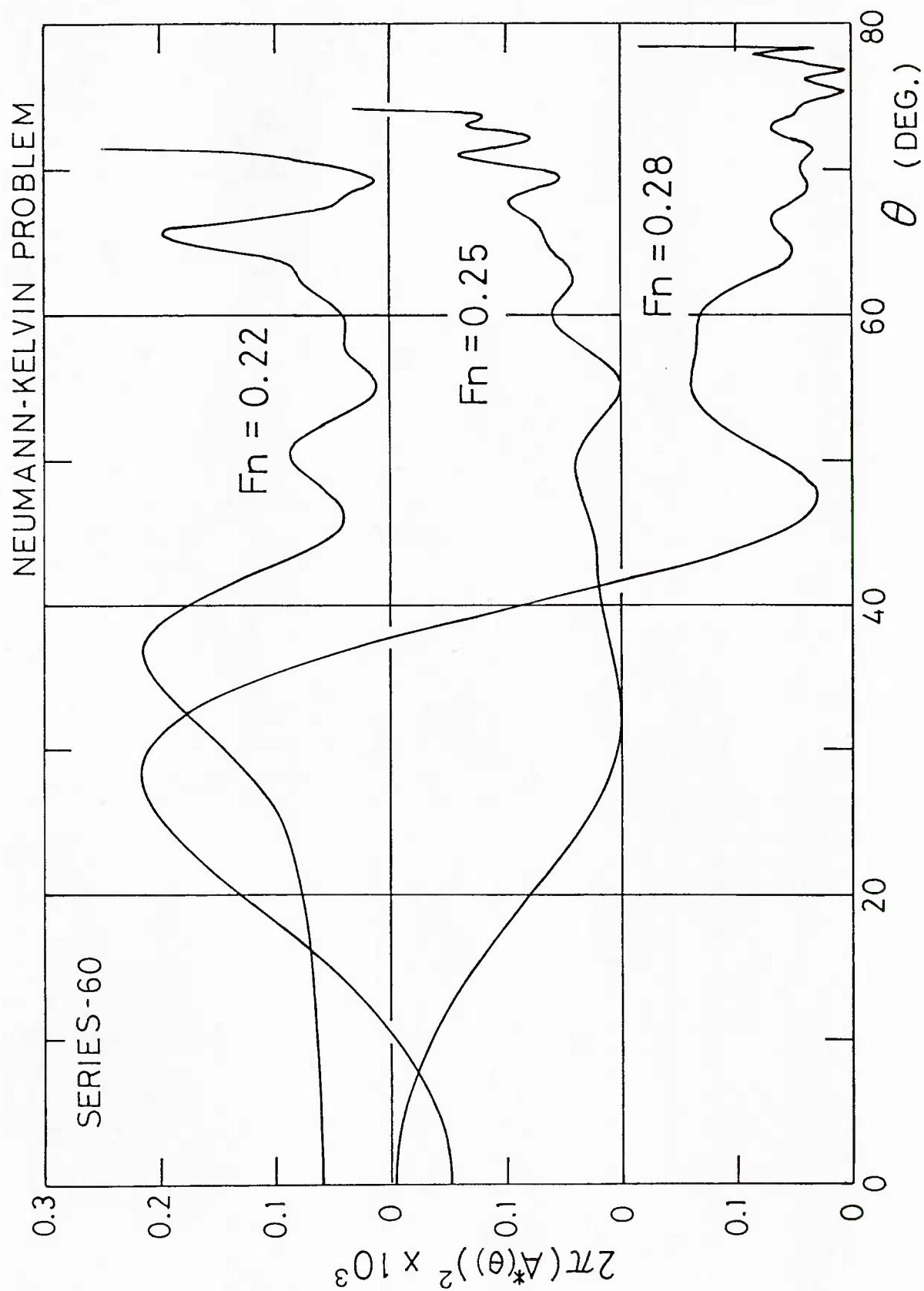


Fig. 11-a Wave Amplitude Function for Series 60, $F_n=0.22, 0.25, 0.28$

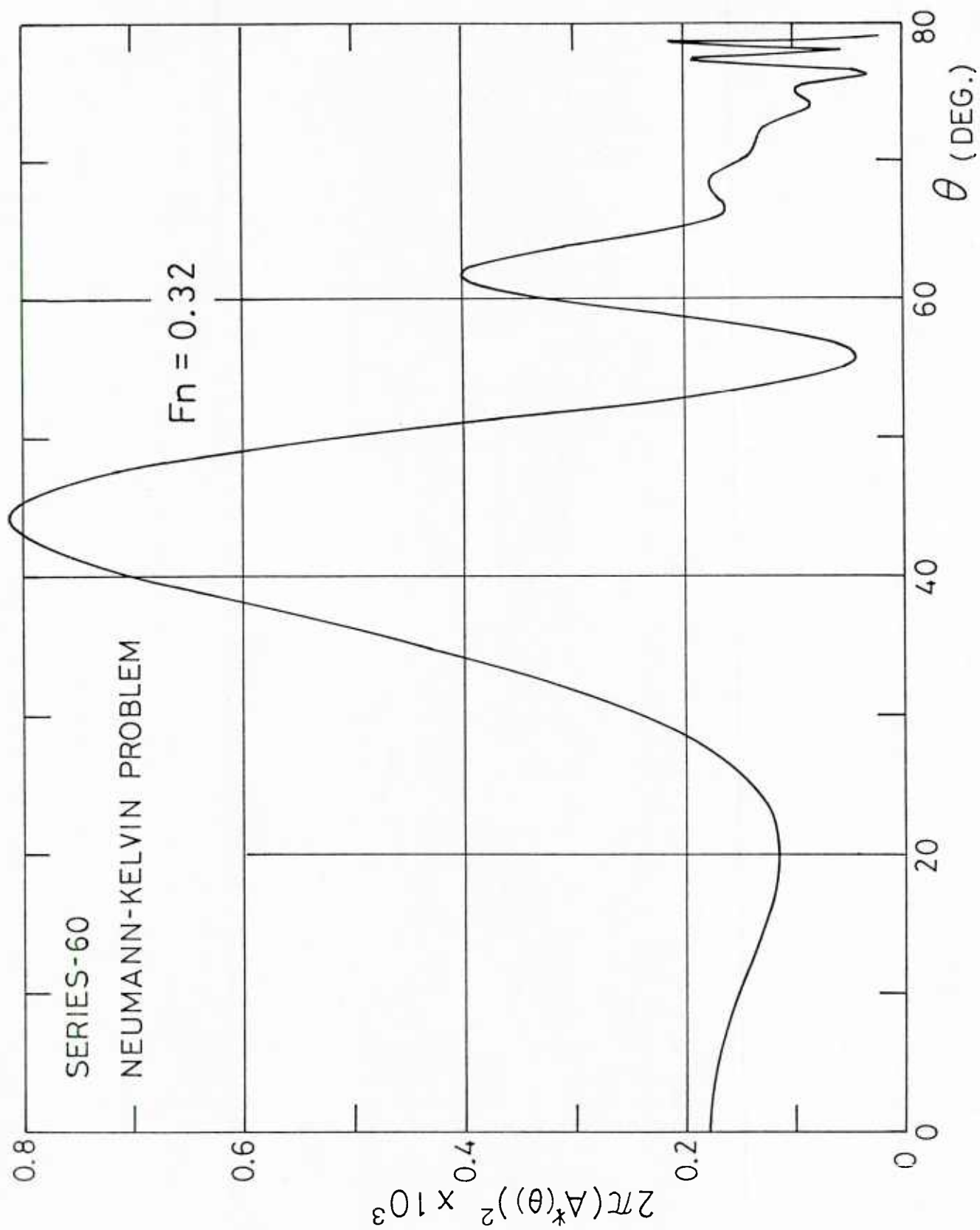


Fig. 11-b Wave Amplitude Function for Series 60, $F_n=0.32$

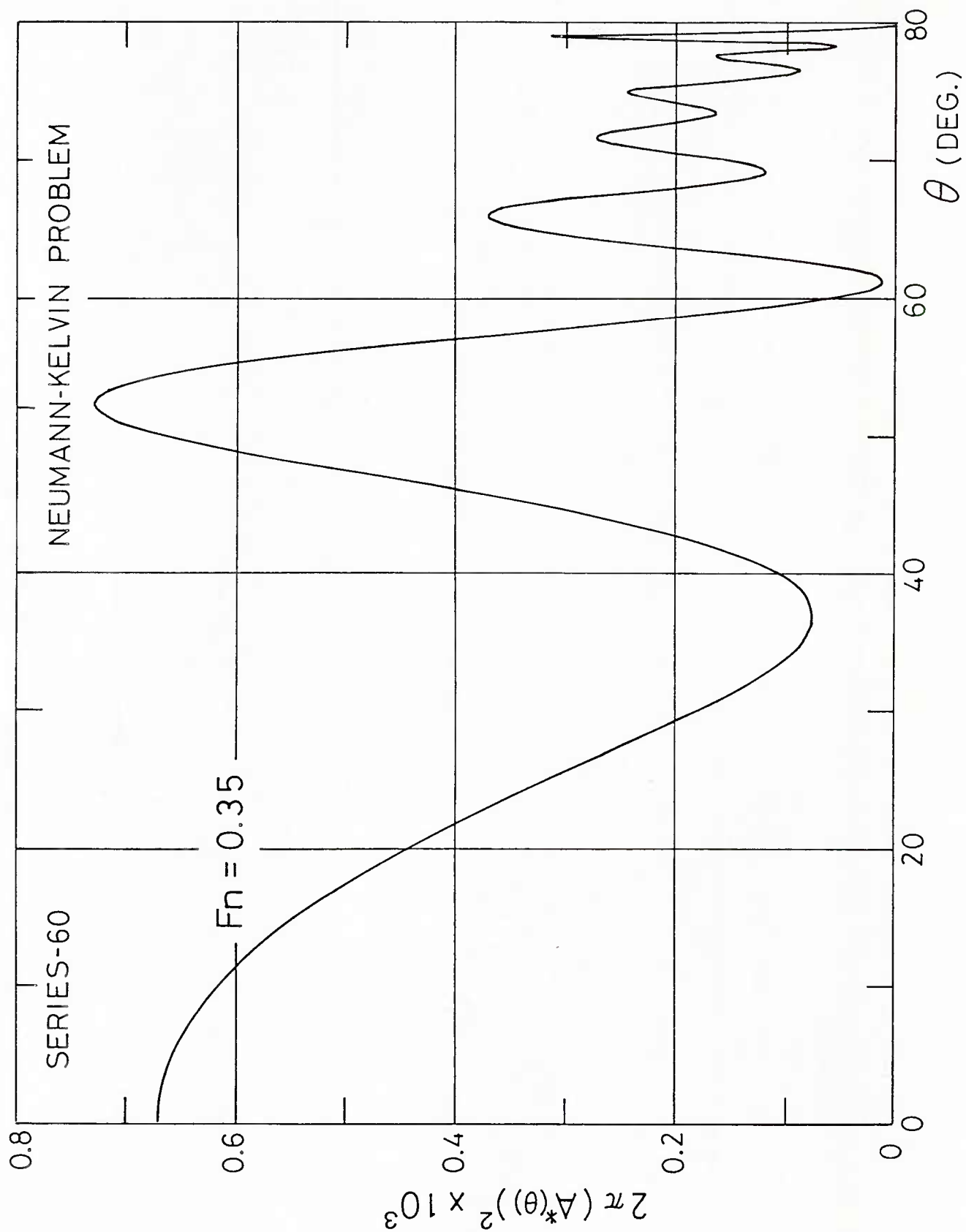


Fig. 11-c Wave Amplitude Function for Series 60, $Fn=0.35$

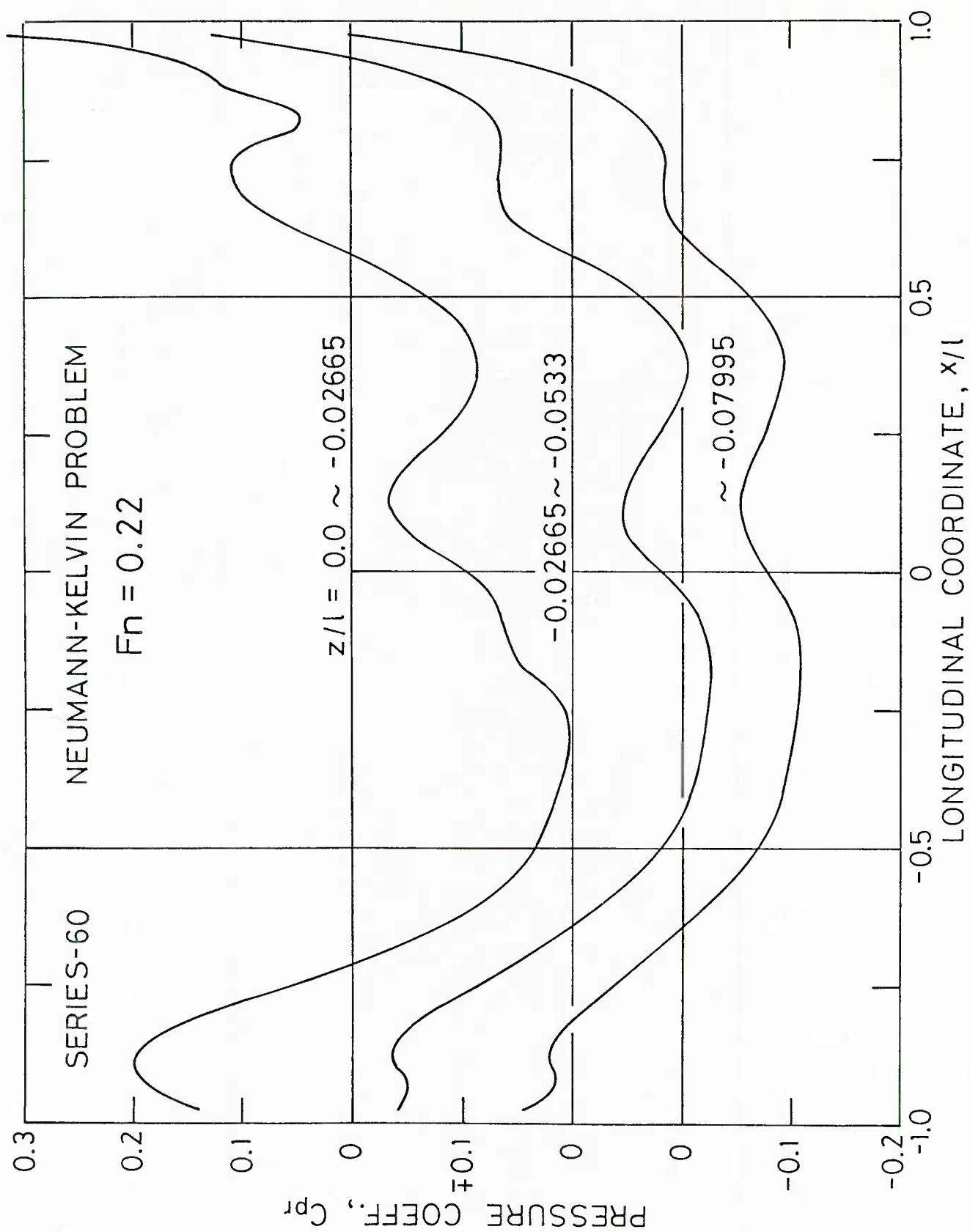


Fig. 12-a Pressure Distribution on the Hull of Series 60, $Fn=0.22$ (Upper Part)

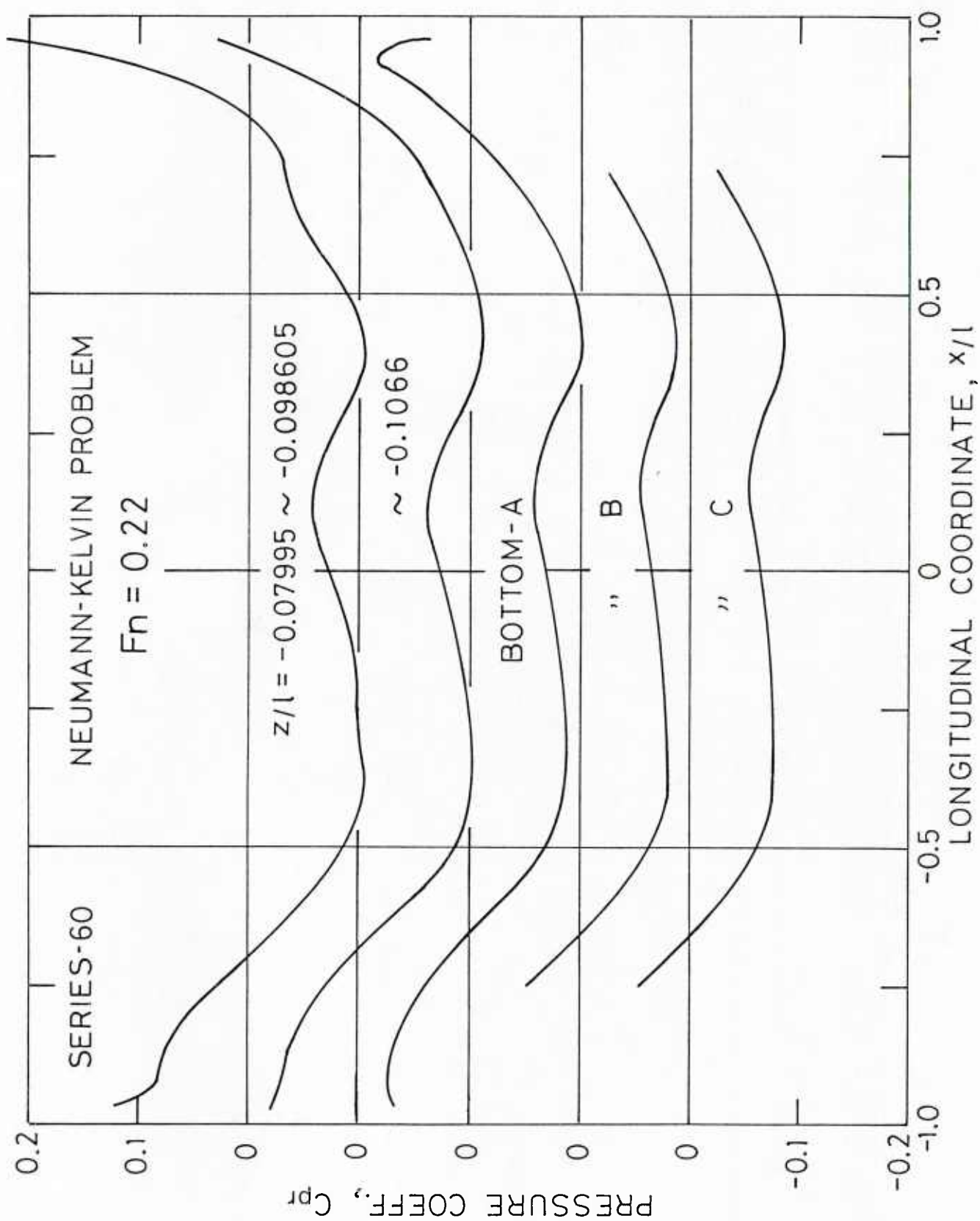


Fig. 12-a Pressure Distribution on the Hull of Series 60, $Fn=0.22$ (Lower Part)

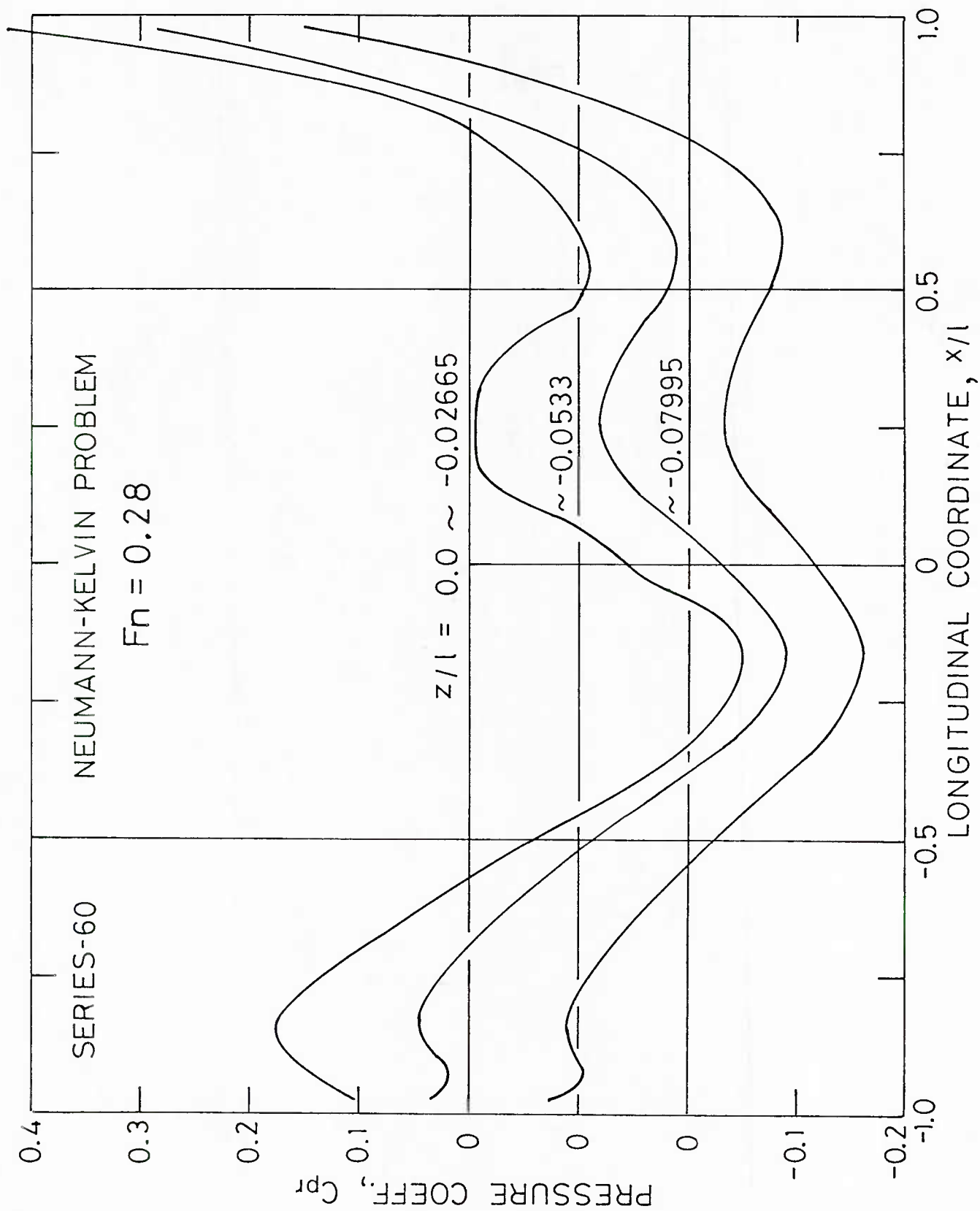


Fig. 12-b Pressure Distribution on the Hull of Series 60, $Fn=0.28$ (Upper Part)

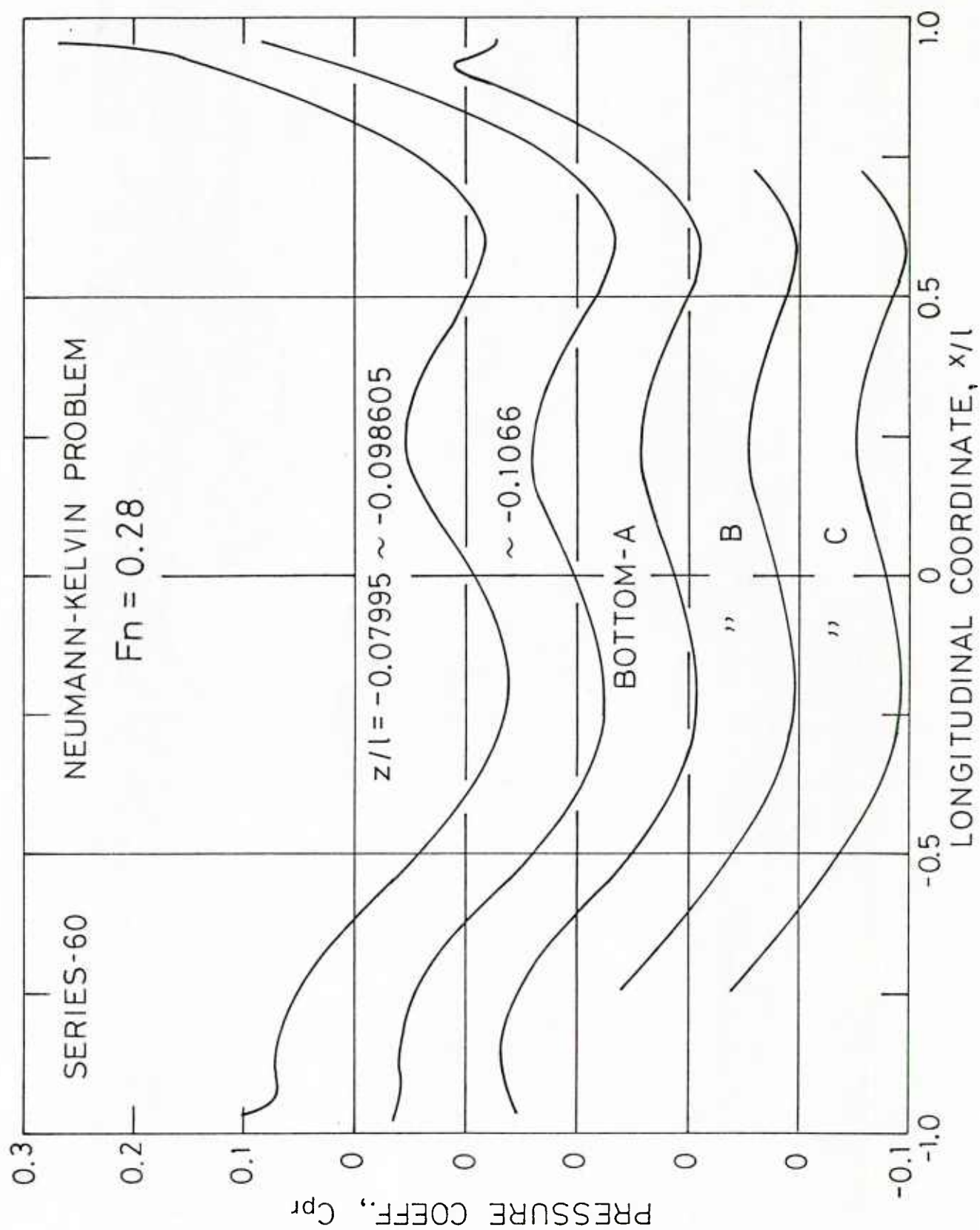


Fig. 12-b Pressure Distribution on the Hull of Series 60, $Fn=0.28$ (Lower Part)

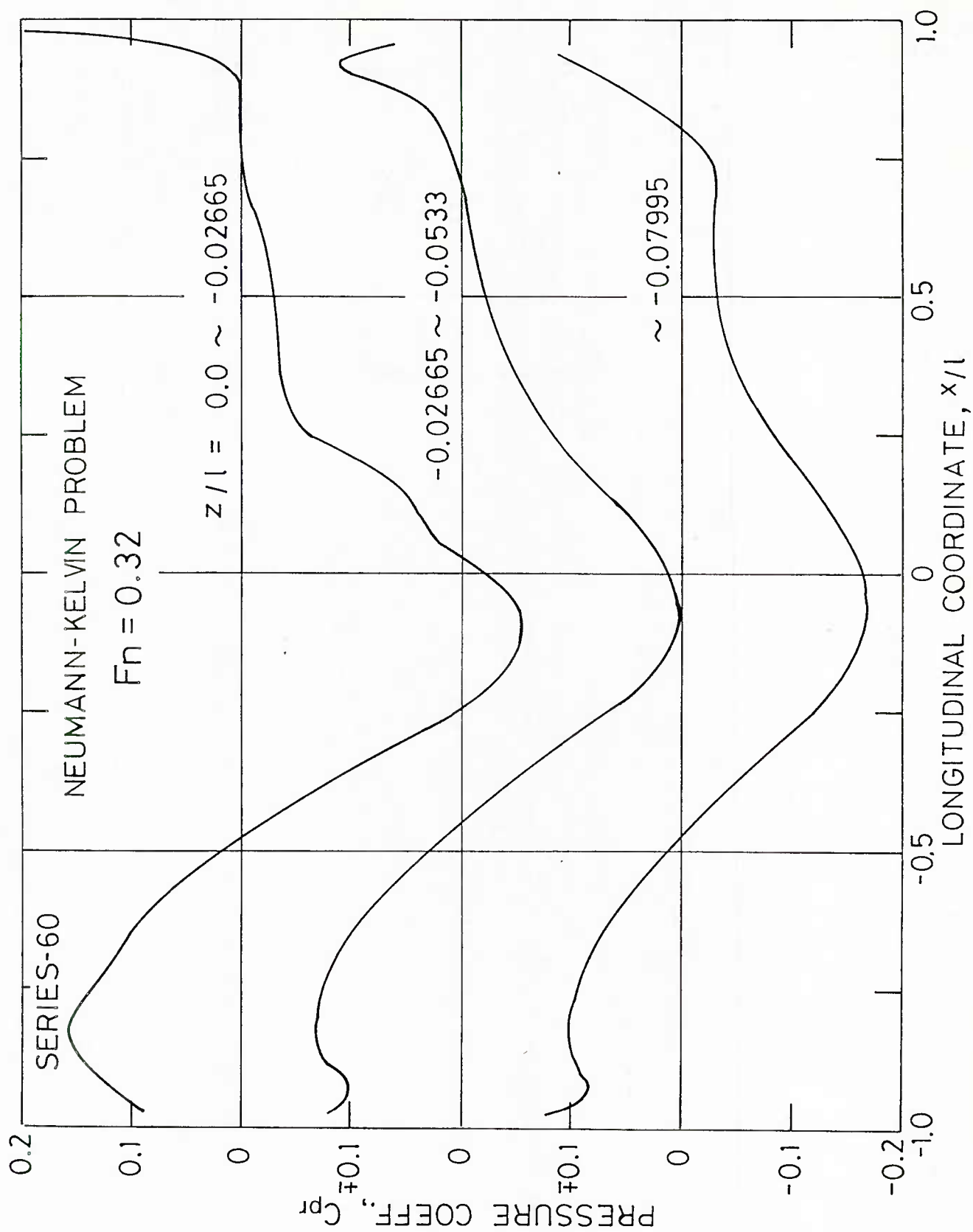


Fig. 12-c Pressure Distribution on the Hull of Series 60, $Fn=0.32$ (Upper Part)

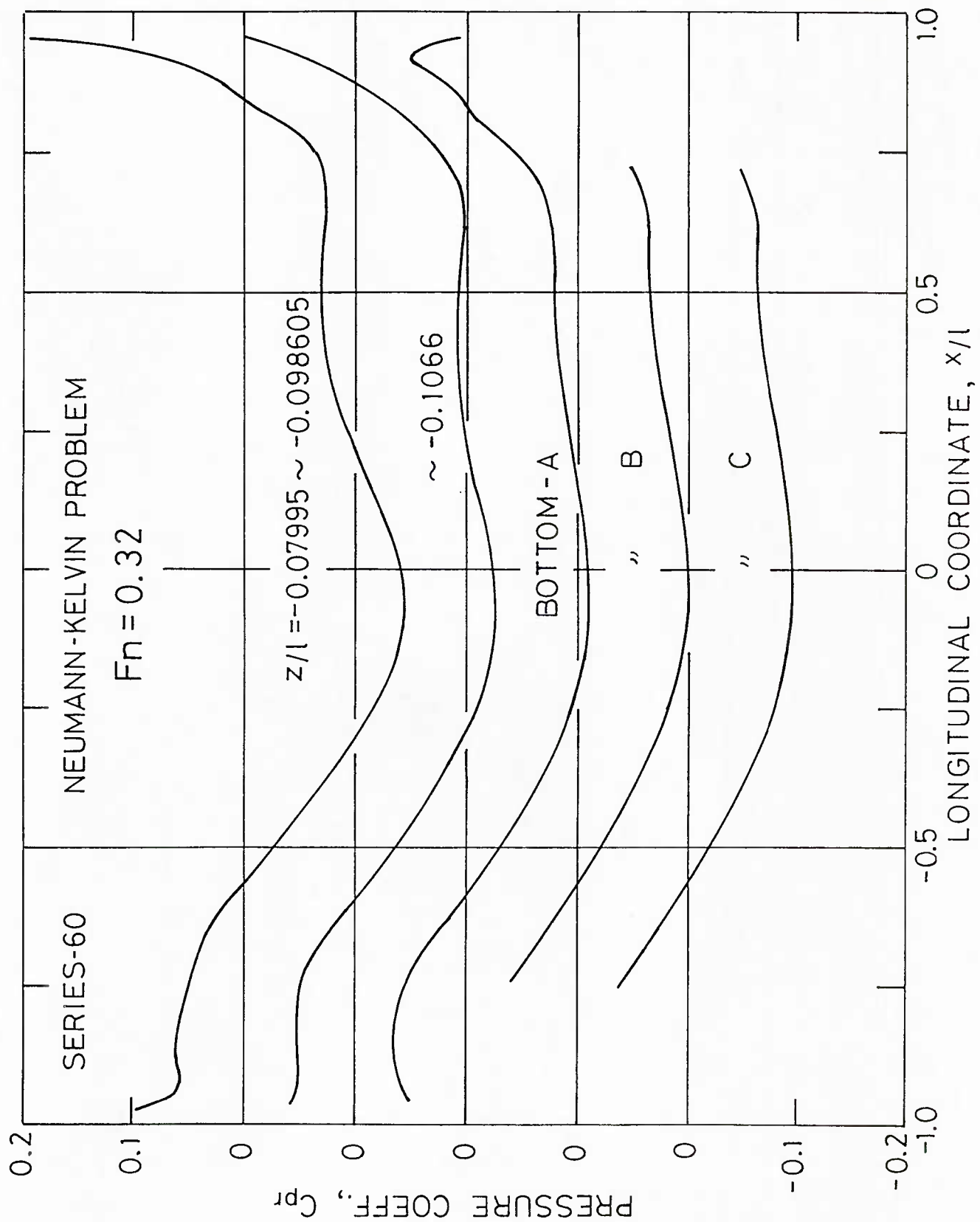


Fig. 12-c Pressure Distribution on the Hull of Series 60, $Fn=0.32$ (Lower Part)

Wave Resistance Calculation by Modified Rankine Source Method

by

Kazuhiro Mori* and Koichi Murata**

1. Introduction

The Rankine source method, where Rankine sources are distributed not only on the hull surface but also on the free surface, was first tried by Gadd(1976)[1]. At the last workshop Dawson(1979)[2] presented encouraging results. In his scheme the double-hull-linearized free surface condition is used together with the exact hull surface condition.

Later Mori(1979)[3] pointed out that the free surface condition used in Dawson's computations is exactly same as Nakatake and et al's(1979)[4] for wall sided vessels, and that, though Nakatake[4] used the double-model hull surface condition, its results agree comparably well with Dawson's.

According to these findings, Mori and Nishimoto(1981)[5] carried out calculations by the modified Rankine source method where the hull surface condition is satisfied only by the hull source and not always by the free surface source. By this modification, the computing time and storage are expected remarkably reduced.

All the computations presented here are carried out by the modified Rankine source method[5]. The wave-resistance is calculated not only by the hull pressure integration but also by an alternative method in terms of Gauss's theorem.

* Hiroshima University

** Nihon Kaiji Kyokai

2. Brief Description of Method

A right-handed Cartesian coordinate system is adopted as shown in Fig.1.

We write the velocity vector \mathbf{q} by

$$\mathbf{q} = iU + \nabla\phi \quad , \quad (1)$$

where U is the uniform velocity and i is the unit vector in the x -direction. By Green's theorem, the velocity potential ϕ is written as follows (see Appendix);

$$\begin{aligned} \phi = & -\frac{1}{4\pi} \iint_{S_H} \sigma_H \left(\frac{1}{r} + \frac{1}{r'} \right) dS - \frac{1}{4\pi} \iint_{S_F} \sigma_F \frac{1}{r} dS \\ & + \frac{1}{4\pi} \iint_{\Sigma_0} \left\{ \phi \frac{\partial}{\partial n} \left(\frac{1}{r} + \frac{1}{r'} \right) - \frac{\partial \phi}{\partial n} \left(\frac{1}{r} + \frac{1}{r'} \right) \right\} dS \quad , \end{aligned} \quad (2)$$

where S_H :hull surface, S_F :free surface, Σ_0 :computing boundary, σ_H, σ_F :source distributions on S_H and S_F , n is the normal vector, and

$$\frac{r^2}{r'^2} = (x-x')^2 + (y-y')^2 + (z-z')^2 \quad . \quad (3)$$

(x, y, z) is a fix point and (x', y', z') an integrating point. In the present modified method σ_H is determined irrelevantly to the second and the third terms of Eq.(2); i.e., the sum of the first terms of Eqs.(1) and (2) realize the double model flow field. Now we denote it by \mathbf{q}_0 and the second term of Eq.(2) by ϕ_w .

The third term of Eq.(2) can be omitted approximately with a proper choice of differenciating scheme (Mori and Nishimoto (1980) [6]). Then the double-hull-linearized free surface condition is written by

$$(\mathbf{q}_0^2 \phi_{w\ell})_{\ell} + g\phi_{wz} = -\mathbf{q}_0^2 \mathbf{q}_{0\ell} \quad , \quad (4)$$

where the suffix ℓ denotes the differentiation along streamlines of \mathbf{q}_0 , and g is the gravity acceleration. The only unknown ϕ_w is determined in order to satisfy Eq.(4).

The wave making resistance R_w and the sinkage force T are given by

$$R_w = - \iint_{S_H} p n_x dS \quad , \quad (5)$$

$$T = \iint_{S_H} P n_z dS \quad . \quad (6)$$

where n_x and n_z are the x- and z-components of the unit vector on S_H respectively, and P is the pressure.

3. Computed Results

Three proposed models are calculated: Wigley's parabolic hull, vertical cylinders with elliptical and lens like waterlines ; here the latter two are called EM-150 and LM-150 respectively.

Fig.2 shows the panel arrangements for Wigley model. The free surface is discretized by 318 panels (53x6) while the hull by 120 (24x5). Fig.3 is the wave making resistance coefficient, where ρ is the density of fluid and S is the wetted surface. Experimental results are referred from Ju(1983)[7] which is obtained by subtracting of the viscous resistance by the wake survey measurements from the total resistance. Both the trim and the sinkage are fixed. The computed results agree well with the measured. Fig.4 shows the comparisons of the wave profiles at $2y/L=0.13$. Behind A.P. the computed results of $Fn=0.289$ are slightly larger than those measured. This fact corresponds to the resistance results; the computed resistance is larger than the measured around $Fn=0.289$. This may be attributed to the viscous effects.

Fig.5 is the wave resistance curves of EM-150 and LM-150 (solid lines). The panel arrangements on the free surface are almost the same as those for Wigley model. More precise panels are required for round-nosed models in order to follow rather sharp changes of velocity around fore stagnation points. It is found, however, that if the same precise panels are used around stern stagnation points, solutions become dissatisfactory and sometimes diverge. This interesting fact may be because that such a sharp velocity change as the ideal flow is not realistic around the stern. A coarse panel arrangement contributed to disguise it, while separations moderate it in real flow. Therefore a coarse size of panels is supposed to play a role of a kind of artificial viscosity in numerical computations.

Fig.6 shows the wave contour of EM-150. The numbers are $2\zeta/L$.

Fig.7 is the total resistance curves of EM-200 and EM-125, which are elliptical waterplane cylinders with the beam length ratios 0.200 and 0.125 respectively. They are calculated for comparisons with the measurements. The calculated wave resistance is added to the viscous resistance based on the Schoenherr friction line (the form factors K are 0.75 and 0.29 for EM-200 and EM-125 respectively). Both curves agree well with measurements in low speed range, $Fn < 0.21$, but poorly in higher range. This may be partially due to significant disturbance of the free surface which makes the double hull linearized free surface condition invalid. The viscous effects are still more possible; the observed and calculated stern flows in Mori and Ito (1983) [8] are no more steady and the separations are quite intensive.

4. Further Discussions

4.1 Effects of sinkage

Usually ships are subjected to sinkage forces and trim moments. The effects of sinkage must be not small. Suzuki(1979)[9] pointed out its importance.

The sinkage force can be calculated by Eq.(6). Assuming a static balance between the buoyant and sinkage forces, the sinkage s is approximately given by

$$s = -T/\rho g A_w \quad , \quad (7)$$

where A_w is the waterplane area.

In Fig.8 a comparison is made for M-21, an Inuid model. The wave resistance is also calculated. The calculated results are both smaller than the measured. Under a 5%L sinkage condition, an iterative calculation is carried out at $Fn = 0.289$ and 0.35 . About 20% increments are realized but they are still insufficient for the existing discrepancies between the calculated and the measured.

Iterative calculations including both sinkage and trim may be useful for practical cases.

4.2 Alternative method for resistance calculation

The force F acting on the hull is written by

$$F = -\rho \iint_{S_H} W dS \quad , \quad (8)$$

where W is a vector given by

$$W = n \left\{ \frac{1}{2} (U^2 - q^2) - \rho g \zeta \right\} + q (n \cdot q) \quad . \quad (9)$$

The first term is the pressure and the second is identically zero on the hull due to the hull surface condition. Applying Gauss's theorem to the domain V_e , surrounded by S_H , S_F and $\Sigma (= \Sigma_0 + \Sigma_1 + \Sigma_2)$, Eq.(8) is transformed into

$$F = \rho \Sigma \iint_{S_i} \mathbf{W} dS + \rho \iint_{\Sigma} \mathbf{W} dS - \rho \iiint_{V_e} \left\{ \frac{1}{2} \nabla \mathbf{q}^2 - \mathbf{q}(\nabla \cdot \mathbf{q}) - (\mathbf{q} \cdot \nabla) \mathbf{q} \right\} dV, \quad (10)$$

where S_i is a small hemisphere surrounding the Rankine source on the free surface and Σ is the terminating plane shown in Fig.1. By virtue of the identity, the integrand of the last term can be transformed into

$$\mathbf{q} \times (\nabla \times \mathbf{q}) + \mathbf{q}(\nabla \cdot \mathbf{q}). \quad (11)$$

The first term is zero if the flow field is irrotational and the second also zero by the continuity condition. Then we have

$$F = \rho \Sigma \iint_{S_i} \mathbf{W} dS + \rho \iint_{\Sigma} \mathbf{W} dS. \quad (12)$$

In the first term of Eq.(12), we split the velocity into two terms;

$$\mathbf{q} = \mathbf{q}_i + \frac{1}{4\pi} \frac{\sigma_{Fi}}{r_0^2} \mathbf{n}, \quad (13)$$

where \mathbf{q}_i is the velocity excluding the contribution by the source σ_{Fi} at $(x_i, y_i, 0)$, the center of S_i , and $r_0^2 = (x-x_i)^2 + (y-y_i)^2 + z^2$. Substituting Eq.(13) into Eq.(9), we have

$$\mathbf{W} = -\frac{1}{2} \mathbf{n} \left(\mathbf{q}_i^2 - \frac{\sigma_{Fi}^2}{4\pi r_0^4} \right) + \mathbf{q}_i \left(q_{in} + \frac{\sigma_{Fi}}{4\pi r_0^2} \right), \quad (14)$$

where q_{in} is the normal component of \mathbf{q}_i on S_i . By making the radius r_0 infinitely small, the integration of the x-component of \mathbf{W} over S_i becomes

$$\iint W_x dS = \frac{1}{2} u_i \sigma_{Fi} , \quad (15)$$

where u_i is the x-component of q_i .

On the other hand, if V_e is taken wide enough, the second term of Eq.(12) is written by the integration only over Σ_0 . Then its x-component R_{w0} is given by

$$R_{w0} = \frac{1}{2} \iint_{\Sigma_0} (v_1^2 + w_1^2 - u_1^2) dS + \frac{1}{2} \rho g \int_{\Sigma_0}^{\infty} \zeta^2 dS , \quad (16)$$

where u_1 , v_1 , and w_1 are disturbance velocity components excluding the uniform velocity.

Finally we have

$$R_w = R_{w0} + \frac{1}{2} \rho \sum_i \sigma_{Fi} u_i . \quad (17)$$

The wave resistance obtained by Eq.(17) is shown by circles with broken lines in Figs.5 and 8. In the calculation of the second term the total source in the computing domain is assumed zero. The results — they are called here those by the free surface integration while those obtained by Eq.(5) is called those by the (hull) pressure integration — are larger by 20% - 30% than the hull pressure integration. The discrepancies stand out when the resistance increases. It can be pointed out for their reasons that the computing domain is suspected not to be enough for the total source to be zero and also for the flux through the lateral terminating planes to be neglected. In the present calculation, all the quantities on Σ_0 are assumed proportional to $g/U^2 z$ in the z-direction. This assumption may be less accurate when the wave making level gets large.

Its practical advantages, however, are immeasurable; the

computing time reduces to less than one fifth if ten speeds are calculated at once, and the resistance computation is free from treating with complicated hull geometries. The reduction of computing time is attained by making use of numerical tables which have been prepared for the calculation of free surface source.

5. Concluding Remarks

Through the present calculations following remarks can be mentioned.

- 1) The modified Rankine source method, where the hull surface condition is approximated by the double hull condition yields satisfactory results within a reasonable computing time.
- 2) Effects of sinkage on the wave making resistance is appreciable. The iterative computation depicts them.
- 3) An alternative method to calculate the resistance is proposed. Though the results are still not satisfactory, its numerical advantage is immeasurable.

The present research is partially supported by the General Hydrodynamics Research Program under the contract No0014-82-K0016 which is highly appreciated. The first author wishes to extend his gratitude to Professor L. Landweber at The University of Iowa who is the principal investigator of the contract. Authors also express their thanks to Professor S. Hatano at Hiroshima University for his discussions.

References

- 1) Gadd, G.E. : A Method of Computing the Flow and Surface Wave Pattern around Full Forms, Trans. of RINA, Vol.118 (1976).
- 2) Dawson, C.W. : Calculations with The XYZ FREE SURFACE Program for five Ship Models, Proc. of the Workshop on Ship Wave-Resistance Computations, Ed. by K. J. Bai and J. H. McCarthy (1979).
- 3) Mori, K. : Comments on Papers Presented at the Workshop on Wave-Resistance Computations, Report of JTTC Panel I, 1980-I-1 (1980).
- 4) Nakatake, K., Toshima, A. and Yamazaki, R. : Wave Resistance Calculation for Wigley, Inuid Hull S-201 and Series 60 Hulls, Proc. of the Workshop on Ship Wave-Resistance Computations, Ed. by K. J. Bai and J. H. McCarthy (1979).
- 5) Mori, K. and Nishimoto, H. : Prediction of Flow Fields around Ships by Modified Rankine Source Method, Jour. of Soc. of Naval Arch. of Japan, Vol. 150 (1981).
- 6) Mori, K. and Nishimoto, H. : On Numerical Techniques of the Rankine Source Method, Proc. of The Continued Workshop on Ship Wave-Resistance Computations, Ed. by K. Mori (1980).
- 7) Ju, S. : Study of Total and Viscous Resistance for the Wigley Parabolic Ship Form, Master Thesis of University of Iowa (1983).
- 8) Mori, K. and Ito, N. : Wake Calculations around 2-Dimensional Elliptic Cylinders by Time-Dependent Vorticity Transport Equation, Jour. of Soc. of Naval Arch. of Japan, Vol.154 (1983).
- 9) Suzuki, K. : Calculation of Ship Wave Resistance with Special Reference to Sinkage, Proc. of the Workshop on Ship Wave-Resistance Computations, Ed. by K. J. Bai and J. H. McCarthy (1979).

Appendix

We consider three subdomains of V_e , \bar{V}_e and V_i which are surrounded by surfaces of Σ_0 , $\bar{\Sigma}_0$, Σ_1 , $\bar{\Sigma}_1$, Σ_2 , $\bar{\Sigma}_2$, S_H , \bar{S}_H and S_F (see Fig.1). $P(x,y,z)$ is a fix point in V_e .

By applying Green's formula to the domain of V_e , \bar{V}_e and V_i , we have

$$4\pi\phi(P) = \iint_{\Sigma_0 + \Sigma_1 + \Sigma_2} \left(\phi \frac{\partial}{\partial n} \frac{1}{r} - \frac{1}{r} \frac{\partial \phi}{\partial n} \right) dS + \iint_{S_F} \left(\phi \frac{\partial}{\partial n} \frac{1}{r} - \frac{1}{r} \frac{\partial \phi}{\partial n} \right) dS \\ + \iint_{S_H} \left(\phi \frac{\partial}{\partial n_H} \frac{1}{r} - \frac{1}{r} \frac{\partial \phi}{\partial n_H} \right) dS, \quad (A-1)$$

$$0 = \iint_{\Sigma_0 + \Sigma_1 + \Sigma_2} \left(\bar{\phi} \frac{\partial}{\partial n} \frac{1}{r} - \frac{1}{r} \frac{\partial \bar{\phi}}{\partial n} \right) dS - \iint_{S_F} \left(\bar{\phi} \frac{\partial}{\partial n} \frac{1}{r} - \frac{1}{r} \frac{\partial \bar{\phi}}{\partial n_H} \right) dS \\ + \iint_{\bar{S}_H} \left(\bar{\phi} \frac{\partial}{\partial n_H} \frac{1}{r} - \frac{1}{r} \frac{\partial \bar{\phi}}{\partial n_H} \right) dS, \quad (A-2)$$

$$0 = - \iint_{S_H + \bar{S}_H} \left(\phi_i \frac{\partial}{\partial n_H} \frac{1}{r} - \frac{1}{r} \frac{\partial \phi_i}{\partial n_H} \right) dS \quad (A-3)$$

where $\bar{\phi}$ and ϕ_i are the velocity potential defined in \bar{V}_e and V_i respectively. The definition of the normal of n and n_H are shown in Fig.1.

The integrands over Σ_1 and $\bar{\Sigma}_1$ vanish when the upstream condition is imposed on ϕ . Then the addition of Eqs.(A-1), (A-2) and (A-3) yields

$$4\pi\phi(P) = \iint_{\Sigma_0} \left(\phi \frac{\partial}{\partial n} \frac{1}{r} - \frac{1}{r} \frac{\partial \phi}{\partial n} \right) dS + \iint_{\Sigma_0} \left(\bar{\phi} \frac{\partial}{\partial n} \frac{1}{r} - \frac{1}{r} \frac{\partial \bar{\phi}}{\partial n} \right) dS \\ + \iint_{\Sigma_2} \left(\phi \frac{\partial}{\partial n} \frac{1}{r} - \frac{1}{r} \frac{\partial \phi}{\partial n} \right) dS + \iint_{\bar{\Sigma}_2} \left(\bar{\phi} \frac{\partial}{\partial n} \frac{1}{r} - \frac{1}{r} \frac{\partial \bar{\phi}}{\partial n} \right) dS \\ + \iint_{S_F} \left\{ (\phi - \bar{\phi}) \frac{\partial}{\partial n} \frac{1}{r} - \frac{1}{r} \frac{\partial}{\partial n} (\phi - \bar{\phi}) \right\} dS \\ + \iint_{S_H} \left\{ (\phi - \phi_i) \frac{\partial}{\partial n_H} \frac{1}{r} - \frac{1}{r} \frac{\partial}{\partial n_H} (\phi - \phi_i) \right\} dS + \iint_{\bar{S}_H} \left\{ (\bar{\phi} - \phi_i) \frac{\partial}{\partial n_H} \frac{1}{r} - \frac{1}{r} \frac{\partial}{\partial n_H} (\bar{\phi} - \phi_i) \right\} dS. \quad (A-4)$$

It can be expected that the contributions from the integrations over Σ_2 and $\bar{\Sigma}_2$, the third and the fourth terms in Eq.(A-4), may cancel each other when Σ_2 and $\bar{\Sigma}_2$ are taken deep enough. We assume that $\bar{\phi}$ is equal to ϕ at the symmetric points; then Eq.(A-4) can be written as follows:

$$4\pi\phi(P) = \iint_{S_H} \left\{ (\phi - \phi_i) \frac{\partial}{\partial n_H} \left(\frac{1}{r} + \frac{1}{r_i} \right) - \left(\frac{1}{r} + \frac{1}{r_i} \right) \frac{\partial}{\partial n_H} (\phi - \phi_i) \right\} dS \\ - \iint_{S_F} \frac{1}{r} \frac{\partial}{\partial n} (\phi - \bar{\phi}) dS - \iint_{\Sigma_0} \left\{ \phi \frac{\partial}{\partial x_i} \left(\frac{1}{r} + \frac{1}{r_i} \right) - \left(\frac{1}{r} + \frac{1}{r_i} \right) \frac{\partial \phi}{\partial x_i} \right\} dS. \quad (A-5)$$

Eq.(A-5) can be expressed in terms of source singularities; putting $\phi = \phi_i$, $\partial/\partial n_H(\phi - \phi_i) = \sigma_H$ and $\partial/\partial n(\phi - \bar{\phi}) = \sigma_F$, we obtain Eq.(2) in the text.

Table 1 Computed Wave-Resistance Coefficients

F _n	Wigley Model ¹⁾		Elliptic Cylinder (EM-150) ²⁾		Lens-Shaped Cylinder (LM-150) ²⁾	
	(P) ³⁾	(P) ³⁾	(F) ⁴⁾	(P) ³⁾	(F) ⁴⁾	
0.170			0.0174		0.0049	
0.180	0.2638		0.0351		0.0073	
0.190	0.3401		0.0609	0.0068		
0.200	0.4251		0.0662		0.0099	
0.210	0.5350	0.0804	0.0876	0.0172	0.0206	
0.220	0.6613	0.1522	0.1757		0.0319	
0.230	0.7331	0.2208	0.2823	0.0265	0.0326	
0.240	0.7462	0.2252	0.3329		0.0253	
0.250	0.7537	0.1771	0.2701	0.0189	0.0265	
0.260	0.8296	0.1552	0.2238	0.0442	0.0703	
0.267	0.9479					
0.270		0.2271	0.3345	0.0929	0.1386	
0.280	1.2251	0.3834	0.5857	0.1440	0.2078	
0.289	1.3728					
0.290		0.5609		0.1702		
0.300	1.4808	0.7006		0.1675	0.3062	
0.310	1.5408			0.1420	0.2761	
0.330	1.5722					
0.350	1.3991					

Remarks 1) $R_w / \frac{1}{2} \rho U^2 S \times 10^3$, 2) $R_w / \frac{1}{2} \rho U^2 L^2 \times 10^2$, 3) by hull pressure integration, Eq. (5),
4) by free surface integration method, Eq. (17).

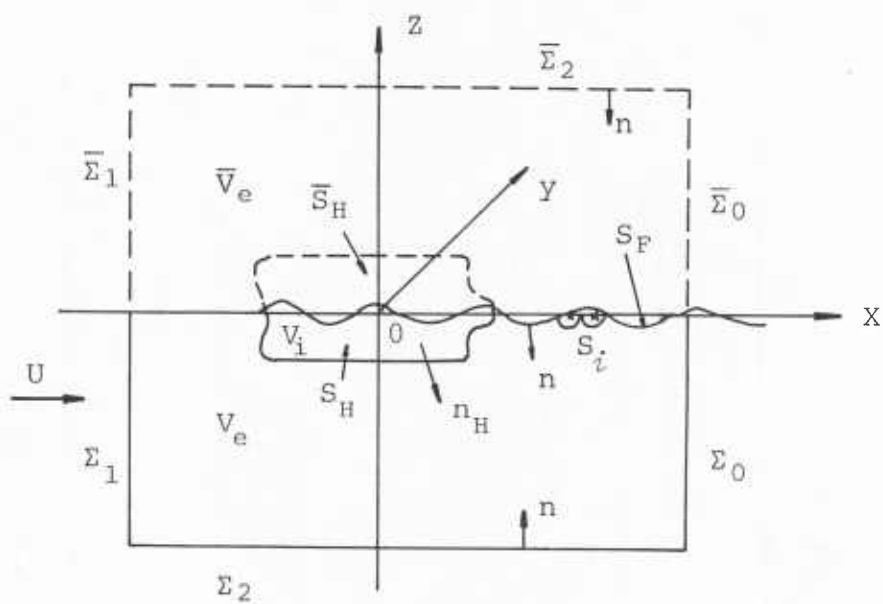


Fig. 1 Coordinate System and Symbols

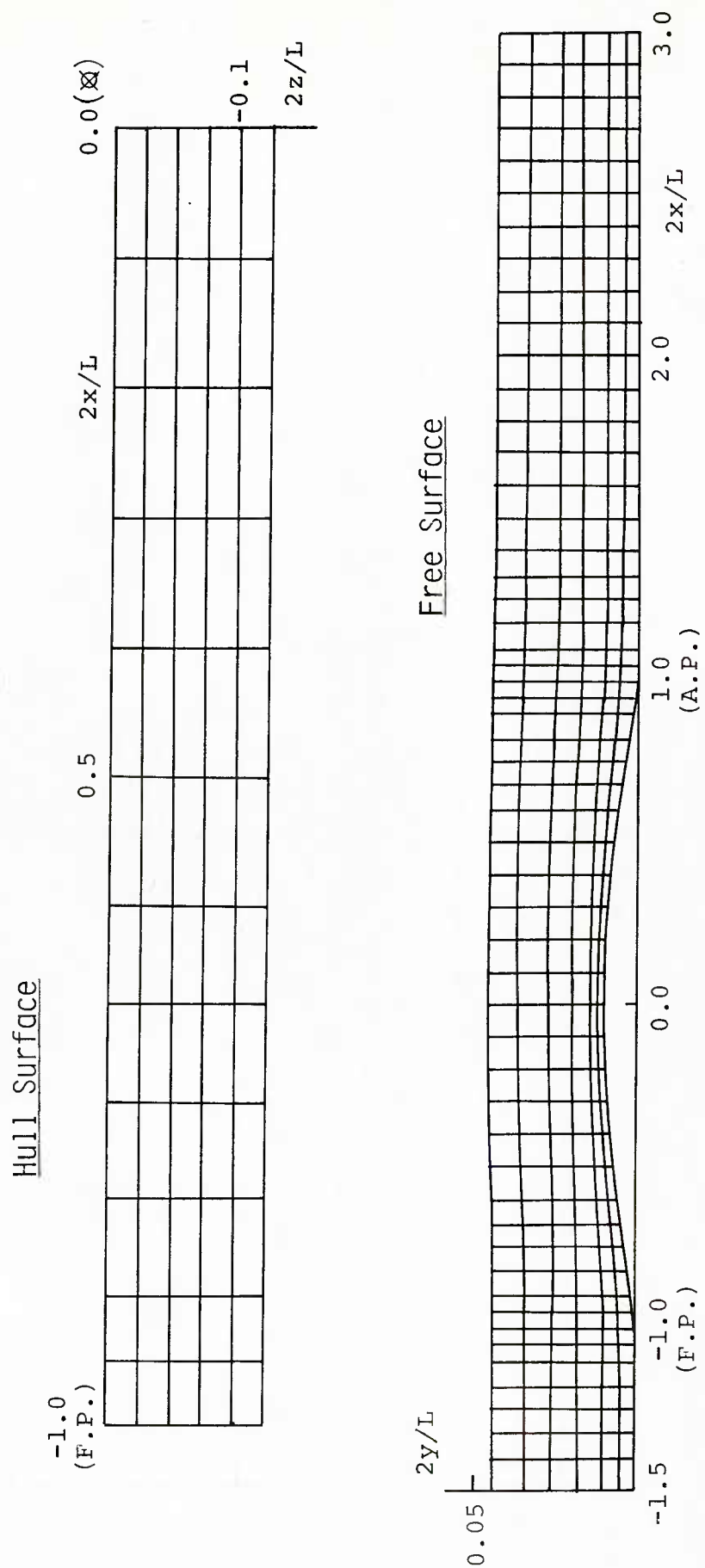


Fig. 2 Panel Arrangements for Wigley Parabolic Model

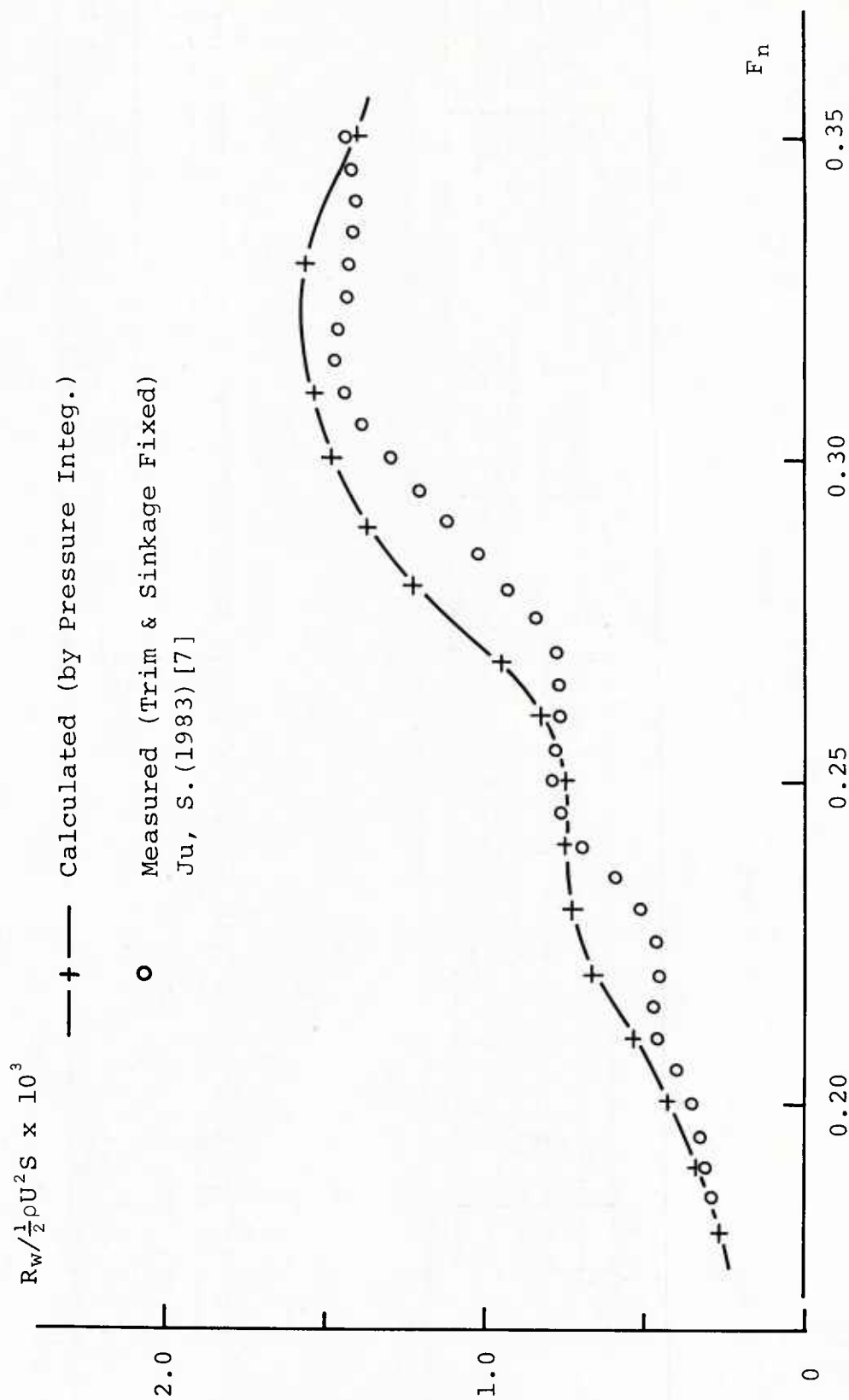


Fig. 3 Wave Resistance of Wigley Parabolic Model

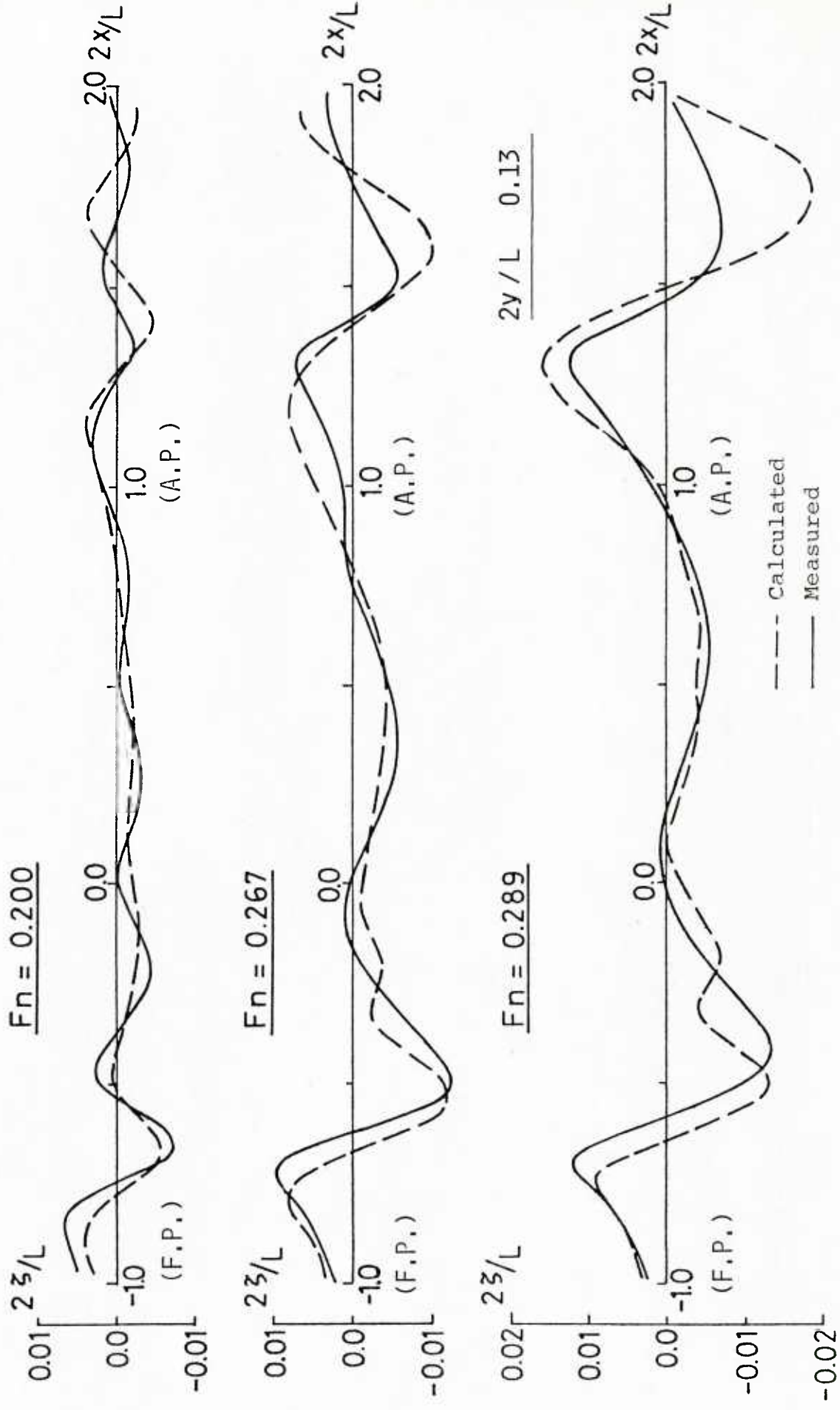


Fig. 4 Wave Profiles of Wigley Model

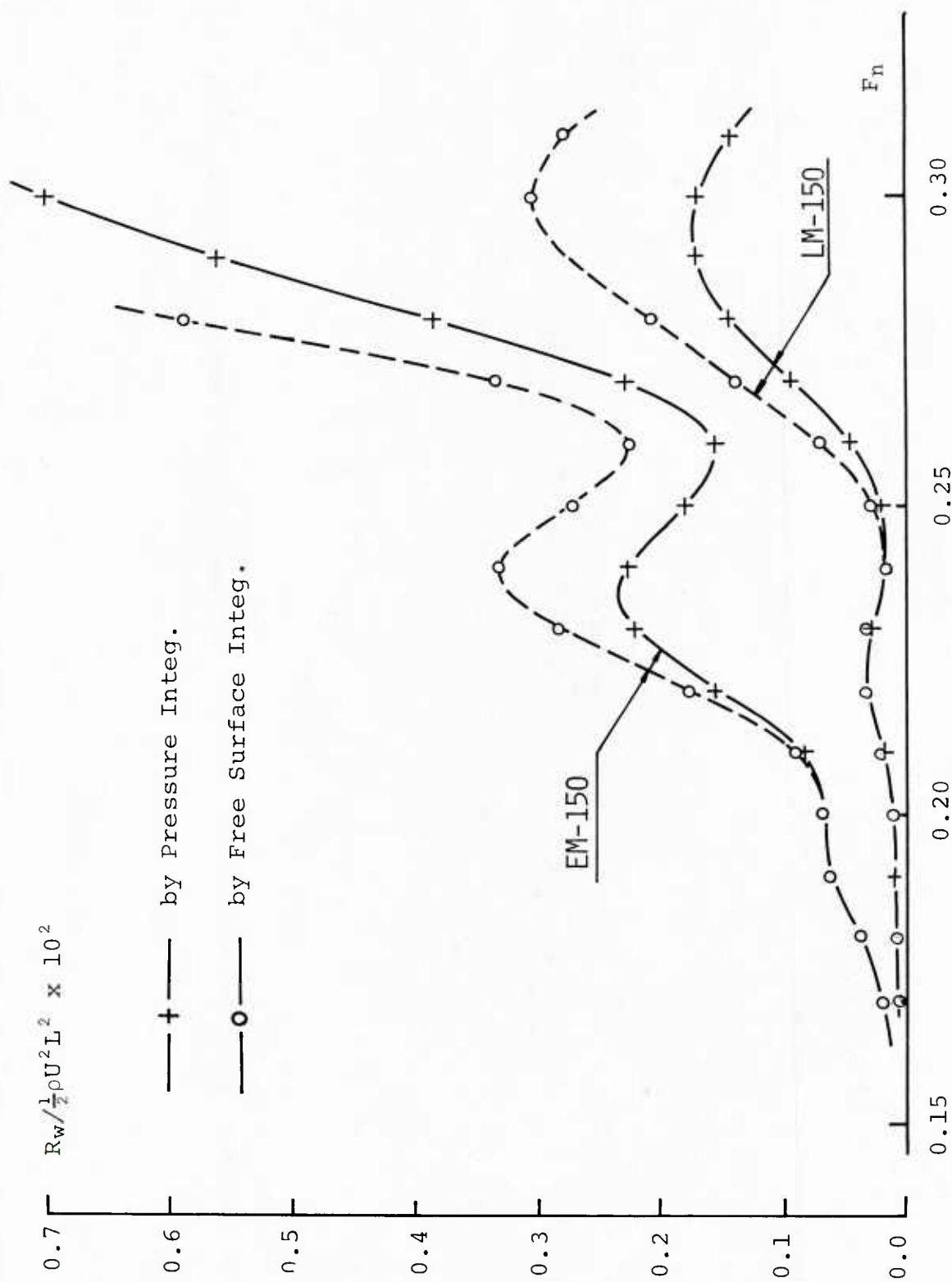


Fig. 5 Calculated Wave Resistance of EM-150 and LM-150

$Fn = 0.250$

Unit : $2\zeta/L$

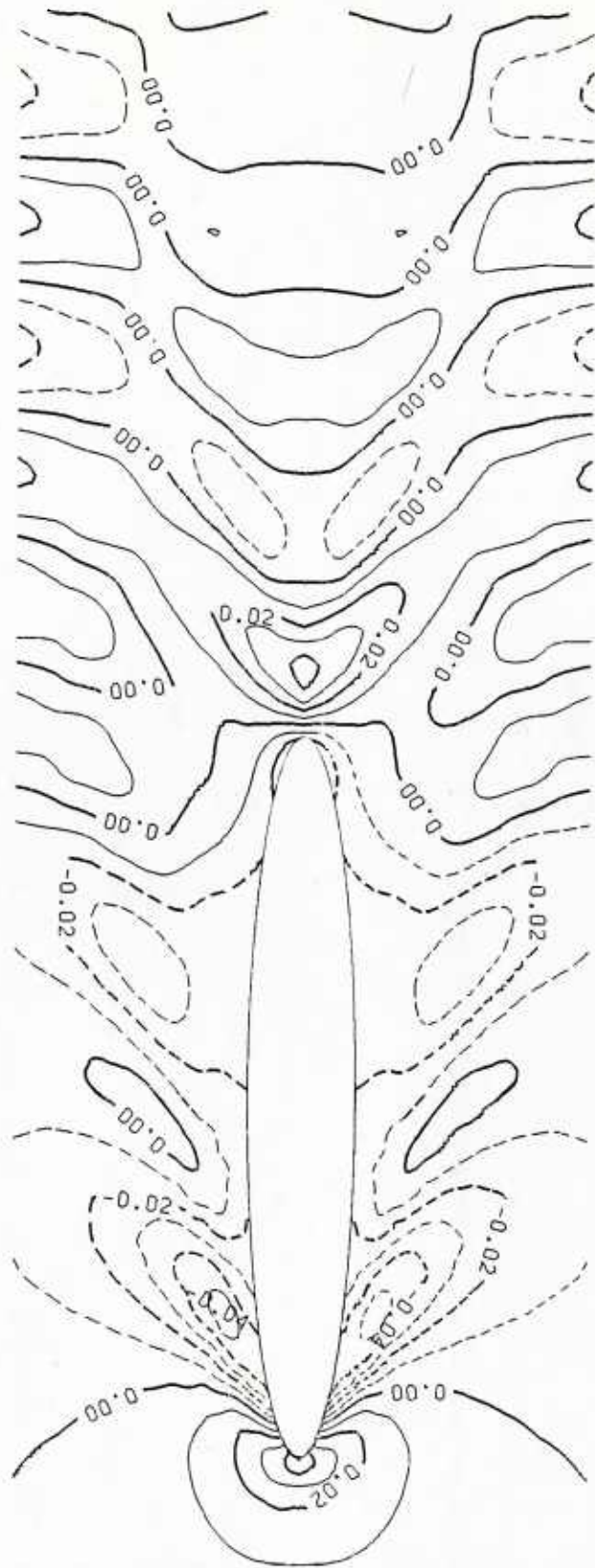


Fig. 6 Wave Contour of Elliptic Cylinder (EM-150)

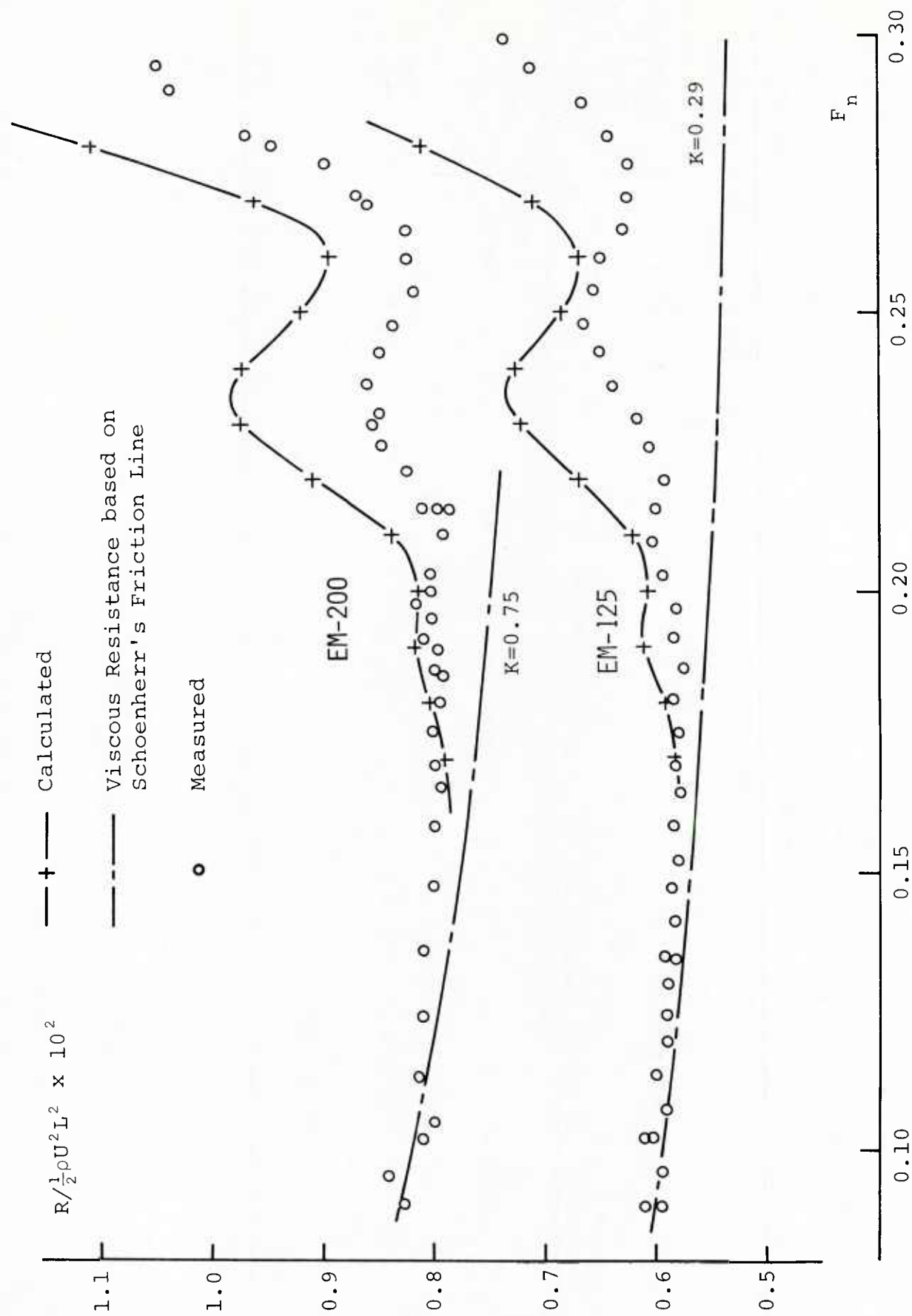


Fig. 7 Comparisons of Resistance of Elliptic Cylinders

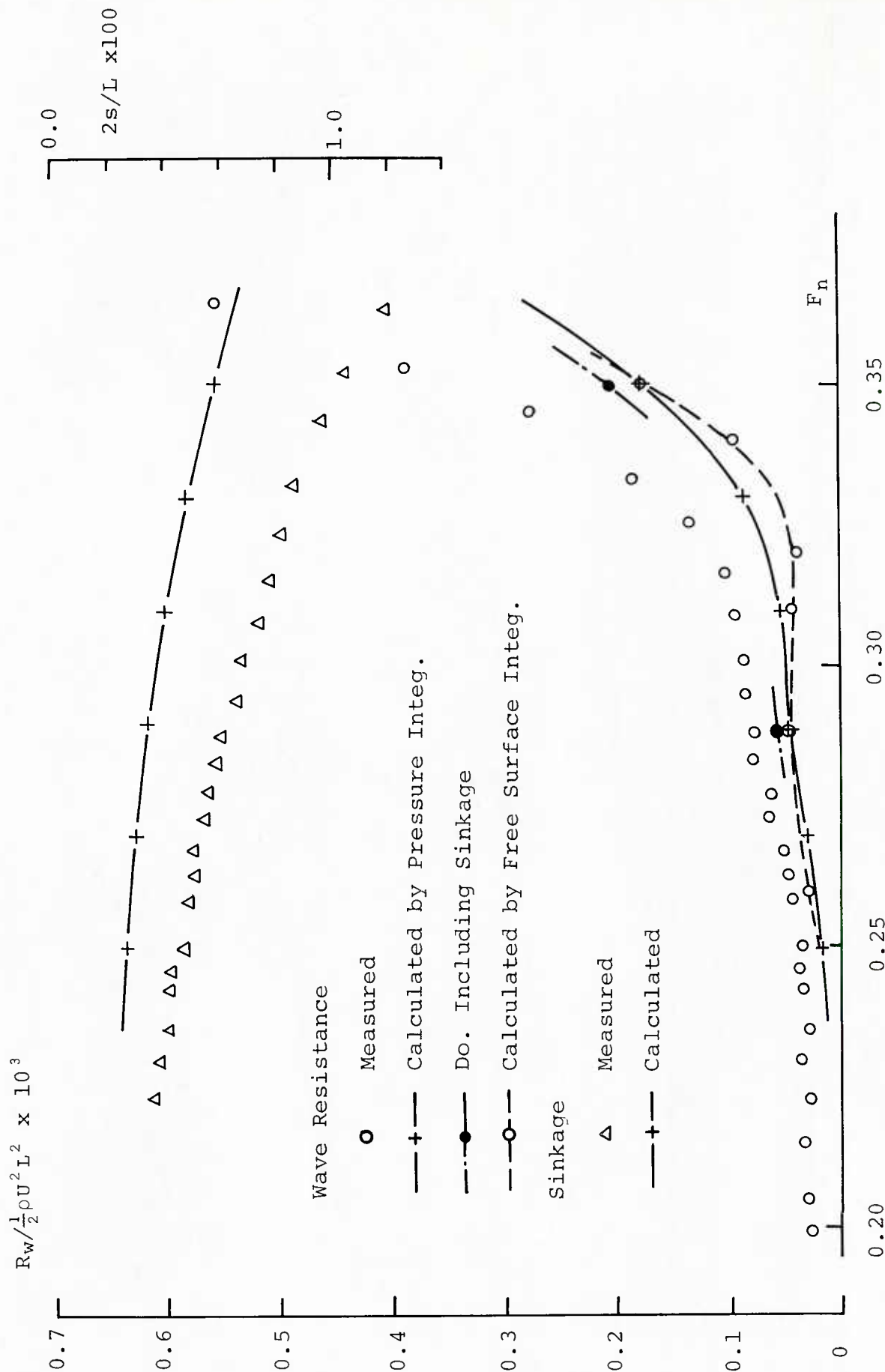


Fig. 8 Wave Resistance and Sinkage of Inuid M-21

Numerical Calculation of Free Surface Flow by Means of Modified Rankine Source Method

S. Ogiwara

Ishikawajima-Harima Heavy Industries Co.,Ltd. ,Japan

Abstract

The free surface flow around a ship is calculated by the method using Rankine Source distribution over the hull surface and undisturbed free surface. The free surface condition is linearized based on the double model flow and is applied at the undisturbed free surface, according to C.W.Dawson¹⁾. The solution of wavy potential that satisfies the boundary condition of the hull surface and the free surface can be obtained by the iterative method²⁾.

The present method is applied to calculate the wave profile, pressure distribution over the hull surface and wave resistance for the Wigley hull and the strut like hull form. The calculated results for the Wigley hull are compared with measured values. For the strut like hull form, the calculation are performed for both cases when the hull is moving with the sharp end ahead and with the blunt end ahead.

Nomenclature

$A_k(i,j), B(i)$; Matrix of the simultaneous equation for Rankine source
on the free surface.

B ; Ship breadth.

$CL_k(i,j)$; Finite difference of $L_k(i,j)$.

C_p ; Pressure coefficient on the hull surface.

C_w ; Wave resistance coefficient $= R_w / (\frac{1}{2} \rho U^2 L^2)$.

d ; Ship draft.

∇_n ; Finite difference operator.

Fn ; Froude number $= U / \sqrt{gL}$.

g ; Gravitational acceleration.

- k ; Three dimensional form factor on flat plate friction.
 K_0 ; Wave number = g/U^2 .
 L ; Ship length.
 ℓ ; Half ship length = $L/2$.
 $L_K(ij)$; Velocity in the direction of double model flow due to a source of unit strength.
 M_0 ; Number of panels on the hull surface of a double model.
 M_1 ; Number of panels on the free surface
 n_x ; x-component of the normal vector on the hull surface
 $N_K(ij)$; Normal velocity on the hull surface due to a source of unit strength.
 S_0 ; Hull surface of a double model
 S_1 ; Undisturbed free surface
 U ; Uniform velocity.
 U_n ; Normal velocity on the hull surface.
 x, y, z ; Cartesian coordinate system fixed to the hull
 ϕ_0 ; Velocity potential of the double model flow
 ϕ_1 ; Velocity potential of the free surface wave
 $\sigma_0, \Delta\sigma_0$; Rankine source strength on the surface of a double model
 σ_1 ; Rankine source strength on the free surface
 ζ ; Wave elevation

1. Basic equations

The coordinate system O-xyz is fixed to the hull with its origin on the midship section, the x-y plane coincides with the undisturbed free surface, the x-axis is in the direction of uniform flow, and the z-axis vertically upward.

The velocity potential is expressed by the sum of a double model velocity potential ϕ_0 and a potential ϕ_1 representing the effect of free surface wave,

$$\phi = \phi_0 + \phi_1 \quad (1)$$

The wavy potential ϕ_1 satisfies the Laplace equation

$$\phi_{1xx} + \phi_{1yy} + \phi_{1zz} = 0 \quad (2)$$

The velocity potential needs to satisfy the dynamical condition and kinematical condition on the free surface,

$$g\zeta + \frac{1}{2} (\phi_x^2 + \phi_y^2 + \phi_z^2 - U^2) = 0 \quad \text{at } z = \zeta \quad (3)$$

$$\phi_x \zeta_x + \phi_y \zeta_y - \phi_z = 0 \quad \text{at } z = \zeta \quad (4)$$

Eliminating ζ from eqs.(3) and (4)

$$\frac{1}{2} \{ \phi_x (\nabla \phi)_x^2 + \phi_y (\nabla \phi)_y^2 + \phi_z (\nabla \phi)_z^2 \} + g \phi_z = 0 \quad \text{at } z = \zeta \quad (5)$$

Substituting eq.(1) into eq.(5), the following linearized free surface condition can be obtained¹⁾ in term of ϕ_i by neglecting the term ϕ_i^2 and assuming that eq.(5) holds for $z=0$,

$$\phi_{0\ell}^2 \phi_{i\ell\ell} + 2 \phi_{0\ell} \phi_{0\ell\ell} \phi_{i\ell} + g \phi_{iz} = - \phi_{0i}^2 \phi_{0\ell\ell} \quad \text{at } z = 0 \quad (6)$$

where the subscript ℓ means the derivative along the stream line of double model flow.

ϕ_i needs to satisfy the boundary condition on the hull surface,

$$\frac{\partial \phi_i}{\partial n} = 0 \quad (7)$$

where n represents a normal to the hull surface in the outward direction.

ϕ_0 and ϕ_i are expressed by using Rankine sources distributed on the hull surface of a double model (S_0) and the undisturbed free surface (S_1) respectively,

$$\phi_0(x, y, z) = Ux - \iint_{S_0} \sigma_0 \frac{1}{r_0} dS \quad (8)$$

$$\phi_i(x, y, z) = - \iint_{S_1} \sigma_1 \frac{1}{r_1} dS - \iint_{S_0} \Delta \sigma_0 \frac{1}{r_0} dS \quad (9)$$

$$r_0 = \sqrt{(x-x')^2 + (y-y')^2 + (z-z')^2}$$

$$r_1 = \sqrt{(x-x')^2 + (y-y')^2 + z^2}$$

The first term of the right hand side of eq.(9) represents the potential of free waves and the second term the effect of waves on the hull surface.

2. Method of numerical solution²⁾

The hull surface of the double model is divided into M_0 panels and the finite domain of the free surface into M_1 panels, and the source intensity is supposed constant within each panel. $\phi_{1\ell}$ and $\phi_{1\ell\ell}$ in the free surface condition, eq.(6), can be expressed as,

$$\phi_{1\ell}(i) = \sum_{j=1}^{M_1} \sigma_1(j) L_1(ij) + \sum_{j=1}^{M_0} \Delta\sigma_0(j) L_0(ij) \quad (10)$$

$$\phi_{1\ell\ell}(i) = \sum_{j=1}^{M_1} \sigma_1(j) CL_1(ij) + \sum_{j=1}^{M_0} \Delta\sigma_0(j) CL_0(ij) \quad (11)$$

where

$$L_\kappa(ij) = \iint_{\Delta S_\kappa} \frac{\{(x-x')\phi_{0x} + (y-y')\phi_{0y}\}}{\phi_{0\ell} \cdot r_\kappa^3} dS \quad (\kappa=0,1) \quad (12)$$

$$CL_\kappa(ij) = \sum_{n=1}^{N-1} e_n L_\kappa(i-n, j) \quad (\kappa=0,1) \quad (13)$$

in which e_n is an N-point upstream difference operator. Substituting eqs.(10),(11) into eq.(6), the simultaneous linear equation for σ_1 and $\Delta\sigma_0$ can be obtained,

$$\sum_{j=1}^{M_1} \sigma_1(j) A_1(ij) + \sum_{j=1}^{M_0} \Delta\sigma_0(j) A_0(ij) - 2\pi g \sigma_1(i) = B(i) \quad (14)$$

($i = 1, 2, \dots, M_1$ on S_1)

where

$$A_K(ij) = \phi_{ol}^2(i) (L_K(ij) + 2\phi_{ol}(i)\phi_{oll}(i)L_K(ij)) \quad (K=0,1) \quad (15)$$

$$B(i) = -\phi_{ol}^2(i)\phi_{oll}(i) \quad (16)$$

Substituting eq.(9) into eq.(7).

$$\sum_{j=1}^{M_1} \sigma_1(j) N_1(ij) + \sum_{j=1}^{M_0} \Delta\sigma_0(j) N_0(ij) = 0 \quad (17)$$

($i=1, 2, \dots, M_0$ on S_0)

where

$$N_K(ij) = - \iint_{\Delta S_K} \frac{\partial}{\partial n} \left(\frac{1}{r_K} \right) dS \quad (K=0,1) \quad (18)$$

The iterative method is used to obtain the solution of eqs.(14) and(17). As the first approximation, the source distribution over the hull surface can be represented by the double model solution σ_0 ,

$$\Delta\sigma_0 = 0 \quad (19)$$

Hence the simultaneous equation for seeking the first order approximation becomes from eq.(14),

$$\sum_{j=1}^{M_1} \sigma_1^{(1)}(j) A_1(ij) - 2\pi g \sigma_1^{(1)}(i) = B(i) \quad (20)$$

($i=1, 2, \dots, M_1$ on S_1)

Mori and et al.⁽³⁾ have used eq.(20) to determine σ_1 . The solution of the first approximation leaves the following flow penetrating across the hull surface,

$$v_h(i) = \sum_{j=1}^{M_1} \sigma_1^{(1)}(j) N_1(ij) \quad (21)$$

The hull surface condition is corrected by adding sources on the hull surface,

$$\Delta\sigma_0(i) = -\frac{1}{4\pi} v_h(i) \quad (22)$$

This will approximately satisfy the boundary condition expressed by eq.(17). Considering the velocity potential, $\Delta\phi_0$ created by $\Delta\sigma_0$, the second order approximation of σ_1 is obtained from the simultaneous equation

$$\sum_{j=1}^{M_1} \sigma_1^{(2)}(j) A_1(ij) - 2\pi g \sigma_1^{(2)}(i) = B(i) - \sum_{j=1}^{M_0} \Delta\sigma_0(j) A_0(ij) \quad (23)$$

($i=1, 2, \dots, M_1$ on S_1)

3. Numerical calculation

The source distribution on the double body and the velocity distribution along streamlines on the still water surface are calculated by the method of Hess and Smith⁴⁾. The division of the still water surface into panels is performed as follows. In the transverse direction, the free surface is divided by the streamlines of double model flow. For the division in longitudinal direction, the hyperbola is used,

$$y(x) = \sqrt{(x - \chi_i + B/2)^2 - (B/2)^2} \quad (24)$$

where χ_i are chosen so that the curves described by eq.(24) intersect the load waterline at the points of division on the hull surface. The features of the free surface panel arrangement are shown in Fig.1. Number of panels on the hull surface and free surface are as follows,

Panel arrangement (half region)		
	Hull surface	Free surface
	Row x Line	Row x Line
Wigley hull	23 x 10	30 x 7
Strut like hull		
Sharp end ahead	20 x 10	30 x 7
Blunt end ahead	20 x 10	30 x 7

In the finite difference approximation expressed by eq.(13), a four-point finite difference

operator is used for the fore part of the free surface and a two-point operator is used for the aft part so that the calculated results of pressure distribution and wave profile on the hull surface become agree with the experimental results²⁾.

The pressure distribution on the hull surface can be expressed as follows by neglecting the higher order terms of ϕ_1 ,

$$C_p = \frac{p - p_0}{\frac{1}{2} \rho U^2} = \frac{1}{U^2} (U^2 - \phi_{0x}^2 - \phi_{0y}^2 - \phi_{0z}^2 - 2\phi_{0x}\phi_{1x} - 2\phi_{0y}\phi_{1y} - 2\phi_{0z}\phi_{1z}) \quad (25)$$

Similarly, the wave height

$$\zeta(x, y) = \frac{1}{2g} (U^2 - \phi_{0x}^2 - \phi_{0y}^2 - 2\phi_{0x}\phi_{1x} - 2\phi_{0y}\phi_{1y}) \quad \text{at } z=0 \quad (26)$$

Assuming that the pressure is constant within a hull surface panel, the wave resistance can be determined by,

$$C_w = \frac{R_w}{\frac{1}{2} \rho U^2 L^2} = \frac{1}{L^2} \sum_{i=1}^{M_0/2} C_p(i) n_{xi} \Delta S_i \quad (27)$$

where ΔS_i is the area of the surface panel and n_{xi} is the x-component of the unit normal on a surface panel.

4. Numerical results

4.1 Wigley hull

The calculated value of pressure distribution are shown in Figs.2-a through 2-d in comparison with measured values, and tabulated in Table 1. The calculated values of wave profiles on the hull surface are shown in Fig.3 and in Table 4-a. The wave resistance obtained by eq.(27) is shown in Fig.4 and Table 5 in comparison with the experimental values.

The results of present calculation of pressure distributions and wave profiles show good agreement with the measured values especially in lower Froude number. The calculated bow wave heights are lower than those of measured value. The calculated wave resistances agree comparatively well with measured values. It is seen that the calculated

wave resistance is somewhat heigher than the pressure resistance obtained from measured pressure distribution on the hull surface. The measured value are reproduced from the report of Cooperative Experiments on Wigley Parabolic Model in Japan⁵⁾ that will be presented to the 17th ITTC Resistance Committee on the request of the Comittee.

4.2 Strut like hull

The numerical results of pressure distribution on the hull surface are shown in Figs.5-a through 5-e and tabulated in Table 2, when the hull is moving with the sharp end ahead. Wave profiles are shown in Fig.6 and tabulated in Table 4-b.

The pressure distribution are shown in Figs.7-a through 7-e, and tabulated in Table 3, when the hull is moving with the blunt end ahead. Wave profiles are shown in Fig.8 and tabulated in Table 4-c. The wave resistances obtained by pressure integration over the hull surface are shown in Fig.9 and Table 5.

In 1978, IHI Ship Model Basen conducted the resistance test of the mathematical model (MS521) similar to the strut like hull given in this workshop. Fig.10 shows the waterline and midship section of MS521 comparing with that of the strut like hull. The wave resistance of MS521 obtained from resistance test is also shown in Fig.10. The difference of wave resistance can be observed for the hull moving with the sharp end ahead and with the blunt end ahead. The numerical results of the strut like hull show the same trend as those of experiments and this result seems to be a significant feature of the present theory.

References

1. Dawson,C.W., A Practical Computer Method for Solving Ship Wave Problems, 2nd Int. Conf. on Numerical Ship Hydrodynamics, Berkeley (1977)
2. Ogiwara S., A Method to Predict Free Surface Flow around Ship by Means of Rankine Sources, (in Japanese) Journal of the Kansai Soc. of Nav. Arch. Japan, No.190 (1983)
3. Mori, K.,Nishimoto,H., Prediction of Flow Fields around Ship by Modified Rankine Source Method,(1st Report), Journal of Soc. Nav. Arch. Japan, Vol.150 (1981)
4. Hess,J.L.,Smith,A.M.O., Calculation of Nonlifting Potential Flow about Arbitrary Three Dimensional Bodies, Journal of Ship Research, Vol.8,No.2 (1968)
5. The Report of Cooperative Experiments on Wigley Parabolic Models in Japan, presented to the Resistance Committee of the 17th ITTC, Varna, Sept. 1983

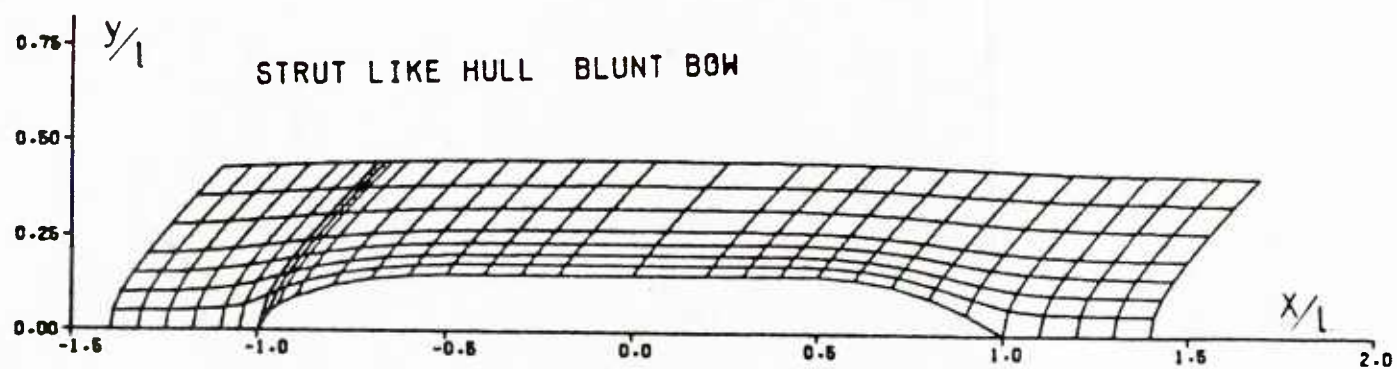
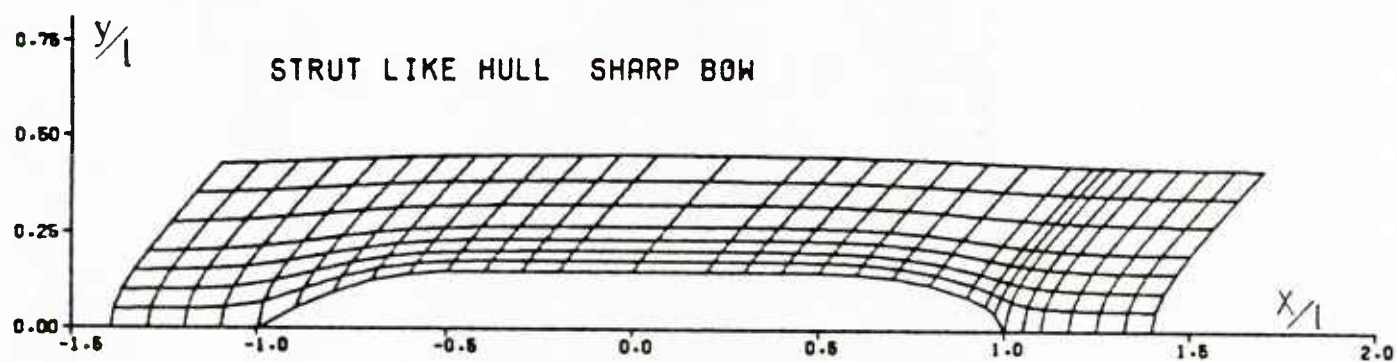
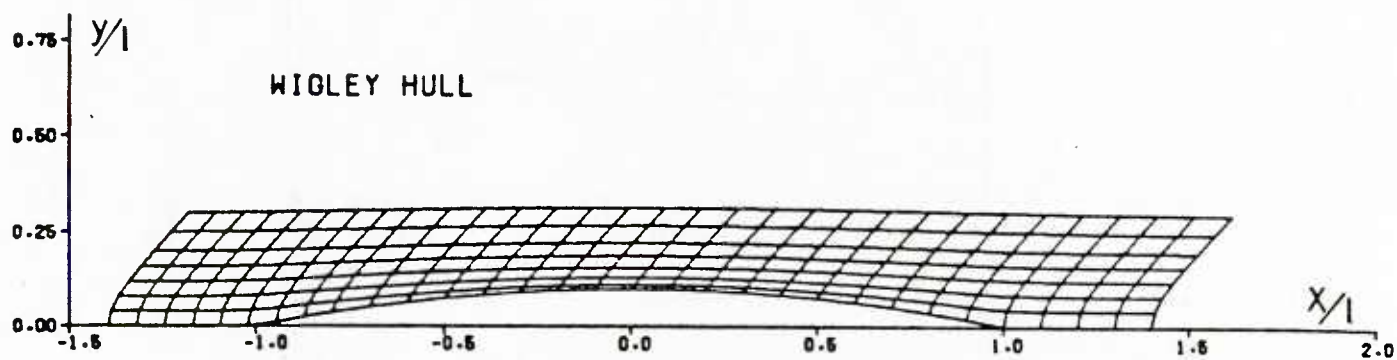


Fig. 1 Panel arrangement on the free surface

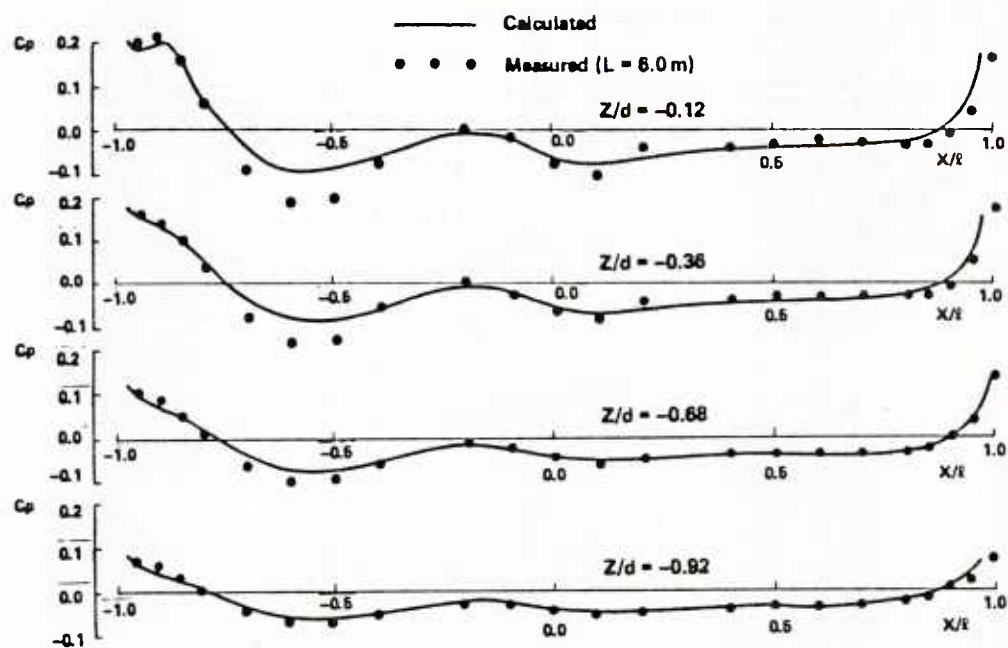


Fig. 2-a Pressure distribution on the surface of Wigley hull at $Fn = 0.250$

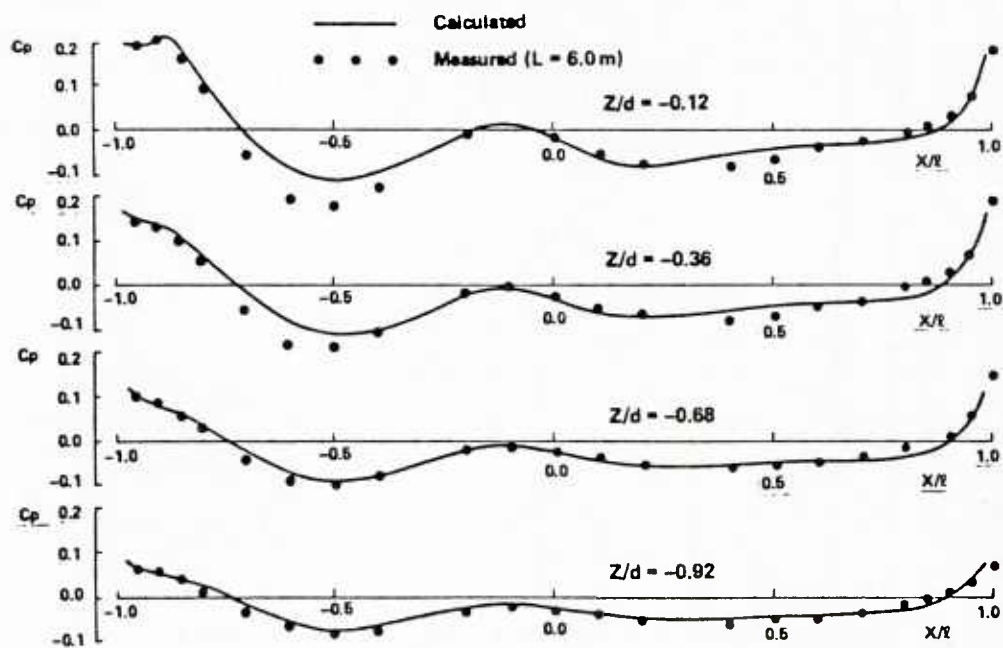


Fig. 2-b Pressure distribution on the surface of Wigley hull at $Fn = 0.267$

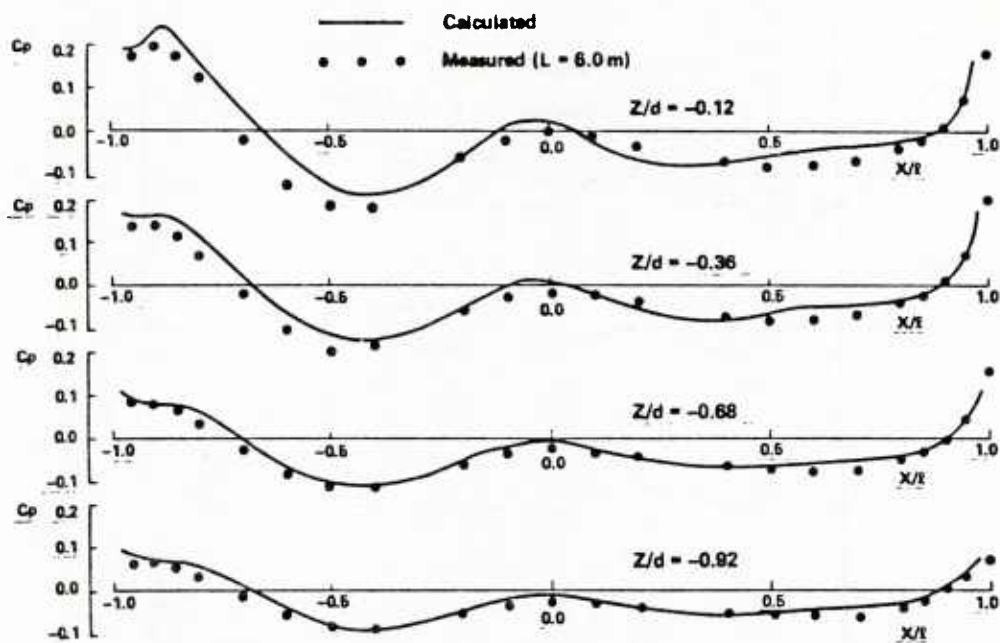


Fig. 2-c Pressure distribution on the surface of Wigley hull at $Fn = 0.289$

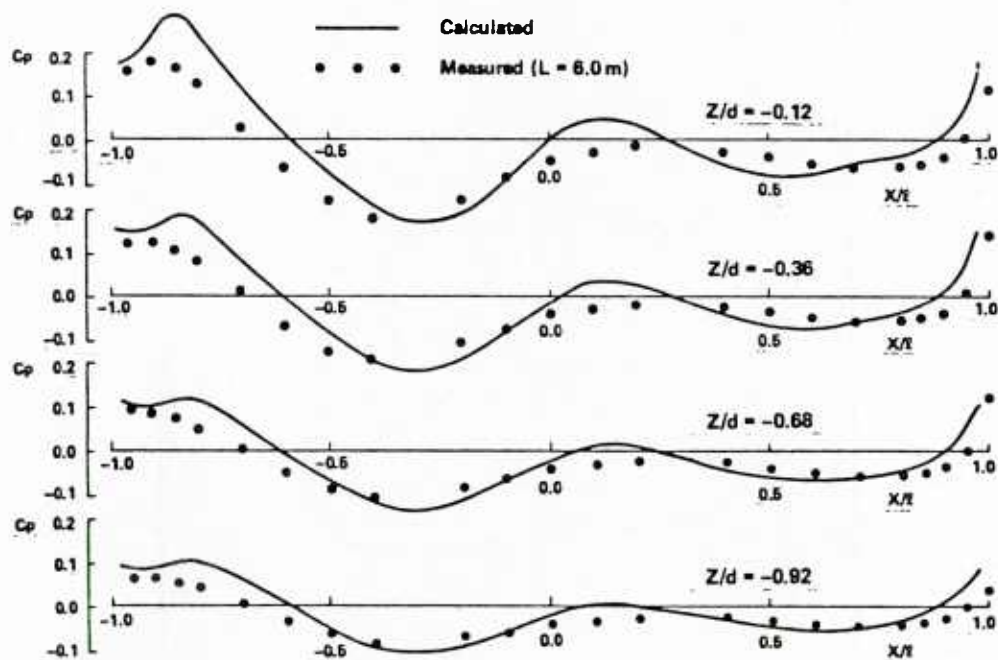


Fig. 2-d Pressure distribution on the surface of Wigley hull at $Fn = 0.316$

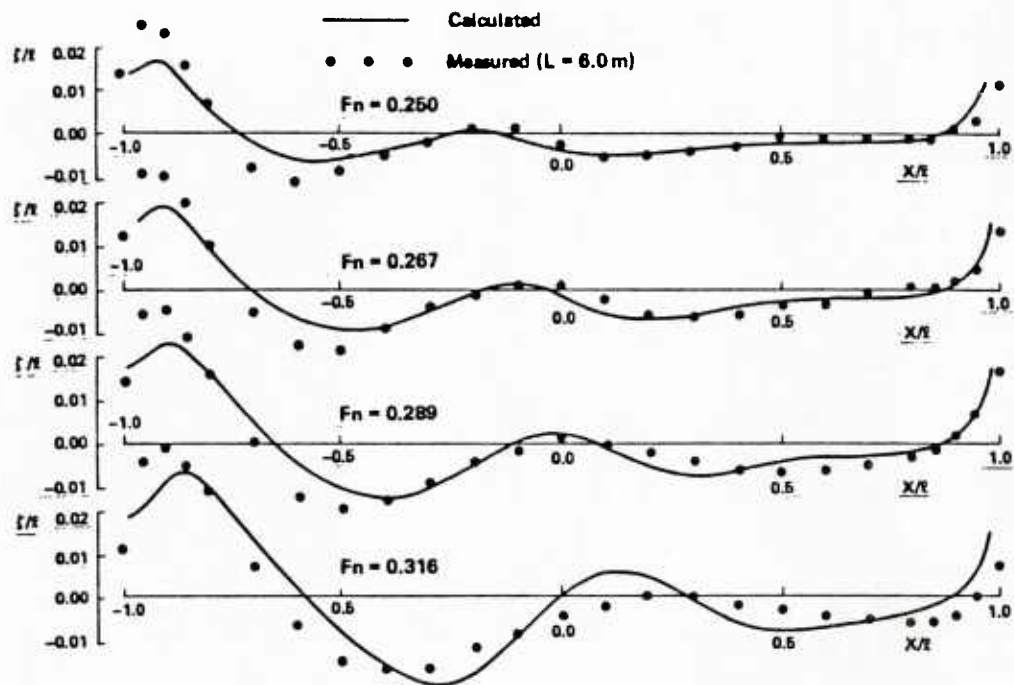


Fig. 3 Wave profiles on the surface of Wigley hull

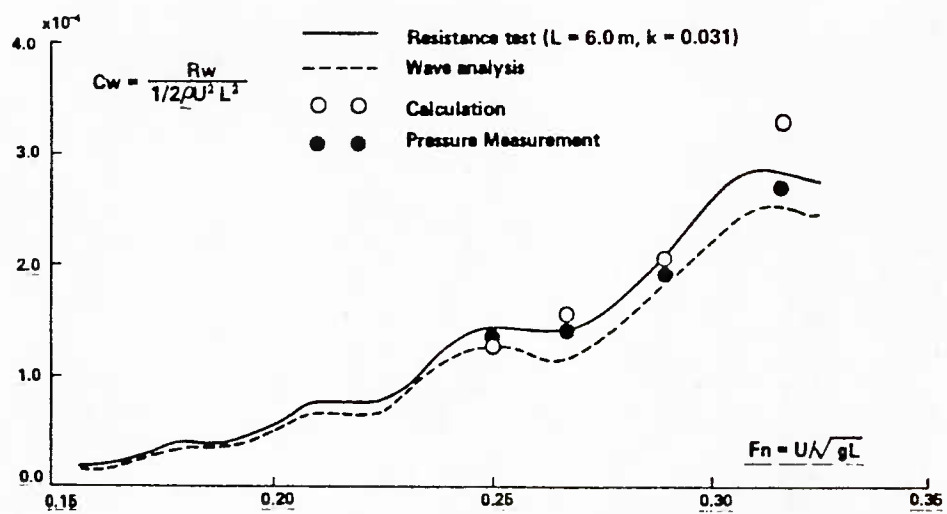


Fig. 4 Comparison of wave resistance of Wigley hull

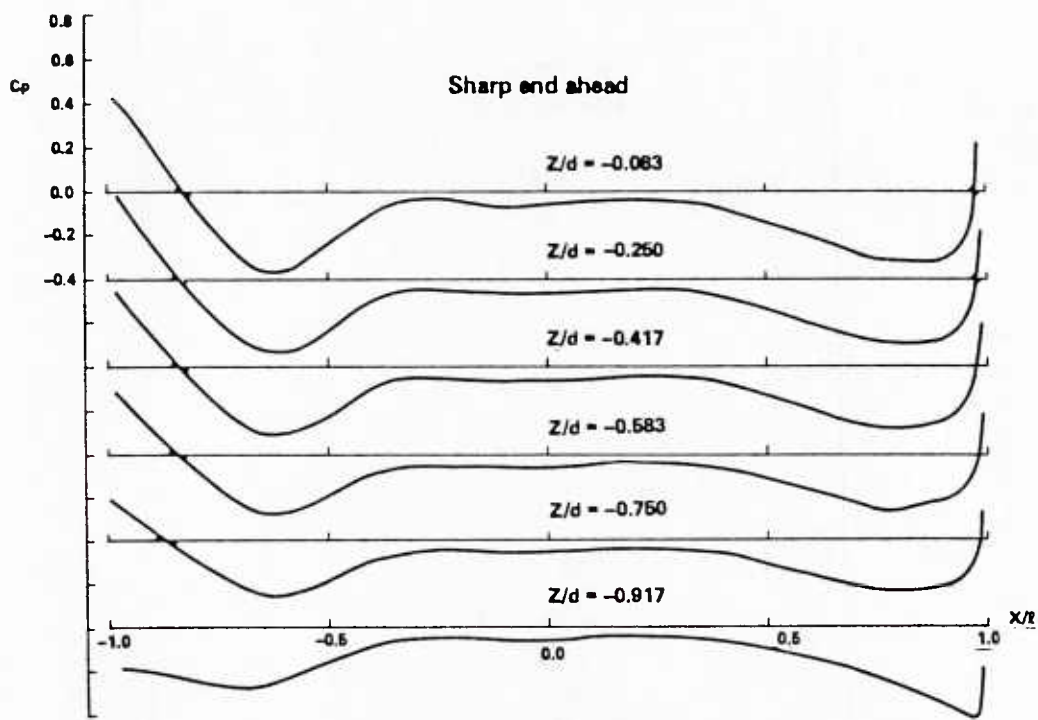


Fig. 5-a Pressure distribution on the surface of strut like hull at $Fn = 0.204$

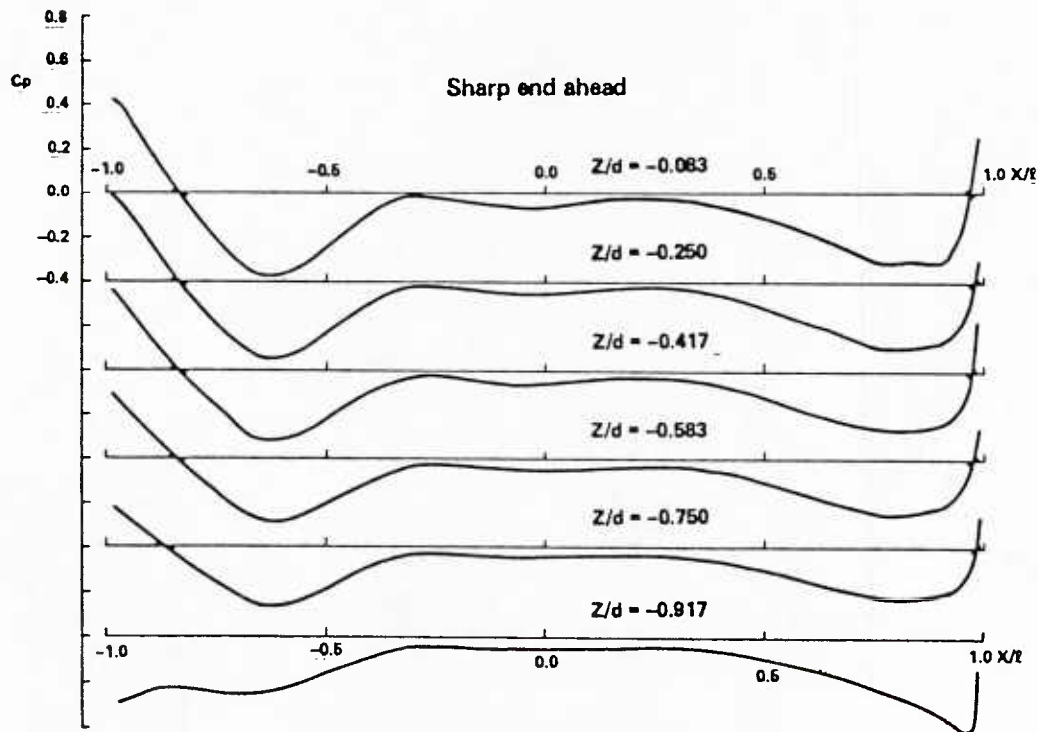


Fig. 5-b Pressure distribution on the surface of strut like hull at $Fn = 0.213$

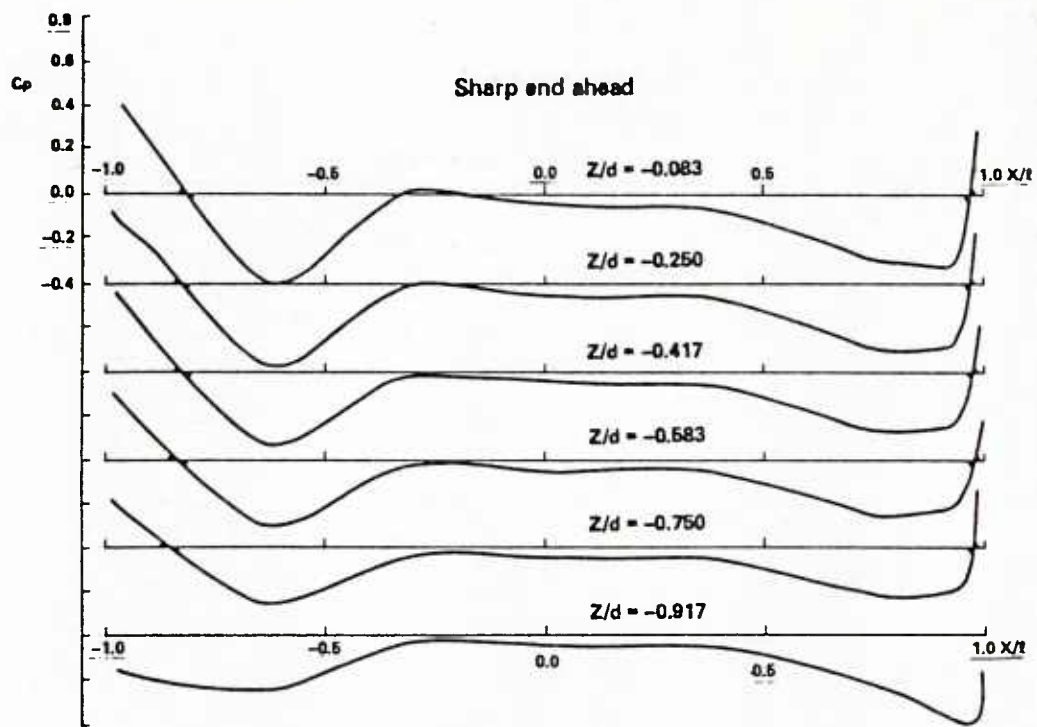


Fig. 5-c Pressure distribution on the surface of strut like hull at $Fn = 0.224$

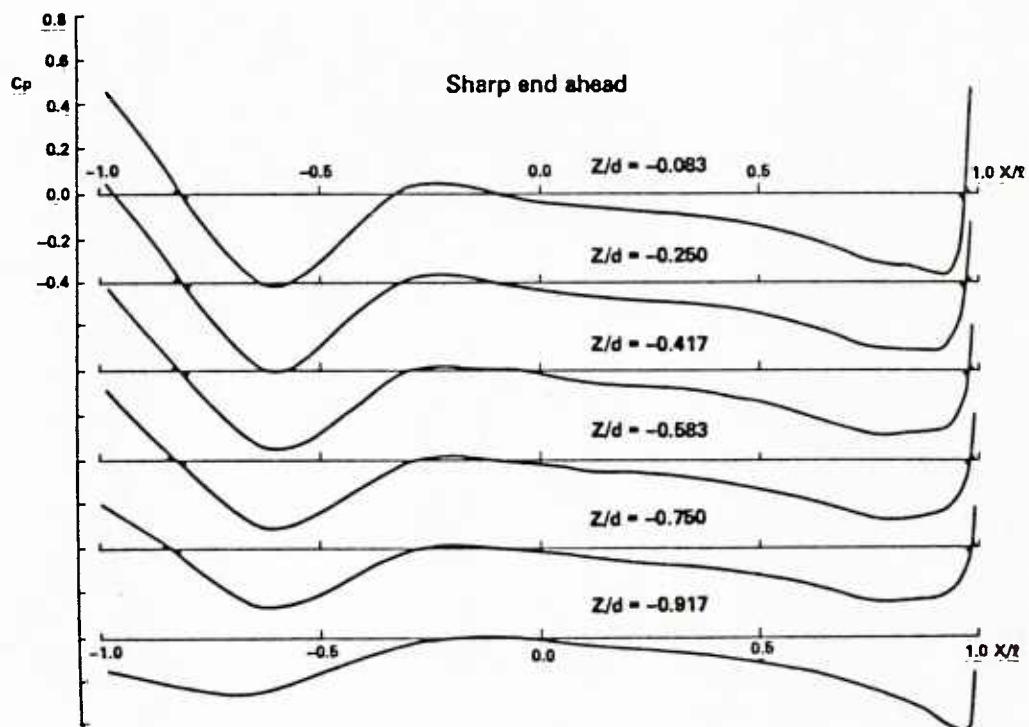


Fig. 5-d Pressure distribution on the surface of strut like hull at $Fn = 0.236$

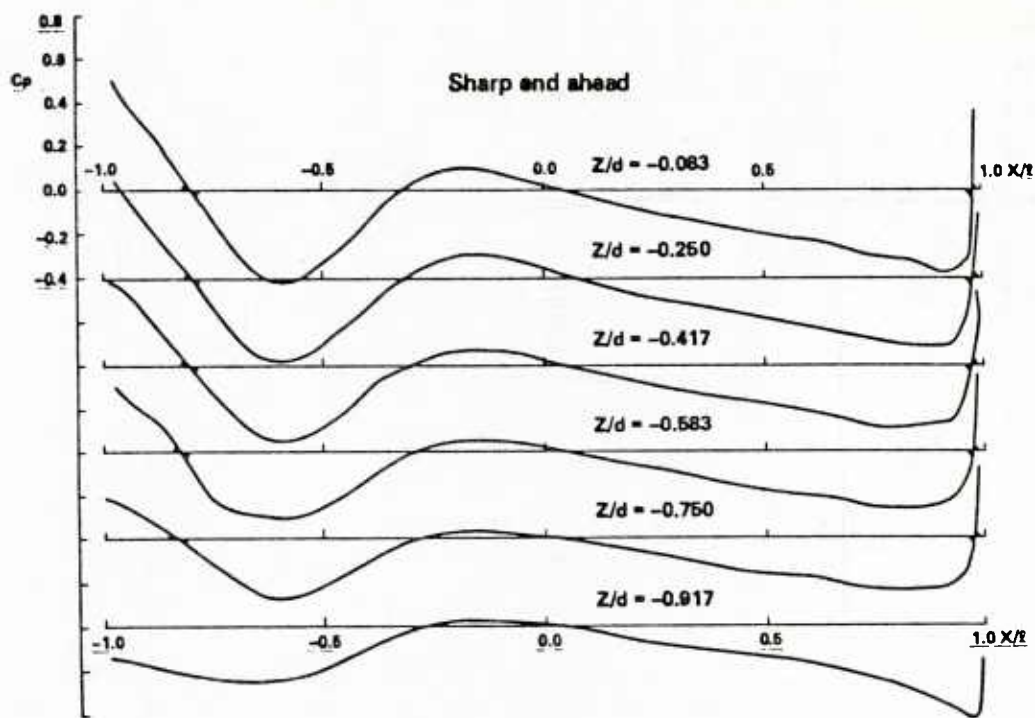


Fig. 5-e Pressure distribution on the surface of strut like hull at $Fn = 0.250$

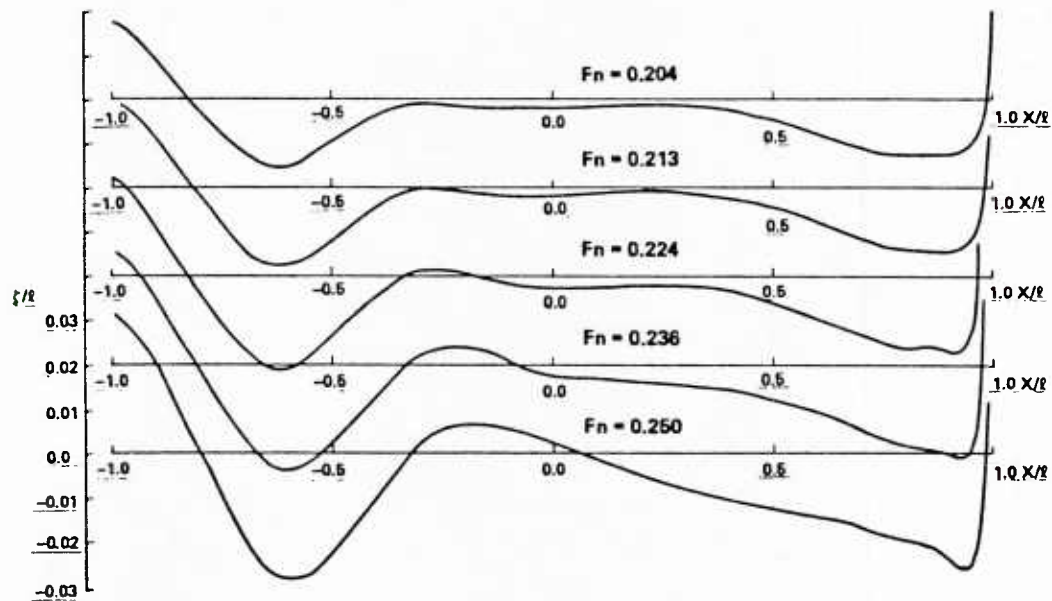


Fig. 6 Wave profiles on the surface of strut like hull (sharp end ahead)

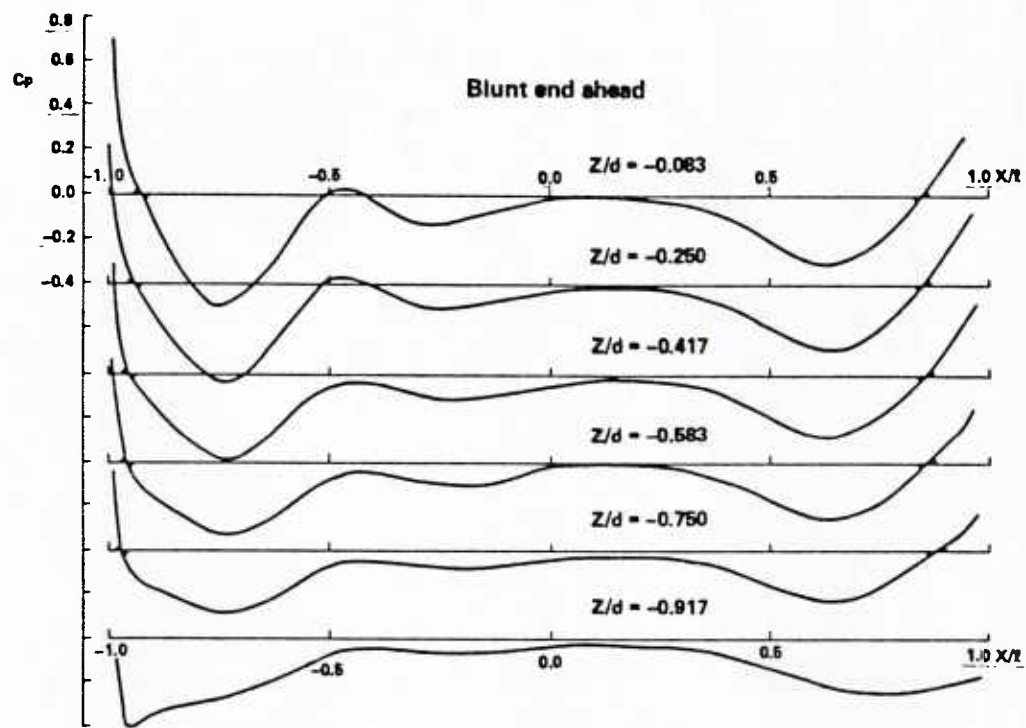


Fig. 7-a Pressure distribution on the surface of strut like hull at $Fn = 0.204$

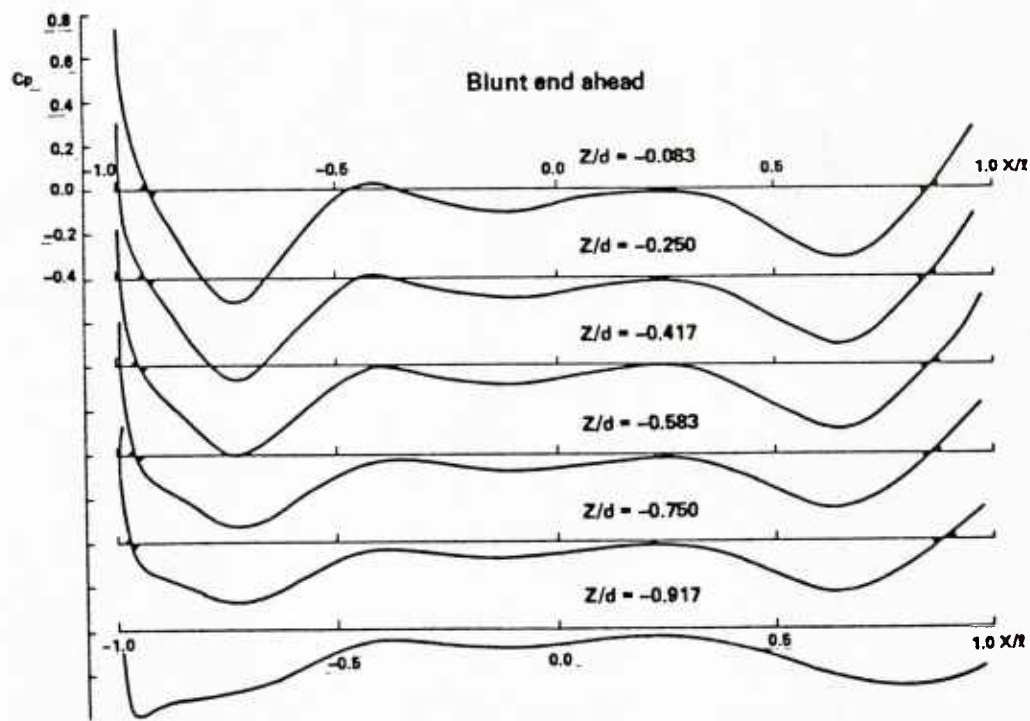


Fig. 7-b Pressure distribution on the surface of strut like hull at $Fn = 0.213$

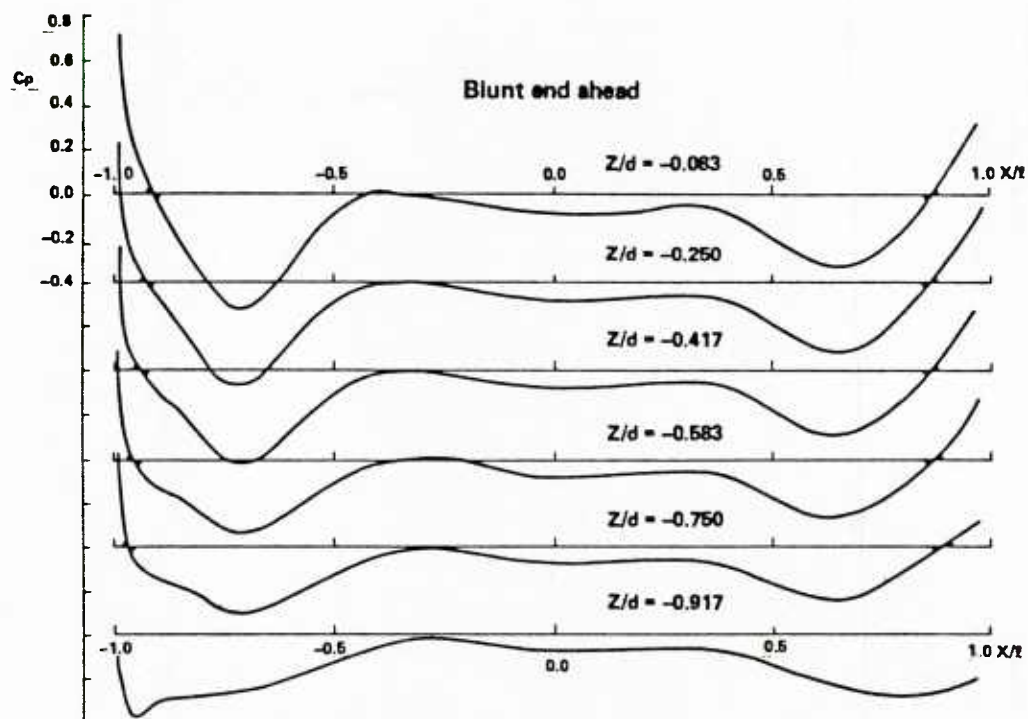


Fig. 7-c Pressure distribution on the surface of strut like hull at $Fn = 0.224$

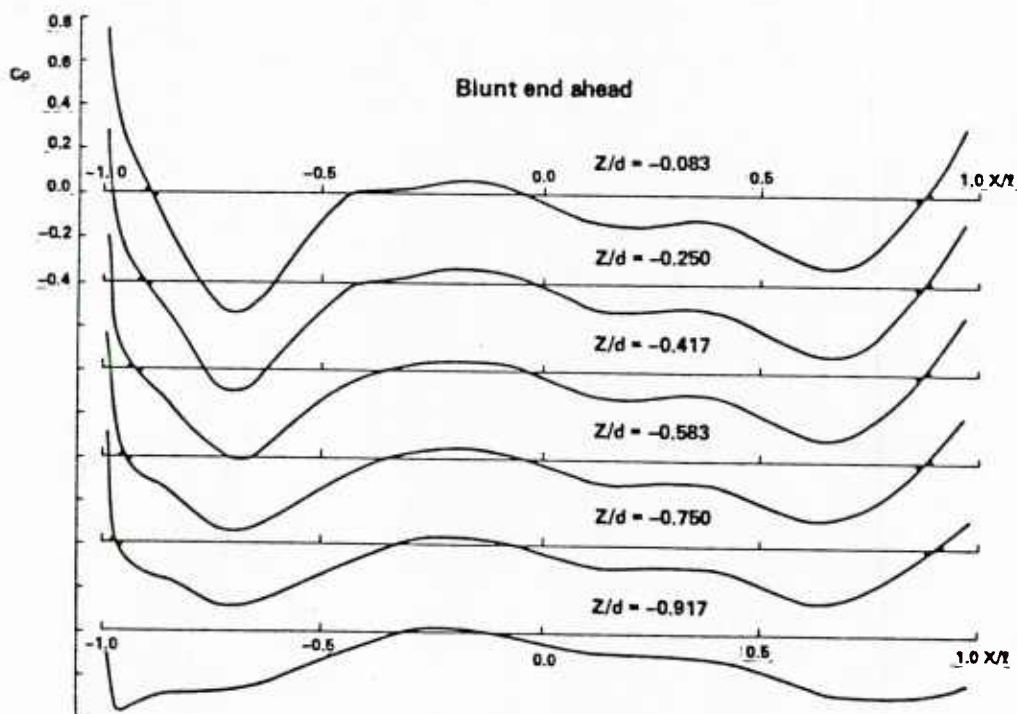


Fig. 7-d Pressure distribution on the surface of strut like hull at $Fn = 0.236$

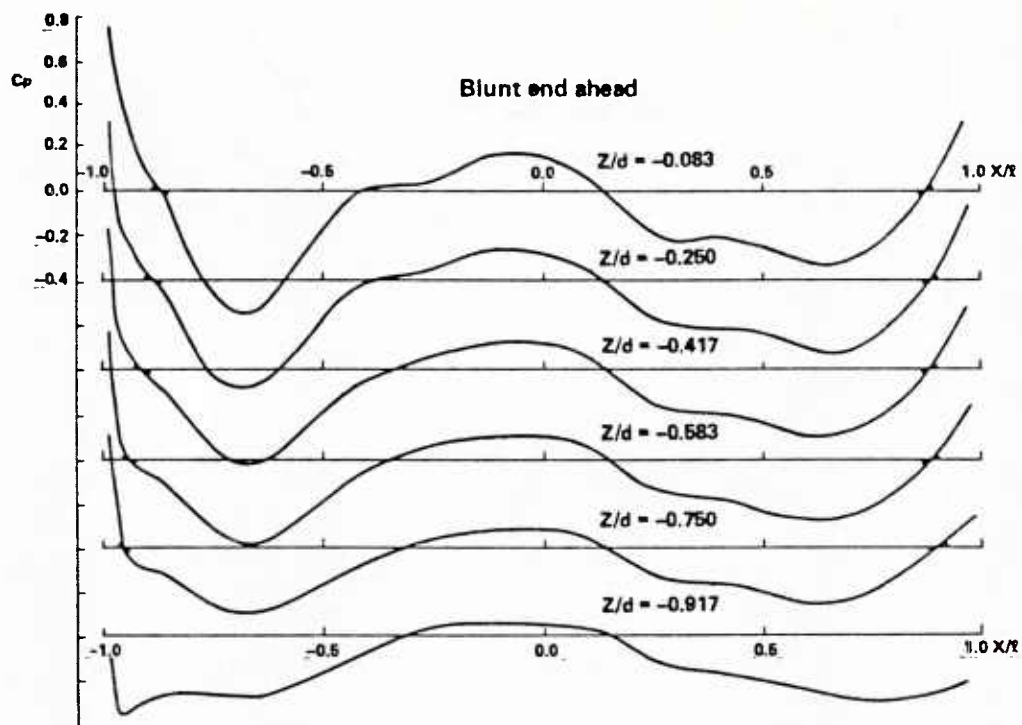


Fig. 7-a Pressure distribution on the surface of strut like hull at $Fn = 0.250$

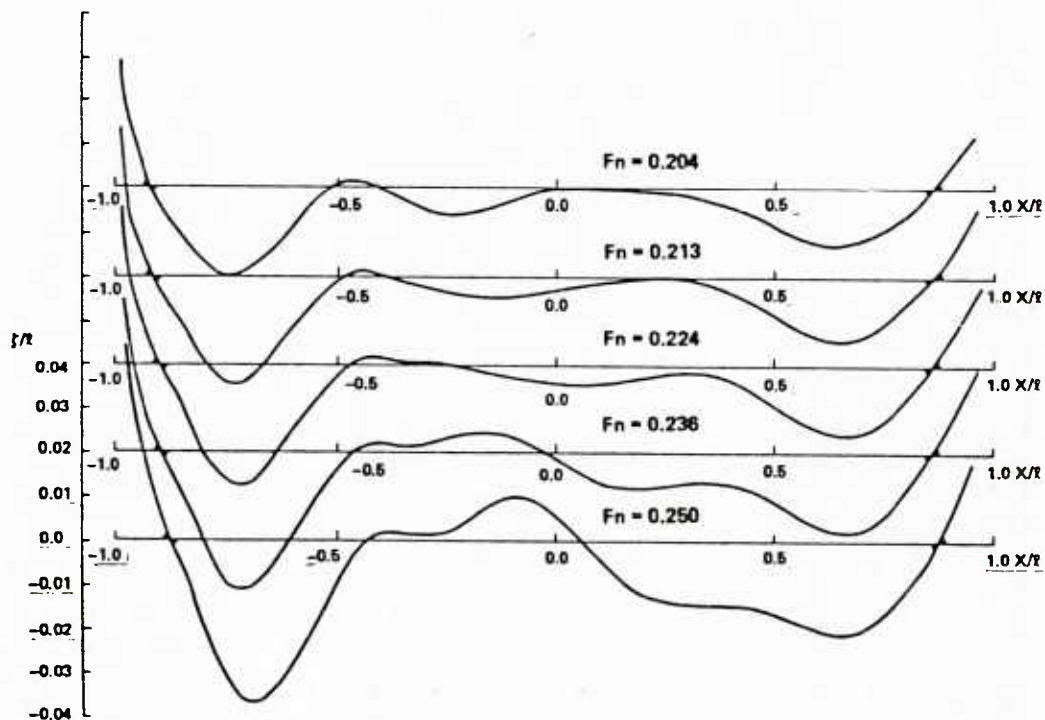


Fig. 8 Wave profiles on the surface of strut like hull (blunt end ahead)

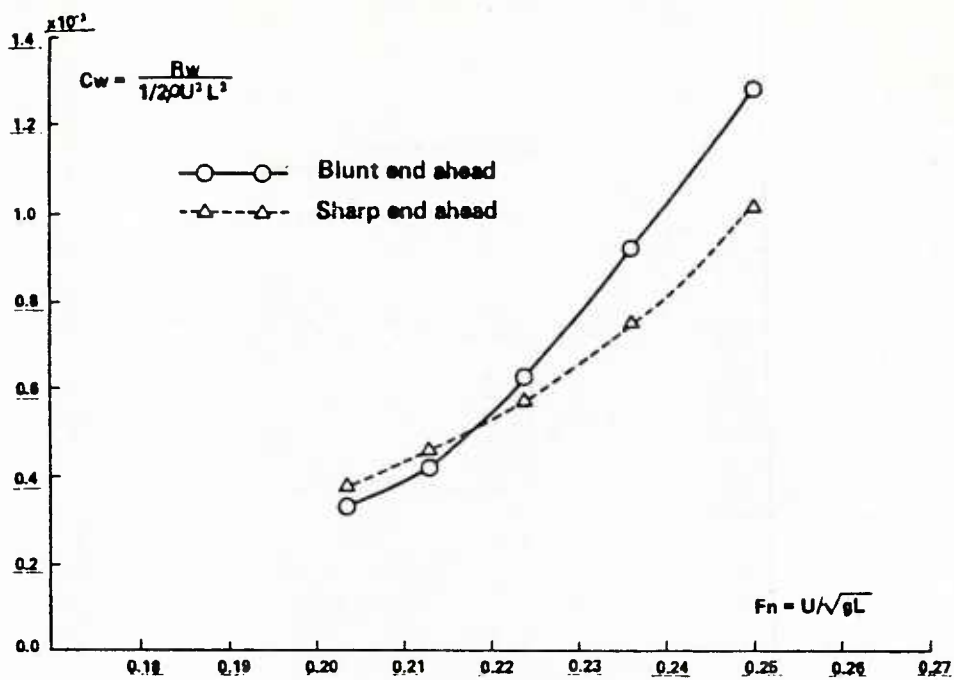


Fig. 9 Calculated wave resistance of strut like hull

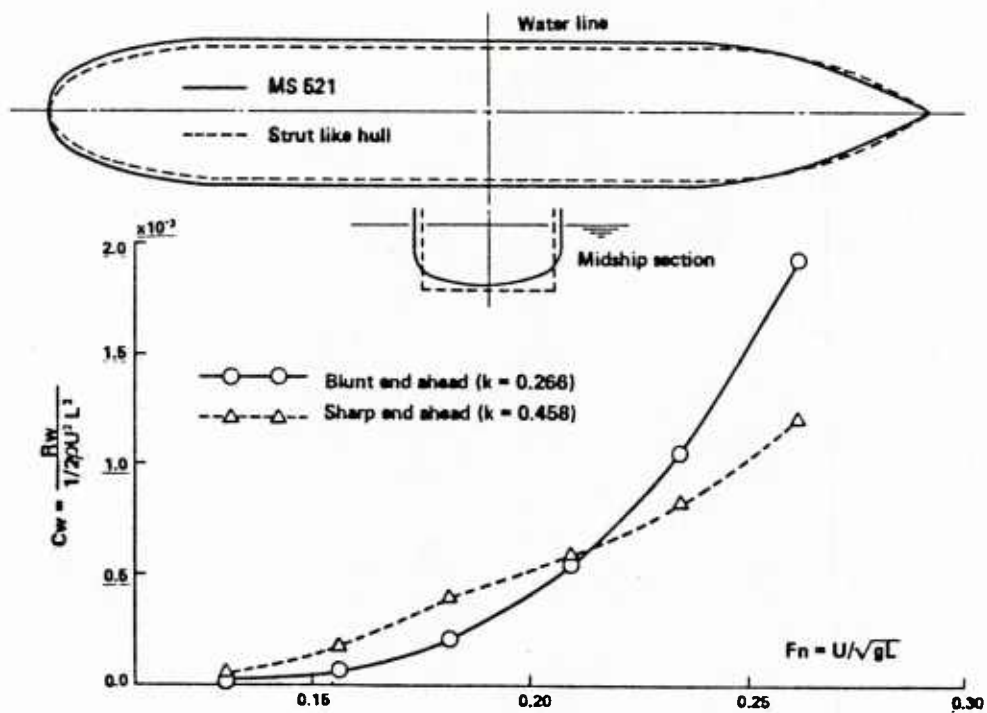


Fig. 10 Results of resistance test of MS 521

Table 1. Calculated pressure coefficients on the hull surface of Wigley hull

$$Fn = 0.250$$

x/l	z/d	- .1200	- .2000	- .3600	- .5200	- .6800	- .8400	- .9200
-.9750	.2141	.2032	.1786	.1526	.1249	.0989	.0881	
-.9250	.1960	.1786	.1427	.1091	.0826	.0648	.0516	
-.8750	.1850	.1590	.1163	.0836	.0608	.0475	.0455	
-.8250	.1002	.0830	.0669	.0462	.0323	.0242	.0264	
-.7500	.0114	.0066	-.0028	-.0104	-.0133	-.0104	-.0050	
-.6500	-.0707	-.0695	-.0577	-.0660	-.0595	-.0506	-.0435	
-.5500	-.0866	-.0851	-.0812	-.0775	-.0719	-.0626	-.0564	
-.4500	-.0714	-.0703	-.0682	-.0648	-.0602	-.0547	-.0514	
-.3500	-.0394	-.0393	-.0411	-.0413	-.0408	-.0376	-.0360	
-.2500	-.0137	-.0158	-.0204	-.0249	-.0260	-.0256	-.0248	
-.1500	-.0152	-.0180	-.0219	-.0254	-.0260	-.0256	-.0263	
-.0500	-.0452	-.0454	-.0455	-.0421	-.0388	-.0356	-.0355	
.0500	-.0720	-.0697	-.0648	-.0572	-.0509	-.0454	-.0445	
.1500	-.0705	-.0689	-.0635	-.0589	-.0531	-.0479	-.0470	
.2500	-.0559	-.0553	-.0546	-.0536	-.0497	-.0453	-.0432	
.3500	-.0463	-.0461	-.0481	-.0476	-.0463	-.0423	-.0403	
.4500	-.0418	-.0430	-.0454	-.0461	-.0447	-.0416	-.0393	
.5500	-.0377	-.0400	-.0428	-.0456	-.0457	-.0414	-.0371	
.6500	-.0339	-.0359	-.0421	-.0452	-.0452	-.0409	-.0358	
.7500	-.0282	-.0297	-.0335	-.0388	-.0399	-.0353	-.0291	
.8500	-.0034	-.0106	-.0143	-.0186	-.0206	-.0152	-.0103	
.9250	.0447	.0428	.0387	.0294	.0209	.0173	.0202	
.9750	.1732	.1664	.1514	.1299	.1055	.0827	.0739	

$$Fn = 0.267$$

x/l	z/d	- .1200	- .2000	- .3600	- .5200	- .6800	- .8400	- .9200
-.9750	.2091	.1991	.1766	.1525	.1261	.1007	.0900	
-.9250	.2039	.1871	.1517	.1179	.0909	.0722	.0587	
-.8750	.2162	.1865	.1385	.1025	.0771	.0613	.0580	
-.8250	.1374	.1239	.0973	.0720	.0541	.0425	.0430	
-.7500	.0489	.0412	.0267	.0151	.0087	.0086	.0126	
-.6500	-.0531	-.0535	-.0543	-.0545	-.0494	-.0413	-.0346	
-.5500	-.0956	-.0942	-.0905	-.0857	-.0788	-.0681	-.0612	
-.4500	-.1043	-.1012	-.0952	-.0877	-.0793	-.0707	-.0662	
-.3500	-.0752	-.0724	-.0688	-.0640	-.0596	-.0535	-.0507	
-.2500	-.0279	-.0285	-.0299	-.0323	-.0320	-.0305	-.0296	
-.1500	.0068	.0028	-.0040	-.0110	-.0147	-.0165	-.0180	
-.0500	-.0004	-.0049	-.0135	-.0177	-.0200	-.0207	-.0218	
.0500	-.0564	-.0549	-.0520	-.0465	-.0416	-.0376	-.0372	
.1500	-.0843	-.0811	-.0722	-.0648	-.0570	-.0504	-.0491	
.2500	-.0759	-.0737	-.0694	-.0650	-.0588	-.0527	-.0501	
.3500	-.0570	-.0564	-.0574	-.0556	-.0533	-.0483	-.0459	
.4500	-.0422	-.0438	-.0470	-.0481	-.0469	-.0437	-.0414	
.5500	-.0339	-.0365	-.0403	-.0438	-.0447	-.0407	-.0366	
.6500	-.0310	-.0333	-.0398	-.0434	-.0438	-.0397	-.0347	
.7500	-.0285	-.0302	-.0338	-.0390	-.0402	-.0356	-.0294	
.8500	-.0142	-.0150	-.0182	-.0217	-.0233	-.0172	-.0122	
.9250	.0372	.0360	.0332	.0253	.0178	.0150	.0183	
.9750	.1684	.1621	.1480	.1273	.1035	.0815	.0728	

Table 1. continued (Wigley hull)

$-Fn = 0.289$

x/l	z/d	$-.1200$	$-.2000$	$-.3600$	$-.5200$	$-.6800$	$-.8400$	$-.9200$
$-.9750$.1968	.1884	.1695	.1485	.1242	.1003	.0896
$-.9250$.2081	.1927	.1589	.1260	.0991	.0800	.0757
$-.8750$.2515	.2181	.1647	.1255	.0971	.0785	.0738
$-.8250$.1858	.1701	.1382	.1075	.0844	.0630	.0564
$-.7500$.1059	.0942	.0732	.0560	.0444	.0394	.0412
$-.6500$.0127	.0157	.0206	.0247	.0231	.0180	.0125
$-.5500$.0831	.0836	.0830	.0802	.0741	.0635	.0564
$-.4500$.1310	.1275	.1206	.1108	.0995	.0879	.0821
$-.3500$.1372	.1309	.1198	.1074	.0965	.0850	.0803
$-.2500$.0911	.0874	.0799	.0737	.0666	.0602	.0574
$-.1500$.0219	.0231	.0244	.0274	.0283	.0281	.0291
$-.0500$.0312	.0244	.0107	.0013	.0053	.0091	.0112
$.0500$.0059	.0023	.0055	.0097	.0124	.0137	.0151
$.1500$.0458	.0450	.0413	.0388	.0349	.0315	.0314
$.2500$.0748	.0718	.0657	.0603	.0533	.0471	.0445
$.3500$.0759	.0734	.0703	.0652	.0598	.0531	.0502
$.4500$.0598	.0603	.0609	.0594	.0562	.0513	.0484
$.5500$.0408	.0434	.0468	.0498	.0500	.0453	.0409
$.6500$.0286	.0313	.0388	.0431	.0439	.0400	.0349
$.7500$.0233	.0252	.0298	.0359	.0377	.0334	.0275
$.8500$.0135	.0144	.0174	.0208	.0222	.0161	.0110
$.9250$.0316	.0311	.0300	.0233	.0166	.0144	.0181
$.9750$.1628	.1573	.1447	.1251	.1024	.0810	.0728

$Fn = 0.316$

x/l	z/d	$-.1200$	$-.2000$	$-.3600$	$-.5200$	$-.6800$	$-.8400$	$-.9200$
$-.9750$.1708	.1690	.1516	.1355	.1151	.0934	.0833
$-.9250$.2012	.1888	.1588	.1281	.1027	.0837	.0791
$-.8750$.2818	.2452	.1881	.1473	.1168	.0954	.0890
$-.8250$.2371	.2201	.1842	.1483	.1197	.0981	.0935
$-.7500$.1787	.1631	.1358	.1125	.0944	.0830	.0814
$-.6500$.0589	.0523	.0418	.0317	.0273	.0270	.0300
$-.5500$.0338	.0370	.0418	.0434	.0412	.0336	.0278
$-.4500$.1118	.1115	.1108	.1045	.0950	.0840	.0782
$-.3500$.1771	.1704	.1586	.1430	.1281	.1127	.1052
$-.2500$.1875	.1786	.1601	.1427	.1257	.1113	.1054
$-.1500$.1332	.1273	.1131	.1013	.0901	.0811	.0787
$-.0500$.0385	.0390	.0401	.0395	.0386	.0373	.0377
$.0500$.0412	.0343	.0199	.0097	.0022	.0022	.0047
$.1500$.0503	.0437	.0317	.0201	.0126	.0081	.0054
$.2500$.0110	.0289	.0036	.0020	.0042	.0049	.0049
$.3500$.0390	.0372	.0362	.0340	.0321	.0283	.0266
$.4500$.0598	.0681	.0646	.0600	.0548	.0492	.0459
$.5500$.0742	.0742	.0722	.0702	.0665	.0591	.0535
$.6500$.0515	.0628	.0670	.0678	.0652	.0583	.0520
$.7500$.0431	.0449	.0488	.0537	.0538	.0477	.0406
$.8500$.0216	.0225	.0257	.0292	.0300	.0228	.0171
$.9250$.0272	.0271	.0267	.0207	.0146	.0131	.0173
$.9750$.1634	.1583	.1463	.1272	.1046	.0835	.0756

Table 2. Calculated pressure coefficients on the hull surface of strut like hull (sharp end ahead)

Fn = 0.204							
x/l	z/d	-.0833	-.2500	-.4167	-.5833	-.7500	-.9167
-.9495	.3528	.3149	.2737	.2155	.1238	-.1816	
-.8490	.0384	.0308	.0223	.0099	-.0217	-.2244	
-.7495	-.2077	-.1913	-.1755	-.1604	-.1545	-.2462	
-.6495	-.3646	-.3352	-.3065	-.2753	-.2430	-.2401	
-.5495	-.3106	-.2897	-.2694	-.2444	-.2145	-.1870	
-.4495	-.1516	-.1483	-.1455	-.1384	-.1268	-.1120	
-.3490	-.0455	-.0505	-.0555	-.0587	-.0593	-.0581	
-.2490	-.0375	-.0398	-.0418	-.0433	-.0437	-.0435	
-.0995	-.0504	-.0483	-.0463	-.0443	-.0422	-.0405	
.1000	.0327	.0329	.0331	.0333	.0333	.0333	
.2500	.0300	.0314	.0326	.0339	.0343	.0343	
.3500	-.0446	-.0457	-.0465	-.0469	-.0461	-.0447	
.4500	-.0951	-.0934	-.0918	-.0883	-.0822	-.0743	
.5500	-.1623	-.1568	-.1518	-.1429	-.1297	-.1153	
.6505	-.2296	-.2194	-.2098	-.1953	-.1760	-.1628	
.7505	-.3020	-.2843	-.2678	-.2462	-.2215	-.2277	
.8500	-.2985	-.2736	-.2509	-.2263	-.2096	-.2937	
.9255	-.2861	-.2516	-.2216	-.2010	-.1963	-.3776	
.9630	-.0881	-.0723	-.0608	-.0755	-.0995	-.4100	
.9875	.6772	.6671	.6525	.6214	.5347	-.1037	

Fn = 0.213							
x/l	z/d	-.0833	-.2500	-.4167	-.5833	-.7500	-.9167
-.9495	.3646	.3246	.2813	.2216	.1288	-.1776	
-.8490	.0509	.0407	.0300	.0155	-.0176	-.2221	
-.7495	-.2061	-.1902	-.1744	-.1598	-.1548	-.2477	
-.6495	-.3792	-.3473	-.3162	-.2830	-.2491	-.2452	
-.5495	-.3319	-.3071	-.2834	-.2555	-.2231	-.1934	
-.4495	-.1599	-.1552	-.1511	-.1429	-.1304	-.1148	
-.3490	-.0337	-.0408	-.0479	-.0529	-.0549	-.0548	
-.2490	-.0193	-.0247	-.0298	-.0339	-.0365	-.0380	
-.0995	-.0514	-.0491	-.0469	-.0445	-.0420	-.0404	
.1000	-.0394	-.0390	-.0384	-.0380	-.0372	-.0365	
.2500	-.0322	-.0333	-.0343	-.0353	-.0357	-.0355	
.3500	-.0424	-.0438	-.0451	-.0457	-.0453	-.0441	
.4500	-.0907	-.0897	-.0887	-.0858	-.0803	-.0728	
.5500	-.1587	-.1537	-.1492	-.1409	-.1282	-.1142	
.6505	-.2295	-.2194	-.2099	-.1954	-.1760	-.1629	
.7505	-.3070	-.2883	-.2715	-.2494	-.2239	-.2297	
.8500	-.3084	-.2822	-.2578	-.2316	-.2137	-.2971	
.9255	-.2999	-.2619	-.2280	-.2052	-.1993	-.3808	
.9630	-.0941	-.0766	-.0528	-.0769	-.1009	-.4122	
.9875	.6783	.6673	.6524	.6209	.5336	-.1065	

Fn = 0.224							
x/l	z/d	-.0833	-.2500	-.4167	-.5833	-.7500	-.9167
-.9495	.3810	.3385	.2923	.2303	.1360	-.1714	
-.8490	.0598	.0561	.0423	.0250	-.0105	-.2175	
-.7495	-.1990	-.1845	-.1699	-.1563	-.1526	-.2473	
-.6495	-.3940	-.3597	-.3259	-.2905	-.2553	-.2507	
-.5495	-.3609	-.3312	-.3026	-.2702	-.2343	-.2019	
-.4495	-.1773	-.1698	-.1624	-.1515	-.1366	-.1192	
-.3490	-.0219	-.0305	-.0391	-.0456	-.0487	-.0496	
-.2490	.0149	.0044	-.0058	-.0142	-.0206	-.0251	
-.0995	-.0349	-.0343	-.0335	-.0327	-.0319	-.0317	
.1000	-.0498	-.0481	-.0463	-.0445	-.0427	-.0428	
.2500	-.0473	-.0465	-.0457	-.0451	-.0439	-.0427	
.3500	-.0529	-.0530	-.0533	-.0531	-.0519	-.0499	
.4500	-.0935	-.0926	-.0918	-.0892	-.0834	-.0759	
.5500	-.1567	-.1528	-.1490	-.1413	-.1292	-.1154	
.6505	-.2279	-.2186	-.2099	-.1960	-.1770	-.1640	
.7505	-.3116	-.2927	-.2757	-.2530	-.2271	-.2523	
.8500	-.3222	-.2937	-.2672	-.2391	-.2194	-.3019	
.9255	-.3211	-.2777	-.2386	-.2122	-.2046	-.3853	
.9630	-.1050	-.0843	-.0672	-.0800	-.1034	-.4159	
.9875	.6794	.6674	.6517	.6196	.5318	-.1102	

Table 2. continued (strut like hull, sharp end ahead)

 $Fn = 0.236$

x/l	z/d	-.0833	-.2500	-.4167	-.5833	-.7500	-.9167
-.9495	.4010	.3556	.3063	.2416	.1461	-.1620	
-.8490	.0963	.0780	.0599	.0390	.0006	-.2093	
-.7495	-.1834	-.1713	-.1587	-.1474	-.1461	-.2434	
-.6495	-.4037	-.3676	-.3316	-.2946	-.2586	-.2539	
-.5495	-.3934	-.3581	-.3239	-.2864	-.2464	-.2108	
-.4495	-.2067	-.1937	-.1813	-.1657	-.1467	-.1263	
-.3490	-.0198	-.0277	-.0357	-.0416	-.0444	-.0449	
-.2490	.0571	.0415	.0261	.0128	.0023	-.0055	
-.0995	.0121	.0083	.0046	.0003	-.0035	-.0074	
.1000	-.0518	-.0496	-.0473	-.0449	-.0425	-.0400	
.2500	-.0776	-.0731	-.0686	-.0647	-.0607	-.0568	
.3500	-.0895	-.0855	-.0816	-.0773	-.0726	-.0676	
.4500	-.1205	-.1172	-.1140	-.1090	-.1010	-.0914	
.5500	-.1680	-.1642	-.1605	-.1524	-.1398	-.1253	
.6505	-.2283	-.2202	-.2129	-.2002	-.1818	-.1691	
.7505	-.3112	-.2934	-.2775	-.2557	-.2303	-.2055	
.8500	-.3338	-.3035	-.2755	-.2459	-.2252	-.2067	
.9255	-.3498	-.2990	-.2524	-.2216	-.2112	-.1912	
.9630	-.1259	-.0993	-.0758	-.0558	-.1077	-.4209	
.9875	.6787	.6659	.6499	.6175	.5291	-.1152	

 $Fn = 0.250$

x/l	z/d	-.0833	-.2500	-.4167	-.5833	-.7500	-.9167
-.9495	.4267	.3776	.3242	.2564	.1595	-.1485	
-.8490	.1336	.1090	.0851	.0594	.0174	-.1958	
-.7495	-.1555	-.1474	-.1384	-.1308	-.1333	-.2344	
-.6495	-.4045	-.3675	-.3303	-.2930	-.2575	-.2537	
-.5495	-.4282	-.3869	-.3465	-.3038	-.2596	-.2210	
-.4495	-.2526	-.2320	-.2118	-.1894	-.1646	-.1392	
-.3490	-.0422	-.0440	-.0480	-.0499	-.0494	-.0472	
-.2490	.0879	.0701	.0520	.0362	.0233	.0130	
-.0995	.0689	.0777	.0666	.0546	.0431	.0327	
.1000	-.0237	-.0233	-.0231	-.0229	-.0229	-.0229	
.2500	-.1029	-.0957	-.0885	-.0818	-.0753	-.0694	
.3500	-.1481	-.1374	-.1267	-.1159	-.1054	-.0956	
.4500	-.1845	-.1747	-.1648	-.1532	-.1394	-.1246	
.5500	-.2158	-.2080	-.2001	-.1882	-.1716	-.1535	
.6505	-.2485	-.2404	-.2327	-.2192	-.2001	-.1868	
.7505	-.3093	-.2942	-.2806	-.2606	-.2370	-.2136	
.8500	-.3341	-.3047	-.2777	-.2488	-.2287	-.2112	
.9255	-.3785	-.3197	-.2552	-.2294	-.2167	-.1967	
.9630	-.1571	-.1204	-.0867	-.0922	-.1122	-.4269	
.9875	.6762	.6625	.6468	.6144	.5253	-.1226	

Table 3. Calculated pressure coefficients on the hull surface of strut like hull (blunt end ahead)

$Fn = 0.204$							
x/l	z/d	-.0833	-.2500	-.4167	-.5833	-.7500	-.9167
-.9870		.7456	.7199	.6852	.6416	.5448	-.0851
-.9620		.1847	.1312	.0713	.0210	-.0395	-.3719
-.9245		-.0072	-.0460	-.0867	-.1163	-.1465	-.3448
-.8490		-.2583	-.2413	-.2232	-.2060	-.1964	-.2964
-.7495		-.5015	-.4390	-.3780	-.3250	-.2786	-.2686
-.6495		-.3595	-.3247	-.2916	-.2568	-.2209	-.1948
-.5495		-.0681	-.0847	-.1021	-.1110	-.1096	-.1029
-.4495		.0314	.0075	-.0164	-.0335	-.0435	-.0476
-.3490		-.0610	-.0572	-.0534	-.0506	-.0485	-.0467
-.2490		-.1292	-.1129	-.0965	-.0828	-.0718	-.0632
-.0995		-.0632	-.0607	-.0581	-.0552	-.0520	-.0491
.1000		-.0064	-.0098	-.0131	-.0166	-.0196	-.0221
.2500		-.0172	-.0207	-.0242	-.0271	-.0290	-.0300
.3500		-.0549	-.0555	-.0562	-.0558	-.0540	-.0516
.4500		-.1471	-.1422	-.1374	-.1293	-.1172	-.1022
.5500		-.2595	-.2469	-.2349	-.2167	-.1922	-.1693
.6505		-.3144	-.2946	-.2763	-.2524	-.2255	-.2262
.7505		-.2186	-.2010	-.1848	-.1679	-.1594	-.2482
.8500		-.0266	-.0220	-.0192	-.0222	-.0462	-.2430
.9500		.2769	.2554	.2313	.1861	.1006	-.2062

$Fn = 0.213$							
x/l	z/d	-.0833	-.2500	-.4167	-.5833	-.7500	-.9167
-.9870		.7542	.7271	.6908	.6458	.5487	-.0814
-.9620		.2121	.1531	.0877	.0331	-.0303	-.3650
-.9245		-.0253	-.0195	-.0664	-.1012	-.1356	-.3374
-.8490		-.2286	-.2182	-.2057	-.1936	-.1879	-.2920
-.7495		-.5099	-.4454	-.3817	-.3280	-.2821	-.2737
-.6495		-.4048	-.3632	-.3236	-.2827	-.2419	-.2121
-.5495		-.1183	-.1280	-.1390	-.1414	-.1340	-.1220
-.4495		.0219	.0010	-.0240	-.0404	-.0494	-.0526
-.3490		-.0176	-.0202	-.0227	-.0262	-.0297	-.0326
-.2490		-.0737	-.0572	-.0507	-.0553	-.0513	-.0480
-.0995		-.0925	-.0863	-.0820	-.0733	-.0668	-.0609
.1000		-.0290	-.0302	-.0314	-.0324	-.0335	-.0339
.2500		-.0074	-.0125	-.0177	-.0220	-.0253	-.0274
.3500		-.0346	-.0381	-.0419	-.0440	-.0445	-.0440
.4500		-.1320	-.1287	-.1258	-.1194	-.1088	-.0951
.5500		-.2556	-.2429	-.2311	-.2128	-.1887	-.1661
.6505		-.3201	-.2993	-.2795	-.2546	-.2268	-.2269
.7505		-.2268	-.2078	-.1901	-.1720	-.1624	-.2510
.8500		-.0298	-.0251	-.0218	-.0245	-.0482	-.2460
.9500		.2784	.2567	.2325	.1871	.1010	-.2073

$Fn = 0.224$							
x/l	z/d	-.0833	-.2500	-.4167	-.5833	-.7500	-.9167
-.9870		.7657	.7369	.6982	.6517	.5541	-.0761
-.9620		.2509	.1837	.1100	.0499	-.0170	-.3547
-.9245		.0695	.0169	-.0377	-.0796	-.1189	-.3255
-.8490		-.1869	-.1847	-.1792	-.1734	-.1733	-.2827
-.7495		-.5095	-.4439	-.3788	-.3251	-.2807	-.2742
-.6495		-.4538	-.4033	-.3554	-.3071	-.2612	-.2273
-.5495		-.1731	-.1745	-.1782	-.1734	-.1593	-.1417
-.4495		.0085	-.0142	-.0370	-.0517	-.0584	-.0532
-.3490		.0092	.0053	.0018	.0038	-.0099	-.0155
-.2490		.0082	.0055	.0026	.0021	-.0070	-.0118
-.0995		-.0526	-.0516	-.0504	-.0487	-.0463	-.0441
.1000		-.0799	-.0752	-.0707	-.0656	-.0612	-.0569
.2500		-.0480	-.0480	-.0482	-.0484	-.0480	-.0472
.3500		-.0480	-.0511	-.0544	-.0561	-.0562	-.0548
.4500		-.1277	-.1269	-.1262	-.1215	-.1122	-.0993
.5500		-.2522	-.2411	-.2307	-.2140	-.1907	-.1687
.6505		-.3290	-.3071	-.2867	-.2609	-.2324	-.2318
.7505		-.2427	-.2216	-.2017	-.1816	-.1707	-.2584
.8500		-.0395	-.0339	-.0293	-.0312	-.0545	-.2529
.9500		.2777	.2557	.2316	.1855	.0990	-.2112

Table 3. continued (strut like hull, blunt end ahead)

$Fn = 0.236$							
x/l	z/d	-.0833	-.2500	-.4167	-.5833	-.7500	-.9167
-.9870		.7794	.7489	.7072	.6589	.5610	-.0688
-.9620		.2995	.2218	.1372	.0705	-.0005	-.3412
-.9245		.1238	.0613	-.0029	-.0523	-.0977	-.3093
-.8490		-.1368	-.1435	-.1454	-.1466	-.1531	-.2685
-.7495		-.4984	-.4334	-.3679	-.3154	-.2734	-.2702
-.6495		-.4991	-.4395	-.3829	-.3274	-.2765	-.2391
-.5495		-.2347	-.2258	-.2198	-.2054	-.1849	-.1611
-.4495		-.0070	-.0302	-.0536	-.0671	-.0713	-.0691
-.3490		.0191	.0156	.0120	.0070	.0015	-.0037
-.2490		.0613	.0590	.0569	.0491	.0393	.0290
-.0995		.0593	.0477	.0359	.0243	.0145	.0055
.1000		-.1131	-.1045	-.0960	-.0868	-.0782	-.0707
.2500		-.1330	-.1220	-.1110	-.1016	-.0929	-.0853
.3500		-.1161	-.1118	-.1077	-.1025	-.0965	-.0899
.4500		-.1575	-.1561	-.1545	-.1486	-.1376	-.1230
.5500		-.2575	-.2491	-.2411	-.2252	-.2041	-.1825
.6505		-.3963	-.3152	-.2958	-.2706	-.2427	-.2123
.7505		-.2617	-.2388	-.2170	-.1949	-.1828	-.2695
.8500		-.0561	-.0493	-.0428	-.0431	-.0657	-.2641
.9500		.2726	.2505	.2267	.1806	.0935	-.2187

$Fn = 0.250$							
x/l	z/d	-.0833	-.2500	-.4167	-.5833	-.7500	-.9167
-.9870		.7968	.7638	.7183	.6676	.5692	-.0599
-.9620		.3663	.2720	.1709	.0955	.0192	-.3251
-.9245		.1929	.1166	.0406	-.0194	-.0721	-.2897
-.8490		-.0764	-.0935	-.1036	-.1138	-.1279	-.2511
-.7495		-.4815	-.4167	-.3516	-.3012	-.2626	-.2638
-.6495		-.5455	-.4769	-.4115	-.3488	-.2928	-.2526
-.5495		-.3133	-.2918	-.2741	-.2495	-.2190	-.1881
-.4495		-.0442	-.0650	-.0867	-.0971	-.0975	-.0910
-.3490		.0225	.0140	.0054	-.0010	-.0057	-.0089
-.2490		.0540	.0615	.0690	.0670	.0598	.0501
-.0995		.1775	.1553	.1329	.1093	.0881	.0695
.1000		-.0699	-.0563	-.0429	-.0384	-.0340	-.0499
.2500		-.2002	-.1814	-.1623	-.1450	-.1295	-.1158
.3500		-.2183	-.2011	-.1843	-.1672	-.1508	-.1358
.4500		-.2351	-.2299	-.2166	-.2032	-.1855	-.1649
.5500		-.2890	-.2807	-.2727	-.2569	-.2336	-.2100
.6505		-.3415	-.3235	-.3068	-.2839	-.2573	-.2376
.7505		-.2731	-.2496	-.2279	-.2058	-.1940	-.2811
.8500		-.0735	-.0648	-.0566	-.0550	-.0771	-.2759
.9500		.2647	.2430	.2199	.1744	.0866	-.2282

Table 4-a Wave profiles on the hull surface (Wigley hull)

	$Fn=0.250$	$Fn=0.267$	$Fn=0.289$	$Fn=0.316$
-.975	.0144	.0159	.0184	.0185
-.925	.0158	.0182	.0215	.0225
-.875	.0139	.0185	.0220	.0275
-.825	.0073	.0113	.0185	.0263
-.750	.0012	.0041	.0103	.0203
-.650	-.0047	-.0039	-.0008	.0070
-.550	-.0057	-.0071	-.0072	-.0032
-.450	-.0046	-.0079	-.0115	-.0115
-.350	-.0025	-.0057	-.0123	-.0188
-.250	-.0007	-.0019	-.0081	-.0200
-.150	-.0007	.0009	-.0017	-.0141
-.050	-.0028	.0005	.0035	-.0037
.050	-.0047	-.0042	.0009	.0051
.150	-.0046	-.0064	-.0039	.0060
.250	-.0036	-.0056	-.0066	.0014
.350	-.0029	-.0041	-.0067	-.0042
.450	-.0025	-.0029	-.0050	-.0073
.550	-.0022	-.0022	-.0031	-.0075
.650	-.0020	-.0020	-.0021	-.0060
.750	-.0017	-.0019	-.0018	-.0042
.850	-.0005	-.0010	-.0011	-.0021
.925	.0029	.0028	.0027	.0027
.975	.0114	.0126	.0142	.0170

Table 4-b. Wave profiles on the hull surface (Strut like hull, sharp end ahead)

	$Fn=0.204$	$Fn=0.213$	$Fn=0.224$	$Fn=0.236$	$Fn=0.250$
-.950	.0155	.0174	.0202	.0236	.0282
-.850	.0018	.0025	.0038	.0059	.0091
-.750	-.0090	-.0097	-.0104	-.0106	-.0100
-.650	-.0158	-.0179	-.0206	-.0235	-.0264
-.550	-.0134	-.0156	-.0189	-.0229	-.0281
-.450	-.0064	-.0074	-.0091	-.0119	-.0164
-.350	-.0018	-.0014	-.0009	-.0009	-.0024
-.250	-.0015	-.0008	.0010	.0036	.0060
-.100	-.0021	-.0024	-.0018	.0008	.0059
.100	-.0014	-.0018	-.0025	-.0029	-.0015
.250	-.0012	-.0014	-.0024	-.0044	-.0067
.350	-.0018	-.0019	-.0026	-.0051	-.0096
.450	-.0040	-.0041	-.0047	-.0068	-.0118
.550	-.0069	-.0073	-.0080	-.0095	-.0137
.650	-.0098	-.0106	-.0117	-.0129	-.0158
.750	-.0129	-.0144	-.0161	-.0178	-.0198
.850	-.0129	-.0146	-.0169	-.0194	-.0218
.926	-.0126	-.0145	-.0172	-.0209	-.0255
.963	-.0040	-.0047	-.0058	-.0077	-.0110
.987	.0284	.0310	.0344	.0382	.0427

Table 4-c. Wave profiles on the hull surface (Strut like hull, blunt end ahead)

	$Fn=0.204$	$Fn=0.213$	$Fn=0.224$	$Fn=0.236$	$Fn=0.250$
-.987	.0316	.0348	.0391	.0443	.0508
-.962	.0088	.0110	.0143	.0188	.0258
-.925	.0005	.0022	.0048	.0086	.0144
-.850	-.0111	-.0106	-.0094	-.0074	-.0042
-.750	-.0222	-.0246	-.0272	-.0296	-.0323
-.650	-.0157	-.0193	-.0241	-.0295	-.0363
-.550	-.0025	-.0051	-.0087	-.0133	-.0203
-.450	.0018	.0015	.0010	.0003	-.0021
-.350	-.0026	-.0007	.0006	.0012	.0017
-.250	-.0057	-.0035	.0005	.0035	.0031
-.100	-.0027	-.0045	-.0027	.0036	.0118
.100	-.0002	-.0013	-.0041	-.0065	-.0045
.250	-.0006	-.0002	-.0024	-.0077	-.0131
.350	-.0023	-.0015	-.0023	-.0066	-.0142
.450	-.0062	-.0061	-.0064	-.0088	-.0150
.550	-.0111	-.0119	-.0129	-.0146	-.0183
.650	-.0135	-.0150	-.0171	-.0193	-.0219
.750	-.0095	-.0107	-.0127	-.0152	-.0178
.850	-.0012	-.0015	-.0021	-.0033	-.0049
.950	.0120	.0131	.0145	.0158	.0172

Table 5. Calculated wave resistance coefficients

Wigley hull

Fn	$K_o L$	$C_w \times 10^3$
0.250	16	0.1269
0.267	14	0.1518
0.289	12	0.2034
0.316	10	0.3289

Strut like hull

Fn	$K_o L$	$C_w \times 10^3$	
		Sharp end ahead	Blunt end ahead
0.204	24	0.3807	0.3303
0.213	22	0.4508	0.4246
0.224	20	0.5717	0.6216
0.236	18	0.7568	0.9209
0.250	16	1.0270	1.2850

THE XYZ FREE SURFACE PROGRAM AND ITS APPLICATION
TO TRANSOM-STERN SHIPS WITH BOW DOMES

Bill H. Cheng
Janet S. Dean
John L. Jayne

David W. Taylor Naval Ship Research and Development Center
Bethesda, Maryland 20084

INTRODUCTION

The XYZ Free Surface Program (XYZFS) is a versatile ship design tool which can be used to predict the wave resistance characteristics of a wide variety of hull forms. XYZFS can analyze surface ships with cruiser or transom sterns as well as submerged vehicles. The program uses a Rankine source panel method to compute three-dimensional, steady potential flow about ship hulls. XYZFS calculates the local flow field, wave resistance and wave patterns for ships moving at a constant speed corresponding to a Froude number of 0.2 to 0.6. An estimate of residual resistance can also be obtained. The program is designed to allow calculations both for ships which are held fixed and for ships which are allowed to sink and trim in response to hydrodynamic forces.

XYZFS was originally developed by the late Charles W. Dawson at the David W. Taylor Naval Ship Research and Development Center (DTNSRDC). He successfully applied the original version of the program to a number of ship hulls including all five of the test cases for the 1979 Workshop on Ship Wave Resistance Computations.¹ These workshop cases consisted of the high-speed Athena transom stern hull, the Wigley parabolic hull, the Inuid hull, the Series 60 cruiser-stern hull, and the low-speed HSVA tanker. XYZFS was one of the most successful programs for predicting wave resistance at the 1979 Workshop. Its flexibility and ease of use contributed to this success, but three other desirable features were most responsible for its accuracy as a ship design tool. First, XYZFS satisfies the Neumann boundary condition exactly on the ship's hull to include what naval architects refer to as the sheltering effect. By contrast classical thin-ship theory satisfies the boundary condition on the ship's centerline. Second, XYZFS takes into account the non-uniform flow generated by the ship hull by using a

double-model linearization of the free-surface boundary condition. Finally, some weakly nonlinear effects are retained in the free-surface boundary condition. In addition to the papers by Dawson,^{2,3} reports by Gadd,^{4,5} Tulin,^{6,7} Dean,⁸ Yeung,⁹ and Mori¹⁰ have covered the program and its methodology. Dawson's free-surface boundary condition was also studied by Katazawa,¹¹ Mori,¹² and Baba.¹³

The present authors have further developed XYZFS by making substantial improvements to its computational techniques. A new method for satisfying the transom boundary conditions has resulted in a more realistic model of the physical problem and an improved prediction of wave resistance. A better procedure for calculating bow and stern heights has led to a closer agreement with experimental values. Conversion of the program to a Cray-1S supercomputer has allowed a greater resolution of the hull and free-surface geometries and a new capability for hulls with bow domes. A direct matrix solver written by Thomas Jordan of the Los Alamos National Laboratory has helped to make the Cray version of the program extremely efficient. The enhanced version of XYZFS has been applied to many additional hull forms. In the current study, the program is used to evaluate the relative merits of two hull designs at various speeds. The results illustrate the usefulness of XYZFS for practical ship design problems involving transom-stern hulls with bow domes.

COMPUTATIONAL PROCEDURE

The application of XYZFS to a specific ship hull begins with the selection of an appropriate geometric modeling technique. For instance, a ship's blueprint can be digitized by using an interactive graphics system and a digitizing board to create the x, y, z coordinates of points on the hull. This hull geometry data and a few parameters are all that is then required to begin the calculation. The program will automatically take care of the panelling of the free surface and the repositioning of the ship for sinkage and trim. Note that only half of the ship and free surface are modeled since a plane of symmetry exists about the ship's centerline ($y = 0$).

The XYZFS calculation begins by using the input hull geometry to perform a surface representation of the ship hull. Flat, four-sided panels are constructed from the ship coordinate data to closely approximate the actual hull geometry.

Each panel is characterized by its centroid, normal vector, and surface area. The influence coefficients are then calculated as a function of panel geometry and the distance between panel centroids. This procedure is based on the panel method developed by Hess and Smith.¹⁴

The double-model problem, consisting of the flow of an infinite fluid about the hull and its reflection above a rigid free surface, is then solved as a boundary-value problem with a matrix formulation. The double-model source densities are found by using Jordan's direct matrix solver and are used to calculate the double-model velocity vectors at the free surface. A Runge-Kutta method is then used to trace double-model streamlines based on these velocity vectors. This technique insures that the streamlines will go around the ship hull rather than penetrate it. Free-surface panels are constructed by using these double-model streamlines as one coordinate of a two-dimensional grid. Smaller panels can be placed near the hull, resulting in computational savings through the use of a variable grid.

XYZFS next proceeds to solve the "complete" problem of flow about the hull and free surface with wave effects included. A new boundary-value problem for the total velocity potential is set up as a matrix formulation using the free-surface boundary condition and four-point upstream finite-difference operator derived by Dawson.² Jordan's direct matrix solver is again used to calculate the source densities. The system of equations being solved is extremely large since its order is the total number of hull and free-surface panels which can be as high as 900.

The velocity vectors and pressures are then calculated from the source densities, and an integration of the pressure along the hull surface completes the calculation of the wave resistance coefficient. The wave profiles are found by computing the wave elevation from the dynamic boundary condition. A prediction of residual resistance is made by approximating viscous effects according to the 1957 ITTC formula and a modification of Granville's form factor.³

The preceding calculations give the results for the fixed model case. The sinkage force and trim moment are also calculated and used to predict the bow and stern levels which the ship would experience if it were left free to sink and trim. These bow and stern levels can then be used to reposition the ship geometry data to correspond to the sunk and trimmed ship. The new hull is then analyzed in the

same way as for the fixed case to determine the wave resistance and local flow field for the sunk and trimmed ship. The wave resistance prediction for the sunk and trimmed hull is not based on a simple correction to the fixed hull results, but rather is based on a complete calculation for the sunk and trimmed hull geometry.

TRANSOM-STERN METHODOLOGY

The last section discussed the XYZFS computational procedure in general. This section presents special considerations for transom-stern hulls. Transom sterns have received considerable attention in the design of high-speed naval ships because of the potential for energy conservation and low drag at high Froude numbers.

Saunders¹⁵ noticed that a depression in the free surface occurs behind a transom-stern hull and forms a phantom afterbody to yield a lower effective Froude number. This implies that the flow detaches smoothly at the edge of the transom for high speeds and no recirculating flow appears in the stern region. In their numerical computations, Gadd⁵ and Chang¹⁶ simulate the surface depression by adding a tapering extension to close the body behind the transom. Their wave resistance calculations consist of contributions from the hull up to the transom location, excluding the tapering extension. Instead of using a tapering extension as a phantom afterbody, Yim¹⁷ models the edge of a transom stern by a line sink where the source density is assumed to be a linear function of transom depth. Dawson³ enforced the condition of flow detachment by requiring that all water flowing across the second column of panels from the transom must pass through the transom edge and then be absorbed by the free-surface panels. A two-point extrapolation formula was used to impose this constraint at the edge of the transom. According to Dawson,³ "the source density on the (free-surface) panels next to the transom is determined so that the pressure at the edge of the transom is approximately zero (atmospheric)". Unfortunately, this original transom boundary condition sometimes caused difficulty in the XYZFS computations. For example, Wilson and Thomason¹⁸ report cases of unreasonably high wave resistance values at certain Froude numbers. Whenever this wave resistance anomaly occurred, high velocities and large jumps in source density were detected directly behind the transom and the pressure in that region was far from atmospheric.

Accordingly a new method for satisfying the transom boundary condition has been incorporated into the current version of the XYZFS Program. The pressure at the edge of the transom is forced to be atmospheric identically from the outset, while the flow leaving the transom edge is assumed to be tangential to the ship hull in a way consistent with the Neumann boundary condition on the hull. It can be shown that the velocity vector at the transom edge is completely determined a priori, depends explicitly on Froude number and transom depth, and is implicitly a function of the transom stern geometry (e.g., buttock angle, deadrise angle, and run angle). On the other hand, the source density on the free-surface panels behind the transom is determined only after the complete problem is solved. This new approach to the boundary conditions gives an excellent prediction of wave resistance and wave profile for transom stern flows, as shown in the following section.

RESULTS

The present study concerns the relative merits of two alternate hull forms over a speed range of interest to the Navy. The two alternate designs, designated as Hull A and Hull B, represent two concepts for the stern design. Hull B has a smaller transom area and transom immersion than Hull A. Hull A and Hull B have identical bow domes. For the XYZFS calculations, a total of 660 panels have been used to model the hull and free surface. Of these, 192 panels (8 panels at each of 24 stations) have been placed on the hull, 100 panels (10 panels at each of 10 stations) have been added for the bow dome, 320 panels (8 panels at each of 40 stations) have been used for the main portion of the free surface, and 48 panels in an 8 by 6 array have been placed on a special portion of the free surface immediately behind the transom stern. This panelling arrangement encompasses a computational domain which extends $1/2$ of a ship's length forward and aft of the hull and $3/8$ of a ship's length to each side. Figure 1 illustrates the XYZFS panelling of Hull A by showing a side view of the forward fifth of the hull with the attached bow dome. Notice that smaller panels are concentrated near the design water line in order to resolve the wave-like motion. For consistency, the spacing and location of the panels have been chosen to be virtually identical for the two hulls being studied.

Table 1 gives the computed wave resistance coefficients for Hull A and Hull B. The Froude number range is from 0.25 to 0.50 with an increment of 0.05. The

wave resistance values corresponding to fixed cases are presented in the first two columns. Similar predictions are given in a parallel study by von Kerczek, Scragg and Stern¹⁹ using a slender-body theory. Unfortunately, wave-cut analysis data are not available for comparison. The wave resistance values corresponding to sunk and trimmed cases are computed after repositioning the ship according to the predictions of bow and stern levels as specified in Table 2.

A comparison with corresponding experimental values²⁰ of bow and stern levels is displayed in Figure 2. Notice the excellent agreement between computed and experimental values below Froude number 0.40. An important feature of this comparison is that the cross-over points, where the trim coefficient is zero, are accurately predicted. Table 2 presents the sinkage and trim coefficients derived from the bow and stern levels. The computation predicts that for both ships the bow trims down for lower Froude numbers and the bow trims up for higher Froude numbers.

Table 3 gives the results of residual resistance coefficients C_R for Hull A and Hull B. The partial form factor K_p , the ratio of wetted surface area, and frictional resistance based on the 1957 ITTC line are also tabulated. A comparison of the computed residual resistance coefficient with the corresponding experimental value is displayed in Figure 3. The agreement is remarkable. In the case of Hull A, the computed values of C_R slightly underestimate the experimental values for Froude numbers above 0.35. At lower speeds the XYZFS results overestimate the experimental values. In the case of Hull B, the agreement above Froude number 0.35 is almost exact, while the computed values overshoot at lower speeds. Based on this comparison, one may conclude that the agreement above $F_n = 0.35$ is excellent while the agreement at lower Froude numbers is encouraging. This conclusion may be related to the assumption of flow breaking clean at the transom edge at high Froude numbers. In the low Froude number range ($F_n < 0.30$) the transom may not clear the water. Additional work is needed to improve these results. Figure 4 gives the relative difference in C_R between Hull A and Hull B as a function of Froude number. The cross-over points are about 0.253 and 0.353, implying that Hull A performs better in terms of resistance consideration above Froude number 0.353 and that Hull B performs better between the range $F_n = 0.253$ and $F_n = 0.353$. The corresponding cross-over points in the experimental data are 0.188 and 0.382.

Table 4 gives the computed wave profiles along the hull from the bow to stern. Figure 5 gives a visual display of the same data in graphical form. Note that the XYZFS predictions show that for ships with bow domes there is a kink in the bow wave system, a fact confirmed by experiments.²⁰ At Froude numbers under 0.40, the kink may be below the mean water line ($z = 0$ line), while at high Froude numbers the kink is above this level. On the other hand, as the Froude number increases, the wave trough behind the bow wave becomes deeper and the maximum amplitude moves toward the stern, indicating longer wave lengths. For all fixed cases, the wave profiles directly at the stern always recover to a small but positive value above the mean level. For sunk and trimmed cases at high Froude numbers, the stern is located significantly below the mean water level, and the wave profiles do not recover to a positive value at the stern. Note that at the stern the amplitude of the wave height for Hull B is equal to or greater than the corresponding value for Hull A, a fact again confirmed by experimental data.²⁰

Table 5 gives the stern wave profiles along a constant y close to the center line. Figure 6 presents the same data in graphical form. Note that the stern wave originates from the edge of the transom with negative values and rises to zero. This is an indication that the fluid immediately behind the transom comes up to the free surface with an upward velocity component, which is related to a distribution of sinks on this part of the free surface. The stern wave profile passes through the zero point, increases to a maximum positive value, and decreases to zero again. The wave length of the stern wave increases with increasing Froude number. Finally, Figure 7 presents the three-dimensional perspective view of the wave pattern for Hull A at Froude number 0.35.

CONCLUSION

The results for the two selected hull forms show that XYZFS can now be used for realistic ship models including transom-stern hulls with bow domes. The excellent wave resistance predictions can be largely attributed to recent improvements in the program's computational techniques. However, the further development of the XYZFS program continues to build on the solid foundation provided by Dawson's pioneering work.

ACKNOWLEDGMENT

This work was supported by the Ships, Subs and Boats Program sponsored by the Naval Sea Systems Command (NAVSEA). The authors wish to thank Mr. William Sandberg of NAVSEA for his support and encouragement during the course of this study. The authors would also like to thank Mr. Samuel Ohring of DTNSRDC for studying available numerical methods and acquiring an appropriate matrix solver and Mr. Michael Brabanski of DTNSRDC for installing the selected routine.

REFERENCES

1. Bai, K.J. and J.H. McCarthy, Proc. of the Workshop on Ship Wave-Resistance Computations, DTNSRDC, Bethesda, Md. 20084, Nov 1979.
2. Dawson, C., "A Practical Computer Method for Solving Ship Wave Problems," Proc. 2nd Int. Conf. on Numerical Ship Hydrodynamics, Sep 1977.
3. Dawson, C., "Calculations with the XYZ Free Surface Program for Five Ship Models," Proc. of the Workshop on Ship Wave Resistance Computations, DTNSRDC, Bethesda, Md. 20084, Nov 1979.
4. Gadd, G.E., "A Method of Computing the Flow and Surface Wave Pattern Around Full Forms," Trans. RINA, vol. 118, 1976, p. 207.
5. Gadd, G.E., "A Convenient Method for Estimating Wave Resistance, and its Variation with Small Changes of Hull Shape, for a Wide Range of Ship Types," Shipbuilding Marine Technology Monthly, vol. 28, Nov 1981.
6. Tulin, M.P., "Wave Resistance - State of the Art 1980," Proceedings of the Continued Workshop on Ship Wave-Resistance Computations, Izu Shuzenji, Japan, Oct 1980.
7. Tulin, M.P., "An Exact Theory of Gravity Wave Generation by Moving Bodies, its Approximation, and its Implications," 14th Symposium on Naval Hydrodynamics, Ann Arbor, Mi., Aug 1982.
8. Dean, J.S., "Ship Wave Resistance Predictions with the XYZ Free Surface Program," Proc. Symposium on Computers in Flow Predictions and Fluid Dynamics Experiments, Am. Soc. Mech. Eng. Winter Annual Meeting, Wash., D.C., Nov 1981.
9. Yeung, R., "Numerical Methods in Free-Surface Flows," Ann. Rev. Fluid Mech., vol. 14, 1982, pp. 395-442.
10. Mori, K., "Calculation of Wave Resistance and Sinkage by Rankine-Source Method," IIHR Report No. 262, May 1983.

11. Katazawa, T., "On the Linearization of the Free Surface Condition," Proc. of the Workshop on Ship Wave-Resistance Computations, DTNSRDC, Bethesda, Md. 20084, Nov 1979, APPENDIX.
12. Mori, K., "On the Double-Hull Linearization Free Surface Condition," Proc. of the Workshop on Ship Wave-Resistance Computations, DTNSRDC, Bethesda, Md. 20084, Nov 1979, APPENDIX.
13. Baba, E., "On the Free-Surface Conditions Used by Nakatake, et al., and Dawson," Proc. of the Workshop on Ship Wave-Resistance Computations, DTNSRDC, Bethesda, Md. 20084, Nov 1979, APPENDIX.
14. Hess, J.L. and A.M.O. Smith, "Calculation of Potential Flow About Arbitrary Bodies," Pergamon Press Series, Progress in Aeronautical Science, vol. 8, 1966.
15. Saunders, H.E., Hydrodynamics in Ship Design, SNAME, vol. 1, 1957, pp. 326-327.
16. Chang, M.S., "Wave Resistance Predictions by Using a Singularity Method," Proc. of the Workshop on Ship Wave-Resistance Computations, DTNSRDC, Bethesda, Md., 20084, Nov 1979.
17. Yim, B., "Wavemaking Resistance of Ships with Transom Stern," 8th Symposium on Naval Hydrodynamics, Pasadena, Ca., 1970.
18. Wilson, M.B. and T.P. Thomason, "Resistance Characteristics of Transom Stern Ships," DTNSRDC, SPD Progress Report, Apr 1982.
19. von Kerczek, C., C. Scragg, and F. Stern, "A Comparative Study of the Resistance of Two Destroyer Hull Forms," NAVSEA Technical Note 051-55W-TN-0001, Mar 1983.
20. von Kerczek, C., F. Stern, C. Scragg, and W. Sandberg, "Resistance Calculation for Destroyer Hull Forms," SNAME, Chesapeake Section, Dec 1983.

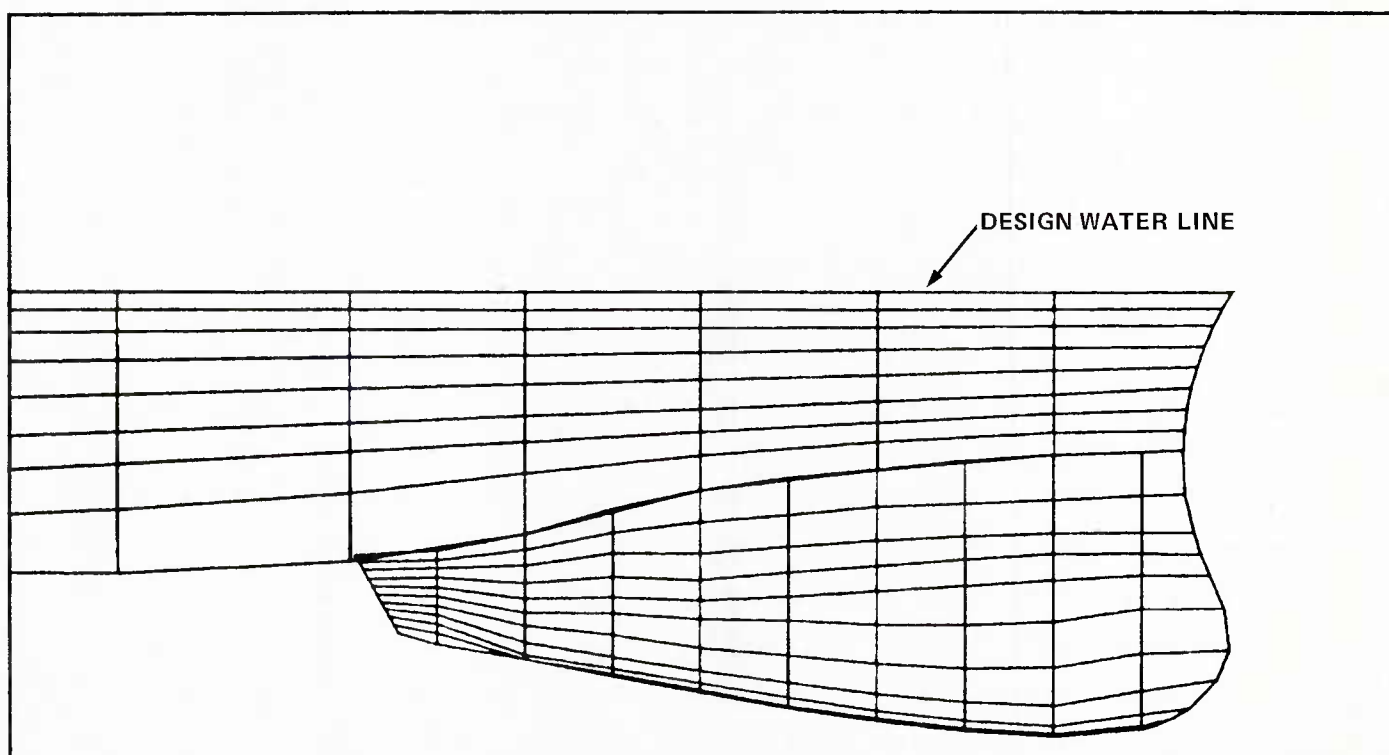


Figure 1 - XYZFS Panelling of Hull A Showing the Forward 1/5 of the Model

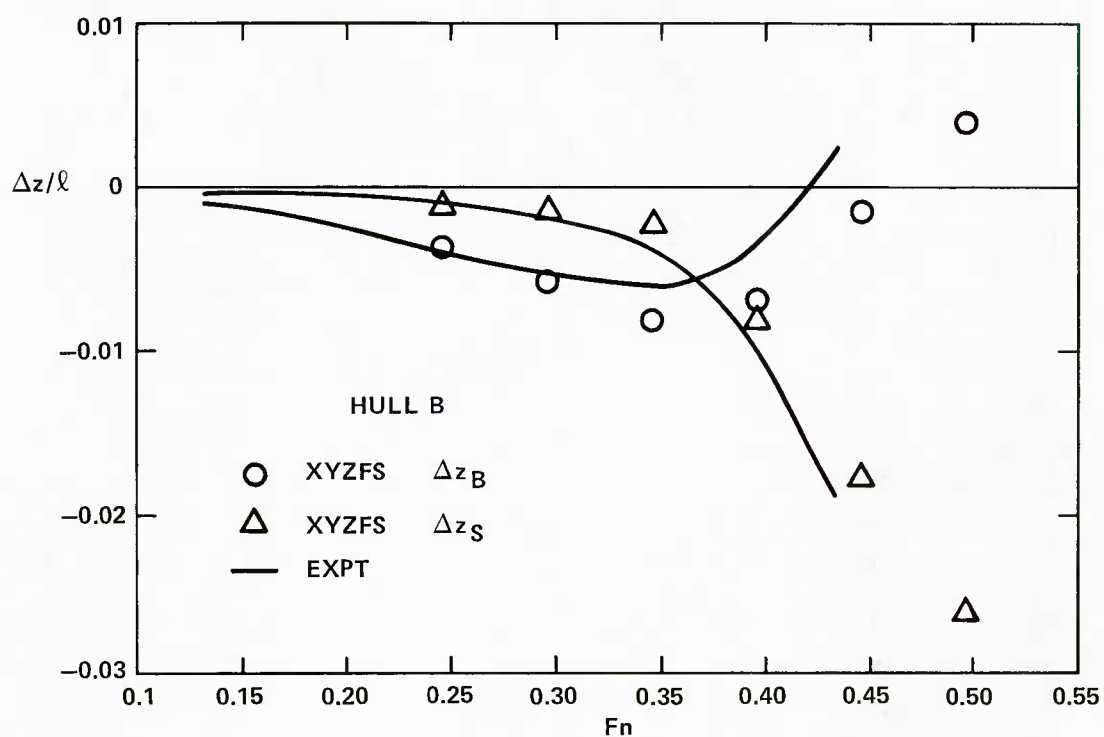
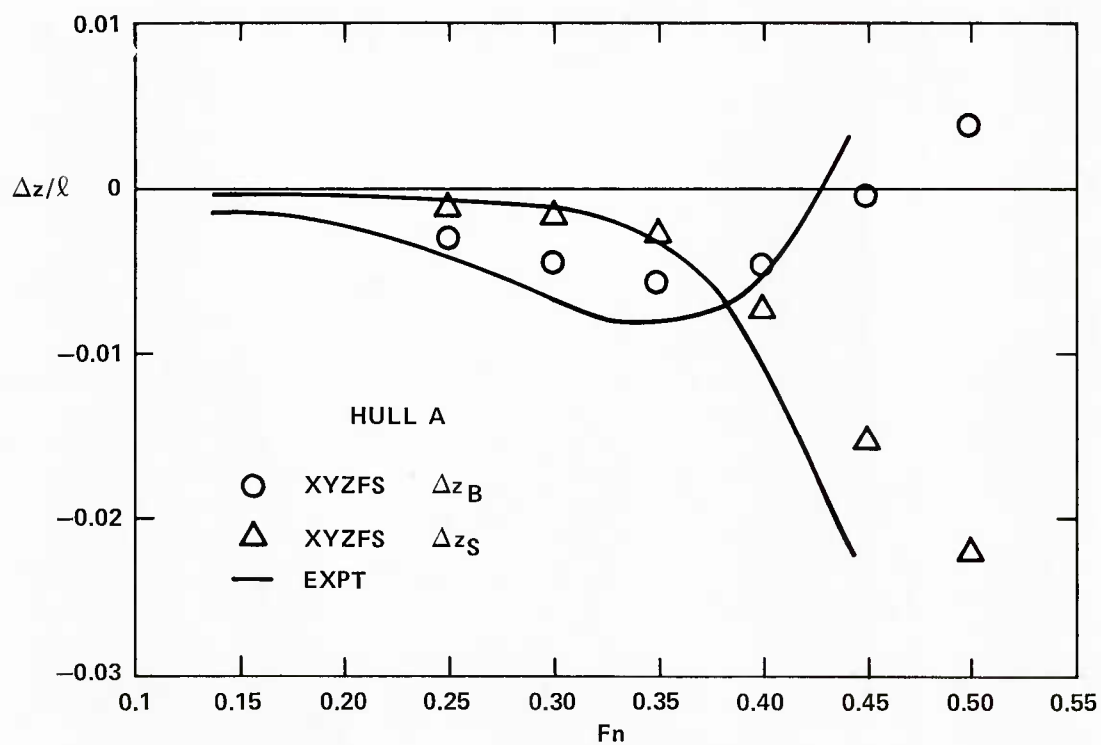


Figure 2 - Comparisons of Calculated and Experimental Bow Levels (Δz_B) and Stern Levels (Δz_S)

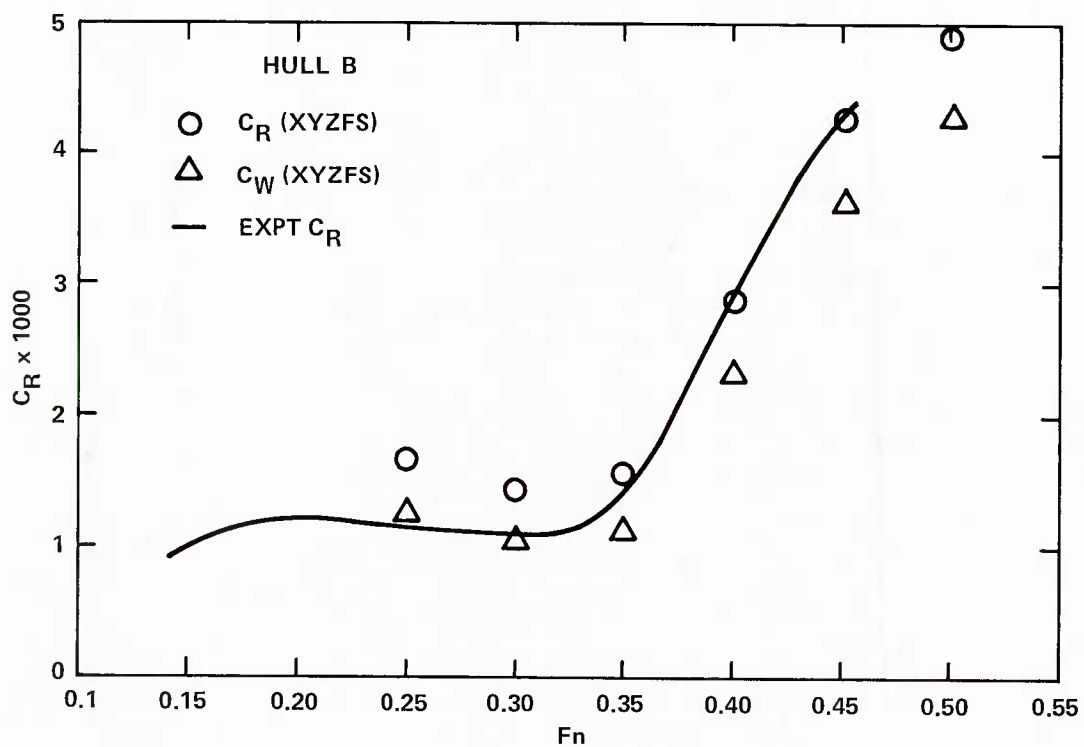
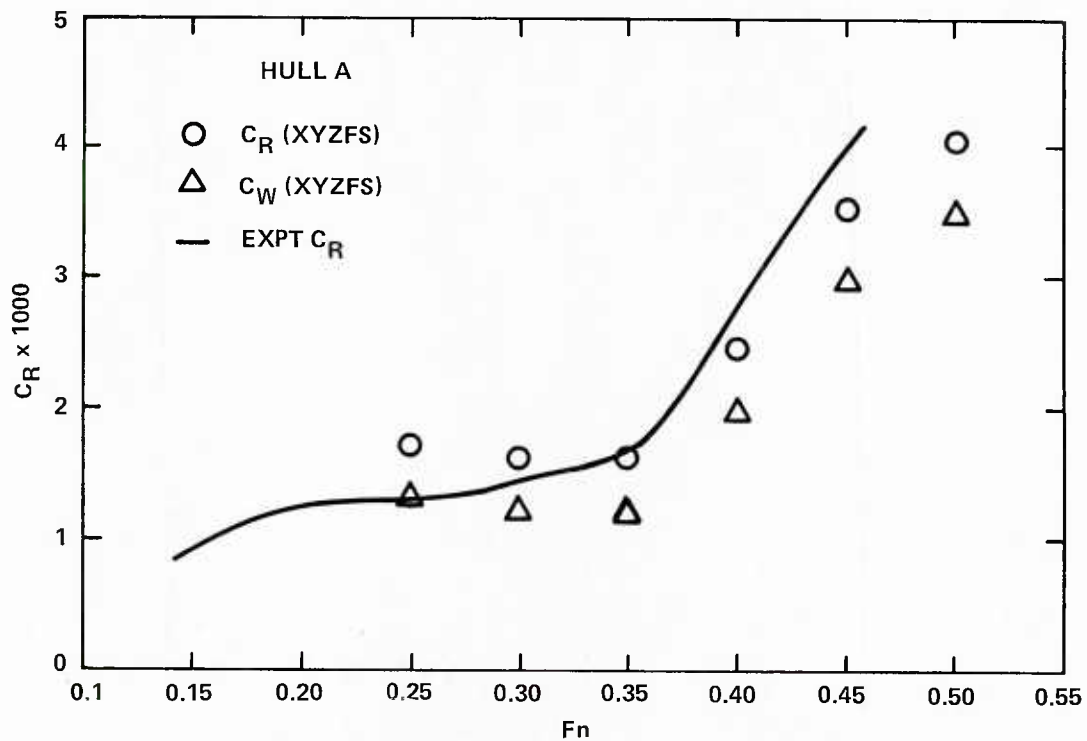


Figure 3 - Comparisons of Calculated and Experimental Residual Resistance Coefficients (C_R) with Wave Resistance Coefficients (C_W)

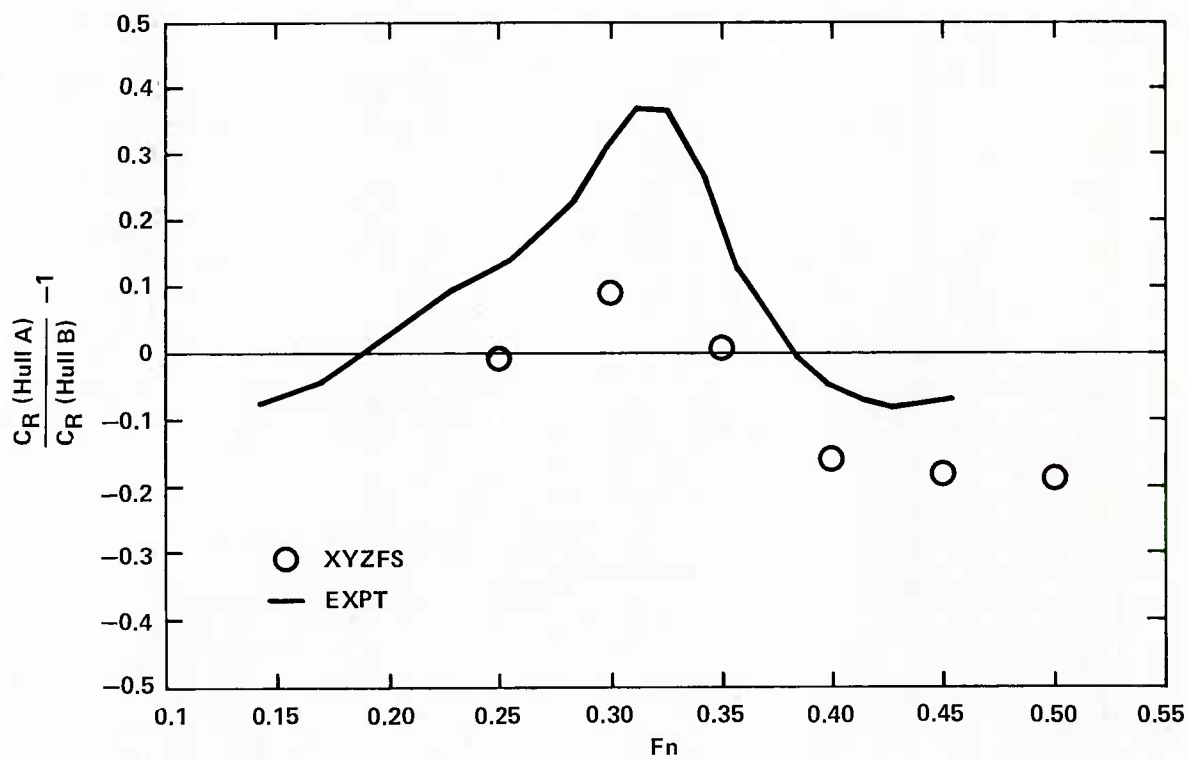


Figure 4 - Normalized Differences in Residual Resistance Coefficients Between Hull A and Hull B

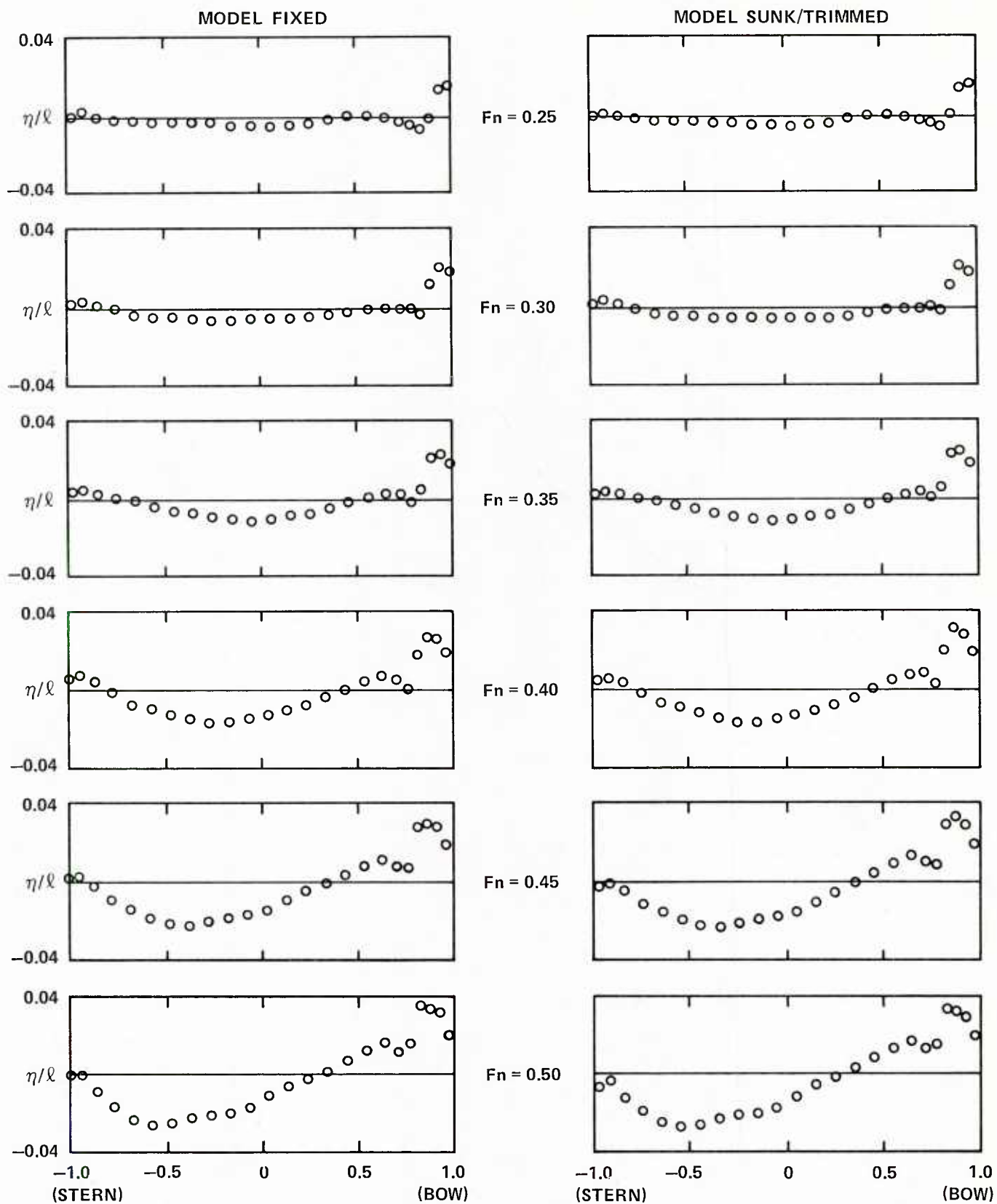


Figure 5a - Wave Profiles Along Hull A at Various Froude Numbers

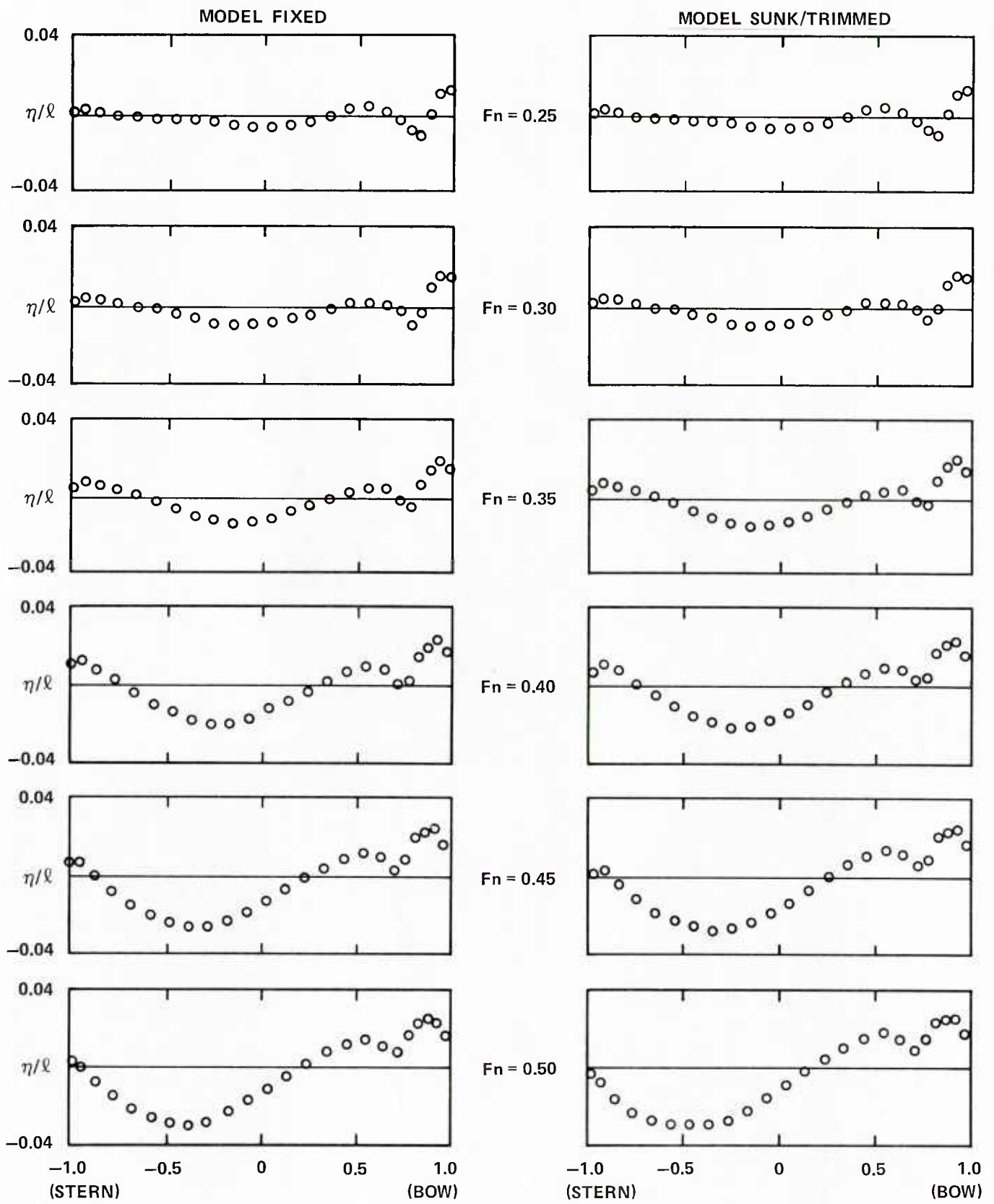


Figure 5b - Wave Profiles Along Hull B at Various Froude Numbers

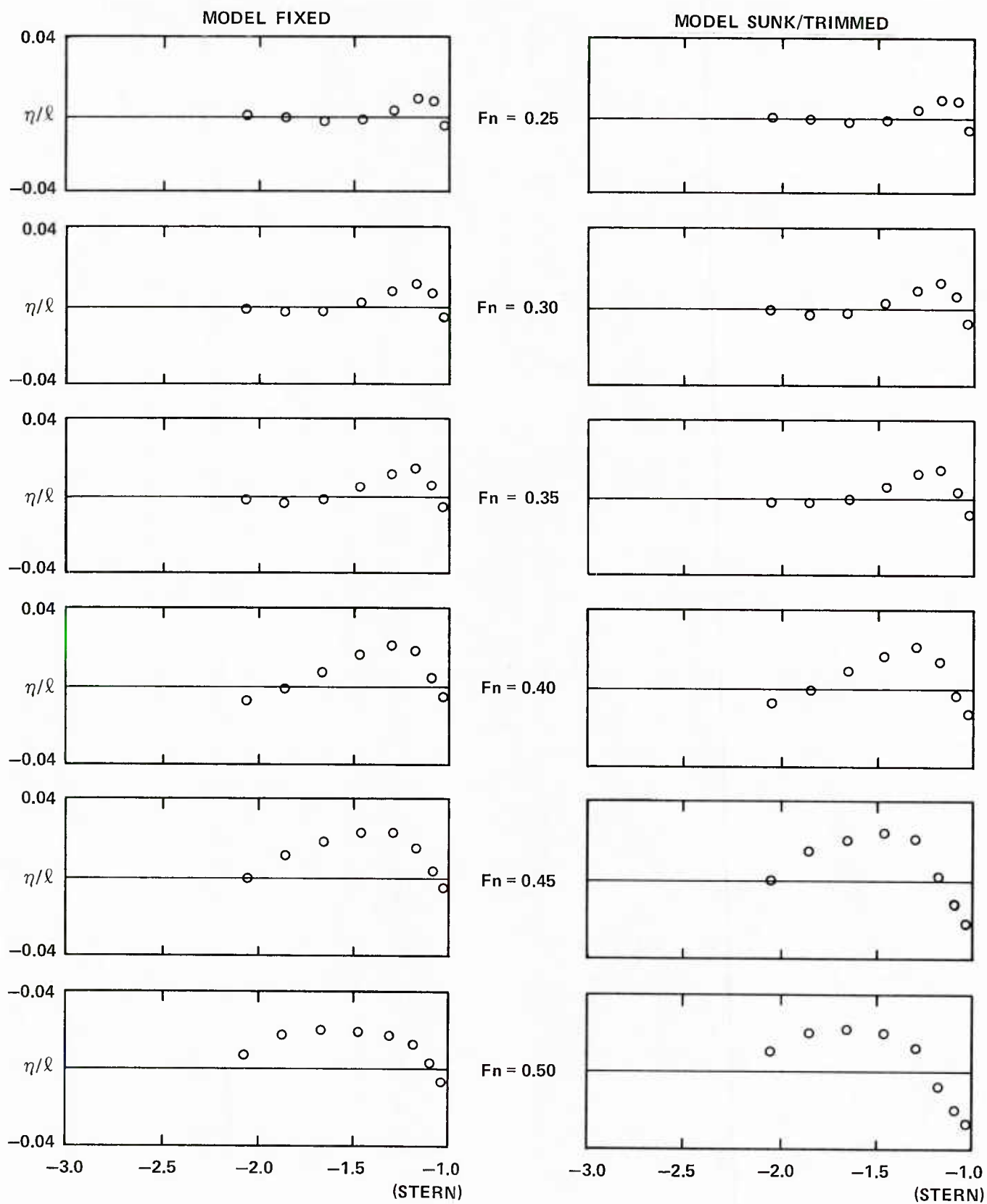


Figure 6a - Stern Wave Profiles for Hull A at Various Froude Numbers

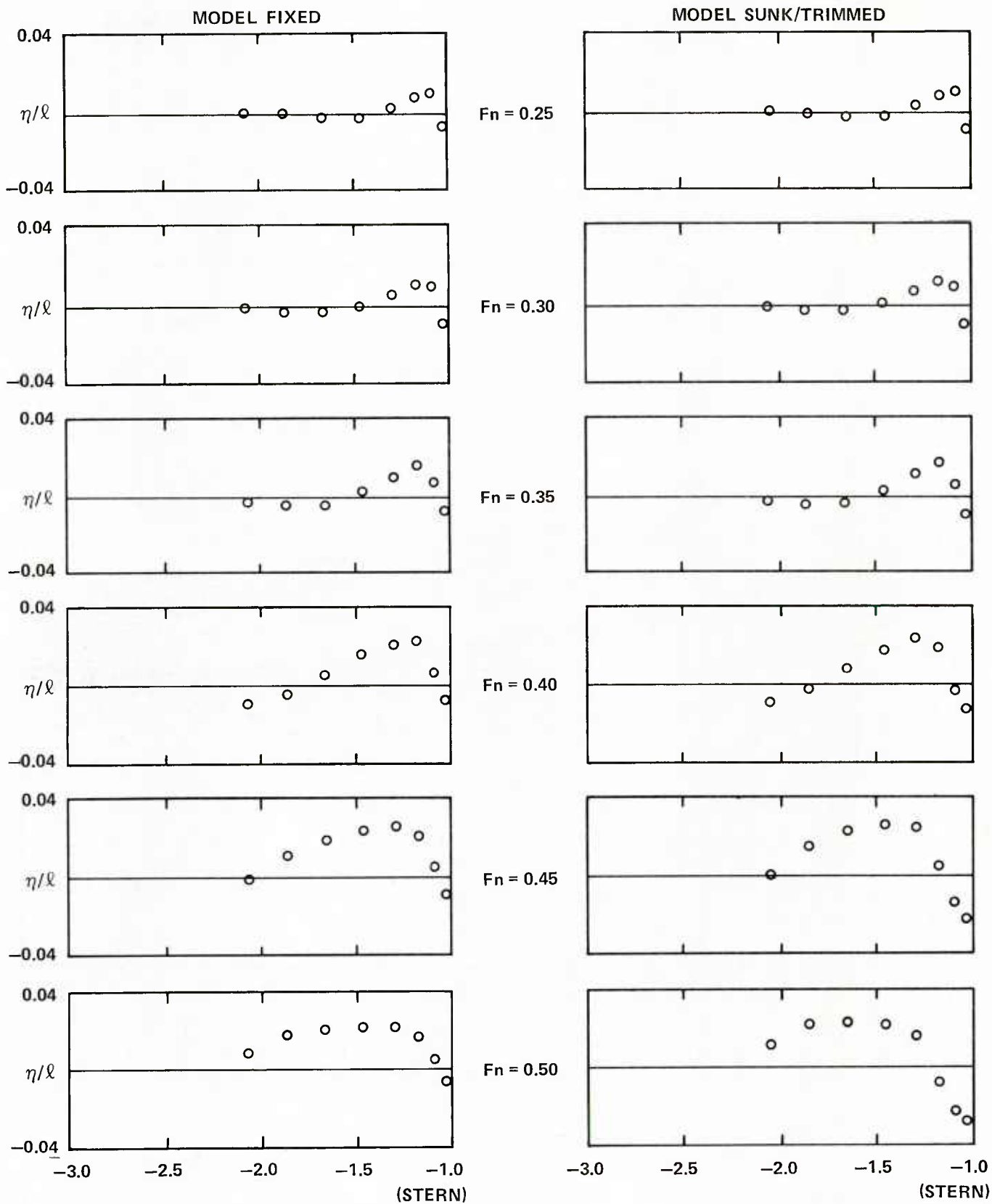


Figure 6b - Stern Wave Profiles for Hull B at Various Froude Numbers

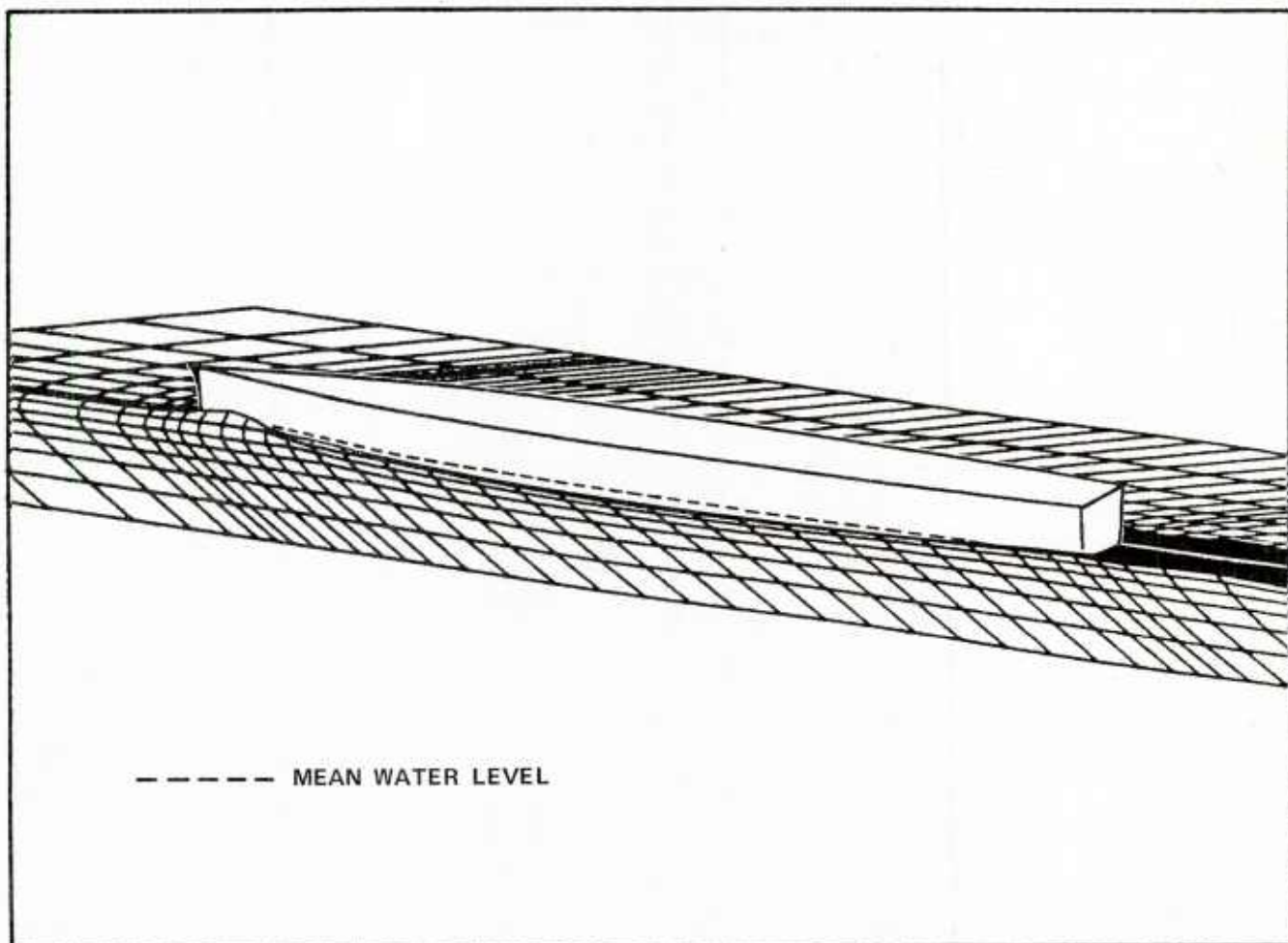


Figure 7 - Perspective View of the Computed Ship Wave Pattern for
Hull A at Froude Number 0.35

TABLE 1 - COMPUTED WAVE RESISTANCE COEFFICIENTS

Fn	Model Fixed		Model Free to Sink & Trim	
	HULL A	HULL B	HULL A	HULL B
	1000 x C_W	1000 x C_W	1000 x C_W	1000 x C_W
0.25	1.24	1.27	1.32	1.32
0.30	1.10	1.01	1.22	1.08
0.35	1.06	1.05	1.20	1.15
0.40	1.69	1.97	1.97	2.36
0.45	2.51	2.97	2.99	3.67
0.50	2.93	3.46	3.49	4.32

TABLE 2 - COMPUTED CHANGES IN LEVELS OF THE BOW AND STERN HEIGHT, SINKAGE AND TRIM COEFFICIENTS

Fn	$\Delta Z_B/\ell$	$\Delta Z_S/\ell$	$-(\Delta Z_B + \Delta Z_S)g/U^2$	$(\Delta Z_B - \Delta Z_S)2g/U^2$
	Bow Ht	Stern Ht	Sinkage Coeff	Trim Coeff
HULL A				
.25	-.00320	-.00146	0.0373	-0.0278
.30	-.00479	-.00207	0.0381	-0.0302
.35	-.00619	-.00316	0.0382	-0.0248
.40	-.00523	-.00788	0.0410	0.0165
.45	-.00106	-.01583	0.0417	0.0730
.50	.00314	-.02280	0.0393	0.1038
HULL B				
.25	-.00375	-.00125	0.0400	-0.0401
.30	-.00594	-.00142	0.0409	-0.0502
.35	-.00826	-.00242	0.0436	-0.0477
.40	-.00701	-.00832	0.0479	0.0082
.45	-.00171	-.01791	0.0484	0.0800
.50	.00368	-.02639	0.0454	0.1203

TABLE 3 - COMPUTATION OF RESIDUAL RESISTANCE COEFFICIENTS

Fn	K _p	S/S ₀	1000 x C _f	1000 x C _w x S/S ₀	1000 x C _R
HULL A					
Model Fixed					
0.25	0.0697	1.00	3.06	1.24	1.56
0.30	0.0678	1.00	2.97	1.10	1.40
0.35	0.0686	1.00	2.89	1.06	1.35
0.40	0.0772	1.00	2.83	1.69	2.02
0.45	0.0826	1.00	2.77	2.51	2.85
0.50	0.0814	1.00	2.72	2.93	3.26
Model Free to Sink & Trim					
0.25	0.0707	1.02	3.06	1.32	1.71
0.30	0.0691	1.03	2.97	1.22	1.62
0.35	0.0697	1.04	2.89	1.20	1.62
0.40	0.0790	1.05	2.83	1.97	2.47
0.45	0.0845	1.06	2.77	2.99	3.54
0.50	0.0814	1.07	2.72	3.49	4.05
HULL B					
Model Fixed					
0.25	0.0711	1.00	3.05	1.27	1.60
0.30	0.0679	1.00	2.96	1.01	1.31
0.35	0.0718	1.00	2.88	1.05	1.36
0.40	0.0829	1.00	2.81	1.97	2.32
0.45	0.0894	1.00	2.76	2.97	3.34
0.50	0.0884	1.00	2.71	3.46	3.82
Model Free to Sink & Trim					
0.25	0.0719	1.02	3.05	1.32	1.72
0.30	0.0693	1.03	2.96	1.08	1.48
0.35	0.0735	1.04	2.88	1.15	1.61
0.40	0.0864	1.06	2.81	2.36	2.92
0.45	0.0931	1.08	2.76	3.67	4.30
0.50	0.0908	1.09	2.71	4.32	4.97

TABLE 4a - WAVE PROFILES ALONG HULL

x	$F_n=.25$.30	.35	.40	.45	.50
HULL A (Model Fixed)						
1.0	Bow					
.972	.017	.019	.020	.020	.020	.020
.923	.015	.021	.025	.027	.029	.032
.874	.000	.012	.023	.028	.031	.034
.824	-.006	-.003	.006	.019	.029	.036
.774	-.003	.000	-.001	.001	.008	.016
.717	-.002	.000	.004	.006	.009	.011
.642	.000	.000	.004	.008	.012	.016
.550	.001	.000	.002	.005	.009	.012
.449	.001	-.002	-.001	.001	.004	.007
.349	-.001	-.003	-.004	-.003	.000	.001
.248	-.003	-.004	-.007	-.007	-.004	-.003
.148	-.004	-.005	-.008	-.010	-.009	-.007
.048	-.005	-.005	-.010	-.012	-.014	-.012
-.052	-.004	-.005	-.011	-.014	-.016	-.018
-.152	-.004	-.006	-.010	-.016	-.018	-.021
-.252	-.003	-.006	-.009	-.016	-.020	-.022
-.353	-.002	-.005	-.007	-.014	-.022	-.023
-.452	-.002	-.004	-.006	-.012	-.021	-.026
-.552	-.002	-.004	-.004	-.009	-.018	-.027
-.652	-.002	-.003	-.001	-.007	-.014	-.024
-.752	-.001	.000	.001	-.001	-.009	-.017
-.845	.001	.002	.003	.005	-.002	-.009
-.920	.003	.004	.005	.008	.003	.000
-.978	.001	.003	.004	.006	.002	.000
-1.0	Stern					
HULL B (Model Fixed)						
1.0	Bow					
.972	.014	.017	.017	.018	.018	.018
.923	.012	.017	.021	.024	.026	.025
.874	.001	.011	.017	.020	.024	.027
.824	-.010	-.002	.008	.015	.021	.024
.774	-.007	-.008	-.004	.002	.010	.018
.717	-.002	-.001	-.001	.001	.004	.009
.642	.002	.002	.006	.008	.011	.012
.550	.005	.003	.006	.010	.013	.016
.449	.004	.003	.004	.007	.010	.013
.349	.000	.000	.000	.002	.005	.009
.248	-.003	-.003	-.004	-.003	-.000	.003
.148	-.005	-.005	-.007	-.008	-.006	-.004
.048	-.006	-.007	-.011	-.012	-.012	-.011
-.052	-.006	-.008	-.013	-.017	-.018	-.017
-.152	-.005	-.009	-.014	-.020	-.022	-.023
-.252	-.003	-.008	-.012	-.020	-.025	-.028
-.352	-.002	-.005	-.010	-.018	-.025	-.030
-.452	-.002	-.003	-.006	-.014	-.023	-.029
-.552	-.002	-.001	-.002	-.010	-.019	-.026
-.652	-.001	.000	.002	-.004	-.014	-.022
-.752	.000	.002	.005	.003	-.007	-.015
-.845	.002	.004	.007	.008	.001	-.008
-.920	.004	.005	.009	.013	.008	-.000
-.978	.002	.003	.006	.011	.008	.003
-1.0	Stern					

TABLE 4b - WAVE PROFILES ALONG HULL

x	$F_n=.25$.30	.35	.40	.45	.50
HULL A (Model Free to Sink and Trim)						
1.0	Bow					
.972	.017	.019	.020	.020	.020	.021
.923	.015	.022	.026	.029	.030	.031
.874	.001	.012	.025	.032	.034	.034
.824	-.005	-.001	.007	.020	.030	.035
.774	-.003	.001	.002	.003	.009	.016
.717	-.002	.000	.005	.009	.011	.014
.642	-.000	-.000	.003	.008	.014	.018
.550	.001	-.001	.001	.005	.010	.014
.449	.001	-.002	-.002	.001	.005	.009
.349	-.001	-.004	-.005	-.004	.000	.003
.248	-.003	-.005	-.008	-.008	-.005	-.002
.148	-.004	-.005	-.009	-.011	-.010	-.006
.048	-.005	-.005	-.010	-.013	-.015	-.012
-.052	-.004	-.005	-.011	-.015	-.017	-.018
-.152	-.004	-.005	-.010	-.017	-.019	-.021
-.252	-.003	-.005	-.009	-.017	-.021	-.022
-.352	-.003	-.005	-.007	-.015	-.023	-.024
-.452	-.002	-.004	-.005	-.012	-.022	-.027
-.552	-.002	-.004	-.003	-.009	-.019	-.028
-.652	-.002	-.003	-.001	-.007	-.015	-.026
-.752	-.001	-.001	.001	-.002	-.011	-.020
-.845	.001	.002	.003	.004	-.004	-.013
-.920	.002	.004	.004	.006	-.001	-.004
-.978	.001	.002	.003	.005	-.002	-.007
-1.0	Stern					
HULL B (Model Free to Sink and Trim)						
1.0	Bow					
.972	.014	.016	.016	.017	.018	.019
.923	.012	.017	.022	.024	.026	.027
.874	.002	.012	.018	.022	.024	.027
.824	-.009	.000	.011	.018	.022	.025
.774	-.006	-.005	-.002	.005	.010	.016
.717	-.002	-.001	.001	.004	.007	.010
.642	.002	.002	.006	.009	.013	.016
.550	.005	.003	.005	.010	.015	.019
.449	.004	.003	.003	.007	.012	.016
.349	.000	-.001	-.001	.002	.007	.011
.248	-.003	-.003	-.005	-.003	.001	.005
.148	-.005	-.006	-.009	-.009	-.006	-.003
.048	-.006	-.008	-.012	-.014	-.013	-.009
-.052	-.006	-.009	-.014	-.018	-.019	-.016
-.152	-.005	-.009	-.015	-.021	-.023	-.023
-.252	-.003	-.008	-.013	-.022	-.026	-.028
-.352	-.002	-.005	-.010	-.019	-.027	-.030
-.452	-.002	-.003	-.006	-.016	-.025	-.030
-.552	-.002	-.001	-.002	-.011	-.022	-.030
-.652	-.001	.000	.002	-.005	-.018	-.028
-.752	.000	.002	.005	.001	-.011	-.024
-.845	.002	.004	.007	.008	-.003	-.017
-.920	.004	.005	.009	.011	.004	-.008
-.978	.002	.002	.005	.007	.002	-.003
-1.0	Stern					

TABLE 5 - STERN WAVE PROFILES ALONG CONSTANT Y CLOSE TO CENTER LINE

x	$F_n=.25$	0.30	0.35	0.40	0.45	0.50
HULL A (Model Fixed)						
-1.0	Stern					
-1.02	-.004	-.005	-.005	-.005	-.005	-.006
-1.08	.019	.008	.007	.005	.004	.004
-1.17	.010	.013	.016	.019	.016	.014
-1.29	.004	.009	.013	.022	.024	.019
-1.45	-.001	.003	.006	.017	.024	.021
-1.65	-.002	-.002	-.001	.008	.019	.022
-1.85	.000	-.002	-.003	-.001	.012	.019
-2.05	.001	-.001	-.002	-.007	.000	.008
HULL A (Model Free to Sink and Trim)						
-1.0	Stern					
-1.02	-.006	-.007	-.008	-.012	-.021	-.027
-1.08	.009	.007	.004	-.003	-.011	-.020
-1.17	.010	.014	.016	.015	.003	-.008
-1.29	.005	.010	.014	.023	.023	.013
-1.45	-.001	.003	.007	.018	.026	.021
-1.65	-.002	-.002	-.000	.010	.022	.023
-1.85	.000	-.003	-.002	-.000	.016	.021
-2.05	.001	-.001	-.002	-.007	.001	.011
HULL B (Model Fixed)						
-1.0	Stern					
-1.02	-.006	-.008	-.007	-.007	-.008	-.006
-1.08	.011	.011	.009	.007	.006	.006
-1.17	.009	.012	.018	.024	.022	.018
-1.29	.003	.007	.012	.022	.027	.023
-1.45	-.002	.001	.004	.017	.025	.023
-1.65	-.002	-.002	-.004	.006	.020	.022
-1.85	.001	-.002	-.004	-.004	.012	.019
-2.05	.001	.000	-.002	-.009	-.001	.009
HULL B (Model Free to Sink and Trim)						
-1.0	Stern					
-1.02	-.008	-.009	-.009	-.012	-.021	-.028
-1.08	.011	.010	.007	-.003	-.013	-.023
-1.17	.009	.013	.019	.020	.006	-.008
-1.29	.004	.008	.013	.025	.026	.017
-1.45	-.002	.002	.004	.019	.027	.023
-1.65	-.002	-.002	-.003	.009	.024	.024
-1.85	.000	-.002	-.004	-.002	.016	.023
-2.05	.001	-.000	-.002	-.009	.001	.012

A Comparison With Experimental Results Of Wave Resistance
Predictions Using A Rankine Source Panel
Method And A Slender Body Theory

by

William C. Sandberg *
and
Carl A. Scragg **

Introduction: This paper will present results from recently completed studies to assess the usefulness of currently available viscous and inviscid computational methods early in the ship design process. The motivation for this effort is the need to develop, for use at an early design stage, a capability for evaluating the effect of local hull form variations on drag and energy consumption.

It was decided to carry out computations for two transom stern hull variants for which model test data existed. Viscous hull drag and wave drag were computed by von Kerczek, Scragg, and Stern¹ and subsequently appendage drag by Stern and von Kerczek². The present paper will discuss only the wave drag computations. The code WAVE-DRAG was developed by Scragg at S.A.I. and applied to the two test case hulls. A description of his method and the results of his calculation are given in reference 1. which is the source of the brief summary we will give here. This method is similar to that

* Naval Sea Systems Command
Washington, D.C. 20362

** Science Applications Inc.
P.O. Box 2351
LaJolla, CA 92038

developed by Noblesse³. The source strengths, determined from the Slender Ship approximation, are proportional to the longitudinal component of the local hull normal. 316 triangular panels were used to model the hull. The transom, following the suggestion of Gadd⁴, was left open. This approach to modelling the transom was checked by an alternative computation where the transom was extended up to the calm waterplane behind the transom. The result of the alternative calculation was approximately one percent higher than that for the open transom. Transom submergence has been computed by Scragg using a near field velocity code which predicts the fluid velocity at the hull surface. Following Chang⁵, the additional contribution to wave resistance due to sinkage and trim was obtained by integrating the pressure over the wetted surface of the hull to obtain the sinkage force and trim moment, from which the additional hydrostatic pressure due to transom wetting was obtained.

Wave resistance was also computed by Cheng, Dean, and Jayne⁶ for the two test case hulls using XYZFS, which is a Rankine source panel method. The code used for the computation includes the capability to handle bow domes and also incorporates the new transom stern boundary condition of Cheng. The modification to the program and the results for these test cases are the subject of the paper by Cheng, Dean, and Jayne at this Workshop. Selected results from that paper will be presented here with those of S.A.I.

Results: The wave resistance coefficients computed by the two methods for both the fixed and sunk and trimmed condition are given in Table 1. These values are plotted in Figures 1 through 4. It can be seen from Figures 1 and

2 that for both hulls in the fixed condition the Slender Body Theory results are lower than those of XYZFS at the two lowest Froude numbers (.25 and .30) and higher over the rest of the Froude number range. For the sunk and trimmed condition Figures 3 and 4 show that the same relative behavior is maintained, however, the differences between the results are now less. This decrease can be accounted for primarily by the larger percentage increase in C_w due to sinkage and trim that is predicted by XYZFS. The percentage changes in C_w for each method due to sinkage and trim are given in Table 2.

Figures 5 and 6 compare the C_w predictions for Hulls 1 and 2 from each method. A significant question from the design point of view is the Froude number at which the two hulls cross. From Figure 6 we see that the S.A.I. computations predict a C_w for Hull 1 that is lower than that of Hull 2 between Froude numbers of .255 and .340 with Hull 2 becoming lower for all higher Froude numbers. From Figure 5 we see that XYZFS also predicts a lower C_w for Hull 1 in the Froude number range of .250 to .355 with Hull 2 higher at all other Froude numbers. For comparison, the residuary resistance coefficients C_R , determined from experiment, are shown in Figure 7. The crossover values from the data are at Froude numbers of 0.185 and 0.394. Thus, both methods have correctly predicted that Hull 2 will have lower wavemaking resistance at the lower Froude numbers with Hull 1 becoming superior at higher Froude numbers. This is a significant accomplishment which indicate that both of these wave resistance computation methods in their present form are of immediate use, not only for research, but also in the design process.

TABLE 1 - COMPUTED WAVE RESISTANCE COEFFICIENTS

Model Fixed	1000 x C _w			
	<u>Hull 1</u>		<u>Hull 2</u>	
F _n	XYZFS	SAI	XYZFS	SAI
0.25	1.24	.644	1.27	.751
0.30	1.10	.913	1.01	.546
0.35	1.06	1.313	1.05	1.499
0.40	1.69	3.026	1.97	3.383
0.45	2.51	3.850	2.97	4.207
0.50	2.93	3.726	3.46	4.054

Model Free to Sink and Trim	<u>Hull 1</u>		<u>Hull 2</u>	
	XYZFS	SAI	XYZFS	SAI
F _n				
0.25	1.32	.741	1.32	.796
0.30	1.22	1.006	1.08	.590
0.35	1.20	1.422	1.15	1.555
0.40	1.97	3.266	2.36	3.530
0.45	2.99	4.218	3.67	4.431
0.50	3.49	4.097	4.32	4.286

TABLE 2 - PERCENTAGE INCREASE IN C_W DUE TO SINKAGE AND TRIM

Fn	<u>Hull 1</u>		<u>Hull 2</u>	
	XYZFS	SAI	XYZFS	SAI
0.25	6%	16%	4%	6%
0.30	11%	10%	7%	8%
0.35	12%	8%	9%	4%
0.40	16%	8%	20%	4%
0.45	19%	10%	23%	5%
0.50	19%	10%	25%	6%

REFERENCES

1. von Kerczek, C., C. Scragg, and F. Stern, "A Comparative Study of the Resistance of Two Destroyer Hull Forms", NAVSEA Technical Note 051-55W-TN-0001, March 1983.
2. Stern, F. and C. von Kerczek, "Calculation of Appendage Drag and Propeller Inflow for Destroyer Hull Forms", NAVSEA Technical Note 051-55W-TN-0002, June 1983.
3. Noblesse, F., "A Slender Ship Theory of Wave Resistance", Journal of Ship Research, October 1983.
4. Gadd, G.E., "Contribution to Workshop on Ship Wave Resistance Computations", Proceedings of the Workshop on Ship Wave Resistance Computations, Vol. 2, 1979.
5. Chang, M., "Wave Resistance Predictions Using a Singularity Method", Proceedings of the Workshop on Ship Wave Resistance Computations, Vol. 2, 1979.
6. Cheng, Bill H., Janet S. Dean, and John L. Jayne, "The XYZ Free Surface Program and Its Application to Transom Stern Ships with Bow Domes", Proceedings of the Second Workshop on Ship Wave Resistance Computations, 16-17 November 1983.

A COMPARISON OF PREDICTIONS FOR HULL 1 IN THE FIXED CONDITION

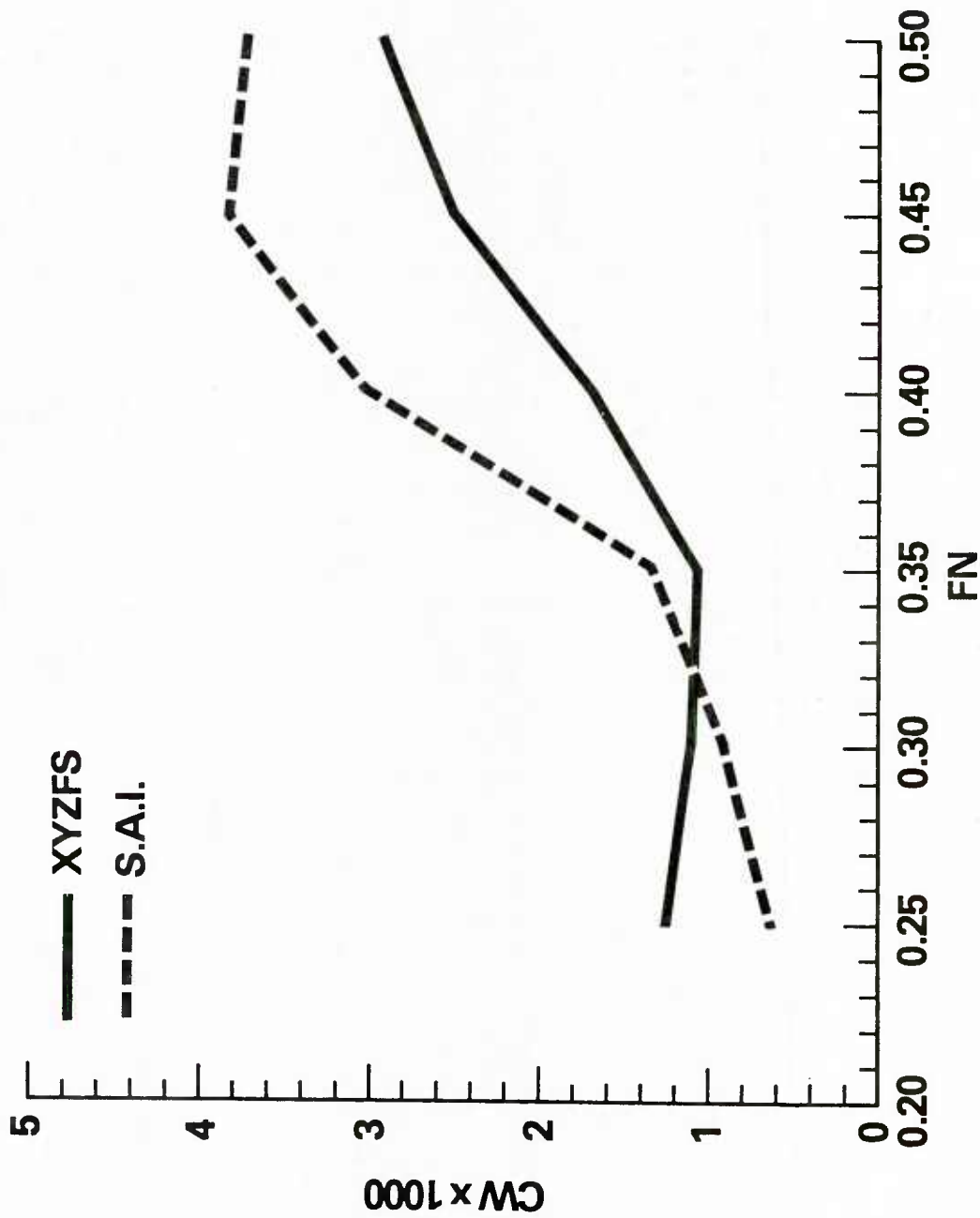


FIGURE 1

A COMPARISON OF PREDICTIONS FOR HULL 2 IN THE FIXED CONDITION

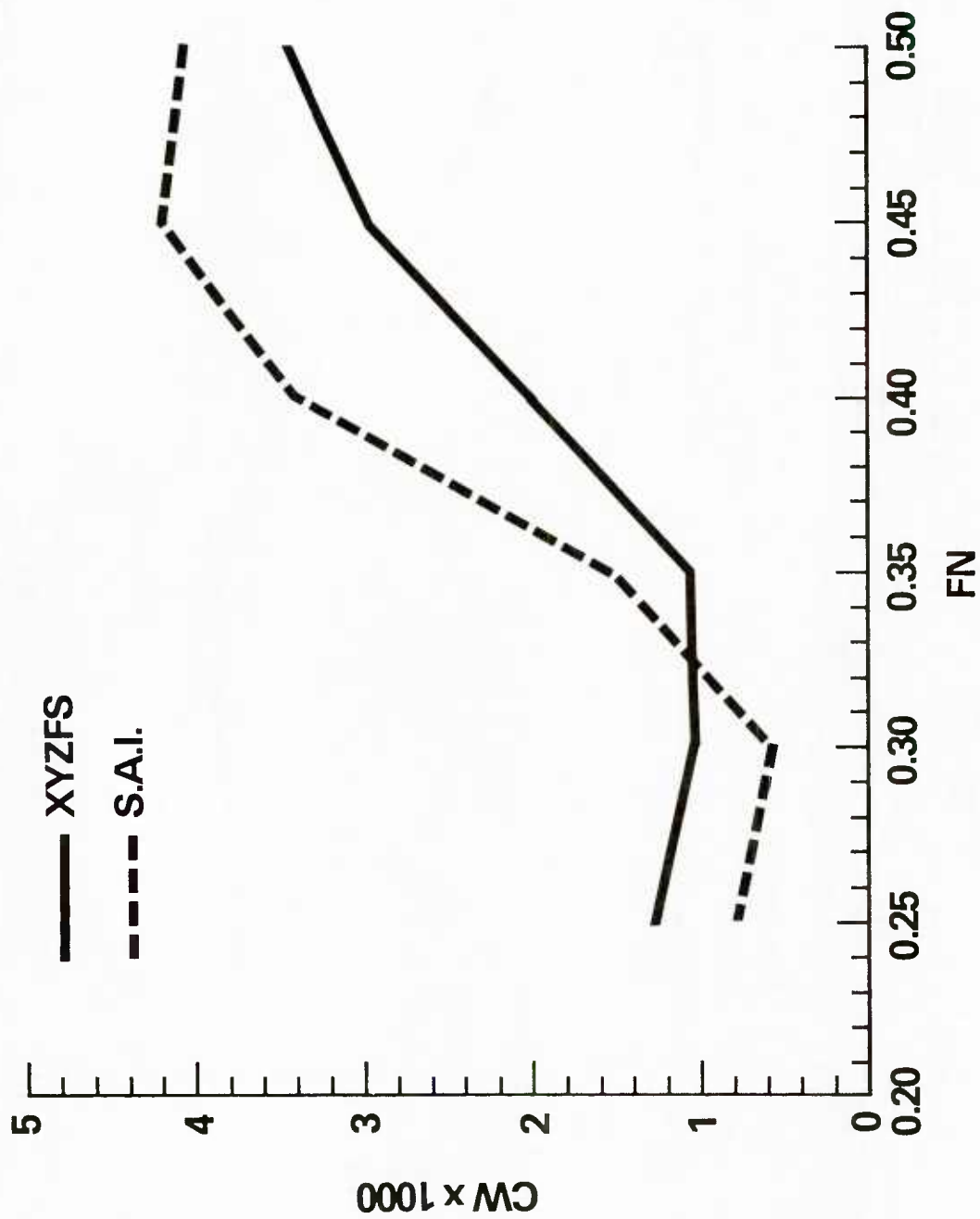


FIGURE 2

A COMPARISON OF PREDICTIONS FOR HULL IN THE SUNK AND TRIMMED CONDITION

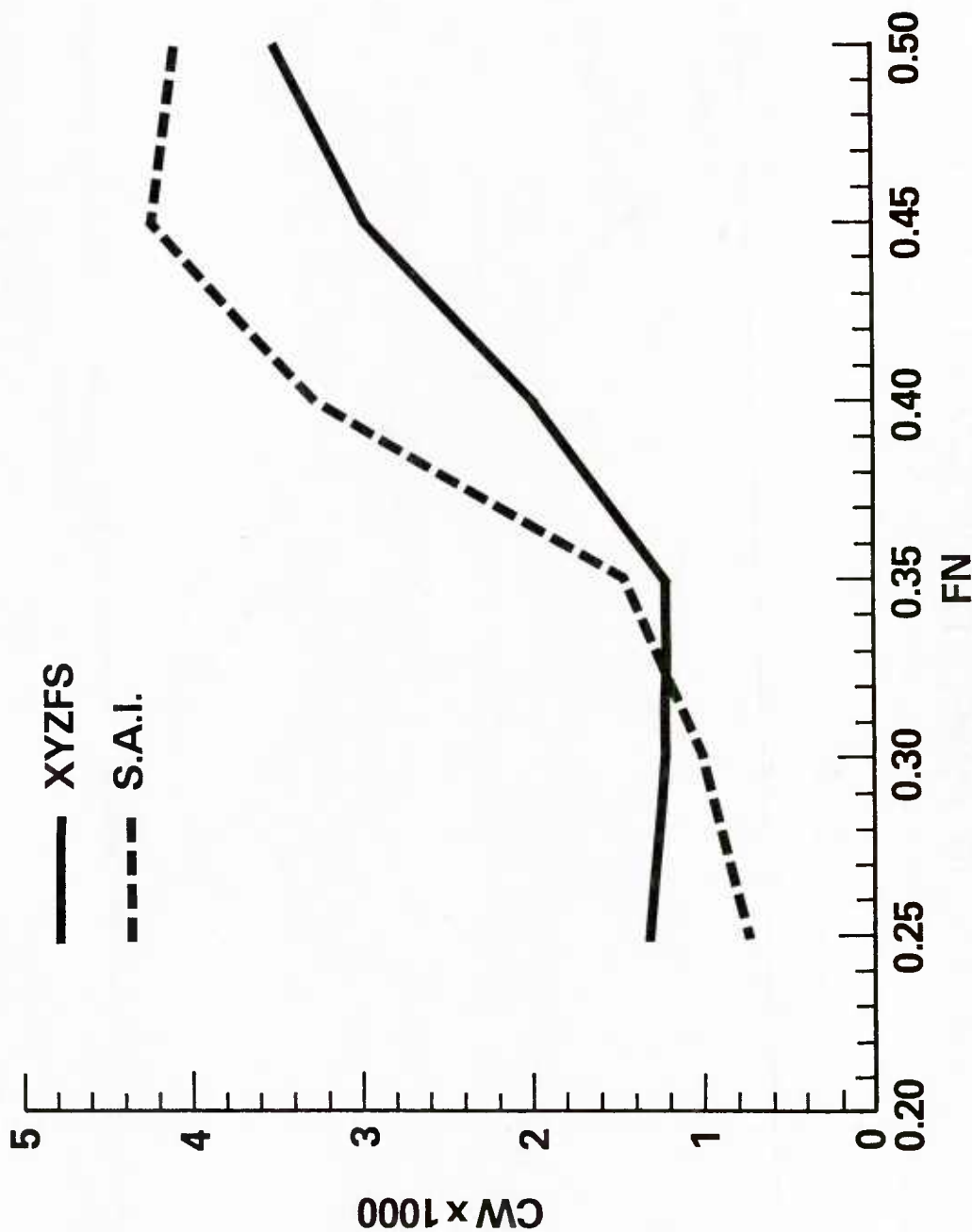


FIGURE 3

A COMPARISON OF PREDICTIONS FOR HULL 2 IN THE SUNK AND TRIMMED CONDITION

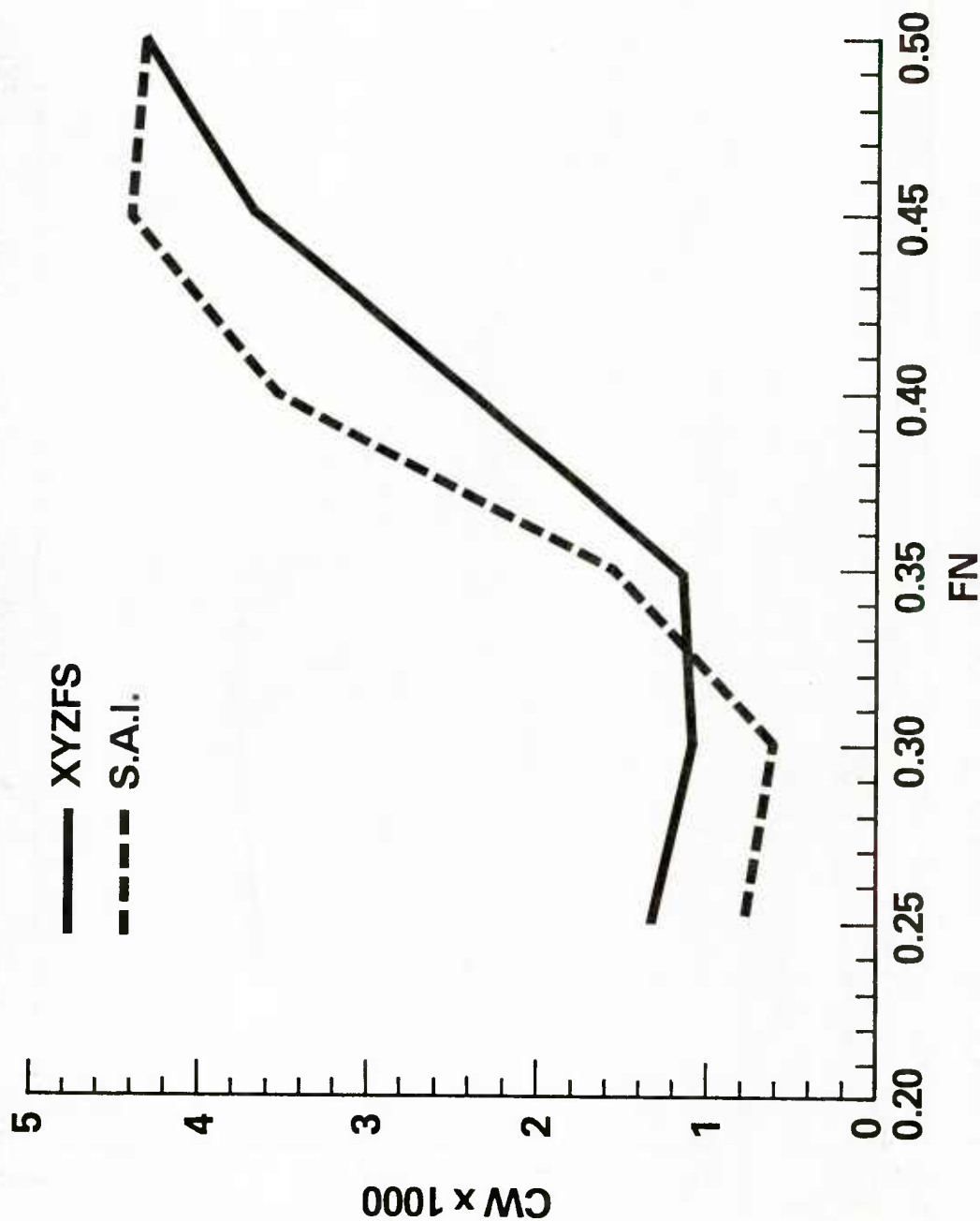


FIGURE 4

A COMPARISON OF XYZFS PREDICTIONS FOR HULLS 1 AND 2 SUNK AND TRIMMED

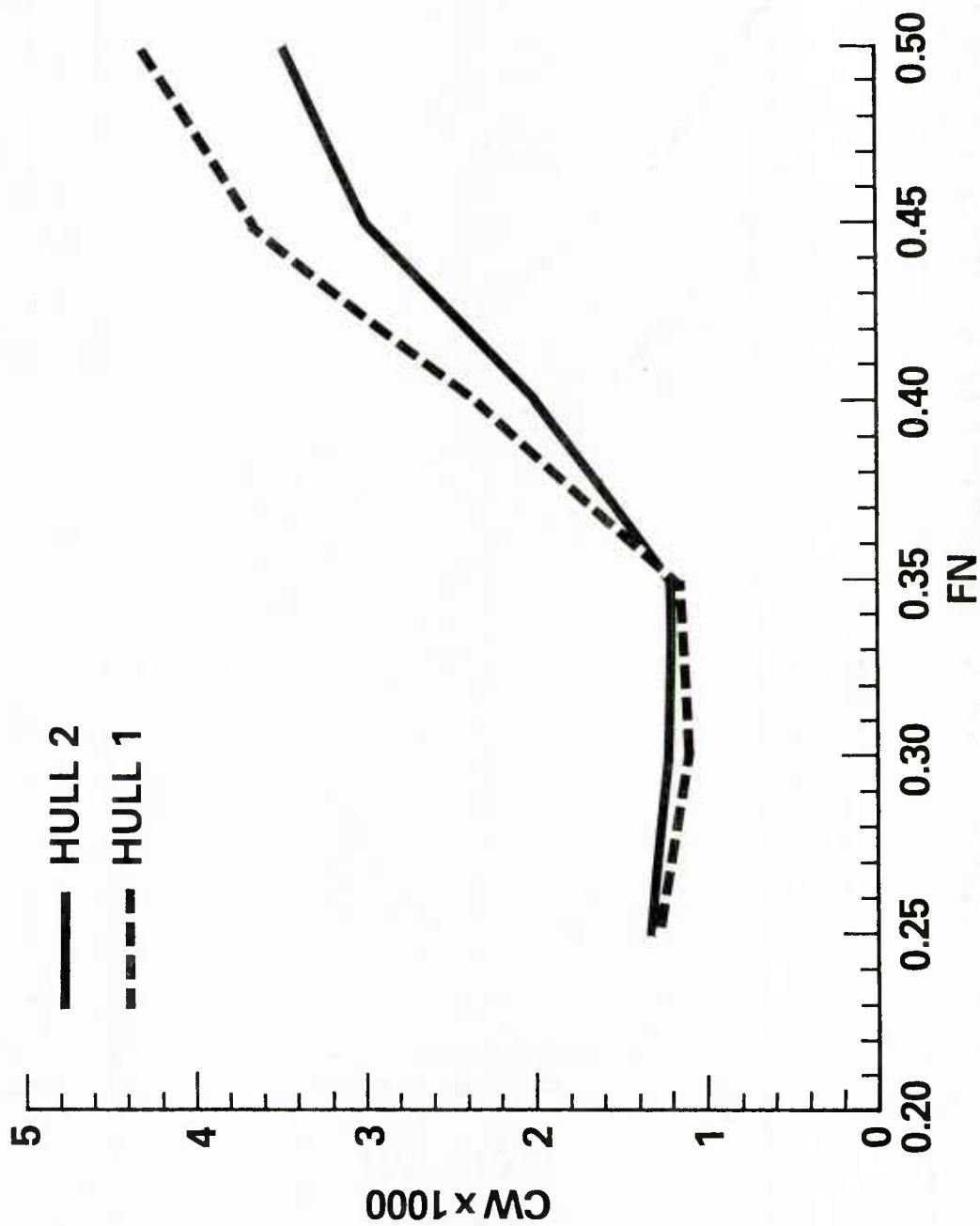


FIGURE 5

A COMPARISON OF PREDICTIONS OF S.A.I. FOR HULLS 1 AND 2 SUNK AND TRIMMED

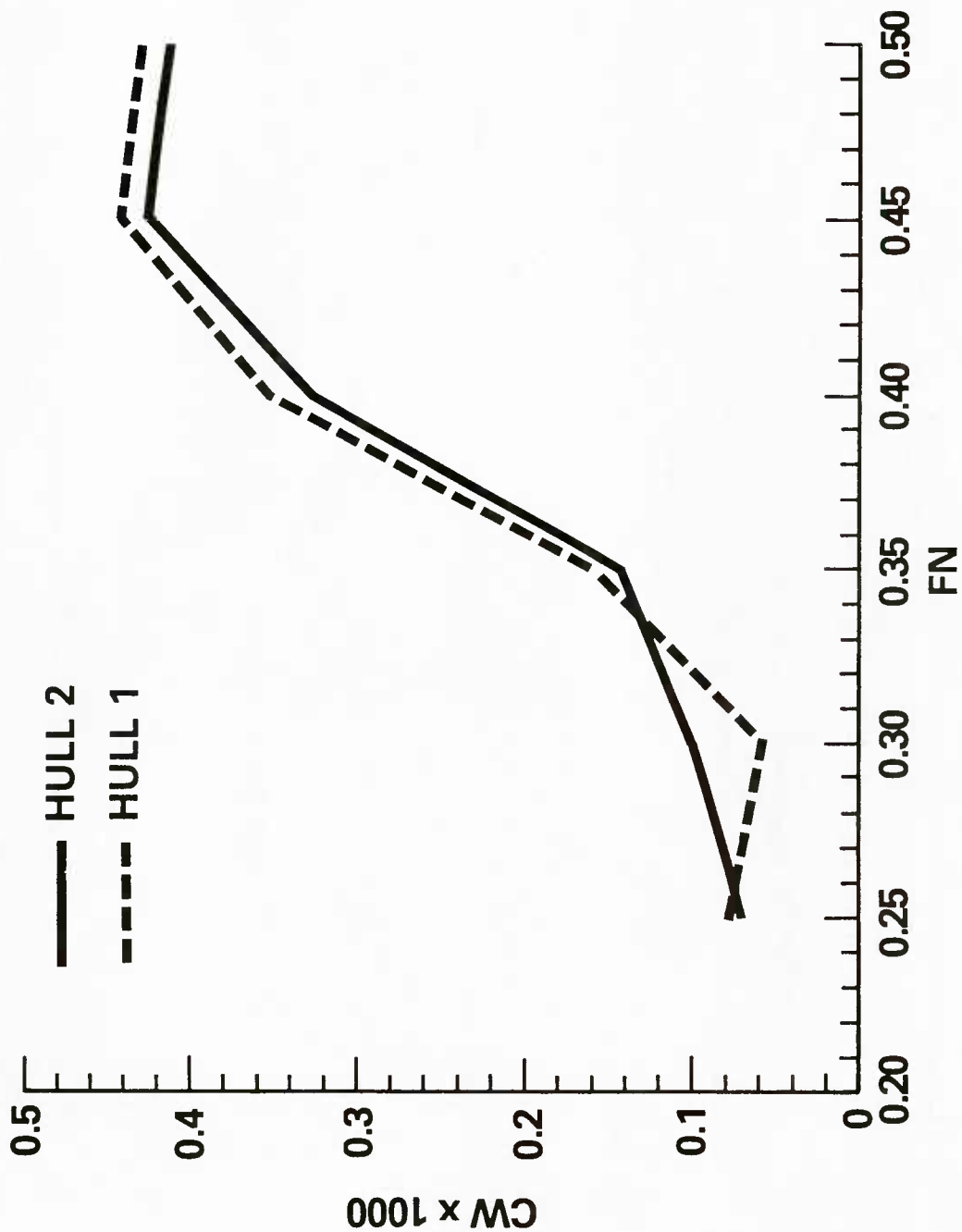


FIGURE 6

RESIDUARY RESISTANCE COEFFICIENT DATA FOR HULLS 1 AND 2 SUNK AND TRIMMED

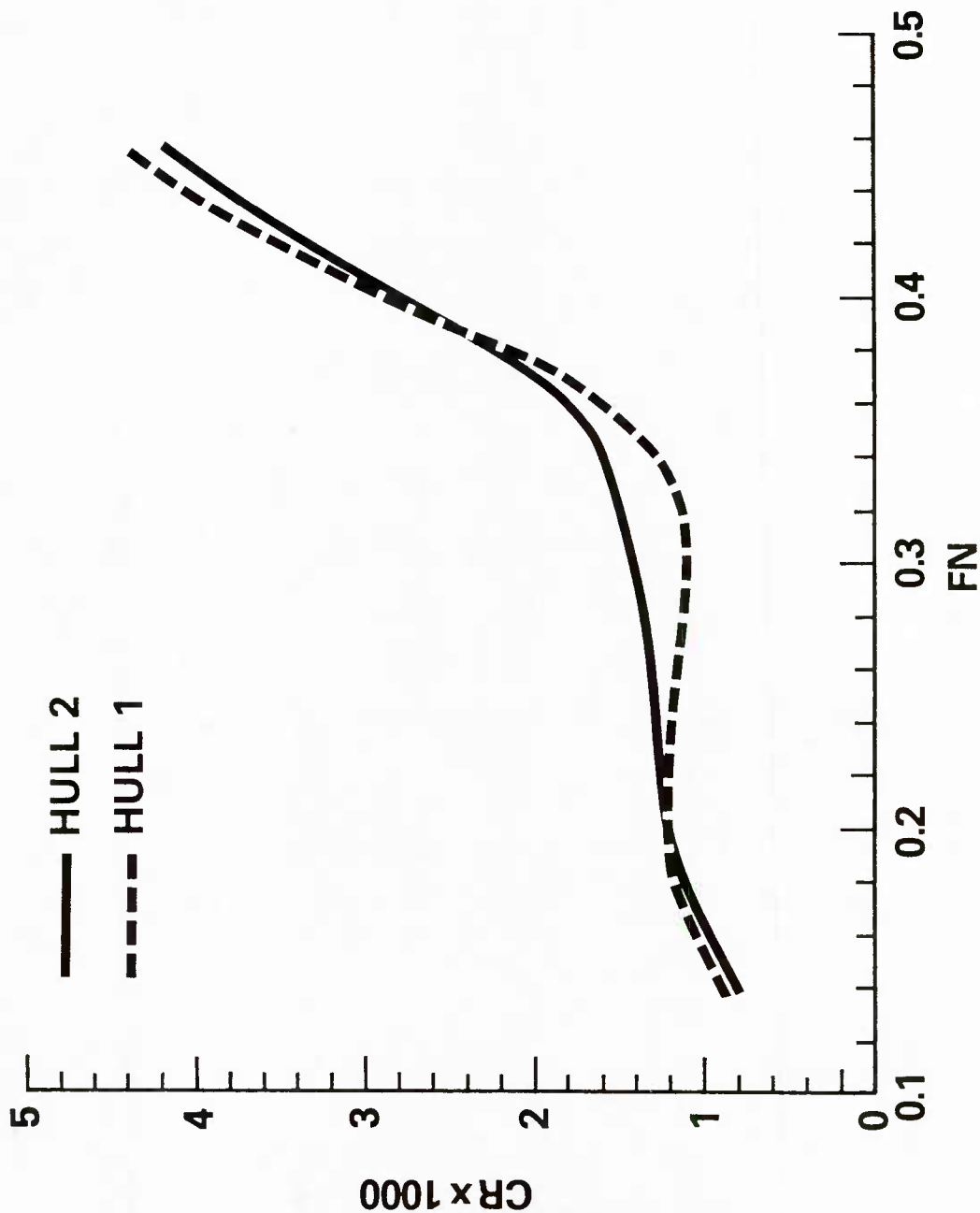


FIGURE 7

Wave Resistance of Vertical Cylinders with Ogival and Elliptical Water Planes

K. Nakatake, A. Nishida and R. Yamazaki

(Kyushu University, Fukuoka, Japan)

1. Introduction

At the first workshop, we presented the results [1] calculated by three kinds of low speed theories, i.e. the modified low speed theory (abbr. MLST) [2], the conventional one (abbr. LST) [3] and Guevel's theory [4]. Among them, the results of MLST agreed comparably well with Dawson's [5]. He used the Rankine source and the same free surface condition as MLST for wall sided hull, as later pointed out by Mori [6]. This fact encouraged us to adopt MLST and LST again for calculating the wave-resistance of the vertical cylinders with an ogival and an elliptical water planes.

In addition to the above-mentioned analytical theories, we present the purely numerical results which are obtained by the fundamental equations of the low speed theory and the Chan's finite difference scheme [7]. Computations are made for the same vertical cylinders.

2. Brief Description of Low Speed Theory

2.1 Wave-Resistance Expressed by Modified Low Speed Theory [MLST]

As an improvement of the conventional low speed theory [3], this method [2] was proposed to take into account the effect of the local non-uniform flow around a ship in the expression of the wave-resis-

tance.

The ship is fixed in the uniform flow of velocity V . The origin of coordinate system O - xyz is fixed at the midship and the xy -plane nearly coincides with the still water surface and the x -axis is in the direction of uniform flow.

Starting from the basic equations of the steady wavemaking theory and repeating order-checking and coordinate transformations three times, we obtained the following expression of wave-resistance R_w [2].

$$R_w = \frac{\rho}{2\pi} k_o^2 \int_{-\pi/2}^{\pi/2} |B(k_o \sec^2 \theta, \theta)|^2 \sec^3 \theta d\theta, \quad (2.1)$$

where

$$B(k, \theta) = - \iint_{F_e} D(x, y) V q_o^{-2} e^{-ikV(\xi \cos \theta + \eta \sin \theta)} dx dy, \quad (2.2)$$

$$D(x, y) = \frac{\partial}{\partial x} \{ \zeta_o (V + \phi_{ox}^o) \} + \frac{\partial}{\partial y} (\zeta_o \phi_{oy}^o) \quad \text{on } F_e, \quad k_o = g/V^2. \quad (2.3)$$

ϕ_o and ζ_o express the velocity potential of the double body flow and the wave elevation due to ϕ_o , respectively. And $\phi_{ox} = \partial \phi_o / \partial x$ and $\phi_{oy} = \partial \phi_o / \partial y$. The strained coordinates ξ and η express the effect of non-uniform flow, and are obtained approximately as

$$\xi = \int_0^x \left[\frac{q_o^{-2}}{\cos \alpha} \right]_{\text{along streamline}} dx, \quad \eta = \int_{y_o(x)}^y \left[\frac{q_o^{-2}}{\cos \alpha} \right]_{\text{along equipotential line}} dy, \quad (2.4)$$

where $y_o(x)$ is the half breadth of a ship at the load water line, and q_o and α are expressed as

$$q_o^2 = (V + \phi_{ox}^o)^2 + \phi_{oy}^o{}^2, \quad \alpha = \tan^{-1} \left\{ \phi_{oy}^o / (V + \phi_{ox}^o) \right\} \quad (2.5)$$

The region F_e means the area of the still water surface outside the

ship hull. Superscript 0 means that the value is evaluated at F_e .

2.2 Wave-Resistance Expressed by Conventional Low Speed Theory

Usual low speed theory is derived from the above-described theory under some assumptions. In this case, the function $B(k, \theta)$ is defined as

$$B(k, \theta) = -\frac{k_0 \sec^2 \theta}{k} \iint_{F_e} D(x, y) e^{-ik(x \cos \theta + y \sin \theta)} dx dy. \quad (2.6)$$

2.3 Expressions of $D(x, y)$ Function

We treat the two-dimensional flow around vertical cylinder with some shape of water plane which is of length L . Since ζ_0 is expressed as

$$\zeta_0 = \frac{1}{2g} \left\{ V^2 - (V + \phi_{0x}^0)^2 - \phi_{0y}^0{}^2 \right\}, \quad (2.7)$$

$D(x, y)$ becomes from Eq. (2.3)

$$D(x, y) = -\frac{1}{g} \left\{ \left\{ (V + \phi_{0x}^0)^2 - \phi_{0y}^0{}^2 \right\} \phi_{0xx}^0 + 2(V + \phi_{0x}^0) \phi_{0y}^0 \phi_{0xy}^0 \right\}. \quad (2.8)$$

Introducing the complex velocity potential $W(\bar{z})$ ($\bar{z} = x + iy$), Eq. (2.8) is transformed to

$$D(x, y) = -\frac{1}{g} \left[\left\{ \overline{\text{RP}\left(\frac{dW}{d\bar{z}}\right)^2} - \overline{\text{IM}\left(\frac{dW}{d\bar{z}}\right)^2} \right\} \cdot \text{RP}\left(\frac{d^2W}{d\bar{z}^2}\right) + 2 \text{RP}\left(\frac{dW}{d\bar{z}}\right) \cdot \text{IM}\left(\frac{dW}{d\bar{z}}\right) \cdot \text{IM}\left(\frac{d^2W}{d\bar{z}^2}\right) \right], \quad (2.9)$$

where RP and IM mean the real and imaginary part of the function in the parenthesis, respectively. Since the mapping functions between the circle and the ogival shape or the elliptical shape are known, we

can calculate $D(x,y)$ function on F_e .

In obtaining the ξ - and η - values, we need to calculate the streamlines and the equi-potential lines around the cylinder. These are obtained by mapping those lines around the circle.

The curves of $D(x,y)$, the weighted amplitude function and R_w are represented in the forms:

$$\begin{aligned} \bar{D}(x,y) &= D(x,y) / (VF_n^2), \quad \text{where} \quad F_n = V/\sqrt{gL}, \\ AMP &= |B(k_0 \sec^2 \theta, \theta)|^2 \sec^3 \theta, \quad C_w = R_w / (0.5 \rho L^2 V^2). \end{aligned} \quad (2.10)$$

3. Brief Description of Finite Difference Method

We treat the steady wavemaking problem as the initial value problem by making use of the double body flow and the finite difference method according to Chan [7].

At first, the disturbed velocity potential ϕ and wave elevation ζ are divided into the double body flow part ϕ_0 , ζ_0 and the wavy part ϕ_1 , ζ_1 , respectively, i.e.

$$\phi = \phi_0 + \phi_1, \quad \zeta = \zeta_0 + \zeta_1, \quad (3.1)$$

ϕ_0 and ζ_0 are known, ϕ_1 and ζ_1 are unknown, and ϕ_1 has to satisfy the Laplace equation,

$$\phi_{1xx} + \phi_{1yy} + \phi_{1zz} = 0. \quad (3.2)$$

From the dynamical condition at the free surface, we get

$$\phi_{1t} + \phi_{0x} \phi_{1x} + \phi_{0y} \phi_{1y} + g \zeta_1 = 0. \quad (3.3)$$

From the kinematic condition at the free surface, we obtain the following two kinds of conditions. One is

$$\zeta_{1t} + \phi_{0x} \zeta_{1x} + \phi_{0y} \zeta_{1y} + \zeta_{0x} \phi_{1x} + \zeta_{0y} \phi_{1y} - \phi_{1z} + D(x, y) = 0. \quad (3.4)$$

At the limit $\phi_t = 0$, Eqs. (3.3) and (3.4) yield the same free surface condition as Dawson's [5]. Then this case corresponds to MLST. The other is

$$\zeta_{1t} + \phi_{0x} \zeta_{1x} + \phi_{0y} \zeta_{1y} - \zeta_{0x} \phi_{1x} - \zeta_{0y} \phi_{1y} - \phi_{1z} + D(x, y) = 0. \quad (3.5)$$

At the steady state, combination of Eqs. (3.3) and (3.5) leads to the same condition as Baba's one [3]. Then this case corresponds to LST.

Since the computation domain is limited, other boundary conditions are necessary:

- (i) $\phi_i = \zeta_i = 0$ at the upstream end and side ends ($\pm y_B$)
 - (ii) $\phi_i = 0$ at the depth (z_B) deeper than a certain depth
 - (iii) radiation condition at the downstream end
- (3.6)

As to last condition, Orlanski's treatment is applied following the Chan's method.

As a result, combination of Eqs. (3.2), (3.3) and (3.4) corresponds to the modified low speed theory, and combination of Eqs. (3.2) (3.3) and (3.5) corresponds to the conventional low speed theory. Use of the body-fitted coordinate system in the y-direction and the finite difference scheme follows the Chan's procedure.

The wave-resistance R_W is obtained by the momentum theorem as

$$R_W = \frac{\rho}{2} \int_{-y_B}^{y_B} dy \int_{z_B}^{\zeta_1} (\phi_{1y}^2 + \phi_{1z}^2 - \phi_{1x}^2) dz + \frac{1}{2} \rho g \int_{-y_B}^{y_B} \zeta_1^2 dy \quad (3.7)$$

at far downstream end.

4. Calculated Results

We select two kinds of vertical cylinders. One is of an ogival

water plane which we name L-15, because it has lens shape and breadth /length=0.15. The other has an elliptical water plane which we name E-15. The length of each cylinder L is 1.0m.

4.1 Low Speed Theory

A finite region of integral is divided into 92 segments in the x-direction and 38 in the y-direction. Figs.1a,b show the mesh divisions around cylinders. Figs.2a,b show the strained coordinates obtained by Eq. (2.4). These values are strained considerably near F.P. and A.P.. Functions $\bar{D}(x,y)$ are shown in Figs.3a,b. This function becomes large and changes violently near F.P. and A.P. Therefore the area near the ends of cylinder is divided very small as in Fig. 1.

The range of θ -integral is from 0° to 65° at $F_n=0.2$ and the upper limit increases until 80° with F_n because exact integration is difficult beyond this limit due to violent change of the integrand. Figs.4a,b and Figs.5a,b show the weighted amplitude functions AMP obtained by MLST and LST. The values of C_W are tabulated in Table 1 and are shown in Figs.8 and 9 in the forms of curves. Difference between MLST and LST are considerable both in magnitude and in phase in the range $F_n < 0.35$.

4.2 Finite Difference Method

The advantage to divide the velocity potential ϕ into ϕ_0 and ϕ_1 is to reduce the number of the mesh points in the depthwise direction. Mesh intervals Δx , Δy , Δz are changed according to F_n as follows:

F_n	Δx	Δy	Δz	Δt
0.23	0.0425	0.021	0.080	0.1
0.25	0.050	0.025	0.085	0.1
0.27	0.056	0.030	0.100	0.1

Numbers of division are 39 in the x-direction, 24 in the y-direction and 6 in the z-direction. And number of iteration is 230. Figs. 6 and 7 show the wave patterns around cylinders. At the first glance, these patterns seem to be plausible. But, if examined in detail, they are not so fine. For example, the first crest of the wave of L-15 shows the phase-lag compared with experimental results. One of reasons for it may be caused by the coarse mesh around F.P. and A.P. And we wish to add the fact that the wave patterns change considerably by changing the mesh intervals. R_w is obtained by Eq. (3.7) which is evaluated at the last 10 sections behind the ship. Since R_w oscillates along the x-direction, we take the mean value as the wave-resistance in the steady state. These values are tabulated in Table 2 and plotted in Figs. 8b and 9b. The agreements between numerical results and analytical ones are not so good.

5. Concluding Remarks and Acknowledgement

Through the computations performed, we have following remarks.

- 1) If the results obtained by the low speed theory are fine, the analytical method is still effective in evaluating wave-resistance, because the computer time is very short.
- 2) Finite difference method needs more know-how, experiences, time and money. But it has big advantage that the whole flow field

becomes clear over the analytical method.

We wish to express our heartfelt gratitude to Messrs. Matoshi Nakamura, Akio Toshima, Tatsuya Eguchi, Kouzou Seta for their developing the computer programs. We are also very grateful to Miss Keiko Matsuki for her making the manuscript. Further we are deeply indebted to the staffs of the Large-Sized Computer Center of Kyushu University for their work using FACOM M-200. This research is partly supported by the Grant-in-Aid for Research of the ministry of Education, Science and Culture.

References

- [1] Nakatake, K., Toshima, A and Yamazaki, R: Wave-Resistance calculation for Wigley, Inuid Hull S-201 and Series 60 Hulls, Proc. of the Workshop on Ship Wave-Resistance Computations, (1979)
- [2] Yamazaki, R., Nakatake, K. and Nakamura, M.: Low Speed Wave-Resistance Theory Making Use of Strained Coordinates, International Joint Research Report (1978)
- [3] Baba, E.: Wave Resistance of Ships in Low Speed, Mitsubishi Tech. Bulletin No. 109 (1976)
- [4] Guevel, P., Vaussy, P. and Kobus, J.M.: The Distribution of Singularities Kinematically Equivalent to a Moving Hull in the Presence of a Free Surface, Int. Ship. Progress, Vol. 21 (1974)
- [5] Dawson, C.W.: Calculations with the XYZ Free Surface Program for Five Ship Models, Proc. of the Workshop on Ship Wave-Resistance Computations, (1979)
- [6] Mori, K.: Comments on Papers Presented at the Workshop on Wave-Resistance Computations, Report of JTTC Panel I, 1980-I-1 (1980)
- [7] Chan, R.K.C.: Finite Difference Simulation of the Planar Motion of a Ship, Second Inter. Conf. on Numerical Ship Hydrodynamics (1977)

Table 1 C_w Values Calculated by the Low Speed Theory

F_n	OGIVAL WATER PLANE		ELLIPTICAL WATER PLANE	
	MODIFIED LOW SPEED THEORY	LOW SPEED THEORY	MODIFIED LOW SPEED THEORY	LOW SPEED THEORY
0.15	0.027×10^{-3}	0.047×10^{-3}	0.291×10^{-3}	0.144×10^{-3}
0.16	0.037	0.046	0.333	0.241
0.17	0.124	0.070	1.283	0.622
0.18	0.054	0.162	0.476	0.429
0.19	0.232	0.094	2.052	0.833
0.20	0.117	0.272	1.742	0.528
0.21	0.228	0.264	1.077	1.539
0.22	0.559	0.185	3.402	0.990
0.23	0.454	0.548	4.705	0.775
0.24	0.197	0.733	3.224	2.119
0.25	0.423	0.511	1.852	2.945
0.26	1.154	0.346	2.789	2.275
0.27	1.886	0.734	5.752	1.200
0.28	2.087	1.494	8.840	1.353
0.29	1.726	2.167	10.500	2.782
0.30	1.128	2.464	10.420	4.748
0.31	0.656	2.305	9.134	6.527
0.32	0.621	1.800	7.082	7.272
0.33	1.287	1.247	5.233	6.872
0.34	2.770	1.005	4.050	5.685
0.35	4.987	1.313	4.000	4.215
0.40	20.29	10.72	16.73	4.120
0.45	32.61	24.61	34.12	17.47
0.50	37.70	33.71	44.27	31.36
0.55	36.18	35.67	45.81	38.14
0.60	31.61	33.05	41.80	38.40
0.65	26.42	29.06	36.11	35.03
0.70	21.76	24.93	30.05	31.12
0.75	17.86	21.35	24.78	26.87
0.80	14.84	18.71	20.76	22.64
0.85	12.29	17.02	17.53	19.22
0.90	10.36	15.98	14.88	16.90
0.95	8.79	15.20	12.54	15.44
1.00	7.40	14.41	10.38	14.50

Table 2 C_w Values Obtained by the Finite Difference Method

F_n	OGIVAL WATER PALNE		ELLIPTICAL WATER PLANE	
	MODIFIED LOW SPEED THEORY	LOW SPEED THEORY	MODIFIED LOW SPEED THEORY	LOW SPEED THEORY
0.22	0.25×10^{-3}	0.58×10^{-3}	0.28×10^{-3}	0.55×10^{-3}
0.23	0.22	0.56	0.25	1.5
0.24	0.17	0.44	0.46	2.8
0.25	0.24	0.14	1.25	2.1
0.26	0.56	0.20	1.9	1.3
0.27	1.1	0.70	2.4	3.0
0.28	1.6	1.4	2.5	4.0
0.29	3.1	3.0	—	3.5
0.30	4.2	4.0	—	5.5

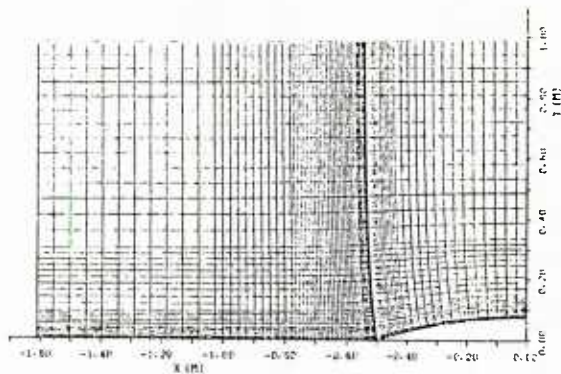


Fig. 1a Mesh Division
around L-15

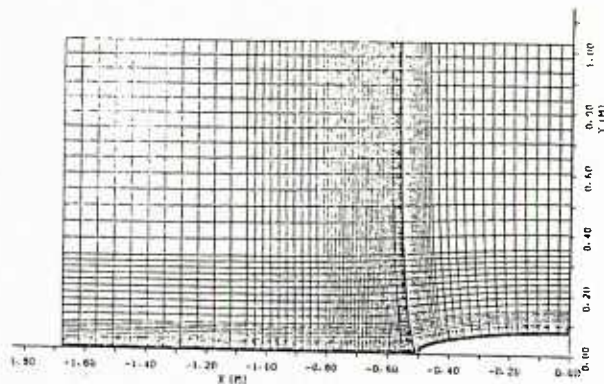


Fig. 1b Mesh Division
around E-15

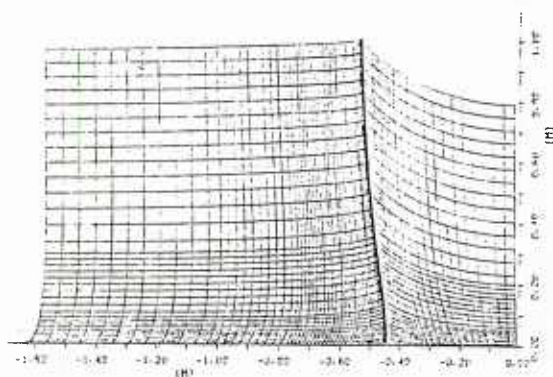


Fig. 2a Strained Coordinates
around L-15

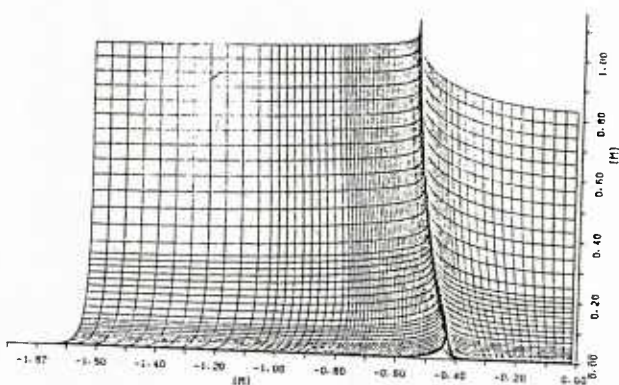


Fig. 2b Strained Coordinates
around E-15

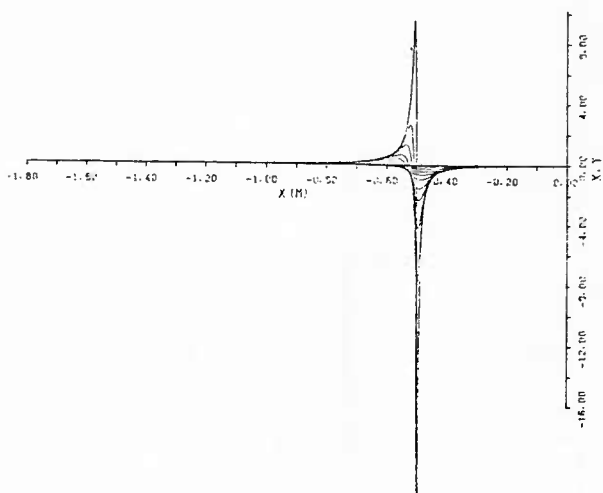


Fig. 3a $\bar{D}(x,y)$ Function of L-15

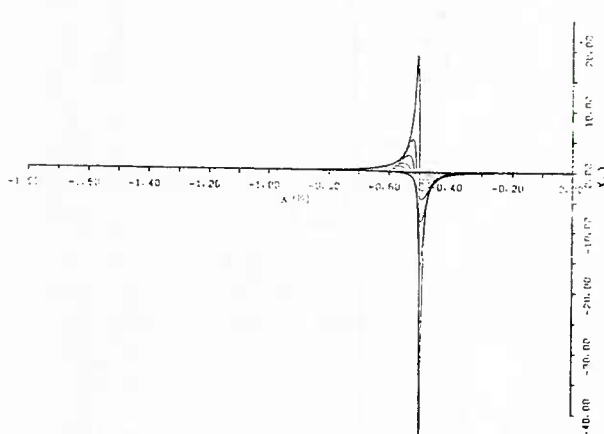


Fig. 3b $\bar{D}(x,y)$ Function of E-15

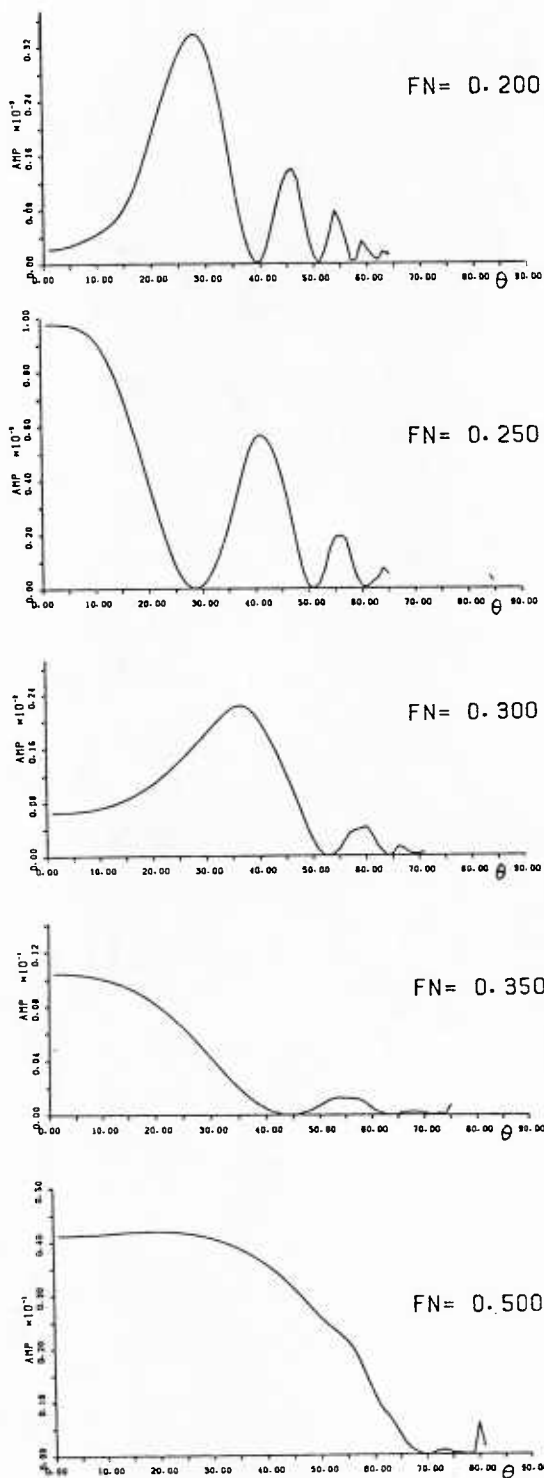


Fig. 4a Weighted Amplitude Functions of L-15 by MLST

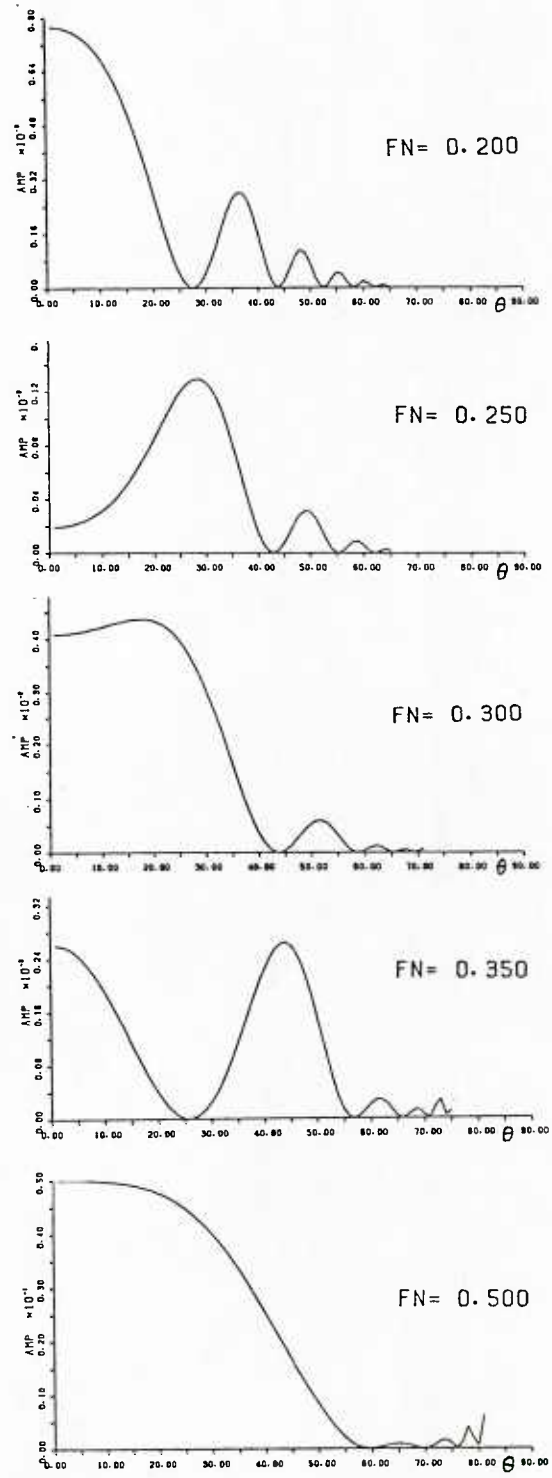


Fig. 4b Weighted Amplitude Functions of L-15 by LST

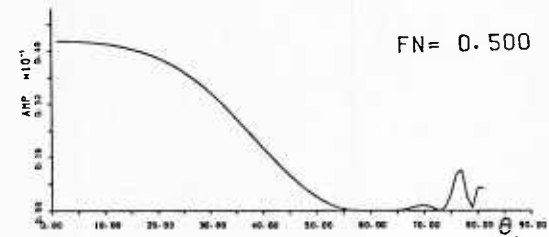
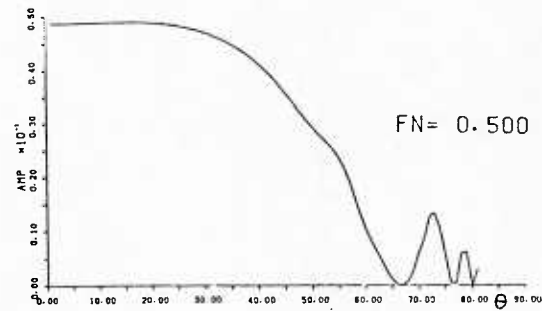
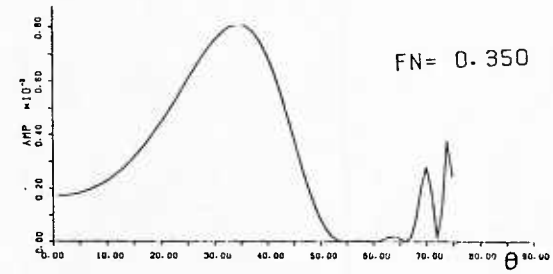
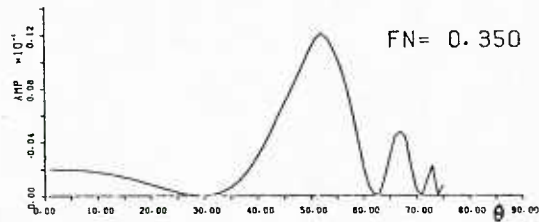
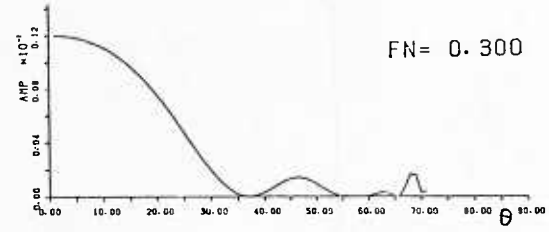
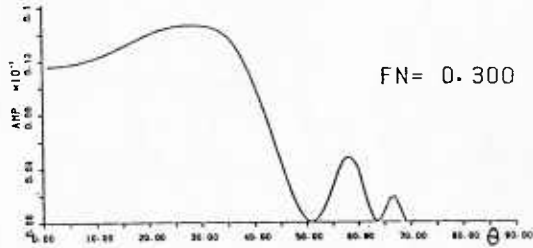
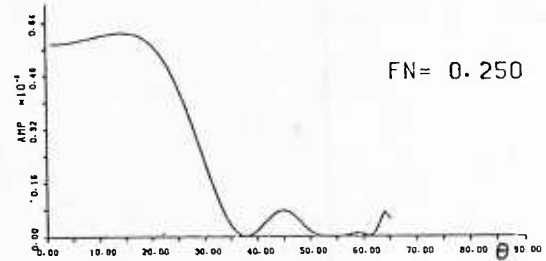
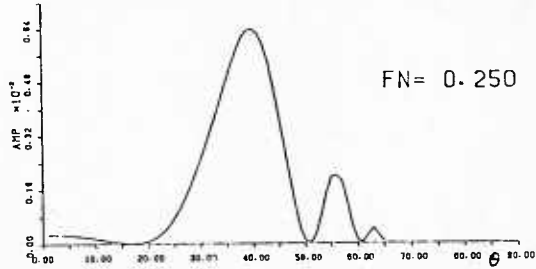
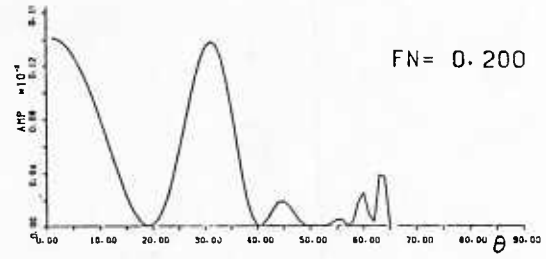
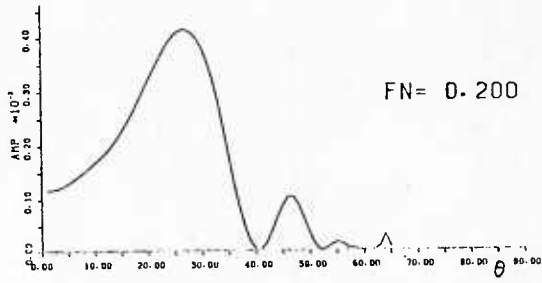
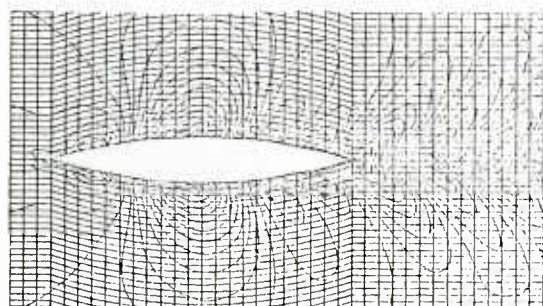
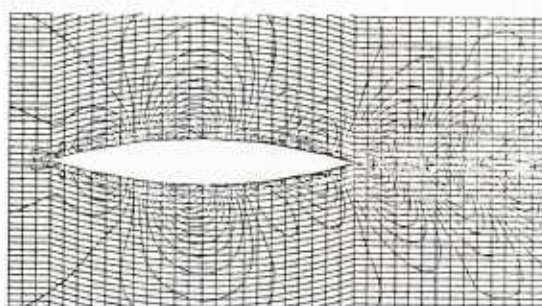


Fig. 5a Weighted Amplitude Functions of E-15 by MLST

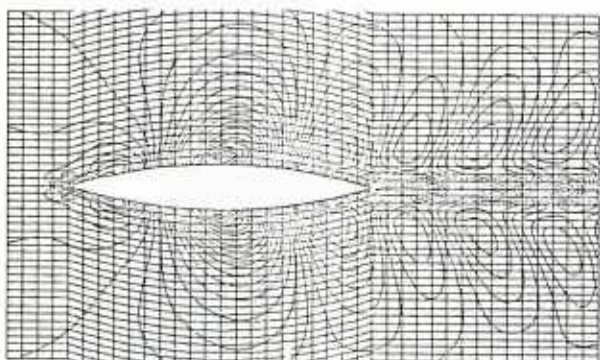
Fig. 5b Weighted Amplitude Functions of E-15 by LST



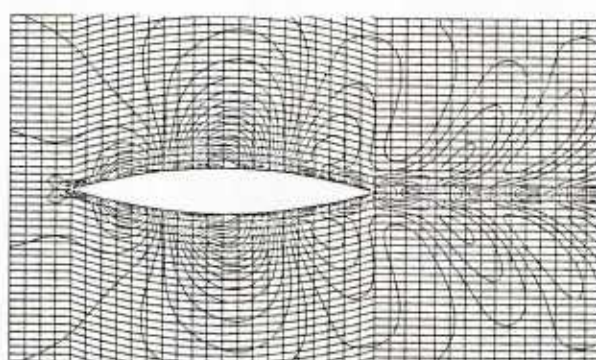
$Fn=0.23$



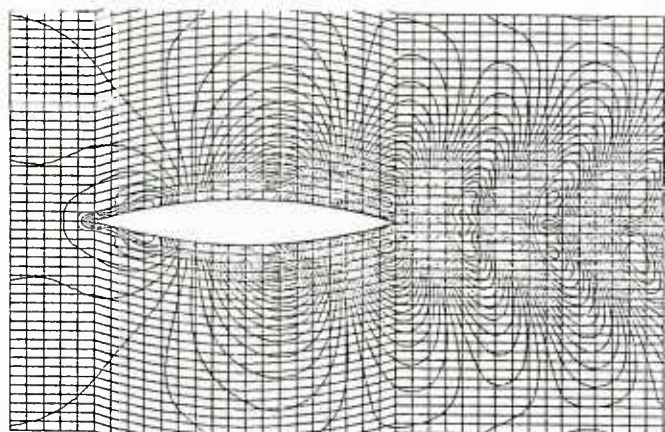
$Fn=0.23$



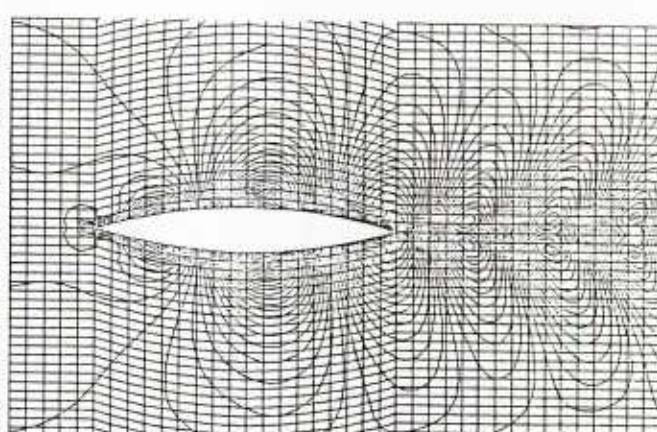
$Fn=0.25$



$Fn=0.25$



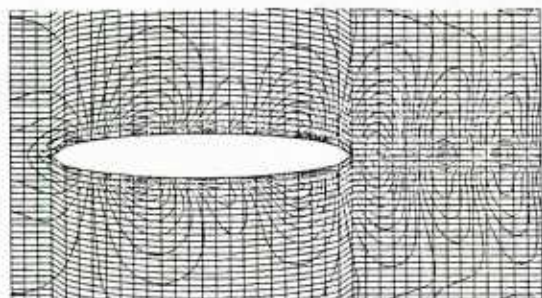
$Fn=0.27$



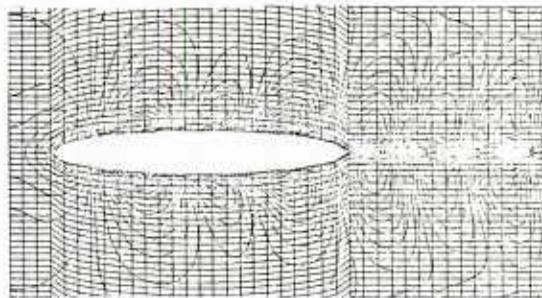
$Fn=0.27$

Fig. 6a Wave Patterns around L-15 by Equations of MLST

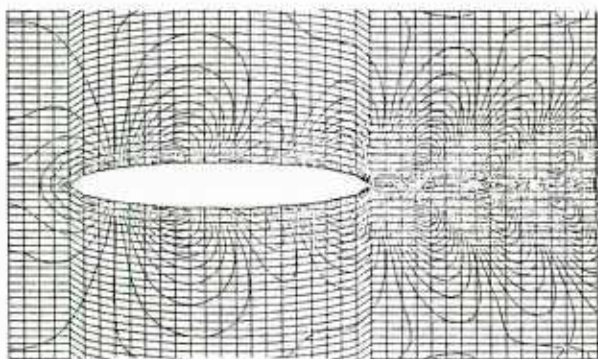
Fig. 6b Wave Patterns around L-15 by Equations of LST



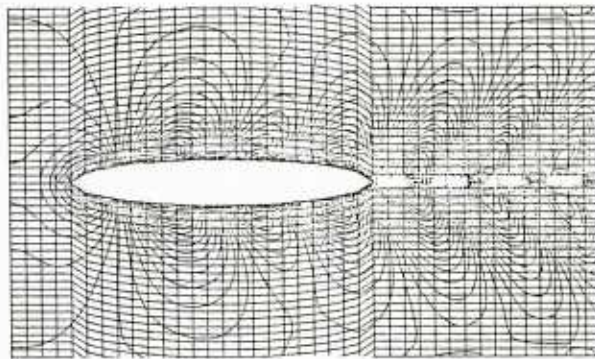
$Fn=0.23$



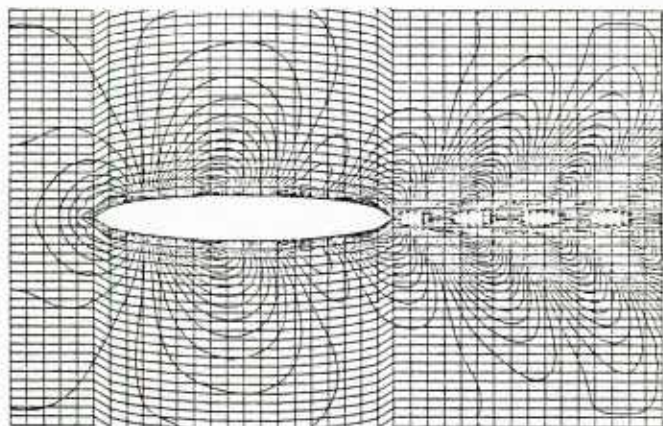
$Fn=0.23$



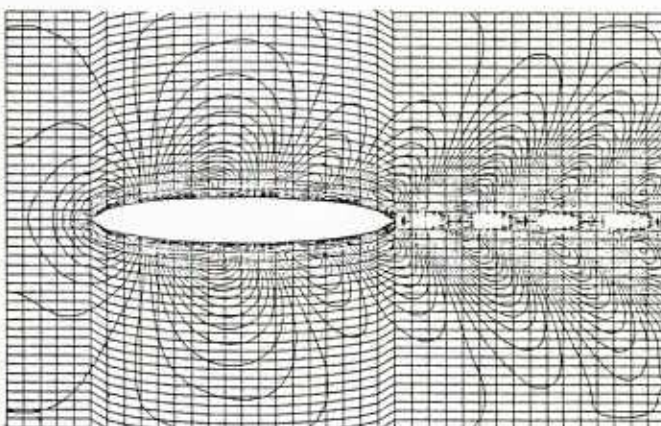
$Fn=0.25$



$Fn=0.25$



$Fn=0.27$



$Fn=0.27$

Fig. 7a Wave Patterns around E-15 by Equations of MLST

Fig. 7b Wave Patterns around E-15 by Equations of LST

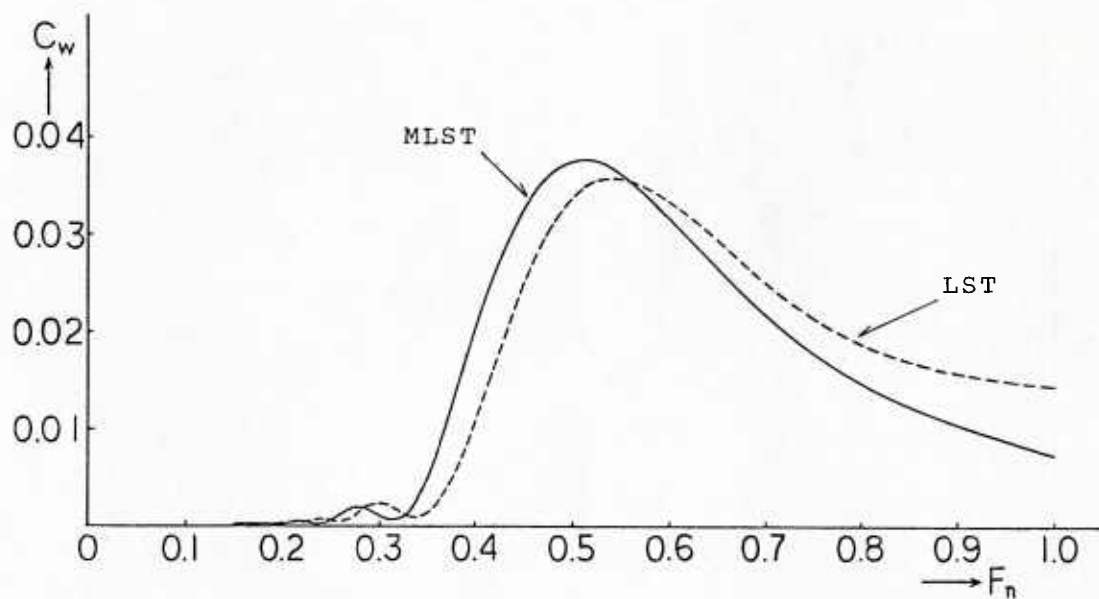


Fig. 8a Comparison of C_w of L-15 between MLST and LST

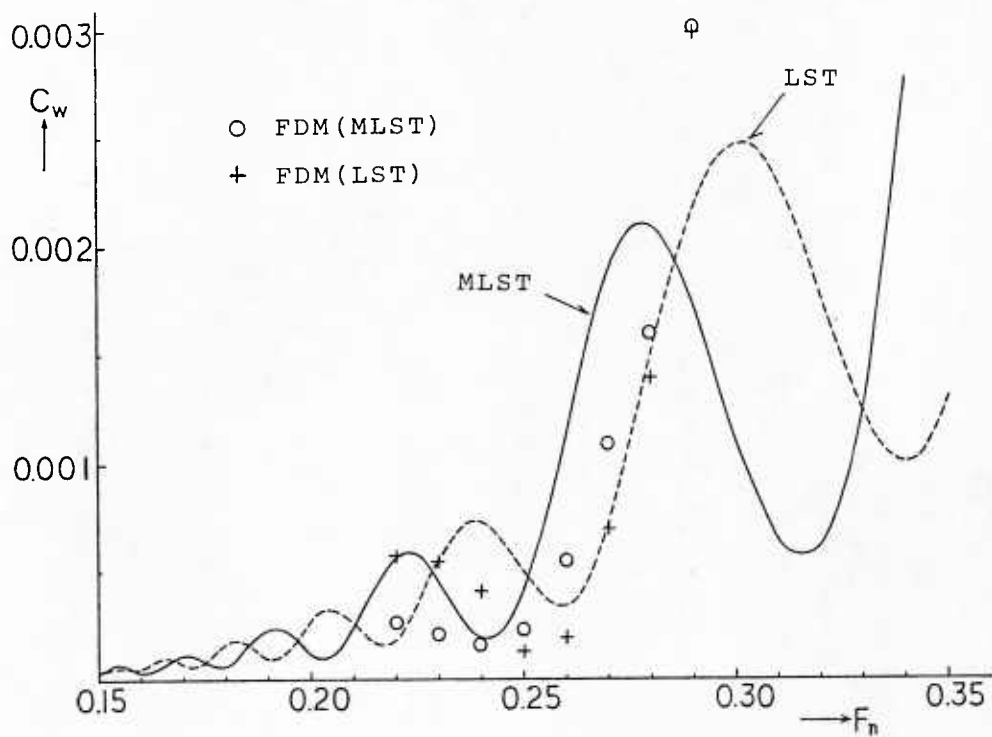


Fig. 8b Comparison of C_w of L-15 among Four Methods

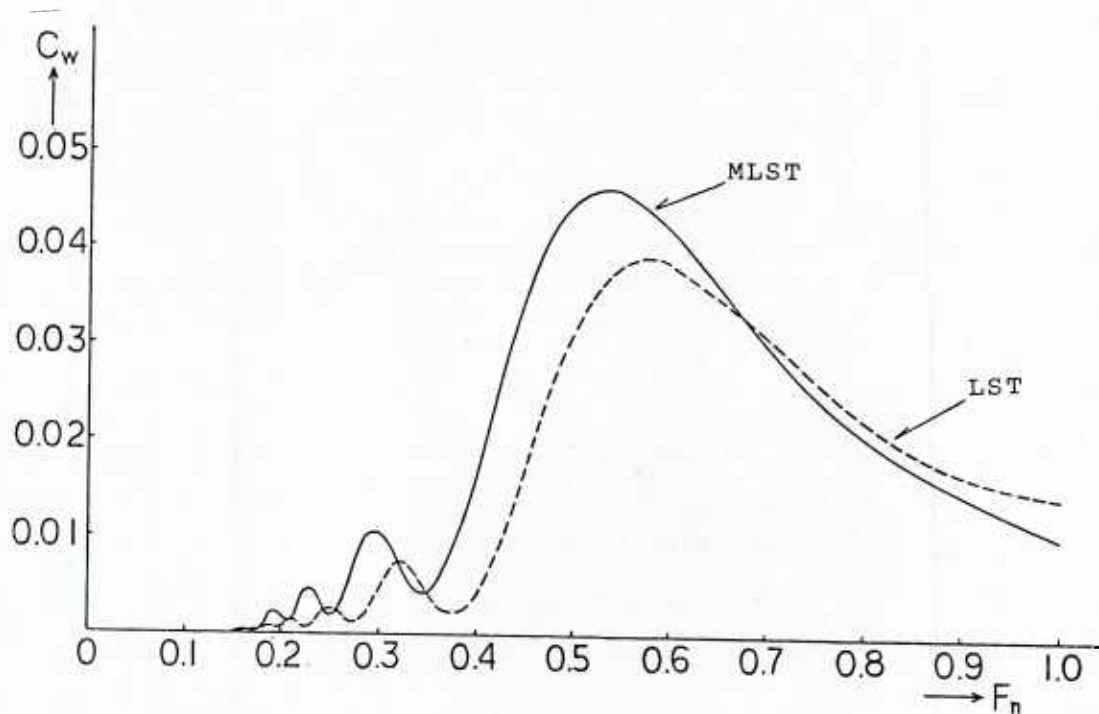


Fig. 9a Comparison of C_w of E-15 between MLST and LST

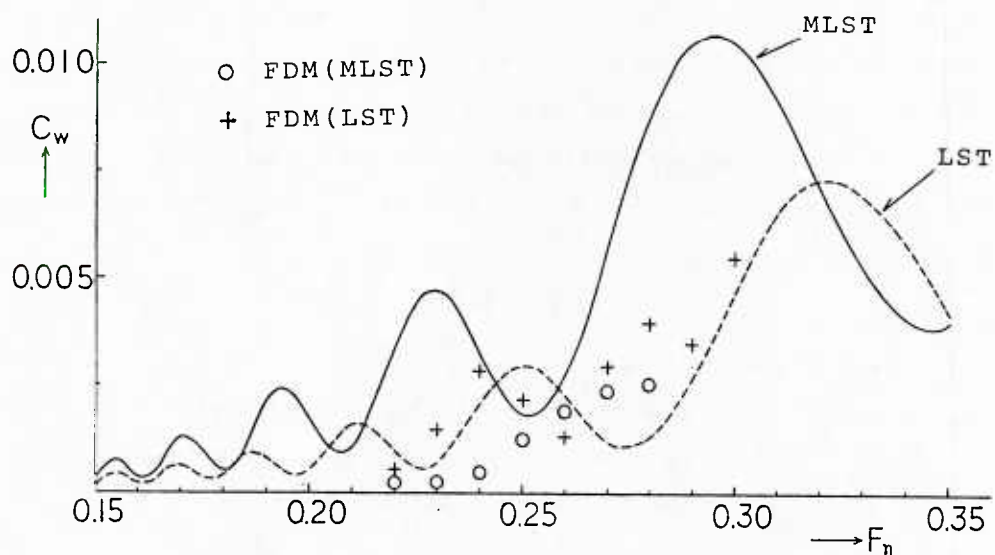


Fig. 9b Comparison of C_w of E-15 among Four Methods

NUMERICAL CALCULATIONS OF THE POTENTIAL FLOW
ABOUT THE WIGLEY HULL*

S. M. Yen and R. R. Chamberlain
Coordinated Science Laboratory
University of Illinois
Urbana, Illinois 61801

Introduction

The objective of our study is to develop a numerical method to solve directly the potential equation for the full nonlinear ship wave problem. In a sense, we attempt to design and construct a numerical towing tank to measure the potential flow field around a ship of arbitrary shape. We have chosen a design of the numerical towing tank which has the following features:

- (1) The computational domain moves with the ship and is bounded by the free surface, the upstream boundary, the downstream boundary, the side boundary, the symmetry boundary, the hull surface and the bottom boundary (See Fig. 1); therefore, only half of the model is tested. The positions of the boundaries can be changed with respect to the hull position.
- (2) The computational mesh system is divided into several regions which are designed to adapt to the hull surface, the free surface and the local property gradient. The mesh near the free surface is time-dependent. The aim of the mesh system is to obtain as uniform as possible an error distribution in the numerical solution. Experimentally, the placement of the nodes determines the positions at which numerical measurements are taken.
- (3) The boundary conditions are set as follows:
 - (a) Upstream boundary: free stream.
 - (b) Downstream boundary: (i) placed close to the ship: nonreflective
(ii) placed at a large distance from the ship:
free stream below the surface.

This work was sponsored by the Office of Naval Research under Contract N00014-80-C-0740

- (c) Symmetry boundary: symmetry condition.
 - (d) Bottom boundary: $\phi_z = 0$ (ϕ = potential function).
 - (e) Side boundary: $\phi_y = 0$.
 - (f) Hull surface: solid body condition.
 - (g) Free surface: kinematic and dynamic conditions.
- (4) The time-dependent approach is used to obtain the long-time (steady state) solution. The free surface condition is updated at each time step by using a stable scheme with as little damping as possible.
- (5) The governing equation, which is complicated due to the complex mesh system and the resulting numerical transformation, may be solved by using an iterative method. The elliptic solver is the numerical instrument to measure the flow variable, i.e., the potential function.

The design features involve several computational difficulties which are characteristic of the free surface wave problem. We have developed methods to deal with these computational difficulties; however, these methods introduced new difficulties, some of which were unforeseen and which have to be resolved. We shall briefly mention two examples of these difficulties and possible ways to alleviate them. The first concerns the implementation of the downstream (open) boundary condition and the other, the solution of the elliptic equation. Orlanski's scheme to implement the open boundary condition, which involves the numerical calculation of the advection speed, is extremely sensitive to numerical errors. A method has been developed to implement this scheme for a nonlinear free surface wave problem [1]; however, its application to the ship wave problem has not been tested. Another alternative is to place the downstream boundary at a large distance from the ship and to apply the free stream condition below the free surface.

The body-fitted coordinate system introduces complexities into the structure of the matrix arising from the elliptic equation. These complexities preclude the use of fast direct solvers. A fast elliptic solver is needed not only to implement both the hull and the free surface conditions accurately, but also to increase the computational efficiency.

In our present phase of study, we tested the Wigley model in our numerical towing tank under the linearized condition. In this situation, we are able to use

a direct method to solve the elliptic equation by employing uniform mesh spacing in the x and y directions. We shall present in this paper the results of the numerical experiments which include the hull wave profile, the contour map of the waves about the ship, the wave resistance, the effect of open boundary and the effect of change in computational parameters. These numerical experiments were conducted on the Wigley ship under linearized conditions in order to study the validity of the basic features of our numerical method. It is our intention that this study will lead to the development of a numerical towing tank for a ship of arbitrary shape under nonlinear conditions.

Numerical Method

The Wigley hull under consideration is defined by the equation

$$f(x, z) = \frac{B}{2}(1 - 4x^2)(1 - z^2/H^2) \quad (1)$$

for $-\frac{1}{2} \leq x \leq \frac{1}{2}$

and $-H \leq z \leq 0$

$$B = 0.10$$

$$H = 0.0625$$

The wetted hull surface area at rest, S (nondimensionalized by L^2), is obtained from the formula

$$S = 2 \int_{-H}^0 \int_{-1/2}^{1/2} [1 + f_x^2 + f_z^2]^{1/2} dx dz \quad (2)$$

All integrations are performed using cubic spline quadrature, and the value for S is 0.1487906.

We wish to numerically solve for the potential function ϕ about the Wigley hull as well as the free surface height η under linearized conditions. Under these conditions, we apply the hull condition on the centerplane of the ship and the kinematic and dynamic conditions on the level of the undisturbed free surface (the plane $z = 0$). With the implementation of the boundary conditions simplified in this way, we may use the Cartesian coordinate system. The governing equation to be solved numerically is, therefore, the Laplace equation.

The domain size in the x , y and z directions is $6.5 \times 2.42 \times 0.61$. (These lengths are nondimensionalized by the ship length L .) The mesh system is shown in Fig. 2. It is uniform in the x and y directions and nonuniform in the z direction. The number of grid points is $131 \times 31 \times 16$. We have also performed numerical experiments using other domain sizes and mesh systems in which nonuniform spacing is used in all directions.

The upstream boundary is located two ship lengths ahead of the bow and the downstream boundary is placed 3.5 ship lengths behind the stern. This placement is based on our early numerical experiments to study the influence of the location of the downstream boundary on the solution near the ship. We should point out, however, that the free stream condition is implemented only below the surface.

In our numerical experiment, the ship accelerates linearly to its final velocity in 10 time steps. The time step Δt is 0.02. (Time t is nondimensionalized by L/U , where U is the final velocity of the ship.) The values of ϕ and η at $t = 0$ are set equal to zero throughout the domain. At each time step, the free surface conditions are updated using a neutrally stable scheme [2]. Values of ϕ on the free surface are used as Dirichlet conditions in the solution of the Laplace equation. A fast direct solver [3] is used in the numerical solution of this equation.

Numerical Results

Long time solutions have been obtained for Froude number = $Fr = 0.266, 0.350$ and 0.452 . The hull wave profiles remain almost the same after $t = 3$. However, other results, including the wave resistance, reach their steady state values after a much longer time, particularly for lower Froude numbers.

The CPU time is 5.7 sec. per time step on the CDC Cyber 175 computer. The numerical calculation consists of the determination of η and ϕ at 4030 points on the free surface and the determination of ϕ at each of the 60,915 interior points. The results for the wave height on the free surface are useful in studying the effects of the location of the downstream and side boundaries and the implementation of the boundary conditions there.

Figs. 3 and 4 show the development of the wave profiles along the centerline for $Fr = 0.266$ and 0.452 . The wave profile on the hull appears to develop very

early while the disturbance barely reaches the downstream boundary. For $Fr = 0.266$, a disturbance appears at the upstream boundary at about $t = 2$. We are currently studying the source of this disturbance.

The hull wave profiles are tabulated in Table 1 and shown in Figs. 5-7. For $Fr = 0.266$ and 0.350 , we compare our results with the Michell profiles. The basic features of these two profiles are similar. However, the amplitudes of the bow waves in our calculations are lower. Also, there seem to be some differences near the stern for $Fr = 0.266$.

Our results of the wave resistance are tabulated in Table 2 for the three Froude numbers considered. Fig. 8 shows the wave resistance as a function of time for $Fr = 0.452$. It appears to reach the steady state value at $t = 7$. Fig. 9 shows the comparison of our results of the wave resistance with the Michell calculation and an experiment. This experiment measured the total resistance with the model fixed. Our values of the wave resistance are lower than the Michell values at higher Froude numbers.

Fig. 10 shows the wave pattern development about the Wigley hull for $Fr = 0.452$. We make the following observations. First, the side boundary is placed far enough away from the model so that the disturbance never reaches it during the course of the calculations. Second, a significant disturbance reaches the downstream boundary about $t = 5$ and is prevented from passing through. The question is whether this disturbance will have any influence on either the hull wave profile or the wave resistance. Our results indicate that there is no effect at all. (For example, see Fig. 8 for wave resistance.) Fig. 11 shows the wave development at a longitudinal cross section of the domain ($y = 1.13$). We observe that some wave reflection at the downstream boundary does occur away from the centerline. This reflection seems to propagate upstream.

References

1. Yen, S. M. and D. R. Hall, Implementation of Open Boundary Conditions for Non-linear Free Surface Wave Problems, 3rd Int. Conf. on Num. Ship Hydrodynamics, Paris, France, 1981, pp. 163-176.

2. Chan, Robert K.-C., Finite Difference Simulation of the Planar Motion of a Ship, Proc. 2nd Int. Conf. on Num. Ship Hydrodynamics, Berkeley, CA, 1977, pp. 39-52.
3. Swartztrauber, P. and R. Sweet, Efficient FORTRAN Subprograms for the Solution of Elliptic Partial Differential Equations, NCAR TN/IA-109, 1975, 139 pp.

Table 1

FORMAT FOR TABULATED VALUE OF WAVE ELEVATION

S. M. Yen and R. R. Chamberlain/Finite Difference

	Wigley Fr=0.266	Wigley Fr=0.350	Wigley Fr=0.452
x/ℓ	η	η	η
-1.0	0.075	0.050	0.032
-0.9	0.124	0.092	0.061
-0.8	0.108	0.109	0.081
-0.7	0.025	0.091	0.085
-0.6	-0.082	0.042	0.072
-0.5	-0.158	-0.023	0.045
-0.4	-0.166	-0.083	0.009
-0.4	-0.112	-0.124	-0.030
-0.2	-0.033	-0.137	-0.065
-0.1	-0.027	-0.123	-0.091
0	-0.041	-0.091	-0.106
0.1	0.012	-0.055	-0.109
0.2	-0.033	-0.027	-0.102
0.3	-0.067	-0.011	-0.090
0.4	-0.074	-0.007	-0.076
0.5	-0.062	-0.011	-0.064
0.6	-0.045	-0.014	-0.057
0.7	-0.033	-0.011	-0.054
0.8	-0.024	-0.011	-0.055
0.9	-0.008	0.013	-0.055
1.0	0.029	0.030	-0.049

Table 2

FORMAT FOR TABULATED VALUE OF WAVE ELEVATION

S. M. Yen and R. R. Chamberlain/Finite Difference

Fr	C_w
0.266	0.970 x 10⁻³
0.350	0.639 x 10⁻³
0.452	2.39 x 10⁻³

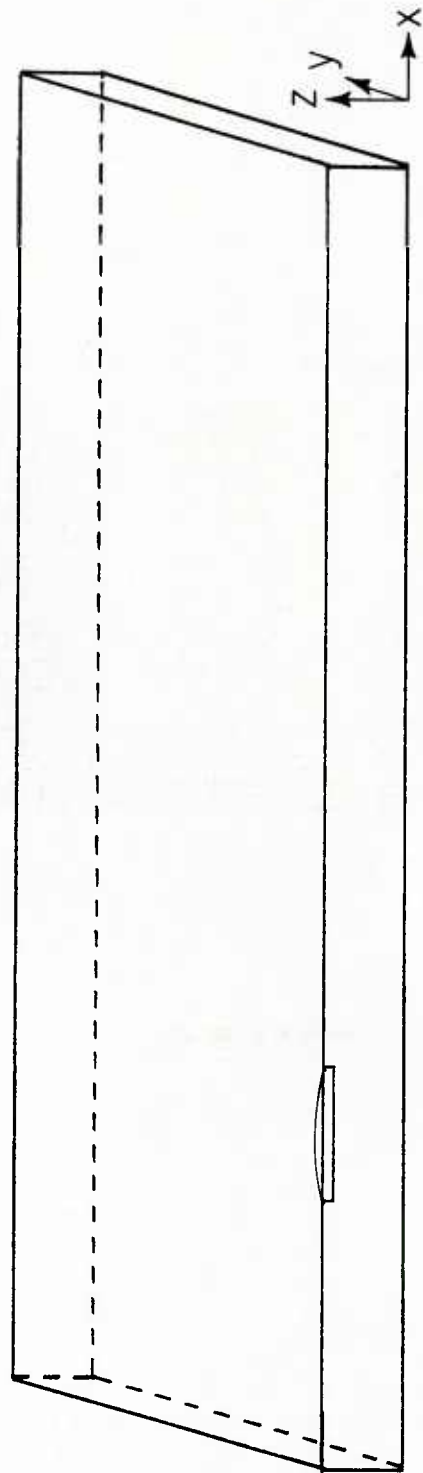


Fig. 1. Computational domain showing the relative placement of the boundaries and the Wigley model.

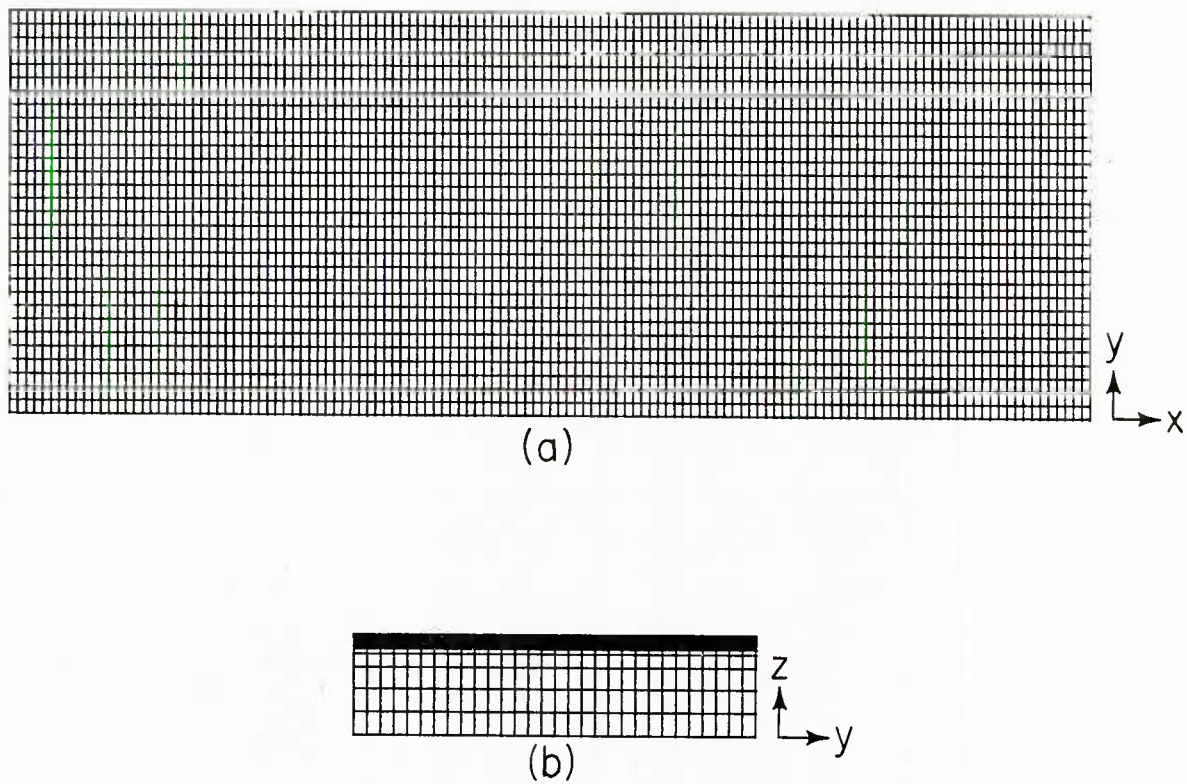


Fig. 2. Computational mesh system:

(a) x-y plane: uniform grid spacing,

(b) y-z plane: nonuniform grid spacing in the z-direction.

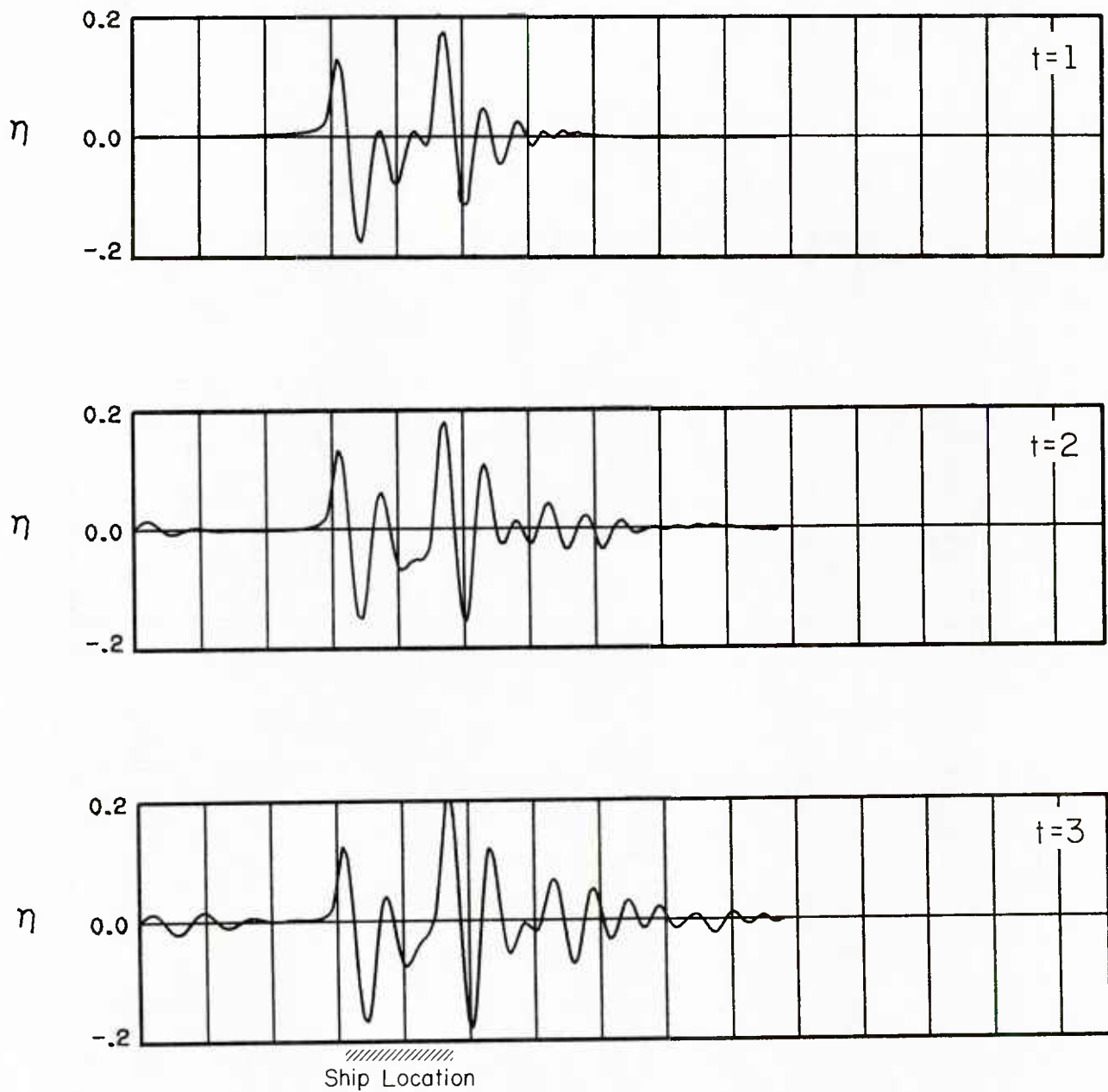


Fig. 3. Wave profile along the centerline at $t = 1, 2$ and 3 . $Fr = 0.266$.

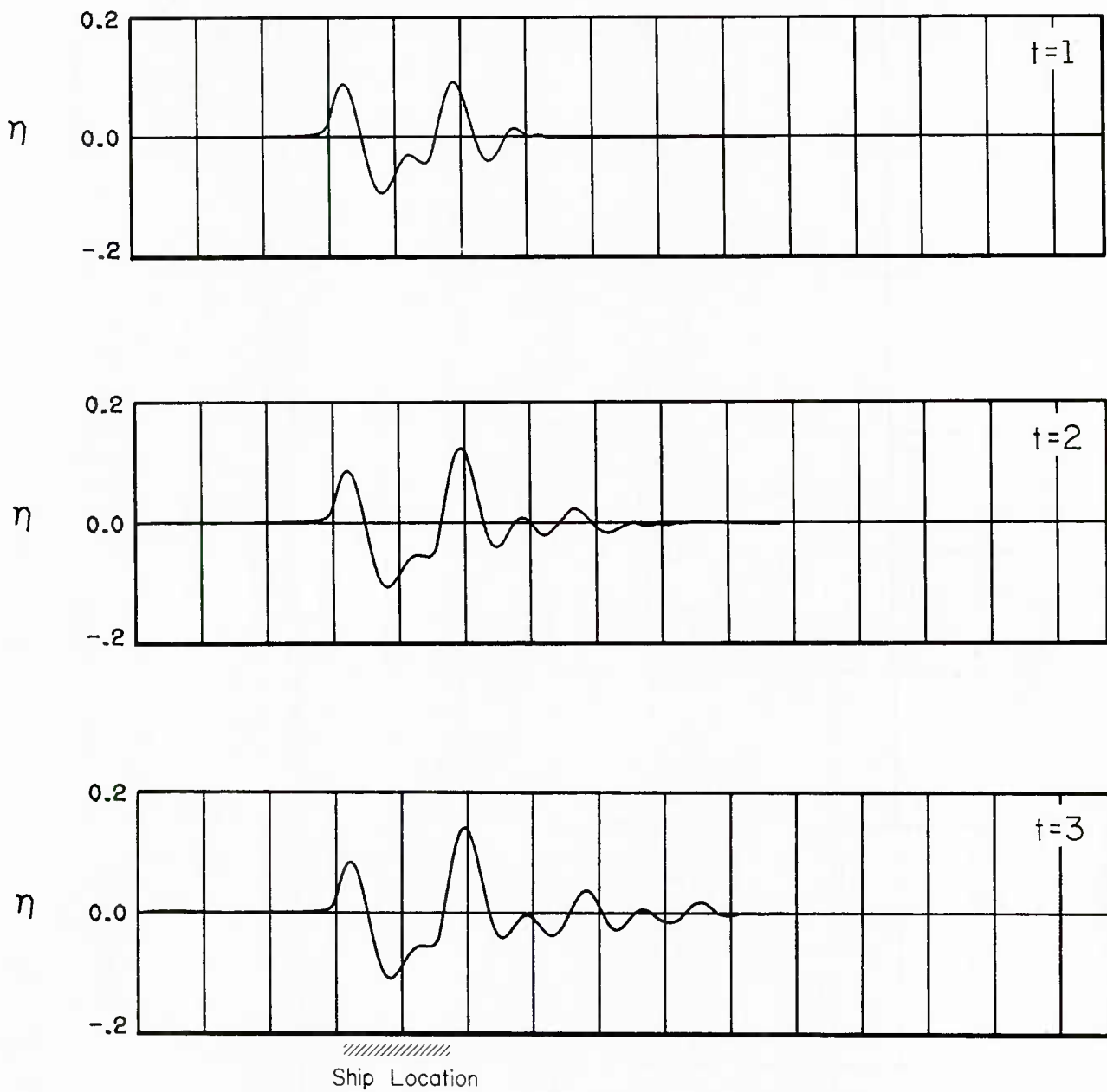


Fig. 4. Wave profile along the centerline at $t = 1, 2$ and 3 . $Fr = 0.452$.

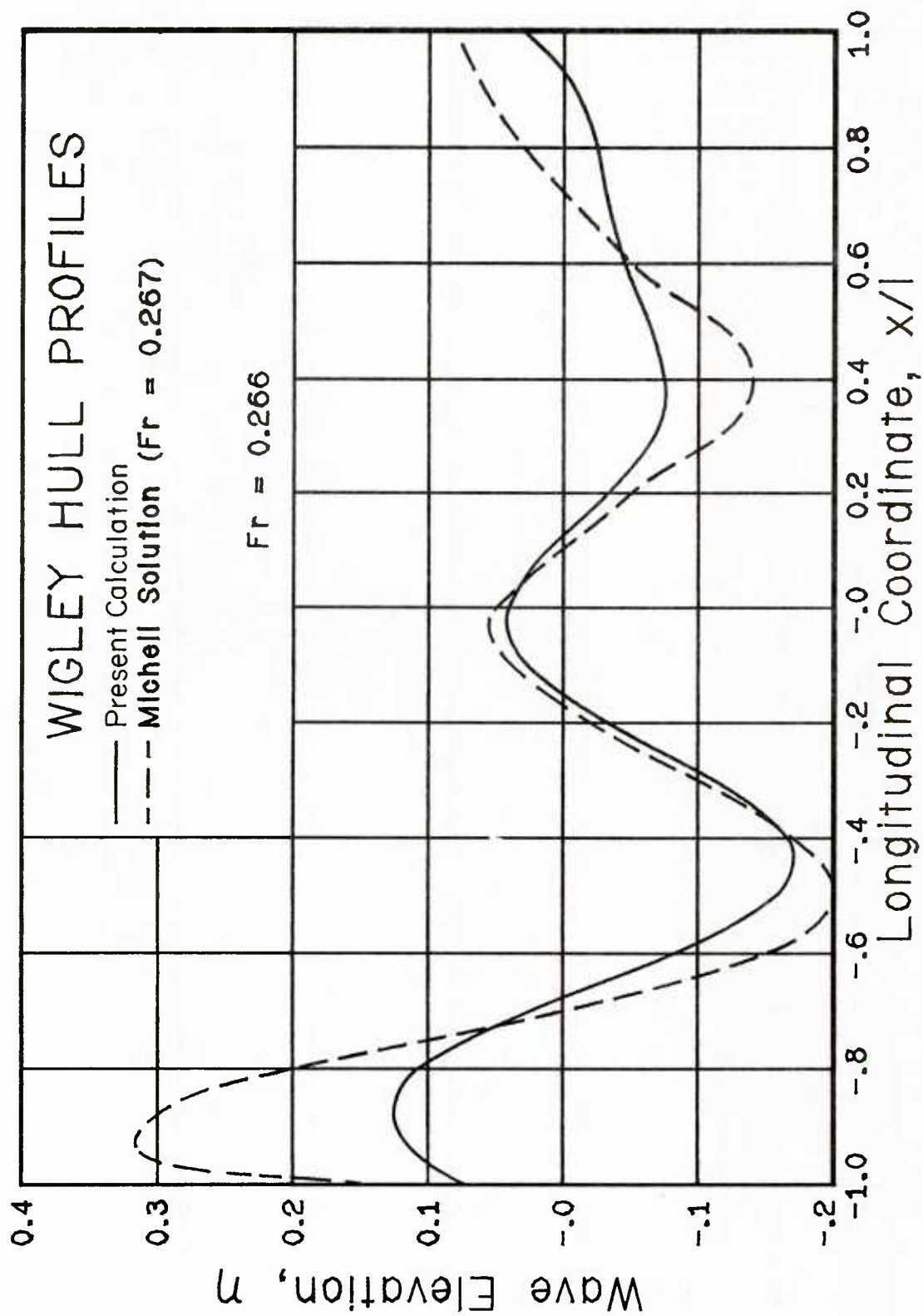


Fig. 5. Comparison of Wigley hull profiles. $Fr = 0.266$.

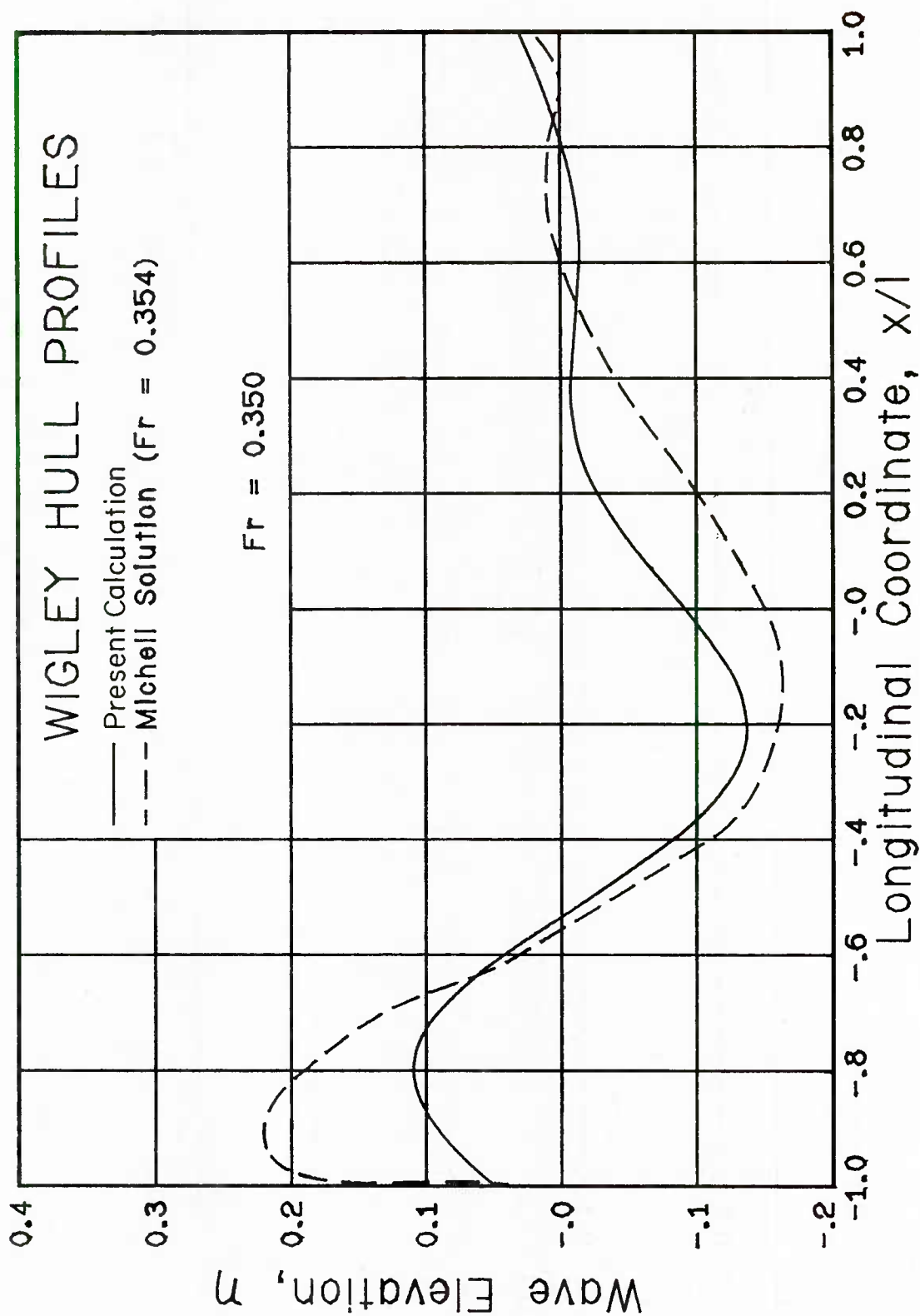


Fig. 6. Comparison of Wigley hull profiles. $Fr = 0.350$.

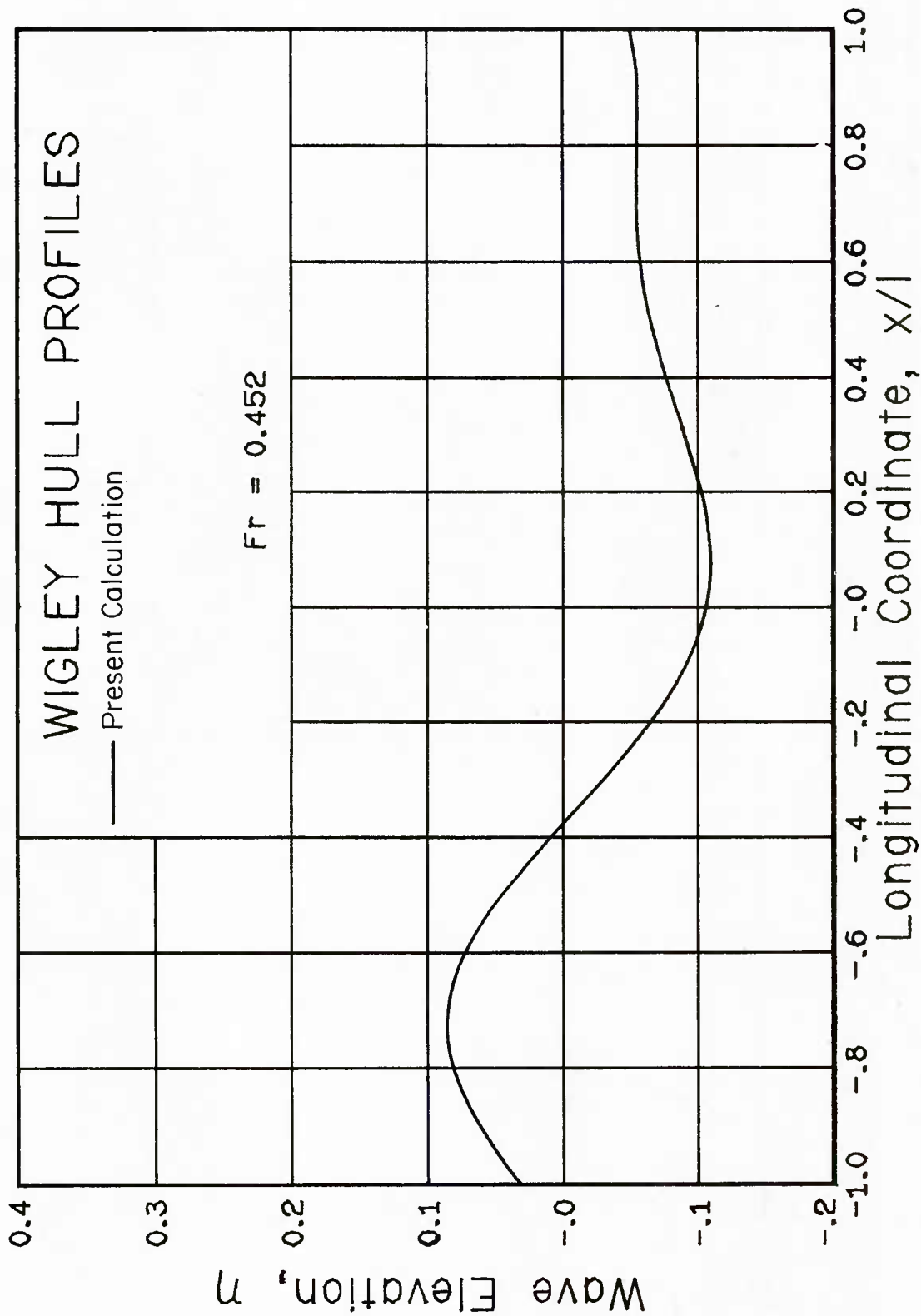


Fig. 7. Wigley hull profile. $Fr = 0.452$.

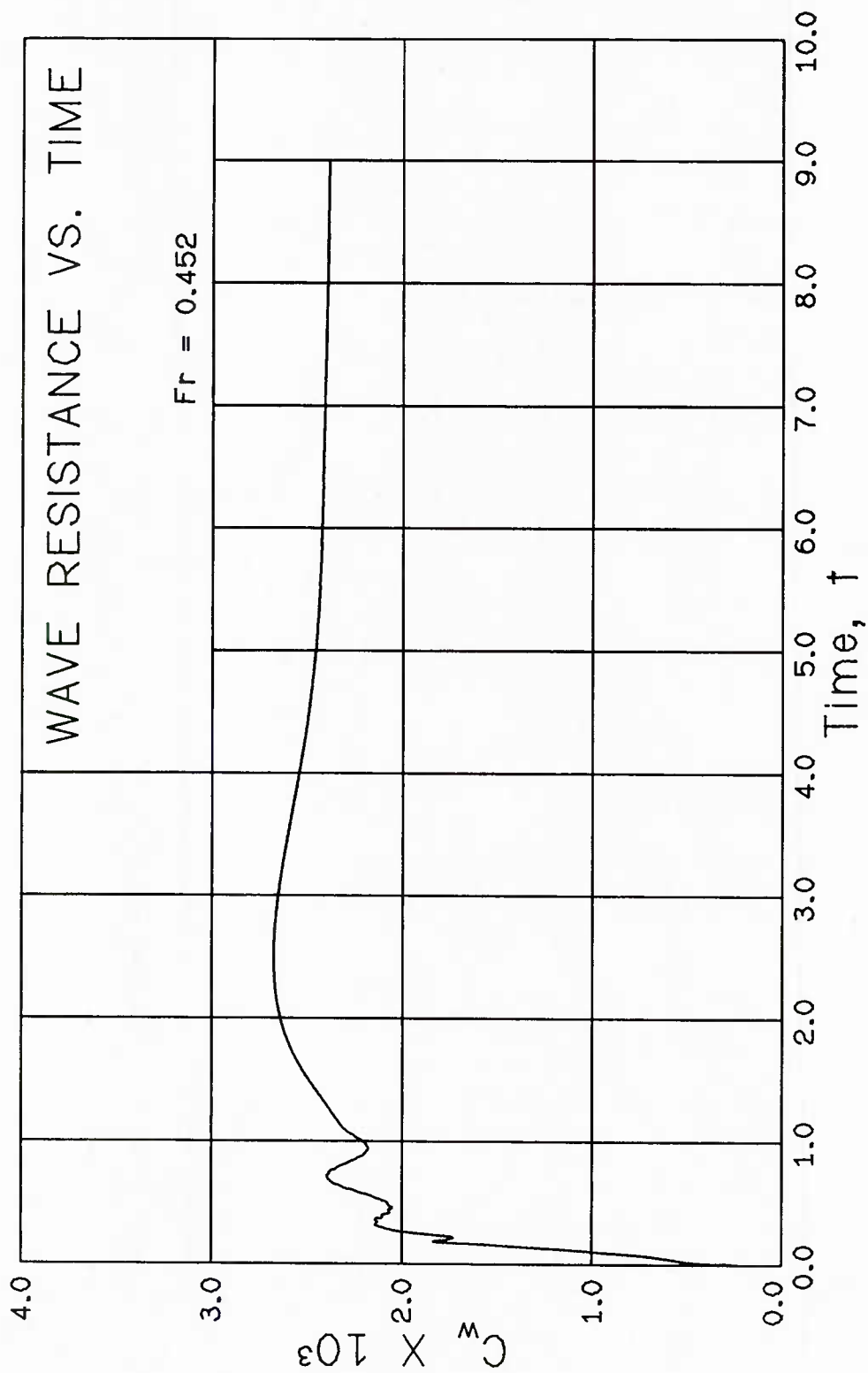


Fig. 8. Wave resistance as a function of time. $Fr = 0.452$.

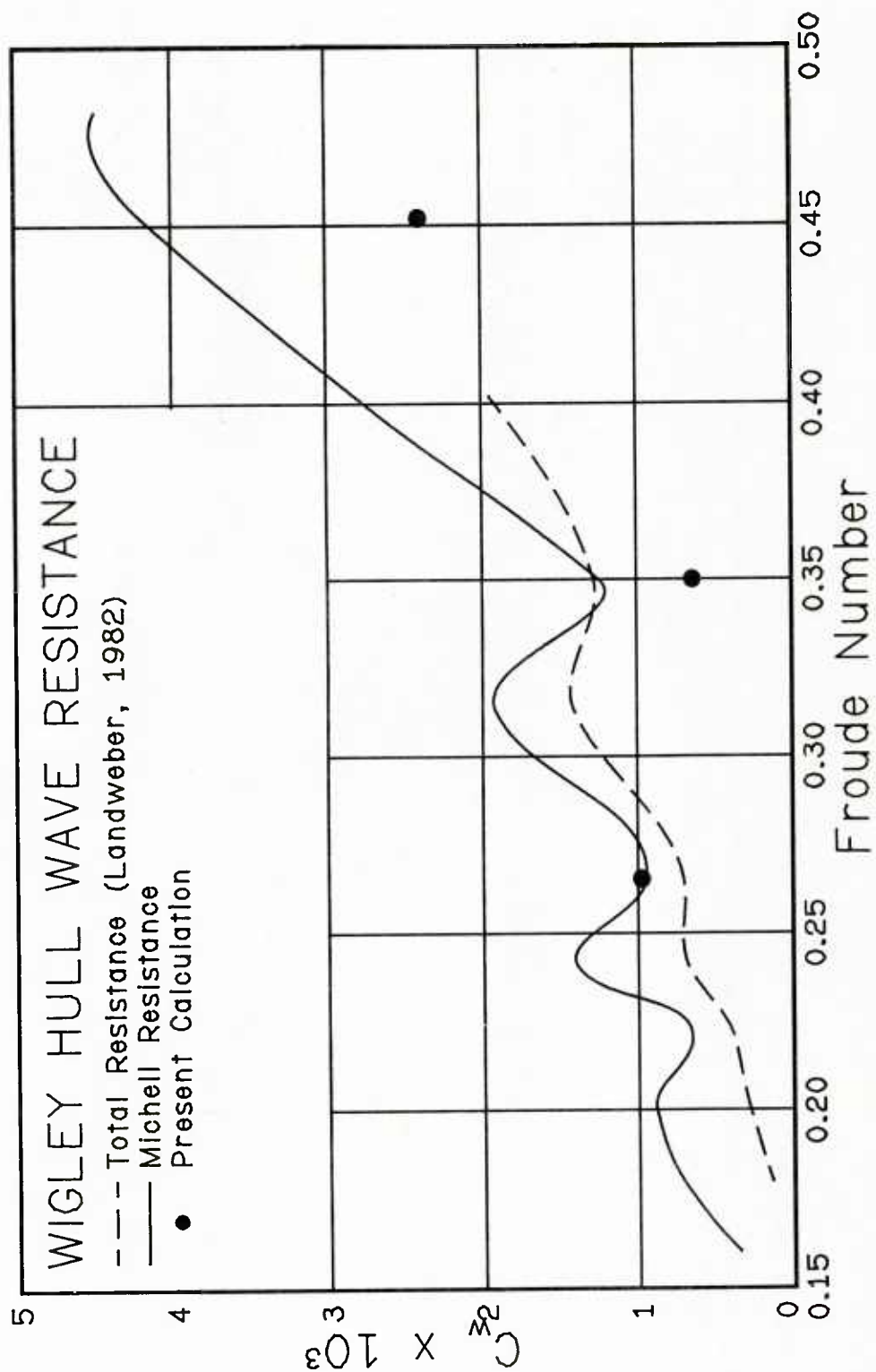


Fig. 9. Comparison of Wigley hull wave resistance vs. Fr.

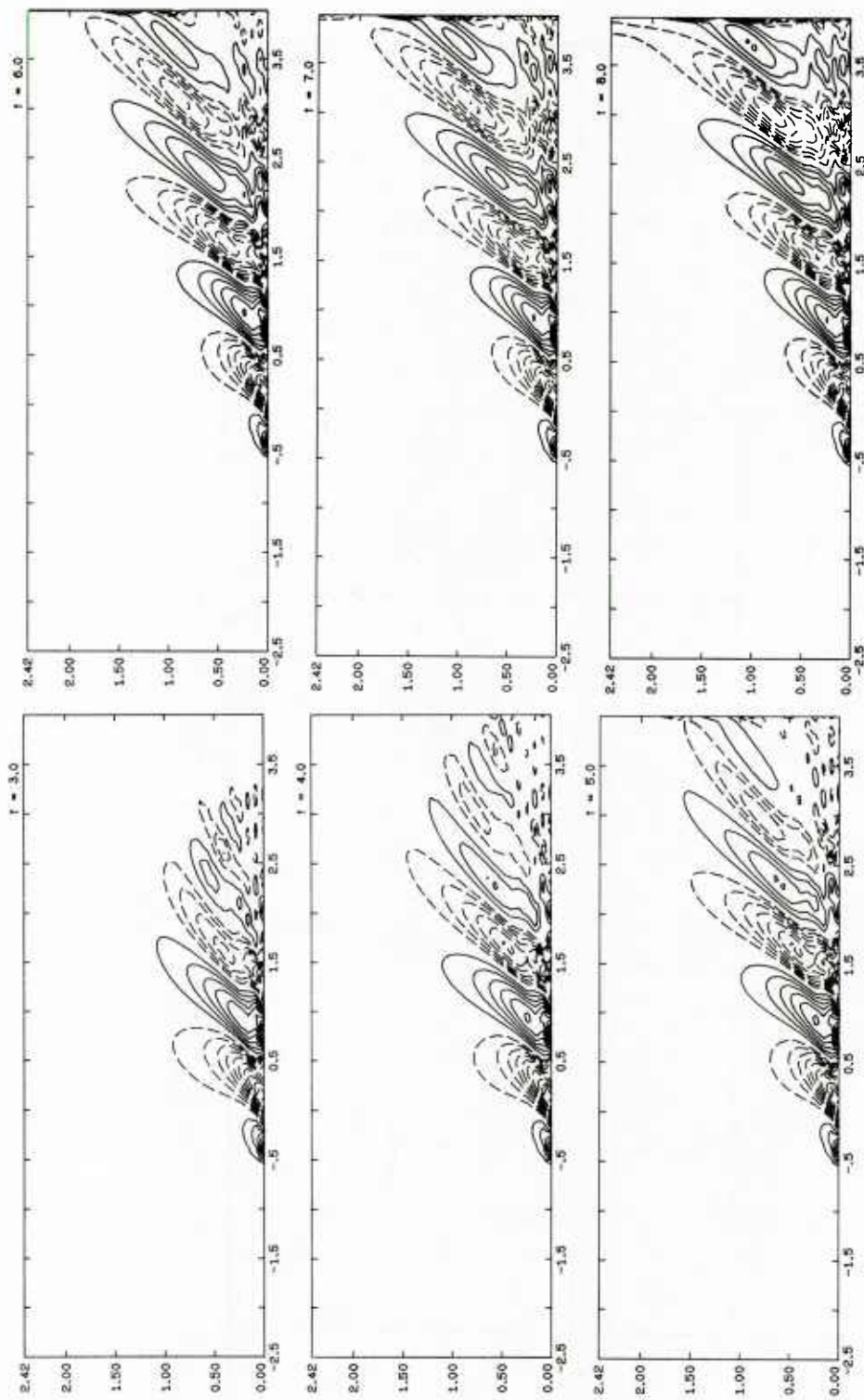


Fig. 10. Wave pattern development about the Wigley hull (located at $x = -0.5$ to $x = 0.5$) at $t = 3, 4, 5, 6, 7$ and 8 . $Fr = 0.452$.

LONGITUDINAL WAVE PROFILE

$Fr = 0.452$ $y = 1.13$

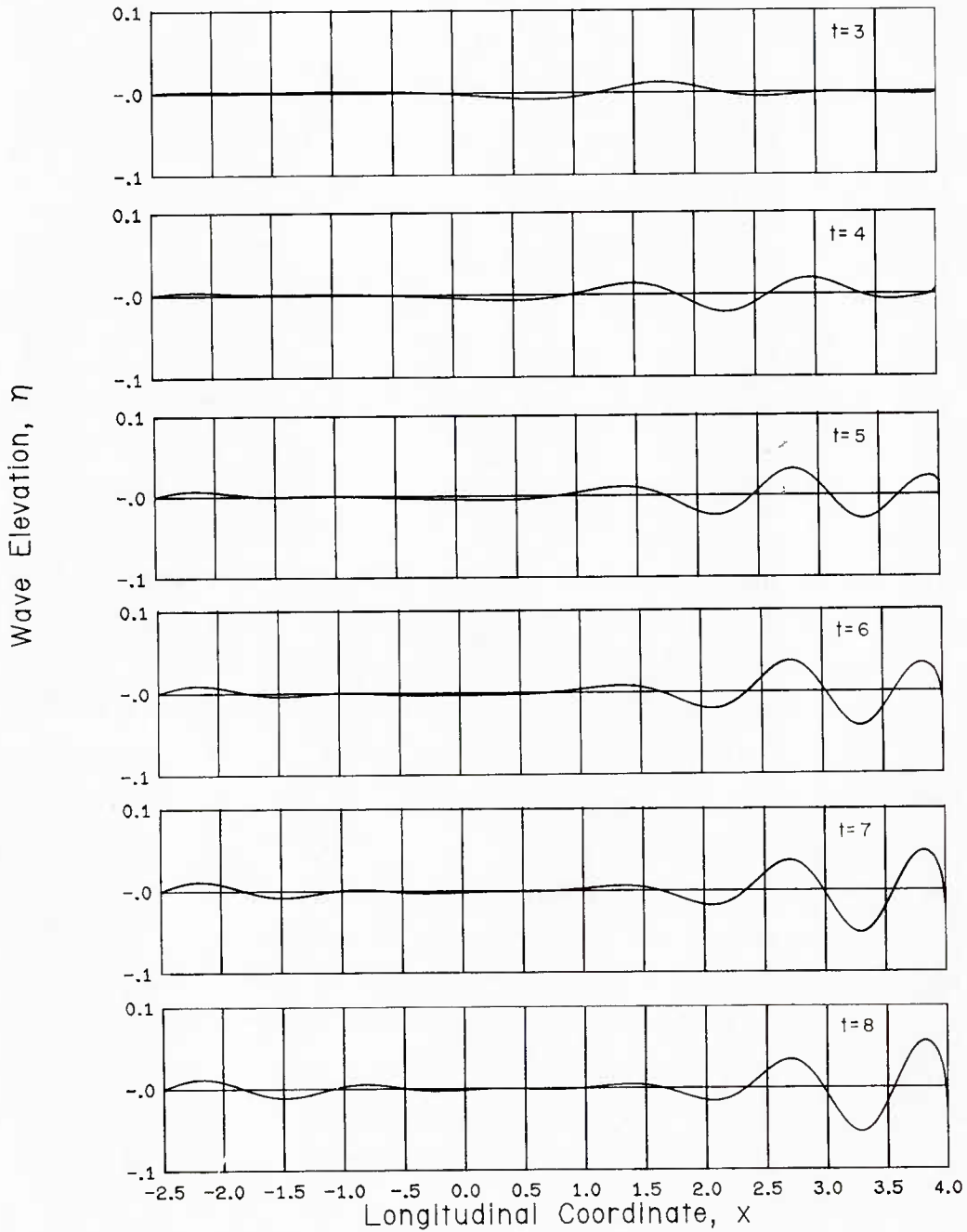


Fig. 11. Surface wave development at a longitudinal cross section ($y = 1.13$). $t = 3, 4, 5, 6, 7$ and 8 . $Fr = 0.452$.

NUMERICAL SIMULATION OF SHIP WAVES BY DIRECT INTEGRATION OF NAVIER-STOKES EQUATIONS

Hideaki Miyata
Shinichi Nishimura
Hisashi Kajitani

Department of Naval Architecture
The University of Tokyo

1. Introduction

Linear wave making theories are usually unsuccessful in the estimation of wave resistance of practical hulls. This is essentially attributable to the nonlinearity of the free surface phenomena. Experimental studies clarified that the generation of steep waves called free surface shock wave (FSSW) is the most significant phenomenon and that it is followed by the energy-deficient phenomena of wave breaking and free surface turbulence [1], [2] and [3]. Because the steep waves are generated in the near-field where disturbance velocities are grossly of the same order of magnitude with the uniform stream, the nonlinearity of the free surface condition must be thoroughly taken into account in the computation of waves and wave resistance.

On the other hand the interaction of wave motion with viscous flow gradually attracts attentions of researchers. Stern waves of practical hull forms cannot be interpreted without sound understanding of the effect of boundary layer and its separation [4]. In the future development of wave theories viscosity must be carefully considered, and the assumption of irrotational flow must be ceased. The effect of sinkage and trim is taken into account in some of the theoretical methods, such as the Dawson's method [5] (in which free surface condition is basically linear). The force that causes sinkage and trim is partly due to viscous fluid motion, and hence a wave making theory that can deal with viscous fluid motion must be developed to complete the theory.

One of the methods that can apply the exact nonlinear free surface condition and can take viscosity into account is the MAC method [6]. At the Experimental Tank of the University of Tokyo the modified MAC method called Tokyo University Modified Marker-And-Cell (TUMMAC) method has been continuously developed mostly for the

simulation of waves generated by advancing bodies in deep water. The TUMMAC-I method was one for the waves of a floating wedge model advancing steadily [7],[8] and the TUMMAC-II method was one for ships of arbitrary waterline [9]. The TUMMAC-V method was a two-dimensional version used in order to simulate the detailed nonlinear wave motion with a fine cell division [10]. In this paper TUMMAC-IV is employed for the simulation of waves and flow field of a Wigley's hull. The TUMMAC-IV, which is under development, is capable of computing waves generated by ships of arbitrary hull form. At the present stage of development of the TUMMAC-IV method, computation of the waves of aft-bodies and estimation of wave resistance are not yet attained, but only the waves of fore-bodies are presented and compared with experiment. The effect of viscosity will require much time to be properly accounted for, as considerable efforts must be devoted for the achievement of adequate resolution of turbulent motion.

2. Computational method

2.1 Solution procedure

The solution method TUMMAC-IV employed here is a modified version of TUMMAC-II which is also an improved version of TUMMAC-I. Therefore, the solution procedure is, in many respects, common to those described in references [7], [8] and [9], and it is described here only briefly.

The Navier-Stokes equations for incompressible fluid and the equation of continuity are represented in finite-difference forms and solved as an initial-value and boundary-value problem by time-marching and iterations.

For discrete treatment a staggered mesh system is used. And then, the Navier-Stokes equations in finite-difference form give the following equations by forward differencing in time. For the convective terms the combined donor-cell and centered differencing is employed and for the diffusive terms centered differencing.

$$\begin{aligned}
 u_{i+\frac{1}{2}jk}^{n+1} &= \xi_{i+\frac{1}{2}jk} - \frac{\psi_{i+1jk} - \psi_{ijk}}{DX} DT \\
 v_{ij+\frac{1}{2}k}^{n+1} &= \eta_{ij+\frac{1}{2}k} - \frac{\psi_{ij+1k} - \psi_{ijk}}{DY} DT \\
 w_{ijk+\frac{1}{2}}^{n+1} &= \zeta_{ijk+\frac{1}{2}} - \frac{\psi_{ijk+1} - \psi_{ijk}}{DZ} DT
 \end{aligned} \tag{1}$$

In Eqs. (1), ξ , η , ζ are sums of terms of convection and diffusion and ψ is pressure divided by the density of water. DT is time increment and DX , DY and DZ are length, width and height of a rectangular cell. Subscripts are used for the cell location and superscripts for the time level. Eqs. (1) are used to give a new velocity field from a new pressure field in the course of time-marching, and at each time step a pressure field is updated by the solution of the Poisson equation below which is iteratively solved by the SOR method.

$$\psi_{ijk}^{m+1} = \frac{1}{2 \left(\frac{1}{DX^2} + \frac{1}{DY^2} + \frac{1}{DZ^2} \right)} \left[\frac{\psi_{i+1jk}^m + \psi_{i-1jk}^{m+1}}{DX^2} + \frac{\psi_{ij+1k}^m + \psi_{ij-1k}^{m+1}}{DY^2} + \frac{\psi_{ijk+1}^m + \psi_{ijk-1}^{m+1}}{DZ^2} - R_{ijk} \right] \quad (2)$$

$$R_{ijk} = \frac{\xi_{i+\frac{1}{2}jk} - \xi_{i-\frac{1}{2}jk}}{DT DX} + \frac{\eta_{ij+\frac{1}{2}k} - \eta_{ij-\frac{1}{2}k}}{DT DY} + \frac{\zeta_{ijk+\frac{1}{2}} - \zeta_{ijk-\frac{1}{2}}}{DT DZ}$$

The computational scheme is shown in block diagram in Fig.1.

2. 2 Boundary condition

It is very significant for the finite-difference method to impose proper conditions at various computational boundaries. The boundary conditions of TUMMAC-IV is essentially common to those of TUMMAC-II described in [9] except for the condition of a body boundary, at which waves are generated.

The hull surface is approximated in the manner illustrated in Figs.2 and 3. The water-line is assumed to be a succession of straight segments, and the frame-line is approximated by a step-like configuration. The body boundary condition is imposed in the cells denoted B. A free-slip condition is applied, and then 1) the velocity normal to the segment is to be zero, 2) the divergence of the boundary cell is to be zero and 3) the normal derivative of the velocity tangential to the segment is to be zero. These conditions are satisfied by the technique extended from that initiated by Vieceilli [11] for a 2-D case. The procedure is described in [9] in the case of ship of vertical walls. The procedure of TUMMAC-IV is contrived to properly take the vertical velocity component into account.

3. Results of computation

3. 1 Condition of computation

The forebody of a Wigley's hull which is 2.5m in full length is chosen for the computation. The computational domain is $0.80 \times 0.30 \times 0.50$ m in x , y , z directions. The cell dimensions $DX \times DY \times DZ$ are $0.025 \times 0.010 \times 0.03125$ m. DX in Fig.2 is 0.050m, which is little coarse cell division and the above finer one is used in the computation in this paper. The number of cell is around 20000. The Froude numbers chosen here are 0.267, 0.289 and 0.316 and the time increment DT is from 0.00300 to 0.00354 sec. The number of time step for the acceleration is 300 steps and the steady state at $F_n = 0.267$ is reached at the 600-th step and again accelerated for 100 steps and the steady state at $F_n = 0.289$ is reached at the 900-th step and once more accelerated to have the steady state of $F_n = 0.316$ at the 1200-th step. The CPU time required by HITAC M-280H for this 1200-th steps is about 71 minutes.

At the end of this paper a computational result of waves around the forebody of a 3m model of a bulk carrier M55FO on ballast condition is presented. This hull form is one of the typical DW 27000 MT bulk carriers with a bulbous bow. In this case $DX \times DY \times DZ$ are $0.020 \times 0.020 \times 0.018$ m.

3. 2 Computed waves and velocity field

Computed wave height contours at three Froude numbers and measured one at $F_n = 0.289$ are shown in Figs.4 and 5. The angle of wave crest line to the centerline is decreased by the increasing Froude number, as experimentally explained [1], [2] and [3]. The comparison with the measured in Figs. 5 and 6 implies quantitative inadequacy, although it is qualitatively satisfactory. The inadequacy can be partly or mostly removed by the adoption of finer cell dimensions though with high computational cost [8]. Computed fields of velocity vector (v - w) components on 6 vertical planes are shown in Fig.7.

Computed wave height contours of M55FO are shown in Fig.8 being compared with the experimental results in Fig.9. The agreement is good with respect to the foremost wave and discrepancy becomes obvious in the wave trough behind it and the second wave crest. This discrepancy is attributable not only to the numerical error but also to the complicated energy-deficient flow caused by wave breaking which the present method is not capable of accounting for. However, this computational results of waves

which are the cause of wave resistance imply that the present method is already useful for the prediction of relative magnitude of waves between hull forms to be compared. Hence, useful information for the design of hull forms of small wave resistance is derived in more detailed manner than the integrated value of wave resistance.

4. Concluding remarks

For finite-difference method the accuracy must be compromised with the economy, when the problem of stability is settled. Although it is certified that high accuracy is attained by finer cells [8], the number of cell greater than 20000 is very costly for the computers of these days. Therefore, the use of this computational method for practical hull form design may be premature.

The other defficulty arises from the complicated nonlinear fluid motion, i. e., wave breaking and turbulence. Both are related to the energy dissipation of fluid flow. A deal of effort is being or going to be dovoted to the numerical simulation of turbulence with proper resolution of sub-grid-scale motions, which will be intimately connected with the computation of stern waves that play a certain role in wave resistance. In this paper a free-slip boundary condition is used and the kinematic viscosity is assumed zero, which is an inevitable consequence of the coarse cell division as well as of the difficulty in the treatment of the turbulent flow at present.

The TUMMAC-IV method is under development, and unfortunately the pressure distribution on the hull surface and the integrated value of wave resistance cannot be included in this paper. In the near future more advanced computations will be carried out by a super-computer HITAC S-810 and will be reported together with pressure distributions and values of wave resistance.

References

- [1] Takahashi, M. et al. (1980). Characteristics of free surface shock waves around wedge models, J. Soc. Naval Arch. Japan 148.
- [2] Miyata, H. (1980). Characteristics of nonlinear waves in the near-field of ship and their effects on resistance, Proc. 13th Sympo. Naval Hydrodynamics.

- [3] Miyata, H. et al. (1982). Characteristics of free surface shock waves around wedge models (2nd report). J. Soc. Naval Arch. Japan 151.
- [4] Doi, Y. et al. (1981, 82). Characteristics of stern waves generated by ships of simple hull form (1st and 2nd report), J. Soc. Naval Arch. Japan 150, 151.
- [5] Dawson, C.W. (1979). Calculations with the XYZ free surface program for five ship models, Proc. Workshop on Ship Wave-Resistance Computations, DTNSRDC.
- [6] Welch, J.E. et al. (1966). The MAC method. Los Alamos Scientific Lab. Univ. California.
- [7] Miyata, H. et al. (1981). Numerical explanation of nonlinear nondispersive waves around bow. Proc. 3rd Intern. Conf. Numerical Ship Hydrodynamics.
- [8] Suzuki, A., Masuko, A., Aoki, K. et al. (1981, 82, 83). Numerical analysis of free surface shock waves around bow by modified MAC-method (1st, 2nd and 3rd report), J. Soc. Naval Arch. Japan 150, 152, 153.
- [9] Aoki, K. et al. (1983). A numerical analysis of nonlinear waves generated by ships of arbitrary waterline (1st report), J. Soc. Naval Arch. Japan 154 (to appear).
- [10] Miyata, H. et al. (1983). Numerical and experimental analysis of nonlinear bow and stern waves of a two-dimensional body (1st report), J. Soc. Naval Arch. Japan 154 (to appear).
- [11] Viecegli, J.A. (1971). A computing method for incompressible flows bounded by moving walls, J. Computational Physics 8.

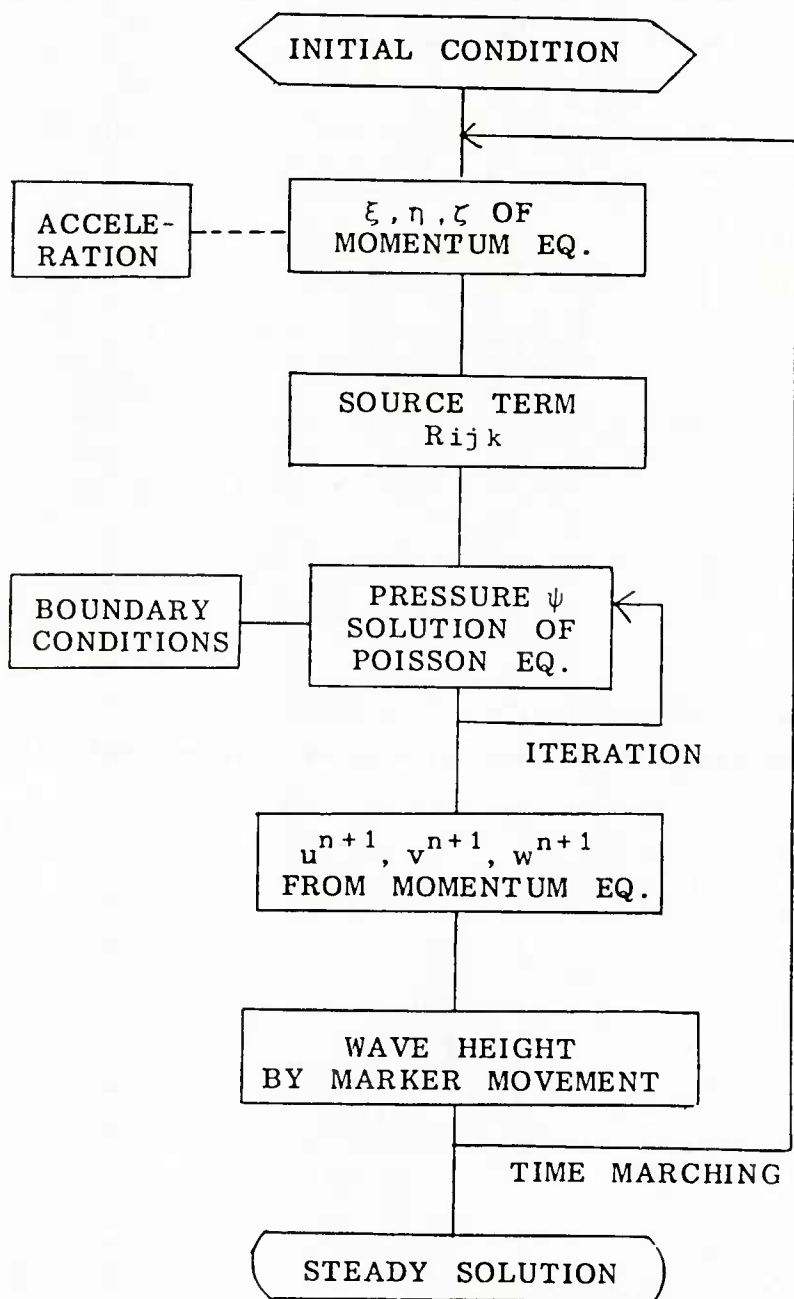
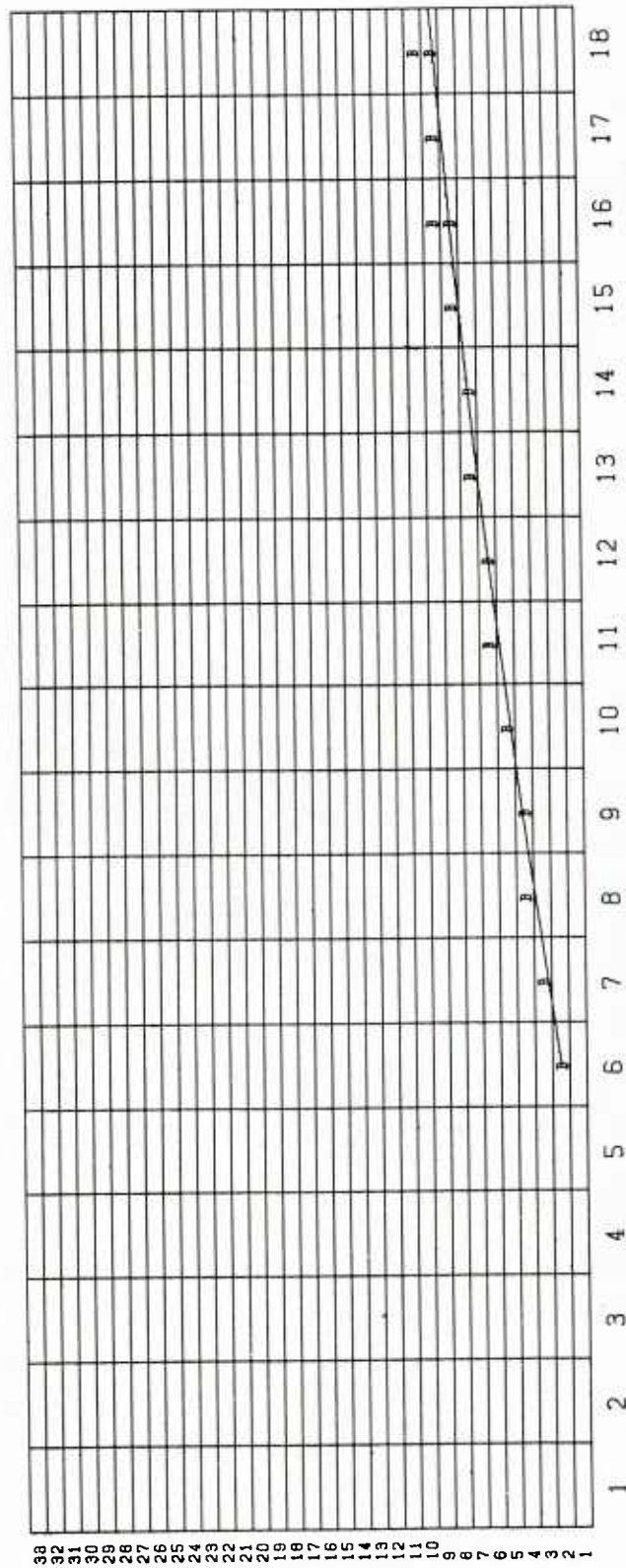


Fig. 1 Block diagram of the TUMMAC method.



$K = 8$ $Z = -0.078125M$

CELL ARRANGEMENT FOR TUMMAC-IV METHOD FOR WIGLEY

Fig. 2 Cell division of a Wigley's hull on a horizontal (x-y) plane.

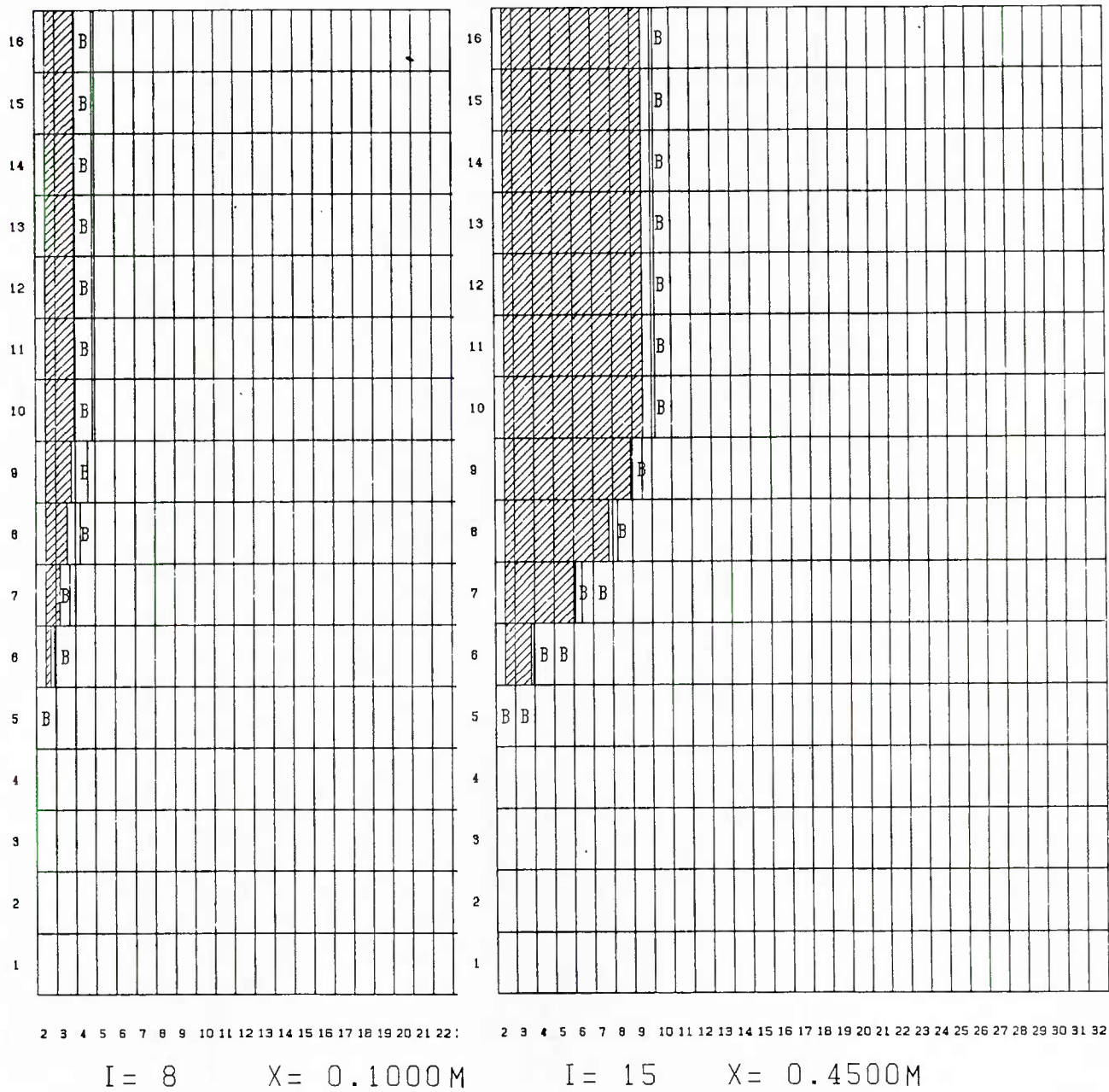


Fig. 3 Cell division of a Wigley's hull on a vertical (y-z) plane.

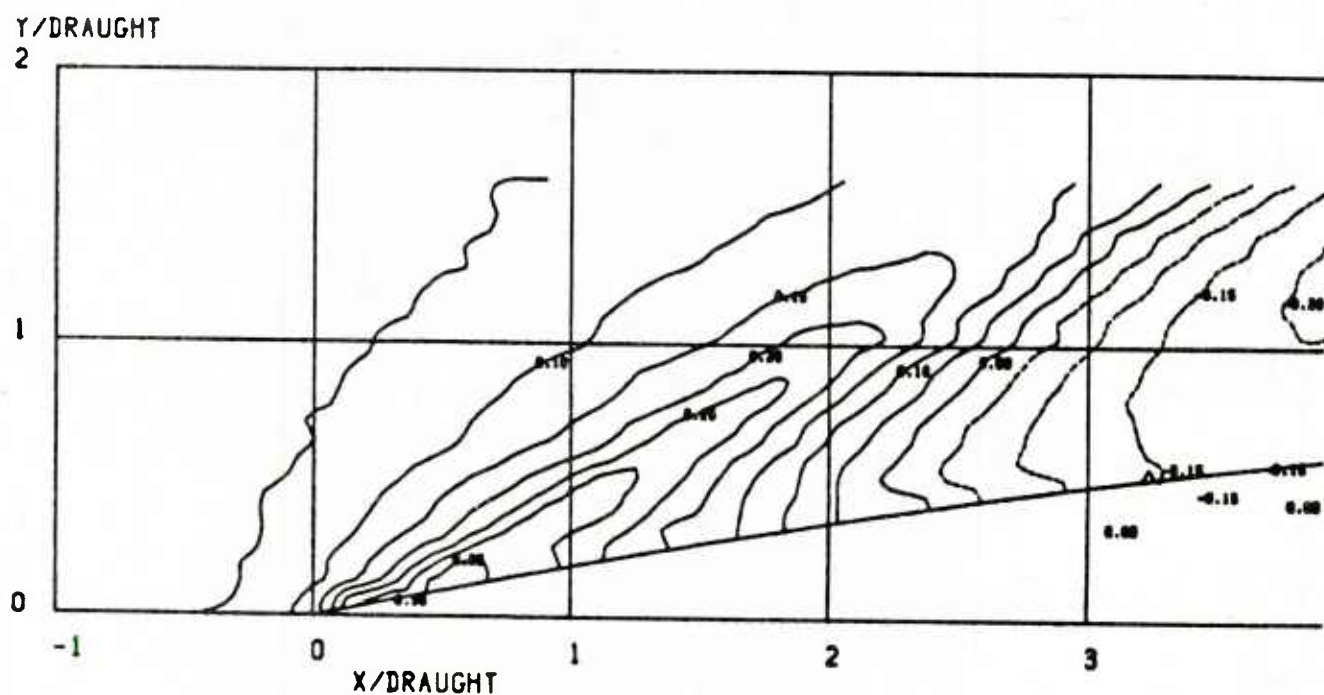
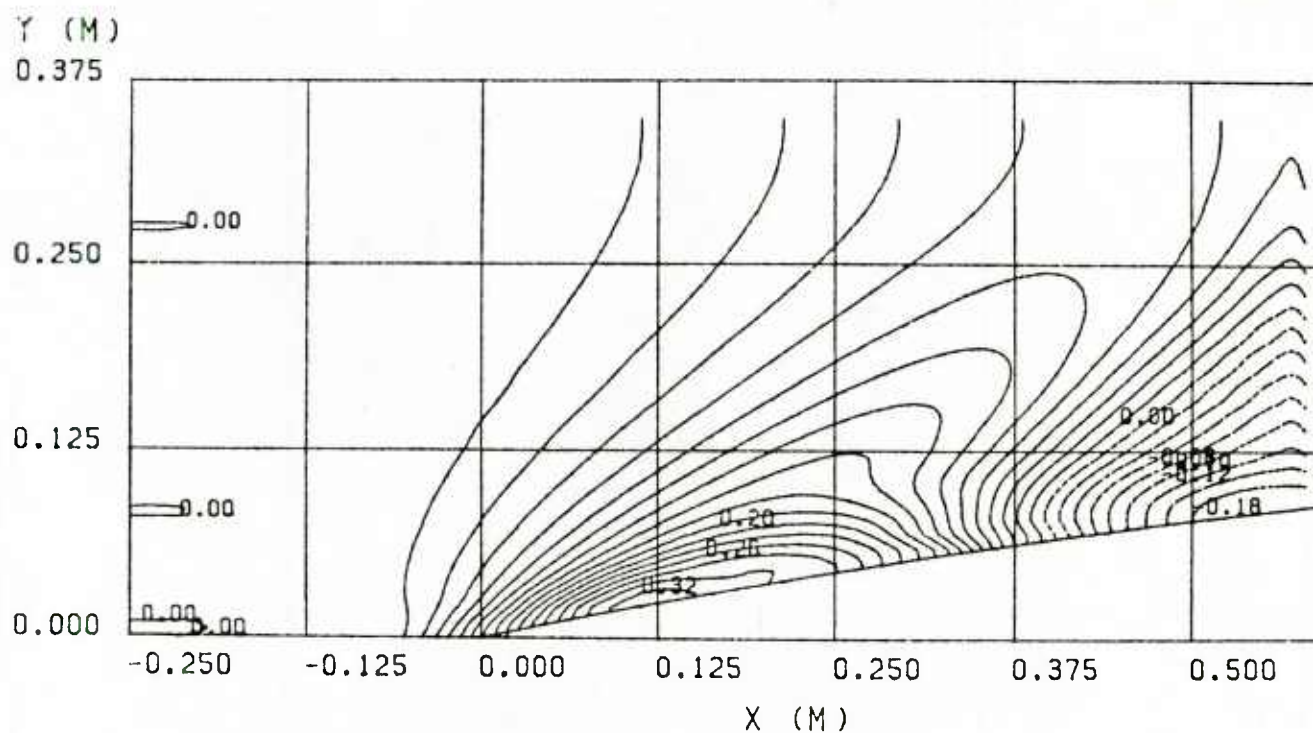


Fig. 5 Computed (above) and measured (below) wave height contours of a Wigley's hull at $F_n = 0.289$.

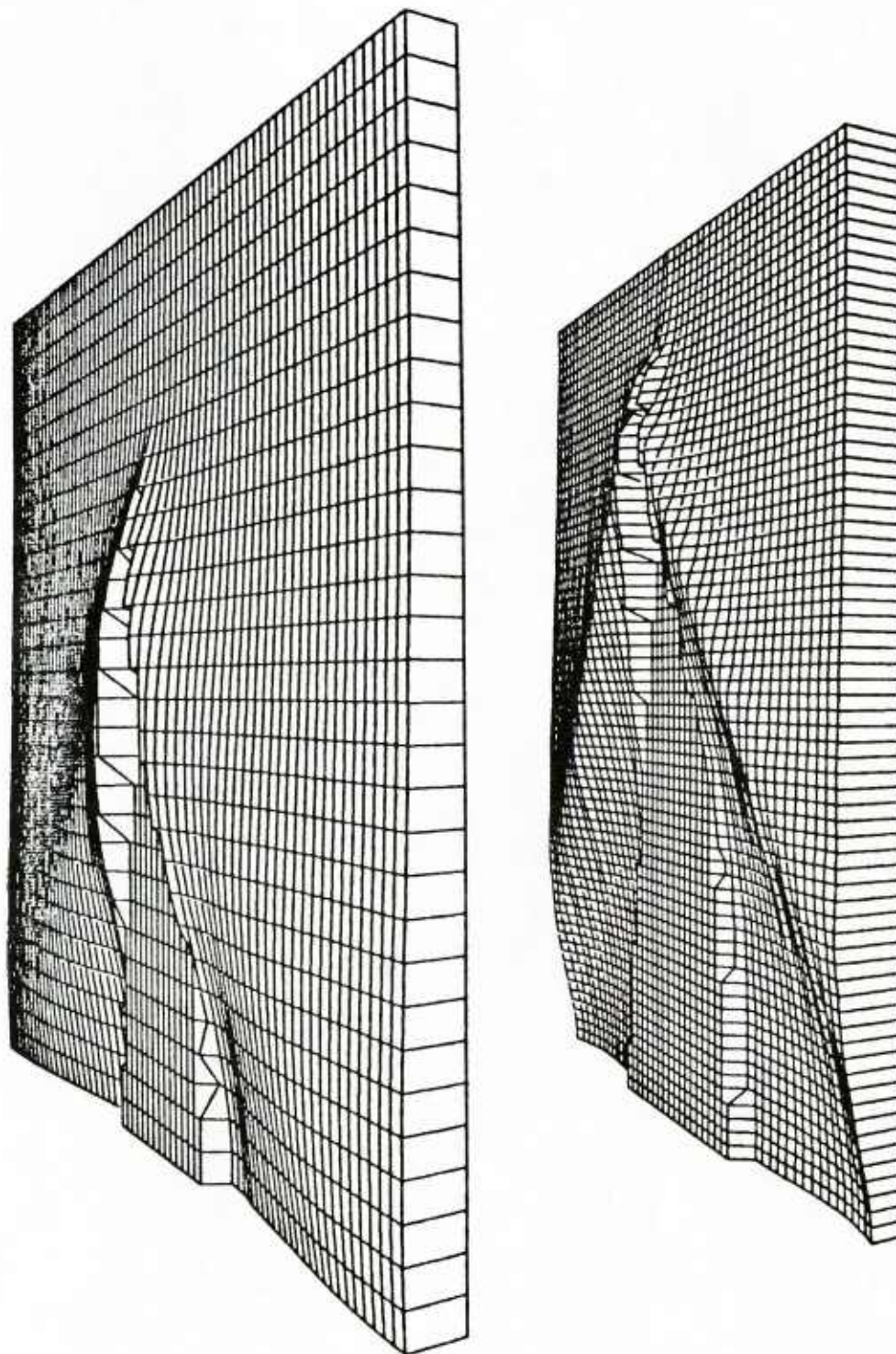


Fig. 6 Computed (above) and measured (below) perspective views of waves generated by a Wigley's hull at $F_n = 0.289$.

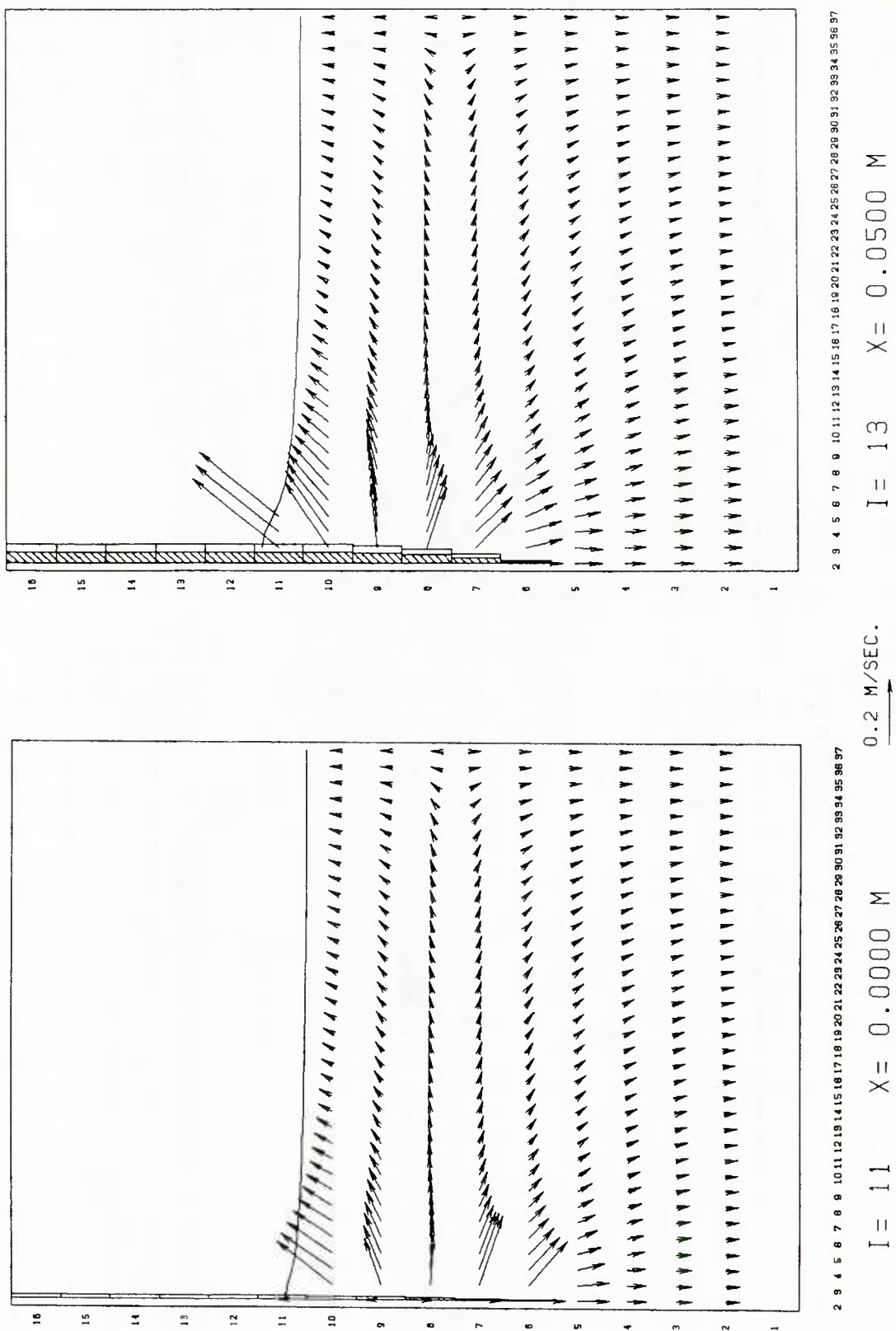
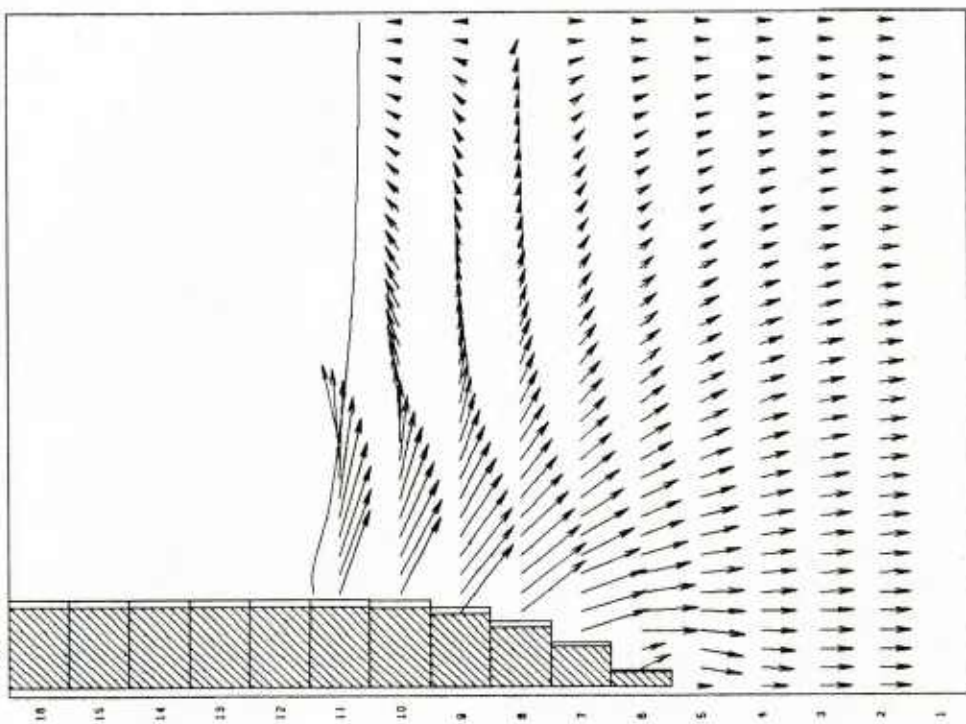
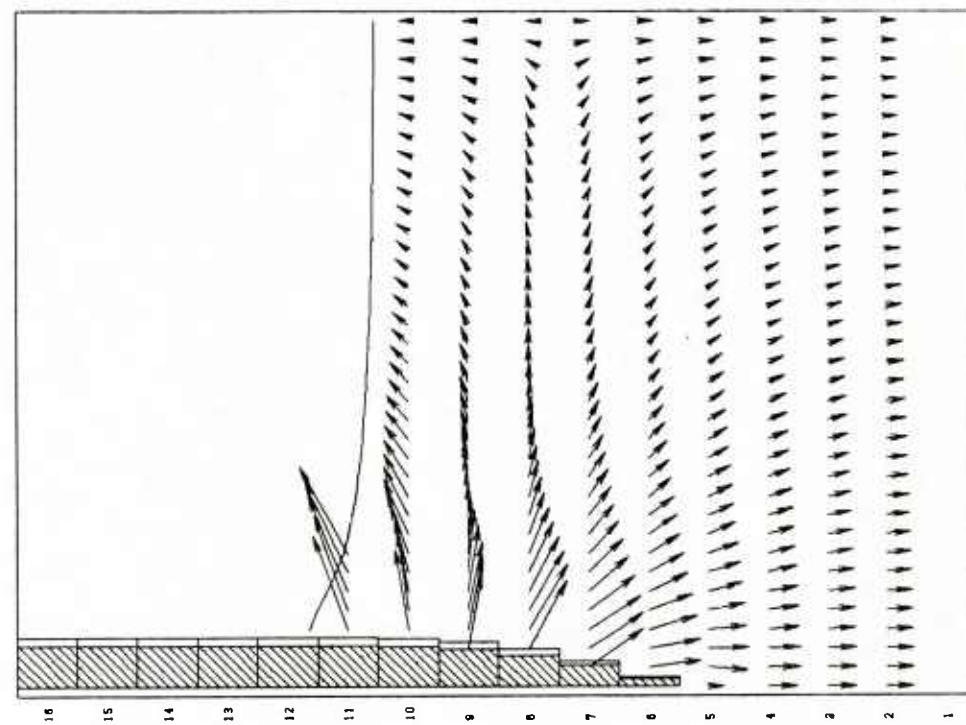


Fig. 7(a) Computed velocity vector (u-w) field on vertical (y-z) planes at $F_n = 0.316$.

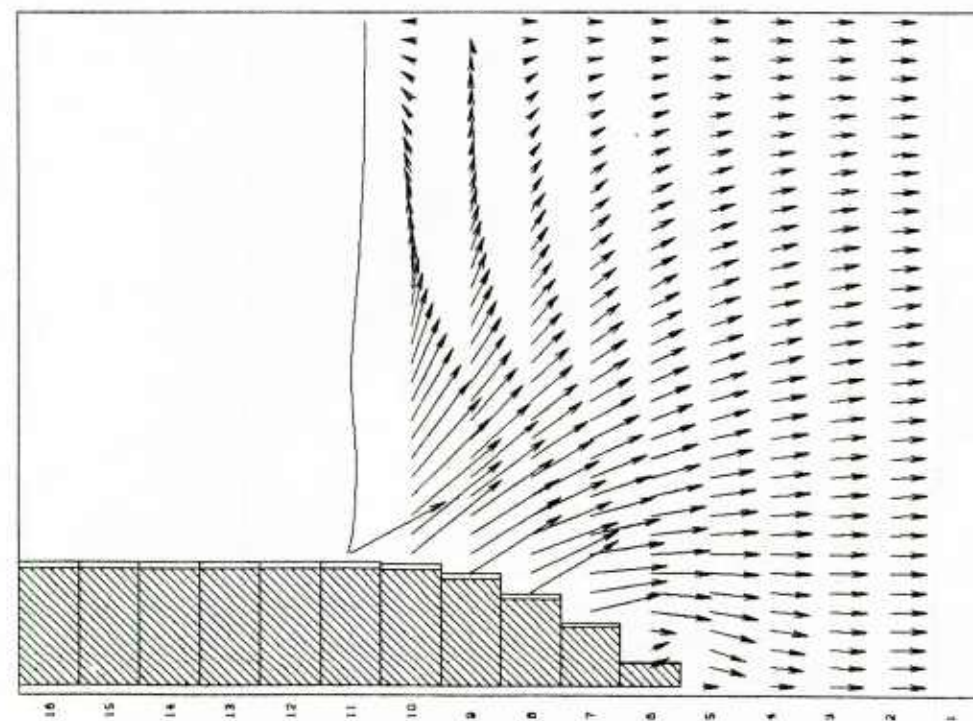


$I = 16$ $X = 0.1250$ M 0.2 M/SEC



$I = 21$ $X = 0.2500$ M 0.2 M/SEC

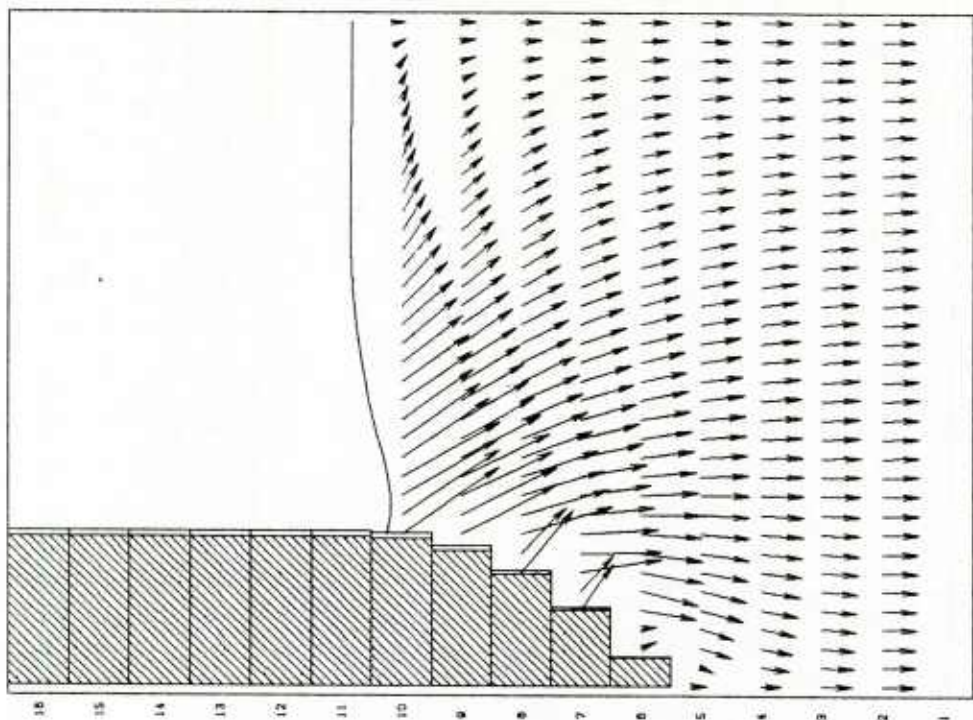
Fig. 7(b) as Fig. 7(a)



2 3 4 5 6 7 8 9 10 11 12 13 14 15 16 17 18 19 20 21 22 23 24 25 26 27 28 29 30 31 32 33 34 35 36 37

I = 26 X = 0.3750 M

0.2 M/SEC.



2 3 4 5 6 7 8 9 10 11 12 13 14 15 16 17 18 19 20 21 22 23 24 25 26 27 28 29 30 31 32 33 34 35 36 37

I = 31 X = 0.5000 M

Fig. 7(c) as Fig. 7(a)

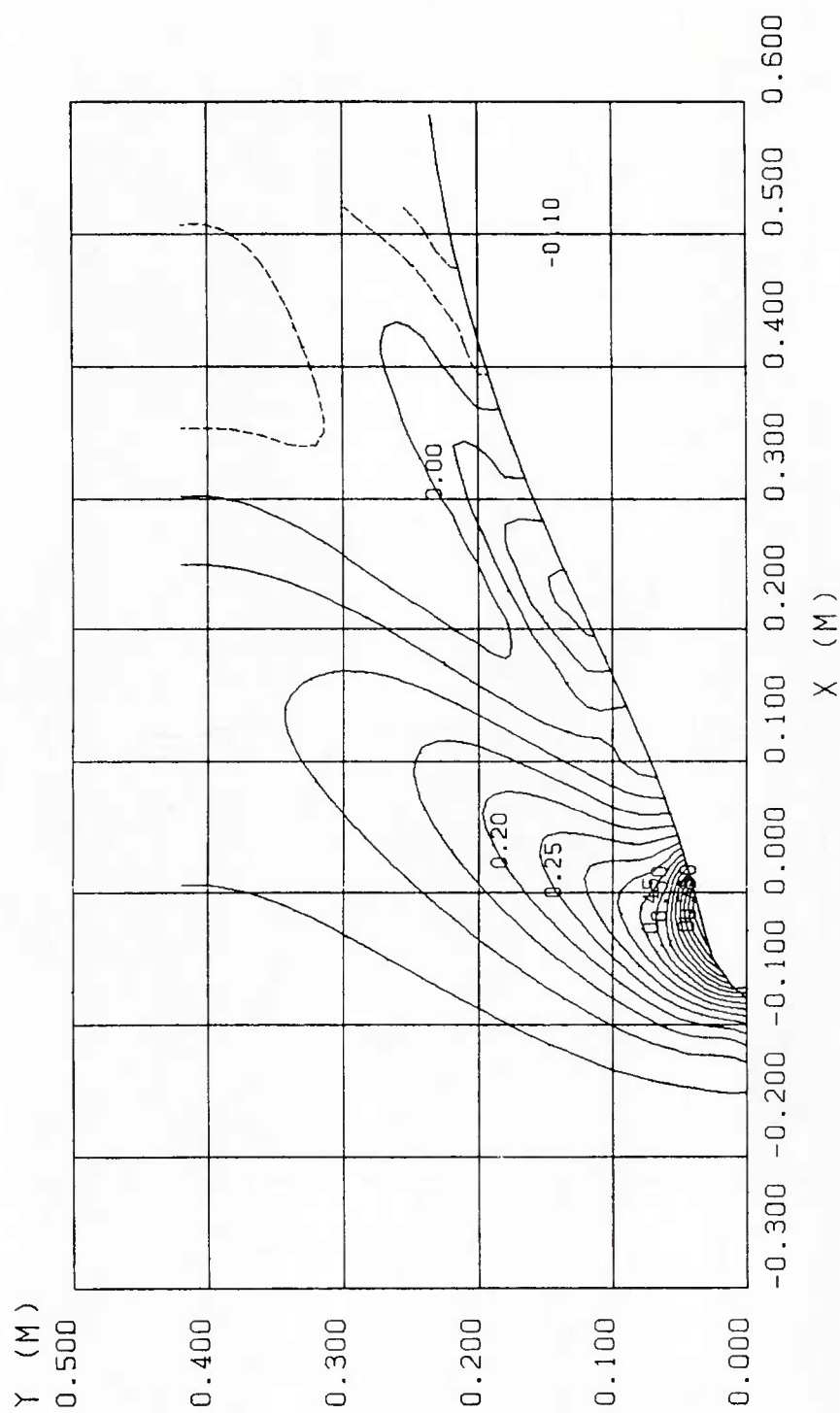


Fig. 8 Computed wave height contours of a ship model of bulk carrier (M55F0) on ballast condition at $F_n = 0.18$, the interval of contour is $0.05H$ ($= U^2/2g$).

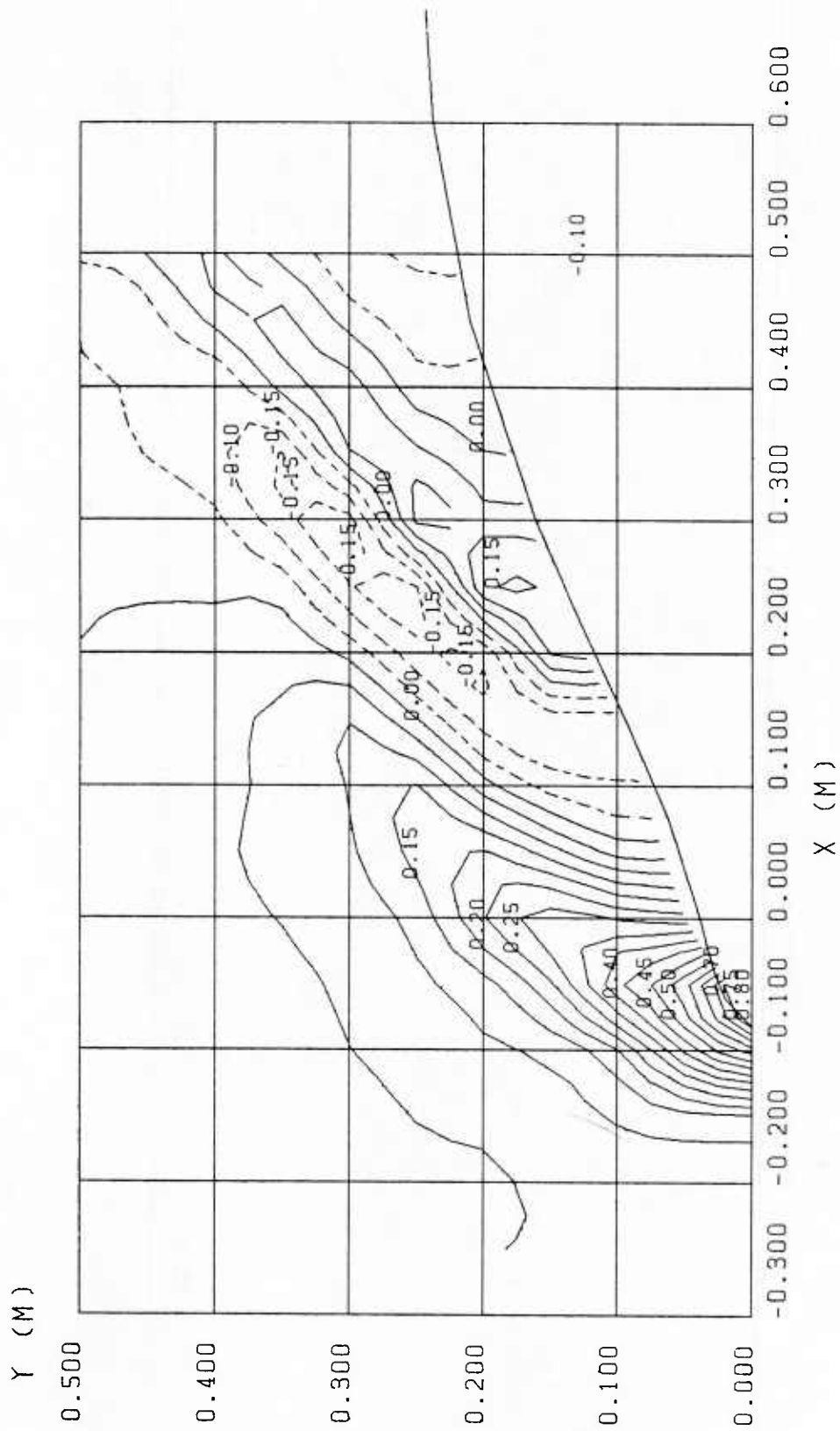


Fig. 9 Measured wave height contours of M55F0 at the same condition with Fig. 8, the interval of contour is 0.05H.

DUDLEY KNOX LIBRARY - RESEARCH REPORTS



5 6853 01002180 1

U211284